Springer Tracts in Civil Engineering

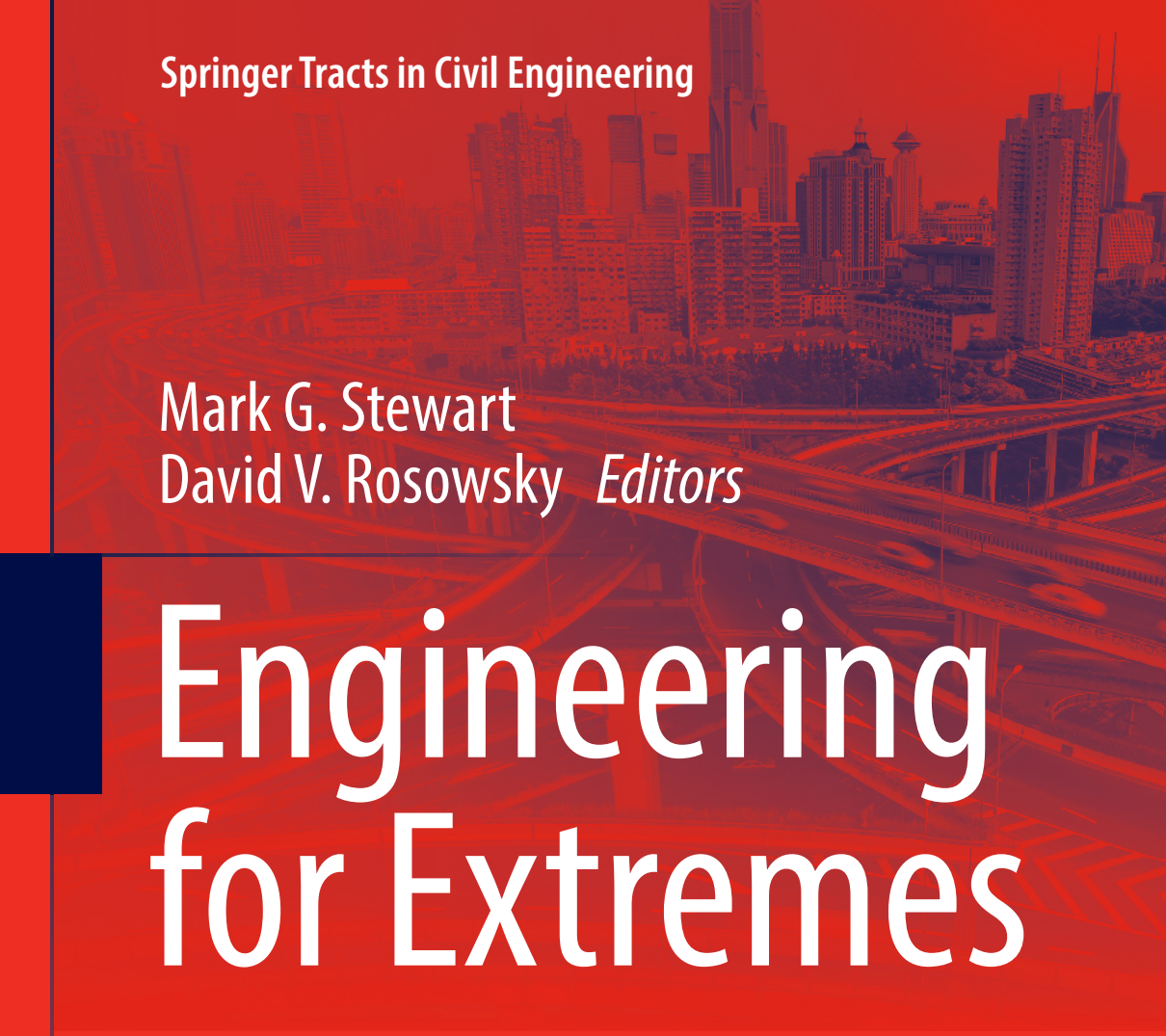

Mark G. Stewart
David V. Rosowsky *Editors*

# Engineering for Extremes

## Decision-Making in an Uncertain World

Springer

# Springer Tracts in Civil Engineering

**Springer Tracts in Civil Engineering** (STCE) publishes the latest developments in Civil Engineering - quickly, informally and in top quality. The series scope includes monographs, professional books, graduate textbooks and edited volumes, as well as outstanding PhD theses. Its goal is to cover all the main branches of civil engineering, both theoretical and applied, including:

- Construction and Structural Mechanics
- Building Materials
- Concrete, Steel and Timber Structures
- Geotechnical Engineering
- Earthquake Engineering
- Coastal Engineering; Ocean and Offshore Engineering
- Hydraulics, Hydrology and Water Resources Engineering
- Environmental Engineering and Sustainability
- Structural Health and Monitoring
- Surveying and Geographical Information Systems
- Heating, Ventilation and Air Conditioning (HVAC)
- Transportation and Traffic
- Risk Analysis
- Safety and Security

**Indexed by Scopus**

To submit a proposal or request further information, please contact:
Pierpaolo Riva at Pierpaolo.Riva@springer.com (Europe and Americas) Wayne Hu at wayne.hu@springer.com (China)

More information about this series at https://www.springer.com/bookseries/15088

Mark G. Stewart · David V. Rosowsky
Editors

# Engineering for Extremes

## Decision-Making in an Uncertain World

Springer

*Editors*
Mark G. Stewart
Centre for Infrastructure Performance
and Reliability
The University of Newcastle
Newcastle, NSW, Australia

David V. Rosowsky
Kansas State University
Manhattan, KS, USA

ISSN 2366-259X ISSN 2366-2603 (electronic)
Springer Tracts in Civil Engineering
ISBN 978-3-030-85017-3 ISBN 978-3-030-85018-0 (eBook)
https://doi.org/10.1007/978-3-030-85018-0



This Springer imprint is published by the registered company Springer Nature Switzerland AG
The registered company address is: Gewerbestrasse 11, 6330 Cham, Switzerland

# Preface

The community has always been worried by extreme weather events and for good reason. In the era before insurance, the personal and financial loss from a flood, storm, fire, hurricane, or earthquake could wreck livelihoods, destroy homes, shops and workplaces, and lead to widespread poverty and destitution that might take generations to recover from. While these devastating consequences are often avoided in the developed world, they remain a sad reality for much of the world.

It is therefore of no surprise that the civil engineering profession has its roots in improving the resilience of the community to extreme events. The desire to build a flood proof river crossing led to the revolutionary cast-iron Iron Bridge being built in Coalbrookdale in England in 1779 for what in its day was an impressive 30 m span. Within a century, civil engineering had advanced to the point where spans of 500 m or longer were possible—the Brooklyn Bridge linking the communities of Manhattan and Brooklyn in New York City being one notable example.

Despite this progress, significant challenges remain today. Buildings, bridges, roads, nuclear power plants, and other infrastructure essential to our economic and social well-being are at an increasing risk from terrorism, climate change, hurricanes, storms, floods, earthquakes, heat waves, fires, and other extreme events. The timing and severity of these extremes are highly uncertain and are characterised as low probability–high consequence events. Risk and cost–benefit analyses of protective measures aim to reduce the vulnerability of infrastructure and hence reduce the future impact of extreme events to reveal protective measures that are cost effective and those that are not. Relevant also are private and public policy imperatives in the decision-making process.

Extreme events and actions taken to reduce the vulnerability of infrastructure are sometimes based on worst-case thinking, probability and cost neglect, and risk aversion. This can result in a frightened public, costly policy outcomes, and wasteful expenditures.

The book will explain how risk and decision-making analytics can be applied to the wicked problem of protecting infrastructure and society from extreme events. There is increasing research that takes into account the risks associated with the timing and severity of extreme events in engineering to reduce the vulnerability or increasing the

resiliency of infrastructure—we refer to this as '*Engineering for Extremes*'. Engineering for extremes is defined as measures taken to reduce the vulnerability or increase the resiliency of built infrastructure to climate change, hurricanes, storms, floods, earthquakes, heat waves, fires, and malevolent and abnormal events that include terrorism, accidental explosion or fire, vehicle impact, and vehicle overload. This may include, for example, enhancement of design standards (higher design loads or flood levels), retrofitting or strengthening of existing structures, utilisation of new materials, and changes to inspection and maintenance regimes.

The book will introduce the key concepts needed to assess the economic and social well-being risks, costs, and benefits of infrastructure to extreme events. This will include hazard modelling (likelihood and severity), infrastructure vulnerability, resilience or exposure (likelihood and extent of damage), social and economic loss models, risk reduction from protective measures, and decision theory (cost–benefit and utility analyses). This will be followed by case studies authored by experts from Australia, USA, Canada, UK, Ireland, France, New Zealand, China, Japan, South Africa, and South America. These case studies will describe succinctly the practical aspects of risk assessment when deciding on the most cost-efficient measures to reduce infrastructure vulnerability to extreme events for housing, buildings, bridges, roads, tunnels, pipelines, and electricity infrastructure in the developed and developing worlds.

The editors have been colleagues and close friends for nearly 30 years. One introduced the other to a lifetime addiction to Dunkin Donuts and the other to the delights of an Aussie favourite—Tim Tams. This book became our COVID project. It was also an excuse to reach out to our friends and colleagues around the globe. Their response to our book proposal was warm and generous. All the more so as, we were all battling the personal trauma and professional disruptions wreaked by COVID-19. In these trying times, their support was something we will not easily forget.

So we are incredibly grateful to the authors of the chapters. The authors shared our enthusiasm for the book and, more importantly, devoted much time and energy to producing chapters that are at the forefront of the latest developments, are engaging to a non-specialist reader, and provide a focus on practical decision outcomes. The chapters reflect the expertise of the authors and the latest developments on engineering for extremes.

Finally, we appreciate the support from the folks at Springer in bringing this book to fruition.

Newcastle, Australia — Mark G. Stewart
Kansas, USA — David V. Rosowsky
May 2021

# Contents

**Part I Introduction**

**1 Extreme Events for Infrastructure: Uncertainty and Risk** . . . . . 3
Mark G. Stewart and David V. Rosowsky

**Part II Decision-Making**

**2 Risks and Compromises: Principled Compromises in Managing Societal Risks of Extreme Events** . . . . . 31
Paolo Gardoni and Colleen Murphy

**3 Risk-Informed Approaches for Mitigating Impacts of Extreme and Abnormal Events in the Built Environment** . . . . . 45
Bruce R. Ellingwood

**Part III Case Studies**

**4 Aviation Resilience to Terrorist Hijackings** . . . . . 69
Mark G. Stewart and John Mueller

**5 Challenges of Effective Blast Protection of Buildings** . . . . . 93
Hong Hao and Xihong Zhang

**6 Adaptation of Housing to Climate Change and Extreme Windstorms** . . . . . 119
Hao Qin and Mark G. Stewart

**7 Risk-Based Management of Electric Power Distribution Systems Subjected to Hurricane and Tornado Hazards** . . . . . 143
Yue Li, Abdullahi M. Salman, Abdullah Braik, Sirrý Bjarnadóttir, and Babak Salarieh

**8 Hurricane Fragility Assessment of Power Transmission Towers for a New Set of Performance-Based Limit States** . . . . . 167
Yousef M. Darestani, Ashkan B. Jeddi, and Abdollah Shafieezadeh

**9 Building Adaptation to Extreme Heatwaves** ..... 189
Dileep Kumar, Morshed Alam, and Jay Sanjayan

**10 Improving Regional Infrastructure Resilience to Earthquakes, Storms and Tsunami** ..... 217
David Elms, Ian McCahon, and Rob Dewhirst

**11 Earthquake-Tsunami Risk Assessment and Critical Multi-hazard Loss Scenarios: A Case Study in Japan Under the Nankai-Tonankai Mega-Thrust** ..... 235
Katsuichiro Goda, Raffaele De Risi, Flavia De Luca, Ario Muhammad, Tomohiro Yasuda, and Nobuhito Mori

**12 Building Resilience in Changing Cryosphere Services** ..... 255
Bo Su, Xiaoming Wang, Cunde Xiao, Jinglin Zhang, and Bin Ma

**13 Extreme Vehicles and Bridge Safety** ..... 271
Colin Caprani and Mayer Melhem

**14 Fire Safety in Road Tunnels** ..... 293
T. D. Gerard Canisius, Dimitris Diamantidis, and Suresh Kumar

**15 Cost-Benefit Analysis of Design for Progressive Collapse Under Accidental or Malevolent Extreme Events** ..... 313
André Teófilo Beck, Lucas da Rosa Ribeiro, and Marcos Valdebenito

**16 Durability and Performance of Wind Turbines Under Climate Extremes** ..... 335
Rui Teixeira, Alan O'Connor, and Dimitri V. Val

**17 Extreme Value Analysis for Offshore Pipeline Risk Estimation** ..... 355
Robert E. Melchers

**18 Reliability Assessment of Corroded Pipelines Subjected to Seismic Activity** ..... 373
Rafael Amaya-Gómez, Mauricio Sánchez-Silva, and Emilio Bastidas-Arteaga

**19 Climate Change Impact for Bridges Subject to Flooding** ..... 393
Boulent Imam

**20 Bushfire and Climate Change Risks to Electricity Transmission Networks** ..... 413
Chi-Hsiang Wang

**21 Provisions for Climate Change in Structural Design Standards** ..... 429
Johan Retief and Celeste Viljoen

**Part IV Conclusions and Recommendations**

**22 Conclusions for Engineers and Policy Makers** . . . . . 449
David V. Rosowsky and Mark G. Stewart

**Correction to: Extreme Vehicles and Bridge Safety** . . . . . C1
Colin Caprani and Mayer Melhem

# About the Editors

**Mark G. Stewart** is Professor of Civil Engineering and Director of the Centre for Infrastructure Performance and Reliability at The University of Newcastle in Australia. Professor Stewart is an international leader in risk assessment, public policy decision-making, and protective infrastructure for extreme hazards. He is Author of *Probabilistic Risk Assessment of Engineering Systems* (Chapman & Hall 1997), *Terror, Security, and Money: Balancing the Risks, Benefits, and Costs of Homeland Security* (Oxford University Press 2011), *Chasing Ghosts: The Policing of Terrorism* (Oxford University Press 2016), *Are We Safe Enough? Measuring and Assessing Aviation Security* (Elsevier 2018), an edited book *Climate Adaptation Engineering: Risks and Economics for Infrastructure Decision-making* (Elsevier 2019), as well as more than 500 technical papers and reports. He has more than 30 years of experience in probabilistic risk and vulnerability assessment of infrastructure and security systems that are subject to man-made and natural hazards. He has attracted more than $10 million in research funding. In the past decade, Stewart has led the way in risk-based assessment of terrorism and climate change impacts on engineering infrastructure with 25 keynotes at international conferences. He is Editor-in-Chief of *Structural Safety* and Fellow of the Australian Academy of Technology and Engineering.

**David V. Rosowsky** is Vice President for Research at Kansas State University where he also holds the title of Professor of Civil Engineering. Prior to joining K-State, he served for six years as Provost and Senior Vice President and Provost at University of Vermont. Prior to that, he served as Dean of Engineering at Rensselaer Polytechnic Institute and before that as Head of the Zachry Department of Civil Engineering at Texas A&M University where he also held the A.P. and Florence Wiley Chair in Civil Engineering. He also previously held Richardson Chair in Wood Engineering and Mechanics at Oregon State University and was Faculty Member at Clemson University. Since 1990, he has conducted research in the areas of structural reliability, performance of wood structural systems, design for natural hazards, stochastic modelling of structural and environmental loads, and probability-based codified design. His current research addresses three topics: (1) behaviour of the built

environment subject to natural hazards, most recently including the effects of climate change and adaptation, (2) modelling and analysis of load effects on buildings and other structures with particular emphasis on complex environmental phenomena, and (3) performance-based engineering for design, post-disaster condition assessment, and loss estimation studies. He has authored or co-authored more than 300 technical papers. A recognised expert in the field of structural reliability, he has been invited to present his research work around the world including invited lecturers in France, Italy, Switzerland, Canada, Japan, Australia, and New Zealand. He has supervised more than 20 masters and doctoral students. He is Recipient of the ASCE Walter L. Huber Research Prize, the T. K. Hseih Award from the Institution of Civil Engineers (UK), and the ASCE Norman Medal.

# Part I
# Introduction

# Chapter 1
# Extreme Events for Infrastructure: Uncertainty and Risk


**Mark G. Stewart and David V. Rosowsky**

**Abstract** Buildings, bridges, roads, and other infrastructure essential to our economic and social well-being are at an increasing risk from hurricanes, storms, floods, earthquakes, tsunamis, heat waves, fires, terrorism, climate change and other extreme events. The timing, severity and combination of these extremes are highly uncertain, and are characterised as low probability-high consequence events. The chapter starts by introducing and reviewing basic concepts about risk and cost–benefit analysis of protective measures aim to reduce the vulnerability of infrastructure, and hence reduce the future impacts of extreme events to reveal protective measures that are cost-effective, and those that are not. This literature review justifies the introduction of risk-based decision support that integrates hazard, engineering, and fragility models, as well as economical decision tools to perform a comprehensive assessment of the cost-effectiveness of protective measures. This risk-based decision support will be illustrated with various study cases of engineering for extremes in the following chapters of this book.

**Keywords** Risk · Decision making · Infrastructure · Extreme events · Hazard · Safety · Cost–benefit analysis · Uncertainty

## 1.1 Introduction

Buildings, bridges, roads, and other infrastructure essential to our economic and social well-being are at an increasing risk from hurricanes, storms, floods, earthquakes, tsunamis, heat waves, fires, terrorism, climate change and other extreme events. The timing and severity of these extremes are highly uncertain, and are characterised as low probability-high consequence events.

M. G. Stewart (✉)
Centre for Infrastructure Performance and Reliability, The University of Newcastle, Newcastle, Australia
e-mail: mark.stewart@newcastle.edu.au

D. V. Rosowsky
Civil Engineering, Kansas State University, Manhattan, KS, USA
e-mail: rosowsky@ksu.edu



M. G. Stewart and D. V. Rosowsky (eds.), *Engineering for Extremes*, Springer Tracts in Civil Engineering, https://doi.org/10.1007/978-3-030-85018-0_1

Extreme events arouse much fear and anxiety in society. And for good reason. The terrorist attacks on 11 September 2001 killed nearly 3000 people in New York and Washington, caused $250 billion in loss of life, infrastructure damage, loss of tourism, reduction in GDP and other direct, indirect and social losses [31]. Since then, over $2 trillion has been spent by the United States on domestic counter-terrorism, and much more on the wars in Afghanistan, Iraq and Syria [33]. The World Bank reports that losses in the built environment from extreme climate hazards are over $300 billion per year, and can rise to $415 billion by 2030 [65], see also Fig. 1.1. Climate change will add to these losses, with the World Bank estimating that sea-level rise and subsidence in the 136 largest coastal cities could result in losses of up to $1 trillion per year by 2050 without further investment in adaptation and risk management. Figure 1.2 shows that fatalities from natural disasters can exceed 300,000 in any one year, and the long-term average is about 100,000 deaths per year. Figure 1.3 shows that the vast majority of losses and fatalities arise from natural disasters (floods, storms, earthquakes, droughts/forest fires/heat waves, cold waves/frost, hail, tsunamis) as these tend to cause widespread damage to large communities or regions. On the other hand, man-made disasters (major fires and explosions, aviation and space disasters, shipping disasters, rail disasters, mining accidents, collapse of buildings/bridges, and terrorism) tend to affect a large object in a very limited space resulting in lower losses when compared to natural disasters. Extreme events, such as climate change, are also deemed by some to be direct threats to national security (e.g., [52]).

While these are staggering losses, they can be ameliorated with targeted strategies to reduce vulnerability, increase resilience or reduce exposure of infrastructure and people to extreme events. For example, the World Bank shows that the net benefit of building more resilient infrastructure in low and middle income countries would be

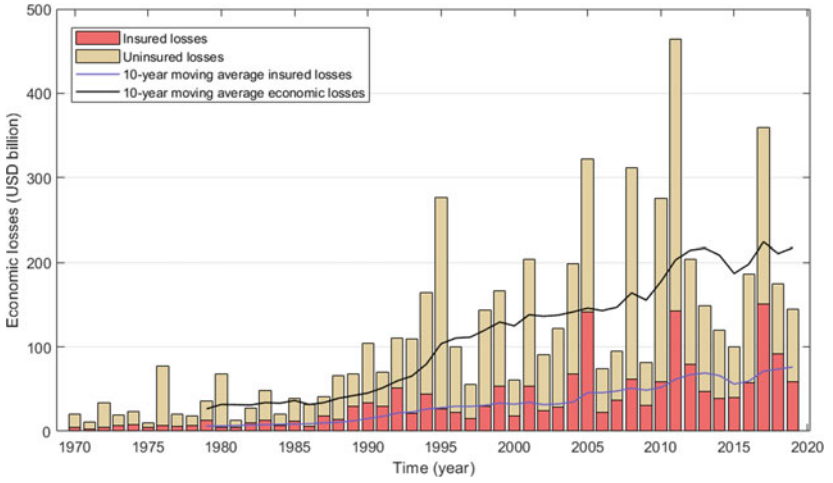


**Fig. 1.1** Losses from extreme events (adapted from Swiss Re [58])

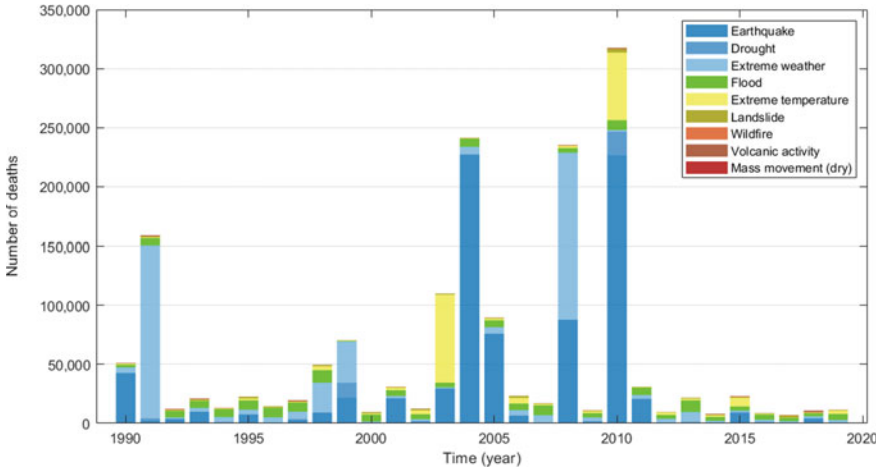


**Fig. 1.2** Number of fatalities based on disaster type (adapted from OWD [39])

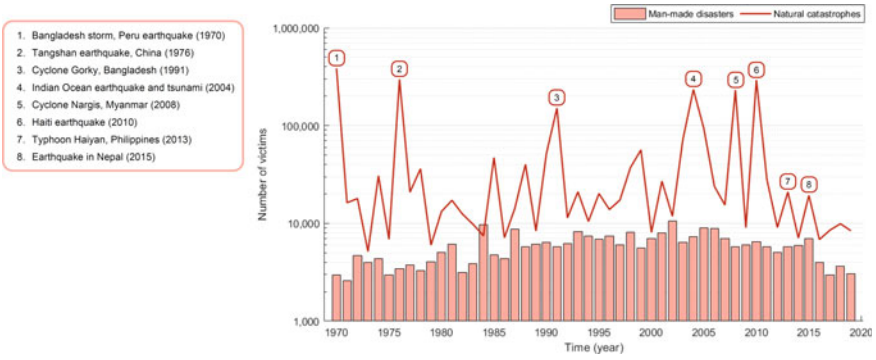


**Fig. 1.3** Number of victims from extreme events (adapted from Swiss Re [58])

$4.2 trillion with $4 of benefit for every $1 invested—i.e. a benefit-to-cost ratio of 4 [15].

There are countless examples where governments can invest wisely in infrastructure programs that provide net lifesaving and economics benefits to society. One is a $27 billion flood protection system for New Orleans that would reap benefits of more than $35 billion, including saving more than 1000 lives [13]. Another is reduced vulnerability of a key airport road to flooding may be achieved by the installation of two additional culverts at a cost of $1.7 million, a risk-based analysis showed a net benefit of $11 million with a benefit-to-cost ratio of 7.3—i.e., $1 of cost buys $7.30 in benefits [35].

It follows that the emphasis of the book is built infrastructure, most notably, housing, buildings, bridges, roads, tunnels, pipelines, and electricity infrastructure

in the developed and developing worlds. This accords with the World Bank [66] for the need for the "construction of buildings, infrastructure, and urban developments should consider how design, construction practices, and construction materials will affect disaster risk in both current and future climates." Risk and cost–benefit analysis of risk mitigation or protective measures aim to reduce the vulnerability of infrastructure, and hence reduce the future impact of extreme events to reveal protective measures that are cost-effective, and those that are not. Relevant also are private and public policy imperatives in the decision-making process.

The focus of this chapter (and this book) is how risk and decision-making analytics can be applied to the complex problem of protecting infrastructure and society from extreme events. There is increasing research that takes into account the risks associated with the timing and severity of extreme events in engineering to reduce the vulnerability or increase the resiliency of infrastructure—we refer to this as '*engineering for extremes*'. Engineering for extremes is defined as measures taken to reduce the vulnerability or increase the resiliency of built infrastructure to climate change, hurricanes, storms, floods, earthquakes, heat waves, fires, and malevolent and abnormal events that include terrorism, gas explosions, vehicle impact and vehicle overload. This may include, for example, enhancement of design standards (higher design loads or flood levels), retrofitting or strengthening of existing structures, utilisation of new materials, and changes to inspection and maintenance regimes. Engineers have a unique responsibility to model infrastructure vulnerability, and these skills will be essential to modelling the impacts of extreme events, and measures to ameliorate these losses.

Engineering for extremes involves quantifying the risks, costs and benefits of infrastructure protection and resilience. Any measures need to be economically and socially viable. There are also uncertainties, risks, upsides, and downsides that need to be factored into any decision. And we are talking about decisions that will involve many hundreds of billions of dollars of expenditures—so there is a need to explore the full range of options to effectively compare costs and benefits. There is no certainty about the future which makes decision-making for extreme events, even those as yet unforeseen or unrecognized, challenging. There is clearly a need for action, the question is what should we be doing now? what decisions can be deferred? and to when? And perhaps most importantly—what information do we need to enable better decisions?

The chapter will describe how risk-based decision support is well suited to optimising the design, construction, operation and maintenance of built infrastructure. Stochastic methods are used to model infrastructure vulnerability, effectiveness of risk mitigation or protective strategies, exposure, and costs. Case studies to follow in other chapters will detail how state-of-the-art risk-based approaches will help 'future proof' built infrastructure to extreme events.

The book will introduce the key concepts needed to assess the economic and social well-being risks, costs and benefits of infrastructure to extreme events. This will include: hazard modelling (likelihood and severity), infrastructure vulnerability, resilience or exposure (likelihood and extent of damage), social and economic loss

models, risk reduction from protective measures, and decision theory (cost–benefit and utility analyses).

## 1.2 Engineering for Extremes

The design and construction of infrastructure has evolved over many millennia so that today we are able to predict with relative ease the likelihood and size of today's natural hazards, and take steps to design houses, buildings, bridges, power stations, dams and other infrastructure to withstand these anticipated hazards. Earthquakes, tropical cyclones or hurricanes, storm surge, floods, and blizzards are often the low probability—high consequence hazards of interest. Over the past century building standards have been developed and continually improved—with the prevention of building collapse and catastrophic loss (ultimate limit state) the main driver for change. And while uncertainties and knowledge gaps still exist, disaster risks in the developed world are, in general, at an acceptable level. This is particularly the case for life-safety risks where, for example, the annual fatality rate from earthquakes in New Zealand is close to the generally acceptable risk of $1 \times 10^{-6}$ or one in a million (e.g. [49, 59]). However, the seismic fatality rate in China in the decade 2001 to 2010 is 50 times higher at $5 \times 10^{-5}$ (data sourced from Li et al. [27]).

Often the huge loss of life in the developing world is due to the poor quality of construction [48]. In Bangladesh, the quality of cement is poor [26]. And in Turkey, higher than expected earthquake damage is attributed to project errors, poor quality of construction, unlicensed modifications to buildings, and so on [22]. A magnitude 7.0 earthquake in Haiti in 2010 killed more than 230,000 people, mainly because of poor building construction, whereas a larger earthquake in densely populated Kobe, Japan, in 1995 killed around 6000, and a magnitude 6.9 earthquake in 1989 in the San Francisco Bay area killed some 63 people. Surveying the damage caused by an earthquake in China in 2008, in which many schools collapsed, killing hundreds of children, a field team of Australian and Hong Kong earthquake experts observed that "many buildings had inadequate construction quality including insufficient reinforcement, poor detailing and poor quality concrete" [63]. In addition, building codes have been bypassed with the complicity of corrupted officials and construction site staff. As Penny Green notes for Turkey, "Violations were part of a well entrenched political process," and she quotes an adviser to the mayor in one of the worst hit earthquake areas of Turkey, who admits, "The project managers, they take bribes, we do it ourselves. There is no project inspection" [10].

On the other hand, large economic losses often arise from natural disasters in the developed world. For example, in 2012 Hurricane Sandy (also known as 'Superstorm Sandy') damaged over 750,000 residences in New Jersey and New York, and caused more than $50 billion in losses [20]. Loss of life numbered around 100, mostly from drownings. The 2010–2011 earthquakes in Christchurch killed 185 people, most of these were victims of the collapse of two multi-storey buildings, and caused over $30 billion in damages—or 20% of the New Zealand GDP. The widespread damage

across the CBD and suburbs led to over 750,000 insurance claims being lodged, 64% of businesses were forced to close temporarily, and 11% were forced to close permanently [42]. With the exception of two buildings that collapsed, other buildings performed as expected and did not collapse—so life-safety was ensured. However, the widespread damage to building reduced their functionality and this loss was the main contributor to the huge economic losses suffered by the New Zealand economy, and to the massive social dislocation of residents.

A key emphasis of this book is to reduce damage to infrastructure that in turn can ameliorate the social and economic disruption of extreme events to the built environment. It aims to provide practical and community-conscious engineering knowledge and solutions to reduce the impact of extreme events on the performance of buildings and infrastructure, including safety, serviceability, and durability. Examples to be presented in this book include:

- installing wind-rated windows to houses to reduce damage from extreme wind events,
- replacing timber power poles with steel or concrete poles to reduce vulnerability to hurricanes,
- installation of additions jet fans for providing mechanical ventilation to reduce fatality risks during a fire in a tunnel,
- use of blast walls and fences to reduce the effects of explosive blast loading,
- construction of a new road to increase the resilience of vulnerable communities to earthquakes, storms and tsunami,
- upgrading building energy efficiency ratings for houses using insulation, sealing, and phase change materials to reduce heat stress during heatwaves,
- increasing foundation depth for bridges to reduce risks of scouring and bridge collapse during extreme floods,
- upgrading construction quality and practices to increase housing resilience,
- and so on.

## 1.3 Decision Challenges for Extreme Events

Cyclones, earthquakes, tsunami and floods are natural hazards that cause significant human, economic and social losses. Added to this are ‘man-made’ hazards such as climate change and terrorism. These hazards are low probability—high consequence events which in recent times are more commonly referred to as ‘extreme events’. Extreme events illicit extreme reactions—risk aversion, probability neglect, cost neglect, worst-case thinking—that may distort the decision-making process in an effort by policy makers to be seen to be ‘doing something’ irrespective of the actual risks involved. Policy-making in these circumstances becomes a “risky business” [17]. If rational approaches to public policy making are not utilised, then politically driven processes “may lead to raising unnecessary fears, wasting scarce resources, or ignoring important problems” [40].

There are a number of issues and questions related to controversial and emotive issues such as terrorism, nuclear power plant accidents, climate change and other extreme events [31–33], and are discussed as follows.

### *1.3.1 Worst-Case Thinking*

Worst-case thinking, or hyperbole, tends to dominate the thinking of many terrorism and climate change experts. In 2008, Department of Homeland Security (DHS) Secretary, Michael Chertoff proclaimed the "struggle" against terrorism to be a "significant existential" one [31]. And in 2014, Mayor Bill de Blasio of New York at a U.N. summit proclaimed that "We know humanity is facing an existential threat" from climate change [11]. The notion that a threat short of all-out nuclear war could be existential to humanity is hard to fathom. If business as usual predictions are biased towards impending doom, then this justifies any response no matter the cost in loss of civil liberties, quality of life, and treasure.

### *1.3.2 Cost Neglect*

While it is not difficult to list hazards and vulnerabilities, what is more challenging is to ascertain the cost to reduce these hazards and vulnerabilities. And to decide who pays, and when. There is a notion that safety is infinitely good, and no cost is too high. There is no attempt to compare costs against benefits.

### *1.3.3 Probability Neglect*

Some analysts base their findings on hazards or scenarios that they assume will occur. There is no consideration of the likelihood that a specific $CO_2$ emission scenario will occur, or that mitigation or adaptation will be effective. For example, a U.S. 2014 climate risk assessment report predicts trillions in dollars of damage due to climate change for the business as usual scenario—i.e., the U.S. continues in its current path [46]. There is no attempt to quantify the likelihood that $CO_2$ emissions will continue unabated for the next 85 years, that $CO_2$ mitigation measures will be implemented, that adaptation measures are implemented, or the impact of improved or game-changing technologies. Sunstein [57] terms this as 'probability neglect' and that "people's attention is focused on the bad outcome itself, and they are inattentive to the fact that it is unlikely to occur." There is no certainty with predictions, nicely summed up by physicist Niels Bohr: "Prediction is very difficult, especially if it's about the future."

### *1.3.4 Opportunity Costs*

Policy-makers that act before they carefully consider the implications of their actions can result in undesirable outcomes which are often referred to as 'opportunity costs'. A $CO_2$ mitigation strategy that reduces economic growth, particularly in developing countries, may reduce their ability to adapt. Or tsunami barriers may have a detrimental effect on tourism and the amenity for the local community.

### *1.3.5 Acceptable Risk*

The notion of acceptable risk is rarely raised in public discussions. The world is not risk free. The generally accepted level of annual fatality risk is 1 in a million (e.g. Stewart and Melchers [49]), see, for example, Gardoni and Murphy [8] for a fuller discussion on risk acceptability. The probability that an American will be killed by a hurricane stands at about one in 7 million per year, and one in 2.8 million per year for a heat-related death [36]. By comparison, an American's chance of being killed in an automobile crash is about one in 9,500 a year, the chance of being a victim of homicide is about one in 20,000, and the chance of being killed by lightning is one in 10 million [53]. The chance of being killed in a natural disaster in the United States is a relatively high one in 500,000 per year [53]. How much should we be willing to reduce a risk, and is the risk reduction worth the cost?

## 1.4 Risk-Based Decision Support

Risk is a measure of expected loss, and quantifies the effect of uncertainty on factors that influence this loss. The standard definition of risk is:

$$\text{(Risk)} = \text{(Hazard)} \times \text{(Vulnerability)} \times \text{(Consequences)} \tag{1.1}$$

The nomenclature can vary from discipline to discipline, but in the context of built infrastructure, these terms are defined as:

1. Hazard—the likelihood and location of a natural or man-made hazard.
2. Vulnerability—how will the infrastructure be damaged?
3. Consequences—what is the life-safety, economic and social costs if the infrastructure is damaged? The criticality of the consequences will depend on the exposure—e.g., the time of day, the location of damage, exposed population, etc.

A risk assessment will combine these three measures in a way to estimate the overall risk to people, operations and infrastructure. The risk assessment process

adopted by the International Organization for Standardization *Risk Management* ISO 31000–2018 is shown in Fig. 1.4.

A number of steps are basic to a risk assessment, and they are independent of the system or issue being considered. The process shown in Fig. 1.5 is also consistent with [23] and can be summarised as [49]:

1. **Define context.** A risk assessment should take place within a well-defined context. This means that the system being examined and the internal and external influences must be known and defined.
2. **Analyse hazard scenarios.** Identification of what might go wrong—and when and where—are crucial to the analysis. Once the potential hazards and scenarios have been identified, it is necessary to identify how and why these threats or scenarios can be realised. It requires the hazard scenarios to be examined (and understood) in considerable detail. Information from databases and other past experience will play an important part in hazard scenario analysis.
3. **Analyse risk.**

$$\text{RISK} = (\text{probability of occurrence}) \times (\text{consequences})$$

This is concerned with determining the occurrence probabilities and the consequences (fatalities, injuries, damages) that would occur if the threat or hazard were realised. Typically, the probabilities are estimated from a combination of relevant data, reliability modelling, and subjective judgments .

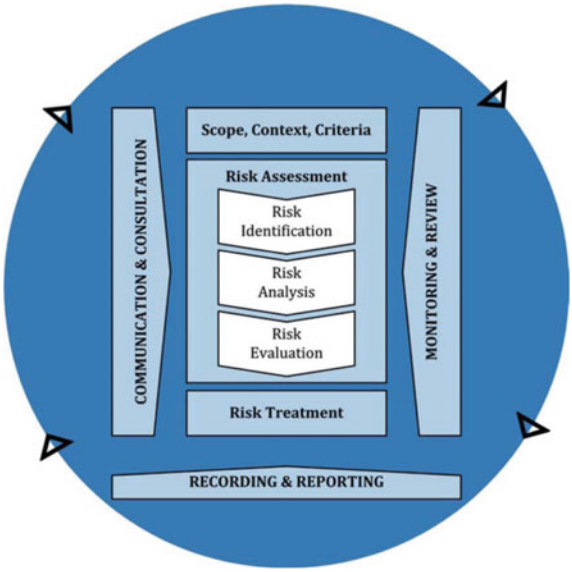


**Fig. 1.4** Risk process (adapted from [23])

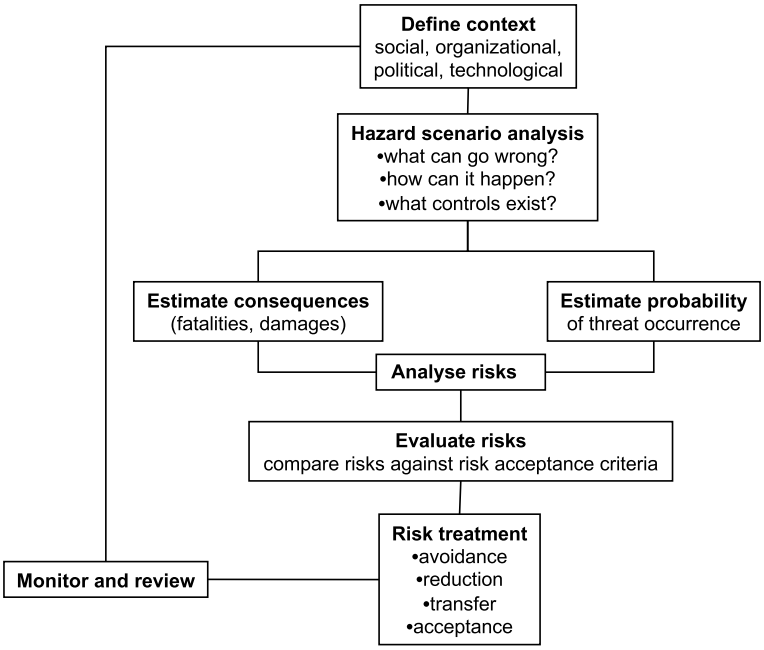


**Fig. 1.5** Risk assessment process [49]

4. **Evaluate risks.**
   Analysed risk must be compared with criteria of risk acceptability, usually applying past experience as a guide.
5. **Treat the risk.**
   If the estimated risk exceeds the risk acceptance criteria, risk treatment is required. This may involve risk avoidance, risk reduction, risk transfer, or risk sharing. In some cases, the risk may be accepted but perhaps only for a limited time until measures can be taken to reduce it. In all cases, the proposed course of action requires careful evaluation. Consideration must be given to possible options and to the likely effect of their implementation, such as opportunity costs. This might involve one or more new risk analyses to gauge the effect of changes.
6. **Monitor and review.**
   Usually a risk analysis presents only a snapshot of the risks—for example, the effectiveness of control procedures may slacken with time. There is a need, then, to monitor the system and to repeat the risk analysis at regular intervals.

A risk assessment needs to be tailored to the needs of the government, community, asset owner, regulator and other stake-holders and decision-makers. There are many tools and methods available for conducting a risk assessment (e.g., [49]). Analysis methods can be qualitative, quantitative or a combination of the two.

The International Organization for Standardization *Bases for Design of Structures—General Principles on Risk Assessment of Systems Involving Structures* [24] provides detailed and critical evidence-based advice on the utility of qualitative and quantitative risk analyses.

In quantitative estimation, numerical values (rather than descriptive scales used in qualitative estimation) are used for both consequences and probability of occurrence based on data and analyses from a variety of sources. Such an assessment is termed a Quantified Risk Analysis (QRA) or a Probabilistic Risk Analysis (PRA). A flowchart of the PRA process for structural systems is shown in Figure 1.6 [24].

A key feature of a PRA (or any other quantitative risk assessment) is that it provides robust and evidence-based advice on the actual level of risk, and this can be compared directly with acceptable risk criteria that are well established in society (e.g., [50]). The process of quantification is fully transparent, as are assumptions and

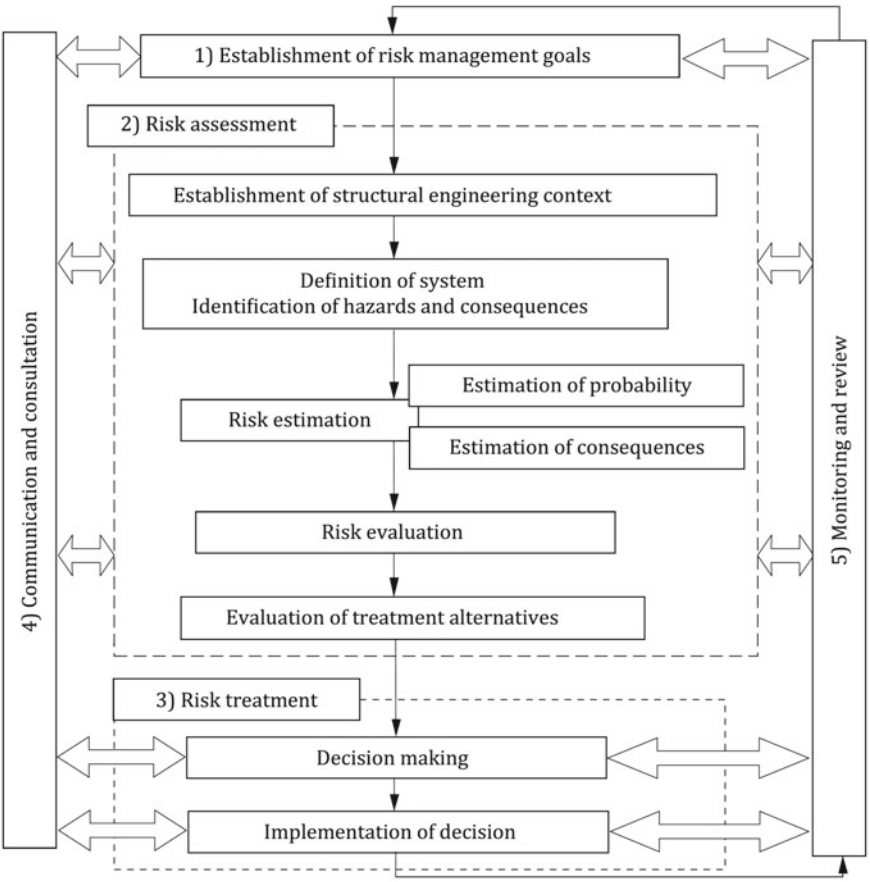


**Fig. 1.6** Flowchart of probabilistic risk assessment. (adapted from [24])

data gaps during this process. Moreover, sensitivity analyses can be conducted to test the robustness of decisions—this is particularly important if there is uncertainty about hazard, vulnerability, exposure or consequences.

The risk shown in Eq. 1.1 can be re-expressed as:

$$\mathrm{E(L)} = \sum \mathrm{Pr(H)Pr(D|H)Pr(L|D)L} \tag{1.2}$$

where Pr(H) is the probability that a specific hazard will occur, Pr(D|H) is the probability of infrastructure damage or other undesired effect conditional on the hazard (also known as fragility) for the baseline case of no extra protection (i.e. 'business as usual'), Pr(L|D) is the conditional probability of a loss (economic loss, loss of life, etc.) given occurrence of the damage, and L is the loss or consequence if full damage occurs. The product Pr(D|H)Pr(L|D)L refers to the expected loss given the occurrence of the hazard. In some cases, 'damage' may equate to 'loss' and so a vulnerability function may be expressed as Pr(L|H) which is equal to the product Pr(D|H)Pr(L|D). The summation sign in Eq. 1.2 refers to the number of possible hazards, damage levels and losses. If the loss refers to a monetary loss, then E(L) represents an economic risk.

In many cases, the probability of occurrence of a threat, hazard, damage or consequence cannot be described adequately by single-point values (best estimates). An example is when there is a large amount of uncertainty about an event frequency. In this case, it is appropriate to retain the uncertainties associated with the event frequency by modelling event frequency as a probability distribution, and allow the risk analysis to propagate these uncertainties throughout the analysis. This may be termed a Probabilistic Risk Analysis (e.g., [49]) or more simply 'uncertainty modelling'. Uncertainty modelling can consider aleatory (random variation inherent in real life events) and epistemic (knowledge uncertainty inherent in the model of the world and associated scientific algorithms) uncertainties.

The expected loss after risk mitigation or other protective measure is derived from Eq. 1.2 as

$$\mathrm{E_{mitigation}} = \sum (1 - \Delta \mathrm{R})\mathrm{E(L)} - \Delta \mathrm{B} \tag{1.3}$$

where $\Delta$R is the reduction in risk caused by risk mitigation or other protective measure, E(L) is the 'business as usual' risk given by Eq. 1.2, and $\Delta$B is the co-benefit such as reduced losses to other hazards, increased energy efficiency of new materials, etc. Costs of protection, timing of these measures, discount rates, future growth in infrastructure and spatial and time-dependent changes in hazards need to be included in any risk analysis.

### *1.4.1 Hazard Assessment*

There are significant challenges in characterizing (in probabilistic terms) the hazard in time and space. While significant advances have been made in doing just that, there remains considerable uncertainty in some aspects of hazard characterization and modelling. These uncertainties, of course, propagate through the risk analysis.

Hazard characterization often is in the purview of disciplinary scientists/experts rather than the engineer conducting the risk analysis. Even modern load standards for structural design (such as ASCE 7 in the US) are developed using critical information provided by, for example, seismologists, meteorologists, hydrologists, and other domain specialists. While this has the advantage of generally more sophisticated models, likely to be more accurate, such hazard models (particularly those that are physics-based) are often very computationally intensive and may be difficult to incorporate into generalized (e.g., regional) risk analysis or time-dependent risk analyses using numerical simulation. The adaptation, simplification, or generalization of these hazard models for such purposes is the responsibility of the engineer.

Hurricane hazard modelling in the last decade has expanded in sophistication to include both temporal and spatial characteristics using event-based simulation models. This has allowed, for example, the characterization of hurricane intensity and spatial extent (size) as a function of time and location [29, 61]. Such models have been successfully coupled with rainfall rate models [30] and, most recently, have been extended to include explicit consideration of projected climate change, specifically warming sea surface temperatures [62]. Nonetheless, uncertainties associated with future $CO_2$ emission scenarios are usually not quantified and future climate projections are produced separately for individual scenarios [55].

As engineers, we are often challenged with selection of appropriate scales, levels of detail, and granularity of both analysis and solution. This is especially true in hazard assessment and modelling where different hazards may be modelled/characterized at different scales, and in cases where hazard models may have vastly different confidence levels from one another and from the embedded mathematical models in the risk analysis framework.

The issues of concurrent or concomitant hazards must also be included in some risk analyses. Examples include hurricane (wind) and coastal flooding, seismic and urban fire, wind and wildfire.

Finally, most risk analyses account only for the hazards we know to exist presently. Failure to consider emerging hazards, and those we may not be able to envision today, may in fact contribute the greatest uncertainty to any risk analysis. Consider, for example, the events of 9/11. No structure had been designed for the direct impact of a fully fuel-loaded passenger jet. It was not even in the realm of possibility. Elms [5] refers to this as ontological uncertainty—a third type of uncertainty after aleatoric and epistemic.

### *1.4.2 Fragility and Vulnerability*

Infrastructure fragility or vulnerability can be expressed in terms of structural damage or other losses, and are derived from fitting curves to damage data from historical damage records (i.e. empirical models and insurance data) or from engineering models (e.g., [49]).

Insurance or building performance data are often used to derive vulnerability models which are often expressed in terms of Pr(L|H). For example, Fig. 1.7 shows a vulnerability model for Australian houses subject to floods derived from insurance loss records. In this case, the hazard H is the water depth above the floor. Empirical models have draw-backs such as, lack of damage data [16], lack of capability to examine the effect of changes in building design and construction methods on damages, lack of ability to examine the effectiveness of building adaptation measures for climate change [67], and they tend to focus on losses (vulnerability) and not damage (fragility). There are also a number of issues associated with utilising claim data such as access to the insurance claim data, insurance valuation cost and the actual damage cost, and insurance claim databases that do not disaggregate losses between building exterior and interior [41]. Most importantly, empirical vulnerability curves are based on what has happened in the past. They cannot assess changes in fragility or vulnerability due to future changes in design standards, materials or construction practices. This highlights the need of developing fragility models based on engineering and structural reliability methods. It is noted however that, as with all models, engineering fragility models should be validated or benchmarked with empirical models based on past events where possible to give more confidence in modelling assumptions and realism.

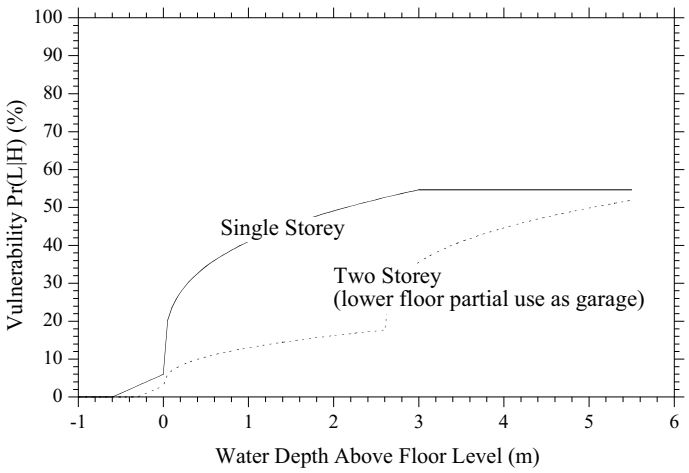


**Fig. 1.7** Flood vulnerability curves for residential construction in Brisbane (data from [28])

The stochastic modelling of infrastructure fragility is Pr(D|H) and is the probability of damage conditional on a specific wind speed, flood level, earthquake or other hazard:

$$\Pr(D|H) = \Pr(R(\mathbf{X}) - H < 0) \tag{1.4}$$

where R(**X**) is the function for resistance or capacity, **X** is the vector of all relevant variables that affect resistance, and H is the known hazard level. Fragility modelling will require probabilistic information on materials, dimensions, model errors, deterioration and other input variables (**X**) into engineering models which define the resistance function R(**X**)—these variables vary in time and space.

A key challenge, at least for engineers, is the development of fragility models for damage prediction. Most damage and loss from floods and storms are not due to major structural failure or collapse, but due to water ingress from damaged roofs or walls, or rising water levels. There is much work on predicting reliabilities for the ultimate limit state (collapse) where life-safety is the major criterion. However, modelling of damage and serviceability limit states is a less tractable problem as this requires advanced simulation modelling to accurately track component and member performance and failure, load sharing, failure of other components/members due to load redistribution, and damage progression leading to economic and other losses.

Another challenge is that infrastructure, particularly houses, are very complex systems comprising of hundreds to thousands of components and members (some engineered, and some not) of differing materials. Poor detailing and workmanship issues contribute to most damage—so the engineering and stochastic models need to consider these variables—such as screw fasteners being spaced too far apart, or some not connected to purlins and battens, etc. (e.g., [43]). These are more challenging to model stochastically than more conventional 'engineered' constructions such as bridges, towers, etc. where materials are more uniform, and workmanship subject to more quality control measures. Stewart et al. [54] have conducted structural reliability analyses to assess the roof envelope fragility Pr(D|H) of contemporary timber-framed houses built in the Australian city of Brisbane, see Fig. 1.8. In this case, Monte-Carlo simulation and structural reliability methods were used to stochastically model spatially varying pressure coefficients, roof component failure for 1600 roof fasteners and 500 battens, load re-distribution and spatial variability across the roof as connections progressively fail, loss of roof sheeting as a critical number of connections fail, and changes in internal pressure coefficient with increasing roof sheeting loss. The fragility of the roof envelope vulnerable to dominant openings on the windward wall, and also to construction defects.

### *1.4.3 Losses*

Exposure and loss data relates to direct and indirect loss or consequence due to location and extent of infrastructure damage, for existing exposure and future projections.

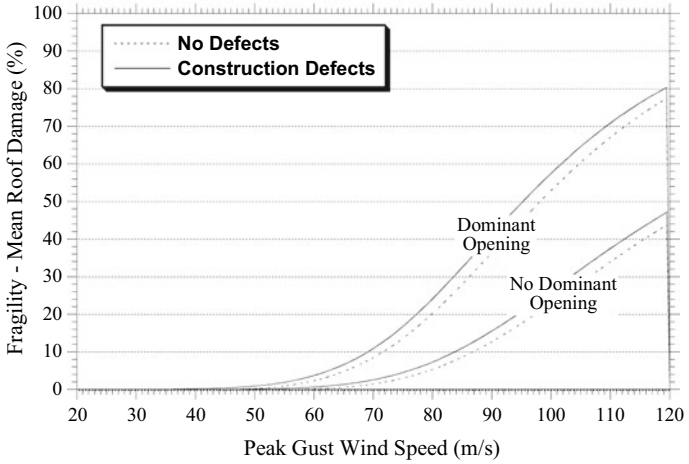


**Fig. 1.8** Fragility curves for Australian timber-framed housing (adapted from [54])

A probability of loss Pr(L|D) and loss L needs to consider direct and indirect losses, however, most existing studies consider direct losses related to infrastructure damage and contents losses. For example, Fig. 1.9 shows a typical direct loss function for wind vulnerability [19], for roofing and building interior losses. It is observed that the trend between extent of damage (D) and loss is non linear, and that losses reach close to their maximum value when damage is only 20%. Clearly, losses accumulate rapidly for low levels of damage because "once the envelope is breached, most of the damage to the interior of the building is a function of the amount of water that enters the building" [19].

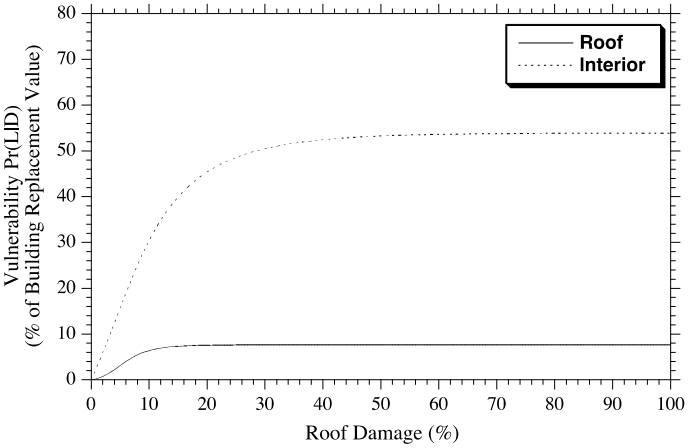


**Fig. 1.9** Components of building loss due to wind

Indirect losses caused by business interruption, clean-up, loss during reconstruction, extra demands on social services, and changes to demand and supply of intermediate consumption goods, post-disaster inflation, etc. can also be significant (e.g. [14, 34, 60]). The data is very limited to accurately quantify how indirect losses increase with vulnerability. Indirect losses were estimated for Hurricane Katrina using an adaptive regional Input–Output model where damage to houses was $20 billion, contents $7 billion, $17 billion damage to government, and $63.5 billion to the private sector—total damage to fixed capital was $107 billion [14]. The total indirect loss is $42 billion or 39% of direct losses. Hallegatte [14] estimates that indirect losses could exceed 100% of direct losses for a damaging event twice as bad as Hurricane Katrina. An Australian assessment of direct and indirect costs shows indirect costs of 9–40% of direct losses for bushfire, cyclones and floods [2].

There is often a high level of post-disaster inflation (or demand surge) of reconstruction costs (e.g., [60]) which can lead to higher insurance and home owner losses. Walker [60] estimates that the post-disaster inflation was close to 100% for Cyclone Tracy.

Finally, resiliency is a term that is increasingly being applied to disaster risk reduction. It may be defined as the ability of the system to restore functionality after a damaging event, and the time needed to achieve full restoration of the system is affected by social, economic, and political aspects (e.g. [7, 47]). Or it may be defined more broadly to capture vulnerability, exposure or loss. Resiliency in one way or another has been included in most risk assessments, particularly for low probability—high consequence events, when assessing loss likelihoods and magnitudes. For example, an urban community that has ready access to emergency services that can temporarily place tarpaulins over damaged roofs will reduce water ingress losses and allow inhabitants to remain in their homes—the community will be able to recover more quickly from such a disaster, and so direct and indirect losses will be minimised. This ‘bouncing back’ implies a return to the status quo, whereas, ‘bouncing forward’ leads to continually improving conditions which is a more desired outcome [21]. While the term ‘resiliency’ may not appear explicitly in risk modelling, it is implied in many cases.

### *1.4.4 Risk Reduction*

A risk treatment or mitigation measure should result in risk reduction ($\Delta$R) that may arise from a combination of reduced fragility or vulnerability (Pr(D|H) or Pr(L|D)) or exposure (L). For instance, changes to planning may reduce the number of new properties built in a flood plain which will reduce L, or more stringent design codes may reduce the fragility of new infrastructure. Systems and reliability modelling are essential tools to quantify the level of risk reduction, and the extent of risk reduction will depend on the hazard, location, and timing of protective measure. For any risk mitigation or protective measure the risk reduction $\Delta$R can vary from 0 to 100% (or even a negative number for an ill-suited measure).

### *1.4.5 Decision Preference and Selection of Risk Mitigation Strategies*

Three criteria may be used to assess the decision preferences of risk mitigation strategies:

1. Net Present Value (NPV)
2. Benefit-to-cost ratio or BCR
3. Probability of cost-effectiveness or Pr(NPV > 0) or Pr(BCR > 1)

These are not mutually exclusive, but complementary. They also refer to a "risk neutral" risk attitude where the decision preference is based on expected outcomes (see Sect. 1.4.5.1).

The 'benefit' is the reduction in damages or losses, and the 'cost' is the cost of the risk mitigation or other protective strategy. The net benefit or net present value (NPV) is equal to benefit minus the cost which is also equivalent to the present value or life-cycle cost of a protective strategy (sum of damage and protection costs) minus the 'business as usual' or 'do nothing' present value. The decision problem is to maximise NPV:

$$\text{NPV} = \sum \text{E(L)}\Delta\text{R} + \Delta\text{B} - \text{C}_{\text{mitigate}} \tag{1.5}$$

where $\text{C}_{\text{mitigate}}$ is the cost of risk mitigation or other protective strategy including opportunity costs that reduces risk by $\Delta$R, $\Delta$B is the co-benefit, and E(L) is the 'business as usual' risk given by Eq. 1.2. The co-benefits ($\Delta$B) may include reduced embodied energy and reduced carbon footprint over the life cycle of the facility, or reduced losses for other hazards due to improved evacuation procedures.

The benefit-to-cost ratio is:

$$\text{BCR} = \frac{\sum \text{E(L)}\Delta\text{R} + \Delta\text{B}}{\text{C}_{\text{mitigate}}} \tag{1.6}$$

If NPV > 0 or BCR > 1 then there is a net benefit and so the risk mitigation measure is cost-effective. Figure 1.10 shows how protective costs increase with risk reduction, while benefits increase linearly with risk reduction according to Eqs. (1.5–1.6). The optimal protection occurs when NPV is a maximum, leading to an optimal risk reduction. It is important to note here that such an analysis is aiming to find the "sweet spot"—that is, the decision where risk reduction or level of protection is optimised—higher protection may be achieved but at a higher marginal cost (law of diminishing returns), and vice-versa for a lower level of protection. Other notations and formulae can be used to provide optimal adaptation (e.g., [12]), but ultimately these also mostly rely on maximising NPV. At what point-in-time the benefits exceed the cost—i.e. the pay back period—is also an important decision metric for policy makers (see Fig. 1.11). For more details see, for example, National Academies of

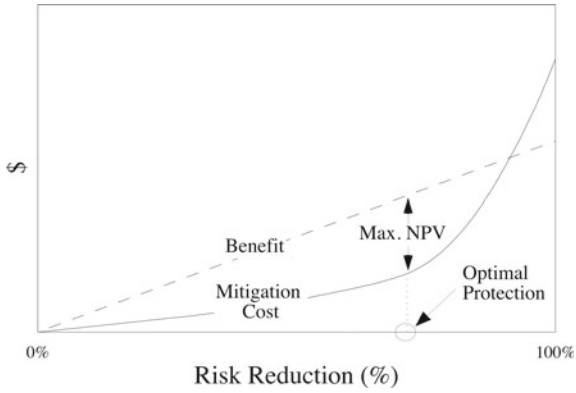


**Fig. 1.10** Schematic of net present value (NPV) showing optimal protection

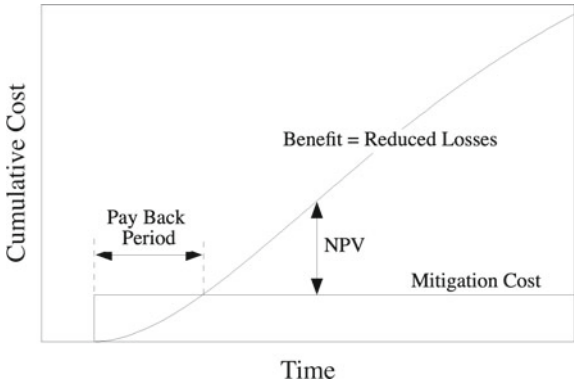


**Fig. 1.11** Schematic of pay back period

Sciences, Engineering, and Medicine [35].

Cost–benefit analyses tend to monetise all costs and benefits to allow comparison of various risk mitigation measures. However, it is important to realise that aggregating costs and benefits may fail to consider that those bearing the risk or cost may not be the same as those sharing the benefits. For example, a nuclear power plant will increase safety risks to local residents, whereas the benefits of energy security will be shared by a much larger population and the profits generated by a new plant will only benefit the utility company and employees. Multi-criteria decision making may be used to consider the various (and competing) risk preferences for all stakeholders—see Sect. 1.4.5.1 for more details.

Confidence bounds of NPV or BCR can then be calculated if input parameters are random variables. The probability that a protective measure is cost-effective denoted herein as Pr(NPV > 0) or Pr(BCR > 1) may also be inferred.

If the probability that a specific hazard will occur Pr(H) is too unreliable, then a decision analysis based on scenario analysis where hazard probability is decoupled from Eq. 1.6 provides an alternative decision-making criteria based on expected costs. If the loss refers to the fatality of an individual, then E(L) represents an individual

annual fatality risk which can be compared with appropriate societal risk acceptance criteria.

#### 1.4.5.1 Risk Preferences

Governments and their regulatory agencies normally exhibit risk-neutral attitudes in their decision-making as described by Eqs. (1.5–1.6) above. This is confirmed by the U.S. Office of Management and Budget (OMB) which specifically states that "the standard criterion for deciding whether a government program can be justified on economic principles is net present value—the discounted monetized value of expected net benefits (i.e., benefits minus costs)" and that "expected values (an unbiased estimate) is the appropriate estimate for use" [37], and also by many practitioners and researchers (e.g., [4, 6, 57]). This entails using mean or average estimates for risk and cost–benefit calculations, and not worst-case or pessimistic estimates. Paté-Cornell [40] elaborates on this point by stating "if risk ranking is recognized as a practical necessity and if resource limitations are acknowledged, the maximum overall safety is obtained by ranking the risks using the means of the risk results (i.e., expected value of losses)."

This type of "rational" approach to risky decision-making is challenging to governments and their agencies which might have other priorities and political concerns. Hardaker et al. [17] note that "policy-making is a risky business", and that "Regardless of the varied desires and political pressures, we believe that it is the responsibility of analysts forcefully to advocate rational decision methods in public policy-making, especially for those with high risk. We believe that more systematic analysis of risky policy decisions is obviously desirable." Probability neglect is a form of risk aversion as decision-makers are clearly averse to events of large magnitude irrespective of the probability of it actually occurring.

Utility theory can be used if the decision maker wishes to explicitly factor risk aversion or proneness into the decision process (e.g. [25, 44, 53]). In this case, utility theory provides a means of evaluating the risk preferences of the interested parties under choice uncertainty. The objective of the decision-making process is to maximise the expected utility, and so an option is preferable if it has a higher utility. Multi-attribute utility theory or multi-criteria decision making is capable of handling more than one interested party (such as federal, state and local governments, residents, infrastructure owners, etc.), non-monetised parameters (such as risk preferences for quality of life), and risk-neutral, risk averse or risk prone decision preferences.

While the appetite for risk will no doubt vary from person from person, governments and regulators need to act in the best interests of the public, and this means ensuring that public policy is geared towards achieving the highest outcomes. This is best achieved by adopting risk-neutral attitudes to decision-making, and not allowing emotion or the political imperative interfere with the process.

It is important to note that the issue of risk aversion is not a new one, but has been well researched and documented for politically sensitive and controversial decisions associated with terrorism, nuclear power safety, aviation safety, pharmaceutical benefits scheme, environmental pollution, etc. In these cases, risk acceptance criteria has been developed based on annual fatality risks and cost–benefit analysis using expected (mean) values. In principle, decisions related to engineering extremes should be made with similar risk-based methodologies.

As noted previously, risk-aversion is often a feature of public policy making [51]. This can lead to very different outcomes depending on the belief system of the decision-maker. For instance, where risk is measured by government expenditures (and less concerned about climate change impacts), a risk averse decision-maker may wish the likelihood of cost-effectiveness to be high before investing in a climate change adaptation measure—for example, that there is 90% likelihood that benefit exceeds the cost ($\Pr(\mathrm{NPV} > 0) = 90\%$) so there is more certainty about a net benefit and small likelihood of a net loss. On the other hand, if the decision maker believes that climate change is the "greatest challenge of the present century" the precautionary principle comes into play, so to avoid the potential risk of catastrophic climate change impacts the decision-maker will support adaptation measures almost irrespective of their cost. Anticipating these types of contradictory risk preferences is not the matter for this book. What is needed, however, is a transparent decision-making framework that outlays in a systematic and rigorous manner risks, costs and benefits. The effect of policy decisions will then be more apparent, as will the trade-offs involved in sub-optimal decisions.

#### 1.4.5.2 Discount Rates

All relevant costs and benefits should be quantified and discounted with an appropriate discount rate applicable to the decision scenario, system boundaries and time horizon. It is generally preferred that cost–benefit analysis results should also be presented in terms of annualised values. The annualised value of a cost (or benefit) becomes:

$$\mathrm{AV} = \frac{PV \cdot \mathrm{r}}{1 - (1 + \mathrm{r})^{-\mathrm{t}}} \tag{1.7}$$

where AV is the annualised value over time t years, PV is the present value, and r is the economic discount rate.

Of particular interest is uncertainty about the level of discount rates. The Australian Government Office of Best Practice Regulation (OBPR) recommends that the discount rate for regulatory interventions is 7%, and that sensitivity analyses consider discount rates of 3% and 10% [38]. Projects with significant effects beyond 30–50 years are considered intergenerational, and so a time-declining discount rate may be appropriate. However, the Australian OBPR states that "there is no consensus

about how to value impacts on future generations" and "Rather than use an arbitrarily lower discount rate, the OBPR suggests that the effects on future generations be considered explicitly" [38]. Nonetheless, the Australian Garnaut Review adopted discount rates of 1.35% and 2.65% [9]. These relatively low discount rates were selected so as to not underestimate climate impacts on future generations. Countries and institutions worldwide use other discount rates. France recommending 2.5% and 1.5% discount rates for short term (lifetime lower than 70 years) and long term investments, respectively [45], and the European Commission recommends a 5% discount rate [18]. Other discount rates vary from 3% (Germany) to over 10% [18, 64].

Discount rates are generally assumed constant with time. However, this may not be appropriate when considering intergenerational effects. For example, the U.K. Treasury recommends time-declining discount rates (e.g., [1]) which places more emphasis on future benefits by reducing the discount rate. While there is some uncertainty about discount rates (e.g. [3]), the selection of discount rates for public policy 'regulatory intervention' is a matter best determined by government regulations specific to each country.

## 1.5 Summary

This chapter introduced the background, basic concepts and principles that constitute the basis for engineering for extremes for built infrastructure that is relevant to housing, buildings, bridges, roads, tunnels, pipelines, electricity infrastructure, etc. Extreme events can result in considerable loss of life, and economic and social losses to communities and countries. These losses may rise in the future due to increased urbanisation and a changing climate. Consequently, there is a need to improve the response of built infrastructure to damage from extreme events based on a risk-based decision support. This decision support starts evaluating risks by combining hazard modelling, to evaluate the demands under different present and future hazard scenarios, as well as engineering and fragility models to quantify the infrastructure response. The outputs of this risk analysis are introduced into a decision framework that allows determining the cost-effectiveness and utility of risk mitigation and other protective measures. The following chapters of this book will present various study cases where this risk-based decision support is applied.

**Acknowledgements** We greatly appreciate the assistance of Reza Filizadeh with the production of Figures 1.1, 1.2 and 1.3.

## References

1. Boardman AE, Greenberg DH, Vining AR, Weimer DL (2011) Cost-benefit analysis: concepts and practice. Pearson, Boston

2. BTE (2001) Economic costs of natural disasters in Australia. Bureau of Transport Economics Report 103, Canberra.
3. Dasgupta P (2008) Discounting climate change. J Risk Uncertain 37(2–3):141–169
4. Ellingwood BR (2006) Mitigating risk from abnormal loads and progressive collapse. J Perform Constr Facil 20(4):315–323
5. Elms D (2004) Structural safety—issues and progress. Prog Struct Mat Eng 6(2):116–126
6. Faber MH, Stewart MG (2003) Risk assessment for civil engineering facilities: critical overview and discussion. Reliab Eng Syst Saf 80(2):173–184
7. Faber MH, Giuliani L, Revez A, Jayasena S, Sparf J, Mendez JM (2014) Interdisciplinary approach to disaster resilience education and research. Proc Econom Finan 18:601–609
8. Gardoni P, Murphy C (2014) A scale of risk. Risk Anal 34(7):1208−1227
9. Garnaut R (2008) The garnaut climate change review: final report. commonwealth of Australia, Cambridge University Press, Cambridge, U.K.
10. Green P (2005) Disaster by design. Br J Criminol 45(4):528–546
11. Grynbaum MM (2014) At U.N., de Blasio Warns of 'Existential Threat' From Climate Change. New York Times, September 23, 2014
12. Hall JW, Brown S, Nicholls RJ, Pidgeon NF, Watson RT (2012) Proportionate adaptation. Nature Clim Change 2(12):833–834
13. Hallegatte S (2006) A cost-benefit analysis of the new orleans flood protection system. AEI-Brookings Joint Center. Regulatory Analysis, 06–02, Washington, DC
14. Hallegatte S (2008) An adaptive regional input-output model and its application to the assessment of the economic cost of Katrina. Risk Anal 28(3):779–799
15. Hallegatte S, Rentschler J, Rozenberg J (2019) Lifelines: the resilient infrastructure opportunity. sustainable infrastructure series. Washington, DC, World Bank. https://doi.org/10.1596/978-1-4648-1430-3
16. Ham HJ, Lee S, Kim HS (2009) Development of typhoon fragility for industrial buidings. In: The Seventh Asia-Pacific conference on wind engineering, Taipei, Taiwan
17. Hardaker JB, Fleming E, Lien G (2009) How should governments make risky policy decisions? Aust J Public Adm 68(3):256–271
18. Harrison M (2010) Valuing the future: the social discount rate in cost-benefit analysis. Visiting Researcher Paper, Productivity Commission, Canberra
19. HAZUS (2014). Multi-hazard loss estimation methodology—hurricane model. Hazus–MH 2.1 Technical Manual. Federal Emergency Management Agency, Mitigation Division, Washington, D.C.
20. Huffington Post (2013) Hurricane sandy's impact. By The Numbers (INFOGRAPHIC), 10/29/2013
21. IPCC (2012) Managing the risks of extreme events and disasters to advance climate change adaptation. In: Field et al. (ed) A special report of working groups i and ii of the intergovernmental panel on climate change. Cambridge University Press, U.K.
22. Irtem E, Turker K, Hasgul U (2007) Causes of collapse and damage to low-rise RC buildings in recent Turkish earthquakes. J Perform Constr Facil 21(5):351–360
23. ISO 31000 (2018) Risk management. International organization for standardization, Geneva
24. ISO13824 (2020) General principles on risk assessment of systems involving structures. International Standards Organization, Geneva
25. Jordaan I (2005) Decisions under uncertainty: probabilistic analysis for engineering decisions. Cambridge University Press
26. Koehn E, Ahmmed M (2001) Quality of building construction materials (Cement) in developing Countries. J Archit Eng 7(2):44–50
27. Li YY, Su GF, Yuan HY (2015) Statistical analysis on earthquake fatality vulnerability in China. In: Proceedings of the World congress on engineering 2015, Vol II WCE 2015, July 1−3, London, U.K.
28. Mason M, Phillips E, Okada T, O'Brien J (2012) Analysis of damage to buildings following the 2010/2011 East Australian floods. Griffith University, Australia, NCCARF

29. Mudd L, Wang Y, Letchford C, Rosowsky DV (2014) Assessing climate change impact on the US East coast hurricane hazard: temperature, frequency, track. ASCE Natural Hazards Rev 15(3):04014001
30. Mudd L, Rosowsky DV, Letchford C, Lombardo F (2016) A joint probabilistic wind-rainfall model for tropical cyclone hazard characterization. ASCE J Struct Eng 04016195
31. Mueller J, Stewart MG (2011) Terror, security, and money: balancing the risks, benefits, and costs of homeland security. Oxford University Press, Oxford and New York
32. Mueller J, Stewart MG (2011) The price is not right: the U.S. spends too much money to fight terrorism. Playboy 58(10):149–150
33. Mueller J, Stewart MG (2016) Chasing ghosts: the policing of terrorism. Oxford University Press, Oxford and New York
34. NAS (1999) The impact of natural disasters: a framework for loss estimation. National Academy of Sciences, Washington, D.C.
35. NAS (2020) Incorporating the costs and benefits of adaptation measures in preparation for extreme weather events and climate change guidebook. National academies of sciences, engineering, and medicine, Washington, DC, The National Academies Press. https://doi.org/10.17226/25744
36. NOAA (2016) Weather fatalities. National weather service, Silver Springs, MD, http://www.nws.noaa.gov/om/hazstats.shtml Accessed 30 Aug 2016
37. OMB (1992) Guidelines and discount rates for benefit-cost analysis of federal programs (Revised). Circular No. A-94, October 29, 1992, Office of Management and Budget, Washington, DC
38. OBPR (2010) Best practice regulation handbook. Office of Best Practice Regulation, Australian Government, Canberra, June 2010
39. OWD (2020) Number of deaths from natural disasters by type, 1990 to 2019, Our World in Data. https://ourworldindata.org/natural-disasters Accessed 19 February 2021
40. Paté-Cornell E (2002) Risk and uncertainty analysis in government safety decisions. Risk Anal 22(3):633–646
41. Pita GL, Pinelli JP, Gurley KR, Hamid S (2013) Hurricane vulnerability modeling: development and future trends. J Wind Eng Ind Aerodyn 114:96–105
42. Potter SH, Becker JS, Johnston DM, Rossiter KP (2015) An overview of the impacts of the 2010–2011 Canterbury earthquakes. Int J Disaster Risk Reduct 14:6–14
43. Qin H, Stewart MG (2020) Construction defects and wind fragility assessment for metal roof failure: a Bayesian approach. Reliabil Eng Syst Safety 197:106777
44. Qin H, Stewart MG (2021) Risk perceptions and economic incentives for mitigating windstorm damage to housing. Civ Eng Environ Syst 38(1):1–19
45. Quinet E (2013) L'évaluation socioéconomique des investissements publics. Commissariat Général à la Strategie et à la Prospective (In French), Paris, France
46. Risky Business (2014) The economic risks of climate change in the United States, June 2014, Riskybusiness.org
47. Rosowsky DV (2020) Defining resilience. Sustain Resilient Infrastruct 5:125–130
48. Sanchez-Silva M, Rosowsky DV (2008) Risk, reliability, and sustainability in the developing World. Struct Build J Instit Civil Eng 160(SB1):1–9
49. Stewart MG, Melchers RE (1997) Probabilistic risk assessment of engineering systems. Chapman and Hall, London
50. Stewart MG (2010) Risk-informed decision support for assessing the costs and benefits of counter-terrorism protective measures for infrastructure. Int J Critical Infrast Protect 3(1):29–40
51. Stewart MG, Ellingwood BR, Mueller J (2011) Homeland security: a case study in risk aversion for public decision-making. Int J Risk Assessment Manage 15(5/6):367–386
52. Stewart MG (2014) Climate change and national security: balancing the costs and benefits. In: Preble C, Mueller J. (eds) Dangerous World? threat perception and U.S. National Security, Cato Institute, Washington, D.C., pp 137–154
53. Stewart MG, Mueller J (2018) Are we safe enough? measuring and assessing aviation security. Elsevier, New York

54. Stewart MG, Ginger JD, Henderson DJ, Ryan PC (2018) Reliability-based fragility assessment of contemporary housing roof sheeting failure due to extreme wind. Eng Struct 171:464–475
55. Stewart MG, Bastidas-Arteaga E (2019) Introduction to climate adaptation engineering. In: Bastidas-Arteaga E, Stewart MG (eds) Climate Adaptation engineering: risks and economics for infrastructure decision-making. Elsevier, Oxford, pp 3–36
56. Sunstein CR (2002) The cost-benefit state: the future of regulatory protection. ABA Publishing, American Bar Association, Chicago
57. Sunstein CR (2003) Terrorism and probability neglect. J Risk Uncertain 26(2–3):121–136
58. Swiss Re (2020) Natural catastrophes in times of economic accumulation and climate change. Sigma 2/2020, Swiss Re Institute, Zurich, Switzerland
59. Taig T (2012) A risk framework for earthquake prone building policy. TTAC Limited and GNS Science, November 2012
60. Walker GR (2011) Comparison of the impacts of cyclone tracy and the newcastle earthquake on the Australian building and insurance industries. Aust J Struct Eng 11(3):283–293
61. Wang Y, Rosowsky DV (2012) Joint distribution model for prediction of hurricane wind speed and size. Struct Saf 35(1):40–51
62. Wang Y, Rosowsky DV (2017) Hazard-based hurricane loss estimation considering storm intensity, size, and sea-surface temperature change. Sustain Resilient Infrast 3(4):151–164
63. Wibowo A, Kafle B, Kermani A, Lam N, Wilson J, Gad E (2008) Damage in the 2008 China Earthquake. In: Proceedings of 2008 Australasian earthquake engineering society conference, Ballarat, Victoria
64. World Bank (2010) Economics of adaptation to climate change: synthesis report. The international bank for reconstruction and development/world bank, Washington DC
65. World Bank (2015) Investing in urban resilience: protecting and promoting development in a changing World. World Bank, Washington, D.C.
66. World Bank (2016) The making of a risker future: how our decisions are shaping future disaster risk. In: Global facility for disaster reduction and recovery, World Bank, Washington, D.C.
67. Zhang S, Nishijima K, Maruyama T (2014) Reliability-based modelling of typhoon induced wind vulnerability for residential buildings in Japan. J Wind Eng Ind Aerodyn 124:68–81

# Part II
# Decision-Making

# Chapter 2
# Risks and Compromises: Principled Compromises in Managing Societal Risks of Extreme Events


**Paolo Gardoni and Colleen Murphy**

**Abstract** Managing the societal risks from extreme events requires making informed decisions. Decisions are in relation to the desired values of probabilities associated with possible consequences, what are unacceptable consequences (including defining their type and duration), and who might be exposed to risks. Different dimensions of risk including probabilities, consequences, and its source have been discussed in the literature. Such dimensions shape decisions about risk. However, in addition to the technical aspects, ultimately managing risk requires socially negotiated rules. This chapter describes how technical risk analysis can be integrated with public values. The chapter starts with a broad definition of risk and defines its different dimensions. Then the chapter defines guidelines for principled compromises in managing societal risks of extreme events. The chapter also defines the roles and scope in this complex process of risk analysis, risk communication, and risk perception. The proposed guidelines can support decision-makers in making more informed and more transparent decisions about safety, sustainability, and resilience.

## 2.1 Introduction

Communities must manage and make decisions about the various risks they face stemming from natural hazards (such as earthquakes, hurricanes, and wildfires), and technological hazards (such as accidental explosions and leak of toxic waste) [16]. Risk management depends on comparative assessments of the relative gravity of diverse risks [8, 17]. Relative assessments influence priorities in mitigation policies and so to which risks limited resources will be devoted [4, 24, 30].

P. Gardoni (✉)
Department of Civil and Environmental Engineering, University of Illinois at Urbana-Champaign, Illinois, USA
e-mail: gardoni@illinois.edu

C. Murphy
College of Law, University of Illinois at Urbana-Champaign, Illinois, USA
e-mail: colleenm@illinois.edu



M. G. Stewart and D. V. Rosowsky (eds.), *Engineering for Extremes*, Springer Tracts in Civil Engineering, https://doi.org/10.1007/978-3-030-85018-0_2

The human and economic losses and social disruption caused by failure of infrastructure systems are often disproportionately high with respect to the actual physical damage to such systems, and the potential exists for even larger losses in the future, given that population and economic development in hazard-prone coastal areas are increasing dramatically while investments in protective systems are lagging [15]. Also, climate change is modifying the likelihoods and magnitudes of natural hazards (in particular heatwaves and droughts and their effects on wildfires; severe precipitation and their effects on floods and large snowfall events; and hurricanes) around the world and creating new exposures to risks. Climate change is also resulting in sea level rise that affects coastal communities where a large population resides (i.e., 50% of the U.S. population lives within 50 miles of the coast) and is exposed to changing extremes as exemplified by recent events like Hurricane Sandy [27].

The importance of public participation in risk analysis has been recognized by, for example, Lynn [19, 21]. Bohnenblust and Slovic [7] developed one of the first policy frameworks for incorporating technical analyses with public values. Webler and Tuler [37] provided a review of the successes and failures of public participation in risk decision-making. Sun and Jones [35] draw analogies and disanalogies been decision making for war and national security, and disaster mitigation and recovery. They also underline the importance of explicitly and deliberately discussing the assumptions and choices in decision making. Woo [40] noted that government decision-making has historically involved the general public to a different degree. He argues that there are several advantages of citizen participation in government decision-making. However, he also highlights the challenges citizens' participation, in particular when dealing with technical or scientific matters of which citizens might not have sufficient understanding and when individual perceptions (like the perception of risk) might lead to irrational decisions.

Woo [40] also offers some principles for citizen participation aimed at overcoming some of these challenges. The principles include (1) the democratic right of citizens to be informed and have a choice, (2) the right of citizens to some basic education on the risks faced, (3) the responsibility of governments to promote rather than forcing citizens into taking specific actions, and (4) the overarching need for decision making to be rational, equitable and defensible.

This chapter describes how technical risk analysis can be integrated with public values. The chapter starts with a broad definition of risk and defines its different dimensions. Then the chapter defines the rules for principled compromises in managing societal risks of extreme events. The chapter also defines the roles and scope in this complex process of risk analysis, risk communication, and risk perception. The proposed framework can support decision-makers in making more informed and more transparent decisions about safety, sustainability, and resilience [18].

## 2.2 Risk Assessment and Risk Evaluation

Decision-making historically has looked strictly at probability (a measure of the likelihood of an event (e.g., undesirable consequences) or more broadly at risk (the *consequences* and *probability* of a set of hazardous scenarios). Below we provide a brief overview of different approaches for risk evaluation and their limitations. We then argue that the evaluation and comparison of risks require information beyond that provided by probability and risk. Murphy and Gardoni [23] and [25] showed that the source of a risk must also be taken into account in decision-making.

### *2.2.1 Review of Some of the Existing Methods for Risk Evaluation and Their Limitations*

Many fields of engineering, including civil, nuclear, and mechanical; the medical profession; and some safety agencies rely on *F-N charts* (like the one if Fig. 2.1) for risk evaluation [6]. Such charts show the frequency or annual probability of occurrence on one axis, where the other axis includes a measure of specific consequences

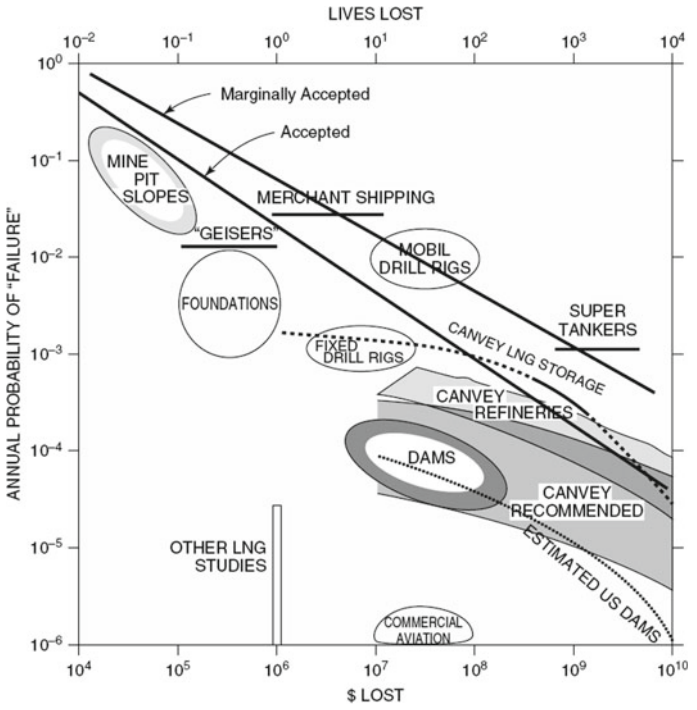


**Fig. 2.1** F-N chart for risks associated with civil facilities and other large structures [5]

(e.g., fatalities and costs). A threshold line is then drawn to distinguish acceptable from unacceptable risks.

F-N charts have three primary limitations [13]. First, they offer a limited picture of the impact of extreme events. Consequences include, but in many cases go significantly beyond, fatalities or other direct losses used in such charts. Second, the relative gravity of a risk is more than a function of probability and consequences. As we discuss more in detail below, the way a risk is created and who stands to bear the negative consequences matter as well. A risk that is voluntarily accepted generates less concern than one involuntarily imposed. Third, there is little room for public involvement in decision-making about risks.

*Cost–benefit analysis* is another common method. From the perspective of cost–benefit (or risk–benefit) analysis, risks are to be permitted if the benefits of allowing them to exceed the costs/risks. Cost–benefit analysis is comparative in nature, examining the costs and benefits of different policies or courses of action. In calculating costs and benefits, a monetary unit of measurement is standardly used (e.g., [9]). The costs of a policy are measured using market information for how much individuals do pay to avoid certain costs or risks. When market information is not available, an assessment of consumer's willingness to pay is done via surveys. Benefits are measured similarly, tracking an individual's willingness to pay for a specific (potential) benefit as ascertained by market data or surveys.

Cost–benefit analysis has the strength of providing a framework for combining and comparing diverse kinds of consequences, which can provide useful information for decision support. However, it also has some limitations. One limitation stems from its characteristic reliance on market data [23]. Such reliance assumes that individuals have full knowledge about the risks they face when paying or when asked how much they would pay to avoid a consequence/risk. Market data also reflect resource constraints, rather than considered judgments about the relative severity of a given risk or value of a particular benefit. An individual's resources set a ceiling for what he or she can or would pay. Thus, differences in the valuation of risks and benefits for poorer and wealthier individuals may not track differences in judgment, but rather differences in available resources. More fundamentally, it is ethically controversial to assume it is appropriate to monetarily quantify all consequences, including loss of human life.

Two additional limitations with the cost–benefit framework are distinct from concerns about its monetary metric. Cost–benefit analysis is indifferent to distributional concerns about who bears risks and who stands to benefit from risks. However, important societal concerns arise when there is no fairness in such distribution. Furthermore, cost–benefit analysis has no principled limit to the risks that societies should accept.

The *psychometric risk paradigm* [10, 11, 33, 34] is another approach focuses on the public perception of risks. Using survey data, psychologists identified the factors that shape public perception. Public attitudes are not shaped strictly by the probability and consequences associated with a risk. For example, dread of a certain risk can inflate the perception of that risks' gravity (as measured by the probability of occurrence of certain consequences); this is unsurprising since dread generates

emotions of terror, catastrophe, and uncontrollability. New risks are often viewed as less acceptable.

One issue with the psychometric risk paradigm, for our purposes, is in explaining why and how risk mitigation policies should take into account public perception of risks. Democratic decision-making may suggest some deference to public viewpoints, but rarely is the public perception on an issue the sole factor shaping decision-making. Moreover, public attitudes are not necessarily comprehensive in identifying the factors that are morally salient in evaluating the relative gravity of risks. Dread and novelty may matter, but it may also matter what the source of dread and novelty is.

Finally, since the 1980s *comparative risk assessment* (CRA) and *multi-criteria decision analysis* have been used in the United States in the context of environmental policy. CRA uses the following method to rank risks. A *Steering Committee* generates a set of hazards that must be ranked. A *Technical Committee* quantifies the risks associated with various hazards and produces an initial ranking. This technical ranking of risks is then sent to a *Public Advisory Committee*, comprised of experts and non-experts, to revise the initial ranking based on consideration of public concern about a hazard and whether potential damage is irreversible. Finally, risks are grouped into high, medium, and low groups.

CRA has the merit of taking into account factors beyond probability and consequences, and importantly the factors that influence public perceptions of risk. CRA also explicitly tries to facilitate discussion among a broad range of stakeholders, including experts and citizens, to ensure the risk evaluation process is transparent and inclusive [3]. As such CRA can provide useful information for decision support.

However, despite its advantages, CRA has also limitations. Cooperation among experts and public stakeholders of the kind required by CRA can be challenging, given the detailed knowledge of risks that is necessary for understanding the basis for the initial ranking of risks under consideration. Absent a comprehensive understanding of the risk determination process, proposed modifications may not reflect an informed understanding. Available versions of CRA do not necessarily account for uncertainties properly. Finally, the source or origins of a risk are not taken into account.

### 2.2.2 Characteristics of the Ideal Method for Risk Evaluation and Decision-Making

Summarizing the discussion so far, an adequate framework for risk evaluation and decision-making must be based on a comparative consideration of three general factors that define what Gardoni and Murphy [13] called a *scale of risk*. First, the *consequences* of a hazardous scenario must be taken into account, where the consequences considered must be broad enough to capture the diverse ways in which extreme events impact communities. Second, the *probability* of occurrence of a

hazard and the associated consequences must be taken into account. Third, how a risk is created and sustained, or its source, must be factored in.

Decision-making in a democratic context must also be sufficiently democratic in two respects. First, consideration must be given to the concerns about risks, which may go beyond the three factors just listed, which the public might expresses. Second, decision-making requires a method for resolving disagreement about the appropriate decision to take given risks posed by extreme events. Such disagreement can exist among members of the public, between the public and experts, as well as among experts.

In the next section, we provide greater detail on the three dimensions that define the *scale of risk* and shape the relative gravity of risks: consequences, probability, and source. Our discussion highlights (1) the ways that consequences vary, (2) the forms uncertainty takes, and (3) the dimensions that shape the source of a risk. The following section then asks how to deal with disagreement and debate over the relative gravity of risks of extreme events and the decisions that should be made.

## 2.3 Dimensions of Risk in Risk Evaluation: Consequences, Probability, and Source

This section looks at the three general *dimensions* that define the *Scale of Risk*. For each dimension, we distinguish the various *sub-dimensions* that are relevant for risk evaluation. This section is intended to only be a brief summary. More details on the *Scale of Risk* can be found in [13].

Consider first consequences. When evaluating a risk and its relative importance, the following five aspects of consequences shape such evaluation:

- ***The kind of consequences:*** Consequences may be of different kinds. Potential death, injury, economic losses, and environmental damage are examples of consequences a hazardous scenario may have. To evaluate a risk, it is necessary to first decide what potential impacts will be predicted. Within considered impact, not all are equally serious. Death is arguably a worse consequence than economic loss or injury.
- ***The extent of consequences***: The amount or extent of a particular consequence varies among risks.
- ***Issues of time***: Some consequences of a hazard are immediate, others are long-term. When determining and then evaluating a risk it is necessary to make a judgment as to how far in the future consequences will be considered. Risks can vary significantly in their gravity depending on the time horizon selected. Climate change and risks associated with climate change are current examples of this.
- ***Whose consequences matter***: In addition to deciding which consequences matter, it is necessary to determine whose consequences matter. Of particular concern in the context of extreme events is future generations. The question of whether to include potential impacts on future generations, and if so, the weight to give to

those impacts relative to the impact on the living generation is the subject of extensive debate. The issue of sustainability foregrounds the potential environmental impacts of extreme events. Whether, and how, to include the environment is an additional question that approaches to risk determination and decision-making must answer.

- ***Issues of distribution of consequences across a population:*** Extreme events often affect segments of a given population differently. Vulnerability studies extensively document how different segments of the population might face greater impacts from extreme events. One challenge that approaches to risk determination and evaluation need to consider is to take into account the differential burdens borne in decision-making about risks.

In terms of probability, there are two different kinds of uncertainty it is necessary to take into account in risk evaluation and decision-making about extreme events: *endodoxastic* and *metadoxastic* uncertainties [26].

Endoxastic uncertainties are a function of intrinsic randomness in the natural world (aleatory) and a function of limitations in our knowledge and understanding (epistemic). Probabilities are used to capture the likelihood of occurrence of specific hazards and associated consequences. Accounting for endodoxastic uncertainty is standard in risk analysis [15].

Metadoxastic uncertainties are a product of limits in confidence in the accuracy of assigned probabilities. Such uncertainties are rarely considered in risk analysis for extreme events. This is problematic. Failure to account for the confidence we should have in a model can result in risk-prone analyses that insufficiently acknowledge the possibility that even the best expert assessment may be mistaken.

Finally, three aspects of the source of a risk, or how a risk is created and sustained, should be taken into account when assessing the relative gravity of risks and engaging in decision-making about extreme events. They are:

- ***Causation and responsibility:*** This sub-dimension focuses on what brings a hazard. In some cases, individual actions and individual or collective decisions are responsible for the creation of certain risks. Risks from nuclear power plants or recreational activities are examples. We are in a position to permit or eliminate the cause of such risks by permitting or eliminating construction or activities. In other cases, we are not in a position to completely eliminate risks. Many risks from extreme natural events are like this. The choice is restricted to whether, and how, to attempt to control or mitigate the risks we face. For example, such control can be exercised through decisions about where we allow dwellings in hazard-prone areas.
- ***Voluntariness:*** In general, risks voluntarily incurred are less grave than risks involuntarily imposed. Voluntariness of a risk is a function of consent or agreement to be exposed to a risk and knowledge about the risk in question. When knowledge and agreement conditions are not satisfied, a risk is involuntarily incurred.
- ***Relation between who is put at risk and who caused the risk:*** The individuals responsible for the creation or control of a risk are not always the same as the individuals or groups that stand to bear the consequences of a hazard. In general,

a risk is graver when those who are put at risk are different than the individuals who stand to benefit from permitting a risk or who generate the risk in question.

Using these dimensions and sub-dimension, Gardoni and Murphy [13] defined a Scale or Risk that can be used for the ranking of risk. Such ranking can inform the decision-making in managing risks. However, as noted earlier, in addition to the technical aspects, ultimately managing risk requires socially negotiated rules. The next section describes how technical risk analysis can be integrated with public values.

## 2.4 Decision-Making in Managing Societal Risks

The previous section provided an overview of a range of considerations that shape the relative gravity of a risk. Decision-making about risk must balance these various considerations to determine whether mitigation actions are necessary in the face of certain risks and what form mitigation action should be taken. Decision-making in a democratic context also requires consideration of whose perspectives should and will count when societal risks are managed and mitigated. Specifically, it is necessary to define who should have a voice in the decision-making process, and how to balance expert opinion with individual/public preferences in cases of conflict. When soliciting public input, risk communication is critical to ensure the public formulates preferences based on an accurate understanding of the risks in question.

Decision-making about risk, we suggest in this section, is best thought of as an exercise in compromise between technical requirements, the opinions of experts, and the preferences of the public. Compromises in decision-making are operative whenever serious practical constraints make the full achievement of normative ideals or values like safety impossible. Full safety is practically impossible. Communities must decide how to deal with risks when necessarily constrained by limits in time, resources, knowledge, and ability. There are also uncertainties that limit our ability to remove certain risks and the options for how safety can best be achieved.

In compromise, it is necessary to balance the different the dimensions of risk discussed in the previous section. For example, prioritizing a principle that individuals bear the consequences for risks voluntarily assumed may lead communities to reduce the public resources used to mitigate risks or available for disaster relief. Sustainability requires protecting ecosystems from damage by disasters and safeguarding their restoration and rehabilitation post-disaster [2, 36]. Damage to ecosystems must be balanced against damage to infrastructure, individuals, and communities. Among individuals, the balance between immediate individuals affected versus damage to future generations must be balanced [22, 41]. Balancing is not always straightforward. MacLean [20] underscores the tension between temporal and spatial aspects of climate change which are relevant to risks from extreme events. Achieving justice in risk decision-making spatially, among presently living members of a community, might be in tension with achieving justice temporally, across generations.

The needs of spatial (or intra-generational justice) and temporal (or inter-generational justice) can pull in different directions [36], and [14].

Finally, the level we reduce or remove risks to achieve safety necessarily carries with it costs of different kinds. Investing resources to mitigate low probability, high impact hazards may limit resources available to mitigate high probability, lower impact hazards [39]. Risk reduction may constrain allowable activities. For risks of extreme events, where one lives and what kind of home one lives in can be more or less constrained to reduce risks. There are other kinds of opportunity costs, for example, the use of resources for safety could be used for other public purposes, such as education.

An example of compromise is the design level of safety of structures (buildings, bridges, nuclear power plants, etc.). In this case, the design level of safety is achieved by experts selecting geometric and material characteristics guided by a codified set of design rules (i.e., the design code). These codes balance safety and costs. However, the actual level of safety achieved through the design code is traditionally implicit, often not even estimated (e.g., when a series of conservative choices are made in the design process), and never the result of a true compromise as defined earlier.

In compromise, it is also necessary to define the scope of inclusion for decision-making about risk. One basis for inclusion when it comes to voices from the public is the extent of the possible consequences of risks. For example, nuclear power plants and dams could bring catastrophic consequences for a large portion of the population. In this case, the process of compromise should be more thorough and involve a larger number of people than in cases when only a few people could be exposed. Also, in cases where those who potentially bear the consequences of a hazard are different than those who benefit from allowing that risk, a decision principle could stipulate that the individuals or community bearing the costs should have a bigger say in the process of compromise than those who benefit.

## 2.5 Guidelines for Principled Compromises in Decision-Making

A framework for principled compromise in decision-making articulates guidelines for defensible ways of balancing the various considerations that are relevant for determining whether, and how, to mitigate certain risks. Such guidelines for managing risks can serve as socially negotiated rules for decision-making and for proceeding in the face of disagreement about the appropriate balance to strike among diverse considerations. In this final section, we provide a sketch of such guidelines. The guidelines integrate technical risk analysis with public preferences and public values.

It is important to recognize that not all approaches to compromises are defensible. Though complete safety is unattainable, it does not follow that anything short of perfection suffices. Decision-making that merely reflects differences in power is not principled. Such decision-making could result in poor and marginalized communities

being unjustifiably exposed to risks from extreme events simply because they lack the political clout to demand public investment in risk mitigation measures and the resources to move to a less risk-prone area.

The criteria we outline in this section provide some resources for distinguishing between justifiable and unjustifiable approaches to risk. The criteria we outline do not imply that there is only one approach to risk that is defensible. But they do allow us to rule out certain approaches as indefensible and help develop viable approaches.

A starting point to thinking through principled compromises [28] with respect to risks is the complaints raised about approaches to risk mitigation or disaster response within communities. We focus here on two distinct, but common, complaints. The first is that victims of disasters or potential victims of future extreme events are sold short. The worry here is that certain individuals or groups are not safe. Whatever minimum protection against risk individuals should enjoy was not met in such cases. For example, living in floodplains (flat areas adjacent to rivers or streams, which are likely to flood during high discharge), while less expensive than other areas, does expose the inhabitants to higher risks (i.e., a higher likelihood of flooding). Similarly living along the coastline, while more desirable for the scenic view might expose the inhabitants to higher risks (i.e., a higher likelihood of wind and storm surge damage). The worry is that victims of disasters or those most vulnerable to future extreme events are unjustifiably harmed or put at risk, even if you take into account other competing or pressing demands and preferences. The worry as expressed does not depend upon the expectation that full safety is achieved. Rather, the worry is that victims are insufficiently protected from harm, even granting all of the balances to be struck discussed above.

To respond to concerns that victims were unjustifiably exposed to risk it is necessary to first understand what a threshold level of protection would be necessary in a given case to count as mitigating risk at all. Here is an analogy. We can ask about whether the rule of law obtains in a given community. Law is governing conduct based on rules [12]. One way of answering this question about whether the rule of law obtains is to examine the extent to which a legal system satisfies the conditions that need to be present for rules to govern conduct. Rules can govern conduct only if, for example, they are known, are known prospectively (or in advance of action), are not contradictory, and do not demand the impossible. A legal system needs to have a threshold level of eight conditions to count as a system of law. In Fuller's words, 'A total failure in any one of these eight directions does not simply result in a bad system of law; it results in something that is not properly called a legal system at all, except perhaps in the Pickwickian sense in which a void contract can still be said to be one kind of contract' [12]. A system of rules that are secret cannot in any meaningful sense govern conduct. With the rule of law, it is only after the threshold level of publicity has been satisfied that it makes sense to talk about balancing. Once that threshold has been satisfied for the criteria for the rule of law, then it makes sense to talk about legal systems satisfying the rule of law to greater or lesser degrees, depending on the extent to which they satisfy the eight criteria for the rule of law.

Similar considerations apply to risk decision-making. We can ask of the considerations discussed in Sect. 2.3 whether they have been sufficiently taken into account

to make it plausible to claim a given value is being balanced. Once that threshold has been passed, we can then talk intelligibly about principled compromises. There are important questions that remain about how to define these thresholds, and by whom such decisions should be made. Here the risk of duplicating patterns of marginalization is especially relevant. Thresholds of acceptable and tolerable risk can be useful in delimiting a baseline for risk mitigation [14, 36].

- A*cceptable threshold*: The minimum level of wellbeing in principle acceptable for individuals to have in the aftermath of an event over any length of time
- *Tolerable threshold:* Below the acceptable threshold, a level of wellbeing can be tolerable if (a) temporary; (b) reversible; and (c) does not fall below the tolerable threshold, which is the absolute minimum level of wellbeing below which no individual in a society should ever fall, regardless of whether that level is temporary and reversible

Decision-making about risk might not provide the same level of safety across the population. For example, as noted earlier, more modest buildings in the floodplains are more likely to experience damage due to riverine flooding. On the other hand, more expensive residencies along the coastline might be more exposed to hurricane damage (wind and storm surge) than more modest buildings built in-land. To deal with the question of intra-generational and inter-generational justice, we can further define ranges of permissible inequality. Gardoni and Murphy [14] argue that if the inequalities are likely to be exacerbated too much then the risk might not be acceptable, if the exacerbation is moderate but not too much then the risk might be tolerable as long as the exacerbation is temporally limited. Similarly, for intergenerational justice, we can have an acceptable and tolerable level to assess the level of change in resilience across generations.

The delimiting of thresholds of acceptable and tolerable risk and permissible inequality still allows for a wide range of options for risk decision-making. In addition to specifying general criteria to satisfy, it is necessary to give some guidance for how differences in decision-making approaches are to be handled. We end this section with a discussion of some of the considerations that allow us to make these distinctions.

First, principled compromises are not just a function of the reasons for the sake of which a decision is made. Compromises that are principled are integrative [38], p. 65, Allen [1]. They take into consideration competing considerations and aim to find a balance among them when all cannot be satisfied fully. When different perspectives exist on the appropriate balance to strike, integration occurs among competing perspectives (e.g., among various stakeholders and risk analysts). Integrative compromises find a balance that includes competing considerations. The contrast between an integrative compromise is a compromise that eschews the views in a conflict in favor of a neutral third alternative. For example, in the face of competing preferences for Japanese or Italian cuisine, a family opts for Thai food as a compromise. By contrast, in principled compromises, an effort is made to respect and incorporate to the extent possible the viewpoints and values in tension. Importantly, this incorporation is not identical to cost–benefit tradeoffs. There may be certain values that cannot be traded against one another.

Second, the reasons behind a particular compromise struck matter [38]. Taking into account the views of various stakeholders with respect to risk decision-making can overcome epistemic limitations associated with any particular view. As the risk perception literature documents (e.g., [29, 31, 32]), differences in the perception of risk among laypeople and risk experts can reflect different underlying valuations. Thus, incorporating multiple perspectives in risk decision-making is one way to ensure that values that should factor into decision-making do factor into decision-making.

Third, a commitment to a democratic community further delimits principled from unprincipled compromises. Democratic communities depend on the willingness of their members to compromise in the face of disagreement. This is signaled by being willing to build bridges in the face of reasonable disagreement over decision-making with respect to risk.

Finally, there can be principled consequentialist reasons to compromise. Refusal to compromise can result in a failure to achieve a given value at all. In the context of democratic decision-making about societal risk, a refusal to compromise can mean inaction and so a failure to promote safety in ways that would otherwise be possible if a compromise was reached.

## 2.6 Conclusions

This book chapter started from the premise that managing societal risks to extreme events requires making informed decisions. Such decisions should be based on sound technical analyses but also socially negotiated principles and integrated with public values. The chapter presented a framework to support decision-makers in making more informed and more transparent decisions about safety. Decisions are in relation to the desired values of probabilities associated with possible consequences, what are unacceptable consequences, and who might be exposed to risks. This chapter described how technical risk analysis can be integrated with public values. The chapter started with a broad definition of risk and defines its different dimensions. Then the chapter defined the rules for principled compromises in managing societal risks of extreme events. The chapter also defined the roles and scope in this complex process of risk analysis, risk communication, and risk perception. The proposed framework can support decision-makers in making more informed and more transparent decisions about safety.

## References

1. Allen J (1999) Balancing justice and social unity: political theory and the idea of a truth and reconciliation commission'. University of Toronto Law J 49(3):315–353

2. Anderson MB, Woodrow PJ (1989) Rising from the ashes: development strategies in times of disaster. Westview Press, Boulder, CO
3. Andrews CJ, Apul DS, Linkov I (2004) Comparative risk assessment: past experience, current trends, and future directions. In: Linkov I, Bakr Ramadan A (eds) Comparative risk assessment and environmental decision making. Kluwer Academic Publishers, Netherlands, pp 3–14
4. Aven T, Renn O (2018) Improving government policy on risk: eight key principles. Reliab Eng Syst Saf 176:230–241
5. Baecher GB (1982) Statistical methods in site characterization updating subsurface samplings of soils and rocks and their in-situ testing. Santa Barbara, CA, Engineering Foundation
6. Bedford T, Cooke R (2001) Probabilistic risk analysis: foundations and methods. Cambridge University Press, Cambridge, UK
7. Bohnenblust H, Slovic P (1998) Integrating technical analysis and public values in risk-based decision making. Reliabil Eng Syst Safety 59(1)
8. Doorn N, Gardoni P, Murphy C (2019) A multidisciplinary definition and evaluation of resilience: the role of social justice in defining resilience. Sustain Resilient Infrast 4(3):112–123
9. Faber MH, Miraglia S, Qin J, Stewart MG (2020) Bridging resilience and sustainability—decision analysis for design and management of infrastructure systems. Sustain Resilient Infrastruct 5(1–2):102–124
10. Fischhoff B, Slovic P, Lichtenstein S (1979) Weighing the risks:which risks are acceptable. Environment 2(4):17–20, 32–38
11. Fischhoff B (1997) Ranking risks. In: Bazerman MH, Tenbrunzel AE, Wade-Benzoni, KA (eds). Environment, ethics, and behavior: the psychology of environmental valuation and degradation. Jason Aroson, pp 342–371
12. Fuller LL (1969) The morality of law, rev. Yale University Press, New Haven, CT
13. Gardoni P, Murphy C (2014) A scale of risk. Risk Anal 34(7):1208–1227
14. Gardoni P, Murphy C (2020) Society-based design: promoting societal well-being by designing sustainable and resilient infrastructure. Sustain Resilient Infrastruct 5(1–2):4–19
15. Gardoni P (Ed.) (2017) Risk and reliability analysis: theory and applications, Springer
16. Gardoni P, LaFave J (Eds.) (2016) Multi-hazard approaches to civil infrastructure engineering, Springer
17. Gardoni P, Murphy C, Rowell A (Eds.) (2016) Societal risk management of natural hazards, Springer
18. Gardoni P (Ed) (2019) Routledge handbook of sustainable and resilient infrastructure, Routledge
19. Lynn FM (1990) Public participation in risk management decisions: the right to define. The Right to Know and the Right to Act, 1 *RISK* 95
20. MacLean D (2016) Climate change and natural hazards. In: Gardoni P, Murphy C, Rowell A (eds) Risk analysis of natural hazards. Springer, pp 81–95
21. McGarity TO (1990) Public participation in risk regulation. 1 *RISK* 103
22. Mileti DS (1999) Disasters by design: a reassessment of natural hazards in the United States. Joseph Henry Press, Washington, D.C.
23. Murphy C, Gardoni P (2006) The role of society in engineering risk analysis: a capabilities-based approach. Risk Anal 26(4):1073–1083
24. Murphy C, Gardoni P (2007) Determining public policy and resource allocation priorities for mitigating natural hazards: a capabilities-based approach. Sci Eng Ethics 13(4):489–504
25. Murphy C, Gardoni P (2011) Evaluating the source of the risks associated with natural events. Res Publica 17(2):125–140
26. Murphy C, Gardoni P, Harris CE (2011) Classification and moral evaluation of uncertainties in engineering modeling. Sci Eng Ethics 17(3):553–570
27. Murphy C, Gardoni P, McKim R (Eds.) (2018) Climate change and its impact: risks and inequalities, Springer
28. Murphy C (2020) On principled compromise. Proceedings of the Aristotelian society CXX, pp 47–70

29. Renn O (1998) The role of risk perception for risk management. Reliab Eng Syst Saf 59(1):49–62
30. Sharma N, Tabandeh A, Gardoni P (2020) Regional resilience analysis: a multi-scale approach to optimize the recovery of interdependent infrastructure. Comput-Aided Civil Infrastruct Eng. https://doi.org/10.1111/mice.12606
31. Sjöberg L (2000) Factors in risk perception. Risk Anal 20(1):1–12
32. Sjöberg L (2001) Political decisions and public risk perception. Reliab Eng Syst Saf 72(2):115–123
33. Slovic P, Fischhoff B, Lichtenstein S (1982) Why study risk perception? Risk Anal 2:83–93
34. Slovic P, Fischhoff B, Lichtenstein S (1981) Perceived risk: psychological factors and social implications. In: Warner F, Slater DH (eds) The assessment and perception of risk. Royal Society, London, pp 17–34
35. Sun LG, Jones RA (2016) War rhetoric and disaster transparency. In: Gardoni P, Murphy C, Rowell A (eds) Risk analysis of natural Hazards, Springer
36. Tabandeh A, Gardoni P, Murphy C, Myers N (2019) Societal risk and resilience analysis: a dynamic Bayesian network approach. ASCE J Risk Uncertainty Anal 5(1):04018046
37. Webler T, Tuler S (2021) Four decades of public participation in risk decision making. Risk Anal 41(3):503–518
38. Weinstock D (2014) On the possibility of principled moral compromise. Reprinted in Wendt 2014, pp 63–82. Originally published in Critical Review of International Social and Political Philosophy 16(4):537–556 (September 2013)
39. Williams RJ, Gardoni P, Bracci JM (2009) Decision analysis for seismic retrofit of structures. Struct Saf 31:188–196
40. Woo G (2016) Participatory decision making on hazard warnings. In: Gardoni P, Murphy C, Rowell A (eds) Risk analysis of natural hazards, Springer
41. World Commission on Environment and Development, Our Common Future (1987) Oxford University, Press, New York

# Chapter 3
# Risk-Informed Approaches for Mitigating Impacts of Extreme and Abnormal Events in the Built Environment


**Bruce R. Ellingwood**

**Abstract** Our built environment is essential for community health and welfare. Even with proper design and construction to withstand demands imposed by occupancy, service requirements and natural environmental hazards, buildings and other civil infrastructure may be susceptible to damage due to events outside the design envelope, which may include extreme windstorms, earthquakes, flooding, accidents or intentional malevolence. The human and economic losses that result from such damage can be significant. Changes in design and construction practices over the past several decades have made some modern structural systems vulnerable to extreme and abnormal events. Social and political factors also have led to an increase in events that may pose a threat to civil infrastructure. Finally, public awareness of infrastructure performance and safety issues has increased markedly in recent years. The move toward risk-informed design, with its formal tools for analyzing uncertainties and consequences of damage or failures in the built environment, promises a level of coherence in decision-making that cannot be achieved by judgment alone, and increases the likelihood that judgements, when necessary, are consistent with logic and the available data. Codes and standards provide a highly visible forum for demonstrating economic and social benefits of risk-informed design. Chapter 3 explores the prospects of improving engineering practices to enhance facility robustness and to manage the risk of unacceptable damage from low-probability, high-consequence threats.

**Keywords** Buildings (codes) · Design (buildings and bridges): probability · Reliability · Risk · Structural engineering

B. R. Ellingwood (✉)
Department of Civil and Environmental Engineering, Colorado State University, Fort Collins, CO 80523, USA
e-mail: bruce.ellingwood@colostate.edu



M. G. Stewart and D. V. Rosowsky (eds.), *Engineering for Extremes*, Springer Tracts in Civil Engineering, https://doi.org/10.1007/978-3-030-85018-0_3

## 3.1 Introduction

Customary design practices for the built environment, involving combinations of dead, occupancy or operating live, flood, wind, snow, rain and ice, and earthquake loads, provide a degree of strength and ductility that is also available to withstand extreme or abnormal loads that are outside the customary design envelope. However, such low-probability events, including extreme environmental effects, accidents, misuse, and sabotage or terrorist attack, may precipitate a disproportionate (or progressive) structural collapse, a catastrophic failure of the facility or a major portion of it, ensuing from local damage that cannot be contained by the inherent continuity and ductility of the structural system and propagates into an extensive partial or total collapse that is disproportionate to the local damage caused by the initiating event [1–4]. Continuous highly redundant steel and reinforced concrete framed structures tend to absorb local damage reasonably well. Large-panel, bearing wall structures and concrete slabs with post-tensioned unbonded reinforcement [5] are inherently more susceptible to damage because continuity between structural elements may be difficult to provide. However, all buildings are susceptible to disproportionate collapse in varying degrees [6, 7]. Many studies worldwide have shown that the risk of structural failure due to such effects as fire, vehicular impact, explosions and other abnormal events may be comparable to the risks associated with hazards that are commonly addressed in structural design. Disproportionate collapses, regardless of cause, are a principal cause of injury and death in building failures [3, 8–10].

Improvements to building and structural engineering practices to enhance robustness and lessen the likelihood of unacceptable damage from low-probability, high-consequence threats or progressive (disproportionate) collapse now are receiving heightened interest among design professionals for a number of reasons. Pressures to achieve economy in design or versatility in building occupancy may lead to systems that have little inherent energy-absorbing capacity and are vulnerable to extreme events outside the design envelope. Construction technologies aimed at minimizing erection costs also may lead to structures with little inherent resistance to disproportionate collapse. Social and political events also have led to an increase in abnormal events that may pose a threat to the built environment. Finally, public awareness of building safety issues has increased markedly during the past thirty years as a result of well-publicized natural and man-made disasters. The growing worldwide acceptance of the concepts of performance-based engineering demands further improvements in design practices to manage risk in the built environment.

The design and construction process involves numerous uncertainties. Some of these uncertainties are inherent (or aleatory) at the customary scales employed in modeling and analysis; these would include material strengths, and occupant and environmental actions. Others are knowledge-based (or epistemic) and arise from limitations in modeling and insufficient databases. No system can be engineered and constructed to be absolutely risk-free in the presence of uncertainty [11]; rather, risk must be managed in the public interest through both technical (codes and standards) and non-technical means (education, public awareness). Risk management often

involves difficult choices; achieving reductions in risk requires additional investment, which must be balanced against competing priorities for those resources. The performance of the built environment during recent natural disasters has drawn attention to deficiencies in current approaches to risk management but appears to have done little to change public expectations that the built environment be essentially risk-free.[1]

Principles of structural reliability and probabilistic risk assessment enable technically feasible and socially acceptable measures for managing risk to the built environment due to extreme or abnormal events. Such principles and their implementation in structural engineering practice have evolved significantly in the past five decades, from their inception in probability-based limit states design to the advanced treatment of impacts of uncertainty on the built environment made possible by conceptual and computational progress in stochastic mechanics.

## 3.2 Probability-Based Limit States Design

The practice of structural engineering in the built environment relies heavily on standards and codes of practice as the basis for defining natural and man-made forces and for identifying structural resistance to these forces. In other fields, such as aerospace, marine and automotive industries, the engineered product is mass-produced, the demands and capacities are relatively predictable, the technology is reasonably controlled, and supporting data are available from component testing. Design development usually involves cycles of product testing and improvement, and performance is governed by the demands of the marketplace. In contrast, most buildings, bridges and other structures in the built environment, are not mass-produced and performance data under repeatable circumstances are hard to obtain; computation supplants testing, uncertainties are very large, and consequences of failure tend to be much more severe in human and economic terms. The framers of these codes on which the structural engineer relies for design must address the question: "How safe is safe enough?" on behalf of society as a whole. Until about 1970, that safety level represented a value judgement by the code-writers based on past experience. About that time, the convergence of research in structural reliability with structural engineering practice enabled structural codes to be developed within a theoretical framework for analyzing uncertainties and addressing safety, leading to quantitative links between structural engineering and its social consequences [11, 12].

[1] A notable exception is in the seismic risk arena, where the surge in interest in performance-based earthquake engineering following the Northridge Earthquake of 1994 stems from the recognition that providing for life safety through building regulation is necessary but not sufficient to mitigate unacceptable economic losses to the residents or the business community affected by the earthquake.

### 3.2.1 Development of Practical Design Criteria

In the simplest formulation of structural reliability, the structural action (tensile force, moment, etc.) due to the combined loads, $Q$, and the structural resistance, $R$, are both modeled as random variables. Failure is defined by the limit state $R—Q < 0$, the limit state being one of, e.g., tension yielding, flexural failure, instability, or connection fracture. The limit state probability (or failure probability), $P_f$, defined as [13, 14]:

$$P_f = P[R - Q] = \int F_R(X) f_Q(x) dx \tag{3.1}$$

becomes the quantitative measure of unsatisfactory structural performance in the presence of uncertain resistance and load. In Eq. 3.1, $F_R(x) = P[R < x]$ is the cumulative distribution function (CDF) of $R$ and $f_Q(q)$ is the probability density function (PDF) of $Q$. More generally, $R$ and $Q$ are functions of other (basic) variables, $\boldsymbol{X}$, derived from structural mechanics and load modeling, such as yield strength, section properties, wind speed, pressure coefficients, etc. The limit state function becomes:

$$G(\boldsymbol{X}) = G(X_1, X_2, ..., X_m) = 0 \tag{3.2}$$

in which $\boldsymbol{X} = (X_1, X_2, \ldots X_m) =$ vector of resistance and load variables that, in general, are random. Consistent with Eq. (3.1), the "failure" event is defined, by convention, such that the limit state is reached when $G(\boldsymbol{X}) < 0$. Thus, the limit state probability becomes:

$$P_f = \int_{\Omega} f_X(x_1, x_2, ..., x_m) dx_1\, dx_2 ... dx_m \tag{3.3}$$

in which $f_X(x) =$ joint probability density function of $\boldsymbol{X}$ and the domain of integration, $\Omega$, is that region of $\mathbf{x}$ where $G(\boldsymbol{X}) < 0$. Equations (3.1)–(3.3) are based on the same fundamental concepts and will not be further distinguished in this chapter.

*First-order reliability methods* were developed in the 1970s to address numerical difficulties in utilizing Eqs. (3.1)–(3.3) in practical structural engineering situations [12]. They enabled the reliability analysis to be performed simply as a function of the means and standard deviations (or coefficients of variation, COV) of resistance and structural actions, and led to a reliability measure known as the reliability index, $\beta$.[2] The reliability index and limit state probability are related as $\beta \approx \Phi^{-1}(1 - P_f)$, in which $\Phi^{-1}() =$ percent point function of the standard normal deviate. With advances

[2] For common structural engineering practice, these numbers usually are on the order of 2 to 6. Many engineers in the last 1960's and early 1970s were more comfortable with such numbers than with probabilities of $10^{-5}$ or less. Moreover, $\beta$ could be computed with only a knowledge of "most likely value" (reflected, approximately, in the means or medians) and "uncertainty" (reflected in the standard deviation or coefficient of variation (COV)), quantities with some familiarity, rather than the entire distribution, which was an unfamiliar concept. Since $\beta$ incorporated uncertainty

in structural reliability theory over the past four decades, the choice of $\beta$ or $P_f$ as measures of structural reliability is a matter of convenience and preference. First-generation probability-based load combinations for limit states design of buildings and other structures, which first appeared in the early 1980s in *ANSI Standard A58-1982* (the predecessor of *ASCE/SEI Standard 7* [15], which now is in its 2016 edition), continue to be based on target reliability indices,[3] which were determined through a complex process of calibration to existing engineering practice rather than ab initio. The current load combinations for dead load, *D*, live load, *L*, snow load, *S,* and wind load, *W,* that resulted from this process define the *required strength* in probability-based limit states design for buildings in the United States:

$$\begin{aligned}
&(1)\ 1.4D_n \\
&(2)\ 1.2D_n + 1.6L_n + 0.5S_n \\
&(3)\ 1.2D_n + 1.6S_n + 0.5L_n + 0.5W_n \\
&(4)\ 1.2D_n + 1.0W_n + 0.5L_n + 0.5S_n \\
&(5)\ 0.9D_n + 1.0W_n
\end{aligned} \tag{3.4}$$

in which the subscripts "*n*" denote *nominal* or *characteristic* value. Probability-based limit states design criteria are completed by the requirement:

$$Required\ strength\ <\ Design\ strength \tag{3.5}$$

in which the *required strength* is defined as $\varphi R_n$, in which $R_n$ = nominal resistance stipulated by code or standard and $\varphi$ = resistance factor, accounting for bias and uncertainty in the determination of resistance. The load combination requirements are designed to achieve $\beta = 3.0$ for ordinary residential, commercial and industrial buildings designed for ductile limit states and chosen, somewhat arbitrarily, for a service period of 50 years (equivalently, a mean annual frequency of failure approximately equal to $3 \times 10^{-5}$/year). Adjustments for other building occupancies, such as temporary structures, public assembly buildings, and critical facilities, such as hospitals and fire stations (termed Occupancy Risk Categories in *ASCE/SEI Standard 7*), are reflected in the return periods for $S_n$ and $W_n$. Adjustments for non-ductile limit states, such as instability or connection fracture, are made through the design strengths $\varphi R_n$ found in the specifications and standards for the various structural materials (e.g. [16, 17]). Load and resistance criteria for bridges were developed independently in the mid-1990s [18].

explicitly, it offered an improvement over the traditional factor of safety, where there was abundant evidence that uncertainty was not treated rationally.

[3] The importance of the reliability index, β, for measuring and communicating risk should be noted. It is unlikely that probability-based limit states criteria would have been accepted in the 1980s by professional structural engineers, let alone the building codes, had they been justified on the basis of a benchmark probability of $10^{-5}$/year. The reliability index is more easily understood and avoids the difficulty that is inherent to explaining such low-probability events.

#### 3.2.1.1 Earthquake Criteria—A Conditional Reliability Approach

Probability-based design for earthquakes (and, more recently, tsunamis) uses a different approach from that described in 3.2.1, for several reasons.[4] First, while design for the hazards in 3.2.1 has traditional been based on elastic behaviour of individual members and systems (local inelastic action, such as plastic hinging is permitted), earthquake engineering in the U.S. traditionally has recognized that nonlinear action of the structural *system* is essential to achieve the desired earthquake performance. This difference in philosophy predates the notions of probability-based design by several decades. Second, while the hazards for the other environmental loads covered by *ASCE/SEI Standard 7* are developed ad hoc by the ASCE 7 Committee, the seismic hazard curves, are developed by the U.S. Geological Survey (USGS) and are used for numerous purposes. Finally, the target reliabilities for earthquake are less than those for the other loads because of the significant economic issues involved in providing seismic resistance and robustness. This difference was first recognized in the initial research leading to *ANSI Standard A58-1982* [19, 20] and has been confirmed in the past four decades by numerous studies.

In probability-based design for earthquake effects, we rewrite Eq. (3.1) as:

$$P_f = P[R - Q] = \int F_R(x)|dH_Q(x)/dx|dx \tag{3.6}$$

in which $H(x)$ = seismic hazard curve developed by the USGS defining the probability that the ground motion intensity (measured by spectral acceleration) exceeds $x$, and $F_R(x)$ = *seismic fragility*, describing the resistance of the structural system expressed in units of spectral acceleration. The design-basis seismic hazard (termed the Maximum Considered Earthquake, or MCE) is defined at a level corresponding to a 2% probability of exceedance in 50 years (equivalently, a return period of 2475 years). The MCE is independent of the structural system. The structural capacity for design is defined at the 10% exclusion limit of the seismic fragility [21],[5] including the effect of inelastic behaviour on structural system capacity. Combining a 2,475-year earthquake with a 10% ile fragility, the probability of incipient collapse of a structure, or a major portion of it, is approximately 1% in 50 years (Eq. 3.6), which is approximately an order of magnitude larger than the limit state probabilities for combinations of dead, live, snow and wind loads in 3.2.1. Note that neither the design hazard nor fragility were selected from the convolution represented by Eq. (3.6). For practical seismic design, these 10% exclusion limits for different structural systems are encapsulated in Chap. 12 of *ASCE/SEI Standard 7-16* in the form of response modification factors on strengths and deformations, $R$, $\Omega_o$ and $C_d$, which are used to modify elastically computed seismic demands and capacities.

[4] We will see subsequently that the approach taken for earthquake effects bears a similarity to the approach for accidental and abnormal loads, making this section a transition between unconditional and conditional reliability approaches.

[5] Reports issued by FEMA, NIST and other Federal agencies of the US Federal Government are available for free download at the agency websites.

### 3.2.2 Closure

The evolution toward probability-based codes and standards has allowed significant improvements in design, particularly in assessment and management of uncertainties. On the other hand, the reliability targets in *ASCE/SEI Standard 7-16* (and similar document worldwide) were determined through a code calibration process involving analysis of reliability of a large number of beams, columns, tension members and connections designed at the code minimums by existing codes of practice of 1960–1970 vintage. This calibration to existing practice provided the continuity that was essential to win the confidence of practicing structural engineers at the time. However, no attempt was made to rationalize the calibrated reliabilities in terms of risk, as we now understand it, and they are related to social expectations of performance only to the extent that reliability benchmarks obtained from calibration can be related to such expectations. Such reliabilities are *notional* and only have meaning when they can be keyed to existing satisfactory practice. In this day and age, probabilistic safety analyses are increasingly directed toward hazards other than those for which the structural system was designed and for which there is little or no experience. Code calibration has little meaning for such situations because such events are not dealt with in current codes.

## 3.3 Engineering Risk Assessment of the Built Environment

The term *risk* is often used interchangeably with *probability* when addressing a potentially hazardous natural or man-made event.[6] The notion of relative likelihood (expressed as an annual probability or mean annual frequency (MAF)) is necessary but insufficient for understanding risk to the built environment. The risk of low-probability events with trivial consequences is negligible, while the risk of events with similar likelihood but with grave consequences may be unacceptable. The fact that the probabilities are so small makes communicating risks to project stakeholders and public regulators or decision-makers especially difficult, even if the potential for human or economic losses are substantial, because there is little information against which the risks can be benchmarked. Thus, one often must look beyond probability for a satisfactory metric of risk, particularly if a substantial investment of public funds must be made for risk mitigation. To most decision-makers concerned with safety of buildings and other infrastructure and representing the public at large, the most important risk metrics are consequences of damage (deaths or injuries, direct economic losses, and deferred opportunity losses). These consequences are reflected

[6] Some agencies and standard-writing groups use probability as a measure of risk. This is especially true in the building codes, which are written to apply to a broad range of buildings or other structures making up the built environment in which the consequences of failure may be vastly different and difficult to characterize for design purposes.

indirectly in building risk categories,[7] for which the MAFs are a reflection of the perceived differences in failure consequences.

### 3.3.1 Fundamental Definitions and Methods of Risk Analysis

Risk can be thought of as involving three components: hazard, consequences, and decision context [22]. The *Hazard* is a threat or peril with the potential for causing harm. The threat posed by an earthquake, hurricane or terrorist attack to a community, in terms of economic damage or loss of life, is a hazard. In some instances (tornado wind speeds or earthquake intensities), the hazardous event (or spectrum of such events) can be defined in terms of a curve describing the annual frequency of the event vs its intensity, a so-called hazard curve (cf Eq. 3.6). *Consequences*[8] are defined in terms of the response of the built environment and inhabitants to the event, including mortality and morbidity, building damage or collapse, direct and indirect economic losses, loss of employment, business downtime, population outmigration, or damage to the environment and other socioeconomic impacts.[9] Finally, the *Decision Context* provides a frame of reference for risk-informed assessment and decision-making and depends on the decision-maker and the overall socioeconomic and political framework in which the decision is made. Stakeholders to a community decision process, including individuals, management groups, government agencies or other decision-makers may view risk differently [23–26]. Most individuals and small groups or communities are reluctant to undertake risky activities without an expectation of some benefit; they are *risk-averse*, implying that they weigh losses more heavily than gains in decision-making. On the other hand, governments and large corporations, with resources large enough to be self-insured, tend to be *risk-neutral*, weighing gains and losses more or less equally. Willingness on the part of individuals to accept risk also depends on whether the risk is undertaken voluntarily or involuntarily and whether the individual *perceives* that the risky situation can be managed [27]. The element of familiarity or dread or the unknown in *perception of risk* plays a significant role in whether the risk is tolerated or accepted [28]. The context also is determined by the necessity for risk management, and how additional investment in risk reduction is balanced against available resources. Different decision-making contexts require different principles and it is important to thoroughly understand the context for the decision at hand.

---

[7] The Building Risk Categories in *ASCE/SEI Standard 7* are identified by: I—buildings representing low risk to human life; II—buildings not identified as I, III or IV; III—Buildings and other structures posing a substantial risk to human life (mainly public assembly structures); and IV—Buildings and other structures designated as essential facilities (e.g., hospitals, fire stations and similar facilities) required to maintain some level of post-disaster functionality.

[8] Some risk analysts replace consequences with vulnerability and consequences [9].

[9] Current building codes are focused on life safety and do not address socioeconomic impacts, which has motivated the developing field of urban resilience, where such effects are considered.

Quantitative measures of risk to the built environment are necessary to achieve (at least) an ordinal ranking of preferences with respect to risk mitigation strategies. Such measures can be couched by the following mathematical framework provided by the theorem of total probability. In the simplest form, the mean annual frequency (MAF) that the *loss metric* - severe injury or death, direct damage costs, loss of housing units, loss of employment, population outmigration, etc.,—exceeds c, $\boldsymbol{\lambda_{Loss>c}}$, is[10]:

$$\lambda_{Loss>c} = \sum_{H} \sum_{DS} P[Loss > c|DS]P[DS|H]\lambda_H \tag{3.7}$$

in which $\lambda_H$ = mean annual frequency (MAF) of event $H$, often expressed as a function of the intensity of the hazard event (wind speed, spectral acceleration, or flood stage); $P[DS|H]$ = conditional probability of damage state, e.g., negligible, minor, moderate, severe [29]; and $P[Loss > c|DS]$ is the conditional probability that the loss exceeds a limit, $c$. For rare events, the MAF and annual probability of the event are virtually identical, but the MAF, as an expectation, is more easily estimated from data maintained by public agencies. The loss metric must be set by community leaders, stakeholders or regulatory authorities. Equation (3.7) also is the starting point for the calculation of expected annual losses[11] should they, rather than mean annual frequencies or probabilities of loss, be the decision variables of interest [30].

The reader may note that Eqs. (3.1) and (3.3) are embedded in Eq. (3.7), since they both are representations of the theorem of total probability: $P_f = \int P[R < Q|Q = x]\, dQ(x)$, with dQ(x) replaced by $\lambda_H$. However, Eq. (3.7) contains the extra dimension of consequences that is missing from the first generation probability-based limit states design criteria, which assumed that the problem of safety was solely a problem of probability [13].

### 3.3.2 Conditional Event Analysis

While statistical data exist to describe the mean rate of occurrence, $\lambda_H$, of some abnormal load events (e.g., fires), more often than not it is necessary to envision a set of *hazardous scenarios*, without regard to their probability or frequency of occurrence [31].[12] These scenarios depend on the concerns of the design team or the judgment of the regulatory authority. Each scenario hazard - e.g., the occurrence of a

[10] Second generation Performance-Based Earthquake Engineering (PBEE-2) utilizes a similar equation expressed in terms of integrals rather than summations [57]. Both approaches are based on the theorem of total probability. The summation form has some conceptual advantages for dealing with extreme and abnormal loads, where the hazard curve is undetermined.

[11] The expected annual loss, obtained by integrating the relation between $\lambda_{Loss>c}$ vs $c$, is a common risk metric in insurance underwriting. Abrahamsen et al. [58] have noted drawbacks in using expected values as the basis for decision-making for low-probability, high-consequence events.

[12] The annual frequency of the threat may be unknown, or it may not be amenable to traditional statistical modeling techniques.

moment magnitude $M_w = 7$ earthquake at an epicentral distance of 40 km from the center of a city at 7:00 am during a morning rush hour or the removal of an exterior corner column of a building due to a detonation of a satchel charge - represents the description of a unique event in time. The MAF of such a scenario cannot be determined and the probability of the loss becomes *conditioned* on the scenario:

$$P[Loss > c|H_s] = \Sigma_{DS} P[Loss > c|DS]\, P[DS|H_s] \tag{3.8}$$

in which $H_s$ = scenario event(s) selected. This is similar to the approach taken for earthquake-resistant design, in which $P[DS|H_s] = P[Collapse|MCE] = 0.10$.

Equations (3.7) and (3.8) each have their advantages and drawbacks. Both deconstruct the risk analysis and enable the design team and decision-makers to focus on strategies where risk mitigation is most likely to be achieved successfully and economically. Equation (3.7) can be used to assess risk due to a spectrum of events, $H$, and to estimate losses over time (often on an annual basis, as that is the most common way of reporting $\lambda_H$). While the MAF calculated from Eq. (3.7) considers (in theory) the complete spectrum of threats, it typically is a small number that may be difficult to interpret; moreover, because of a paucity of data, the associated epistemic uncertainties may be very large. Furthermore, it may not be possible or practical to identify and/or analyze the full spectrum of hazards, especially when dealing with low-probability events. Moreover, most public decision-makers who control the resources for project risk mitigation are not expert in probabilistic risk analysis, especially when rare events are involved. To these decision-makers, a scenario event may be more understandable than an event with a return period (RP) of 10,000 years, which doesn't convey the same level of priority in public decision-making. Scenarios often are selected by reviewing the historical record to identify events that severely impacted the community or similar communities—loss of life, economic damage, population dislocation, time to recovery, etc.—and that must be avoided in the future to maintain community well-being. This approach has the advantage of familiarization with past events, which is facilitates communicating the threat to a city council and for mobilizing financing for risk mitigation.

To summarize, the scenario approach has significant advantages in the context of public decision-making and risk mitigation in the context of risk communication to public decision-makers. As a side issue, the uncertain future impacts of climate change are very large, making it attractive to remove that source of uncertainty from the risk assessment. On the other hand, the probability of overall loss cannot be annualized or benchmarked against other commonplace risks using common risk metrics such as expected annual loss (EAL) or probable maximum loss (PML) [30] because the probabilities in Eq. (3.8) are conditional in nature. Furthermore, scenario identification requires a great deal in skill and insight. Either way, it is important that decision-makers arrive at a common understanding of how risk is to be measured in a risk-informed decision.

### 3.3.3 Risk Measurement, Tolerance and Communication

Assessment of $P[Loss > c]$ or $P[Loss > c|H_s]$ (Eqs. (3.7) or (3.8) and decisions regarding risk mitigation depend on the decision-maker's view on the acceptability of risk and on whether/how investments in risk reduction should be balanced against available resources [32–34]. There is evidence that the public is not entirely irrational when it comes to risk, but rather worries about different things than professional risk analysts. Thus, if quantitative risks or explicit numerical safety goals are to be used as a basis for policy decisions, these worries must be acknowledged, and acceptable risks must be considered as outcomes of acceptable decision processes. Most public decision-makers are unfamiliar with concepts of quantitative risk assessment. Accordingly, risk must be measured and communicated in such a way that non-technically trained decision-makers can understand its full dimensions and can devise effective strategies for its management. Recent studies, summarized by Corotis [35], have indicated that *acceptance* of risk is based more on its *perception* than on the actual probability of occurrence and that biases in perception, whether or not they are well-founded, shape decisions. Although mortality statistics from disease and accidents are often used to benchmark risks (e.g., automobile traffic fatalities in the United States have remained relatively constant for many years), comparisons of annual frequencies from disparate events must consider differences in exposure, consequences and whether the risk is incurred voluntarily; attempts to correct for such effects are subjective [36].

While design procedures for the built environment nowadays often are risk-informed [37, 38], *acceptable risk* in the built environment at the community level remains undefined, a fact that is becoming increasingly relevant to risk-informed decisions regarding emerging concerns about community resilience [39]. Risks associated with rare extreme events invariably are relative, in the sense that they can be determined only in the context of what is acceptable in other activities, what investment is required to marginally reduce the risk, and what losses might be incurred if the risk were to increase. May [40] has observed that we should aim at developing tools that would allow a decision-maker to make *informed choices about how to manage and mitigate the risk* rather than argue about what is acceptable risk. This eminently sensible approach will be adopted in the remainder of this chapter.

## 3.4 Abnormal Loads

Abnormal loads may be grouped as pressures (e.g., explosions and detonations),[13] impacts (e.g., vehicular collision, aircraft or missile impact, debris, swinging objects during construction or demolition, or self-straining actions (fire). Characteristically, the loads usually act over a short period of time in comparison with ordinary design

[13] *ASCE/SEI Standard 7-22* contains a new chapter on tornado-resistant structural design. Formerly, tornadoes were also considered an abnormal load.

loads. The loads generally are time-varying but may be static or dynamic in their structural action, depending on the frequency content of the load and the dynamic response characteristics of the structural system affected. Two other factors distinguish them from the ordinary loads contained in *ASCE/SEI Standard 7* and similar standards worldwide: (1) their mean annual frequencies usually are less than $10^{-4}$/year, and (2) they typically are caused by accidents or human malevolence. Both factors make them difficult to characterize statistically. In the first category would be building fires caused by occupant carelessness or malfunctioning building service equipment; the MAF of such events depends on the building occupancy and area [41]. In the second category would be acts of arson or sabotage directed at a target for an intended (often political) purpose. The latter depends on an intelligent perpetrator. Statistics from the U.S. Federal Bureau of Investigation suggest that the MAF of explosive detonations directed at buildings is approximately $2 \times 10^{-6}$/year, a number which is obtained by dividing the number of incidents by the number of buildings. However, certain buildings are far more likely to be targets than others, and such estimates must be viewed with skepticism when applied to a specific building project.

As best as can be determined from limited data, MAFs are reasonably independent of building construction but are dependent on occupancy. Data reported for buildings in the United States are comparable, in order of magnitude, to similar data reported in other industrialized countries. There have been no attempts to examine the dependence of MAF on whether the building is symbolic, is a government facility, or has special occupancy characteristics. However, in the twenty-first century, it should be anticipated that symbolic, iconic or supertall buildings, or buildings representing or housing government agencies, financial or corporate authority will become more attractive targets for terrorist attack than the building inventory at large. Buildings associated with domestic issues that are socially or politically volatile also are at increased risk. Since estimates of MAFs are unreliable, a scenario analysis may be a better approach to risk mitigation in such cases.

## 3.5 Reliability Bases for Disproportionate Collapse-Resistant Design

The risk-informed approach to implement the above considerations in building design is different from that used to develop the first generation of probability-based limit states design criteria, represented by Eqs. (3.1) and (3.3), but is philosophically similar to modern earthquake-resistant design. In particular, the notion of damage control rather than damage prevention is common to both approaches.

### 3.5.1 Design for Conditional Limit States

We begin by rewriting Eq. (3.7) using terms that are familiar to the structural engineering community [3, 42, 43]:

$$\lambda_C = \Sigma_H \Sigma_{LD} P[C|LD]\, P[LD|H]\lambda_H \tag{3.9}$$

in which $\lambda_H$ = mean annual frequency of a hazard event, $P[LD|H]$ = conditional probability of local damage (yielding or rupture, buckling, crushing), given the occurrence of the hazard, $P[C|LD]$ = conditional probability of incipient collapse of the structure or a major portion of it, given the occurrence of local damage, and $\lambda_C$ = mean annual frequency of collapse. The overarching goal of structural design is to keep $\lambda_C$ at or below the *de minimis* threshold for public safety [44], which is believed to be on the order of $10^{-6}$/year.

Management of risk to the built environment involves an evaluation of each of the terms in Eq. (3.9): (a) to prevent the occurrence of abnormal loads through social or political means; (b) to prevent the occurrence of local significant structural damage that is likely to initiate a disproportionate collapse; and (c) to prevent the collapse of the structural system or a major portion of it. The design team must focus on appropriate strategies for hazard prevention, withstanding local damage, and absorbing local damage without disproportionate collapse. Facility performance objectives and loss metrics must be clearly identified and agreed upon, and uncertainty analysis should be a central part of the decision model. Tradeoffs that occur between investment and risk reduction must be treated candidly[14] and the entire decision process must be made as transparent as possible. While structural engineering can mitigate local damage or incipient collapse, hazard mitigation requires a different skillset and an interdisciplinary team is best positioned to achieve the most cost-effective risk mitigation strategy.

***Event control*** involves preventing the *occurrence* of the hazard (or, equivalently, taking actions to limit $\lambda_H$ to the *de minimis* threshold) for a spectrum of threats for which the MAF is difficult to determine quantitatively. Such actions might include changes in the building site or access to it, e.g., by imposing a minimum stand-off distance through placement of physical barriers and similar devices, preventing access to certain building zones, etc., by controlling hazard substances within the building, and by educating the building occupants on the need for caution with dangerous substances or unauthorized access. These measures are non-technical in nature and do not require professional engineering services, but often are the most cost-effective route to risk reduction.

***Structural engineering*** is focused on the terms *P(C|LD)* and *P(LD|H)* in Eq. (3.9), assuming that the hazard scenarios have been defined. Design options include: (1)

[14] In protective structure design and construction, quantitative benefit/cost analyses, when performed, often are cursory in nature [59, 60], perhaps because many of the facilities are managed by the Federal government. Safety at any cost is not a risk-informed decision stance; the implication is that buildings should be safe at any cost is a position of extreme risk aversion.

designing the structure to withstand specific loads (control $\boldsymbol{\lambda_C}$ by limiting *P[LD|H]* and the likelihood of damage initiating) or (2) designing the structural system to withstand local damage without collapse (control $\boldsymbol{\lambda_C}$ by limiting *P[C|LD]* [3, 4, 7, 45], termed alternative path design). The first approach requires that a specific threat be identified in order to determine the demand placed on the structural member, component or subsystem. The second approach generally requires the design team to envision certain initial structural damage scenarios, without regard to cause, and to design the system as a whole to be sufficiently robust that it can absorb such damage without general disproportionate collapse. Modern design guidelines and code officials favor the latter threat-independent approach because it is not possible to identify or characterize all sources of abnormal loads [46]. Instead, the officials ask that the structure be designed to withstand various threat-independent damage scenarios—removal of a first-story corner column or exterior bearing wall as surrogates for robustness.

Practical structural design criteria then can be developed by rewriting Eq. (3.9) to take $\lambda_H$ out of the analysis:

$$\Sigma_{LD} P[C|LD]P[LD|H] \; < 10^{-6}/\lambda_H \approx 0.01 - 0.1 \tag{3.10}$$

bearing in mind that if $\lambda_C$ is on the order of $10^{-6}$/year and $\lambda_H$ is on the order of $10^{-5}$ to $10^{-4}$/year, the conditional probability of failure should be in the range 0.01–0.1. These conditional reliability targets are the bases for the abnormal load provisions found in a number of standards and guidelines in which extreme or abnormal events are addressed [15, 17, 47–50].

### *3.5.2 Risk-Consistent Load Factors and Load Combinations*

Two basic situations encountered in designing for extreme or abnormal loads must be addressed in probability-based limit states design for disproportionate collapse resistance. In the first, load combination requirements are devised to check the capability of the structure to withstand a specific abnormal load event (or events) identified from the above scenario analysis.[15] In the second, we consider load combinations for evaluating the capability of a damaged structure to bridge over or around the damaged volume or area without a disproportionate collapse developing from the local damage. Normally, only the main load-bearing structure is checked.

In the first situation, the objective is to calculate the resistance required to resist a postulated accidental load (given that it occurs). The basic load combination on which to base the reliability analysis is:

[15] Progressive collapse usually starts with a member failure, even though it develops into a system-wide failure.

$$\begin{aligned}&\text{Dead} + \text{abnormal load} + \text{point} - \text{in} - \text{time live load}\\&+ \text{annual maximum snow load}\end{aligned} \tag{3.11}$$

This analysis is conservative because the abnormal load is unlikely to occur at the same time as the annual maximum snow load. However, the companion action live and snow load in *ASCE/SEI Standard 7-16* are $0.5L_n + 0.2S_n$ and the same companion actions have been used for consistency. As will be shown subsequently, the following load combination is consistent with the conditional reliability requirement $P[LD|H] < 0.01 - 0.1$ from Eq. (3.10):

$$(0.9 \text{ or } 1.2)\, D_n + A_n + 0.5\, L_n + 0.2\, S_n \tag{3.12}$$

in which $A_n$ = structural action due to the postulated abnormal load and $D_n$, $L_n$ and $S_n$ are the nominal dead, live and snow loads in *ASCE/SEI Standard 7-16*. The structural action, $A_n$, can be a force, as in the case of explosion or impact, or a self-straining action, as in the case of fire. The load factor on $A_n$ is 1.0, under the assumption that $A_n$ will be scenario-based since statistical data on its intensity are limited or non-existent. The dead load on the structure is the same, regardless of load combination, and its load factor is 1.2 (or 0.9 when dead load stabilizes the structural system), as with other load combinations in *ASCE/SEI Standard 7–16*. The load factors on $L_n$ and $S_n$ are less than unity in both cases because the means of the companion actions in Eq. (3.11) are substantially less than the nominal loads specified in *ASCE/SEI Standard 7-16*.[16] Equation (3.12) has been adopted by *AISC/ANSI 360* [17] for fire-resistant design, in which $A_n$ (replaced by $T$) is the self-straining structural action due to the design-basis fire.

In the second situation, the objective is to determine an appropriate load combination for assessing the integrity of a building structural system that has sustained local damage. The basic load combination on which to base the reliability analysis is:

$$\text{Dead} + \text{point} - \text{in} - \text{time} + \text{annual maximum snow} \tag{3.13}$$

As before, the conditional reliability requirement $P[C|LD] < 0.01–0.1$ using Eq. (3.10) is used to justify the following load combination:

$$(0.9 \text{ or } 1.2)\, D_n + 0.5\, L_n + 0.2\, (L_r \text{ or } S \text{ or } R) \tag{3.14}$$

Probability-based limit states design (or LRFD) is based on Eq. (3.5):

$$\text{Required strength} < \text{Design strength} \tag{3.15}$$

[16] For example, the nominal live load for general and clerical offices is 2.4 kPa (50 psf), reducible as the influence area increases, while the survey mean live load is 0.58 kPa (12 psf) and is virtually independent of area. For an influence area of 279 $m^2$ (3000 $ft^2$), the mean point-in-time life load has a mean of approximately $0.4L_n$ and a coefficient of variation (COV) of 0.60.

in which the required strength is based on either Eq. (3.12) or Eq. (3.14), depending on the design approach, and the design strength equals $\varphi R_n$ in which $R_n$ = nominal (or characteristic) strength (e.g., strength in tension, flexure or shear) based on material standards and specifications and $\varphi$ = resistance factor, which is a function of the bias and uncertainty associated with the design strength.

We assume in the following illustration of the above concepts that the resistance is associated with an inelastic stability limit state and that $\varphi$= 0.85. The reliabilities associated with Eqs. (3.12) and (3.14) are determined using Eqs. (3.1) or (3.3). The resistance and load random variables are defined in Table 3.1:

The statistics in Table 3.1 for *R, D,* $L_{apt}$ and $S_{ann}$ are taken from Ellingwood [12]; those for A are taken from Netherton and Stewart [51] and [52] simply for illustration; no implication that Eqs. (3.12 and (3.14) are applicable only to a situation where the damage is caused by the detonation of a military-grade explosive is intended.

Conditional limit state probabilities for structures designed using load combinations 3.13 and 3.15 for typical ranges of $L_{n/}D_n$, $S_n/D_n$ and$A_n/D_n$ are presented in Tables 3.2 and 3.3. Considering that $\lambda_H$ is on the order of $10^{-5}$ to $10^{-4}$/year, the corresponding limit state probabilities are comparable to the reliability targets in Table 1.3-1 of *ASCE/SEI Standard 7-16* for Risk Category II (ordinary habitable) buildings.

A disproportionate collapse, once initiated, is driven by gravity. Building structural systems rarely are perfectly symmetric or symmetrically loaded by gravity loads; nor

**Table 3.1** Random variables used in illustration of reliability-based conditional limit states for structural design

| Random variable | Mean | COV | CDF |
|---|---|---|---|
| Resistance, $R$ | 1.15 $R_n$ | 0.15 | Lognormal |
| Dead load, $D$ | 1.05 $D_n$ | 0.10 | Normal |
| Live load, $L_{apt}$ | 0.4 $L_n$ | 0.60 | Type I largest |
| Snow load, $S_{ann}$ | 0.2 $S_n$ | 0.60 | Type I largest |
| Abnormal load, $A$ | 0.95 $A_n$, 0.65 $A_n$ | 0.50 | Type I largest |

**Table 3.2** Conditional limit state probabilities for design by Eq. (3.12) $(0.9 or\ 1.2)D_n + A_k + 0.5L_n + 0.2S_n \leq 0.85R_nA_n/D_n$

| $L_n/D_n$ | 1.0 | 2.0 | 4.0 | 10.0 | 20.0 |
|---|---|---|---|---|---|
| 0.25 | 0.063 (0.012) | 0.105 (0.021) | 0.140 (0.030) | 0.168 (0.038) | 0.179 (0.041) |
| 0.40 | 0.060 (0.011) | 0.101 (0.020) | 0.137 (0.029) | 0.167 (0.037) | 0.178 (0.041) |

Values in parentheses correspond to a case where $A_n$ is 65% rather than 95% of the mean of A

**Table 3.3** Conditional limit state probabilities for design by Eq. (3.14) $(0.9 or\ 1.2)D_n + 0.5L_n + 0.2(L_r or\ S\ or\ R) \leq 0.85\ R_nS_n/D_n$

| $L_n/D_n$ | 0.5 | 1.0 | 2.0 |
|---|---|---|---|
| 0.5 | 0.030 | 0.036 | 0.056 |
| 1.0 | 0.042 | 0.045 | 0.057 |
| 2.0 | 0.066 | 0.067 | 0.070 |

are columns and beams perfectly straight; nor are fabrication and erection procedures perfect. Consequently, even a "perfect" frame is subject to sway under gravity forces. If this sway is not considered, large secondary ($P$-$\Delta$) forces may develop and lead to overall instability of the frame under gravity loads. Section 2.5.3 of A*SCE/SEI Standard 7-16* stipulates that in addition to the above load combinations, stability shall be provided for the structure as a whole and for each of its elements.

Resistance criteria are outside the scope of *ASCE/SEI Standard 7-16*. Resistance criteria to be used with Eqs. (3.12) or (3.14) should focus on mean or median strength rather than nominal strength, similar to earthquake-resistant design, since the objective of the analysis should be to obtain as realistic an estimate of the distribution of forces and structural performance as possible. Load-carrying mechanisms not normally utilized in building design (e.g., catenary action on floors; arching in wall systems) may be permitted when designing to withstand abnormal loads. While the details of the required analysis are outside the scope of this chapter, it should be remarked that advances in structural engineering computation (e.g. [53–56]) have made it feasible for high-visibility building projects.

## 3.6 Performance-Based Engineering and Design

The climate of structural engineering practice has changed in recent years, with increasing levels of attention being paid to economic and social as much as technical issues in design. The performance concept is a new design paradigm, made possible by advances in engineering technologies and computation, which has evolved to match new building technologies with increased public expectations. The performance concept encourages designers to devise alternative and innovative solutions that meet performance expectations equally well, enhancing beneficial competition in the building community. Moreover, it provides a rational framework for evaluating existing structures, where the role of available information and data are different from in new construction. Better understanding of the relation between building design, behavior and performance, coupled with risk analysis, leads to better allocation of resources, focuses research on topics that will enhance future performance, and provides a communications interface between building professionals and the public.

In the past two decades, performance-based design has gained traction in three areas: earthquake engineering, wind engineering, and fire-resistant structural design. A new *ASCE/SEI Standard on Disproportionate Collapse Mitigation of Building Structures* is nearing completion, with an anticipated release date in 2021. The technical basis for its chapter on risk assessment builds on the material presented previously in this chapter. One of its distinguishing feature is its introduction of *Collapse Resistant Design Categories* (CRDCs),[17] which are presented in a simplified form in

[17] ASCE/SEI Standard 7-16 identifies Seismic Design Categories (SDCs), which serve a similar purpose as the CRDCs. The SDCs place limits on the nature of structural design of buildings based on ground motion intensity and Building Risk Category. Such categories appear to be necessary

**Table 3.4** Collapse-resistant design categories building risk categories

| Consequences | I | II | III | IV |
|---|---|---|---|---|
| Minor | N/A | A | A | B |
| Moderate | N/A | A | B | B |
| Major | N/A | B | C | C |
| Extreme | N/A | C | D | D |

Table 3.4 in terms of building risk categories and consequences in *ASCE/SEI Standard 7-16*, which are based on Eq. (3.9) and serve as pointers to the provisions in the remainder of the Standard.

Buildings in CRDC A simply requires provision of general structural integrity through a continuous load path and a complete lateral force-resisting system. CRDCs B, C and D require progressively more stringent design measures and design documentation, which are stipulated in the remaining sections of the *Standard.* In addition, structures in CRDC D require a peer review.

## 3.7 Concluding Remarks

Proper structural design involves looking beyond the minimum design code requirements. The need for structural robustness to withstand extreme or abnormal loads must be acknowledged explicitly in codes, standards, and other regulatory documents. The building design team should document that steps have been taken to achieve a measure of robustness sufficient that the occurrence of events outside the design envelope, accidents or human malevolence will not precipitate a disproportionate structural collapse or unacceptable human or economic losses. The technical feasibility and effectiveness of specific provisions depend on specific building design practices and construction technologies. The client, developer, and owner must be educated during the conceptual project development stage on issues related to structural robustness.

Achieving reductions in risk for competing hazards generally requires additional investment, which must be balanced against competing demands for finite resources and temporal constraints. The structural engineer must be clear as to what can be achieved at reasonable cost by good engineering practice. The building team must acknowledge that uncertainty in achieving the project performance goals and objectives cannot be eliminated; that risks therefore cannot be avoided; and that reduction in risk can be achieved through both technical and non-technical measures. Finally, competing risks must be measured and communicated to non-technically trained decision-makers in such a way that the full dimensions of risk can be understood, and effective policies can be implemented for its management.

---

for design in which nonlinear actions are permitted and the design objective is to mitigate damage rather than to prevent it entirely.

**Acknowledgements** The reliability analyses summarized in Tables 3.2 and 3.3 were performed by Dr. Yue Li, Professor of Civil & Environmental Engineering at Case Western University, Cleveland, Ohio, as part of an assessment of load combinations for extraordinary events that appear in Section 2.5 of *ASCE/SEI Standard 7-16*. Dr. Li's assistance with these analyses is gratefully acknowledged.

## References

1. Adam J, Parisi F, Sagaseta J, Lu X (2018) Research and practice on progressive collapse and robustness of building structures in the 21st century. Eng Struct 173:122–149
2. Kiakojouri F, de Biagi V, Chiai B, Sheidaii MR (2020) Progressive collapse of framed building structures: current knowledge and future prospects. Eng Struct 206:110061
3. NISTIR 7396 (2007) Best practices for reducing the potential for progressive collapse in buildings. National Institute of Standards and Technology, Gaithersburg, MD
4. Starossek U, Haberland M (2011) Approaches to measures of structural robustness. Struct Infrastructure Eng 7(7–8):625–631
5. Yang T, Liu Z, Lian J (2021) Progressive collapse of RC flat slab substructures with unbonded posttensioning strands after the loss of an exterior column. Eng Struct 234:111989
6. Allen D, Schriever WR (1973) Progressive collapse, abnormal loads and building codes. Structural Failures: Modes. Responsibilities, American Society of Civil Engineers, New York, NY, Causes, pp 21–48
7. Ellingwood B, Leyendecker EV (1978) Approaches for design against progressive collapse. J Struct Div ASCE 104(3):413–423
8. Cormie D (2013) Manual for the systematic risk assessment of high-risk structures against disproportionate collapse. Institute of Structural Engineers, London, UK
9. FEMA (2005) Risk assessment—a how-to guide to mitigate potential terrorist attacks (FEMA 452). Federal Emergency Management Agency, Washington, DC, p 2005
10. NRC (2001) Protecting people and buildings from terrorism, committee for oversight and assessment of blast-effects and related research, National Research Council, National Academy Press, Washington, DC
11. Ellingwood BR (2007) Strategies for mitigating risk to buildings from abnormal load events. Int J Risk Assessment Mgt
12. Ellingwood B (1994) Probability-based codified design: past accomplishments and future challenges. Struct Saf 13(3):159–176
13. Freudenthal AM, Garrelts J, Shinozuka M (1966) The analysis of structural safety. J Struct Div ASCE 92(1):267–325
14. Melchers RE, Beck AT (2018) Structural reliability analysis and prediction (3rd edn). John Wiley and Sons, Ltd., Chichester, UK
15. ASCE/SEI Standard 7-16 (2016) Minimum design loads and associated criteria for buildings and other structures. American Society of Civil Engineers, Reston, VA
16. ACI 318-19 (2019) Building code requirements for structural concrete. American Concrete Institute, Farmington Hills, MI
17. AISC/ANSI 360-16 (2016). *Specification for Structural Steel Buildings.* American Institute of Steel Construction, Chicago, IL
18. AASHTO LRFD bridge design specifications (9th edn). American Association of State Highway and Transportation Officials, Washington, DC, 2020
19. Ellingwood B et al (1982) Probability based load criteria: load factors and load combinations. J Struct Div ASCE 108(5):978–997
20. Galambos TV et al (1982) Probability based load criteria: assessment of current design practice. J Struct Div ASCE 108(5):959–977

21. FEMA (2009) Quantification of building seismic performance factors (P695). Federal Emergency Management Agency, Washington, DC, p 2009
22. Elms DG (1992) "Risk assessment" In: Blockley D (ed) Engineering safety. McGraw-Hill International, Berkshire, UK, pp 28–46
23. Cha EJ, Ellingwood BR (2012) Risk-averse decision-making for civil infrastructure exposed to low-probability, high-consequence events. Rel. Eng Syst Safety 104(1):27–35
24. Menezes CF, Hanson DL (1970) On the theory of risk aversion. Int Econ Rev 11:481–487
25. Slovic P (2000) The perception of risk. Earthscan Publications, Sterling, VA
26. Tversky A, Kahneman D (1992) Advances in prospect theory: cumulative representation of uncertainty. J Risk Uncertainty 5:297–323
27. Starr C (1969) Social benefits versus technological risk. Science 168:1232–1238
28. Wilson R, Crouch EAC (1987) Risk assessment and comparisons: an introduction. Science 237:267–290
29. FEMA (2017) Multi-hazard loss estimation methodology—Flood Model. HAZUS-MH-MR4 Technical Manual. Federal Emergency Management Agency Washington, D.C., 2017
30. Grossi P, Kunreuther H (2005) Catastrophe modeling; a new approach to managing risk. Springer, New York, NY
31. Garrick BJ et al (2004) Confronting the risks of terrorism: making the right decisions. Rel Eng Syst Safety 86:129–176
32. Ellingwood BR (2001) Acceptable risk bases for design of structures. Progress Struct Eng Mat 3(2):170–179
33. Vrijling JK, Van Hengel W, Houben RJ (1998) Acceptable risk as a basis for design. Rel Eng Syst Safety 59:141–150
34. Faber MH, Stewart MG (2003) Risk assessment for civil engineering facilities: critical review and discussion. Rel Eng Syst Safety 80(2003):173–184
35. Corotis RB (2003) "Socially relevant structural safety," Applications of Statistics and Probability in Civil Engineering, Proceeding. ICASP 9 (Der Kiureghian, Madanat and Pestana, eds.), Millpress, Rotterdam, pp 15–26
36. Reid SG (2000) Acceptable risk criteria. Progress Struct Engrg Mat 2:254–262
37. Aven T (2010) How to define, understand and describe risk. Rel Eng Syst Safety 95:623–631
38. Aven T, Ylonen M (2018) A risk interpretation of sociotechnical safety perspectives. Rel Eng Syst Safety 175:13–18
39. Lounis Z, McAllister TP (2016) Risk-based decision making for sustainable and resilient infrastructure systems. J Struct Eng ASCE 142(9):F4016005
40. May PJ (2004) Making choices about earthquake performance. Nat Hazards Rev 5(2):64–70
41. NISTIR 7563 (2009) Best practices guidelines for structural fire resistance design of concrete and steel buildings. National Institute of Standards and Technology, Gaithersburg, MD
42. Ellingwood BR, Dusenberry DO (2005) Building design for abnormal loads and progressive collapse. Comput-aided Civ Infrastruct Eng 20(5):194–205
43. Ellingwood BR (2006) Mitigating risk from abnormal loads and progressive collapse. J Perf Constructed Fac ASCE 20(11):315–323
44. Pate-Cornell E (1994) Quantitative safety goals for risk management of industrial facilities. Struct Saf 13(3):145–157
45. Starossek U (2018) Progressive collapse of structures, 2nd edn. ICE Publishing/Thomas Telford Ltd., London, UK
46. Marchand KA, Stevens DJ (2015) Progressive collapse criteria and design approaches improvement. J Perf Constructed Fac ASCE 29(5):B4015004
47. EN 1991 (2006) Eurocode 1- Actions on structures, Part 1-7: General actions—accidental actions (EN 1991-1-7:2006). Comite Europeen de Normalization 250, Brussels, Belgium
48. GSA (2016) General services administration alternate path analysis & design guidelines for progressive collapse resistance, General Services Administration, Washington, D.C
49. SFPE (2007) Guide to performance-based fire protection analysis and design of buildings. National Fire Protection Association, Washington, DC

50. Unified Facilities Criteria UFC 4-023-03 (Change 3, 2016). Design of buildings to resist progressive collapse. US Department of Defense, Washington, DC
51. Netherton MD, Stewart MG (2010) Blast load variability and accuracy of blast load prediction models. Int J Protect Struct 1(4):543–570
52. Stewart, M.G. (2018). Reliability-Based Load Factor Design Model for Explosive Blast Loading, Struct Safety 71:13–23
53. Izzuddin B, Vlassis AG, Elghazouli AY, Nethercot DA (2007) Assessment of progressive collapse in multi-story buildings. Proc Inst Civil Engrs Struct Build 160(4):197–205
54. Marjanishvili SM (2004) Progressive analysis procedure for progressive collapse. J Perf Constructed Fac ASCE ASCE 18(2):79–85
55. Scott MH, Fenves GL (2010) Krylov subspace accelerated Newton algorithm: application to dynamic progressive collapse simulation of frames. J Struct Engrg ASCE 136(5):473–480
56. Stylianidis PM, Nethercot DA, Izzuddin BA, Elghazouli AY (2016) Study of the mechanics of progressive collapse with simplified beam models. Eng Struct 117:287–304
57. Porter K.A. (2003). An overview of PEER's performance-based earthquake engineering methodology *Proc., 9$^{th}$Int. Conf. on App. of Stat. and Prob. in Civil Engrg. (ICASP9) July 6–9, 2003*, San Francisco
58. Abrahamsen EB, Aven T, Vinnem JE, Wiencke H (2004) Safety management and the use of expected values. Risk, Dec Pol 9:347–357
59. Mueller J, Stewart MG (2011) Terror, security, and money: balancing the risks, benefits and costs of homeland security. Oxford University Press, Oxford, UK
60. Stewart MG (2017) Risk of progressive collapse of buildings from terrorist attacks: are the benefits of protection worth the cost? J Perf Constructed Fac ASCE 31(2)

# Part III
# Case Studies

# Chapter 4
# Aviation Resilience to Terrorist Hijackings


**Mark G. Stewart and John Mueller**

**Abstract** Approximately $50 billion is spent annually world-wide in the quest to deter or disrupt terrorist attacks to aviation, significant expenditures that have rarely been subject to systematic cost–benefit or risk analysis. This chapter applies that approach, assessing the risks, costs, and benefits of security measures designed to disrupt terrorist hijackings of airliners assuming terrorists arrive at the airport undeterred and undetected. Under those conditions, existing security measures reduce the risk of a terrorist success by over 88%. Another security measure could be added to the existing array: secondary flight deck barriers, lightweight devices that are easy to deploy and stow, installed between the passenger cabin and the cockpit door to block access to the flight deck whenever the cockpit door is opened in flight. These barriers are highly cost-effective and raise total risk reduction to over 96%. The benefit-to-cost ratio of the measure is high at 5.1, and it remains cost effective even if risk reduction is halved and costs are doubled. On the other hand the expensive Federal Air Marshal Service fails a cost–benefit analysis, whereas the Federal Flight Deck Officer program proves to be cost-effective.

**Keywords** Aviation security · Terrorism · Risk · Cost–benefit analysis · Transportation security administration · Risk reduction · Airline bombing

M. G. Stewart (✉)
Centre for Infrastructure Performance and Reliability, The University of Newcastle, Newcastle, Australia
e-mail: mark.stewart@newcastle.edu.au

J. Mueller
Mershon Center for International Security Studies, Department of Political Science, Ohio State University, 1501 Neil Avenue, Columbus, OH 43201, USA

Cato Institute, 1000 Massachusetts Avenue, Washington, DC, NW 20001, USA



M. G. Stewart and D. V. Rosowsky (eds.), *Engineering for Extremes*, Springer Tracts in Civil Engineering, https://doi.org/10.1007/978-3-030-85018-0_4

## 4.1 Introduction

The attacks of September 11, 2001, by far the most destructive in history, highlighted the vulnerability of airliners and infrastructure to terrorism. The attack directly resulted in the deaths of nearly 3000 people. Following the widely-applied value of statistical life (VSL) approach, the best estimate for homeland security analysis is about $8 million in 2020 dollars [1]. Using that leads to a direct loss of approximately $25 billion arising from nearly 3000 fatalities. In addition 9/11 caused approximately $35 billion in physical damage including rescue and clean-up costs. Indirect costs were even more substantial. Thus, the International Monetary Fund and others estimate that the 9/11 attacks cost the US economy up to 1% in lost GDP ($200 billion in 2020 dollars) in that year alone. An upper bound estimate of the losses of 9/11, then, might exceed $250 billion [2].

Thus, the protection of airliners seems to be particularly important because the downing of one does seem to carry with it the special dangers of a widespread and at least somewhat lingering impact on the airline industry, as well as on related ones such as tourism. Particularly in the few years after 2001, it was commonly said that if terrorists were able to down two or three more airliners, they would destroy the airline industry, and an attack on aviation is considered by some to be the "gold standard" for terrorists.

However, contrary to anticipations, there have been few terrorist attempts on airliners since 9/11 anywhere in the world, even though security measures in many places are considerably more lax than in the United States. Indeed, averaged over the past 44 years, the chance worldwide that an individual airline passenger will be killed by terrorists on an individual flight is 1 in 25 million, while for the post-9/11 period the odds are 1 in 110 million [3].

Approximately $50 billion—about $10 billion in the United States—is spent annually world-wide in the quest to deter or disrupt terrorist attacks to aviation [3]. But these significant expenditures have rarely been subject to systematic cost–benefit or risk analysis, and this lack of scrutiny may lead to risk-averse and costly counterterrorism policies.

This chapter assesses the degree to which security measures currently in place provide safety. In particular, it focuses on determining the likelihood under current conditions that a 9/11-like attempt by terrorists to hijack an airliner in the United States, commandeer it, and fly it into a pre-designated target could succeed. Another aim is to assess the cost-effectiveness of security measures by evaluating the risk reduction of each and its cost, as well as the losses from a successful terrorist attack, and the probability that there will be a terrorist attack.

Previous research has compared the costs and benefits of some aviation security measures, and recommended where savings can be made without unduly sacrificing risk reduction as in [2, 4]. This work was then considerably extended by applying utility theory to quantify levels of risk aversion finding that a very risk averse decision-maker is 48% likely to prefer to retain the expensive FAMS program even if the attack probability is as low as 1% per year—a very high level of risk aversion that

is exhibited by few, if any, other government agencies [5, 6]. Stewart and Mueller [7] then conducted a risk analysis that a terrorist organisation could down an airliner with a passenger-borne bomb or IED—an improvised explosive device. The cost–benefit assessment found that efficiencies in checkpoint screening are needed for this layer to be deemed cost-effective. A systems reliability analysis and a cost–benefit assessment of Advanced Imaging Technologies (AIT) full-body scanners found the technology to be a questionable expense [8]. Later studies have also assessed the risks and cost-effectiveness of Transportation Security Administration (TSA) PreCheck, airport policing, measures to protect airport terminals, and the counter-terrorism efforts of the Federal Bureau of Investigation [9–13].

There is other research that looks at the risks and efficiencies of aviation security.[1] Few of these studies, however, estimate absolute risk and risk reduction. A key component of assessing absolute risk is to include the probability of an attack in the calculations. A relative risk assessment, in contrast, is often conducted conditional on an attack occurring and then ranking risks based on the relative likelihood of threats.

A potential security measure is a *secondary flight deck barrier* (Installed Physical Secondary Barrier or IPSB). This is a lightweight device that is easy to deploy, installed between the passenger cabin and the cockpit door that blocks access to the flight deck whenever the reinforced door is opened in flight for rest breaks, meals, etc. (see Fig. 4.1). It will reduce the vulnerability of another 9/11 type attack. In 2018 the United States Congress reauthorized the Federal Aviation Administration (FAA) that included a mandate that the FAA issue a rule by 5 October 2019 to require the installation of secondary flight deck barriers on all new passenger aircraft. However, the FAA is now studying the requirement and has yet to issue a final rule on this legislation. Hence, the life saving and risk reducing potential of secondary flight deck barrier and its cost-effectiveness is assessed in this chapter.

The system reliability model used in this chapter is taken from our latest book [3]. However, this chapter extends that work by considering risks from hijacking that are not deterred in the first place. Some of the numerical estimates will differ from those listed in the book due to updated information and to feedback from the book [15].

Throughout, costs and benefits are taken as mean values—that is, as single-point or deterministic values. An advantage of this is that the calculations are straightforward. They can also be readily replicated and checked by others. However, this simplified approach ignores the uncertainties and variabilities in the parameter estimates—and uncertainties in the realm of terrorist intentions and predictions are large. Stewart and Mueller [6, 8] have used Monte Carlo simulation methods to propagate vulnerability, risk reduction, and loss uncertainties in the calculation of net benefits. However, results from a probabilistic analysis shows similar trends to those obtained from a deterministic analysis.

[1] For a full review of probabilistic terrorism risk assessment see Stewart and Mueller [16].

**Fig. 4.1** Secondary Flight Deck Barrier (Installed Physical Secondary Barrier or IPSB) [14]

## 4.2 The Risk Framework

The standard definition of risk used by the Department of Homeland Security is:

$$(\text{Risk}) = (\text{Threat}) \times (\text{Vulnerability}) \times (\text{Consequence}) \tag{4.1}$$

Threat:

- A 9/11-like attempt by terrorists to hijack an airliner in the United States, commandeer it, and flying it into a pre-designated target.
- We assume that the terrorists arrive at the airport undeterred and undetected.

Vulnerability:

- Probability that the attack will be disrupted at the airport or on the airliner.

Consequences:

- Economic and human losses, direct, indirect and social, from a successful hijacking attack.

To determine the benefit-to-cost ratio for a security layer the *benefit* is calculated as:

$$\begin{aligned} &Benefit\ of\ a\ security\ measure \\ &\quad = probability\ of\ a\ successful\ attack \\ &\quad \times losses\ sustained\ in\ the\ successful\ attack \\ &\quad \times reduction\ in\ vulnerability(risk\ reduction) \\ &\quad furnished\ by\ the\ security\ measure \end{aligned} \tag{4.2}$$

This *benefit* is then divided by the *cost* of the security measure to generate an easy to understand decision-making metric—the benefit-to-cost ratio (BCR).

## 4.3 Vulnerability and Reliability Analysis of the Existing Layers of Security Against a Hijacking

The TSA has arrayed 21 "Layers of Security" to "strengthen security through a layered approach" (see Fig. 4.2).

Rates of deterrence are more difficult to quantify than disruption rates because the former depends more on the motivation and adaptive capability of the terrorist. And deterrence rates also depend on the ability of a terrorist to game the system. Our approach is to consider those terrorists who arrive at the airport undeterred and undetected. In this case, the deterrence rates for all layers are set at zero, and disruption rates are set to zero for the first four layers on TSA's list: intelligence, international partnerships, customs and border protection, and Joint Terrorism Task Force. Also ignored are several layers that play little or no role in a hijacking consideration: crew vetting, VIPR, canines, checked baggage, random employee screening, and bomb appraisal officers. In our analysis, we thus include ten of the TSA's security layers and add two more for the post-hijacking stage.

The effectiveness at disrupting a terrorist effort is estimated for each of these 12 layers. Since there is little quantitative data on disruption rates, it is more tractable to assign words of estimative probability such as "probably not" and "chances about even" as in Table 4.1, and to translate them into probabilities.

Many of the disruption rates are taken from previous studies [3, 6, 8, 13, 16]. The results of this examination are summarised in Table 4.2 and the overall model of the system is shown in Fig. 4.3.

### *4.3.1 Pre-boarding Security Layers*

1. *No-fly list and passenger pre-screening*
2. *Behavior Detection Officers (BDOs)*
3. *Travel document checkers*
4. *Checkpoint screening with Transportation Security Officers (TSOs).*
   The disruption rates for the pre-boarding layers are mostly modest, with the most effective being the passenger screening at the TSA checkpoints.

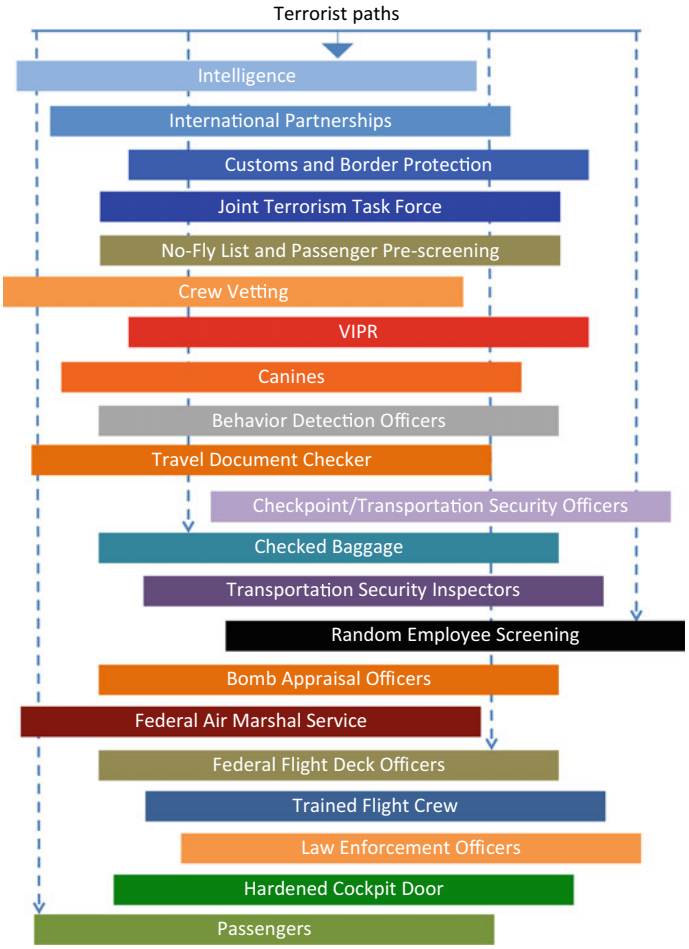


**Fig. 4.2** TSA's 21 Layers of security. *Source* Transportation Security Administration

**Table 4.1** Words of estimative probability

| | |
|---|---|
| Certain | 100% |
| Almost certain | 95% |
| Highly probable | 85% |
| Probable | 75% |
| Chances about even | 50% |
| Less likely than not | 40% |
| Probably not | 25% |
| Highly improbable | 15% |
| Almost certainly not | 5% |
| Impossible | 0% |

**Table 4.2** Disruption rates for existing aviation security measures, for a hijacking attack

| | Disruption rate |
|---|---|
| Pre-boarding Security: | |
| 1. No-fly list & passenger pre-screening | 5% |
| 2. Behavior Detection Officers | 1% |
| 3. Travel document checkers | 5% |
| 4. Checkpoint/TSOs | 15% |
| In Flight Security: | |
| 5. Passenger resistance | 15% |
| 6. Cabin crew resistance | 15% |
| 7. Law enforcement officer | 1% |
| 8. Federal Air Marshal Service (FAMS) | NA |
| Probability that air marshals are on-board: 20% | |
| 9. Hardened cockpit door | |
| FAMS on board | 75% |
| No FAMS on board | 50% |
| 10. Flight deck resistance and FFDOs | 40% |
| 11. Unable to fly airliner into target | 5% |
| 12. Anti-aircraft measures | 15% |

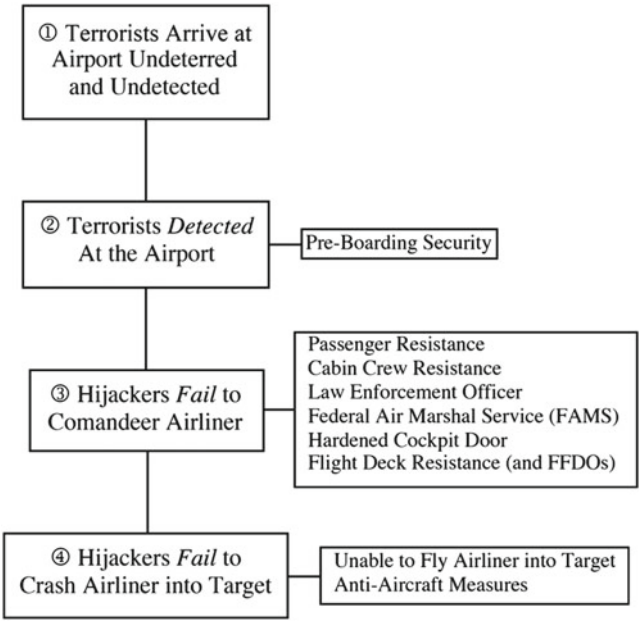


**Fig. 4.3** System model of existing aviation security measures

### 4.3.2 In-Flight Security Layers

5 and 6. *Passenger and cabin crew resistance*

As pilot Patrick Smith points out, what the 9/11 attacks "actually exploited was a weakness in our mindset—a set of presumptions based on the decades-long track record of hijackings. In years past, a takeover meant hostage negotiations and standoffs; crews were trained in the concept of 'passive resistance'" [17].

This policy was obviously shattered by the 2001 hijackings as was demonstrated on the fourth plane in which passengers and crew, having learned of what had happened on the three earlier flights, fought to overcome the hijackers and were successful in that they were able to prevent the terrorists from flying the plane into its intended target. That is, any terrorists seeking to actually commandeer the aircraft would face not only a considerable number of security measures designed to counter such a threat, but "a planeload of angry and frightened people ready to fight back" [17].

Nonetheless, there have been a number of airliner hijackings by passengers since 2001, although none of them took place in the United States and none have involved a concerted effort to commandeer the plane.

Bruce Schneier concludes that passenger resistance combined with secure cockpit doors is likely to be enough, by itself, to disrupt a hijacking attempt, while Smith suggests that crew and passenger resistance alone is likely to do the trick [17, 18].

Others disagree, Captain Tom Walsh rates it as "unlikely" that "passengers will come to the rescue of crew members and fighting back against attackers" [19]. Most reported incidents of fighting back have occurred when the terrorist was acting alone, not the coordinated resistance needed to overwhelm a team of hijackers spread throughout an aircraft—and a team of hijackers is what would be required for a 9/11 type of attack to be repeated. The time it takes for hijackers to take over an aircraft could be a matter of seconds, which could conceivably be less than passengers need to assess the situation, realize the dire threat, communicate with other passengers, and process other information needed for them to summon the courage to assault armed and dangerous terrorists. Moreover, there is little formal training of cabin crew in effective techniques to fight back.

With this in mind, we estimate that for the passenger resistance layer, the rate of disruption is 15% and that the rate of disruption for the cabin crew is also 15%.

7. *Law enforcement officers on board*

Law enforcement officers are on some flights for reasons other than countering terrorism, such as escorting prisoners or protecting VIPs. However, their numbers are small and their impact on security is also likely to be low. Largely because of the low likelihood of one being on an individual flight, we estimate that the layer reduces the risk of a successful hijacking by only 1%.

8. *The Federal Air Marshal Service (FAMS)*

There are now some 3000–4000 air marshals [20, 21]. It has been estimated that air marshals ride on less than 5% of flights in the United States [21]. Although these are deemed to be high-risk flights based on intelligence reports, it is unclear exactly how that risk has been determined—after all, since 9/11, no airline flight in the U.S. has had an active terrorist on board.

It might be argued that some crew and passengers may be reluctant to be the first to confront a hijacker if they believe an air marshal is on board, a hesitation that could conceivably give hijackers the time they need to execute their plans. On the positive side, air marshals may provide more flexibility than many other security measures because they can be deployed at short notice for emerging threats.

Although FAMS are on no more than 5% of flights, they are not placed randomly but rather on flights deemed to be 'high risk.' Consequently, and perhaps rather generously, we assume a high 20% effective coverage.

9. *Hardened cockpit door*

While the effectiveness of the hardened cockpit door in restricting cockpit access to a determined hijacker has sometimes been questioned [19], there is little doubt that they will have an impact on the likelihood that a hijacking will succeed.

We assume that the hardened cockpit door will be attacked during a time of its opening and closing—i.e., when it is most vulnerable. In this case, the odds that the attack will be disrupted by the door is "about even" or 50%. While there is a vulnerability, an attack would only succeed if the terrorist(s) could launch their attack at precisely the right moment to exploit what is a momentary vulnerability during a door transition. As the presence of air marshals near the cockpit door is likely to complicate a terrorist attempt, a door's disruption rate increases in that case to 75%.

However, if attackers are somehow able to get into the flight deck, the doors could be used to protect them. Something like this happened in deliberate crashes on a Germanwings flight in 2015 and on a LAM Mozambique Airlines flight in 2013—neither of them terrorist events.

10. *Flight Deck Resistance Enhanced by the Federal Flight Deck Officer (FFDO) Program*

An invasion of the cockpit by terrorists determined to take over the controls would, in the aftermath of 9/11, be met with determined resistance by the flight crew.

The cockpit is a small place and, unlike any hijackers, the flight crew knows every square inch of it. In addition, they have, of necessity, access to tools, some of which can be used as weapons of defence like screwdrivers, hammers, chisels, hatchets, and they are likely to know exactly where each of these is. Added to this are less lethal defensive measures. For example, there was an attempt in 1994 to hijack and crash a FEDEX cargo flight by an employee of the company flying as a passenger. Even though both pilots and the flight engineer suffered head blows from a hammer

during a violent struggle in the cockpit, they successfully restrained the hijacker and landed the aircraft safely [22].

As an enhancement, TSA instituted the Federal Flight Deck Officer (FFDO) program in which flight crew members are trained and armed with firearms to be able to defend the cockpit from intruders. This program, not FAMS, provides the "last line of defense" against a hijacking, and it has dramatically increased in size since its inception in 2003 [23]. It is estimated that up to 20% of pilots in the United States are FFDOs [21]. (Data on the number of FFDOs is classified). It seems reasonable to assume that if FFDOs are present on the flight deck, they are likely to be as effective as any air marshals who happen to be on board.

If FFDOs are in the cockpit, we suggest they are likely to be highly effective in foiling a hijacking. If the probability that FFDOs are on a plane is 15–20%, we estimate that the FFDO program, when combined with flight deck resistance more generally, reduces the risk of a successful hijacking by 40%—i.e., their ability to foil a hijacking is "less likely than not".

### *4.3.3 Post-Hijacking Security Layers*

11. *Terrorists are unable to fly the airliner into the target*

Piloting a large commercial airliner is difficult and so perhaps is the challenge confronting a hijacker trying to steer an airliner to a pre-designated target on the ground. Assuming that a hijacker has the time, resources, and ability to learn to pilot large aircraft, the odds of successfully striking a ground target will be high, as evidenced by the attacks on the World Trade Center and Pentagon. Of course, if an aircraft misses its intended target when it crashes into the ground, it can still do damage, though probably not as much as might be imagined.

We estimate that the difficulty for terrorists to fly the airliner into their intended target or to inadvertently hit a mass casualty target reduces the risk of a successful hijacking by 5%.

12. *Anti-aircraft measures*

If a pilot is able to transmit to air controllers that the plane is under a violent hijacking attempt (or if passengers or cabin crew members can use their phones to warn authorities), anti-aircraft measures might immediately be deployed to shoot down or ground the captured airliner before it can reach an intended target.

Despite these efforts, Associated Press report that "U.S. military officials have concluded it would be very difficult to intercept a hijacked plane within a certain radius of major cities like Washington unless fighter jets were already airborne". Surface-to-air missiles have been deployed around Washington DC, but these are a "measure of last resort for protecting a limited number of key locations against an aerial attack" [21]. The 9/11 hijackers were able to disable the aircraft's transponders,

making the detection of the aircraft the more difficult, but not impossible as the aircraft were still tracked by ground-based radar [21].

We estimate that the anti-aircraft layer reduces the risk of a successful hijacking by 15%.

## 4.4 Adding a Security Layer: Installed Physical Secondary Barriers

An additional security measure to disrupt airline hijackers is a *secondary flight deck barrier* (Installed Physical Secondary Barrier or IPSB). The installation of this security barrier has been supported by the Airline Pilots Association (ALPA) because, "the reinforced flight deck door, together with supplementary crew procedures, does not provide a complete solution for securing the flight deck" [24].

One analysis examines a hijacking scenario positing "a team of highly trained, armed, athletic individuals" who might, in a matter of seconds, be able to take over the flight deck during a door transition. Under those circumstances, passengers and crew would scarcely have time to assess the situation, realize the dire threat, communicate with other passengers, and process the information needed for them to summon the courage to fight back. Accordingly, it concludes that "passengers are not considered a predictably reliable option for preventing an attempted violent or sudden breach of the flight deck," and it completely excludes "the possibility of passenger intervention as a mitigating measure" from its consideration. Although flight attendants receive little or no training in the use of force, many airlines have instituted procedures during door transition, such as galley trolleys to block access to the flight deck. The study found, however, that this did "not produce satisfactory results" [25].

An IPSB could deal with this concern. Further security is provided by the fact that a cabin crew member is generally required to be at the scene when the secondary barrier is put into place, something that adds a complication for would-be hijackers.

The cost of an IPSB for a new aircraft has been estimated to be less than $10,000 [21], with some estimates as low as $3500 [26]. However, more recent cost date obtained by the Aviation Rulemaking Advisory Committee [27] suggest that the production cost is significantly higher at $35,000 per aircraft. Added to this are design, testing and certification costs ($9 million one-time), flight attendant and pilot training costs (60 min initial, 30 min recurrent), maintenance (up to $700), supply chain/spares ($10,000 per unit), added fuel burn due to additional weight of an IPSB, and time out of service (delay cost is $4800 per hour). FAA [27] does not provide a definitive total cost estimate. However, as a starting point we assume that the one-off costs over the life of the aircraft are approximately $45,000. Since there are approximately 6000 commercial aircraft in the United States, and if we take the $45,000 estimate, this equates to $270 million. If we annualize this cost over the 25 year design life of an aircraft with a 7% discount rate, this equates to a cost of $23.2 million per year for the entire U.S. commercial airline fleet. If we then add

in annual costs (training, maintenance, etc.) of approximately $2500 per aircraft per year, this equates to a cost of $15 million per year. Total cost is then rounded up to $40 million per year for the entire U.S. commercial airline fleet.

The IPSB layer (excluding the effects of a hardened cockpit door or FAMS) will have a high disruption rate if deployed properly. However, this may not always be the case, so we consider an IPSB to be "probably" effective leading to a disruption rate of 75%. If the IPSB is foiled, the hardened cockpit door is still a potential obstacle to a hijacking. The disruption rate for the door is reduced from 75 to 65% if an air marshal is on a flight, which is further reduced to 40% in the absence of FAMS. In this case, the failure of one layer of security (IPSB) affects the effectiveness of another layer (hardened cockpit door). Similarly, the presence of an IPSB may mean that the flight crew are less careful during door transitions, so if the IPSB is foiled by a hijacker, there is less opportunity for flight or cabin crew to close the hardened cockpit door in time, hence we assume a reduced rate of disruption for the hardened cockpit door. The risk reduction from an IPSB, hardened cockpit door and FAMS is calculated as 86%, and in the absence of an IPSB the risk reduction drops to 55%.

Thus, we add IPSB to the existing array of security measures as listed in Table 4.2, estimating its disruption rate to be 75%. And we add a further consideration: If IPSB fails, the risk reduction rate for hardened cockpit doors declines to 65% if FAMS is on board and to 40% if it is not.

## 4.5 Calculations of Reduction in Vulnerability

We apply a reliability analysis to the system. The probability that a hijacking attempt will be disrupted (that is, the degree to which the risk of a hijacking attack has been reduced by the security layers) is

$$R_{hijacking} = 1 - \left\{ \begin{array}{l} \left[1 - Pr(\text{disrupted by pre - boarding measures})\right] \\ \times \left[1 - Pr(\text{disrupted by in - flight measures})\right] \\ \times \left[1 - Pr(\text{unable to fly airliner into target})\right] \\ \times \left[1 - Pr(\text{disrupted by anti - aircraft measures})\right] \end{array} \right\} \tag{4.3}$$

where the term Pr() represents a probability, such that, for example, Pr(disrupted by pre-boarding measures) is the probability that pre-boarding security measures will disrupt, foil or prevent a terrorist attack.

The elements behind the probabilities shown in Eq. (4.3) are arrayed in full detail in Appendix A. An example shows the benefits of multiple layers of security: if each of the four probabilities in Eq. (4.3) is 25%, the risk reduction (or reduction in vulnerability) is a high $R = 68.4\%$ (this is equal to $1 - (1 - 0.25)^4$). If other layers

of security are added to the array, this risk reduction will increase, but the additional risk reduction of each layer will become progressively smaller.

Applying the data from Table 4.2, the probability that a hijacking attempt by a well-organised and undeterred terrorist organisation will be disrupted by existing security measures is 88.2%. This represents the existing level of protection. This suggests that, because of existing security measures, even a well planned and executed terrorist hijacking attempt has perhaps at best one chance in ten of being successful. If the rates of deterrence are estimated using a similar procedure and then added in for all layers, vulnerability is reduced by over 99%. A similar analysis for bombing attacks reveals an overall risk reduction of over 98% (for more details see [3]).

That the risk is low is borne out by the data—there have been no successful terrorist attacks on US airliners since 2001, and, as noted earlier, a statistical analysis of the Global Terrorism Database shows that the probability that an airline passenger will be killed in a single flight in a terrorist attack world-wide is 1 in 110 million for the years since 2001 [3].

Table 4.3 shows that if IPSBs are installed on all aircraft, the probability that a hijacking attempt will be disrupted increases to 96.4%—i.e., the additional risk reduction furnished by IPSBs is 96.4–88.2 = 8.2%.[2] This is an impressive reduction in vulnerability from a security measure that will only cost about $40 million per year.

The analysis does not directly include one important impediment to a successful hijacking attack: the general incompetence and poor tradecraft of most terrorists, particularly in complicated plots [10, 28–32]. As Brian Jenkins [33] puts it, "their numbers remain small, their determination limp, and their competence poor." Some of the disruption rates presented in the analysis do in part take terrorist inadequacies into account in that a high rate of disruption implies less than perfect terrorist competence and tradecraft.

**Table 4.3** Risk reductions in the United States

| | Reduction in vulnerability (%) |
|---|---|
| Existing security layers | 88.2 |
| Existing security layers with the addition of IPSBs | 96.4 |
| Reduction in risk due to IPSBs | 8.2 |

[2] Note that some results are rounded so as not to imply a precision higher than the precision of input detection rates and costs.

### 4.5.1 Substitution Effects and Adaptive Behaviour by Terrorists

As noted, the analysis has assumed that disruption rates are statistically independent. This assumption may not hold in every instance [6, 16]. Thus, security measures may not be perfectly substitutional: removing one layer of security may alter the systems model and/or detection rates of other layers of security. For example, if passengers or crew know there is an air marshal aboard, they may be less willing to jump a would-be hijacker. However, for the most part it seems correct to assume that the layers are statistically independent. Checkpoint screening effectiveness, for example, is not influenced by whether FAMS are on-board. Canines do not care whether there is an air marshal aboard. Do TSOs work less hard because there are BDOs around?

If it is believed that complete independence may not be strictly correct for some layers, the sensitivity analysis suggests that disruption rates can be doubled or halved with little effect on overall risk reduction. This high level of robustness strongly suggests that substitution and/or independence issues wouldn't make much difference even insofar as they may be valid.

It is also important to recognise that some terrorists may exhibit adaptive behaviour. Jackson and LaTourrette [34] have developed a set of adaptation strategies: substitute target or location, substitute tactic or attack mode, hide from or deceive defence, avoid defence at the target, attack defence directly, and absorb defence effects. Adaptive behaviour is inherently difficult to model in a risk analysis, but scenario-based analyses can be enlightening by considering changes such behaviour might make in rates of disruption. Duping someone into unwittingly boarding an aircraft with a bomb concealed in their carry-on luggage is one way to avoid detection from intelligence services, no-fly lists, JTTF, FBI or police. However, Stewart and Mueller [3] show that the overall risk reduction for a passenger-borne bombing declines by about 5% for this scenario. The insider threat is another example of adaptive behaviour. Overall, the results suggest that it is difficult to imagine a scenario in which an adaptive terrorist working with an organisation is likely to be able to dramatically alter the odds of pulling off a passenger-borne bombing or hijacking attack.

### 4.5.2 Comparisons with Other Countries

The aviation security layers in Europe, Canada, and Australia are very similar to those in the United States. Although the nomenclature may vary, the intent remains the same. For example, the JTTF is unique to the United States, but the concept of coordination between security services, police, airports, and airlines is not.

However, many European Union countries have fewer air marshals on flights, or even none at all, and they do not require the removal of shoes at the screening checkpoint. The sensitivity analysis in the American case shows that, if the likelihood

that air marshals are on board is reduced from 20 to 5%, the overall risk reductions are essentially unchanged. Thus, risk reductions estimated for the United States are most likely to apply as well to other Western countries, including Australia.

It is often argued that Israel has the most effective aviation security. All passengers are interviewed by Israeli security officials, air marshals are on every flight, secondary barriers to the cockpit (or double doors) are fitted to all aircraft, and each is equipped with anti-missile defences [21]. When Richard Reid, the December 2001 shoe bomber, flew on El Al in the summer of 2001, Israeli security "didn't like the look of him, so they checked everything in his bags, and everything he was wearing, and then put an armed sky marshal in the seat right next to him" [35]. While Reid was not carrying a bomb at the time, it could be argued that Israeli authorities were perceptive enough to recognise a potential threat and deal with it appropriately. In 1986, a six months pregnant Irish woman was interviewed by Israeli security officials at London's Heathrow Airport before her planned El Al flight to Tel Aviv. The interview was "inconclusive," so officials searched her bags, discovering a bomb hidden in the lining of her luggage [22]. The bag had been given to her by her Jordanian fiancé. This, and other examples, may attest to the effectiveness of the interview process—there has been no successful attack on an El Al airliner in nearly 50 years, which is, as [21] observes, "a somewhat remarkable feat given terrorist animosities toward Israel."

The Israeli approach comes at a considerable cost, however. TSA Administrator John Pistole estimates that Israel spends "about 10 times as much as we spend here in the U.S. per passenger" [36]. To duplicate the Israeli approach in the United States would roughly require boosting U.S. government and private spending on aviation security from its current level of $10 billion per year to $100 billion per year. It is highly doubtful that such a spending increase is a worthwhile investment if it reduces risk only by an additional 3–5%. The laws of diminishing returns applies—the first dollars spent on counterterrorism measures are likely to be more worthwhile than the last ones.

### *4.5.3 Security Measures in Place in the US Before 2001*

A key value of our reliability model of the overall system of aviation security is that risk reductions can be estimated when some layers of security are removed or have reduced effectiveness. This allows for an evaluation that compares aviation security measures for the 1973–2001 period with those currently in place.

To establish a match, we make the following adjustments to the model:

- Since the ability to trace weapons at the checkpoint was lower because detection technologies were less advanced, we reduce disruption rates for this layer by half.
- We reduce disruption rates for resistance by passengers and crew to zero percent because the crew were instructed to cooperate with hijackers before 9/11, not to fight back.

- We halve the proportion of flights that air marshals are on from 20 to 10%. The U.S. Customs Air Security Officers Program (or sky marshals as they were then called) comprised nearly 1800 recruits when established in 1970, but the program was discontinued in 1974, only to be re-established in the mid-1980s [21]. There were only 33 air marshals in 2001, which was rapidly expanded to several thousand soon after [37].
- Hardened cockpit doors were only introduced in 2003, so this layer can be removed from the analysis entirely.
- However, we assume that, if air marshals are on board, their ability to foil a hijacking attempt is a high 50%.
- Since anti-aircraft measures would have a much lower chance of success before the shocking events of 9/11, we reduce the probability for disruption to 5% for this layer.
- Travel document checkers, Behavior Detection Officers, and the FFDO program were introduced after 2001, so these layers can be removed from the analysis entirely.

With these revised measures in place, the risk reduction is lowered: from 88.2 to 23.5%. The odds of a successful hijacking attack before 9/11 thus become quite high.

We can also evaluate aviation security in the United States prior to 1973 when it was minimal. In-flight measures might include law enforcement officers, and anti-aircraft measures and ability to fly the airliner. With these revised measures in place, overall risk reduction for hijackings is lowered again: from 23.5% (as established for the 1973–2001 period) to 10.6%. The odds of a successful hijacking before 1973 become quite high—the likelihood that a terrorist who arrives at the airport undeterred and undetected will be successful is a high 90%. Under these conditions hijackings are easier to accomplish, something that, sadly, is borne out by the historical record for this period.

## 4.6 Benefit-to-Cost Ratio for IPSBS

To determine the benefit-to-cost ratio for IPSBs the *benefit* is calculated as:

$$\begin{aligned} &Benefit\ of\ IPSBs \\ &\quad = probability\ of\ a\ successful\ attack \\ &\quad \times losses\ sustained\ in\ the\ successful\ attack \\ &\quad \times reduction\ in\ vulnerability\ (risk\ reduction)\ furnished\ by\ IPSBs \end{aligned} \tag{4.4}$$

An easy to understand decision-making metric—the benefit-to-cost ratio (BCR)—is simply the benefit divided by the cost. If the ratio exceeds one, the benefits exceed

the cost and the measure is cost-effective. The most cost-effective measures are those with high risk reduction, low cost, or a combination of the two.

*Losses sustained in a successful attack*

A loss of $10 billion for the 9/11 attack on the Pentagon gives a reasonable lower bound, and $100 billion per airliner for the World Trade Center attack on 9/11 represents an upper bound.

In our analysis, mean losses for a hijacking is taken as $50 billion.

*Probability of an otherwise successful terrorist attack*

No terrorist hijackings or bombing attacks have been disrupted at U.S. airports for several decades.

An attempt was made to hijack and crash a FEDEX cargo flight from Memphis to San Jose in 1994 by an employee of the company flying as a passenger; after a violent struggle in the cockpit in which all three flight crew were seriously injured, he was restrained and the aircraft landed safely [22].

If we count the 9/11 attacks as a single attack and the failed FEDEX attack, there have been two hijacking attacks over the last 26 years (1994–2019) in the United States.

The likelihood of a hijacking attack, then, is two divided by 26 years which is 7.7% which we conservatively round down to 5% or one attack every 20 years.

*Cost of the security measure*

The cost of IPSBs to be installed in new aircraft is $40 million per year for the entire U.S. commercial airline fleet.

Applying these numbers, the benefit-to-cost ratio (BCR) for IPSBs assuming a risk reduction of 8.2% is 5.1—i.e., $1 of cost buys $5.10 of benefit. If public safety is paramount the decision-maker may wish to ensure that decisions are risk averse. In this case, the BCR would increase if a Disproportionate Factor is applied to life-safety benefits [38] or if risk-averse utility function are utilised [6].

The results of this model are robust. Table 4.4 shows that changing the disruption rates in Table 4.2, often very substantially, alters risk reduction mostly by no more than ±7%. For example, if the rate of disruption for IPSB is halved to 37.5%, the risk reduction provided by IPSBs declines from 8.2 to 2.8%—with a BCR of 1.7 where $1 of cost returns nearly $2 in benefit. Doubling the rates of disruption for passengers, cabin crew and flight deck crew reduces risk reduction of IPSBs to 1.9%, with a BCR of 1.2. Even if there were only one terrorist hijacking attack in a hundred years (annual attack probability of 1%) and the terrorists arrived at the airport undeterred and undetected, secondary barriers would still be cost-effective.

Therefore, at just about all reasonable combinations of security measure effectiveness, costs and attack likelihood, the IPSB is an effective and cost-efficient security measure.

**Table 4.4** Sensitivity analysis of risk reductions

| | Reduction in vulnerability due to IPSBs (risk reduction) (%) | Benefit-to-cost ratio BCR |
|---|---|---|
| Addition of secondary flight deck barriers or IPSBs | 8.2 | 5.1 |
| Rate of disruption for hardened cockpit door reduced by 50% | 15.4 | 9.6 |
| Rate of disruption flight deck resistance reduced by 50% | 11.0 | 6.8 |
| Rate of disruption by passengers and cabin crew reduced to 5% | 10.3 | 6.4 |
| Rates of disruption for anti-aircraft measures is 0% | 9.7 | 6.0 |
| Rate of disruption by passengers reduced from 15 to 5% | 9.2 | 5.7 |
| Rate of disruption for checkpoint screening reduced by 50% | 9.0 | 5.6 |
| Probability of air marshals on flight reduced from 20 to 5% | 9.0 | 5.6 |
| Rate of disruption for checkpoint screening increased by 50% | 7.5 | 4.7 |
| Passenger and cabin crew resistance increased by 50% | 6.8 | 4.3 |
| Rate of disruption for hardened cockpit door increased by 25% | 5.5 | 3.4 |
| Rate of disruption flight deck resistance increased by 50% | 5.5 | 3.4 |
| IPSB installed in 50% of aircraft | 4.1 | 2.6 |
| Rate of disruption for IPSB reduced by 50% | 2.8 | 1.7 |
| Doubling the rates of disruption for passengers, cabin and flight crew | 1.9 | 1.2 |
| Rate of disruption for IPSB reduced from 75 to 25% | 1.0 | 0.62 |
| IPSB cost halved to $20 million per year | – | 10.2 |
| IPSB cost doubled to $80 million per year | – | 2.6 |
| Attack probability reduced to 2.5% per year | – | 2.6 |
| Attack probability reduced to 1% per year (1 attack every 100 years) | – | 1.0 |
| Loss from successful attack doubled to $100 billion | – | 10.2 |
| Loss from successful attack halved to $25 billion | – | 2.6 |
| Loss from successful attack reduced to $10 billion | – | 1.0 |

Assumes that the probability that terrorist are undeterred and undetected is 5% per year.
The losses sustained in a successful terrorist hijacking attack are assumed to be $50 billion.

**Table 4.5** Cost-Effectiveness of FAMS, FFDOs and IPSBs

| | Reduction invulnerability (risk reduction) (%) | Cost (millions) | Benefit-to-cost ratio BCR |
|---|---|---|---|
| FAMS | 1.2 | $1000 | 0.03 |
| FFDOs | 4.0 | $20 | 5.0 |
| IPSBs | 8.2 | $40 | 5.1 |

## 4.7 Benefit-to-Cost Ratio for FFDOS and FAMS

Table 4.5 shows that the FFDO program passes a cost–benefit assessment for terrorist attacks.[3] However, we also find that the FAMS, at a combined cost of about $1 billion per year, fails to be cost-effective by a considerable margin. Terrorists would need to arrive at an airport in the United States, undeterred and undetected at least two times per year for FAMS to be cost-effective.

Stewart and Mueller [3, 7, 15] provide more details and discussion about these and other security measures and their cost effectiveness.

## 4.8 Discussion

This approach should not be seen as all or nothing. What is important is to determine what levels of expenditure and risk reduction furnish the greatest benefit and when the law of diminishing returns kicks in. Security measures that are at once effective and relatively inexpensive are generally the first to be implemented (e.g., hardened cockpit doors and FFDOs), and thus the first dollars spent on counterterrorism measures are often more likely to be worthwhile—that is, to be cost-effective—than are the last. This may even be the case for the expansion of FAMS which began right after 9/11. Quickly boosting the number of air marshals was sensible given understandable fears that there might soon be more hijacking attempts and it might as well have helped assuage the public's fears about flying a bit. However, the continued expansion of the program thereafter is likely to have done far less good per dollar expended.

The analysis provides a snapshot of risk reductions and cost-effectiveness under present conditions. Of course, terrorists may adapt their threats in reaction to new security measures, security measures may lose effectiveness with time, evolving threats may lead to the potential for higher losses, and so forth. Nevertheless, it does not seem that the competence of terrorists and the destruction they inflict are on the rise, and 9/11 is increasingly standing out as an aberration, not a harbinger—indeed, scarcely any terrorist attack anywhere in the world has managed to do even one-tenth as much total damage. Also, it is difficult to imagine a scenario in which an adaptive terrorist would be able to dramatically alter the odds of pulling off a hijacking or passenger-borne bombing attack. It might be added that the layer of security we find to be particularly cost-ineffective—FAMS—is unlikely to be any more effective when dealing with insider and other threats, and so our conclusions are likely to hold true for those conditions as well. Reducing the budget for this expensive security measure and transferring some of the savings into more cost-effective security measures could maintain current security levels while substantially reducing the cost to taxpayers and the airlines.

[3] Assumes that in the absence of FFDOs, the disruption rate for flight deck resistance drops from 40 to 20%.

It should be stressed as well that our calculations are for terrorists who arrive at the airport undeterred and undetected by other security measures. Since security measures surely do deter and some provide pre-flight detection, the overall impact of existing security measures in preventing hijackings is likely much higher than our analysis would suggest.

The systems model provides a starting point for aviation risk analysis and helps to begin to flesh out some other concerns including the data requirements that become more challenging as the systems model increases in detail and complexity. A more detailed and comprehensive study may be required to fully model the interactions and interdependencies between different threats in aviation security. Nonetheless, the analysis provides a basis for assessing the influence and sensitivity of policy options on risk reduction.

We recognise that risk and cost–benefit considerations should not be the sole criterion for public decision making. Nonetheless, they provide important insights into how security measures may (or may not) perform, their effect on vulnerability and risk reduction, and their cost-effectiveness. They can reveal wasteful expenditures and allow limited funds to be directed to where the most benefit can be attained.

Finally, Western airlines or passengers have comprised about 50% of the victims of successful terrorist attacks worldwide in the past 48 years, but zero percent during the 20 years after 9/11. With the heightened awareness and enhancements in security and expenditures, particularly since 9/11, Western airlines and airports are quite resilient to terrorists attacks [32]—a person would need to fly once per day for 30,000 years before being involved in a terrorist attack.

## 4.9 Conclusions

In this analysis, we have assessed the full array of security measures designed to protect an airliner from being hijacked, and we have used that to evaluate the risk reduction supplied by each security measure. The analysis is presented in a fully transparent manner: readers who wish to challenge or vary the analysis and assumptions are provided with the information, data, and framework with which to do so. This analysis finds that existing layers of aviation security reduce the risk of a successful hijacking attack by undeterred and undetected terrorists to be near 90%. Secondary flight deck barriers reduce the remaining vulnerability quite considerably to over 95%. This level of risk reduction is very robust: security remains high even when the parameters that make it up are varied considerably. Their relatively low cost and high risk reduction lead to very high benefit-to-cost ratios. Hence, there is little doubt that secondary flight deck barriers are an effective and cost-efficient security measure.

**Acknowledgements** The support of the Australian Research Council grant DP160100855 is acknowledged.

## Appendix A: Reliability Analysis of Aviation Security

### Existing Security Measures

The probability that an attack is disrupted, foiled or prevented by pre-boarding security measures assuming that the terrorists have arrived at the airport undeterred and undetected is:

$$\Pr\begin{pmatrix}\text{disrupted by}\\ \text{pre - boarding measures}\end{pmatrix} = 1 - \left\{\begin{array}{l}\left[1 - \Pr(\text{disrupted by no fly list \& passenger pre-screening})\right]\\ \times\left[1 - \Pr(\text{disrupted by Behavior Detection Officers})\right]\\ \times\left[1 - \Pr(\text{disrupted by travel document checkers})\right]\\ \times\left[1 - \Pr(\text{disrupted by checkpoint/TSOs})\right]\end{array}\right\} \quad (4.5)$$

In the absence of a secondary barrier, the probability that an attack is disrupted or prevented by in-flight security measures is

$$\Pr\begin{pmatrix}\text{disrupted by}\\ \text{in-flight}\\ \text{measures}\end{pmatrix} = 1 - \left\{\begin{array}{l}\left[1 - \Pr(\text{foiled by passengers})\right]\\ \times\left[1 - \Pr(\text{foiled by cabin crew})\right]\\ \times\left[1 - \Pr(\text{foiled by Law Enforcement Officer})\right]\\ \times\left[1 - \Pr(\text{foiled by hardened cockpit door})\right]\\ \times\left[1 - \Pr(\text{foiled by flight deck resistance and FFDOs})\right]\end{array}\right\} \quad (4.6)$$

where

$$\Pr\begin{pmatrix}\text{foiled by}\\ \text{hardened}\\ \text{cockpit door}\end{pmatrix} = \left\{\begin{array}{l}\Pr(\text{FAMS on flight})\\ \times\Pr(\text{foiled hardened cockpit door if FAMS on flight})\\ +\Pr(\text{no FAMS on flight})\\ \times\Pr(\text{foiled hardened cockpit door if no FAMS on flight})\end{array}\right\} \quad (4.7)$$

### Addition of Installed Physical Secondary Barriers (IPSBs)

The probability that in-flight security measures will disrupt an attack, and now including the effect of IPSBs, is a modified version of Eq. (4.6):

$$\Pr\left(\begin{array}{c}\text{disrupted by}\\ \text{in-flight}\\ \text{measures}\end{array}\right) = 1 - \left\{\begin{array}{l}\big[1 - \Pr(\text{foiled by passengers})\big]\\ \times\big[1 - \Pr(\text{foiled by cabin crew})\big]\\ \times\big[1 - \Pr(\text{foiled by Law Enforcement Officer})\big]\\ \times\big[1 - \Pr(\text{foiled by IPSB})\big]\\ \times\big[1 - \Pr(\text{foiled by hardened cockpit if IPSB fails})\big]\\ \times\big[1 - \Pr(\text{foiled by flight deck resistance and FFDOs})\big]\end{array}\right\} \tag{4.8}$$

where

Pr(foiled by hardened cockpit door if IPSBfails)

$$= \left[\begin{array}{ll}\Pr\left(\begin{array}{c}\text{FAMS}\\ \text{on flight}\end{array}\right) & \times \Pr\left(\begin{array}{c}\text{foiled hardened cockpit door}\\ \text{if IPSB fails and FAMS on flight}\end{array}\right)\\ +\left(1 - \Pr\left(\begin{array}{c}\text{FAMS}\\ \text{on flight}\end{array}\right)\right) & \times\left(\begin{array}{c}\text{failed hardened cockpit door}\\ \text{if IPSB fails and no FAMS on flight}\end{array}\right)\end{array}\right] \tag{4.9}$$

where Pr(foiled by IPSB) is the probability that the IPSB is deployed and will function as intended and delay a hijacker sufficiently to allow the cockpit door to be closed.

## References


1. Robinson LA, Hammitt JK, Aldy JE, Krupnick A, Baxter J (2010) Valuing the risk of death from terrorist attacks. J Homel Secur Emerg Manage 7(1):Article 14
2. Mueller J, Stewart MG (2011) Terror, security, and money: balancing the risks, benefits, and costs of homeland security. Oxford University Press, New York
3. Stewart MG, Mueller J (2018) Are we safe enough? measuring and assessing aviation security. Elsevier, New York
4. Stewart MG, Mueller J (2008) A risk and cost-benefit assessment of U.S. Aviation security measures. J Transp Secur 1(3):143–159
5. Stewart MG, Ellingwood BR, Mueller J (2011) Homeland security: a case study in risk aversion for public decision-making. Int J Risk Assess Manage 15(5/6):367–386
6. Stewart MG, Mueller J (2013) Aviation security, risk assessment, and risk aversion for public decisionmaking. J Policy Anal Manage 32(3):615–633
7. Stewart MG, Mueller J (2018) Risk and economic assessment of U.S aviation security for passenger-borne bomb attacks. J Transp Secur 11:117–136
8. Stewart MG, Mueller J (2011) Cost-Benefit analysis of advanced imaging technology fully body scanners for airline passenger security screening. J Homel Secur Emergency Manage 8(1):Article 30
9. Mueller J, Stewart MG (2014) Evaluating counterterrorism spending. J Econ Perspect 28(3):237–248
10. Mueller J, Stewart MG (2016) Chasing ghosts: the policing of terrorism. Oxford University Press, Oxford and New York
11. Stewart MG, Mueller J (2014) Risk and cost-benefit analysis of police counter-terrorism operations at Australian airports. J Policing, Intell Counter Terrorism 9(2):98–116

12. Stewart MG, Mueller J (2014) Cost-Benefit analysis of airport security: are airports too safe? J Air Transp Manag 35(March):19–28
13. Stewart MG, Mueller J (2017) Risk and economic assessment of expedited passenger screening and TSA PreCheck. J Transp Secur 10(1):1–22
14. ALPA (2020) Take action to secure the flight deck. http://www.alpa.org/advocacy/cta/secondary-barriers
15. Stewart MG, Mueller J (2019) Security risk and cost-benefit assessment of secondary flight deck barriers. Research Report No. 285.11.2019, Centre for Infrastructure Performance and Reliability, The University of Newcastle, NSW, Australia
16. Stewart MG, Mueller J (2013) Terrorism risks and cost-benefit analysis of aviation security. Risk Anal 33(5):893–908
17. Smith P (2007) The airport security follies. nytimes.com, December 28
18. Schneier B (2003) Beyond Fear: Thinking sensibly about security in an uncertain world. Copernicus, New York
19. Walsh T (2016) 15 Years Since 9/11: why are we still vulnerable to this type of attack? Aviation Security International June, 29–30
20. Black N, Devine C, Griffin D (2015) Sleep-deprived, medicated, suicidal and armed: federal air marshals in disarray. CNN Invest, August 14
21. Elias B (2010) Airport and aviation security. CRC Press, Boca Raton, FL
22. Baum P (2016) Violence in the skies: a history of aircraft hijacking and bombing. Summerdale Publishers, Chichester, U.K.
23. Moak L (2011) Letter to house subcommittee on transportation security, president of airline pilots association international, July 12, 2011
24. ALPA (2013) Secondary flight deck barriers and flight deck access procedures: a call for action. White paper, Airline Pilots Association International, Washington, DC, July
25. RTCA (2011) Aircraft secondary barriers and alternative flight deck security procedures, final report. Radio Technical Commission for Aeronautics, Special Committee 221, RTCA DO-329, Washington, D.C., September 28
26. Brennan C (2016) 15 years after 9/11, a pilot's widow still seeks aviation security. The Inquirer, September 12
27. FAA (2020) Recommendation report to aviation rulemaking advisory committee for implementation of section 336 of P.L. 115–254. Flightdeck Secondary Barrier Working Group, Federal Aviation Administration, Washington, D.C., February 27
28. Aaronson T (2013) The terror factory. Ig Publishing, Brooklyn, NY
29. Kenney M (2010) 'Dumb' yet Deadly: local knowledge and poor tradecraft among Islamist Militants in Britain and Spain. Stud Conflict and Terrorism 33(10):911–932
30. Mueller J (2020) Terrorism Since 9/11: The American Cases. Mershon Center, Ohio State University, Columbus, OH. http://politicalscience.osu.edu/faculty/jmueller/SINCE.pdf
31. Mueller J, Stewart MG (2012) The terrorism delusion: America's overwrought response to september 11. Int Secur 37(1):81–110
32. Stewart MG, Mueller J (2020) Terrorism risks chasing ghosts, and infrastructure resilience. Sustain Resilient Infrastruct 5(1–2):78–89
33. Jenkins BM (2011) Stray dogs and virtual armies: radicalization and recruitment to Jihadist Terrorism in the United States Since 9/11. RAND Corporation, Santa Monica, CA
34. Jackson BA, LaTourette T (2015) Assessing the effectiveness of layered security for protecting the aviation system against adaptive adversaries. J Air Transp Manag 35(March):26–33
35. Kohn D (2002) The safest airline: a security example set by Israel's El Al. 60 Minutes, CBS, January 15
36. Balakrishnan A (2016) Would you pay more for extra airport security? CNBC, March 24
37. Meckler L, Carey S (2007) Sky patrol: U.S. Air Marshal service navigates turbulent times. The Wall Street J, February 9
38. Grant MJ, Stewart MG (2019) Postal IEDs and risk assessment of work health and safety considerations for postal workers. Int J Risk Assess Manage 22(2):152–169

# Chapter 5
# Challenges of Effective Blast Protection of Buildings


**Hong Hao and Xihong Zhang**

**Abstract** Effective building protections against blast loading are important for the protection of people and property. This chapter summarizes existing guidelines for blast load prediction and structural design to resist blast loading effects. Different approaches for explosion source separation and isolation and their effectiveness on reducing blast loading effects on structures are presented and discussed. The blast resistance performances of structural components as well as building strengthening methodology and their effectiveness are discussed. Uncertainties in blast load prediction and reliability analysis of structures with and without strengthening measures against blast loading are presented and discussed.

## 5.1 Introduction

Terrorist bombing attacks and accidental explosion incidents have caused many casualties and damages to structures. As a result, effective protections of building structures against such extreme loads have attracted attentions of decision makers, architects, and engineers. Government agencies and design guides provide definitions of different blast threat levels, and the corresponding recommended practices for blast protection. Intensive research also has been reported in the open literature on developing technologies for effective structural protection against blast loads. The primary approaches for structural protection can be classified as: (i) blast load isolation; (ii) blast loading energy absorptions for structure response mitigation; and (iii) structure strengthening. This chapter discusses the needs for building protection against blast loadings, current practices and challenges, and possible future technology developments for more effective building protection.

H. Hao · X. Zhang (✉)
Centre for Infrastructure Monitoring and Protection, School of Civil and Mechanical Engineering, Curtin University, Bentley, Australia
e-mail: xihong.zhang@curtin.edu.au



M. G. Stewart and D. V. Rosowsky (eds.), *Engineering for Extremes*, Springer Tracts in Civil Engineering, https://doi.org/10.1007/978-3-030-85018-0_5

### 5.1.1 Design Requirements

Different governmental agencies and standard committees specify blast resistance design requirements for different types of buildings. For example, for structural design against military weapon effects, ASCE Manual-42 [1] provides the design guide against nuclear weapon effects, and UFC 3-340-01 [2] provides design methods for hardened structures to resist conventional weapon effects. FEMA-426 [3] provides basic concepts for protective structures against terrorist attack, UFC 4-010-01 [4] defines minimum anti-terrorism requirements for building protection; ASCE Structural Design for Physical Security (1999) covers threat assessment, load estimations, structural response and design methods; and [5] defines minimum stand-off distance for structural safety against terrorist attacks. For progressive collapse, UFC 4-023-03 [6] details buildings protection requirements, and GSA-Alternate load path analysis and design guideline for progressive collapse resistance [7] provides tie force and alternate path methods. For chemical explosions, ASCE Design of Blast Resistant Buildings in Petrochemical Facilities [8] provides guidelines for blast resistant design of petrochemical facilities.

Among these design manuals and recommended practices, UFC 3-340-02 [9] is one of the most widely used guidelines for design and analysis of structures against blast loading. This manual defines 'close-in' and 'far' explosion ranges for predicting the response mode of structures. The response limits or design criterion for structural components such as slabs and roofs are defined in terms of support rotations. Another widely used manual is ASCE-59 [10], in which element damage levels are classified as superficial, moderate, heavy and hazardous. Compared to UFC 3-340-02, the angle of rotations corresponding to different damage levels is slightly conservative. For superficial damage, ductility ratio is limited to 1.0 (elastic deformation). Another difference between these two design guides is that double-reinforcement design is always required in UFC 3-340-02 for resisting rebounds, while in ASCE-59 single- and double- reinforced elements are separately considered. Dynamic increase factors (DIF) of concrete and reinforcing steel strengths are considered in both standards. While UFC 3-340-02 lists DIFs for far-range and close-in explosion scenarios, in ASCE-59 only DIFs for far-range are provided. For the design of RC structures subjected to close-in explosion, ASCE-59 suggests performing explicit numerical modeling.

Analyses specified in most design guides are based on the Single Degree of Freedom (SDOF) model, and the equivalent SDOF system is derived with the assumption that flexural response governs the structural response. Therefore, these design approaches and criteria in the current guides are not necessarily suitable for modelling structural responses subjected to contact or close-in explosions where structural responses are governed by localized damages associated with concrete crushing and spalling, or governed by direct or diagonal shear response (Fig. 5.1). In such situations, high-fidelity numerical simulation or modified SDOF analysis is needed to predict structural responses in the design analysis. Furthermore, the current design guides, e.g., UFC 3-340-02 assumes elastic-perfect-plastic resistance of structures.

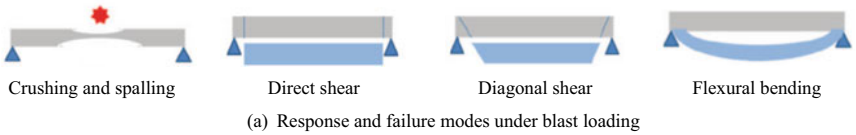


(a) Response and failure modes under blast loading


(b) Local indentation of CFDST (concrete filled double skin tubular) column under close-in blast [40]

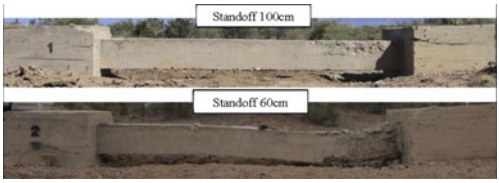


(c) Scabbing and shear damage of RC column [39]

**Fig. 5.1** Different damage modes of structural elements subjected to blast loading

The strain hardening or softening effect, as well as the secondary structural response effects such as membrane effect and P-Δ effect are neglected. As large deformation of structures subjected to blast load may occur, such nonlinear effects could be significant. Neglecting these effects may lead to inaccurate structural response predictions in design analysis.

## 5.2 Blast Load Estimation, Separation/Isolation

To better design structures against blast loading, it is essential to accurately predict the blast load. In this section, blast load estimation methods, and the state-of-the-art blast load separation and isolation measures including blast wall, blast fence, and blast separation landscaping technique are introduced and discussed.

### *5.2.1 Blast Load Estimation*

Explosions are associated with a rapid release of a large amount of energy. The amplitude and distribution of blast loading on a structure are a function of the explosive type, weight and shape of the explosive, distance and location of the explosive from the structure and the interaction of the blast wave with the structure. For different

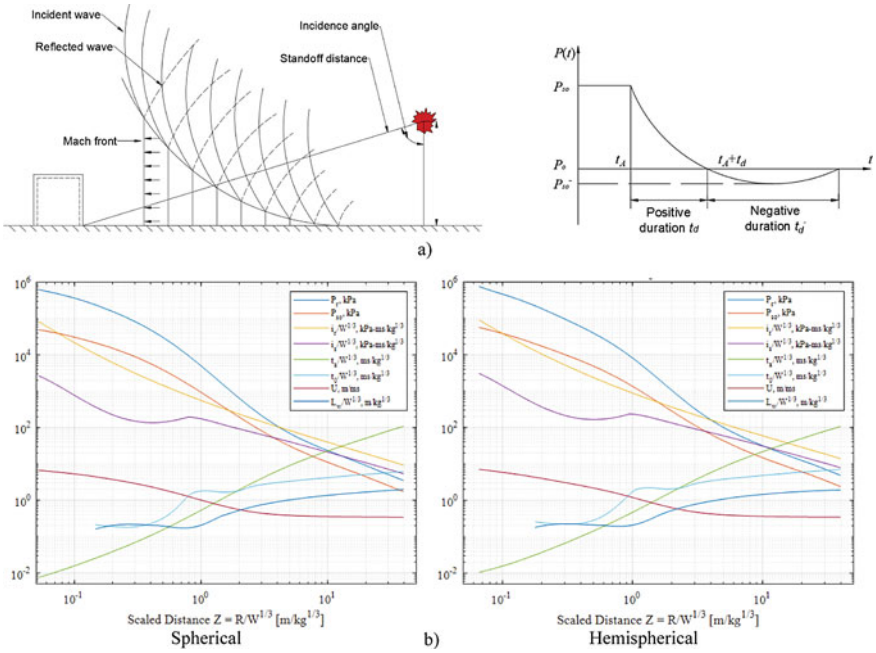


**Fig. 5.2** **a** Unconfined air burst and typical pressure–time profile; **b** shock wave parameters for spherical and hemispherical TNT explosions. Reproduced from UFC 3–340-02

solid high explosives, it is a common practice to convert the charge weight to an equivalent weight of Trinitrotoluene (TNT). The blast effects are given as a function of scaled distance $Z = R/W^{1/3}$, where R is the stand-off distance and W is the weight of TNT equivalence [9]. Figure 5.2a shows a typical air blast pressure profile from a TNT explosion. Until now, the most extensive data about blast load parameters are for TNT spherical airbursts and hemispherical surface bursts. The blast parameters can be scaled and plotted versus the scaled stand-off distance in the form of a series of curves as shown in Fig. 5.2b. A number of computer tools, design charts, empirical formulae, and computational fluid dynamics models can be used to estimate blast loadings. For example, design charts in UFC 3-340-02 [9] are most commonly used to estimate reflected peak pressure $P_r$ and impulse $I_r$ corresponding to an explosion scenario (Fig. 5.2b), which are the blast loading acting on the structure.

### *5.2.2 Blast Separation and Isolation*

When considering structural protections against blast loading, the primary strategy is to keep the explosive detonation point as far away from the building as possible. This is usually the easiest and least costly way to achieve a desired level of protection in

comparison to strengthening the structural system. Increasing the distance between possible locations of an explosion and the target reduces the peak overpressure and the impulse acting on structures from an explosion, which consequently reduces the damage and risk to the structures. Different approaches are discussed herein.

#### 5.2.2.1 Blast Wall

A blast wall provides a stand-off distance to protect the structure from an external explosion, which also acts as an obstacle in the direction of the blast wave propagation. Therefore, some portion of the explosive energy is reflected, and then the distribution of the blast pressure on the structure behind the barrier is changed and the peak pressure is reduced. Both experimental and numerical results showed that a blast wall can effectively protect buildings from external explosion [11, 12]. A barrier between an explosion and a building not only can reduce the peak reflected pressure and impulse on the building, but also delay the arrival time of the blast wave. Based on the numerical results, analytical formulae have been derived to estimate the reflected pressure–time history on a structure behind a barrier [12]. As illustrated in Fig. 5.3, the critical parameters that affect the blast loading behind a blast wall, include the TNT equivalent charge weight W, the distance from charge to the building D, the height of the building $H_B$, the height of point of interest on the structure H, the blast wall height $H_1$ and the ratio of the distance between the blast wall and the explosion to that between the building and the explosion $L_1/D$ are incorporated in the formulae as

$$A_{P,\max} = -0.1359 + \left(0.3272 + 0.1995 \log\left(\frac{H_1}{D}\right)\right) \log Z - 0.5626 \log\left(\frac{H_1}{D}\right) + 0.4666 \frac{L_1}{D} \tag{5.1}$$

$$A_{I,\max} = 0.0274 + \left(0.4146 + 0.2393 \log\left(\frac{H_1}{D}\right)\right) \log Z - 0.5044 \log\left(\frac{H_1}{D}\right) + 0.2538 \frac{L_1}{D} \tag{5.2}$$

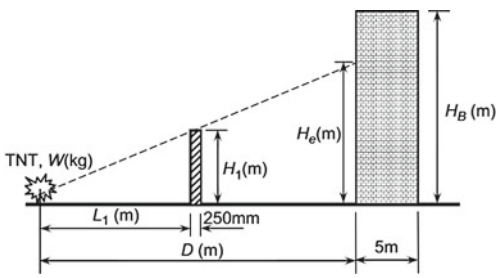


**Fig. 5.3** Configuration of explosive, blast wall, and structure for the design of blast wall in [12]

where $A_{P,\max}$ and $A_{I,\max}$ are the de-amplification factors for the maximum peak reflected pressure and peak reflected impulse behind the blast wall, which can be used together with [9] to estimate the peak reflected overpressure and impulse. Detail procedures for predicting blast loadings behind a solid barrier can be found in [12].

#### 5.2.2.2 Blast Fence

Solid blast barriers normally need to be designed with high structural resistance and ductility. This often requires bulky and heavy protective barriers which are not only highly costly but also often not appropriate for application in downtown areas. Moreover, damage of solid blast barriers generates debris hazards, which endangers structures and people behind the barrier. Based on the principle that blast wave diffracts when interacting with obstacles, blast fence was proposed as a potential blast protection technology. Considering a series of identical obstacles/columns evenly spaced side by side, diffracted waves from adjacent columns could cancel each other, which would significantly weaken the wave amplitude. Niollet et al. [13] experimentally demonstrated that placing cylindrical bars between the target structure and a charge resulted in faster blast wave attenuation. Chaudhuri et al. [14] numerically investigated shock wave attenuation with a matrix consisting of rigid obstacles. It was found that reverse triangular columns could effectively attenuate blast wave, and staggered arrangement of columns could bring further enhanced effectiveness. Recently, Hao and his co-workers carried out extensive field blast tests and numerical modeling to study the performance of blast fences [15–17]. To achieve the balance between reducing the net blast load on elements of fence poles and satisfactory blast wave attenuation, the effects of geometry, spacing, dimension and separation distance, and number of layers of fence poles on mitigating blast pressures were investigated as shown in Fig. 5.4a, b. It was found that poles with circular or triangular (with angle facing the explosion) cross sections gave the balanced performance of net blast load on fence barrier and blast pressure mitigation. A blast fence is more effective at a distance away from the barrier owing to the interaction and self-cancellations of pressure wave energies diffracted from the fence poles. The corresponding reduction in peak overpressure could be more than 80% and impulse can be around 70% as compared to those in free field (Fig. 5.4d). These results demonstrate that fence barriers could be a possible alternative of solid walls to provide stand-off distance and mitigate blast loading behind the fence. Empirical formulae were proposed to estimate the blast overpressure and impulse behind the blast fence as

$$A_{P,\max} = \frac{11.7H_1^2}{D^2} + \frac{0.48L_1^2}{D^2} - \frac{0.14ZH_1}{Z_0 D} - \frac{1.5H_1L_1}{D^2} + 0.06\frac{Z}{Z_0} - \frac{5.25H_1}{D} + \frac{0.16L_1}{D} + 1.1 \tag{5.3}$$

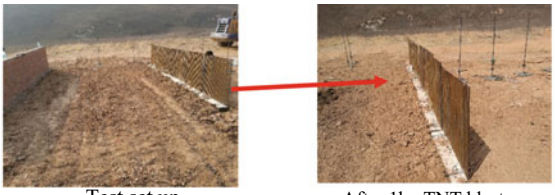

Test set up After 1kg TNT blast

(a) Field blast test

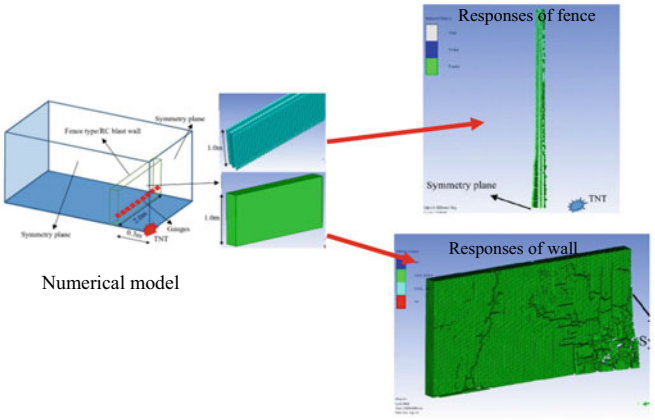


(b) Numerical modeling of blast fence and blast wall

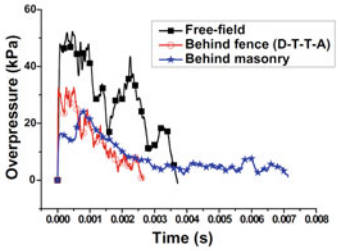


(c) Comparison of measured blast overpressure time histories

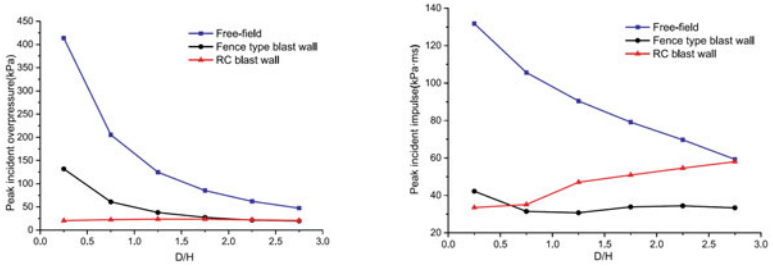


(d) The peak overpressures and impulses with respect to the normalized distance D/H
(D: distance behind the wall; H: height of wall)

**Fig. 5.4** Field tests and numerical simulation of blast pressure mitigations with fence and solid barriers [15–17]

$$A_{I,\max} = \frac{4.9H_1^2}{D^2} + \frac{0.037L_1^2}{D^2} + \frac{0.18ZH_1}{Z_0D} - \frac{1.05H_1L_1}{D^2} - 0.026\frac{Z}{Z_0} - \frac{2.43H_1}{D} + \frac{0.5L_1}{D} + 0.8 \quad (5.4)$$

$$A_{I,\max} = \frac{16.1H_1^2}{D^2} - \frac{0.97L_1^2}{D^2} + \frac{0.086ZH_1}{Z_0D} - \frac{3.6H_1L_1}{D^2} - 0.011\frac{Z}{Z_0} - \frac{8.2H_1}{D} + \frac{1.5L_1}{D} + 1.6 \quad (5.5)$$

where $A_{P,\max}$ and $A_{I,\max}$ are the de-amplification factors for the maximum peak reflected pressure and peak reflected impulse behind the blast fence, which can be used together with [9] to estimate the peak reflected overpressure and reflective impulse, in which $H_1$ is the height of the blast fence in meter, $L_1$ is the distance between the explosive centre and the blast fence in meter, Z is the scaled distance in ($m/kg^{1/3}$), D is the distance between the explosive centre and the target measurement point in meter. Both Eqs. (5.4) and (5.5) estimate the de-amplification factors of the maximum peak reflected impulses. The larger value estimated should be used in design. Detail procedures for predicting blast loading behind fence wall can be found in [16].

#### 5.2.2.3 Protective Plants/Landscaping

Gebbeken and his team proposed the concept of employing landscaping and plants to provide blast protection. Both field blast tests [18, 19], and simplified numerical modeling [18, 20] were conducted to investigate the effectiveness of employing plants/landscaping to achieve blast protection.

Field blast tests and numerical modeling (Fig. 5.5) found the biomass density above ground is the governing parameter for blast wave mitigation. For example, when using cherry laurel hedging with 3.5% biomass density, the peak overpressure could be reduced by 38.6% comparing to no hedging protection when a 5 kg TNT equivalent charge is detonated at 5.5 m stand-off distance. When using thuja hedging with a 5% larger biomass, over 56% of reduction was observed for the peak overpressure. A denser biomass from plants could provide more inertia resistance against blast, and it also provides a larger surface to reflect the blast wave. In the meanwhile, larger leaves, which are favorable for noise reduction, lead to more damages and make the plants more vulnerable, especially against small parts of debris. In comparison, narrow needle shape plants with a much smaller surface reduces the stresses within the structure. The blast wave is effectively mitigated due to the sheer number of needles. Therefore, coniferous and deciduous trees with small leaves are suitable as protective plants.

Based on their studies, the following principles of blast protection plants were proposed: (a) evergreen plants to provide year-round protection; (b) opaque plants

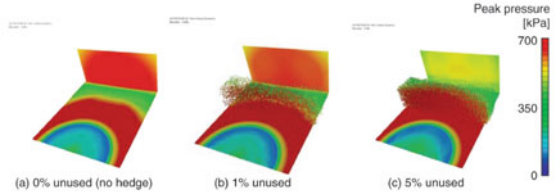


(a) Simplified numerical modeling (Gebbeken and Döge, 2010)

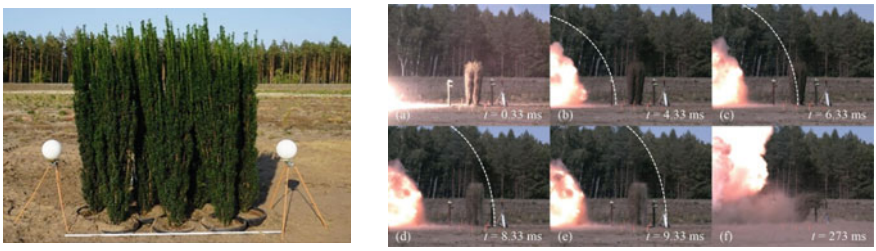


Test setup High speed camera images

(b) Field blast test using yew tree hedge (Warnstedt and Gebbeken, 2020b)

**Fig. 5.5** Simplified numerical modeling and field blast test on hedge as blast barrier

to ensure the existence of biomass in each possible direction towards an explosion; (c) non-brittle behavior enabling the plant to withstand large deflections without sustaining vital damage; (d) needle shape leaves to reduce the vulnerability of plants in front of blast wave and debris; and (e) most importantly of all, having a large amount of biomass to provide inertia resistance against blast.

## 5.3 Structure Resistance Analysis and Strengthening

To achieve a reliable analysis and design of structures subjected to blast loading, it is important to properly understand the behavior of structures under blast loading. Since blast loading normally generates localized responses on structural elements instead of global responses of the entire structure, studies are therefore primarily conducted on the responses of structural elements such as beam, column, slab, and progressive collapse of the structure should gravity load-carrying components fail. In this section, the responses of structural columns and slabs under blast loading are presented, which are followed by strengthening and mitigation retrofits.

### 5.3.1 RC Columns

Columns are one of the most targeted structural components in bombing attacks. It is also the most crucial load-bearing component in a structural system. Failure of a column could trigger progressive collapse of part or the entire structure. Therefore, many attentions have been paid to study the performance of structural columns under blast loading. Shi et al. [21] used a numerical method to assess the performance of RC columns under blast loads. "Residual load-bearing capacity" was used as an indicator to quantify the damage level and performance of a column. In general, when subjected to blast loads, there are two damage modes for RC columns: shear and flexural governed damages. Sometimes the failure could be a combination of these two modes. Figure 5.6 illustrates these typical damage modes derived from numerical simulation. When subjected to impulsive load, it is inclined to be damaged by shear; while in the quasi-static region, the column is likely damaged by flexural mode. This is because, in the impulsive region, a blast load is usually of high peak overpressure and short duration. Shear stress develops quickly to a high value before the development of flexural deflection. Therefore, shear damage is likely to happen. On the other hand, in the quasi-static region the blast load has relatively long duration. The loading effect is more similar to that of quasi-static loading, and therefore flexural response governs (Fig. 5.8b). However, it should be mentioned that these are some general observations only. The damage modes also depend on the column properties.

Design guides such as UFC 3-340-02 [9] employs the SDOF method for design analysis of RC columns under blast loading. Typically, UFC 3-340-02 provides both a step-by-step numerical approach to solve the differential equations for analyzing column dynamic response, and design charts for structural response estimation. It is

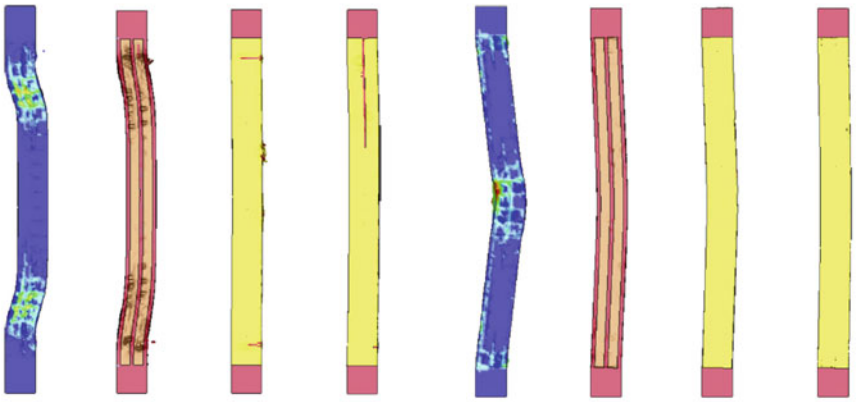


**Fig. 5.6** Responses of RC columns subjected to **a** impulsive loading; **b** quasi-static loading: (i) un-strengthened; (ii) longitudinal FRP strips; (iii) FRP wrap; (iv) FRP wrap and strips [22]

worth noting that the current design charts and criteria given in the design guides were derived by assuming flexural governed structural response mode and elastic or elastic-perfect-plastic resistance functions. These assumptions do not necessarily represent the possible response modes and structural resistances, which may therefore lead to inaccurate design analysis [23]. Considering strain hardening and softening effect, as well as the shear failure mode, an improved analysis approach and design charts can be developed [24]. Typically, in the analysis the direct shear response is firstly examined. When the structure survived shear damage, its flexural response would then be analyzed with modified resistance functions considering strain hardening or softening effects. Non-dimensional design charts with various levels of elastic–plastic-hardening/softening resistances were generated and shown in Fig. 5.7, in which H/S represents the hardening ratio. These charts could be used to consider the appropriate hardening ratios in design of structures against blast loading.

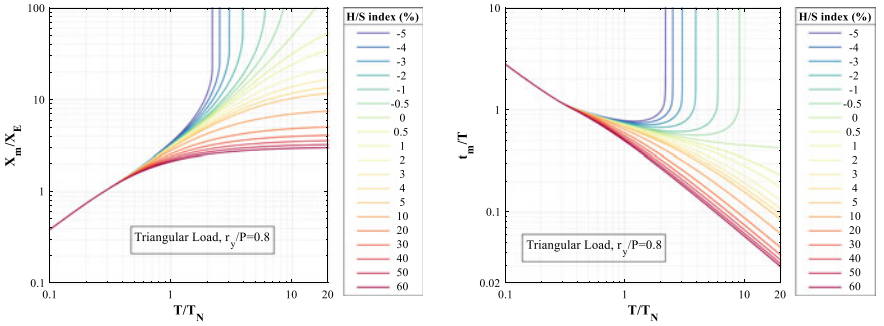


**Fig. 5.7** Design charts using improved SDOF analysis method considering strain hardening and softening

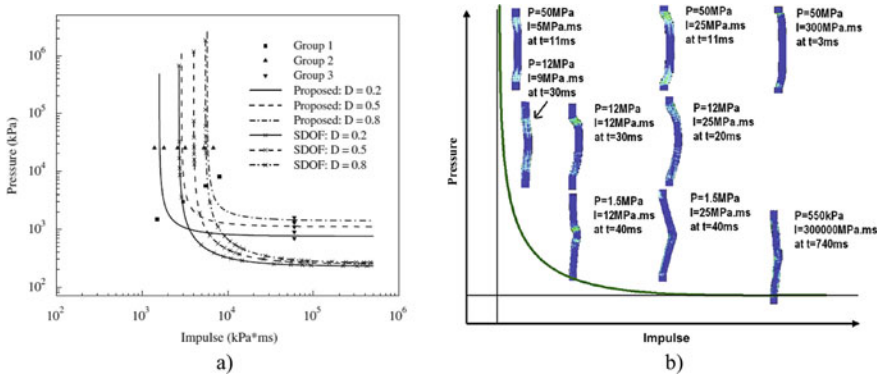


**Fig. 5.8** Pressure-Impulse diagrams for RC columns (4 m tall, 0.5 m × 0.5 m squared cross-section, $fc' = 40$ MPa, and $\rho = 0.01$): **a** un-strengthened and SDOF analysis; **b** damage modes of un-strengthened RC columns [21, 22]

P-I diagrams are also available which are generated from either SDOF model or comprehensive numerical modeling for RC columns. As shown in Fig. 5.8a, Shi et al. [21] derived P-I diagrams for RC columns with different design parameters, in which D = 0.2 represents minor damage with a remaining axial loading capacity of 80% after an explosive event, and D = 0.8 indicates severe damage with a remaining axial loading capacity of only 20%. Compared with those generated using SDOF methods, the diagrams from Shi et al.'s numerical method have similar impulse asymptotes as those from SDOF analysis in the impulsive region, but much higher pressure asymptotes in the quasi-static loading region. This is probably because the material idealization, the neglect of strain rate effects, and inability of modelling the combined shear and flexural damage in the SDOF approach underestimates the blast-loading resistance capacity of the column.

#### 5.3.1.1 Strengthening with FRP

To improve the blast resistance performance of RC columns, fibre reinforced polymer (FRP) can be applied as strips along the column, or wrap around the column, or combined. Figure 5.6a shows the failure modes of RC columns retrofitted with FRP under impulsive loading. The damage mode of the RC column strengthened with longitudinal FRP strips is similar to that of the un-strengthened RC column because FRP strips act as additional longitudinal reinforcements which mainly increase column flexural resistance capacity, but do not improve much of its shear resistance. FRP wraps could help to prevent the concrete from expanding, and therefore produce a tensile hoop stress imitating the behavior of a column with closely spaced stirrups. Therefore, FRP wraps increase the column shear resistance capacity. As shown in Fig. 5.6a (iii), the RC column strengthened with FRP wrap remains almost elastic with negligible damage, indicating the effectiveness of the FRP wrap on improving column shear resistance. When the column is subjected to a blast load in the quasi-static region (as shown Fig. 5.6b), the un-strengthened RC column fails primarily due to flexural damage. Both FRP strips and wraps increase the column capacity to resist such blast load. However, the FRP wrap is less effective because the response mode is primarily flexural, although FRP wrap confines concrete and increases column ductility. Therefore, applying both FRP strip and wrap together to strengthen RC columns could provide the best retrofitting performance to enhance column load-carrying capacity. Similarly, P-I diagrams are available for FRP strengthened RC columns [22].

### *5.3.2 RC Slabs*

The failure modes of RC slabs can be categorized into one-way and two-way slabs depending on the boundary condition and span ratio. Figure 5.9 illustrates the different failure modes of one-way and two-way slabs. For one-way slabs, at the

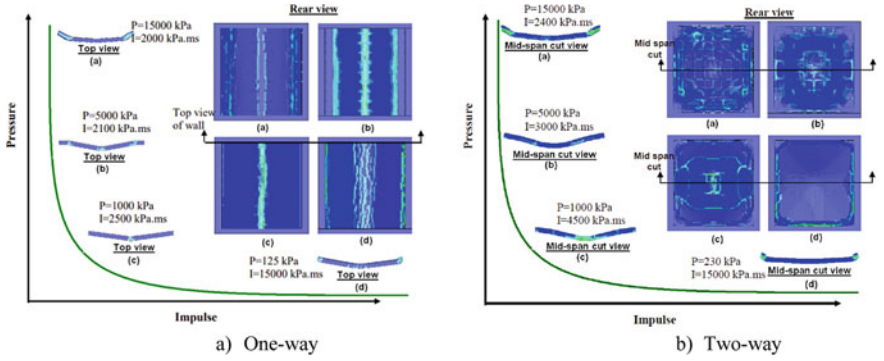


**Fig. 5.9** Damage modes of RC slabs [25]

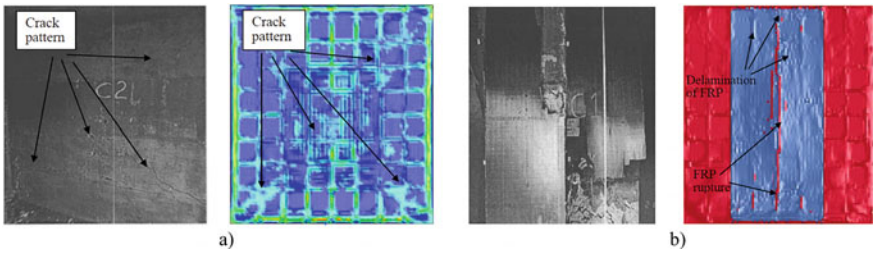


**Fig. 5.10** Comparison of **a** un-strengthened and **b** FRP strengthened RC slab/wall [26]

impulsive range, shear damage near the boundary dominates the failure of the slab when flexural bending deformation is negligible; in the dynamic range, combined shear and flexural failure modes dominate the failure mode; and in the quasi-static range, a maximum deflection is observed at mid-span of the slab which governs the failure of the slab. For two-way slabs, shear damage along the boundary is the primary failure mode in the impulsive range; the shear response becomes smaller and flexural deflection begins to develop with tensile tearing developed along the support due to negative bending moment when the slab is subjected to blast load in the dynamic loading range; in the quasi-static region, the mid-point deflection increases and the residual velocity causes transverse shear deformation at the support. From the failure modes, it can be found that the damage criteria based on flexural deflection at the mid-span may not reliably reflect the case when slab suffers shear damage. Based on intensive numerical modelling, P-I diagrams were generated for assessing the performance of RC slabs subjected to blast loading [25].

#### 5.3.2.1 Strengthening with FRP

Similarly, FRP can be applied to improve the blast resistance of RC slabs. Figure 5.10 compares the damage of RC slabs subjected to blast load with and without FRP strengthening. It was observed that the damage and cracks in the un-strengthened slab could be effectively mitigated by the application of FRP sheet [26]. Nevertheless, when applying FRP to strengthen a RC slab, a primary concern is debonding between the FRP and RC slab. The FRP-concrete bond strength is significantly affected by epoxy strength, consistency of epoxy thickness, quality of workmanship and concrete surface preparation. Figure 5.11 illustrates the different damages of FRP-strengthened RC slabs [26], from which it can be observed with a 2.8 MPa bond strength, almost the entire FRP sheet debonded from the RC slab when subjected to blast loading. When the bond strength increases to 5 MPa, both the FRP debonding and FRP rupture occur mainly at the mid-span of the slab. Only a very small delamination of FRP is observed when the bond strength is 10 MPa, hence a substantial increase in the blast resistance capacity of the slab is achieved. The above comparison clearly demonstrates the importance in reducing the debonding and maintaining the composite behavior of FRP strengthened slabs. Figure 5.11d depicts the damage of the slab when the FRP is anchored along its boundaries, where it can be found that FRP delamination is greatly reduced which improves the blast resistance of the slab. Nevertheless, when FRP is both anchored along its boundary and at mid-span, it leads to FRP rupture (Fig. 5.11e). These results indicate that proper anchorage for FRP to strengthen RC slabs is needed, but it should be noted that more anchorages are not necessarily always more beneficial. Similar to un-strengthened RC slabs, P-I diagrams were developed to assess the performance of FRP strengthened RC slabs [25].

### *5.3.3 P-I Diagrams*

The above studies showed the vulnerabilities of RC columns and slabs under blast loading and demonstrated the effectiveness of FRP strengthening in enhancing their

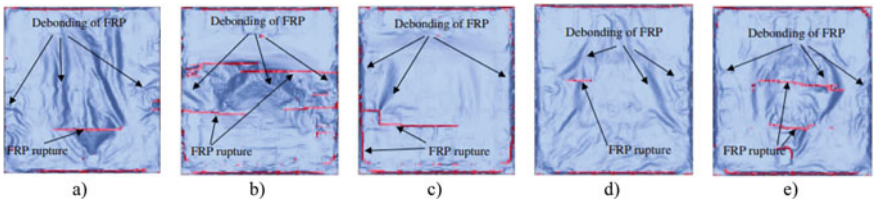


**Fig. 5.11** Damages of FRP-strengthened RC slabs with different FRP-concrete bond strengths, **a** 2.8 MPa; **b** 5 MPa; **c** 10 MPa; **d** 2.8 MPa with boundary anchorage; **e** 2.8 MPa with boundary and mid-span anchorages [26]

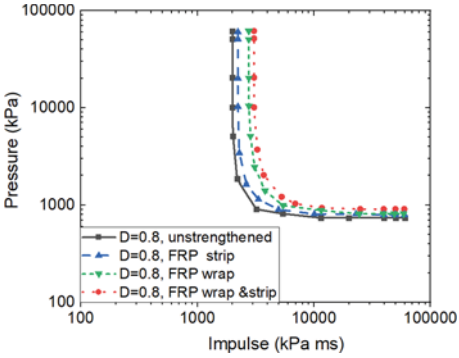


**Fig. 5.12** Comparison of P-I diagrams of un-strengthened and FRP strengthened RC columns [25]

blast resistance. Based on intensive numerical simulations, P-I diagrams and the corresponding formulae were developed to construct the P-I diagrams of different damage levels. The developed formulae are functions of structural dimension, material properties, with or without FRP strengthening and loading conditions. Detailed formulae and their applications can be found in [22, 25, 26]. Without loss of generality, considering a RC column of 4600 mm in height, 600 mm $\times$ 400 mm in cross-section, concrete strength of 40 MPa and the longitudinal and transverse reinforcement ratio of 0.01 and 0.003, respectively and yield strength of 550 MPa, FRP strength of 2280 MPa, longitudinal FRP strip of 1 mm thick and FRP wrap of 3 mm thick, the P-I diagrams of RC column with or without FRP strengthening subjected to the same axial load of 20% of column design axial load-carrying capacity are derived and shown in Fig. 5.12. It can be observed that strengthening the RC column with either FRP strips, or wraps could both effectively improve the blast resistance performance. In comparison to the un-strengthened RC column, both the impulse and pressure asymptotes are increased. Better strengthening effect could be achieved for the column with both FRP strip and wrap. Since it is relatively straightforward to apply FRP strengthening, and FRP has the advantages of light weight, high strength and does not prominently increase the structural size, FRP strengthening could be a good choice for strengthening structures to resist blast loadings for building protection.

## 5.4 Uncertainty and Reliability

The probabilities of terrorist bombing attack or accidental explosion on civilian structures are often low, but the consequence is enormous. Moreover, many uncertainties exist for blast load predictions and structural response calculations. Instead of using a large safety factor to account for uncertain variations, reliability analyses could be employed in design. In this section, uncertainties for blast load and reliability analysis of blast performances of RC columns and slabs with and without FRP strengthening are presented and discussed, which is followed by analysis on frame structures.

### 5.4.1 Blast Load

The variations of blast load are very significant because many factors may affect the shock wave propagation and interaction with structures. For instance, the blast load on structures could be affected by explosive material, detonation centre, charge shape, temperature, and humidity, and most prominently the interaction of shock with the surrounding environment, etc. Low and Hao [27] compared the peak reflected overpressures and positive phase duration of blast loads estimated from eight different sources including empirical relations, attenuation curves and computer tools, and found that the average coefficient of variation (COV) of peak reflected pressure in the scaled distance range of 0.24 m/kg$^{1/3}$ to 40 m/kg$^{1/3}$ is 0.3227, and that of positive loading duration is 0.130, indicating significant variations of the blast loadings estimated from different empirical relations. Using blast loads predicted from any of these empirical relations without considering the possible variations in analysis might not lead to accurate structural response predictions.

Considering the random variations of estimated peak reflected pressure and duration are scaled distance dependent, the mean and COV of the peak reflected pressure and duration estimated from empirical relations and design charts as a function of scaled distance are derived. Figure 5.13 shows the mean, standard deviation and COV, and their corresponding fitted functions of the peak reflected pressures. When the scaled distance is smaller than 1.0 m/kg$^{1/3}$ or larger than 10 m/kg$^{1/3}$, the variations are very significant, with the standard deviations comparable to the mean values and the COV approaches to 1.0. Therefore, ideally variations in blast loadings should be taken into consideration in predicting the structural responses. This is particularly

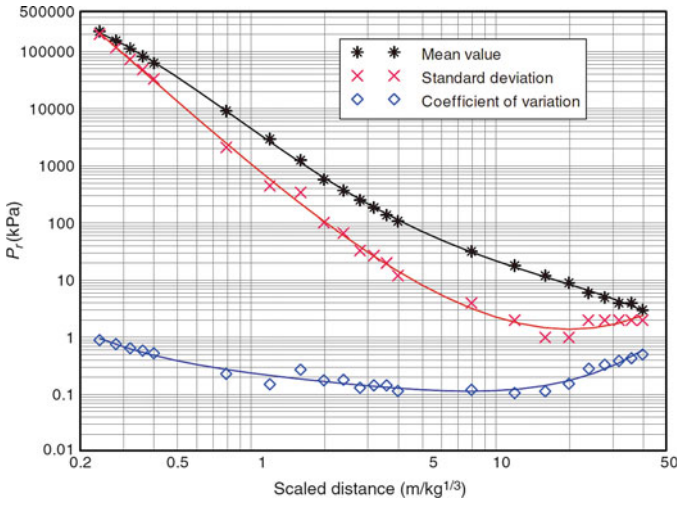


**Fig. 5.13** Mean, standard deviation and COV of the predicted peak reflected pressures and best fitted curves [29]

important for terrorist improvised explosive devices which have high variability of range and explosive mass (e.g., [28]).

## 5.4.2 *Structural Performance*

Owing to the workmanship, environmental condition and material deterioration, structural parameters such as stiffness, material strength and dimensions inevitably vary from their respective design values. Reliability and failure probability analyses of structural components to blast loading can be employed.

### 5.4.2.1 RC Columns

For RC columns, Hao et al. [30] carried out reliability analysis, where P-I diagrams corresponding to different column damage levels with consideration of random fluctuations of geometrical and material parameters were used to define column performances. The random variations of estimated blast loading are modelled as those described above. Figure 5.14 presents the results of an example column (column details shown in accompanying table). The failure probabilities of the RC column obtained by assuming deterministic RC column parameters are close to those obtained by considering random variations in both the blast loading and column parameters, whereas assuming deterministic blast loading results in very different predictions of column damage probabilities, indicating the statistical variations in blast loading estimations dominate the statistical variation effects on structural responses. However, these results are obtained because only the random variations in structural parameters induced mainly by construction quality control are considered. If considering structural property deterioration or poor construction quality, more intensive fluctuations of structural parameters are to be expected and different results might be observed.

Mean and COV of the example column

| | Mean | COV | Distribution |
|---|---|---|---|
| $\rho_s$ | *0.016* | 0.15 | normal |
| $\rho$ | 0.02 | 0.10 | normal |
| $f_{cu}$ (MPa) | 40 | 0.11 | normal |
| $d$ (mm) | 600 | 0.03 | normal |
| $b$ (mm) | 600 | 0.03 | normal |
| $H$ (mm) | 4600 | 0.03 | normal |

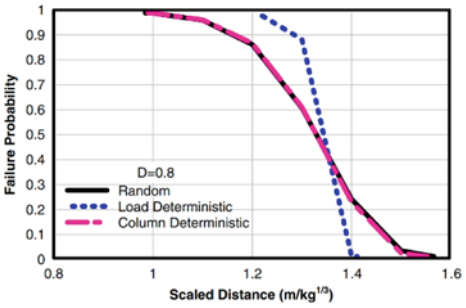


**Fig. 5.14** Failure probabilities of un-strengthened columns obtained by considering either blast loading or column parameters deterministically [30]

FRP could effectively improve the blast resistance capacity of RC columns, but significant variations in the effectiveness of FRP strengthening have been reported. Apart from the large uncertainties in blast loading and RC material properties, FRP properties and workmanship in preparation could also have a strong influence. Reliability analysis on the blast resistance capacity of FRP strengthened RC columns was conducted by [30], where the failure probabilities of columns corresponding to different damage levels were calculated. The statistical variations of blast loading, RC column dimension, longitudinal and transverse reinforcement ratio, and concrete, steel, and FRP material strength and FRP thickness were all considered. Figure 5.15 shows the failure probabilities of the un-strengthened column (as in Fig. 5.14) and FRP strengthened columns (details in Table 5.1). It can be found that FRP strengthening is effective in increasing the column blast resistance capacity. However, it has different influences on columns at different failure probabilities corresponding to different damage levels. Under minor damage (D = 0.2), increasing the FRP strength has an insignificant effect on column threshold failure probabilities, because only concrete experiences damage. Under moderate (D = 0.5) and severe damage levels (D = 0.8), both concrete and FRP are damaged. Increasing FRP strength and thickness therefore have pronounced effects on column failure probabilities.

Ultra-high Performance Concrete (UHPC) columns may also be used to help mitigate the effects of blast loads on structures. For example, Stewart and Li [31] found that for a UHPC column designed for blast the probability of major damage given an explosive blast load varies from $1 \times 10^{-2}$ to $1 \times 10^{-5}$ for explosive ordnance and terrorism blast scenarios. This provides a reasonable margin of safety against major structural damage.

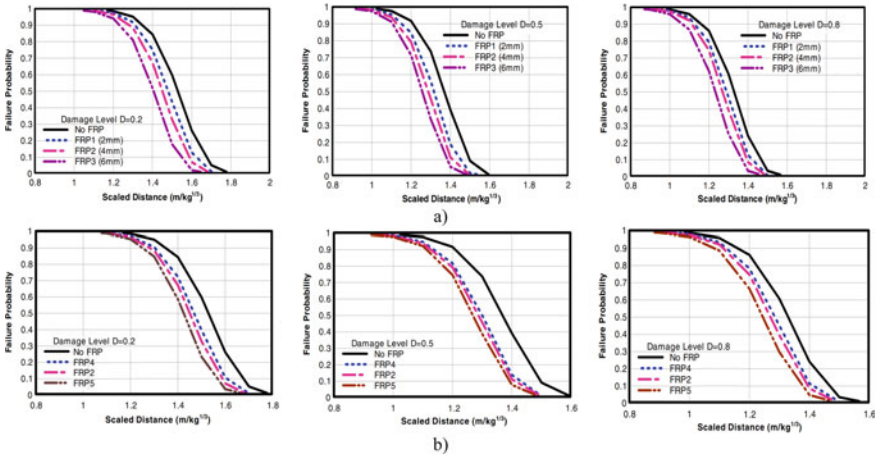


**Fig. 5.15** Failure probability of un-strengthened and FRP strengthened RC columns: **a** with different FRP thicknesses; **b** with different FRP strengths [30]

**Table 5.1** Mean and COV of the unstrengthened and FRP strengthened columns

| Column | $f_{strip}$ (MPa) | | | $f_{wrap}$ (MPa) | | | $t_{wrap}$ (mm) | | |
|---|---|---|---|---|---|---|---|---|---|
| | Mean | COV | Distribution | Mean | COV | Distribution | Mean | COV | Distribution |
| No FRP | – | – | – | – | – | – | – | – | – |
| FRP1 | 1700 | 0.05 | Normal | 1700 | 0.125 | Normal | 2 | 0.07 | Normal |
| FRP2 | 1700 | 0.05 | Normal | 1700 | 0.125 | Normal | 4 | 0.07 | Normal |
| FRP3 | 1700 | 0.05 | Normal | 1700 | 0.125 | Normal | 6 | 0.07 | Normal |
| FRP5 | 1000 | 0.05 | Normal | 1000 | 0.125 | Normal | 4 | 0.07 | Normal |
| FRP6 | 2400 | 0.05 | Normal | 2400 | 0.125 | Normal | 4 | 0.07 | Normal |

#### 5.4.2.2 RC Slabs

For RC slabs, Low and Hao [32] performed reliability analysis to predict the failure probabilities of the flexural and direct shear responses of one-way reinforced concrete slabs subjected to blast loading. The slab was simplified into 2-equivalent SDOF systems respectively representing flexural or shear failure modes. The failure probabilities and the boundary between direct shear and flexural failures as a function of the blast loading duration were determined. With a flexural dominated failure mode, the variation in the Young's modulus of concrete has the greatest influence on the failure probability. The yield strength of reinforcement has a smaller contribution while the crushing strength of concrete has the least effect. Parametric studies showed the length of the slab has no influence on the failure probability. Increasing slab thickness and the reinforcement ratio, and reducing the slab rigidity by changing its supporting conditions, all have positive effects on the performance of the flexural response of RC slabs. In a following study, Hao [33] carried out reliability analysis on the blast resistance capacity of RC slabs, where the limit state functions were derived using P-I diagrams developed in Mutalib [25]. Figure 5.16 illustrates the typical failure probabilities of one-way and two-way RC slabs subjected to blast loading of different scaled distances. Table 5.2 lists the slab design parameters and statistical variations of these parameters. Increasing the slab reinforcement ratio from 0.87 to 4.0% could effectively reduce slab failure probabilities.

For FRP strengthened RC slabs, Fig. 5.16 compares the failure probabilities of one-way and two-way slabs. FRP strengthening is very effective to protect RC slabs against blast loads. Applying a 1 mm thick layer is more effective than increasing the reinforcement ratio from 0.87 to 4.0%. However, any additional benefit by further increasing the FRP layer thickness to 2 and 3 mm is not prominent. Without FRP

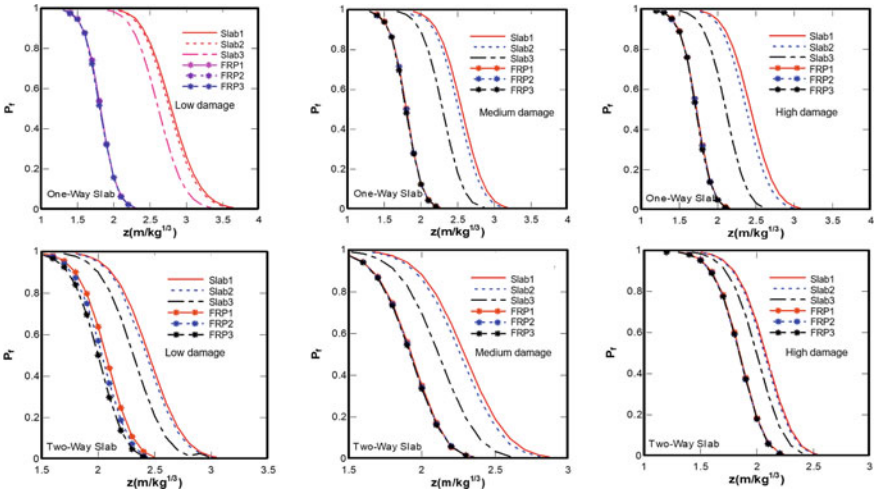


**Fig. 5.16** Failure probabilities of RC slabs with and without FRP strengthening [33]

**Table 5.2** Design and statistical parameters for RC slabs

| Slap | Reinforcement ratio $\rho$ (%) | Concrete strength $f_{cu}$ (MPa) | Slap thickness $D$ (mm) | Slap length $H$ (mm) | Slap with $b$ (mm) | FRP strength $f_{frp}$ (MPa) | FRP thickness $f_{frp}$ (mm) | FRP deboning strength $f_e$ (MPa) |
|---|---|---|---|---|---|---|---|---|
| *(a) Slab design parameters* | | | | | | | | |
| Slap1 | 0.87 | 30 | 200 | 2700 | 2500 | – | – | – |
| Slap2 | 1.4 | 30 | 200 | 2700 | 2500 | – | – | – |
| Slap3 | 4.0 | 30 | 200 | 2700 | 2500 | – | – | – |
| FRP1 | 0.87 | 30 | 200 | 2700 | 2500 | 2085 | 1 | – |
| FRP2 | 0.87 | 30 | 200 | 2700 | 2500 | 2085 | 2 | 2.8 |
| FRP3 | 0.87 | 30 | 200 | 2700 | 2500 | 2085 | 3 | 2.8 |

*(b) Statistical variations of slab parameters*

| Variation | $\rho$(%) | $f_{cu}$ | $d$ | $H$ | $B$ | $f_{frp}$ | $t_{frp}$ | $f_e$ |
|---|---|---|---|---|---|---|---|---|
| COV | 0.1 | 0.11 | 0.03 | 0.03 | | | | 0.1 |
| Disribution | Normal | Normal | Normal | Normal | Normal | Normal | Normal | Normal |

strengthening, the one-way RC slab with 0.87% reinforcement might experience some low damage when the scaled distance is about or less than 3.5 m/kg$^{1/3}$. With FRP strengthening, this scaled distance reduces to about 2.2 m/kg$^{1/3}$. Without FRP strengthening the slab will collapse when the scaled distance is less than or equal to about 2.0 m/kg$^{1/3}$, whereas it is about 1.3 m/kg$^{1/3}$ when the slab is strengthened with a FRP layer.

#### 5.4.2.3 Progressive Collapse Analysis

The preceding component reliability study can be extended to a system reliability analysis to estimate the progressive collapse probability of a structure when subjected to blast loading [30]. Using a 2-bay six-storey RC frame structure as an example, which is designed following Australian Standard [34, 35]. The dimension and detailed design parameters are provided in Fig. 5.17.

The failure of the frame structure can be evaluated using the column capacity corresponding to the different damage levels. Following the damage or failure of a column, if the imposed loading is larger than the capacity of the column, the system is remodelled, where load and moment redistributions are considered. The frame structure is deemed to collapse when the bending moment in the beam exceeds its capacity. Detail analysis can be found in [30]. The table in Fig. 5.18 shows the failure combinations of the frame as a result of column damage. For example, if the damage level of Column 1 is 0.5 or above, irrespective of the damage level of the other two columns, the structure will collapse. Combining the collapse combinations, system reliability analysis can be performed using the following equation

$$P_f = 1 - \prod_{i=1}^{3}(1 - P_{fi}) = 1 - (1 - P_{f1})(1 - P_{f2})(1 - P_{f3}) \tag{5.6}$$

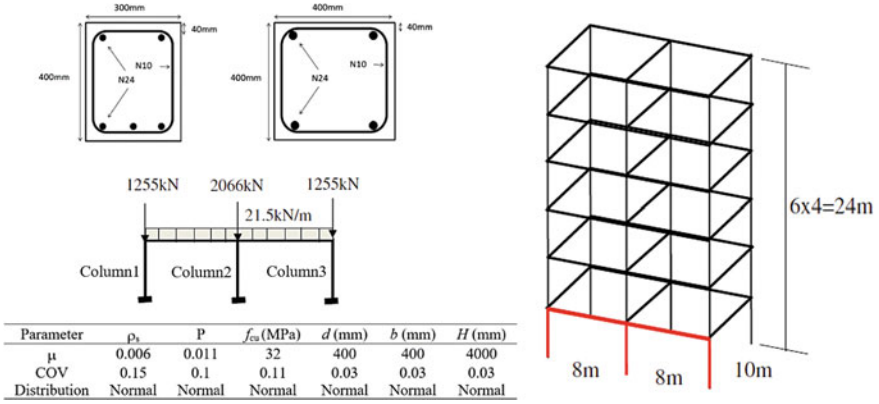


| Parameter | $\rho_s$ | P | $f_{cu}$ (MPa) | $d$ (mm) | $b$ (mm) | $H$ (mm) |
|---|---|---|---|---|---|---|
| μ | 0.006 | 0.011 | 32 | 400 | 400 | 4000 |
| COV | 0.15 | 0.1 | 0.11 | 0.03 | 0.03 | 0.03 |
| Distribution | Normal | Normal | Normal | Normal | Normal | Normal |

**Fig. 5.17** Example RC frame structure for reliability analysis [30]

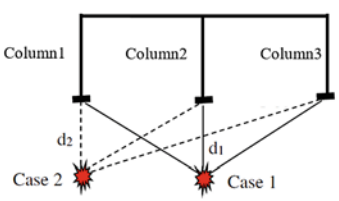


| Failure combination | Column1 | Column2 | Column3 |
|---|---|---|---|
| 1 | D≥0.5 | Any | Any |
| 2 | | D≥0.8 | Any |
| 3 | Any | Any | D≥0.5 |

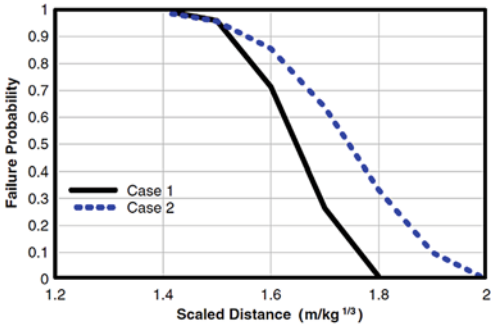


**Fig. 5.18** Collapse probabilities of the RC frame [30]

where $P_{fi}$ is the damage probability of the $i$th column.

Without loss of generality, two explosion cases as shown in Fig. 5.18 are considered. The collapse probability of the frame structure in these two explosion cases at different scaled distances by considering all parameters randomly can be calculated. As can be seen in Fig. 5.18, at a scaled distance smaller than 1.5 m/kg$^{1/3}$, both explosion scenarios give almost identical collapse probabilities; however, when the scaled distance is larger than 1.5 m/kg$^{1/3}$, Case 1 induces a lower collapse probability indicating a lower risk to the structure when explosion occurs at the centre of the structure. Similarly, the effectiveness of FRP strengthened structures in reducing the structural collapse probability can be analysed. More details can be found in reference [30]. The effect of column removal on progressive collapse probabilities is clearly an important area for research (e.g., [36–38]).

## 5.5 Summary

Effective protection of building structures against extreme loading from terrorist bombing attacks and accidental explosion incidents are important for the protection of people and property. This chapter summarizes existing design guidelines for blast protection of buildings. Different approaches for building protection against blast loads, including blast barriers and their effectiveness on reducing blast loading effects on structures are discussed. Commonly used analysis methods including blast loading estimations, simplified analysis and detailed numerical modeling of structural components are briefly presented and discussed. Building protection methodologies using FRP strengthening of structural components, and their effectiveness on enhancing blast loading resistant capacities of structures are discussed. Uncertainties to blast load prediction and reliability analysis of RC column and slab with and without FRP strengthening against blast loading are presented and discussed. Reliability analysis of structure progressive collapse due to structural element failure is also introduced.

## References


1. ASCE-42 (1985) Design of structures to resist nuclear weapons effects. *ASCE-42.* American Society of Civil Engineers, Engineering Mechanics Division
2. UFC-3-340-01 (2002) Design and analysis of hardened structures to conventional weapons effects. UFC-3-340-01. Department of Defense Washington, DC
3. FEMA-426 2003. Reference Manual to Mitigate Potential Terrorist Attacks against Buildings. *FEMA-426.* Federal Emergency Management Agency Washington, DC.
4. UFC-4-010-01 (2003) Minimum antiterrorism standards for buildings. UFC-4-010-01. Department of Defense, Washington, DC, USA: Department of Defense
5. FEMA-428 2003. Primer to design safe school projects in case of terrorist attacks. *FEMA-428.* Federal Emergency Management Agency Washington, DC
6. UFC-4-023-03 (2009) Design of buildings to resist progressive collapse. UFC-4-023-03. Department of Defense, Washington, DC, USA
7. GSA (2013) Alternate path analysis and design guidelines for progressive collapse resistance. General Services Administration
8. ASCE. Design of blast-resistant buildings in petrochemical facilities (2010) Task committee on blast-resistant design of the petrochemical committee of the energy division of american society of civil engineers
9. UFC-3-340-02 (2014) Structures to resist the effects of accidental explosions. UFC-3-340-02. Department of the Army, Navy and Air Force Technical Manual
10. ASCE-59-11 (2011). Blast protection of buildings. ASCE-59-11. American Society of Civil Engineers: American Society of Civil Engineers
11. Rose T, Smith P, Mays G (1998) Protection of structures against airburst using barriers of limited robustness. Proc Inst Civil Eng Struct Build 128:167–176
12. Zhou X, Hao H (2008) Prediction of airblast loads on structures behind a protective barrier. Int J Impact Eng 35:363–375
13. Niollet J, Yuen SCK, Nurick G (2015) A study to assess the use of cylindrical bars as blast barriers. Int J Protect Struct 6:263–286
14. Chaudhuri A, Hadjadj A, Sadot O, Ben-dor G (2012) Study of shock-wave mitigation through solid obstacles. In: 28th international symposium on shock waves. Springer, pp 493–498
15. Hao Y, Hao H, Shi Y, Wang Z, Zong R (2017) Field testing of fence type blast wall for blast load mitigation. Int J Struct Stab Dyn 17:1750099
16. Jin M, Hao Y, Hao H (2019) Numerical study of fence type blast walls for blast load mitigation. Int J Impact Eng 131:238–255
17. Zong R, Hao H, Shi Y (2017) Development of a new fence type blast wall for blast protection: numerical analysis. Int J Struct Stab Dyn 17:1750066
18. Gebbeken N, Warnstedt P, Rüdiger L (2018) Blast protection in urban areas using protective plants. Int J Protect Struct 9:226–247
19. Warnstedt P, Gebbeken N (2020a) Innovative protection of urban areas—experimental research on the blast mitigating potential of hedges. Landscape Urban Plann 202:103876
20. Gebbeken N, Döge T (2010) Explosion protection—architectural design, urban planning and landscape planning. Int J Protect Struct 1:1–21
21. Shi Y, Hao H, Li Z-X (2008) Numerical derivation of pressure–impulse diagrams for prediction of RC column damage to blast loads. Int J Impact Eng 35:1213–1227
22. Mutalib AA, Hao H (2011) Development of PI diagrams for FRP strengthened RC columns. Int J Impact Eng 38:290–304
23. Hao H (2015) Predictions of structural response to dynamic loads of different loading rates. Int J Protect Struct 6:585–605
24. Cui L, Zhang X, Hao H (2021) Improved analysis method for structural members subjected to blast loads considering strain hardening and softening effects. Adv Struct Eng 0:13694332211007382
25. Mutalib AA (2011) Damage assessment and prediction of FRP strengthened RC structures subjected to blast and impact loads. University of Western Australia

26. Mutalib AA, Hao H (2011) Numerical analysis of FRP-composite-strengthened RC panels with anchorages against blast loads. J Perform Constr Facil 25:360–372
27. Low HY, Hao H (2001) Reliability analysis of reinforced concrete slabs under explosive loading. Struct Saf 23:157–178
28. Stewart MG (2018) Reliability-based load factor design model for explosive blast loading. Struct Saf 71:13–23
29. Hao H, Stewart MG, Li Z-X, Shi Y (2010) RC column failure probabilities to blast loads. Int J Protect Struct 1:571–591
30. Hao H, Li Z-X, Shi Y (2016) Reliability analysis of RC columns and frame with FRP strengthening subjected to explosive loads. J Perform Constr Facil 30:04015017
31. Stewart MG, Li J (2021) Risk-based assessment of blast-resistant design of ultra-high performance concrete columns. Struct Safety 88:102030
32. Low HY, Hao H (2002) Reliability analysis of direct shear and flexural failure modes of RC slabs under explosive loading. Eng Struct 24:189–198
33. Hao H (2014) Reliability analysis of rc slabs with or without frp strengthening to blast loads. In: 23rd Australasian conference on the mechanics of structures and materials. Byron Bay, Australia
34. AS1170 (2011) Structural design actions. Standards Australia
35. AS3600 (2018) Concrete structures. Standards Australia
36. Beck AT, Da Rosa Ribeiro L, Valdebenito M (2020) Risk-based cost-benefit analysis of frame structures considering progressive collapse under column removal scenarios. Eng Struct 225:111295
37. Stewart MG (2017) Risk of progressive collapse of buildings from terrorist attacks: are the benefits of protection worth the cost? J Perform Constr Facil 31:04016093
38. Stewart MG (2021) Simplified reliability-based load design factors for explosive blast loading, weapons effects, and its application to collateral damage estimation. J Defense Model Simul. https://doi.org/10.1177/1548512920977737
39. Codina R, Ambrosini D, De Borbón F (2016) Experimental and numerical study of a RC member under a close-in blast loading. Eng Struct 127:145–158
40. Li M, Zong Z, Hao H, Zhang X, Lin J, Xie G (2019) Experimental and numerical study on the behaviour of CFDST columns subjected to close-in blast loading. Eng Struct 185:203–220

# Chapter 6
# Adaptation of Housing to Climate Change and Extreme Windstorms


**Hao Qin and Mark G. Stewart**

**Abstract** This chapter presents a probabilistic approach to assess the long-term economic risk and cost-effectiveness of relevant adaptation measures for Australian housing exposed to non-cyclonic extreme windstorms under a changing climate. The proposed method provides decision-support for the long-term adaptation of residential communities to extreme windstorms and climate change. The cost–benefit analysis suggests that, for all considered climate scenarios, strengthening roof cladding connections is not cost-effective, while improving window resistance or installing window shutters is more cost-effective.

## 6.1 Introduction

Non-cyclonic extreme windstorms (e.g. synoptic storms associated with low-pressure systems; severe thunderstorms) account for nearly 25% of annual economic losses caused by natural hazards in Australia [5] with substantial damage occurring to housing (e.g. [12, 16]). The three states, Victoria, Queensland and New South Wales, in the southeastern region of Australia have more than half of the country's population, where the residential communities are susceptible to damage from non-cyclonic extreme windstorms. For example, the 2008 Brisbane storms occurring on November 16 and 19 caused significant housing damage from high wind pressure, rainwater ingress, windborne debris, hailstones and fallen trees [16] with an estimated economic loss of $309 million [13]. The 2010 Victorian storms brought strong winds,

H. Qin (✉) · M. G. Stewart
Centre for Infrastructure Performance and Reliability, The University of Newcastle, Callaghan 2308, Australia
e-mail: hao.qin@newcastle.edu.au

M. G. Stewart
e-mail: mark.stewart@newcastle.edu.au

H. Qin
School of Civil Engineering, The University of Queensland, Brisbane 4072, Australia



M. G. Stewart and D. V. Rosowsky (eds.), *Engineering for Extremes*, Springer Tracts in Civil Engineering, https://doi.org/10.1007/978-3-030-85018-0_6

large hailstones, heavy rainfall and flood to the Greater Melbourne area during March 6–7 causing extensive property damage and approximately $1044 million loss [13].

To improve the resilience of residential communities, risk assessment for housing under extreme windstorms is evidently essential and the key to assessing the cost-effectiveness of relevant risk mitigation and reduction measures. For a stationary climate, the risk assessment generally includes the modelling of wind and associated environmental hazards (e.g. rainfall, storm surge), fragility assessment for structural and non-structural damage, and estimation of economic losses and vulnerability (e.g. Qin and Stewart [25]; Qin and Stewart [28]). Both aleatory and epistemic uncertainties are involved in these components of risk assessment and the outputs are the probabilistic distributions of economic losses at building component, single-building and community levels. The risk assessment can be conducted considering different risk reduction measures applied to housing, which enables the cost–benefit evaluation for windstorm mitigation (e.g. Qin and Stewart [26]).

The latest IPCC AR5 report released in 2013 [14] predicts that extreme windstorms generally become more intense under a changing climate leading to intensified wind, rainfall, storm surge and flooding associated with extreme wind events. However, climate change projections are subjected to large uncertainty, which highly depend on carbon emission scenarios and accuracy of general circulation models (GCM) [33]. When assessing the climate change impact on extreme windstorms in a regional scale for residential communities, the climate projections are more uncertain than those for a global scale due to localized weather and climate fluctuations. Therefore, climate change imposes significant uncertainty in assessing windstorm damage to housing and cost-effectiveness of risk mitigation and reduction measures in the long term. To suit the context of decision-making under climate change, 'risk mitigation and reduction' is hereafter rephrased as 'climate adaptation' [7, 33].

There are a considerable number of models available for tropical cyclones or hurricanes that can be applied to the risk assessment for residential buildings. These cyclone or hurricane models can integrate both the underlying physics and empirical relations to simulate landfall statistics and associated environmental hazards such as wind, rainfall and storm surge (e.g. [15, 17, 21, 36]). Moreover, these models typically include parameters depending on climate change, such as sea surface temperature (e.g. [18]), for which the climate projections are generally with relatively high confidence. On the other hand, the physical mechanisms for non-cyclonic extreme windstorms are complex and diverse, which include but are not limited to synoptic winds generated by extra-tropical depressions and severe local thunderstorms originated from convective effects [12]. To this end, in contrast to cyclones or hurricanes, it is not unexpected that there is a very limited number of models having the capacity to stochastically simulate the generation, track and intensity of non-cyclonic extreme windstorms that can be readily applied to the risk assessment for residential buildings. Climate change impact on concurrent extremes (e.g. wind speed and rainfall intensity) during non-cyclonic windstorms is also unclear [38].

Therefore, the risk assessment and climate adaptation for housing under non-cyclonic extreme windstorms face strong challenges mainly arising from highly uncertain climatic impact projections, and a lack of physics-based and empirical

models for non-cyclonic extreme windstorms. To overcome these difficulties, this chapter presents a probabilistic risk assessment (PRA) approach for housing exposed to non-cyclonic extreme windstorms, which enables the estimation of annual risks based on statistical modelling of the annual maximum windstorm intensity, and long-term economic risks under climate change based on possible carbon emission scenarios and climate projections. The proposed PRA approach provides an effective vehicle for the cost–benefit evaluation of relevant climate adaptation measures. Climate adaptations for reducing windstorm risks to housing include measures to either enhance the design during initial construction or retrofit (i.e. upgrade or strengthen) an existing house. According to post-disaster damage observations for suburban houses (e.g. [16]), the economic risks are primarily resulting from wind damage to the building envelope, and subsequent rainwater intrusion via breaches of building envelope causing damage to building interior and contents during non-cyclonic extreme windstorms. A set of climate adaptation measures are thus proposed to reinforce the building envelope against wind: (i) strengthening connections for metal roof cladding, (ii) installing shutters for windows, and (iii) improving window resistance. A case study is presented to assess economic risks from wind and rainfall hazards associated with non-cyclonic extreme windstorms for the representative contemporary housing in suburbs of Brisbane, Australia. Based on the PRA results, the cost-effectiveness of proposed climate adaptation measures is evaluated under possible scenarios of climate change impact, which offers decision-support for the long-term adaptation of residential communities to extreme windstorms and climate change.

## 6.2 Risk Assessment Under Climate Change

### *6.2.1 General Framework for Windstorm Risk*

The risk from extreme windstorms under a changing climate is expressed as [26, 32]

$$E(L) = \sum \Pr(C) \Pr(H|C) \Pr(DS|H) \Pr(L|DS) L \tag{6.1}$$

where $\Pr(C)$ is the annual probability that a specific climate scenario will occur, $\Pr(H|C)$ is the annual probability of a windstorm hazard conditional on the climate, $\Pr(DS|H)$ is the probability of a damage state conditional on the hazard (also known as fragility), $\Pr(L|DS)$ is the conditional probability of a loss given the occurrence of damage, and $L$ is the loss or consequence if full damage occurs. Wind speed is a representative parameter to characterize the intensity of a windstorm hazard. Other environmental hazards (e.g. rainfall, windborne debris, storm surge, hail, flood, etc.) may also be associated with or induced by extreme windstorms. If the loss refers to a monetary loss, then $E(L)$ represents an economic risk. The summation sign in

Eq. (6.1) refers to the summation of a number of possible climate scenarios, hazards, damage states and losses. If the probability that a specific climate scenario will occur, Pr($C$), is too uncertain, then a scenario-based analysis where climate scenario probability is decoupled from Eq. (6.1) is typically adopted for risk assessment and decision analysis (e.g. [26, 32, 34]).

### *6.2.2 Representative House in Brisbane*

The risk assessment framework described in Sect. 6.2.1 is concretized for the representative house in suburban Brisbane exposed to extreme wind and associated rainfall hazards. The representative contemporary house is a timber-framed brick-veneer construction with 21.5° timber roof trusses at 600 mm spacings on a complex hip-end roof. Windows are generally horizontal sliding aluminum or timber awning with a brick on edge or terracotta tiled window sill. Roof cladding is 762 mm wide corrugated metal sheeting. Metal top-hat battens are attached to timber roof trusses at 900 mm spacings. The dimension, shape and construction type of the representative house were determined by field surveys completed by the Cyclone Testing Station (CTS), James Cook University (JCU) (see Parackal et al. [19] for more details). Figure 6.1 shows the 3D and plan view of the representative one-storey house [19]. The design of structural members and components for the representative house subjected to wind loading is based on the design wind classifications specified in AS4055 [3] for different site conditions. According to AS 4055 [3], most suburban houses in Brisbane have a design wind classification of N2 or N3 excluding those built on the top-third zone of a hill, ridge or escarpment.

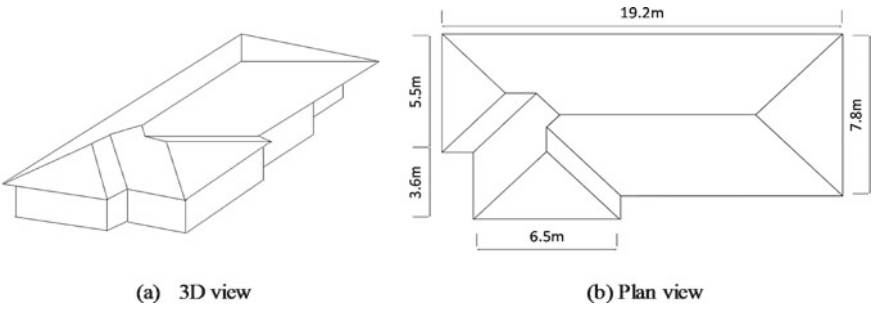


**Fig. 6.1** One-storey representative contemporary house

### 6.2.3 Economic Risks

The cumulative expected loss (or risks) over the 50-year service life of the representative house from 2020 to 2070 is given by

$$E(L) = \sum_{t=2020}^{2070} E_{annual}(t)/(1+r)^{(t-2020)} \tag{6.2}$$

where $E_{annual}(t)$ is the annual expected loss in year $t$, and $r$ is the discount rate. The annual risk, $E_{annual}(t)$ under a changing climate is given by

$$E_{annual}(t) = \int\int\int f(R_h, t|v, D_{ur}) f(v,t) f(D_{ur}) \frac{1}{n_d} \sum_{j=1}^{n_d} \left[ \Pr(DS|D_{Nj} T_N v, R_h, D_{ur}) \sum_{i=1}^{n_c} \Pr(L_i|DS) L_i \right] dv dR_h dD_{ur} \tag{6.3}$$

where $f(v, t)$ is the probability distribution of the annual maximum gust wind speed in year $t$, $f(R_h, t|v, D_{ur})$ is the probability distribution of the average rainfall intensity of a severe windstorm corresponding to a given duration $D_{ur}$ in year $t$, $f$ $(D_{ur})$ is the probabilistic distribution of the windstorm duration which is assumed to be independent of climate change, $n_d$ is the number of wind directions considered for wind damage assessment, $n_c$ is the number of components/subassemblies considered in the loss estimation, $\Pr(DS|v, R_h, D_{ur})$ is the probability of damage state (e.g. extent of roof damage, amount of rainwater intrusion) given the gust wind speed, rainfall intensity and storm duration, $D_{Nj}$ is the wind directionality factor, $T_N$ is the topographic factor, $S_N$ is the shielding factor, $\Pr(L_i|DS)$ is the loss likelihood for the $i$th component/subassembly for a given damage state, and $L_i$ is the maximum probable loss for the $i$th component/subassembly. It is noted that Eq. (6.3) assumes that damage is caused by the largest wind event in any calendar year, which will slightly underestimate damage risks in the event of a lesser damaging windstorm in the same year.

According to post-disaster damage observations (e.g. [16, 20]), the majority of losses to contemporary houses subjected to non-cyclonic extreme windstorms result from wind damage to roof and fenestrations (especially windows), and the subsequent rainwater intrusion causing damage to building interior and contents. The damage to other housing components (e.g. walls) is rare for contemporary houses in non-cyclonic regions of Australia. In light of this, the economic losses considered for the representative house arise from wind damage to metal roof cladding and timber roof framing, windward windows, and rainwater damage to building interior and contents as well as the loss of use (i.e. a total of six housing components/subassemblies are considered). The probabilistic risk assessment (PRA) method by Qin and Stewart [25] is employed to assess the annual economic losses through a Monte Carlo Simulation

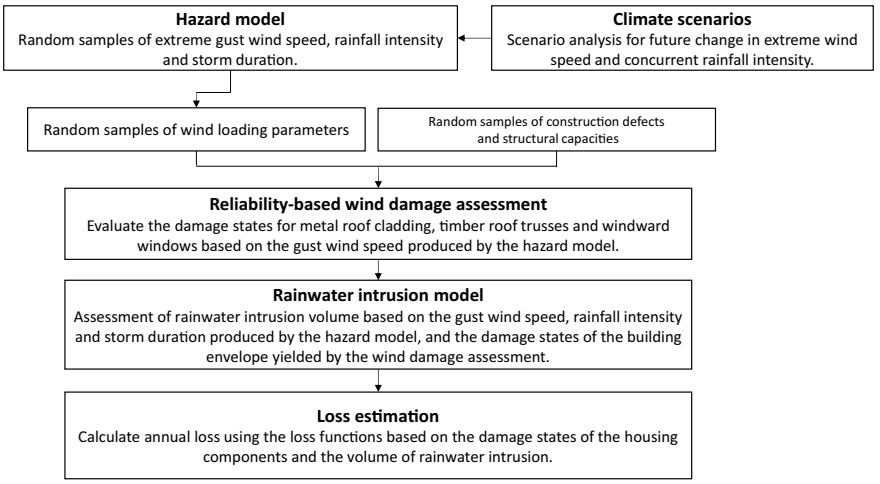


**Fig. 6.2** Outline of the risk analysis method under climate change

(MCS) analysis. This simulation-based risk assessment method consists of four major components, i.e. (i) hazard modelling for extreme wind and associated rainfall, (ii) reliability-based wind damage assessment for roof and windows, (iii) evaluation of rainwater intrusion, and (iv) loss estimation. The effect of construction defects on roof damage is also incorporated by randomly generating the defect rate and capacity reduction for defective roof connections in the MCS analysis [27]. The climate scenarios for wind and rainfall change in the future climate can also be included. Figure 6.2 shows an outline to illustrate the risk analysis method. The following sections describe each component of the PRA framework.

#### 6.2.3.1 Hazard Modelling

The hazard model of the simultaneous occurrence of extreme wind and rainfall is based on statistical analyses of regional meteorological data [25]. The peak gust wind speed, $v$ (m/s), is modelled by the Gumbel distribution [34, 37]. The cumulative distribution function (CDF) for annual maximum non-cyclonic gust wind speed is then given by

$$F_V(v) = e^{-e^{-\frac{v-v_g}{\sigma_g}}} \tag{6.4}$$

where $v_g$ and $\sigma_g$ are the location and scale parameter, respectively. The gust wind speed $v$ is the maximum 0.2 s gust velocity at 10 m height in Terrain Category 2 (open terrain defined in AS/NZS 1170.2 [4]). Figure 6.3 shows the relationship between gust wind speed and return period for Brisbane. The location and scale

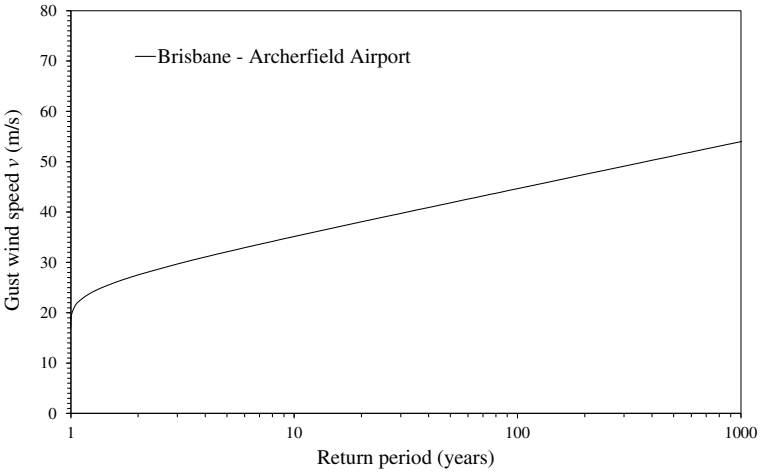


**Fig. 6.3** Extreme gust wind speed vs return periods for Brisbane

parameters are given as $v_g = 26.0326$, $\sigma_g = 4.0488$ according to statistical analysis of meteorological data by Wang et al. [37].

When assessing rainwater intrusion and the consequent damage to building interior and contents, it is ideal to have the joint probability of wind speed and rainfall intensity (e.g. [17] rather than treating these two weather variables independently. In addition, the average rainfall intensity ($R_h$) during a windstorm is typically dependent on the duration, e.g. intense burst of rainfall is more likely to occur in a short event. A two-parameter exponential distribution is adopted to model the windstorm duration ($D_{ur}$) with the CDF given by

$$F(D_{ur}) = 1 - e^{-\kappa(D_{ur}-\mu)} \tag{6.5}$$

where $\kappa$ and $\mu$ are the rate and location parameter, respectively.

A gamma distribution is used to model the average rainfall intensity during an extreme windstorm. The probability density function (PDF) of the gamma distribution is given by

$$g_a(R_h) = \frac{R_h^{\gamma-1} e^{\frac{R_h}{\beta(D_{ur})}}}{\Gamma[\gamma]\beta(D_{ur})^{\gamma}} \tag{6.6}$$

where $\Gamma(\cdot)$ is the gamma function, $\gamma$ is the shape parameter, and $\beta(D_{ur}) = a_0 + a_1(1/D_{ur})$ is the scale parameter which is assumed to have a linear relationship with the reciprocal of $D_{ur}$. Note that $R_h$ in Eq. (6.6) is greater than zero, and hence the gamma distribution is only used when rainfall concurs with strong winds. Accounting for the probability of no rain ($P_{no}$) during a windstorm, the CDF of $R_h$ ($R_h \geq 0$) is

given by

$$F(R_h) = P_{no} + (1 - P_{no})G_a(R_h) \tag{6.7}$$

where $G_a(R_h)$ is the CDF of the gamma distribution given by Eq. (6.6) to model the non-zero $R_h$, and $P_{no}$ can be estimated from the meteorological data.

The model parameters of the exponential and gamma distribution are estimated using the meteorological data from a weather station, i.e. Archerfield airport in Brisbane. A windstorm with the maximum gust wind speed greater than 36 knots (i.e. 18.5 m/s or 66.7 km/hr) is considered as an extreme wind. A total of 86 severe windstorms from 1996 to 2015 are then extracted from the meteorological data for Archerfield airport, and for each storm event, the duration and average rainfall intensity (accumulative rainfall depth divided by storm duration) are obtained. The number of storm events with no rain (i.e. $R_h = 0$) is also obtained to estimate $P_{no}$.

Figure 6.4 shows the exponential probability plots for $D_{ur}$, which suggests that the two-parameter exponential distribution given by Eq. (6.5) fits well to the storm duration data. It is estimated that $P_{no} = 25.6\%$ for Brisbane. The model parameters in the gamma regression formulation given by Eq. (6.6) are estimated using the generalized linear model in the **R** software package [29]. Figure 6.5 shows the mean and quantile values of $R_h$ produced by the gamma model as a function of $D_{ur}$. The average rainfall intensity data is also plotted in the same figure, which indicates that Brisbane tends to have windstorms with relatively short duration and intense rainfall (e.g. severe thunderstorms). Figure 6.5 suggests a good predictability of the gamma model to capture the average rainfall intensity during windstorms. Note that the estimated model parameters for $D_{ur}$ and $R_h$ can only be rigorously applied to the risk assessment for houses in the surrounding or nearby suburbs of Archerfield airport,

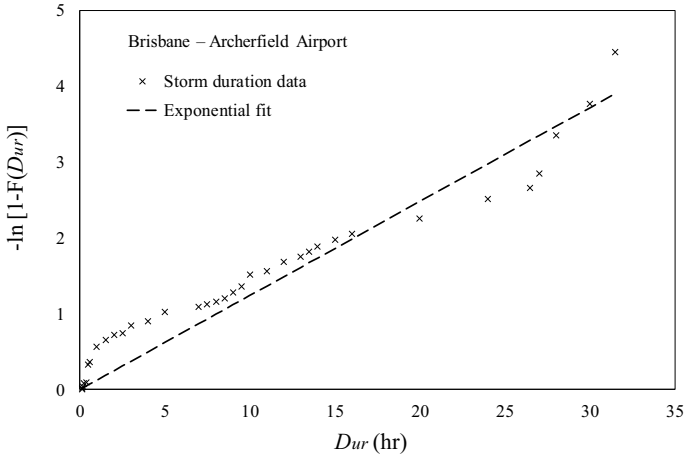


**Fig. 6.4** Exponential probability plots for storm duration $D_{ur}$

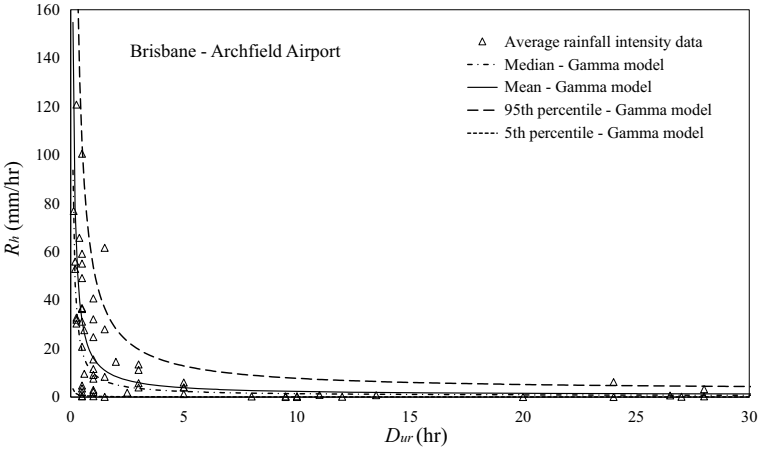


**Fig. 6.5** Average rainfall intensity $R_h$ from the observed data and gamma regression model

however it can be further extended to incorporate more weather stations in Brisbane, and account for the spatial variations and patterns of rainfall across the entire urban areas. The accuracy of estimation can be further improved by incorporating more years of data, if available.

#### 6.2.3.2 Climate Change Impact

Climate change influences extreme wind speed and associated rainfall intensity, and thus affects the risk assessment and climate adaptation for housing. The latest projections [8] for changes in extreme wind speed in Brisbane are summarised in Table 6.1 for medium and high $CO_2$ emission scenarios RCP 4.5 and RCP 8.5, respectively, to 2090. Note that the climate projections are relative to 1995 levels (1986–2005 average). A drying trend with declining annual average rainfall is predicted for Brisbane, while extreme rainfall is projected to become more intense due to increasing water-holding capacity of the atmosphere under a warmer climate [8]. However, the quantitative projections for rainfall concurred with extreme winds in a future climate are not available because the climate change impacts on extremes of compound events (e.g. simultaneous occurrence of extreme wind and rainfall) in Australia remains unclear [38]. A high level of uncertainty is also involved in

**Table 6.1** Climate projections for extreme wind speed (percentage change relative to 1995 levels) to 2090 under two $CO_2$ emission scenarios

| | RCP 4.5 | | | RCP 8.5 | | |
|---|---|---|---|---|---|---|
| | 10th | Median | 90th | 10th | Median | 90th |
| Wind speed change (%) | −8.0 | −1.5 | +1.0 | −5.0 | −2.0 | +2.0 |

the projected magnitudes of change in wind speed due to the limitation of general circulation models [33]. To this end, a scenario analysis is adopted for the future change in extreme wind speed and concurrent rainfall. The median, 10th and 90th percentile projections for wind speed change under RCP 4.5 and RCP 8.5 shown in Table 6.1 are used, and the changes in concurrent rainfall intensity to 2090 for all the wind speed change scenarios are assumed to be −20%, −10%, 0%, +10% and +20%. Information is scarce to non-existent on time-dependent changes in extreme wind speed and concurrent rainfall for Australia. A time-dependent linear change [34] is then assumed for both wind speed and rainfall intensity. These climate change scenarios can be applied to the extreme wind speed and concurrent rainfall intensity generated by the hazard modelling for current climate as described in Sect. 6.2.3.1. The climate change impact is then incorporated in the risk assessment given by Eqs. (6.2) and (6.3) based on a scenario analysis.

#### 6.2.3.3 Wind Damage

A reliability-based fragility method developed by Qin and Stewart [23] and Qin [24] is used to assess the wind damage to metal roof cladding, timber roof trusses and windward windows for the representative house. The fragility of the roof system is defined as the extent of the roof sheeting loss and the roof truss failures as a function of the peak gust wind speed. The fragility of windward windows is the probability of exceeding window resistances as a function of the peak gust wind speed. High wind pressure is considered to cause window damage, while windborne debris is less of a concern during non-cyclonic extreme windstorms [4]. Since the roof connections are generally the 'weakest links' of the roof system [10], the overloading of cladding-to-batten (CTB), batten-to-rafter/truss (BTR) and rafter/truss-to-wall (RTW) connections is considered as the limit states, the exceedance of which leads to the failure of roof cladding and trusses.

The uplift capacities for roof connections are modelled to follow a lognormal distribution [23]. For CTB and BTR connections, the uplift capacities are taken as the lower of the pull-out and pull-over strengths, and the uplift capacities for triple grip RTW connections fastened using hand nails and gun nails are the peak loads in the load–deflection curves obtained from experiment tests [31]. Note that the RTW connections are different for houses with design wind classifications of N2 and N3, while the CTB and BTR connections are identical for N2 and N3 designs. The window resistance includes the ultimate strength and water penetration resistance. According to AS 2047 [2], windows shall not fail when tested under the ultimate limit state pressure, and shall have no penetration of uncontrolled water when tested under the water penetration resistance test pressure. The ultimate glazing strength and water penetration resistance of windows are assumed to follow a normal distribution. The ultimate strength and water penetration resistance statistics for windows are different for N2 and N3 design wind classifications (see Qin [24] for detailed statistics). The spatially varying wind uplift pressures acting on the roof surface and windward windows are calculated from the peak gust wind speed and the wind

loading parameters mainly including the terrain and height factor, shielding factor, wind directionality factor, external and internal pressure coefficients, etc. All the wind loading parameters are modelled as random variables with mean-to-nominal ratios and coefficient of variation (COV) values given in Qin and Stewart [23] and Qin [24]. The corresponding nominal values of these factors can be obtained from AS/NZS 1170.2 [4] for different site conditions. See Qin and Stewart [23] and Qin [24] for more details about roof connection and window resistances as well as the probabilistic wind loading modelling.

Two typical scenarios are assumed for the internal pressurization in the roof fragility analysis, i.e. (i) dominant openings existing on windward wall and (ii) without any wall openings. These two scenarios depend on whether there are damaged windward windows, the probabilities of which are obtained from the windward window fragility. The MCS to evaluate wind fragility for windward windows is straightforward that both the window resistances and wind pressures acting on windward windows are randomly generated from corresponding probability distributions. In each simulation run, whether the wind pressure exceeds the window resistances is checked, and fragility curves are then obtained for the windward windows. A MCS analysis in conjunction with the FE approach are employed to evaluate the wind fragility for roof cladding and trusses under the two wall opening scenarios, which enables the stochastic characterization of spatially varying wind uplift pressure, structural demands and resistances for roof connections, failure progression and load redistribution, and evolution of internal pressure with increasing sheeting loss. A total of 75 roof sheets, 17 trusses, and 1646 CTB, 532 BTR and 38 RTW connections are involved in the MCS analysis and FE approach. In each run of the MCS, the spatially distributed wind pressures and structural resistances of roof connections are randomly generated as the input to the FE model of the roof system. The wind uplift loads acting on all roof connections are then obtained from the FE analysis, and a single connection is deemed to fail if the wind load exceeds the connection resistance. Any overloaded (failed) CTB, BTR and RTW connections are then deactivated in the FE model, and the FE analysis is further conducted to evaluate the load redistribution and failure progression of other connections. The damage states for metal roof sheeting and timber roof trusses can then be obtained from the fragility assessment. The MCS and FE approach enables the development of two fragility curves: (i) the extent of roof sheeting loss, and (ii) proportion of roof truss failures. Refer to Qin and Stewart [23] and Qin [24] for more details about the MCS analysis, FE approach and fragility analysis. The occurrence of construction defects reduces the wind resistance of housing components and thus increases housing vulnerability. The construction defects are generally difficult to quantify due to the complex mechanism of human error and a lack of relevant data. Qin and Stewart [27] developed a probabilistic model for construction defects in roof connections, which systematically integrates the human reliability analysis method, engineering judgement and limited construction error data through a Bayesian approach. This construction defects model is further incorporated in the reliability-based fragility method to account for the effects of construction error on wind damage to the roof. The mean proportions of roof sheeting loss and roof truss failures produced by the

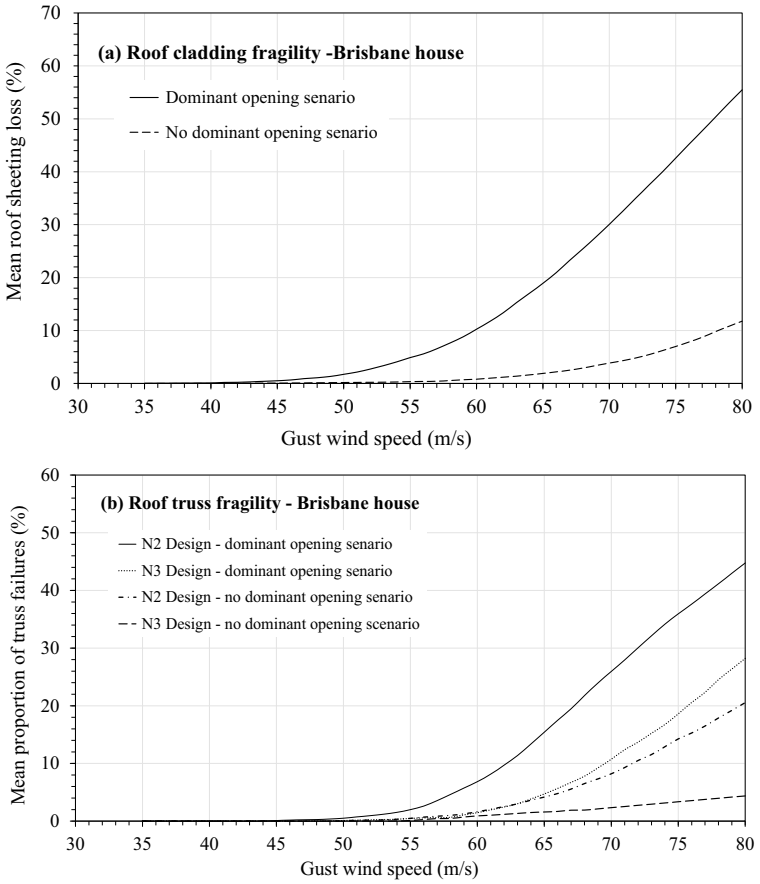


**Fig. 6.6** Mean proportions of roof sheeting loss and roof truss failures vs gust wind speed

roof fragility assessment for the representative house are shown in Fig. 6.6. The fragility curves for windward windows are shown in Fig. 6.7.

#### 6.2.3.4 Rainwater Intrusion

The volumetric rate of rainwater intrusion is mainly dependent on the wind speed, rainfall intensity, and damage states of the building envelope (especially roof and windows). A semi-empirical rainwater intrusion model [21, 35] is modified by Qin and Stewart [25] and adapted to quantify the amount of rainwater intrusion into the damaged metal roof and windward windows for the representative house in Brisbane. The quantification of rainwater intrusion is also conducted under the two wall opening scenarios: (i) presence of windward wall dominant openings, and (ii) absence of any wall openings. For the windward dominant opening scenario, the main source of

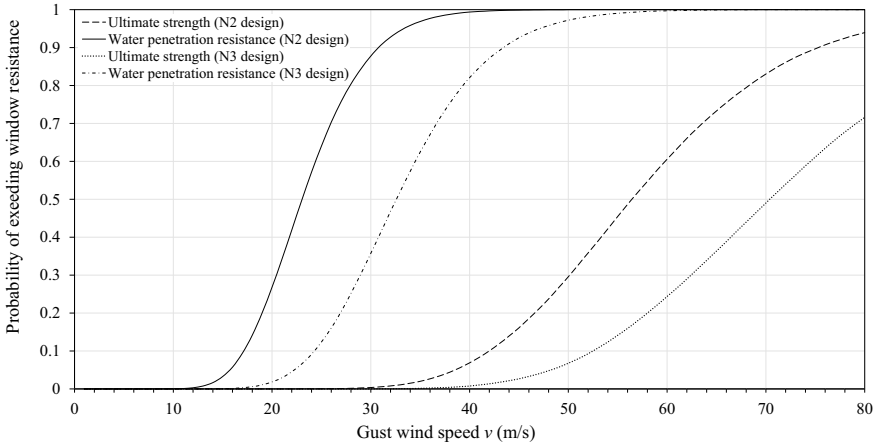


**Fig. 6.7** Fragility curves for windward windows

rainwater intrusion considered is water entering from roof and window breaches. For the scenario without any wall openings, rainwater is considered to enter through roof breaches and gaps around undamaged windward windows when the water penetration resistance of window is exceeded. The number and locations of failed roof sheets at a given wind speed obtained from the reliability-based fragility assessment described in Sect. 6.2.3.3 are subsequent used in the MCS analysis by applying the semi-empirical rainwater intrusion model. The total volumetric rate of rainwater intrusion can then be obtained. The volume of rainwater intrusion is calculated by the multiplication of the volumetric rate and the rainfall duration after wind damage. See Qin and Stewart [25] for more details about the quantification of rainwater intrusion. Figure 6.8 shows the mean volumetric rate of rainwater intrusion as a function of both the gust wind speed and rainfall intensity for the two wall opening scenarios. This figure suggests that the mean rainwater intrusion rate increases with wind speed and rainfall intensity. The nonlinearity of rainwater intrusion with increasing wind speed is because there is more roof sheeting loss at a higher wind speed allowing for more water ingress.

#### 6.2.3.5 Loss Estimation

The loss estimation uses an assembly-based approach (e.g. [9, 22]). The representative house is divided into components/subassemblies based on specific building details as shown in Table 6.2. The loss estimation takes into account the direct losses from wind damage to windward windows, metal roof cladding and timber roof framing, and the losses to building interior and contents caused by subsequent rainwater intrusion as well as the loss of use.

The losses are estimated in terms of cost ratios, which is defined as the ratio of the cost to complete the subassembly to the building value. The estimated total

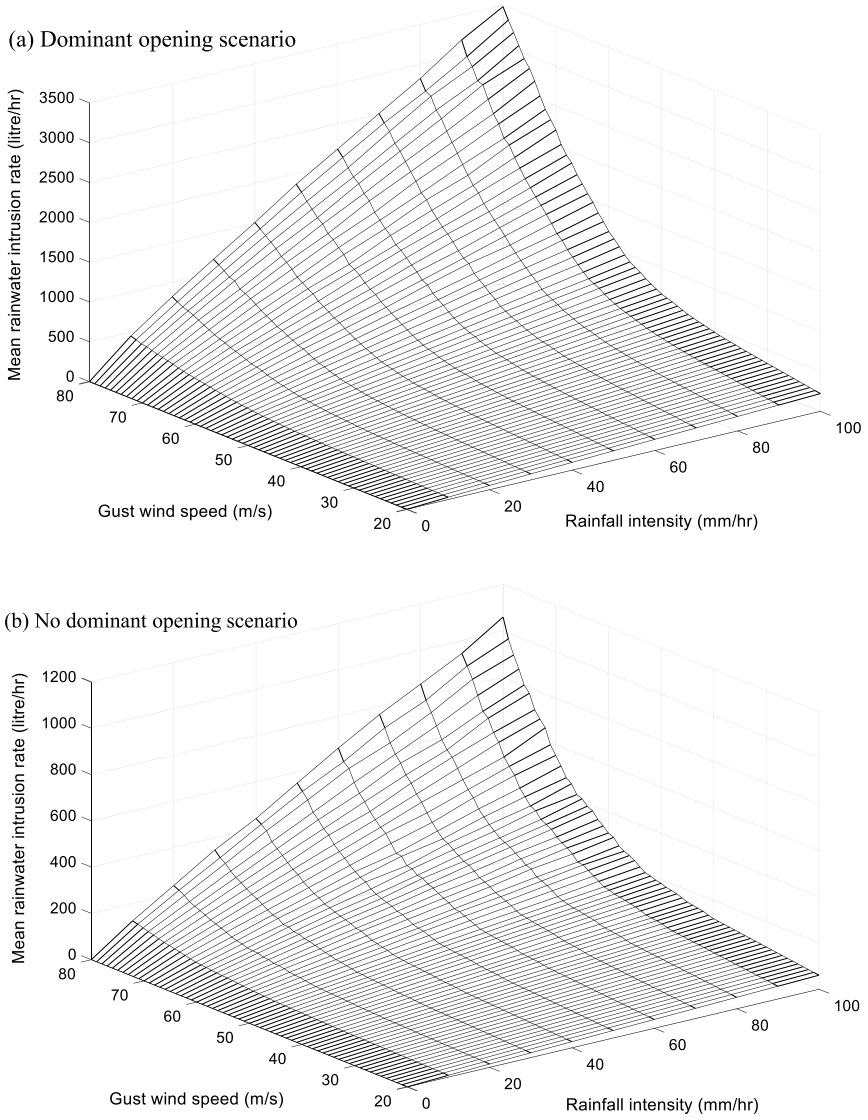


**Fig. 6.8** Mean volumetric rate of rainwater intrusion

cost to build a new representative house with an approximate floor area of 150 $m^2$ is $L_{building}$ = \$300,000 Australian Dollars [11]. Based on cost data provided by Australian housing cost guides [30] and subjective judgement, the subassembly cost ratios for new construction are estimated for a representative house built to an average standard. The cost ratios are adjusted to account for the additional costs associated with removal, repair and remodelling of an existing house [9]. The adjusted cost ratios

**Table 6.2** Subassembly cost ratios for the representative house

| Subassembly | | Description | Cost ratio (%) | Adjusted cost ratio (%) |
|---|---|---|---|---|
| Roof | Roof cladding | Mainly including corrugated metal roof sheets, metal top-hat battens and insulation | 4.1 | 5.4% |
| | Roof framing | Timber trusses, rafters, ceiling joists, fixings, etc | 15.9 | 20.9% |
| Windward windows | | Single glazed, aluminum sliding or awning windows | 0.8 | 1.0% |
| Internal finishes, fittings | Wall | Mostly plasterboard, also include ceramic tiles and painting | 6.8 | 51.2% (building interior) |
| | Floor | Mixed use of timber, carpet and ceramic tiles | 3.5 | |
| | Ceiling | Mostly plasterboard, also including painting | 4.7 | |
| | Fittings and fixtures | Built-in wardrobes/cupboards, kitchen units, bathroom suites, shelving, internal doors, etc | 10.0 | |
| Mechanical | | Air conditioning, heaters, ventilation, etc | 10.0 | |
| Electrical | | Lighting, conduits, cables, etc | 4.0 | |
| Other | | Site preparation, foundation, wall framing, other fenestrations, plumbing, etc | 37.0 | n/a |

are also given in Table 6.2. The building interior herein includes internal finishes and fittings, mechanical and electrical systems. The cost ratio of contents is estimated to be 25% of the building value [1].

The empirical loss functions are given by Qin and Stewart [25] to relate economic losses with the damage states of housing components, which are mainly based on engineering judgement and existing loss models given in HAZUS [9]. The losses to roof cladding and framing are directly expressed as a function of the roof damage states, whereas the building interior and contents losses are expressed as a function of the amount of rainwater intrusion, which is indirectly related to roof cladding and window damage. The window losses are estimated based on the window damage model described in Sect. 6.2.3.3. The proportions of roof sheeting loss and roof truss

failures are obtained from the reliability-based fragility assessment as described in Sect. 6.2.3.3. The loss function for loss of use is taken from HAZUS [9] which is a function of the expected total building loss. See Qin and Stewart [25] for more details about the loss functions.

#### 6.2.3.6 Cumulative Risks for Climate Scenarios

The annual economic risks by Eq. (6.3) are calculated using the simulation-based PRA method considering various climate scenarios for the change in extreme wind and concurrent rainfall. The cumulative risks over the 50-year service life of the representative house from 2020 to 2070 are then obtained using Eq. (6.2). Figure 6.9 shows the cumulative expected losses to 2070 for the representative house in Brisbane with N2 and N3 designs under different climate scenarios. Compared to the scenario with no change in wind speed and concurrent rainfall, the worst climate scenario considered herein, i.e. +2% change in wind speed (RCP 8.5–90th percentile) and + 20% change in concurrent rainfall intensity, increases the cumulative expected loss only modestly by 4.6% and 4.7% respectively for N2 and N3 designs. Compared to the most favourable climate scenario herein, i.e. −8% change in wind speed (RCP 4.5–10th percentile) and −20% change in concurrent rainfall intensity, the cumulative expected losses to 2070 corresponding to the worst climate scenario are up to 16.9% higher.

## 6.3 Cost-effectiveness of Climate Adapation

### *6.3.1 Climate Adaptation Measures*

The adaptation measures proposed for the representative house mainly aim to protect roof and windows from high wind pressure, and thus reduce rainwater intrusion and damage to building interior and contents. The fragility analysis in Sect. 6.2.3.3 show that wind damage to roof cladding is highly likely to occur for the representative house in Brisbane. The failure of metal roof sheets can further incur rainwater intrusion through the roof breaches, though the direct loss from roof cladding damage is limited due to a small cost ratio as shown in Table 6.2. Window breakage by high wind pressure creates windward dominant openings, which allows for more rainwater intrusion and roof damage due to significantly increased internal pressure. Rainwater intrusion via small gaps around undamaged windows may also occur when the water penetration resistance of window is exceeded. Therefore, strengthening roof cladding and windows not only decreases the direct losses from wind damage to the building envelope, but also reduce the amount of rainwater intrusion.

To this end, three climate adaptation measures are proposed herein: (i) increase of uplift capacities for roof cladding connections (RF), (ii) protection of windows by

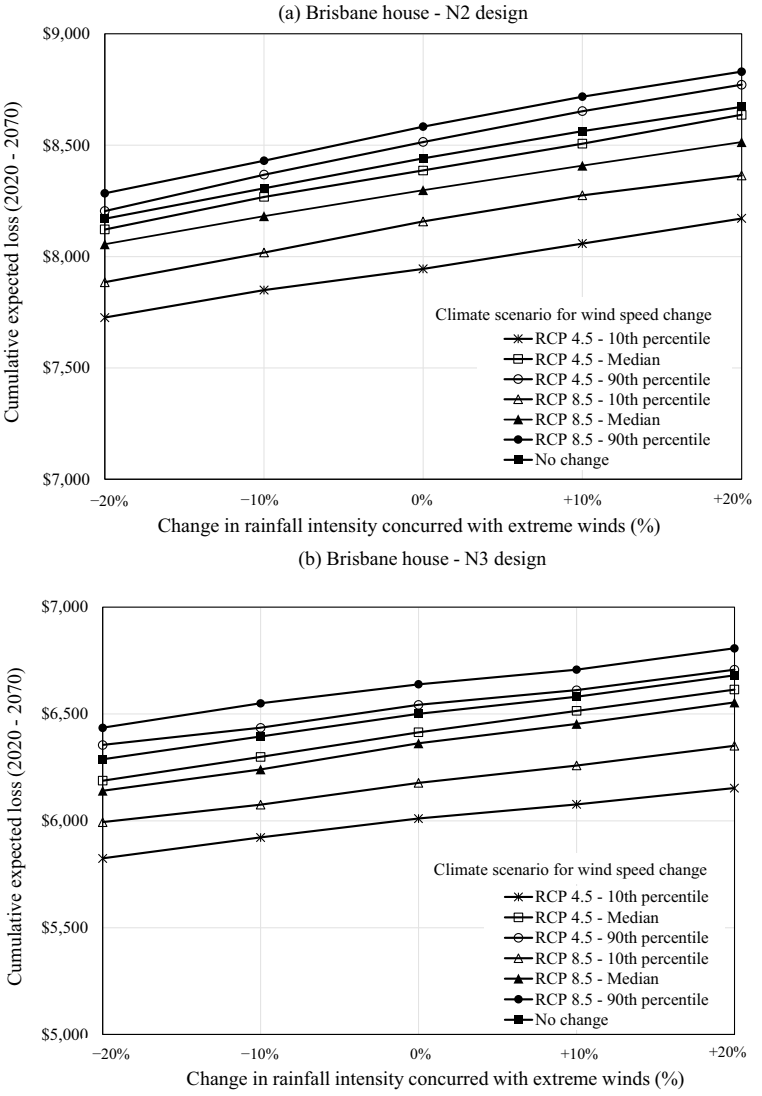


**Fig. 6.9** Cumulative expected losses to 2070 under different climate scenarios

shutters (WS), and (iii) improvement of window resistances (WR). Table 6.3 summarizes the proposed climate adaptation measures. The adaptation cost (normalized by building value) and the improved performance due to the adaptation measure (i.e. benefit) are also shown in Table 6.3. The adaptation measures applied at the initial design and construction are RF and WR, whereas window shutters (WS) can be installed at any time during the service life to retrofit an existing house. The cost is the additional money spent on the adaptation measure, which is considered as a

**Table 6.3** Climate adaptation measures for the representative house in Brisbane

| Housing component | Adaptation measure | Description | Cost (%) | Benefit |
|---|---|---|---|---|
| Roof cladding | **RF**. Strengthen roof cladding connections | Increase BMT of metal roof sheets from 0.42 to 0.48 mm, and upgrade the screw fastener from M6–11 to 14–12 | 0.7 | Improve the uplift capacities of CTB connections with the mean pull-over and pull-out capacity increased by 25% and 7% respectively |
| Window | **WS**. Install shutters | Cyclone-rated steel roller shutters tested for wind pressure up to 2500 Pa | 2.0 | Reduce wind pressure and the amount of wind-driven rain acting on windows by 50–100% [26], and hence decrease the probability of windward dominant openings |
| | **WR**. Improve window resistance | Increase the window rating to a higher level (N2 to N3, N3 to N4) | 0.4 | Increase the mean ultimate strength and water penetration resistance of windows by up to 100%, see Qin and Stewart [26] for more details |

one-off expense. The adaptation costs presented in Table 6.3 are estimated from an Australian housing construction cost guide [30].

### *6.3.2 Cost–benefit Analysis*

The cost-effectiveness of a climate adaptation measure is evaluated based on the net present value (NPV), which is calculated as

$$\text{NPV} = E(L)\Delta R + \Delta B - C_{\text{adapt}} \tag{6.8}$$

where $\Delta R$ is the reduction in risk due to the adaptation measure, $E(L)$ is the risk for the house without any adaptation measures (i.e. 'business as usual') given by Eq. (6.1), $\Delta B$ is the co-benefit of adaptation such as reduced losses to other hazards, increased energy efficiency, etc., and $C_{\text{adapt}}$ is the cost for climate adaptation. For an adaptation measure, $\Delta R$ can vary from 0 to 100%. If the adaptation measure is applied at the initial design/construction stage, $C_{\text{adapt}}$ is the extra money spent on a stronger design/construction. For retrofitting, $C_{\text{adapt}}$ is the cost to remove the

old housing component, if applicable, plus the cost to upgrade the component. The present chapter focuses on climate adaptation for extreme windstorms, and therefore the quantification of $\Delta B$ is not included. The NPV is a dependent variable mainly due to the variability of $\Delta R$ that can be assessed by the PRA approach and climate scenarios described in Sect. 6.2.3. The confidence bounds of NPV or the probability of NPV > 0 can also be calculated (e.g., [32]).

It is noted that Eq. (6.8) can be generalised for any time period, discounting of future costs and detailed time-dependent cost and damage consequences. Hence, for the representative house during a 50-year service life from 2020 to 2070, $E(L)$ in Eq. (6.8) is the cumulative risks calculated by Eq. (6.2) and the corresponding risk assessment results are given in Sect. 6.2.3.6. The cumulative risks corresponding to a given climate adaptation measure can be obtained by incorporating the benefit of the adaptation measure (see Table 6.3) into the risk assessment. The risk reduction $\Delta R$ can then be calculated by comparing the cumulative risks with and without implementing the adaptation measure. See details in Qin and Stewart [26]. The results suggest that installing window shutters (WS) is the most effective adaptation measure that the mean $\Delta R$ is approximately 95%. Strengthening roof cladding connections (RF) provides up to 9% and 4% mean risk reduction respectively for the representative house with N2 and N3 designs, while improving window resistance (WR) offers up to 55% and 12% mean risk reduction respectively for the representative house with N2 and N3 designs under various climate scenarios. The cost–benefit analysis in this chapter is based on a maximum expected net benefit/return criterion for risk-neutral decision-makers, and hence only the mean NPV is of interest. If the mean NPV is greater than zero, then the corresponding climate adaptation measure is deemed as cost-effective. The cost–benefit assessment results are shown in Table 6.4. This table suggests that strengthening roof cladding connections (RF) is not cost-effective for the representative house with both N2 and N3 designs under all considered climate scenarios. Improving window resistance (WR) is cost-effective for the Brisbane house with N2 design but not cost-effective for the N3 design under all considered climate scenarios. Installing window shutters (WS) is cost-effective for the N2 design under all considered climate scenarios, while for the N3 design, the cost-effectiveness depends on climate scenarios. As shown in Fig. 6.10, the mean NPV to 2070 corresponding to shutter installation for the representative house with N3 design generally increases as the climate impact on extreme wind speed and concurrent rainfall intensity becomes more adverse. Under the RCP 4.5–10th percentile scenario for wind speed change, installing window shutters (WS) is not cost-effective regardless of the possible change in concurrent rainfall intensity considered herein. Under the RCP 8.5–10th percentile scenario for wind speed change, installing window shutters (WS) is only cost-effective when the concurrent rainfall intensity increases in a future climate. Installing window shutters (WS) is cost-effective for most climate scenarios other than RCP 4.5–10th percentile and RCP 8.5–90th percentile. Compared to the most favourable climate scenario considered herein, the mean NPV to 2070 under the worst climate scenario are approximately $1000 higher. Whether to adopt a climate adaptation measure under this situation depends on how decision makers weigh the possible climate scenarios and

**Table 6.4** Mean NPV and cost-effectiveness assessment for the representative house in Brisbane

| Adaptation measure | Design wind classification | Mean NPV | Cost-effective? |
|---|---|---|---|
| **RF**. Strengthen roof cladding connections | N2 | Less than zero for all considered climate scenarios | No |
| | N3 | Less than zero for all climate scenarios | No |
| **WS**. Install shutters | N2 | Greater than zero for all considered climate scenarios | Yes |
| | N3 | Greater than zero for some considered climate scenarios, whereas less than zero for other climate scenarios. See Fig. 6.10 | Depends on climate scenario |
| **WR**. Higher window rating | N2 | Greater than zero for all considered climate scenarios | Yes |
| | N3 | Less than zero for all considered climate scenarios | No |

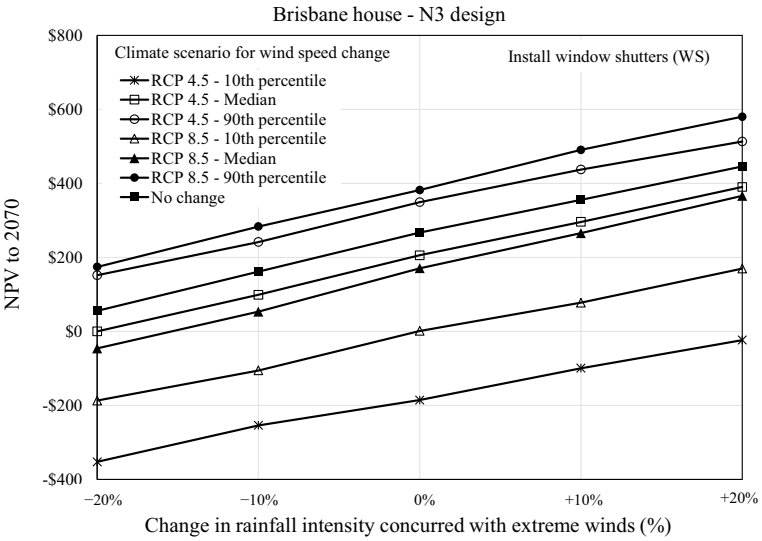


**Fig. 6.10** Mean NPV to 2070 corresponding to shutter installation for the representative house with N3 design under different climate scenarios

the decision makers' risk appetite towards disaster risks under climate change (e.g. [6, 28]).

## 6.4 Summary

This chapter presents a probabilistic risk assessment (PRA) approach for housing exposed to non-cyclonic extreme windstorms, which enables the estimation of annual economic risks based on statistical modelling of the annual maximum windstorm intensity, and long-term economic risks under climate change based on possible climate scenarios. This simulation-based risk assessment method consists of four major components, i.e. (i) hazard modelling for extreme wind and associated rainfall, (ii) reliability-based wind damage assessment for roof and windows, (iii) evaluation of rainwater intrusion, and (iv) loss estimation. The effect of construction defects on roof damage is also incorporated. The climate scenarios for wind and rainfall change in the future climate are included to examine the climate change impact. A set of climate adaptation measures are subsequently proposed aiming to reinforce the building envelope against wind: (i) strengthening roof cladding connections, (ii) installing shutters for windows, and (iii) improving window resistance. A case study is presented to assess long-term economic risks from wind and rainfall hazards associated with non-cyclonic extreme windstorms for the representative contemporary housing in suburbs of Brisbane, Australia. Based on the PRA results, the cost-effectiveness of the proposed climate adaptation measures is evaluated under possible climate scenarios according to the mean net present value (NPV). The cost–benefit analysis suggests that, for all considered climate scenarios, strengthening roof cladding connections is not cost-effective, while improving window resistance is cost-effective for the Brisbane house with a design wind classification of N2 but not cost-effective for the house with a design wind classification of N3. Installing window shutters is cost-effective for the Brisbane house with a N2 design, while its cost-effectiveness for the house with a N3 design depends on the considered climate scenarios.

When the cost-effectiveness of an adaptation measure varies with climate scenarios, whether to adopt this adaptation measure depends on how decision makers weigh the possible climate scenarios and the decision makers' risk appetite towards disaster risks under climate change. The PRA method and cost–benefit analysis presented in this chapter provide decision-support for long-term adaptation of residential communities to extreme windstorms and climate change.

## References

1. ABS (2011) Australian social trends December 2011: components of household wealth. Australian Bureau of Statistics, Canberra, Australia

2. AS 2047 (2014) Windows and external glazed doors in buildings. Standards Australia, Sydney
3. AS 4055 (2012). Wind loads for housing. Standards Australia, Sydney
4. AS/NZS 1170.2 (2011) Structural design actions, part 2: wind actions, Standards Australia, Sydney
5. BITRE (2008) About Australia's regions. Bureau of Infrastructure, Transport and Regional Economics, Canberra, Australia
6. Cha EJ (2018) Discrepancy in perceived hurricane risks in a changing climate. Nat Hazard Rev 19(2):04018002
7. Contento A, Xu H, Gardoni P (2019) Risk analysis for hurricanes accounting for the effects of climate change. In: Bastidas-Arteaga E, Stewart MG (eds) Climate adaptation engineering: risks and economics for infrastructure decision-making. Butterworth-Heinemann, UK
8. Dowdy A et al (2015) East coast cluster report, climate change in Australia projections for Australia's natural resource management regions: cluster reports. In: Ekström M et al (eds) CSIRO and Bureau of Meteorology. Australia
9. HAZUS (2014) Multi-hazard loss estimation methodology—hurricane model. In: Hazus-MH (ed) 2.1 Technical Manual, Federal Emergency Management Agency, Mitigation Division, Washington, DC
10. Henderson DJ, Ginger JD (2007) Vulnerability model of an Australian high-set house subjected to cyclonic wind loading. Wind Struct 10(3):269–285
11. HIA (2018) Window into housing 2018. The Housing Industry Association, Canberra, Australia
12. Holmes JD (2015) Wind loading of structures, 3rd edn. CRC Press Boca Raton, Florida, USA
13. ICA (2012) Catastrophe disaster statistics. Insurance Council of Australia, Sydney, Australia
14. IPCC (2013) Climate change 2013: the physical science basis. In: Stocker TF, Qin D, Plattner G-K, Tignor M, Allen SK, Boschung J, Nauels A, Xia Y, Bex V, Midgley PM (eds) Contribution of working group I to the fifth assessment report of the intergovernmental panel on climate change. Cambridge University Press, Cambridge and New York, NY, USA
15. Lee KH, Rosowsky DV (2007) Synthetic hurricane wind speed records: development of a database for hazard analyses and risk studies. Nat Hazard Rev 8(2):23–34
16. Leitch C, Ginger J, Harper B, Kim P, Jayasinghe N, Somerville L (2009) Investigation of performance of housing in Brisbane following storms on 16 and 19 November 2008. Technical Report No. 55. Cyclone Testing Station, James Cook University
17. Mudd L, Rosowsky D, Letchford C, Lombardo F (2017) Joint probabilistic wind–rainfall model for tropical cyclone hazard characterization. J Struct Eng 143(3):04016195
18. Mudd L, Wang Y, Letchford C, Rosowsky D (2014) Assessing climate change impact on the US East Coast hurricane hazard: temperature, frequency, and track. Nat Hazard Rev 15(3):04014001
19. Parackal KI, Humphreys MT, Ginger JD, Henderson DJ (2016) Wind loads on contemporary Australian housing. Aust J Struct Eng 17(2):136–150
20. Parackal KI, Mason M, Henderson D, Stark G, Ginger J, Somerville L, Harper B, Smith D, Humphreys M (2015) Investigation of damage: Brisbane, 27 November 2014 severe storm event. Technical Report No. 60. Cyclone Testing Station, James Cook University
21. Pita G, Pinelli JP, Cocke S, Gurley K, Mitrani-Reiser J, Weekes J, Hamid S (2012) Assessment of hurricane-induced internal damage to low-rise buildings in the Florida Public Hurricane Loss Model. J Wind Eng Ind Aerodyn 104:76–87
22. Porter KA, Kiremidjian AS, LeGrue JS (2001) Assembly-based vulnerability of buildings and its use in performance evaluation. Earthq Spectra 17(2):291–312
23. Qin H, Stewart MG (2019) System fragility analysis of roof cladding and trusses for Australian contemporary housing subjected to wind uplift. Struct Saf 79:80–93
24. Qin H (2020) Risk assessment and mitigation for Australian contemporary houses subjected to non-cyclonic windstorms. PhD thesis, The University of Newcastle, Australia
25. Qin H, Stewart MG (2020a) Wind and rain losses for metal-roofed contemporary houses subjected to non-cyclonic windstorms. Struct Saf 86:101979
26. Qin H, Stewart MG (2020b) Risk-based cost-benefit analysis of climate adaptation measures for Australian contemporary houses under extreme winds. J Infrast Preserv Resilience 1(1):1–19

27. Qin H, Stewart MG (2020c) Construction defects and wind fragility assessment for metal roof failure: a Bayesian approach. Reliab Eng Syst Saf 197:106777
28. Qin H, Stewart MG (2021) Risk perceptions and economic incentives for mitigating windstorm damage to housing. Civ Eng Environ Syst 38(1):1–19
29. R Core Team (2019). R: a language and environment for statistical computing. R Foundation for Statistical Computing. Vienna, Austria. http://www.R-project.org/
30. Rawlinsons (2015) Rawlinsons construction cost guide 2015. Rawlinsons Publishing, Perth, Australia
31. Satheeskumar N, Henderson DJ, Ginger JD, Wang CH (2016) Wind uplift strength capacity variation in roof-to-wall connections of timber-framed houses. J Archit Eng 22(2):04016003
32. Stewart MG (2015) Risk and economic viability of housing climate adaptation strategies for wind hazards in southeast Australia. Mitig Adapt Strat Glob Change 20(4):601–622
33. Stewart MG, Bastidas-Arteaga E (2019) Introduction to climate adaptation engineering. In: Bastidas-Arteaga E, Stewart MG (eds) Climate adaptation engineering: risks and economics for infrastructure decision-making. Butterworth-Heinemann, UK
34. Stewart MG, Ginger JD, Henderson DJ, Ryan PC (2018) Fragility and climate impact assessment of contemporary housing roof sheeting failure due to extreme wind. Eng Struct 171:464–475
35. Straube JF, Burnett EFP (2000) Simplified prediction of driving rain on buildings. In: Proceedings of the international building physics conference. Eindhoven, Netherlands
36. Vickery PJ, Skerlj PF, Twisdale LA (2000) Simulation of hurricane risk in the US using empirical track model. J Struct Eng 126(10):1222–1237
37. Wang CH, Wang X, Khoo YB (2013) Extreme wind gust hazard in Australia and its sensitivity to climate change. Nat Hazards 67(2):549–567
38. Zscheischler J, Westra S, Zhang X et al (2018) Future climate risk from compound events. Nat Climate Change 8:469–477

# Chapter 7
# Risk-Based Management of Electric Power Distribution Systems Subjected to Hurricane and Tornado Hazards


**Yue Li, Abdullahi M. Salman, Abdullah Braik, Sirrý Bjarnadóttir, and Babak Salarieh**

**Abstract** Extreme events, especially weather-related events, are the leading cause of power outages in many countries around the world. Hurricanes and tornadoes are especially destructive and have caused billions of dollars in direct losses due to damage to power systems and indirect losses due to power outages. There is, therefore, a need to implement risk management strategies to reduce such losses and ensure that power systems are reliable and resilient. This chapter presents a framework for risk management of electric power distribution systems subjected to hurricane and tornado hazards. Methods for hazard analysis and component- and system-level risk analysis are discussed. Two case studies are presented to demonstrate the application of the framework. Various risk mitigation strategies such as the use of alternative pole material, targeted hardening of systems, regular preventive maintenance, and enhancement of design are considered in the case studies. Risk and cost-benefit analysis methods are presented to evaluate the effectiveness of the various mitigation strategies. A methodology for optimizing the preventive and corrective maintenance of distribution poles to reduce risk and minimize cost is also presented.

Y. Li (✉)
Department of Civil and Environmental Engineering, Case Western Reserve University, Cleveland, OH 44106, USA
e-mail: yxl1566@case.edu

A. M. Salman · B. Salarieh
Department of Civil and Environmental Engineering, The University of Alabama in Huntsville, Huntsville, AL 35899, USA

A. Braik
Engicon, Amman, Jordan

S. Bjarnadóttir
Department of Civil and Environmental Engineering, University of Iceland, Reykjavik, Iceland



M. G. Stewart and D. V. Rosowsky (eds.), *Engineering for Extremes*, Springer Tracts in Civil Engineering, https://doi.org/10.1007/978-3-030-85018-0_7

## 7.1 Introduction

Extreme events such as hurricanes, storms, tornadoes, floods, earthquakes, and fires are the leading cause of power outages around the world. Hurricanes and tornadoes are among the most destructive extreme events that can cause extensive damage to power systems resulting in prolonged outages. For example, after hurricane Maria in 2017, it took more than five months for about 90% of customers in Puerto Rico to be reconnected to the power distribution systems. Hurricane Sandy in 2012 caused power outrage for about 10 million residents. In the same year, more than 730,000 homes and businesses along the gulf coast were left without electricity after Hurricane Isaac. In 2011, Hurricane Irene left approximately 6 million residents without power along the east coast of the U.S., causing an estimated $5–7 billion in damages [28].

Tornadoes are another cause of frequent power outages. Tornadoes are columns of air in contact with cumulonimbus clouds and the Earth's surface, rotating rapidly and violently. Although tornadoes could occur anywhere on Earth, they are more common in the U.S. Goliger and Milford [20], where Tornado Alley and Florida are the most tornado active regions [29]. Despite tornadoes being one of the most violent extreme events, there is still a lack of research focusing on the impact of tornadoes on infrastructure such as power systems, which is mainly due to their low probability of occurrence. However, after the occurrence of many strong tornadoes in the last few years (such as in Tuscaloosa, Alabama and Joplin, Missouri in 2011; Moore and El Reno in Oklahoma in 2013; Nashville in Tennessee in 2020) that resulted in billions of dollars in damage and social disruption, it became necessary to better understand the behavior of tornadoes and their interaction with buildings and infrastructures.

This chapter focuses on the management of risk posed by hurricanes and tornadoes to power distribution systems. A brief description of power systems is first presented. This is followed by a description of the hurricane and tornado hazards analysis methods, the risk assessment process, and common risk mitigation strategies to reduce damage to power systems. Two case studies on hurricanes and tornadoes are then presented.

## 7.2 Electric Power Systems

Electric power systems are subdivided into generation, transmission, and distribution subsystems as shown in Fig. 7.1. The transmission system transports bulk power through high voltage conductors supported by steel lattice towers, H-frame towers, or single poles, which can be wood, steel, or concrete. The distribution system is the downstream part of the system that transports power to the customers. Distribution lines consist of two systems, the structural support system (single-pole structures) and the wire system (conductors, third-party attachments such as telecom wires, ground wires). The structural support system supports the loads from the wires and provides resistance to lateral loads due to wind on the wire system. All three subsystems of the

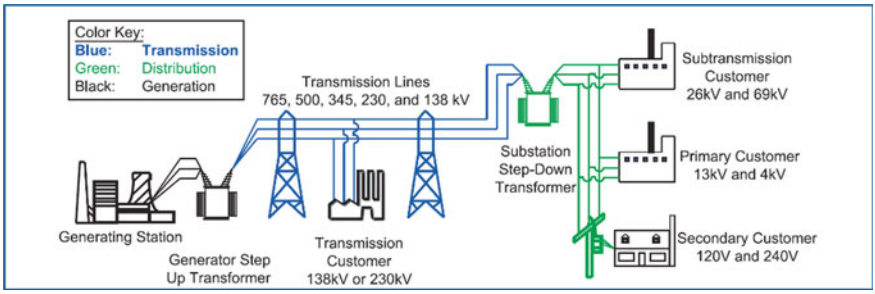


**Fig. 7.1** Basic structure of the electric power system [17]

electric power system can be susceptible to damage due to extreme events, especially hurricanes and tornadoes. However, the distribution subsystem is typically the most vulnerable [16] because:

i Distribution poles are designed to a lower standard compared to transmission structures.
ii There are more miles of distribution lines exposed to hurricane winds.
iii Distribution system rights-of-way are typically narrower compared to transmission systems, which leads to more treefall-related damage.

In a survey of the damage to distribution and transmission structures by Brown [12] for storms in Texas, the most common causes of damage were found to be strong wind, falling trees, and flying debris. Foundation failures have also been observed in some instances [21].

## 7.3 Hazard Analysis

Hazard analysis for structures and infrastructure systems can be carried out in two ways: probabilistic analysis and scenario-based analysis. Probabilistic analysis considers the aggregated effect of all possible hazard levels. In a probabilistic analysis, hazard levels are weighted by their respective probability of occurrence. In a scenario-based approach, the effect of a specific hazard level is considered (e.g., 200-year return period hurricane or an EF 3 tornado). Application of probabilistic hazard analysis to spatially distributed infrastructure systems has been shown to be limited because the spatial variation of intensity is lost in the aggregation process of probabilistic analysis. The probabilistic approach, however, allows risks to be annualized which is essential in decision making regarding long-term investment in mitigation strategies.

### 7.3.1 Hurricane Hazard Analysis

In probabilistic hurricane analysis, historical hurricane records are used to develop probability density functions for key hurricane parameters such as location of origin, translation speed, heading angle, central pressure, and radius to maximum wind location. The wind speeds from the simulation are then modeled using an extreme value distribution which can be used to calculate the probability of exceeding a certain wind speed in a given period. Weibull distribution has been shown to be appropriate for modeling hurricane annual maximum wind speeds [23].

Scenario-based hurricane hazard analysis can be carried out using historical hurricanes. Hurricane track data and recorded wind speeds for historical hurricanes can be obtained from the North Atlantic Hurricane Database (HURDAT) compiled by the National Oceanic and Atmospheric Administration [30]. The spatial variation of the wind speed can be considered by using a wind-field model which will give the wind speed at any distance from the hurricane eye at any given time.

### 7.3.2 Tornado Hazard Analysis

Using probabilistic hazard analysis for tornadoes could result in underestimating the frequency of tornadoes in a region, and more importantly, the vulnerability of a spread-out power distribution system. This is because the probabilities of occurrence of all tornado scales are relatively low, and they become extremely low for strong tornadoes of EF4 and EF5 ratings. When comparing the number and ratings of tornadoes hitting a region with the probabilities of occurrence obtained from current hazard maps, it is clear that the high frequency of tornadoes is not reflected in the hazard maps because of the small path area of tornadoes. For this reason, tornado risk-based studies in tornado-active regions are better performed using scenario-based analysis [10].

Tornado scenarios can be created by assuming the tornado intensity scale (Enhanced Fujita (EF) category), starting point, and path angle. Using these assumptions, the tornado total path width and length can be estimated using historical data. Data has been systematically gathered for tornadoes since the 1950s by the National Weather Service (NWS), and statistics based on this data for the length and width of 40,000 tornadoes that occurred in the United States between 1973 and 2011 can be found in [41]. These statistics can be used to model the width and length of each EF tornado scale as random variables.

## 7.4 Risk Assessment and Management

### *7.4.1 Component-Level Risk Assessment*

Risk assessment of power distribution systems under extreme winds can be approached at a component-level or system-level. In component-level risk assessment, risk is evaluated for the system's components that are vulnerable or critical to the continued functionality of the system during hazard events. However, the impact of a component failure on system performance is not explicitly evaluated. The most vulnerable components of distribution systems under extreme wind events are the support structures (poles). Hence, utility companies have focused on implementing strategies to mitigate the risk to distribution poles.

One of the most common distribution pole materials is wood. As a natural material, wood is susceptible to decay over time due to fungal attack. The rate of decay is site- and material-specific and affected by factors such as wood specie, climatic conditions (temperature, rainfall, humidity), soil properties, initial preservative treatment, and nature of the fungal attack. Examples of decay models for wood poles include Wang et al. [43] model and [24] model. The vulnerability of the poles is quantified using fragility analysis performed using Monte Carlo Simulation. The limit state function for the fragility analysis is given by Eq. (7.1).

$$G(t) = R(t) - S(t) \tag{7.1}$$

where $G(t)$ is the limit state function; $R(t)$ is the time-dependent strength of the poles; and $S(t)$ is the time-dependent load demand (i.e. bending stress) at the ground line caused by hurricane wind load. To get the stress demand, $S(t)$, at the ground line, the wind force acting on the pole and the wires can be calculated using equations from [2]. For tornadoes, some modification of the equations might be necessary as discussed in detail in [10].

In the probabilistic hazard analysis, the risk to distribution poles can be evaluated as the annual probability of failure of the poles using Eq. (7.2).

$$P_f = \int_0^\infty F_R(v,t)\, f_v(v,t) dv \tag{7.2}$$

where $F_R(v,t)$ is the time-dependent cumulative distribution function (CDF) of the structural fragility, and $f_v(v,t)$ is the time-dependent probability density function (PDF) of the annual maximum hurricane wind speed. $f_v(v,t)$ can be modeled using the Weibull distribution as mentioned earlier while $F_R(v,t)$ can be modeled using the Lognormal distribution [7, 9, 35].

### 7.4.2 System-Level Risk Assessment

In system-level risk assessment and management, the effectiveness of mitigation strategies in reducing the impact of hazards on system performance is considered. Such an approach requires explicitly quantifying system performance or reliability through topological methods or power flow methods. The system-level approach enables the identification of critical components or lines that have a greater impact on system performance. Hence, it allows mitigation strategies to be focused on such critical components.

For electric power systems, models of performance measure can range from purely topological-based models to complex alternating current (AC) power flow models. Topological- or connectivity-based models only consider the manner in which system components are arranged (topology) to describe the behavior of the system. Physical constraints that govern power flow within the system are ignored. Power flow-based models, on the other hand, consider the physics of power flow, power capacity limits of components and other engineering details of the system.

Topological-based models have two main advantages: (i) they are computationally efficient especially for complex systems or in a case where system performance under various scenarios is desired, and (ii) significantly less data about a system is required to evaluate reliability. While power flow-based models provide more accurate description of system performance, they are computationally complex and often impractical. Furthermore, detailed information about engineering properties of system components is required for such analysis. In studies where the focus is mainly on structural components (poles) of the power system, which define the topology, the topological-based method can suffice, especially if the system topology or power flow is not altered by any risk mitigation strategy. Detailed reviews of system performance measures for power systems can be found in Salman [34].

### 7.4.3 Risk Management

Various risk management strategies involve regular maintenance, repair, periodic replacement, and the use of alternative pole materials. One strategy is the use of fiber-reinforced polymers (FRP) to repair and strengthen decayed poles. FRP are strands of carbon-fiber reinforcement arranged in parallel and cast into an epoxy coating and applied to the exterior of structural elements. Merschman et al. [26] investigated the effectiveness of using FRP sleeves to reinforce wood poles subjected to decay to restore their lost strength and extend their useful service life.

The undergrounding of lines has also been explored as a means of reducing risk and improving the resilience of power systems. Advantages of undergrounding include potentially lower storm damage and restoration costs, fewer outages during normal weather, fewer momentary interruptions, lower tree-trimming costs, reduced live-wire contact, and improved aesthetics. Potential disadvantages include susceptibility

to flooding, reduced flexibility of operations and system expansion, longer duration interruptions, higher maintenance and operating costs, stranded asset cost for existing overhead facilities, etc.

Another risk management method is distribution automation. Many distribution systems have radial topologies or are radially operated where there is a unique path from the source of power to each component or customer. Consequently, if there is a fault at any point in a line, all customers downstream of the point will lose power. To overcome this shortcoming, a network topology with a large number of automatic and remotely controlled switches can be adopted. Distribution automation can significantly improve system reliability and reduce the number of customers experiencing outages during extreme events, as power can be rerouted around failed lines. The use of Distributed generation (DG) units such as fuel cells, microturbines, wind turbines, and photovoltaic panels is also being studied to reduce risk and improve grid resilience by improving generation availability. To efficiently manage DGs, microgrids can be utilized. Due to their potential for improving grid resilience, microgrids are being actively studied by government agencies, industries, and research institutions.

A cost-benefit analysis can be used to evaluate the cost-effectiveness of the proposed strategy. The direct cost (repair cost, maintenance cost, and revenue loss by utilities) and indirect cost (societal economic losses) are considered in the cost-benefit analysis. Multi-criteria decision making can be used to investigate the effectiveness of risk mitigation measures considering various criteria such as vulnerability, resilience improvement, and cost.

## 7.5 Case Studies

### *7.5.1 Case Study 1: Power Distribution Systems Subjected to Hurricanes*

#### 7.5.1.1 Component-Level Risk Management

Risk Assessment

A typical wood distribution pole that is 13.7 m high is chosen for the case study. The pole is assumed to be a Class 4 southern pine pole buried 2 m below ground per [1]. The pole supports three Aluminum Conductor Steel Reinforced (ACSR) conductor wires with diameters of 18.3 mm and located 0.61 m below the pole tip. A conductor span of 91.44 m is assumed for wind pressure calculations. To evaluate the time-dependent decrease in strength of the pole, the decay model developed by [24, 40] is adopted. Risk is quantified as the annual probability of failure given by Eq. (7.4). More details on the evaluation of annual failure probability and statistics of random variables can be found in [36].

### Mitigation Strategy

The mitigation strategy considered is the use of alternative pole material, specifically steel poles. The use of steel poles is becoming more popular due to various reasons, including the high cost of maintenance and environmental and durability concerns associated with timber poles. To facilitate comparison, a steel pole with similar strength to the wood pole is selected. To evaluate the time-dependent decrease in strength for the steel pole, the corrosion model developed by Romanoff [33] is adopted.

### Cost-Effectiveness Analysis

To evaluate the effectiveness of the mitigation strategy, lifecycle cost analysis is performed. For a pole network with $n$ number of poles, the present value of the lifecycle cost can be calculated using Eq. (7.3) [8, 45].

$$LCC = nC_o + \left[\sum_{t=1}^{\tau} nP_f(\mathrm{t})\right]\frac{C_{rep}}{(1+r)^t} + \int_0^t \frac{C_m}{(1+r)^t}d\tau \tag{7.3}$$

where $n$ is the number of poles, $C_o$ is the initial cost per pole, $\tau$ is the total number of years being considered, $P_f(\mathrm{t})$ is the time-dependent annual probability of failure, $C_{rep}$ is the replacement cost, $(1+r)^t$ is a discount factor, r is a constant discount rate/year, and $C_m$ is the operation and maintenance cost per year.

A network of 100,000 poles in Miami, Florida, is considered over a timeframe of 60 years. The cost parameters used can be found in [36]. Figure 7.2 shows the

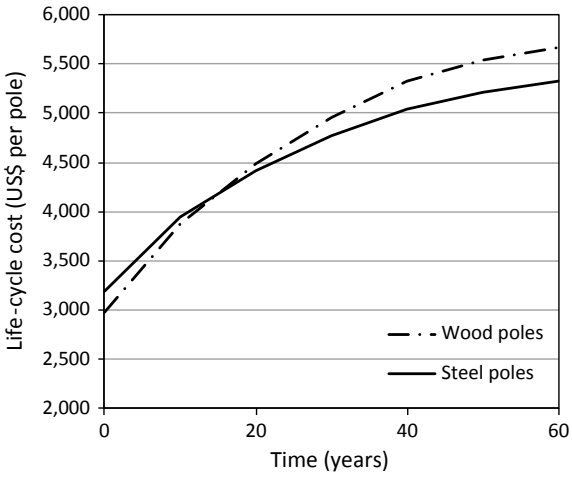


**Fig. 7.2** Cumulative lifecycle cost of poles over time

result of the lifecycle cost analysis. While the steel poles' initial cost is higher, their lifecycle cost is lower than the wood poles. The wood and steel poles' lifecycle costs are $5670 and $5320 per pole, respectively. After about 15 years, excessive decay in the wood poles will increase the replacement cost, increasing the total cost.

#### 7.5.1.2 Maintenance Optimization for Poles to Reduce Risk

A key aspect of risk management for distribution systems is periodic maintenance. Such maintenance involves replacing or strengthening poles when their strength falls below a certain threshold. Periodic maintenance reduces the likelihood that poles will fail during extreme wind events and can be cost-effective by reducing repair costs, revenue loss by utility companies, and losses to businesses and other customers due to power outages. Hence, the National Electrical Safety Code (NESC) requires poles to be replaced once their strength falls below two-thirds of the initial strength due to decay [27]. Models for the periodic maintenance of poles can be divided into age-based and condition-based maintenance.

Age-Based Maintenance

Age-based maintenance involves replacing or strengthening decayed poles after a specific number of years in service. Age-based models are based only on the observation of failure times or rates. Data on the past failures of a component is used to determine its failure rate, which can then be used to optimize the maintenance. Such an approach is appropriate for components with a well-defined aging process. Age-based models can lead to the uneconomical use of resources as maintenance actions are carried out without explicit regard to the components' condition. However, the models are relatively easy to implement and can be an adequate decision-making tool. The objective of the model is to find the optimal replacement age of the poles that will minimize the total maintenance cost over a period. The optimization problem can be solved using renewal theory. For an infinite period, the objective function is given by Eq. (7.4) [5, 6].

$$C(T) = \frac{C_p R_s(T) + C_c F(T)}{\int_0^T R_s(t)dt} \tag{7.4}$$

where $C(T)$ is the annual total maintenance cost; $T$ is the cycle length or the time between renewals; $C_p$ is the preventive maintenance cost, $C_c$ is the corrective maintenance cost. $F(T)$ is the cumulative distribution function (CDF) of the service life of the pole, which models the probability that failure will occur before renewal, and $R_s(T)$ is the survival function of the pole. More details of the solution to the age-based maintenance problem can be found in [37]. To solve the optimization, the

probability distribution of the service life (time to failure) of the poles is required. The distribution can be obtained from statistical analysis of pole failures in a network. In this case study, it is assumed that the service life follows a Weibull distribution. The parameters of the Weibull distribution can be obtained, knowing the mean and standard deviation of the time to failure.

Figure 7.3a shows the results of the optimization assuming a mean value of the time to failure of 32 years and a coefficient of variation (COV) of 25% [37]. The cost ratio on the vertical axis is the ratio of the cost of preventive maintenance to the additional cost incurred if failure were to occur, i.e., $C_p/(C_c - C_p)$. For example, if the cost of preventive maintenance is $3000 and the cost of corrective maintenance is $15,000, then the cost ratio is 0.25. Based on the cost ratio, the optimal replacement age is 19, which is lower than the mean service life of 32 years. Hence, it is more economical to replace the pole much earlier in its life. Figure 7.3b shows the impact of varying mean service life on the optimal replacement age. The COV is kept constant at 25%. Figure 7.3c shows the impact of the variation in COV on the optimal results. The mean time to failure is kept constant at 32 years.

### Condition-Based Maintenance

Condition-based maintenance (CBM) models account for the condition of the poles at the time of maintenance. Hence, the models require periodic or continuous inspection/condition monitoring. A case study is considered to find the optimal inspection interval that minimizes the expected total cost per unit time. If the poles are inspected after regular intervals of length $\tau$; the cost of inspection, preventive replacement, and additional cost of corrective replacements are $C_i$, $C_p$, and $C_c$; and the mean number of inspections before preventive replacement is $n_p$, then following [32], the expected total cost per unit time is then given by Eq. (7.5).

$$C(\tau) = \frac{C_p + C_i \cdot (n_p) + C_c \cdot \left[1 - F(y_c - y_p)\right]}{(n_p + 1) \cdot \tau} \tag{7.5}$$

$F(y_c - y_p)$ is the probability of failure of the poles. To determine $F(y_c - y_p)$, two deterioration or condition levels are set: the 'critical' level, $y_p$, and the 'failure' level, $y_c$. Once the condition of the pole reaches the 'critical' level, it is preventively replaced to avoid failure. The 'critical' level, in this case, is based on the NESC requirement mentioned earlier. The 'failure' level, $y_c$, is higher than $y_p$, and is the deterioration level that can jeopardize the functionality of the pole. The value of $y_c$ can be set based on experience or field observations. As the deterioration of the poles is monotonic and gradual, it is modeled with a gamma process. Hence, $F(y_c - y_p)$ has a gamma distribution. More details on the modeling of pole decay with the gamma process can be found in [39].

In this case study, a network of 200,000 Class 4 southern pine poles in Miami and New York City (NYC) is considered. The age distribution of the poles is shown

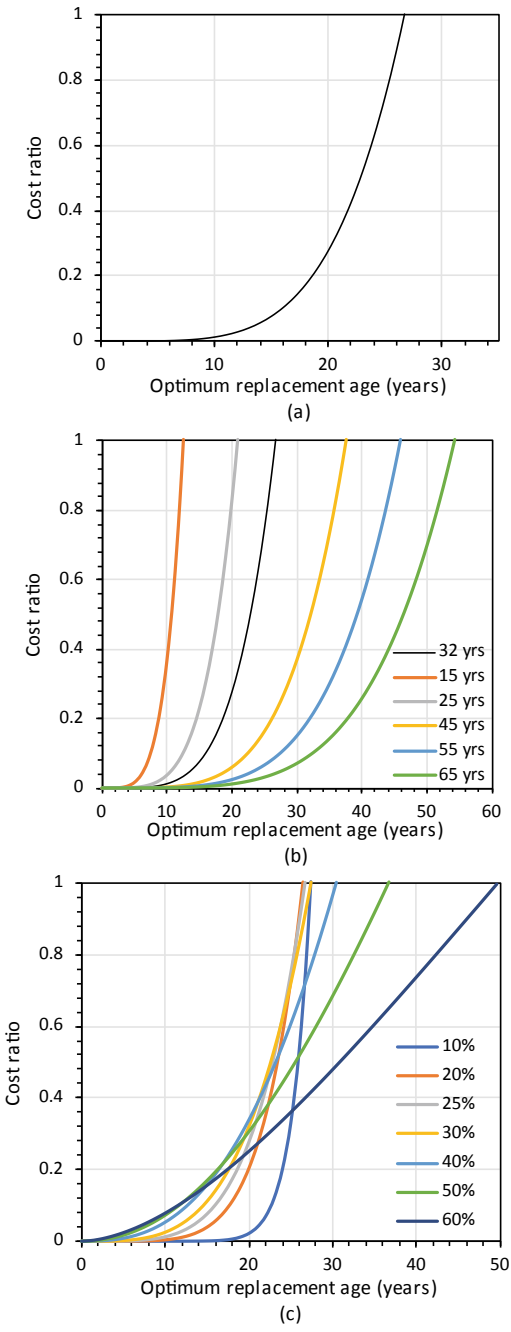


**Fig. 7.3** Age-based optimization results, **a** Mean service life of 32 years and COV of 25%, **b** varying mean service life and COV of 25%, and **c** mean service life of 32 years and varying COV

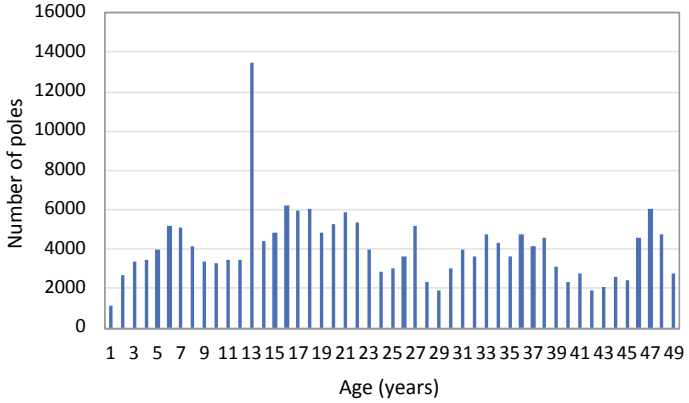


**Fig. 7.4** Age distribution of poles

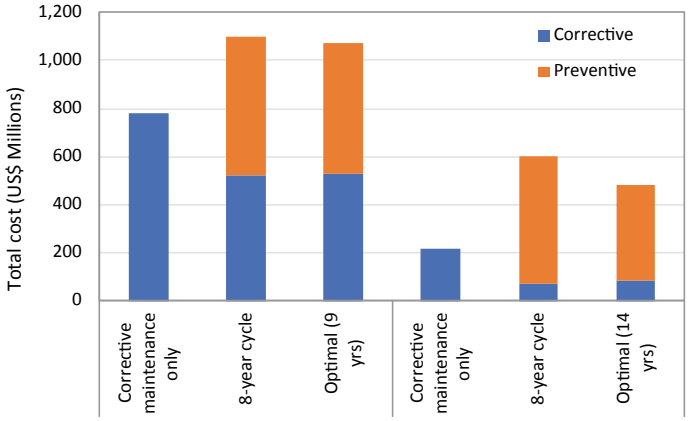


**Fig. 7.5** Comparison of discounted total pole replacement costs from 2010–2099 (Note: bars are stacked)

in Fig. 7.4. The optimal inspection interval is determined and compared with an inspection cycle of 8 years, typical for utilities in the U.S. The results are shown in Fig. 7.5. 'Corrective maintenance only' implies a strategy in which poles are only replaced when they fail due to hurricanes. The 8-year cycle and optimal cycle results include both preventive and corrective replacements. The optimal inspection intervals in Miami and NYC are 9 years and 14 years, respectively. Including preventive replacement increased the total discounted costs because of the high number of poles that need to be replaced. Figure 7.5 also shows that the presented method led to an optimal inspection cycle that decreased the total discounted replacement cost. For more details on the CBM model presented here, including cost parameters used for optimization, see [39].

#### 7.5.1.3 System-Level Risk Management

Power Distribution Model

The power system model adopted for demonstrating the framework is shown in Fig. 7.6 [4]. For this case study, the city is assumed to be located on the east coast of Florida and is assumed to be 20 years old.

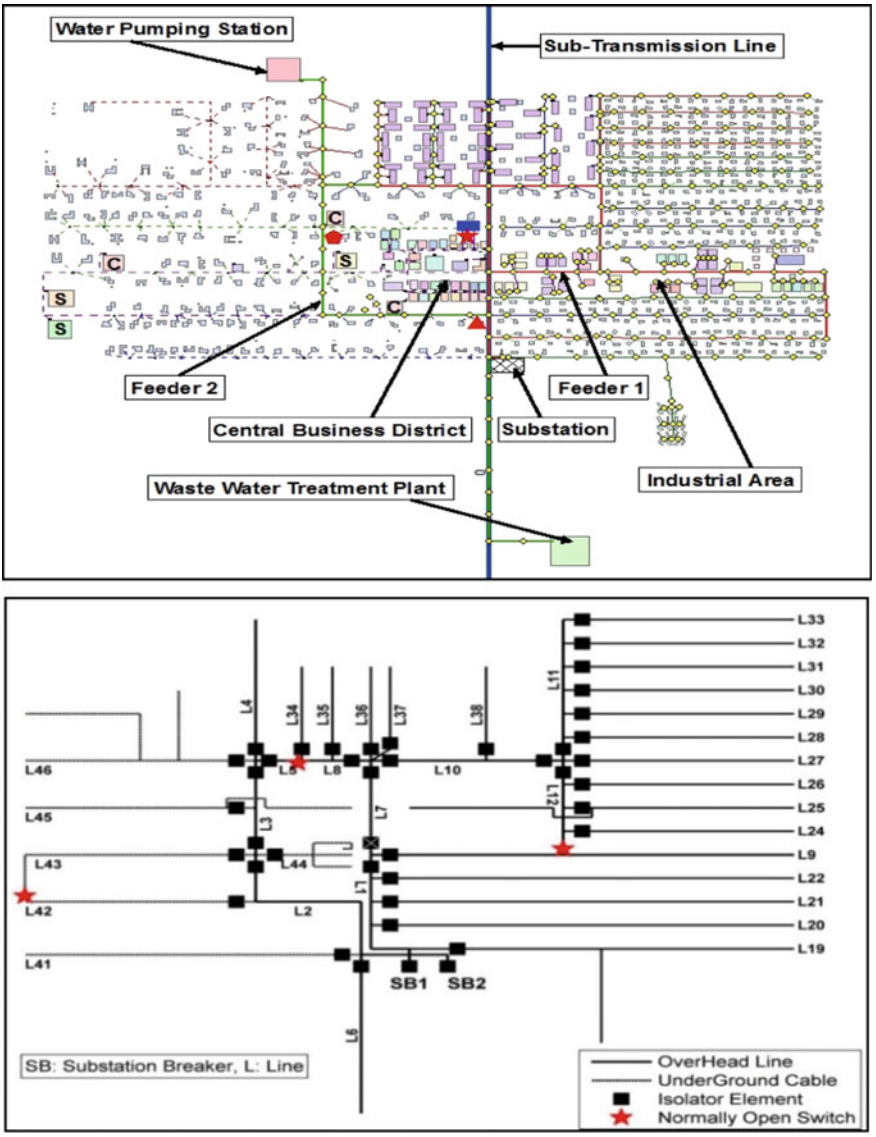


**Fig. 7.6** Micropolis power distribution system. Top: system details. Bottom: line diagram [4]

Mitigation Strategies

To determine critical lines in the system that can be the focus of mitigation measures, Risk Achievement Worth (RAW) is employed [32, 38]. Three mitigation strategies are then considered:

i Strategy 1: Hardening only the main feeder lines
ii Strategy 2: Hardening all lines with RAW $\geq 2.5$
iii Strategy 3: Hardening all lines.

Hardening means using a pole that is one class higher than required by structural design. Both probabilistic hurricane analysis and scenario-based analysis are considered. For the scenario-based analysis, Hurricane Jeanne (2004) is selected for the case study. To evaluate the cost-effective of the mitigation strategies, cost-benefit analysis is employed. Costs considered include mitigation cost, periodic maintenance costs, repair cost, revenue loss by utilities, and societal economic losses. Parameters and details of the cost analysis can be found in [38].

Cost-Effectiveness Analysis

The results of the cost-benefit analysis are shown in Fig. 7.7. In the probabilistic analysis, all three strategies are cost-effective. Strategies 1 and 2, however, resulted in higher net benefit compared to Strategy 3. Hence, the targeted hardening of the system is more beneficial. In the scenario-based analysis, only Strategies 1 and 2 are cost-effective. Strategy 3 is not cost-effective because of the high cost of mitigation (hardening all lines). The cost–benefit analysis results will be different depending on the time of mitigation—see [38] for more details.

## *7.5.2 Case Study 2: Power Distribution Systems Subjected to Tornados*

### 7.5.2.1 Tornado Scenario

In this case study, a slightly simplified version of "Micropolis" virtual city discussed earlier is used and assumed to be located near Norman, Oklahoma which is one of the most tornado-prone regions in the world. More details on the city can be found in [11, 13]. Similar to the hurricane case study discussed above, distribution poles are class 4 southern pine wood poles. The age of poles is modeled as a random variable following log-normal distribution with mean 31.2 years and coefficient of variation of 0.47. In this study, an Enhanced Fujita scale 2 (EF2) tornado is considered with width of 197 m, which is the mean width of EF2 tornadoes. Out of this width, 21.1% have EF0 intensity (with mean wind speed of 34 m/s), 31.4% have EF1 intensity

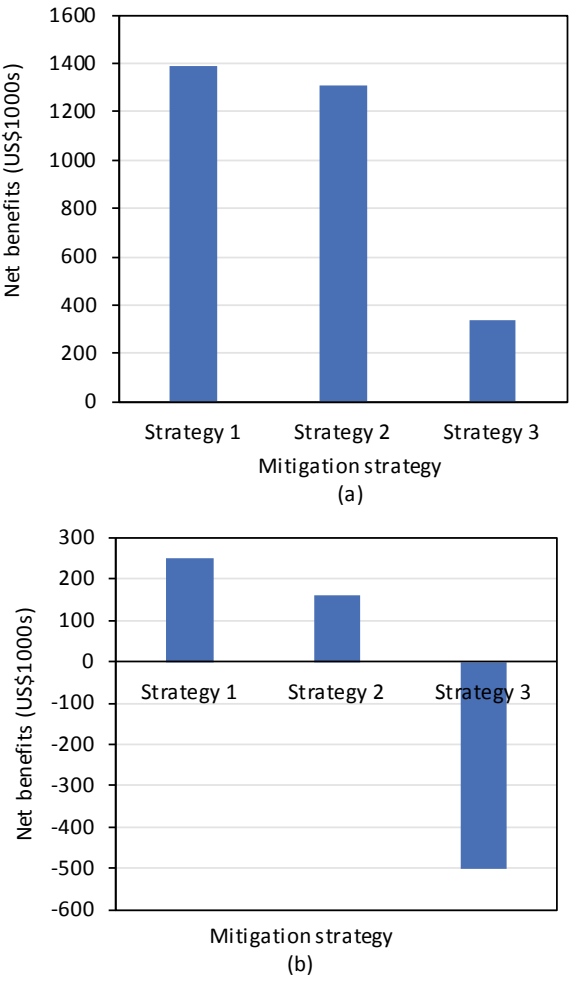


**Fig. 7.7** Cost-benefit analysis results **a** probabilistic hazard analysis **b** scenario-based analysis (Hurricane Jeanne 2004)

(with mean wind speed of 44 m/s), and 47.5% have EF2 intensity (with mean wind speed of 55 m/s) [18, 25, 41]. The system and tornado scenario are shown in Fig. 7.8.

#### 7.5.2.2 Component-Level Risk Management

Mitigation Strategy

The mitigation strategy considered is the use of alternative pole material, specifically steel and prestressed concrete (PC). PC poles are popular because of their high strength, light weight, and low permeability which helps protect the reinforcement from corrosion. To facilitate comparison, a steel pole and a PC pole with similar

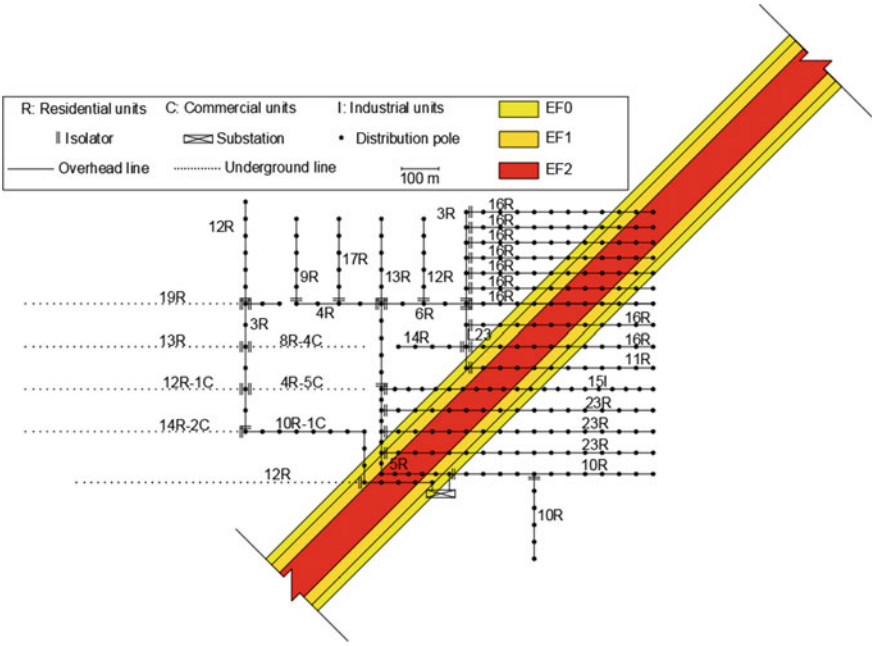


**Fig. 7.8** Micropolis tornado scenario

strength to the wood pole are selected. To evaluate the time-dependent decrease in strength for the poles, the decay model developed by Wang et al. [44] is adopted for wood poles, the corrosion model developed by [14] is adopted for steel poles, and the corrosion model developed by [15] is adopted for PC poles. More details can be found in [10]. Figure 7.9 shows the fragility curves for new and aged poles. The fragility curves are similar for all 3 types of new poles because the poles were designed to have similar dimensions and strengths at age 0, while wood poles become more vulnerable to tornadoes when aged compared to other poles.

### Scenario-Based Cost Analysis

The total cost of poles replacement can be calculated using Eq. (7.6).

$$C_R = \sum_{p=1}^{n} C_r P_{f-p} \tag{7.6}$$

where $n$ is the number of poles within the system (284 total), $P_{f-p}$ is the probability of failure of pole $p$, and $C_r$ is the replacement cost of failed poles. To estimate the probability of failure of poles, we can determine the number of poles within each

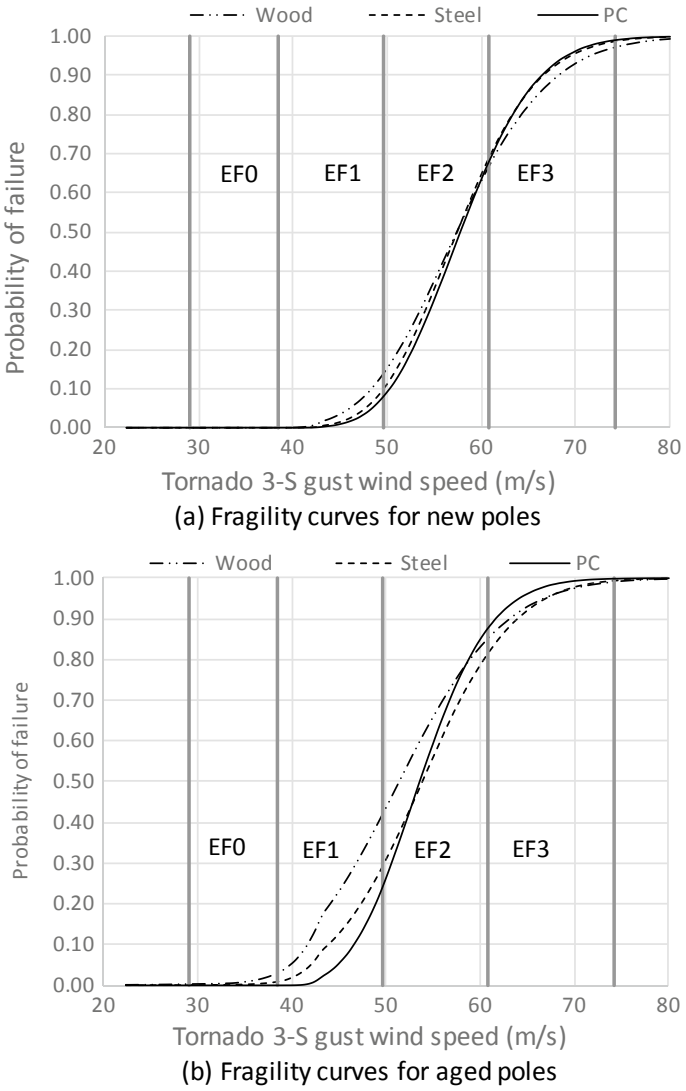


**Fig. 7.9** Tornado fragility curves for new and aged poles

tornado EF category, and assume $P_{f-p}$ using the average velocity of the category. Moreover, $C_r$ is assumed equal to \$4000/pole for all three types of poles [35]. $C_R$ results are shown in Fig. 7.10. Both steel and PC poles result in lower total replacement costs compared to wood poles, with steel poles total replacement cost being the lowest.

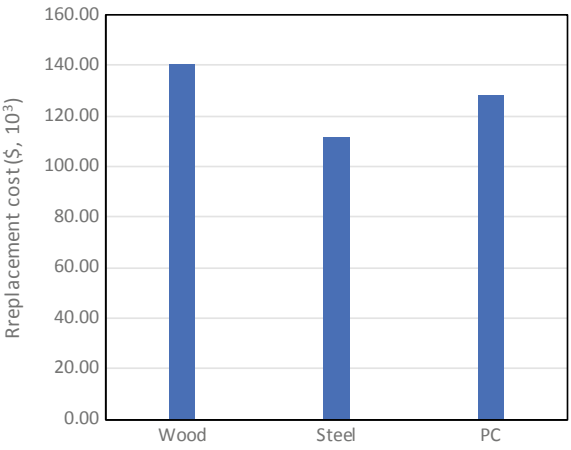


**Fig. 7.10** Total replacement cost for wood, steel, and PC poles

#### 7.5.2.3 System-Level Risk Management

Reliability Analysis

The system-level approach uses different fragility functions for each pole depending on the span length of conductors and the conditional probability of failure of adjacent poles. This approach allows to calculate the probability of failure of lines within the system. It can be assumed that a line fails if two adjacent poles fail within the line itself, or if any line upstream to the line fails, which can be determined using fault-tree analysis because the system studied here is radial. More details on this method can be found in [11].

Mitigation Strategy

The mitigation strategy considered is the hardening through replacing class 4 poles with stronger class 2 poles. The worth of the hardening is measured through the risk reduction worth (RRW). RRW allows for targeted hardening of a small proportion of the poles while achieving the target reliability. Using the results of RRW, lines L1, L7, L8, and L28 are hardened.

Scenario-Based Cost Analysis

The direct costs considered are the cost of poles replacement ($C_R$), the service interruption cost ($C_L$), and the hardening cost ($C_H$). $C_R$ can be calculated using the same formula used in the component-level method, while $C_L$ can be calculated using Eq. (7.7).

**Table 7.1** Scenario-based system reliability and costs before and after targeted hardening

| | Before hardening | After hardening |
|---|---|---|
| Reliability | 0.013 | 0.823 |
| $C_R(\$, \times 10^3)$ | 147.8 | 122.6 |
| $C_L(\$, \times 10^3)$ | 1533.2 | 88.5 |
| $C_H(\$, \times 10^3)$ | 0.0 | 168.4 |
| $C_{Total}(\$, \times 10^3)$ | 1681.0 | 379.5 |

$$C_L = \sum_{l=1}^{\mathrm{m}} P_{f-l} C_l t_l \tag{7.7}$$

where $P_{f-l}$ is the failure probability of line $l$; m is the number of distribution lines (38 total); $C_l$ is the average cost per hour customers incur when line $l$ is out of electricity. This cost was estimated by [22] to be \$2.7/h, \$886/h, and \$3253/h for residential, commercial, and industrial units respectively. $t_l$ is the recovery time of the line $l$, and assumed equal to 25.5 h [11]. $C_H$ is the sum of both the installation cost (assumed \$2500/pole) and the purchase cost (assumed \$619/pole) [3, 11, 42]. Therefore, the total cost can be calculated using Eq. (7.8).

$$C_{Total} = C_R + C_L + C_H \tag{7.8}$$

Table 7.1 shows a comparison of the reliability and costs before and after the targeted hardening and shows that hardening results in a considerable increase in system reliability and decrease in total cost. While the replacement of poles caused some additional costs, the considerable decrease in the other costs, especially the service interruption cost, resulted in a much lower total cost.

### Comparison of Different Tornado Scenarios

Because the tornado path area is smaller than the total area of the system, it is necessary to consider different paths covering different regions. In addition to the path studied above, five other paths are considered. While all paths are assumed to follow the same path angle, each path shifts 80 m in both the x and y direction from the adjacent path. Figure 7.11 shows the six path scenarios considered, where path four is the one considered earlier. Moreover, Fig. 7.12 shows the costs and reliability comparison for the six scenario paths both before and after targeted hardening. In general, the reliability is low, and the costs are high before hardening, except for scenario six because its tornado path is far from the main feeders and the industrial units. After targeted hardening, the reliability increases to exceed 0.8 for all paths, and the total costs reduce considerably.

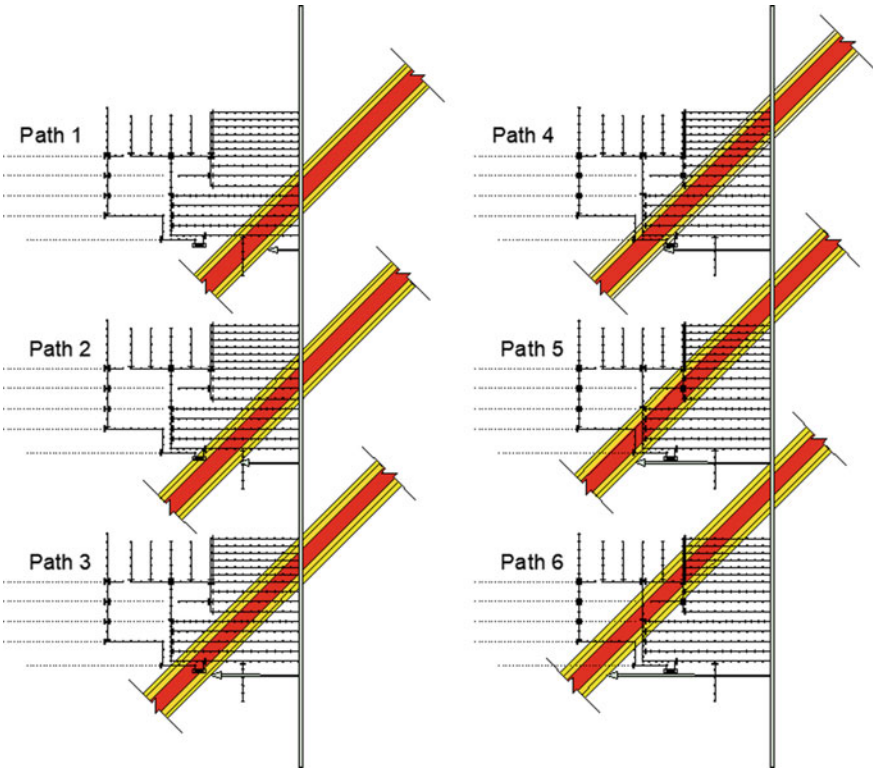


**Fig. 7.11** Tornado paths

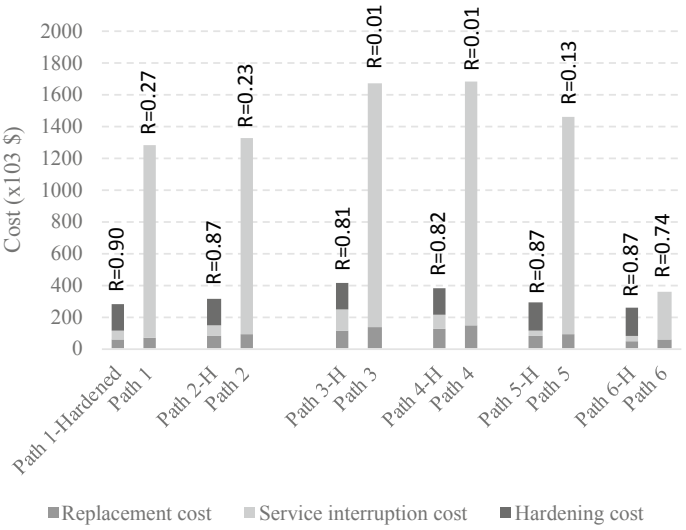


**Fig. 7.12** Cost and reliability comparison for different tornado paths

### 7.5.3 Discussion/Comparison of Both Hazards

Hurricanes and tornadoes differ in crucial aspects, such as their nature, how and where they are formed, size and duration. During an Atlantic hurricane season starting from June to the end of November, an average of 12 tropical storms form over the Atlantic basin, of which six become hurricanes [31]. Hurricanes are typically hundreds of miles in diameter causing high winds and heavy rains over an entire coastal region for days or even weeks. Major hazards associated with hurricanes are high winds, storm surge, and heavy rainfall which may cause inland flooding [19]. On the other hand, the United States records about 800–1,400 tornadoes per year [11]. Unlike hurricanes, tornadoes can occur at any time of the year and in any area, although some parts of US (e.g. Central Plains and the southeastern US) are more prone to high intensity tornadoes. The life span of tornadoes are typically no more than few minutes and their radius is about few hundred feet. Tornadoes are accompanied by very strong cyclonic winds as well as heavy rain and large hail.

Risk assessment and management for power systems under hurricanes and tornadoes differ in the hazard analysis approach. For hurricanes, mathematical simulation approach has been widely accepted for estimating wind speeds for structural design and hurricane risk assessment. Among the available methods, probabilistic models (site-specific method and track model) and hurricane wind field models are of crucial importance and has been widely used in recent studies. In site specific modeling, key hurricane parameters are assessed by sampling from statistical distributions obtained from historic hurricanes using a Monte Carlo approach. For tornadoes, the annual probability of tornado occurrence for a given location can be calculated by employing different tornado hazard models which are based on historical data [41]. Statistical characterization of tornadoes like occurrence rate, intensity, width, track, and path length can also be assessed. Multiple scenarios for tornado modeling are available depending on whether each of the tornado characteristics and properties are considered as a deterministic parameter or assessed as a random variable from the probability distributions. As mentioned in the case study, since the actual shape of a tornado path is difficult to model, it is typically assumed to be rectangular in shape. The area inside the rectangular path is then classified into multiple EF ratings which relates each tornado scale to a lower and upper bound of 3-s average gust wind speed [10], which can then be used to derive the fragility curves for the power poles and lines.

## 7.6 Conclusions

Reducing the tremendous losses due to power outrage and the high replacement costs of aging poles requires the cost-effective management of the systems. This chapter demonstrates risk-based management of electric power distribution systems subjected to hurricane and tornado hazards. It presents the framework to perform risk analysis and cost analysis of power distribution systems subjected to the extreme wind hazard. The framework includes reliability analyses of the power poles and

the distribution system using fragility analysis considering various sources of uncertainties, the effects of degradation of timber poles, probabilistic wind models, and a life-cycle analysis to investigate the economic viability of various mitigation strategies. Various mitigation strategies to reduce replacement costs and damage risks are proposed. The deterioration of the strength of the poles is found to be the critical elements within the power distribution lines.

The results of the case studies showed that the use of alternative pole materials such as steel and concrete can be a cost-effective risk management strategy. However, such results depend on site and material-specific factors that affect deterioration of power distribution poles. Deterioration models for specific areas can be developed to obtain results that can be useful in decisions regarding future investments by utility companies. The results also show that the current maintenance practice by utility companies may not be the optimal approach based on cost. The optimal inspection/replacement cycle depends on location, which dictates the decay rate and hurricane hazard level. The results from system-level risk management showed the importance of evaluating system performance and component importance measures. It was shown that targeted hardening of the system can be a cost-effective risk mitigation strategy, whereas hardening an entire system may not be cost-effective.

## References

1. ANSI-O5.1 2002. Wood poles specifications and dimensions. American National Standards Institute, Washington, DC
2. ASCE-111 2006. Reliability-based design of utility pole structures. American Sociaety of Civil Engineers, Reston, VA
3. ATS. 2019. Products and Pricing (Online). American Timber and Steel. Available: http://www.americantimberandsteel.com/poles-pilings-utility-poles-unframed-cca.html. Accessed 6/4/2019 2019
4. Bagchi A, Sprintson A, Singh C (2009) Modeling the impact of fire spread on the electrical distribution network of a virtual city. In:North American Power Symposium (NAPS), IEEE, pp 1–6
5. Barlow RE, Proschan F (1965) Mathematical theory of reliability. SIAM Publications, Philadelphia
6. Ben-Daya M, Kumar U, Murthy DP (2016) Introduction to maintenance engineering: modelling, optimization and management. Wiley, West Sussex, UK
7. Bjarnadottir S, Li Y, Stewart M (2013) Hurricane risk assessment of power distribution poles considering impacts of a changing climate. J Infrastruct Syst 19:12–24
8. Bjarnadottir S, Li Y, Stewart MG (2014) Risk-based economic assessment of mitigation strategies for power distribution poles subjected to hurricanes. Struct Infrastruct Eng 10:740–752
9. Bjarnadottir S, Li Y, Stewart MGJJOIS (2012) Hurricane risk assessment of power distribution poles considering impacts of a changing climate 19:12–24
10. Braik AM, Salman AM, Li Y (2019) Risk-based reliability and cost analysis of utility poles subjected to Tornado hazard. J Aerosp Eng 32:04019040
11. Braik AM, Salman AM, Li Y (2020) Reliability-based assessment and cost analysis of power distribution systems at risk of Tornado hazard. ASCE-ASME J Risk Uncertainty Eng Syst Part A: Civil Eng 6:04020014

12. Brown RE (2009) Cost-benefit analysis of the deployment of utility infrastructure upgrades and storm hardening programs. Quanta Technology, Raleigh
13. Brumbelow K, Torres J, Guikema S, Bristow E Kanta L (2007) Virtual cities for water distribution and infrastructure system research. In: World Environmental and Water Resources Congress, pp 15–19
14. Caleyo F, Velázquez J, Valor A, Hallen J (2009) Probability distribution of pitting corrosion depth and rate in underground pipelines: a Monte Carlo study. Corros Sci 51:1925–1934
15. Darmawan MS, Stewart MG (2007) Spatial time-dependent reliability analysis of corroding pretensioned prestressed concrete bridge girders. Struct Saf 29:16–31
16. Davidson RA, Liu H, Sarpong IK, Sparks P, Rosowsky DV (2003) Electric power distribution system performance in Carolina hurricanes. Nat Hazard Rev 4:36–45
17. DOE (2004) Final Report on the August 14, 2003 Blackout in the United States and Canada: Causes and Recommendations. U.S.-Canada Power System Outage Task Force
18. Edwards R, Ladue JG, Ferree JT, Scharfenberg K, Maier C, Coulbourne WL (2013) Tornado intensity estimation: past, present, and future. Bull Am Meteor Soc 94:641–653
19. Fang Y-P, Zio E (2019) An adaptive robust framework for the optimization of the resilience of interdependent infrastructures under natural hazards. Eur J Oper Res 276:1119–1136
20. Goliger AM, Milford R (1998) A review of worldwide occurrence of tornadoes. J Wind Eng Ind Aerodyn 74:111–121
21. Kwasinski A, Andrade F, Castro-Sitiriche M, O'neill-Carrillo E (2019) Hurricane Maria effects on Puerto Rico electric power infrastructure. IEEE Power Energy Technol Syst J
22. Lacommare KH, Eto JH (2006) Cost of power interruptions to electricity consumers in the United States (US). Energy 31:1845–1855
23. Li Y, Ellingwood BR (2006) Hurricane damage to residential construction in the US: importance of uncertainty modeling in risk assessment. Eng Struct 28:1009–1018
24. Li Y, Yeddanapudi S, Mccalley JD, Chowdhury AA, Moorehead M (2005) Degradation-path model for wood pole asset management. In: Proceedings of the 37th Annual North American Power Symposium, 23–25 Oct 2005, pp 275–280
25. Masoomi H, van de Lindt JW (2018) Restoration and functionality assessment of a community subjected to tornado hazard. Struct Infrastruct Eng 14:275–291
26. Merschman E, Salman AM, Bastidas-Arteaga E, Li Y (2020) Assessment of the effectiveness of wood pole repair using FRP considering the impact of climate change on decay and hurricane risk. In: Advances in Climate Change Research
27. NESC (2017) National electric safety code. Institute of Electrical and Electronics Engineers
28. NOAA (2012a) Service assessment—Hurricane Irene, August 21–30, 2011. U.S. Department of Commerce, National Oceanic and Atmospheric Administration, National Weather Service
29. NOAA (2012b) US tornado climatology/tornado alley (Online). National Oceanic and Atmospheric Administration. Available: https://www.ncdc.noaa.gov/climate-information/extreme-events/us-tornado-climatology/tornado-alley. Accessed 07 April 2018
30. NOAA (2016) Revised Atlantic hurricane database (HURDAT2) (Online). Available: http://www.aoml.noaa.gov/hrd/hurdat/hurdat2-1851-2015-070616.txt. Accessed
31. NOAA (2020) Tropical cyclone climatology (Online). National Hurricane Center and Central Pacific Hurricane Center. Available: https://www.nhc.noaa.gov/climo/. Accessed 23 Dec 2020
32. Rausand M, Høyland A (2004) System reliability theory: models, statistical methods, and applications. John Wiley & Sons
33. Romanoff M (1957) Underground corrosion, US Government Printing Office Washington, DC
34. Salman AM (2016) Risk-based assessment and strengthening of electric power systems subjected to natural hazards. Michigan Technological University
35. Salman AM, Li Y (2015) Age-dependent fragility and life-cycle cost analysis of wood and steel power distribution poles subjected to hurricanes. In: Structure and Infrastructure Engineering, pp 1–14
36. Salman AM, Li Y (2016) Age-dependent fragility and life-cycle cost analysis of wood and steel power distribution poles subjected to hurricanes. Struct Infrastruct Eng 12:890–903

37. Salman AM, Li Y, Bastidas-Arteaga E (2017) Maintenance optimization for power distribution systems subjected to hurricane hazard, timber decay and climate change. Reliab Eng Syst Saf 168:136–149
38. Salman AM, Li Y, Stewart MG (2015) Evaluating system reliability and targeted hardening strategies of power distribution systems subjected to hurricanes. Reliab Eng Syst Saf 144:319–333
39. Salman AM, Salarieh B, Bastidas-Arteaga E, Li Y (2020) Optimization of condition-based maintenance of wood utility pole network subjected to hurricane hazard and climate change. Front Built Environ 6
40. Shafieezadeh A, Onyewuchi UP, Begovic MM, Desroches R (2014) Age-dependent fragility models of utility wood poles in power distribution networks against extreme wind hazards. IEEE Trans Power Delivery 29:131–139
41. Standohar-Alfano CD, van de Lindt JW (2015) Empirically based probabilistic tornado hazard analysis of the United States using 1973–2011 data. Nat Hazard Rev 16:04014013
42. Taras A, Ratel G, Chouinard L (2004) A life-cycle cost approach to the maintenance of overhead line supports. In: Reliability and optimization of structural systems: Proceedings of the 11th IFIP WG7. 5 Working Conference, Banff, Canada, 2–5 November 2003. CRC Press, p 241
43. Wang C-H, Leicester RH, Nguyen MN (2008) Manual 3—decay in ground contact. Forest & Wood Products Australia, Melbourne
44. Wang C, Leicester R, Nguyen M (2008b) Manual No. 3: decay in ground contact. Forest & Wood Products Australia
45. Wen Y, Kang Y (2001) Minimum building life-cycle cost design criteria. II: applications. J Struct Eng 127:338–346

# Chapter 8
# Hurricane Fragility Assessment of Power Transmission Towers for a New Set of Performance-Based Limit States


**Yousef M. Darestani, Ashkan B. Jeddi, and Abdollah Shafieezadeh**

**Abstract** With the increasing reliance on the constant flow of electricity, risk-based management strategies are increasingly needed to ensure that with limited available resources, the grid can maintain high reliability and resilience. A growing concern in meeting this objective is the impact of climatic extremes, as the wide exposure of the power grid infrastructure has resulted in a system that is inherently vulnerable to extreme climatic hazards which are exacerbated by climate change. Analyzing the likelihood of damage induced by extreme hazards is critical for developing risk-informed strategies. Overhead structures, in particular, may experience a wide spectrum of damage types and degrees during hurricanes. Beyond the collapse state of transmission towers, which has been investigated in the past, non-collapse damage states in lattice towers require further attention as they can assist with performance-based design, grid recovery planning, and hardening decisions in preparation for extreme events. The present study establishes a set of performance-based limit states for lattice transmission towers subject to wind-induced extreme loadings. Specifically, five damage states including no damage, slight, moderate, and extensive damage, and collapse are defined. These limit states are founded on the nonlinear behavior of lattice towers and the type and severity of failures in tower elements and connections, as they relate to the repair or replacement requirements of towers. Focusing on a double circuit vertical steel lattice transmission tower as a case study, the proposed limit states are evaluated by generating a large number of random realizations of a diverse set of uncertain variables including those related to wind

Y. M. Darestani
Department of Civil, Environmental, and Geospatial Engineering, Michigan Tech University, Houghton, MI 49931, USA
e-mail: ydaresta@mtu.edu

A. B. Jeddi · A. Shafieezadeh (✉)
Risk Assessment and Management of Structural and Infrastructure Systems (RAMSIS) Lab, Department of Civil, Environmental, and Geodetic Engineering, The Ohio State University, Columbus, OH 43210, USA
e-mail: shafieezadeh.1@osu.edu

A. B. Jeddi
e-mail: bagherijeddi.1@osu.edu



M. G. Stewart and D. V. Rosowsky (eds.), *Engineering for Extremes*, Springer Tracts in Civil Engineering, https://doi.org/10.1007/978-3-030-85018-0_8

pressure and material properties using Latin Hypercube sampling method. The generated realizations are used in a set of nonlinear pushover analyses to investigate the performance of the tower at various loading levels. Subsequently, multi-state fragility functions are developed via logistic regression. These fragility models constitute a key step toward reliable extreme wind hazard risk assessment of the transmission grid and can assist with risk-informed decision-making in support of a resilient power grid.

## 8.1 Introduction

Long-span high-voltage conductors in geographically spread transmission systems transfer bulk electricity from power plants to distant substations. The overhead conductors are supported by poles, frames or lattice towers. Commonly, lattice towers are the economic choice when high reliability and clearance limits are required. These structures and supported conductors are widely exposed and therefore are vulnerable to climatic extremes such as hurricanes. Figure 8.1 shows two cases of collapsed transmission towers during hurricanes Michael, 2018 and Maria, 2017. While collapse prevention has been the focus of the design of lattice towers, these structures may also sustain a wide spectrum of other damage types and degrees ranging from minor to severe. In maintaining or enhancing the resilience of the power grid, grid planners and engineers are confronted with decisions about how to design and prepare the infrastructure to withstand future uncertain extreme hazards. The ability to project the performance of the power grid under such hazards is critical for such decisions. A key decision concerns the recovery of the power grid in the aftermath of hurricanes. While collapsed towers are scheduled for immediate replacement, towers that have sustained a lower degree of damage are scheduled for repair or replacement to ensure that the system remains safe when facing future


**Fig. 8.1** Damaged transmission towers during hurricanes, **a** Michael, 2018 in Florida [19] and **b** Maria, 2017 in Puerto Rico [20]

extreme wind events. The resources and time needed to repair the system or, if it has collapsed or reached a state where repair is no longer feasible or economic, to replace the system are different. Quantifying the probability of towers experiencing different levels of damage during hurricanes is essential for analyzing the state of the grid and the resources and time needed to recover the system and resume the transmission of electricity. The ultimate products of this reliability analysis in the form of fragility models assist with post-event recovery planning for the restoration of the power grid. They also enable risk-based life-cycle management and decision making in the power infrastructure [7, 10].

A handful of studies have investigated the failure of transmission towers under hurricane hazards. These studies can be categorized into three groups. In the first group, it is assumed that any yielding or buckling in the tower results in a failure that disrupts the transmission of electricity (e.g., [16, 18, 21]). This assumption is overly conservative as towers collapse when a collapse mechanism is developed in the structure. A collapse mechanism is often developed when multiple elements are failed such that the tower becomes unstable, i.e., it is no longer able to resist against any further loading [13]. In the second group, failure events are defined based on the displacement responses of transmission towers during extreme wind events (e.g., [12, 24]). Although excessive deformations are intuitively associated with damage and potentially collapse of towers, a displacement threshold may not reliably represent a collapse mechanism, as the form of the pathway to collapse in lattice towers and thus the displacement at the time of collapse can vary by the load, configuration, and uncertainties. In the third group of studies, the load bearing capacity of the tower is obtained from nonlinear pushover analysis where the maximum load before the stiffness of the tower permanently drops is assumed as the collapse load of the tower [6, 15, 14]. In this case, the true collapse is captured as the load bearing capacity indicates the load beyond which the tower cannot withstand the wind-induced and gravity loads. However, this representation of failure only applies to the extreme nonlinear regimes of tower behavior, and it does not capture incipient or intermediate states of damage in towers. Therefore, fragility analysis of lattice towers especially for non-collapse damage states is still an underexplored territory.

To address the existing gaps, this study proposes a set of performance-based structural damage states including slight, moderate, extensive, and collapse for lattice transmission towers. These states are defined to correspond to repair and replacement requirements of towers in the aftermath of extreme wind events. For slight and moderate damage, the number of lattice elements and connections exhibiting inelastic behavior is used to define the limit state, while for extensive and complete damage, the load bearing capacity of the tower is used. This process is drawn from the structural and electrical performance of towers. For the case of slight and moderate damage, the ability of towers in transmitting the electricity is not compromised. However, the spread of inelastic behavior in tower components, although not significant, reaches a state that degrades the reliability of the structure to future events. The spread of damage in tower elements in these damage states is limited and therefore the economic solution is to repair damaged elements of the tower. Extensive damage, on the other hand, represents a state where the tower has not collapsed,

but it is severely damaged such that it cannot be repaired, and it must be replaced. Finally, we define collapse as the state where the stability of the tower is compromised and the structure is no longer able to withstand wind-induced and gravity loads. Based on these damage states, fragility models are developed using a high-fidelity finite element model of a double circuit vertical steel lattice transmission tower. The computational model of the tower accounts for several key complexities including post-buckling and post-yielding behavior of steel elements, and joint slippage and joint failure effects. A large number of random realizations of uncertain parameters corresponding to material and joint properties of the tower model and wind pressure parameters are generated using Latin Hypercube Sampling (LHS) method. Subsequently, the extreme wind performance of the tower is evaluated for each realization through a nonlinear pushover analysis. Using logistic regression, fragility curves are developed from the results of pushover analyses. As the incurred cost and recovery process of towers in hurricanes are directly related to the type and extent of the sustained damage, the developed fragility models are essential tools for risk-based decision making for managing the transmission infrastructure.

## 8.2 Finite Element Modeling of Transmission Towers

Lattice transmission towers are made of a large number of components that may undergo inelastic behavior under severe wind-induced loadings during hurricanes. Various damage types such as failure of legs, cage, and cross arms, as well as joint failures may occur in transmission towers. These damages may affect the local or global structural performance of towers during hurricanes, the ability of towers to support the transmission of electricity, and the restoration of the grid in the aftermath of hurricanes. In order to capture the complex behavior of lattice transmission towers, computational models should be able to account for various types and sources of nonlinearity such as geometric nonlinearities due to large deformations, material nonlinearities, imperfections, and elastic and inelastic buckling of lattice elements. For this purpose, a physics-based modeling approach in OpenSEES finite element platform [17] proposed by the authors in [5] is adopted in this study. A sketch of the 27.4 m double circuit vertical lattice tower used in this study is provided in Fig. 8.2 along with the transverse and longitudinal loading directions. The tower carries two lines of three-phase conductors at three cross arm levels and two lines of neutrals at the top. The conductors' span is 258 m. Various aspects of the finite element modeling approach are briefly discussed next. Further details can be found in [5].

### *8.2.1 Steel Elements*

Lattice towers are constructed commonly from galvanized steel elements. 'Displacement-based beam-column' elements in OpenSEES are used to model lattice

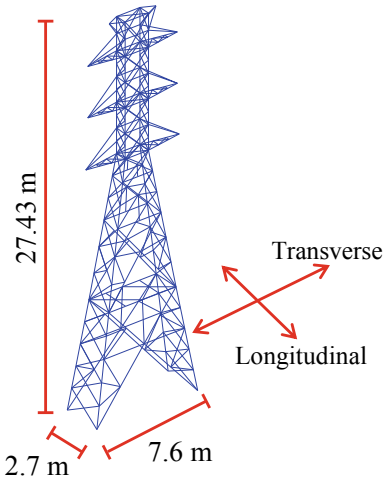


**Fig. 8.2** A sketch of the 27.4 m double circuit vertical lattice tower

elements of the tower. This element formulation considers plasticity at multiple integration points along the length of the element. In this study, each 'displacement-based beam-column' element is defined via five integration points. The section at each integration point is defined using fiber sections with ten fibers along the length of the section and three fibers along the thickness of the section. To capture the inelastic and post-yielding behavior of these elements, particularly the spread of plasticity under flexural and axial loads, a bilinear steel material model ('steel01' element) is used for defining fiber sections.

### *8.2.2 Buckling*

Buckling refers to the instability of an element under compressive forces due to geometrically nonlinear effects. According to [5], buckling can be captured by accounting for imperfections, P-$\Delta$ and P-$\delta$ effects, and large deformations. In order to account for these factors in OpenSEES, Uriz et al. [23] have suggested dividing each lattice element to at least two sub-elements with a camber displacement of 0.05–0.1% applied to the mid-point of the lattice element. In addition, to account for large deformations, the geometric transformation in OpenSEES is set to 'corotational'. In corotational transformation, kinematics of elements are defined in the local system and transferred to the global system via transformation matrices. This approach enables accurate derivation of geometrically nonlinear finite element formulations.

### 8.2.3 *Joint Slippage and Joint Failure Model*

Steel elements in lattice towers are commonly connected through bolted joints. In these joins, bolt holes are often made slightly larger than the bolt diameter in order for the elements to be assembled easily. Subsequently, when a lattice tower is subjected to strong wind loads, joint slippage may occur. Darestani et al. [5] observed that joint slippage can considerably increase the lateral displacement of towers during strong winds. These excessive deformations can change the failure mechanism and the load bearing capacity of the tower. In this study, the joint slippage model developed by [5] is adopted. This model consists of three hysteretic material models (Fig. 8.3a) that are set parallel to each other to closely follow the experimentally derived force–deformation model for bolted joints by [22]. A scheme of this model is provided in Fig. 8.3b. The studied tower includes five types of connections that are illustrated in Fig. 8.4. These connections are used for lap splices in leg elements (Type A), connection of bracing elements (Type B), and connection of bracing elements to main elements with one, two, and three bolts (Type C1, C2, and C3, respectively).

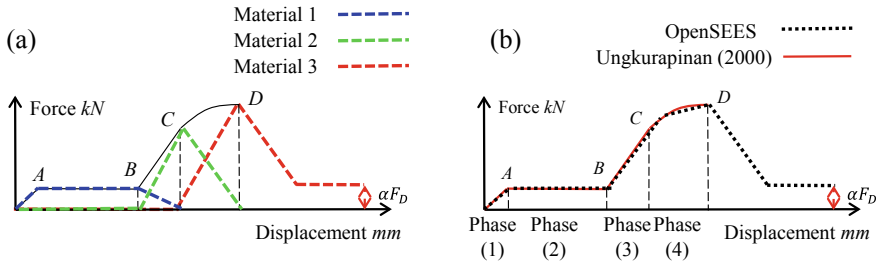


**Fig. 8.3** Joint slippage and failure model: **a** parallel hysteretic materials and **b** implemented joint slippage model in OpenSEES (adopted from [5])

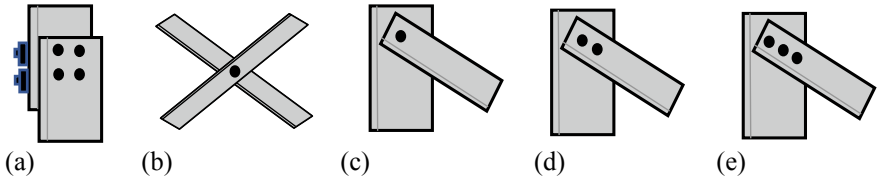


**Fig. 8.4** Types of connections in transmission tower: **a** Type A, **b** Type B, **c** Type C1, **d** Type C2, and **e** Type C3 (adopted from [5])

## 8.3 Wind Load on Transmission Towers

This study adopts the equivalent static wind model by the American society of civil engineering (ASCE) wind load standard ASCE [1]. In this code, the wind loading per unit length for non-building structures is defined as:

$$f_w = q_z G C_f D \tag{8.1}$$

where $q_z$ is the wind velocity pressure at height $z$ on the tower, $G$ is the gust-effect factor, $C_f$ is the force coefficient, and $D$ is the diameter perpendicular to the wind direction. The wind velocity pressure is calculated from:

$$q_z = 0.613 K_z K_d K_{zt} K_e V^2 \tag{8.2}$$

where $K_z$ is the exposure coefficient, $K_d$ is the wind directionality factor, $K_{zt}$ is the wind topographic factor, $K_e$ is the elevation factor, and $V$ is the 3-s gust wind velocity at 10 m above the ground line. $K_z$ is a function of the height from the ground line and exposure category, and is calculated from:

$$K_z = 2.01\left(\frac{\max(4.75, z)}{z_g}\right)^{2/\alpha} \tag{8.3}$$

where $z$ is the height from the ground line. Assuming that the transmission line is located in an open terrain area, the exposure category is C, and $\alpha$ and $z_g$ are 9.5 and 274.32 m, respectively [1]. $K_d$, $K_e$, and $K_{zt}$ are taken as 1.0 [1]. The gust-effect factor, $G$, accounts for the effects of the dynamic nature of wind forces on the tower. In the case of the transmission tower, $G$ is set as 0.85. According to ASCE No. 07 [1] the force coefficient, $C_f$, for squared truss towers is calculated as:

$$C_f = 4\varepsilon^2 - 5.9\varepsilon + 4 \tag{8.4}$$

where $\varepsilon$ is the ratio of solid area to gross area of the tower face under consideration. In addition, a force coefficient equal to 1.0 is considered for conductors [2].

## 8.4 Uncertainties and Probabilistic Simulation

Uncertainties in demand and capacity of steel elements can play a critical role in performance assessment of transmission towers. Uncertainties can be associated with material properties, imperfection and eccentricity in elements and joints, and wind-induced loadings, among others. These uncertainties can change the balance

between structural demand and capacity in towers and therefore, impact the mode of failure.

The geometric uncertainty associated with imperfection effects is considered through the camber displacement in the midpoint of lattice elements. This uncertainty is modeled with a uniform distribution between 0.1% and 0.5% of the length of the element. Uncertainties in steel material are considered through probabilistic models for the modulus of elasticity of steel, yield stress of main and bracing elements, and post yield elasticity of steel material. The mean, coefficient of variation (COV), and the type of the distribution for each variable is presented in Table 8.1. Moreover, uncertainties in wind-induced loading are accounted for using probabilistic models for the parameters that convert wind speed to wind loading (defined in Sect. 8.3). These parameters, their mean and COV and the type of distribution are also presented in Table 8.1.

For bolted joints in transmission towers, Darestani et al. [5] adopted an experimentally validated probabilistic model. This model is applied here to generate realizations of uncertain variables defining the backbone curve of bolted connections defined in Sect. 2.3. Table 8.2 presents the uncertain variables, their mean and COV and the type of distribution used for modeling connections.

**Table 8.1** Uncertain variables defining material behavior and wind loading

| Properties | | Notation | Type of Distribution | Mean | COV | References |
|---|---|---|---|---|---|---|
| Steel material | Modulus of elasticity | $E$ | LogNormal | 2.0e11 ($N/m^2$) | 0.06 | ASCE No. 07 [1] and ASCE No. 74 [2] |
| | Yield stress of main leg | $f_{ym}$ | LogNormal | 4.02e8 ($N/m^2$) | 0.1 | |
| | Yield stress of bracing members | $f_{yb}$ | LogNormal | 2.9e8 ($N/m^2$) | 0.1 | |
| | Post yield elasticity | $E_{st}$ | LogNormal | 0.02E ($N/m^2$) | 0.25 | |
| Buckling | Imperfection of element | | Uniform | 0.075 (%) | 0.192 | |
| Wind load | Gust effect factor | $G$ | Normal | Section 8.3 | 0.11 | ASCE No. 07 [1] and [9] |
| | Force coefficient | $C_f$ | Normal | Section 8.3 | 0.12 | |
| | Velocity pressure exposure coefficient | $K_z$ | Normal | Section 8.3 | 0.16 | |
| | Wind directionality factor | $K_d$ | Normal | Section 8.3 | 0.08 | |

**Table 8.2** Uncertain variables defining connections [22]

| Properties | | Notation (Fig. 8.3) | Type of Distribution | Mean | COV |
|---|---|---|---|---|---|
| Connection Type A | Load at onset of slip | Force @ A | LogNormal | 86.6 (kN) | 0.109 |
| | Load at end of slip | Force @ B | LogNormal | 197.3 (kN) | 0.23 |
| | Load at onset of plasticity | Force @ C | LogNormal | 317 (kN) | 0.13 |
| | Maximum load | Force @ D | LogNormal | 440 (kN) | 0.017 |
| | Dis. at elastic frictional load transfer | Phase 1 | LogNormal | 0.29 (mm) | 0.35 |
| | Slippage length | Phase 2 | Uniform | 1.9 (mm) | 0.61 |
| | Dis. at elastic load transfer | Phase 3 | LogNormal | 2.95 (mm) | 0.27 |
| | Dis. at nonlinear load transfer | Phase 4 | LogNormal | 0.36 (mm) | 0.34 |
| Connection Type B | Load at onset of slip | Force @ A | LogNormal | 23.95 (kN) | 0.1 |
| | Load at onset of plasticity | Force @ C | LogNormal | 132.17 (kN) | 0.09 |
| | Maximum load | Force @ D | LogNormal | 205.08 (kN) | 0.02 |
| | Dis. at elastic frictional load transfer | Phase 1 | LogNormal | 0.11 (mm) | 0.1 |
| | Slippage length | Phase 2 | Uniform | 0.45 (mm) | 0.15 |
| | Dis. at elastic load transfer | Phase 3 | LogNormal | 2.09 (mm) | 0.22 |
| | Dis. at nonlinear load transfer | Phase 4 | LogNormal | 3.99 (mm) | 0.16 |
| Connection Type C1 | Load at onset of slip | Force @ A | LogNormal | 9.29 (kN) | 0.084 |
| | Load at onset of plasticity | Force @ C | LogNormal | 65.03 (kN) | 0.098 |
| | Maximum load | Force @ D | LogNormal | 107.78 (kN) | 0.039 |
| | Dis. at elastic frictional load transfer | Phase 1 | LogNormal | 0.39 (mm) | 0.29 |
| | Slippage length | Phase 2 | Uniform | 1.28 (mm) | 0.43 |
| | Dis. at elastic load transfer | Phase 3 | LogNormal | 2.74 (mm) | 0.175 ara> |

(continued)

**Table 8.2** (continued)

| Properties | | Notation (Fig. 8.3) | Type of Distribution | Mean | COV |
|---|---|---|---|---|---|
| | Dis. at nonlinear load transfer | Phase 4 | LogNormal | 6.04 (mm) | 0.158 |
| Connection Type C2 | Load at onset of slip | Force @ A | LogNormal | 20.14 (kN) | 0.219 |
| | Load at onset of plasticity | Force @ C | LogNormal | 97.51 (kN) | 0.115 |
| | Maximum load | Force @ D | LogNormal | 157.71 (kN) | 0.062 |
| | Dis. at elastic frictional load transfer | Phase 1 | LogNormal | 0.25 (mm) | 0.26 |
| | Slippage length | Phase 2 | Uniform | 1.32 (mm) | 0.44 |
| | Dis. at elastic load transfer | Phase 3 | LogNormal | 1.73 (mm) | 0.225 |
| | Dis. at nonlinear load transfer | Phase 4 | LogNormal | 2.55 (mm) | 0.235 |
| Connection Type C3 | Load at onset of slip | Force @ A | LogNormal | 29.28 (kN) | 0.069 |
| | Load at onset of plasticity | Force @ C | LogNormal | 152.85 (kN) | 0.095 |
| | Maximum load | Force @ D | LogNormal | 204.4 (kN) | 0.117 |
| | Dis. at elastic frictional load transfer | Phase 1 | LogNormal | 0.28 (mm) | 0.28 |
| | Slippage length | Phase 2 | Uniform | 1.11 (mm) | 0.37 |
| | Dis. at elastic load transfer | Phase 3 | LogNormal | 2.4 (mm) | 0.192 |
| | Dis. at nonlinear load transfer | Phase 4 | LogNormal | 2.18 (mm) | 0.174 |

## 8.5 Performance-Based Damage States for Transmission Towers

Transmission towers may experience various levels of damage during strong wind related hazards such as hurricanes. However, the criteria that define these levels of damage have not yet been established. In this section, five distinct levels of damage for transmission towers are defined. These damage levels can help researchers, designers, and utility owners in performance-based design, reliability analysis, and restoration planning of transmission lines. In order to investigate damage states, a set of 1000 realizations of uncertain variables were generated using LHS method. The generated realizations were used to perform 1000 nonlinear static pushover analyses of the

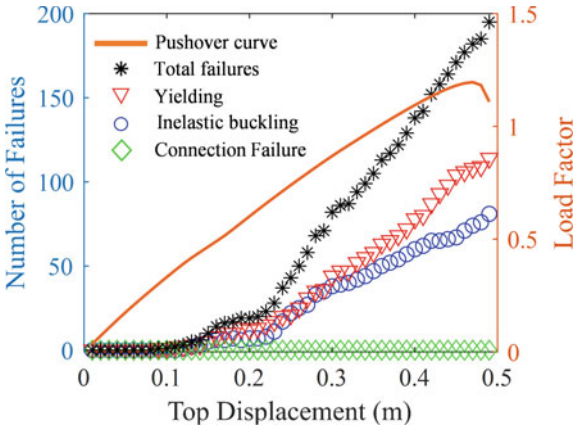


**Fig. 8.5** Pushover curve and failures for a sample realization of uncertain parameters

tower in longitudinal and transverse directions. As an example, the pushover curve for one of the 1000 pushover analyses in the longitudinal direction is provided in Fig. 8.5. The computational model tracks various types of damage in towers. The number of yielded elements, inelastic buckling of elements, and connection failures as well as total number of failures at each instant of pushover analysis are provided in Fig. 8.5. The tower used in this study is designed for a 130 mph (209.2 km/h) wind speed. Therefore, in the pushover analysis, the load factor of 1.0 corresponds to wind speed of 130 mph. As the wind-induced force relates to the second power of wind speed, i.e., Eq. (8.2), other load factors are scaled to 130 mph as:

$$V = 130\sqrt{F} \tag{8.5}$$

where $F$ is the load factor and $V$ is the wind speed in mph.

For the particular pushover analysis provided in Fig. 8.5, the maximum load bearing capacity of the tower is 1.15 times the design load indicating that the tower will fail under a 139.4 mph (224.3 km/h) wind. In addition, the tower will experience its first inelastic behavior under a load factor of 0.28, which corresponds to the wind speed of 68.8 mph (110.7 km/h). Therefore, for any wind speed equal to or less than this value, the tower would not undergo any permanent damage. Based on the present capability to track damage in the tower, a set of performance-based damage states are proposed, which are explained in detail next.

### *8.5.1 Slight Damage*

Although a tower might completely collapse under severe hurricane scenarios, in most weak to moderate hurricanes, transmission towers will not experience collapse; however, they may undergo some levels of damage. When the wind-induced loadings

on towers increases, they initially undergo elastic deformations. Prior to the occurrence of the first nonlinear deformation, the tower has not experienced any damage. Therefore, until the onset of the experience of the first nonlinear behavior in elements or connection failures, the tower is in 'no damage' state. As the loading on the tower increases, yielding and inelastic buckling may occur in lattice tower elements. In this state, the tower elements need patches or a handful of replacements to restore the reliability of the tower against future hazard events. In this context, slight damage is defined as the state where the spread of damage in the tower is limited and only a handful of patches or replacements of damaged elements are needed to repair the tower. The indication of this state is the first inelastic buckling, yielding or connection failure in the tower.

For the single tower realization provided in Fig. 8.6, the slight damage occurs at 0.28 load factor, which corresponds to 68.8 mph (110.7 km/h) wind speed (shown with the blue colored asterisk in Fig. 8.6). In addition, the top displacement of the tower corresponding to the onset of the slight damage is 9 cm. According to Saffir-Simpson Hurricane category (Table 8.3), the lowest gust wind speed for a hurricane is 81 mph (130.4 km/h) [1], indicating that the tower can undergo slight damage even for category 1 hurricane scenarios.

As the evaluation of the number of failures in towers requires complex computational models of the structure which may not be readily accessible for use in industry, the characterization of slight damage is presented here also in terms of the top displacement of the tower. This approach is commonly used in conventional

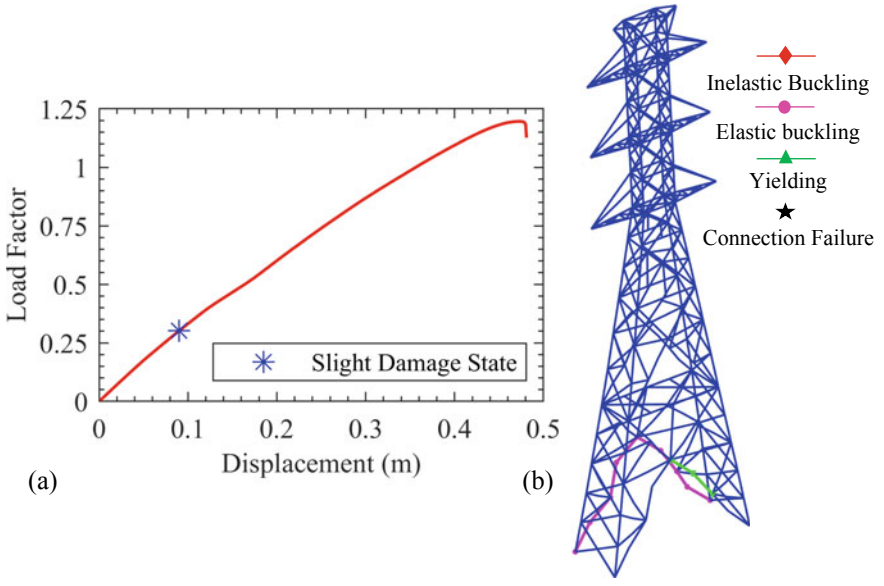


**Fig. 8.6** Identification of slight damage state in longitudinal direction: **a** pushover curve and **b** the state of the tower for the analysis demonstrated in Fig. 8.5

**Table 8.3** Saffir-Simpson hurricane categories [1]

| Saffir-Simpson Hurricane category | Sustained wind speed over water | | Gust wind speed over water | | Gust wind speed over land | |
|---|---|---|---|---|---|---|
| | mph | m/s | mph | m/s | mph | m/s |
| 1 | 74–95 | 33–42 | 90–116 | 40–51 | 81–105 | 36–47 |
| 2 | 96–110 | 43–49 | 117–134 | 52–59 | 106–121 | 48–54 |
| 3 | 111–129 | 50–57 | 135–157 | 60–70 | 122–142 | 55–63 |
| 4 | 130–156 | 58–69 | 158–190 | 71–84 | 143–172 | 64–76 |
| 5 | >157 | >70 | >191 | >85 | >173 | >77 |

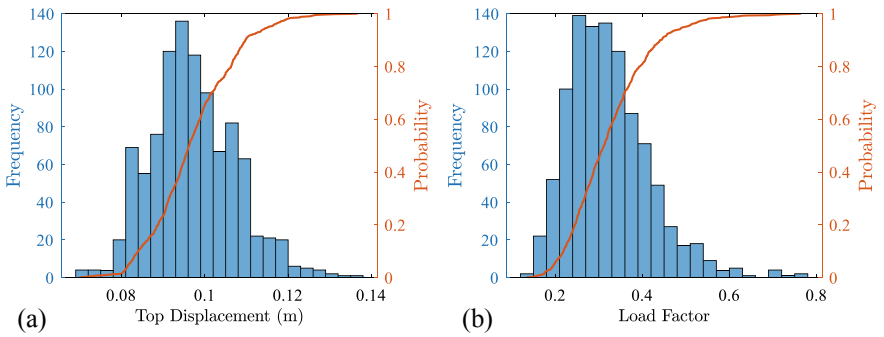


**Fig. 8.7** Histograms of 1000 pushover analyses in longitudinal direction for the slight damage state: **a** top displacement and **b** load factor

performance-based design guidelines. The displacement of the top of the tower and the load factor corresponding to the emergence of the first nonlinear behavior in the tower are studied here. The histograms of load factors and top tower displacement are provided in Fig. 8.7. The first failure occurs at a top displacement between 8 and 14 cm with a mean of 9.7 cm. The load factor corresponding to the slight damage has a mean of 0.32 and a standard deviation of 0.094. Converting the load factor to wind speed using Eq. (8.5), the mean wind speed and the standard deviation for the slight damage are 73.5 mph (118.3 km/h) and 39.9 mph (64.2 km/h), respectively, which again confirms that the tower on average undergoes a slight damage during category 1 hurricane scenarios. Although the slight damage state does not compromise the transmission of the electricity under the experienced wind hazard scenario, it may degrade the reliability of the tower against future extreme events and therefore must be considered for risk analysis of transmission systems over long horizons. In addition, for life-cycle cost assessments, slight damage should be considered as the repair or replacement of tower elements following each hurricane event may impose a substantial cost for the maintenance and the overall life-cycle cost of the transmission infrastructure.

### 8.5.2 Moderate Damage

If the loading on the tower increases, inelasticity will spread to a considerable number of elements or connections in the tower, however, the damage is not to a degree that threatens the stability of the tower under gravity loads. On the hand, the induced damage can considerably degrade the reliability of the tower for future extreme events. In this context, moderate damage is defined as the event where the ratio of the number of elements and joints with inelastic behavior including yielding, inelastic buckling, and connection failure to the total number of elements in the tower exceeds a preestablished threshold. This limit depends on factors that are relatively subjective and depend on the owner of the tower. Here, a set of thresholds rather than a single threshold are considered including 2, 3, and 5%. These thresholds are informed by the degree of inelasticity observed in pushover curves of the tower. For the same analysis provided in Fig. 8.5, the pushover curve and the state of the tower are presented in Fig. 8.8. The points corresponding to each threshold are above the slight damage. From the 1000 pushover analysis results for the longitudinal wind direction, the mean of the top tower displacement corresponding to 2, 3, and 5% limits are 18 cm, 21 cm, and 26 cm, respectively. Moreover, the color-coded deformed tower plots in Fig. 8.8b indicate that while multiple elements in the tower have experienced inelasticity, no collapse mechanism has been developed in the tower and the structure is functional. The histogram of top displacement and the load factor for the case where the number of failures is set to 5% of the total number of elements and connections in the tower, is provided in Fig. 8.9. A comparison of this figure with Fig. 8.7 for the slight damage reveals that the load factor and the top displacement of the tower are roughly doubled for moderate damage.

### 8.5.3 Extensive Damage

Extensive damage is the state where the tower has not yet experienced global failure and therefore the transmission of power has not been interrupted. However, the tower has reached a condition where the stability of the tower may be compromised under combined effects of future moderate winds and gravity, and therefore the structure requires immediate attention. In this state, while the tower has not collapsed, the degree of damage in the structure is extensive and repairing damages is either not feasible or not economic (i.e., the tower needs to be replaced). In this context, the extensive damage is defined as the state where the number of elements and connections with inelastic behavior exceeds 80% of the corresponding number when the tower reaches its load bearing capacity. As seen in Fig. 8.10, in this damage state, a large number of elements experience inelastic behavior, but since no global failure mechanism has formed, the tower has not yet collapsed. The histogram of the top displacement and load factor at the onset of extensive damage state for all pushover analyses performed for the longitudinal wind direction are presented in Fig. 8.11. For

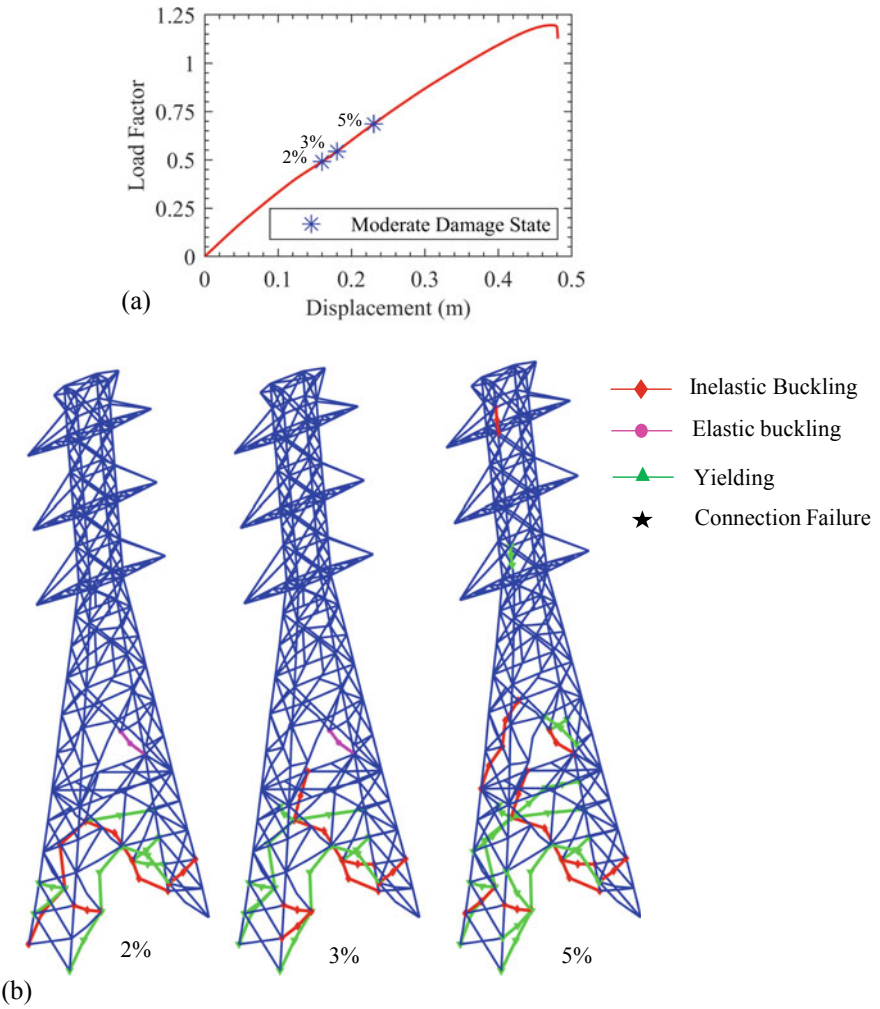


**Fig. 8.8** Identification of 2%, 3%, and 5% moderate damage states in longitudinal direction: **a** pushover curve and **b** the state of the tower for the analysis demonstrated in Fig. 8.5

the extensive damage, both displacement and load factor are again almost doubled compared to the moderate damage.

### *8.5.4 Collapse*

The tower reaches the collapse damage state when a global failure mechanism is developed and the tower is unable to carry additional loadings. Lattice towers may

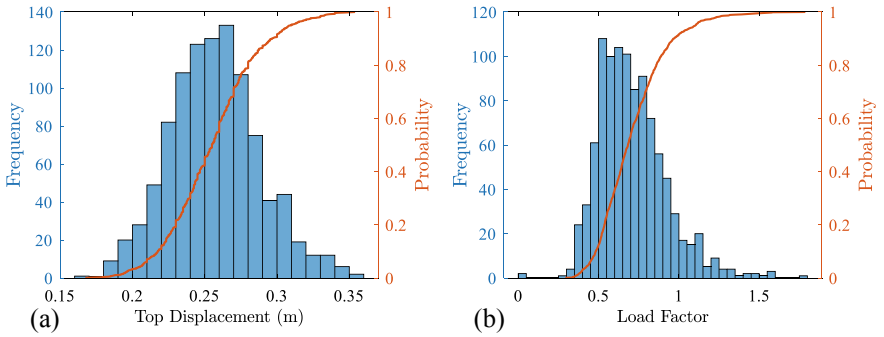


**Fig. 8.9** Histograms of 1000 pushover analyses in longitudinal direction for moderate damage state: **a** top displacement and **b** load factor for 5% failure corresponding to moderate damage

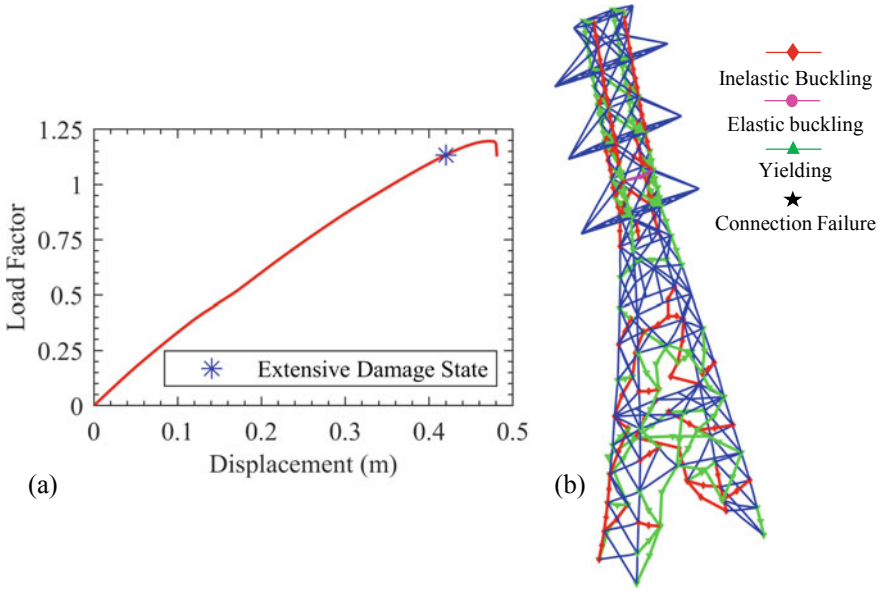


**Fig. 8.10** Identification of extensive damage state in longitudinal direction: **a** pushover curve and **b** the state of the tower for the analysis demonstrated in Fig. 8.5

experience two general patterns of collapse including complete and partial collapse. In the partial collapse, the upper portion of the tower including the cage and cross arms may fail while the bottom portion of the tower is intact. The complete collapse occurs often when the legs of the tower fail resulting in the collapse of the entire tower. It should be noted that in pushover analysis (Fig. 8.12a), the load factor increases until a significant drop is observed. The maximum load factor is considered as the load bearing capacity of the tower as the tower cannot resist against any additional loading. For the analysis that was shown in Fig. 8.5, the tower fails under a load

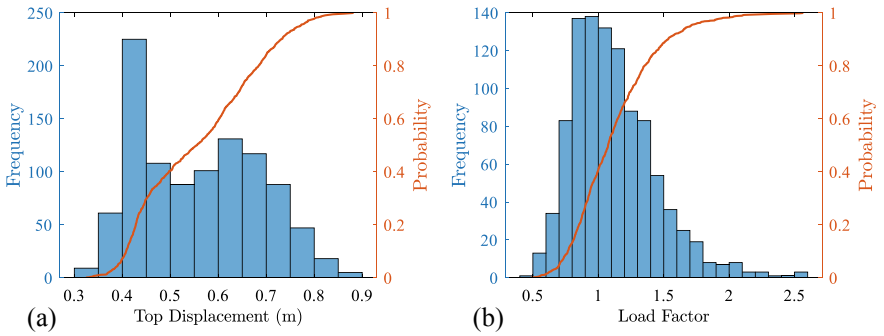


**Fig. 8.11** Histograms of 1000 pushover analyses in longitudinal direction for extensive damage state: **a** top displacement and **b** load factor

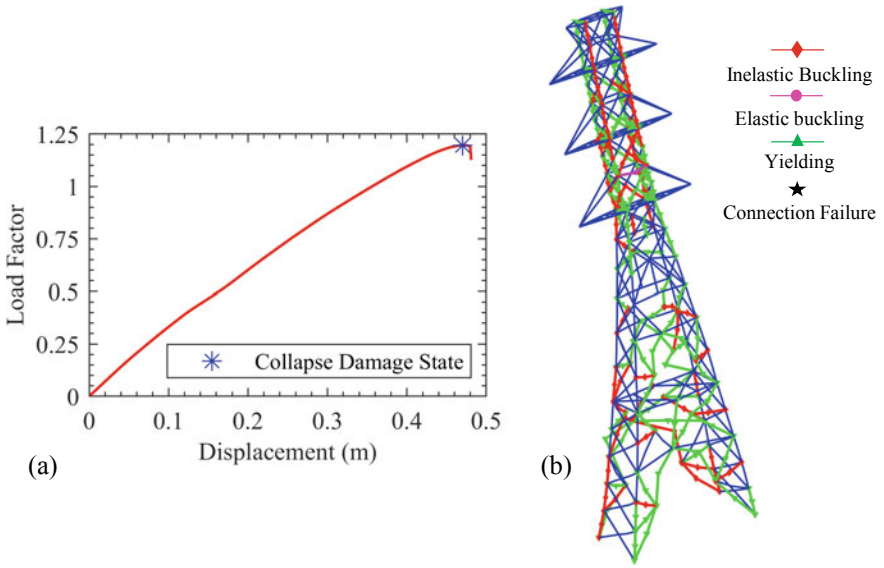


**Fig. 8.12** Identification of collapse state in longitudinal direction: **a** pushover curve and **b** the state of the tower for the analysis demonstrated in Fig. 8.5

factor of 1.15 which corresponds to a wind velocity of 139.4 mph (224.3 km/h). The collapse is partial and due to a failure mechanism that is developed in the cage of the tower. The histogram of the top displacement and the load bearing capacity for the 1000 pushover analyses are provided in Fig. 8.13 for the longitudinal wind direction. As expected, the values of load factor and top displacement are slightly higher than those for the extensive damage as the onset of the extensive damage is defined as when 80% of failures for the collapse state are developed in the tower.

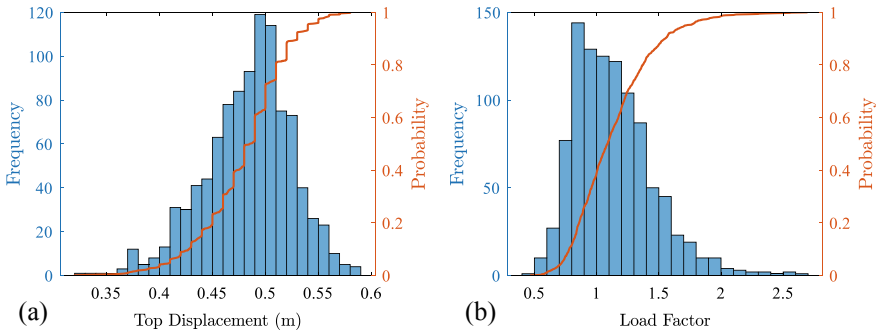


**Fig. 8.13** Histograms of 1000 pushover analysis in longitudinal direction for collapse state: **a** top displacement and **b** load factor

## 8.6 Fragility Modeling via Logistic Regression

A logistic regression model [11] is used to develop fragility models based on the survival-failure outcomes of the transmission tower simulations. This approach provides explicit mathematical expressions for representation of fragility models and thus facilitates the application of the developed fragility models in hurricane risk and resilience studies of power infrastructures [4, 7, 8, 13]. The probability of failure based on the logistic regression model with wind speed as the input parameter is as follows:

$$p_f = {}^{1}\!/_{1 + e^{-(\beta_0 + \beta V)}} \tag{8.6}$$

where $V$ is wind speed in terms of mph, and $\beta = \{\beta_0, \beta_1\}^T$ is the vector of regression coefficients. The form of the regression function is selected using the stepwise logistic regression process. Based on the Akaike Information Criterion (AIC) [3], a linear function of the feature was shown to be appropriate for this regression problem. The outputs of this regression model, which are the probabilities of the transmission tower being in a particular damage state, are illustrated in Fig. 8.14 for the transverse and longitudinal wind directions. The regression coefficients of this model are presented in Table 8.4. According to the developed fragility models, in response to a hurricane with design wind speed (i.e., 130 mph) in transverse direction, the transmission tower will be in slight, moderate, extensive, and collapse damage states with a probability of 0.8406, 0.1104, 0.0857, and 0.0581, respectively. Therefore, the tower can most likely continue to operate with little or no repairing. For the longitudinal direction, the tower will be in minor, moderate, extensive, and collapse damage states with probabilities of 1.0, 0.9234, 0.4512, and 0.2734, respectively. Therefore, it is more likely that the tower will be in moderate to collapse damage states. This is because in the longitudinal direction, the width of the tower is 2.7 m, while in the transverse direction the width of the tower is 7.6 m. Therefore, it is stronger in the transverse direction.

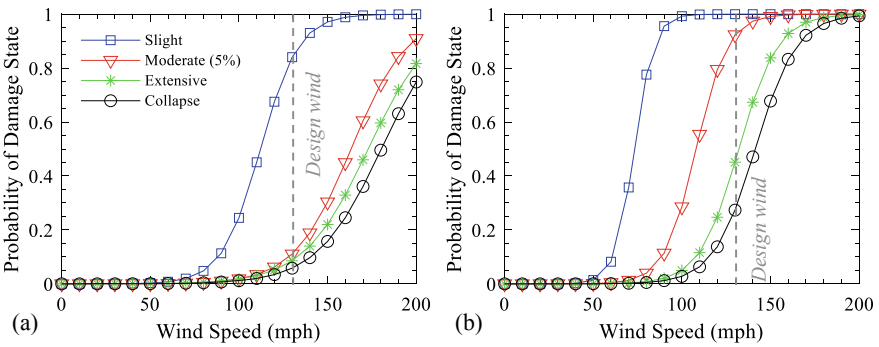


**Fig. 8.14** Hurricane fragility models for the 27.43 m double circuit vertical lattice tower for: **a** transverse and **b** longitudinal wind directions

**Table 8.4** Coefficients of the logistic regression models

| Wind direction | Damage state | $\beta_0$ | $\beta_1$ |
|---|---|---|---|
| Transverse | Slight | −10.4262 | 0.0930 |
| | Moderate (2%) | −10.0458 | 0.0784 |
| | Moderate (3%) | −10.1901 | 0.0742 |
| | Moderate (5%) | −10.2445 | 0.0628 |
| | Extensive | −9.5395 | 0.0552 |
| | Collapse | −9.9818 | 0.0554 |
| Longitudinal | Slight | −13.3875 | 0.1829 |
| | Moderate (2%) | −12.7250 | 0.1346 |
| | Moderate (3%) | −12.3704 | 0.1240 |
| | Moderate (5%) | −12.2771 | 0.1136 |
| | Extensive | −12.1438 | 0.0919 |
| | Collapse | −12.1615 | 0.0860 |

It should be noted that the wind-induced loads on conductors are only applied to the tower when the wind is applied in the transverse direction. Nonetheless, because the width is less than half in the longitudinal direction, the tower is significantly more vulnerable in the longitudinal direction. Moreover, in the transverse direction, the median wind speeds (i.e., wind speed associated with 50% probability of damage state) are 112, 163, 173, and 180 mph (180.2, 262.3, 278.4, and 289.7 km/h) for slight, moderate, extensive, and collapse damage states, respectively. In comparison, median wind speeds in longitudinal direction are 73, 108, 133, and 141 mph (117.5, 173.8, 214, 226.9 km/h) for slight, moderate, extensive, and collapse damage states, respectively. This implies 22–35% decrease in the median wind speed which further indicates higher vulnerability of the tower in the longitudinal direction (Fig. 8.14).

## 8.7 Summary and Conclusion

The power grid, especially the overhead infrastructure, faces substantial risks from extreme climatic hazards. In this environment, risk-informed decision making can guide limited available resources to where they can have the largest impact. A key element of grid risk analysis is the ability to project the future state of the power grid when facing extreme hazards. These projections can be facilitated via integration of hazard models with fragility models that express the likelihood of damages in structures conditional on the intensity of the event. As grid infrastructure decisions for preparing against hazards as well as the recovery of the system post hazards depend on the type and degree of damage sustained by the infrastructure, fragility models are needed for damage states that correspond to key states of overhead structures for repair and replacement decisions.

The current study proposed a set of performance-based limit state functions for various levels of damage in lattice transmission towers subjected to extreme wind loads. Specifically, five distinct levels of damage including no damage, slight, moderate, and extensive damage, as well as collapse were defined. Slight damage corresponds to the case where an element or connection of the system experiences the first damage. The state preceding slight damage is known as no damage state. The damage may occur due to yielding, inelastic buckling or connection failure. While these damage forms in an element or connection are local and alone may not jeopardize the integrity of the structure under gravity loads, they need to be repaired to ensure the reliability of the tower against future extreme wind events. Furthermore, moderate damage state is defined as the case where the tower experiences a considerable number of failures and therefore damaged tower elements may need to be repaired or replaced to ensure the reliability of the tower. Extensive damage state corresponds to the case in which the tower has not yet experienced collapse; however, the number of damaged elements and connections in the tower is considerably high to a degree that repairing the tower is not economic compared to replacing the tower, or the repair may not be feasible. This damage state is defined as the case where the number of damages in the tower exceeds 80% of the number of damages when the tower reaches its load bearing capacity. The last level of damage is the collapse state in which the tower is partially or completely failed due to instability. This state of damage is identified as when the tower reaches its load bearing capacity, which corresponds to the maximum load factor in pushover analysis.

The proposed definitions of damage states were applied to the nonlinear model of a double circuit vertical tower. A large number of random realizations of uncertain parameters including yield stress, modulus of elasticity, imperfection, joint slippage properties, and wind loading were generated using Latin Hypercube Sampling method. A nonlinear pushover analysis was conducted for each realization and the damage in the tower was tracked for each simulation. Based on the defined damage states, fragility models were developed via logistic regression for both transverse and longitudinal wind directions of the tower. The developed fragility models indicated high probability of slight damage state for the tower at the design wind speed for the

transverse direction and high probability of moderate damage for the longitudinal direction at the same wind speed.

The outcomes of this research in terms of multi-state fragility models enable accurate quantification of the type and extent of damage to transmission towers, which is essential for risk and resilience assessment. The proposed fragility models which represent a key component of probabilistic risk models can be used by utility owners and planners to support risk-informed decisions vis-à-vis long-term planning for hardening the grid as well as the distribution of grid recovery resources across the coverage area based on the anticipated types and degrees of damage to the infrastructure.

**Acknowledgements** This paper is based upon work supported by the Division of Civil, Mechanical and Manufacturing Innovation, National Science Foundation under Grants Nos. CMMI-1635569, CMMI-1762918, and CMMI-2000156. These supports are greatly appreciated.

## References

1. ASCE No. 07 (2016) Minimum design loads for buildings and other structures. American Society Civil Engineers (ASCE). Reston, VA, USA
2. ASCE No. 74 (2009) Guidelines for electrical transmission line structural loading. American Society of Civil Engineers (ASCE). Reston, VA, USA
3. Akaike H (1998) Information theory and an extension of the maximum likelihood principle. In: Selected papers of hirotugu akaike. Springer, New York, pp 199–213
4. Darestani YM, Shafieezadeh A (2019) Multi-dimensional wind fragility functions for wood utility poles. Eng Struct 183:937–948
5. Darestani YM, Shafieezadeh A, Cha K (2020) Effect of modelling complexities on extreme wind hazard performance of steel lattice transmission towers. Struct Infrastruct Eng 16(6):898–915
6. Darestani YM, Wang Z, Shafieezadeh A (2019) Wind reliability of transmission line models using kriging-based methods. In: Paper presented at the13th International Conference on Applications of Statistics and Probability in Civil Engineering (ICASP13), Seoul, South Korea, 26–30 May 2019
7. Dehghani NL, Darestani YM, Shafieezadeh A (2020) Optimal life-cycle resilience enhancement of aging power distribution systems: a MINLP-based preventive maintenance planning. IEEE Access 8:22324–22334
8. Dehghani NL, Jeddi AB, Shafieezadeh A (2021) Intelligent hurricane resilience enhancement of power distribution systems via deep reinforcement learning. Appl Energy 285: 116355
9. Ellingwood BR, Tekie PB (1999) Wind load statistics for probability-based structural design. J Struct Eng 125(4):453–463
10. Fereshtehnejad E, Shafieezadeh A (2016) Multiple hazard incidents lifecycle cost assessment of structural systems considering state-dependent repair times and fragility curves. Earthquake Eng Struct Dynam 45(14):2327–2347
11. Hosmer DW, Lemeshow S, Sturdivant RX (2013) Applied logistic regression, vol 398. Wiley
12. Huang M, Wu L, Xu Q, Wang Y, Lou W, Bian R (2020) Bayesian approach for typhoon-induced fragility analysis of real overhead transmission lines. J Eng Mech 146(9):04020092
13. Jeddi AB, Shafieezadeh A, Hur J, Kim M, Ha J (2020) Fragility assessment of overhead transmission towers under typhoon and earthquake multi-hazard events. In: Transactions of the korean nuclear society, autumn meeting

14. Jiang WQ, Liu YP, Chan SL, Wang ZQ (2017) Direct analysis of an ultrahigh-voltage lattice transmission tower considering joint effects. J Struct Eng 143(5):04017009
15. Jiang WQ, Wang ZQ, McClure G, Wang GL, Geng JD (2011) Accurate modeling of joint effects in lattice transmission towers. Eng Struct 33(5):1817–1827
16. Kroetz HM, Tessari RK, Beck AT (2017) Performance of global metamodeling techniques in solution of structural reliability problems. Adv Eng Softw 114:394–404
17. McKenna F (2011) OpenSees: a framework for earthquake engineering simulation. Comput Sci Eng 13(4):58–66
18. Rezaei SN (2017) Fragility assessment and reliability analysis of transmission lines subjected to climatic hazards (Doctoral dissertation, McGill University)
19. Roueche D, Cleary J, Gurley K, Marshall J, Pinelli J, Prevatt D, Smith D, Alipour A, AngelesK, Davis B, Gonzalez C (2018) StEER—hurricane Michael: field assessment team 1 (FAT-1) early access reconnaissance report (EARR). DesignSafe-CI. https://doi.org/10.17603/DS2G41M
20. StEER (2017) NSF Structural Extreme Events Reconnaissance (StEER) Network, Fulcrum Community, Accessed 1 Mar 2021
21. Tessari RK, Kroetz HM, Beck AT (2017) Performance-based design of steel towers subject to wind action. Eng Struct 143:549–557
22. Ungkurapinan N (2000) A study of joint slip in galvanized bolted angle connections
23. Uriz P, Filippou FC, Mahin SA (2008) Model for cyclic inelastic buckling of steel braces. J Struct Eng 134(4):619–628
24. Xue J, Mohammadi F, Li X, Sahraei-Ardakani M, Ou G, Pu Z (2020) Impact of transmission tower-line interaction to the bulk power system during hurricane. In: Reliability engineering & system safety, vol 203, p 107079

# Chapter 9
# Building Adaptation to Extreme Heatwaves


**Dileep Kumar, Morshed Alam, and Jay Sanjayan**

**Abstract** Climate change is aggravating the summer heatwaves, making them more severe, frequent and prolonged. During the heatwave period, buildings are overheated due to heat gain from surroundings which poses significant risks to the occupants. Therefore, adapting our buildings to extreme heatwaves is of paramount importance. This chapter aims to identify the factors contributing to overheating buildings and the associated mitigation measures. The identified overheating factors are low energy building design, lightweight construction materials, internal heat gain, occupant behaviour and urban heat island effect. The overheating mitigation measures are divided into four categories (1) Modification of local microclimate, (2) resistance to heat transfer from outdoor to indoor (3) Absorption of transferred heat through thermal mass, and (4) Release of trapped heat from indoor to outdoor. The effectiveness of each mitigation measure category depends on indoor and outdoor environmental conditions. Numerical analysis showed that the risk of experiencing heat stress during extreme heatwave decreases with increasing energy star rating of the houses in Melbourne, Australia. If the entire existing lower energy star rated houses can be upgraded to 5.4 star, the percentage of Melbourne population experiencing six severe heat stress hours will decrease from 50% to only 4% at 36 °C mean outdoor temperature. The heat-related mortality and morbidity also decreases with increasing house energy rating. Net-benefit analysis showed that upgrading the lower energy rated houses to 5.4 star is highly beneficial with net-benefit becoming positive within 2–5 years. Emerging technology like dynamic insulation material (DIM) which changes the resistance of the external walls and ceilings depending on the indoor and outdoor temperature can help to minimise overheating in a highly insualted and air-tight building. Numerical simulation showed that DIM reduces the indoor air temperature in bedroom and living room by up to 1.1 °C and 1.2 °C, respectively, in the case study building in Melbourne, Australia.

D. Kumar · M. Alam (✉) · J. Sanjayan
Centre for Smart Infrastructure and Digital Construction, Department of Civil and Construction Engineering, Swinburne University of Technology, Hawthorn, VIC 3122, Australia
e-mail: mmalam@swin.edu.au



M. G. Stewart and D. V. Rosowsky (eds.), *Engineering for Extremes*, Springer Tracts in Civil Engineering, https://doi.org/10.1007/978-3-030-85018-0_9

## 9.1 Introduction

Climate change is resulting in a hotter and longer summer period and more frequent heatwaves across the globe [1]. As a result, buildings are overheated during those hot summer periods, particularly in temperate climate zones, where retention of winter heat has been the principal focus of dwelling design and construction. Overheating poses a significant threat to human health, particularly the elderly occupants and babies.

Heatwaves have caused thousands of deaths around the world in the past. In Europe, over 70,000 casualties were reported, including 14,000 in French buildings and 2000 in British homes during the heatwave in August 2003. Eastern Europe and Russia reported 56,000 heat-related mortalities in July and August 2010. Another heatwave period was responsible for 863 excess mortalities in the UK, and a significant portion of the deceased was over 65 age group residents [2]. In Australia, extreme heat events caused at least 4,555 deaths since 1900, which is more than the combined total deaths from all other natural hazards [3]. The 2009 heatwaves in Victoria and South Australia resulted in 432 death [3]. Another scorching heatwave in 2014 caused 167 excess death in Victoria [4]. During the heatwave period of 2003, the peak indoor temperature exceeded 30 °C across 20 terraced apartments in Lindas, Sweden [5]. In the same period, the indoor temperature of British homes was on average 2.3 °C higher, with a peak indoor temperature of 39.2 °C [6]. The average indoor temperature was recorded as 27 °C in South East England and over 35 °C in major Australian cities (Melbourne, Canberra, and Adelaide) [7]. During a heatwave, most of the heat-related deaths occured to those people who stayed at home in overheated indoor environment and don't have access to air-conditioning.

The Zero Carbon Hub (ZCH) defines Overheating as "the phenomenon of excessive and prolong high indoor temperature in buildings which is responsible for occupants' thermal dissatisfaction and thermal degradation of processes undertaken within the space" [8]. According to the 2006 definition of the Chartered Institution of Building Services Engineers (CIBSE) guide, overheating occurs when the indoor operative temperature over 28 °C in the living room and 26 °C in the bedroom for 1% of occupancy hours in households.

A national survey on summertime temperatures and overheating risks in England reported that new homes (post-1990) have a higher risk of overheating than existing building stock [9]. Moreover, the Zero Carbon Hub found that the risks of overheating is maximum in urban apartments based on survey responses of 70% of the housing provider organisation [10]. The CIBSE adaptive criteria-I is breached by 30% of flats and communal area, with 70% held operative temperature over 28 °C for 1% of occupied hours in English dwellings [11]. McGill et al. [12] recorded indoor operative temperature over 28 °C in living rooms of 27% of the selected low-energy buildings constructed between 2012 and 2014. Considering Passivhaus criteria, overheating was determined in 57% and 75% of monitored bedrooms and living rooms, respectively. Another study in Melbourne, Australia reported 11–46% overheating hours in heavyweight two-story student accommodation with insulated external and internal

walls, floor, and single glazed windows. Apartments with a reinforced concrete structure and lightweight cladding, insulated internal and external walls, ceiling, and operable double-pane window allowing natural ventilation cooling, has the lowest overheating of 6%–23% following four international standards: CIBSE UK, NF-HQE France, Passivhaus Germany and ASHRAE USA [13]. The post-occupancy survey of apartments in Melbourne has identified that residents have a high level of satisfaction with overall building design and performance, excluding the two main issues: summertime overheating and outdoor noise [14].

This chapter aims to identify the factors contributing to building overheating and discuss possible strategies to mitigate overheating risks. It then presents the risks of experiencing heat stress in different energy rated houses in Melbourne, Australia and cost–benefit analysis of upgrading the energy star rating of a house. Furthermore, it explores potential new technologies to reduce building overheating and highlights future research needs.

## 9.2 Factors of Overheating

Based on an extensive literature review, the major causes of summertime building overheating have been identified and presented in Fig. 9.1.

### *9.2.1 Low Energy Building Measures*

Various energy efficiency measures were introduced in the building sectors around the world to reduce energy consumption and greenhouse gas emissions. Adoption of energy-efficient measures in Australian dwellings has reduced average daily electricity use by 64% and 62% in Canberra and Melbourne [15]. However, those energy-efficient measures were also responsible for 7.1% overheating under the current climate of Canberra and Melbourne in the absence of mechanical cooling [15]. The following section describes the influence of different low energy building measures on overheating.

#### 9.2.1.1 Insulation

Insulated buildings consume less energy in the heating-dominated region, whilst it may increase energy use in the cooling-dominated region [16]. Insulating the external wall of the building has dropped heating demand by up to 70% depending on climatic conditions [17], reducing $CO_2$-emissions by 42% [18]. However, the insulated external wall of the UK dwelling has also exacerbated overheating by 15–17% [19]. The use of insulation close to indoor conditions in a lightweight concrete

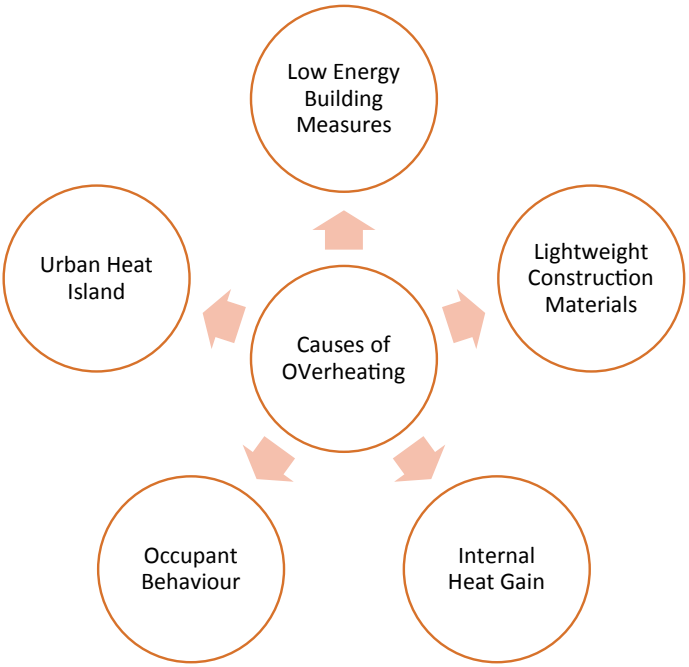


**Fig. 9.1** Major causes of summer overheating in buildings in a temperate climate

wall had a higher risk of overheating than insulation applied close to outdoor environment because of low heat rejection at nighttime [20]. Another experimental study showed that the mean operative temperature in the living room and bedroom of an internally insulated house were 2.2 °C and 1.5 °C higher than that of an identical uninsulated house during summer in the absence of night ventilation [21].

#### 9.2.1.2 Window to Wall Ratio

Modern buildings have a glassy appearance with large windows that are difficult to open, creating thermal discomfort during summer. In a UK passive house, the percentage of overheating in the living room increased from 10 to 38% when the window-to-wall ratio was changed from 25 to 55% in similar climatic conditions. The predicted percentage of overheating is expected to be 47% by 2030 if the climate change scenario is considered [22].

#### 9.2.1.3 Coatings

High-emissivity (low-reflective) coatings materials are preferred in cold and temperate climates during winter because it can absorb more solar energy during the

daytime and thereby lowers heating energy use in buildings [23]. However, during the summer period, those low-reflective coating materials may increase indoor air temperature by absorbing more solar radiation. Cheng et al. [24] showed that low-reflective paint increased the mean indoor air temperature by 4 °C in winter, benefiting with heating energy savings. However, in summer, the mean indoor temperature increased by 6 °C that not only overheats the passive houses but also increases the cooling load of active buildings.

#### 9.2.1.4 Airtightness

Air-tightness in a building refers to unintentional heat and mass transfer between indoor and outdoor environments through any cracks, crevices, or gaps around doors and windows. Sealing existing buildings to improve airtightness was found to decrease infiltration by 18% and increase energy savings by 10% in an active building and reduce mean summer temperature by 1.2 °C in Passivhaus house [25]. However, airtight buildings were also found to experience significant overheating. A recent study on airtight apartment buildings showed CIBSE overheating criteria was exceeded for 30–77% of occupied hours even after using a mechanical ventilation system [26].

### *9.2.2 Lightweight Construction Materials*

The post-occupancy survey of two prefabricated timber houses revealed that 75 and 81% of occupants felt warm during summer. Floor-to-ceiling height was the most influencing factor exacerbating the summer overheating. According to CIBSE comfort criteria, 67% of the spaces were subjected to extreme summer overheating during the monitoring period. The comparative analysis of previous studies identified that the overheating was more frequent in timber houses because of the lightweight structure than previously surveyed buildings built with heavyweight materials [27].

### *9.2.3 Occupant Behaviour*

Occupant behavior in buildings refers to human-building interaction related to energy use, their conscious or unconscious adaptation related to the indoor environment or personal situation, and actions. Occupant's behavioral adaptation includes the use of passive measures such as nighttime ventilation cooling by opening the window, mitigating daytime overheating by shading and closing the window, changing clothes to feel comfortable using less energy, and others. They are equally important to common structural adaptations such as insulation, thermal mass, window glazing, external shading, and efficient appliance. They vary with occupant types in a household e.g.

vulnerable occupants (over 65 years old, disabled, and prolong illness) may have limited control over passive measures due to physical mobility and social isolation. The vulnerable homes were reported to have 34% overheating hours compared to18% in non-vulnerable dwellings confirming the ventilation effect of window openings [28]. However, natural ventilation through opening windows is not always available or desirable due to security concerns and noise pollution.

### *9.2.4 Internal Heat Gain*

The internal heat gain in buildings refers to the heat generated by occupants, appliances, lightings, and building services such as heating and cooling systems. In a compact building, the overcrowding has reduced heating demand by accumulating occupant heat within the building. The kitchen was found to have more risk of overheating (18%) than the living room (5%) due to the heat generated by cooking activities [28]. In offices, computer monitors, televisions, and other electronics and miscellaneous devices were responsible for higher cooling energy use than residential buildings [29].

### *9.2.5 Urban Heat Island Effects*

In urban areas, the surfaces capture, absorb, and store more short-wave solar radiation compared to rural areas. The urban street canyon is confined with smaller sky view reducing the nighttime cooling effect of long-wave radiation. Additionally, anthropogenic heat emissions also exacerbate urban microclimate [30]. As a consequence, the ambient air in urban areas can be up to 10 °C hotter than in rural areas [31]. Santamouris et al. [32] showed that the ambient air temperature in the central part of Sydney is 6 °C higher than coastal areas due to high anthropogenic heat emission and smaller sky views. Magli et al. [33] reported that the monthly average ambient temperature in urban areas of Modena was 1.6 °C higher than its suburban area with the highest temperature difference of 6 °C during the nocturnal period. The high outdoor temperature exacerbates summer overheating and reduces the natural ventilation cooling effect. Palme et al. [34] found that urban heat island reduces the cooling capability of natural cross ventilation by up to 20–30% in Valparaíso and Guayaquil, South America. Consequently, overheating hours ($\geq$28 °C) in urban buildings were higher than in suburban and rural areas.

## 9.3 Overheating Mitigation Measures

Overheating mitigation measures can be divided into four categories as shown in Fig. 9.2.

### *9.3.1 Modifying Surrounding Micro-Climate*

This category focuses on cooling down the surrounding micro-climate and minimise the occurrence of the urban heat island. To reduce urban heat island effects, advanced materials including reflective materials (Low-E and retro-reflective, thermochromic and fluorescent, photonic and plasmonic) and thermal storage materials (PCM coating), have been developed by the researchers which reduced building envelope surface temperature by up to 12% [35]. The use of reflective coating [36] and thermal storage materials [37] were shown to reduce the peak ambient temperature up to 1.5–2.0 °C and 8 °C, respectively. Moreover, introducing green infrastructures, such as green roofs and vertical vegetation on a city scale, may on average decrease the ambient temperature between 0.3–3 °C through transpiration cooling and maintain average leaf temperature at about 21 °C irrespective of weather conditions [38].

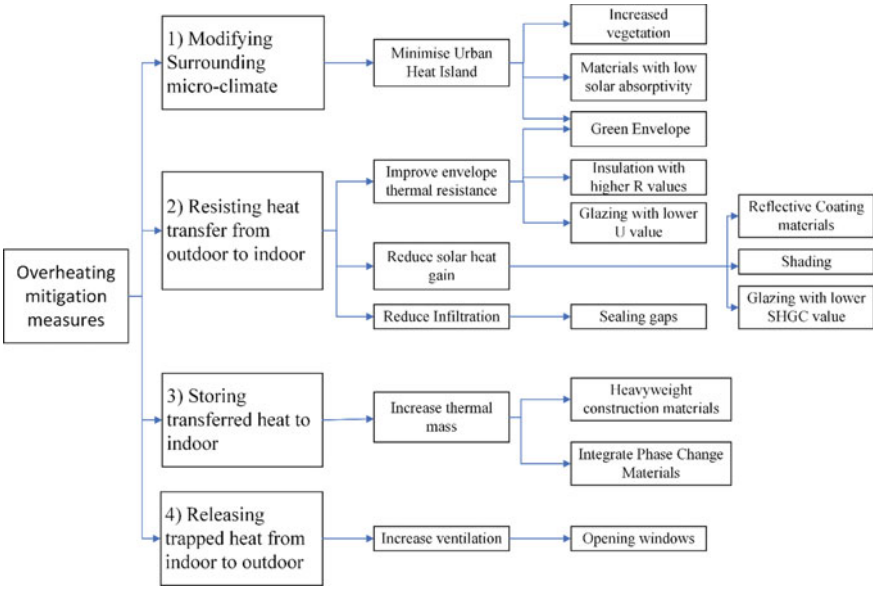


**Fig. 9.2** Categories of overheating mitigation measures

### *9.3.2 Resisting Heat Transfer from Outdoor to Indoor*

This step focuses on reducing conduction, convection, and radiation heat transfer through the building envelope. This step is effective when the indoor temperature is lower than the outdoor temperature during a hot summer day.

#### 9.3.2.1 Improving Envelope Thermal Resistance to Minimise Conduction Heat Transfer

Insulation materials are predominantly used in the building envelope to resist conduction heat transfer through the building envelope. Barnett et al. [39] also showed that annual severe discomfort hours (Discomfort index over 28 °C) could be reduced by 24–78% by insulting the traditional residential building in Australian climates. The heat stress level was measured using the Discomfort index (DI) scale, which is the average of wet-bulb and dry-bulb temperature. The heat stress is considered severe if the DI is over 28. Applying insulation close to indoor conditions reduced heating load by retaining heat inside, which exacerbates the risk of summer overheating. Contrarily, the use of insulation in the exterior wall close to surrounding conditions reduces overheating hours because it mainly resists daytime heat gain, reducing indoor air temperature [31].

A green envelope can also reduce the heat transfer due to increased thermal resistance with the addition of soil layer, increased thermal mass with the moisture content of the soil, higher surface reflectivity with green leaves and evapotranspiration [40]. Integration of a vegetated roof reduced heat transfer by up to 25% as compared to without plantation [41] resulting in an average reduction of an indoor air temperature of 0.6 °C and peak indoor temperature up to 1.1 °C [42]. Hoof et al. [40] found that green roofs reduced overheating hours over the CIBSE threshold. To eliminate the negative impact of soil layer thermal resistance, Lesjak et al. [43] developed an independent green façade that reduced the indoor operative temperature by 1.8–6.3 °C and kept the indoor temperature below 26 °C throughout the day.

#### 9.3.2.2 Reducing Solar Heat Gain

Radiative solar heat gain in buildings can be reduced by using reflective coatings, shading, and Low SHGC (solar heat gain coefficient) windows. A light colour coating absorbs less solar radiation compared to dark colors which results in lower heat transfer through the building envelope [44]. The high reflective coating materials was found to reduce heat transfer through the envelope by 18% [45] and improve thermal comfort by 22% [24] in traditional German buildings depending on structure heat storage and resistance capacity, and climatic conditions. Retrofitting the detached Dutch house with low-emissivity coating dropped the overheating hours by 89% [40].

Solar shading refers to the prevention of unwanted solar energy gain in a building through a transparent envelope. Shadings can be classified as fixed and moveable. Fixed shading includes overhang and awning, whilst available movable shadings are blinds and shutters. A 1.2 m overhang reduced the overheating hours from 75% (with no overhang) to 42% in an English dwelling [46]. Sometimes, fixed shadings are difficult to retrofit or refurbish thereby the moveable shadings are easy to install and operate. Moveable shadings were found to reduce overheating hours by 39% for external shutters and 20% for internal blinds. Internal blinds were less effective than external shutters because of their direct contact with indoor air. The major drawback of moveable shading is the loss of external view [40].

Replacing the single-glazing window with a double and triple-glazing window reduces conduction and radiation heat gain because of lower U-value and lower solar heat gain coefficient values without sacrificing external visibility. A reflective double glazing window increased the number of hours with comfortable indoor temperature by 107% and 14% in unventilated and ventilated rooms, respectively, compared to a traditional single clear glazing [47]. Moreover, Porritt et al. [31] also reported that in a naturally ventilated house, replacing the double-glazed window with a low-E triple-glazed window reduced overheating by 20% depending on building orientation. Combing insulation with solar shading and window rules had eliminated the summer overheating in monitored dwellings in south England [21].

### *9.3.3 Absorbing the Transferred Heat*

When the hot weather continues for some time, the heat slowly transfers through the building envelope and starts to increase the indoor air temperature. In this scenario, thermal mass can absorb the transferred heat and inhibits the indoor temperature rise. Thermal mass is the ability of a building envelope to store heat per unit surface area and per unit rise in material temperature. It is classified as a lightweight, medium weight, and heavyweight with a heat storage capacity of 38, 281, and 520 kJ/m$^2$K, respectively. It passively absorbs, stores, and release thermal energy suppressing the indoor temperature peak and swing with diurnal temperature fluctuation. A net-zero-energy townhouse in Toronto [48] and low-energy timber house in the UK [49] have been shown to have the lowest heating demand in winter, but the risk of summer overheating in these dwellings were higher due to low thermal mass. Replacing lightweight wall material with cellular concrete lowered severe discomfort from 18.6 days to only 8 h in an experimentally designed test house, in central-western Poland [50].

Building envelope thermal mass can also be increased by integrating latent heat thermal energy storage materials, also known as Phase change materials (PCM). PCM stores energy in the form of latent heat and therefore have higher heat storage capacity compared to sensible heat storage. The PCM integrated building envelope had improved occupant thermal satisfaction by 10.7% in Athens and 18.1% in Marseille [17]. Figure 9.3 shows that the combination of PCM and nighttime venti-

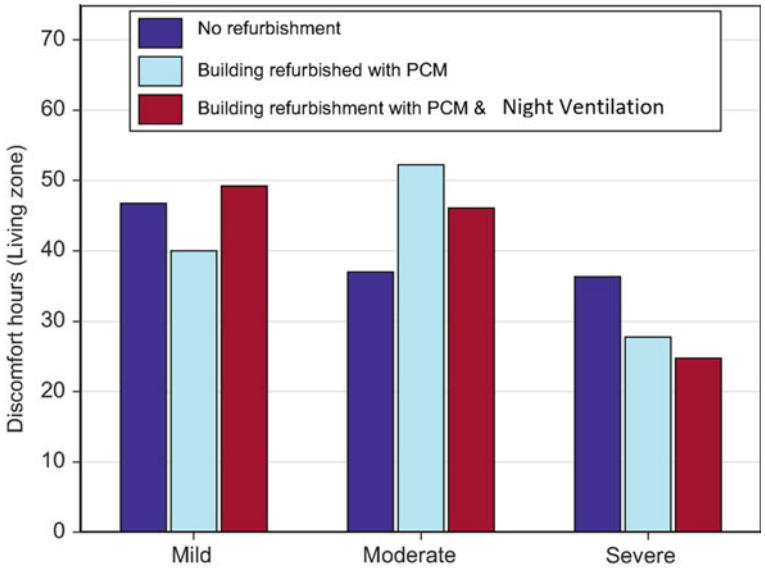


**Fig. 9.3** Hours of different heat risk levels for five consecutive days in a typical Melbourne house during extreme heatwave conditions [49]

lation (NV) could reduce severe discomfort hours by 65% in a typical residential building in Melbourne, Australia in extreme heatwave conditions [51]. In another study, PCM integrated external wall, where PCM was applied closer to the exterior surface, has maintained indoor temperature below 26 °C in an English dwelling. Hence, PCM has passively mitigated overheating in buildings [52].

### *9.3.4 Releasing the Heat from Indoor to Outdoor*

This category is essential when the outside air temperature drops in the evening, but the indoor temperature is still considerably higher than the outdoor and is over the thermal comfort threshold. It is crucial to release the trapped heat from indoor to outdoor, through passive measures such as natural ventilation via opening windows or active measures such as air-conditioning. However, the use of air-conditioning is not sustainable as it will increase the peak cooling demand and may also result in a power shortages because the existing energy infrastructure may not be sufficient to meet the peak cooling demand during a hot summer period. Therefore, passive measures to release trapped heat are the more preferred options. Passive strategies, including thermal insulation and mass, reflective coating, and ventilation, have reduced the heat stress hours in different apartment buildings up to 85% [53]. Natural ventilation cools down a building having a high thermal mass structure by releasing the daytime

absorbed heat back into the surroundings. The nighttime ventilation reduced the discomfort hours over the CIBSE threshold up to 67% in UK dwellings [31].

## 9.4 Mitigation of Heat Stress Risk Through Building Energy Retrofitting

Alam et al. [54] numerically investigated the risk of experiencing heat stress in different energy star rated houses in Melbourne, Australia using EnergyPlus. The simulaitons were carried out using a typical single storey and double storey brick veneer house with floor areas of 232 $m^2$ and 326 $m^2$, respectively. Different energy star rated houses were represented by changing the insulation value and infiltration rate as shown in Table 9.1.

ACH = Air change per hour, U = Heat transfer coefficient (Wm-2 K-1), SHGC = Solar heat gain coefficient.

The level of heat stress in different energy rated houses were calculated using Wet Bulb Glove Temperature (WBGT) index which is widely used around the world and is the basis for ISO 7243 heat stress standard (Parsons, 2006, [55, 56]. WBGT is calculated using Eq. (9.1).

$$WBGT = 0.67T_{wb} + 0.33T_{db} - 0.048 \log v(T_{db} - T_{wb}) \tag{9.1}$$

Here, $T_{wb}$ is the wet bulb temperature, $T_{db}$ is the dry bulb temperature and $v$ is the indoor air velocity.

**Table 9.1** Modifications of the base house to represent different energy star-rated houses in Melbourne [54]

| | 0.9 star | 1.8 star | 2.3 star | 3.7 star | 4.5 star | 5.4 star |
|---|---|---|---|---|---|---|
| Energy consumption ($MJ/m^2$/year) | 571 | 421 | 348 | 217 | 170 | 137 |
| External wall insulation ($m^2K/W$) | No | No | No | No | R 2.0 | R 4.0 |
| Ceiling insulation ($m^2K/W$) | No | No 60% R 1.0 40% | R 1.0 | R 2.0 | R 4.0 | R 6.0 |
| Infiltration (ACH) | Average = 1.7 ACH | Average = 1.15 ACH | Average = 0.96 ACH | Average = 0.4 ACH | Average = 0.4 ACH | Average = 0.3 ACH |
| Window glazing | U = 5.75 SHGC = 0.69 | U = 5.75 SHGC = 0.69 | U = 5.75 SHGC = 0.69 | U = 5.75 SHGC = 0.69 | U = 5.75 SHGC = 0.69 | U = 5.75 SHGC = 0.69 |

The indoor environment is considered to be exposed to severe heat stress when WBGT $\geq$ 25. Figure 9.4 shows the number of hours with WBGT $\geq$ 25 in different star rated house corresponding the to mean outdoor temperature (Mean T). Mean outdoor temperature is the average of daily maximum and minimum temperature. The figure shows that the number of severe heat stress hours (WBGT $\geq$ 25) are higher in the case of a lower star-rated houses compared to a higher star-rated houses at a constant meant T.

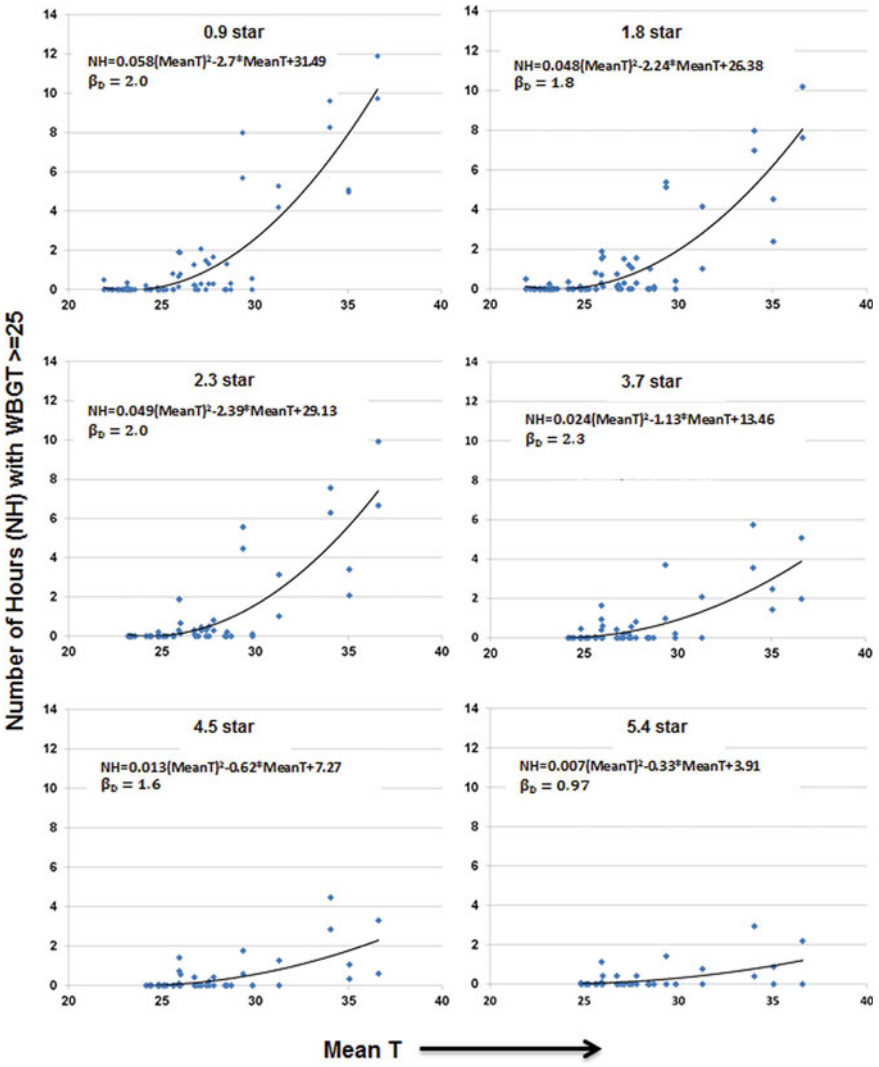


**Fig. 9.4** Heat stress hours against mean outdoor temperature (Mean T) in different star rated houses [54]

The probabilities of experiencing heat stress by the occupants in different energy star rated houses were calculated using the following formula [57]:

$$Probability\ of\ exposure = 1 - \phi\left(\frac{\log C - \log\left(A * (MeanT)^2 - B * MeanT + C\right)}{\beta_D}\right) \tag{9.2}$$

where, $\boldsymbol{C}$ is the tolerance limit of heat stress hours. $\boldsymbol{A}$, $\boldsymbol{B}$ and $\boldsymbol{C}$ are regression coefficients and were determined from the relationships show in Fig. 9.5 for different energy star rated houses. $\boldsymbol{\beta_D}$ is the standard deviation of actual data from the calculated data.

Figure 9.5 shows the percentage of total Melbourne population exposed to severe heat stress conditions under a typical 2009 Melbourne heatwave condition. Three different curves were calculated for three different tolerance limits. The higher the tolerance limit, the lower is the vulnerability to heat stress. Generally, strong healthy young persons will have a higher tolerance limit whereas e older people and babies have a lower tolerance limit. Figure 5a shows that when Mean T reaches 36 °C (typical of 2009 heatwave in Melbourne), over 80% of total population are exposed to 1 heat stress hours and approximately 50% of total population are exposed 6 heat stress hours. Approximately 1.9 million of the existing houses were built before 2005 which represents nearly 86% of the total houses [58]. The average energy star rating of those existing houses is onle 1.81 star compared to current standards of 6 star. If the entire existing lower energy star rated houses can be upgraded to 5.4 star, percentage of Melbourne population exposed to 1 and 6 heat stress hours will reduce to 54% and 4% respectively at 36 °C Mean T (Fig. 5b). In another study, Alam [59] investigated heat-related heath hazard in different energy star rated houses and reported that heat related mortaility and morbidity can be reduced significantly through energy efficiency retrofitting as shown in Table 9.2.

## 9.5 Net-Benefit Analysis of Heatwave Adaptation Measures

In case of non-air-conditioned houses, the benefits of upgrading house star rating are gained from reduced mortality and morbidity from heatwave, reduced heating cost and extended thermal comfort period during summer. Whereas in an air conditioned house, benefit is gained from reduced heating and cooling cost and reduced peak energy consumption. There is no reduced mortality and morbidity benefit in case of air-conditioned houses. The net-benefit of upgrading the house star rating was calculated according to the following formula:

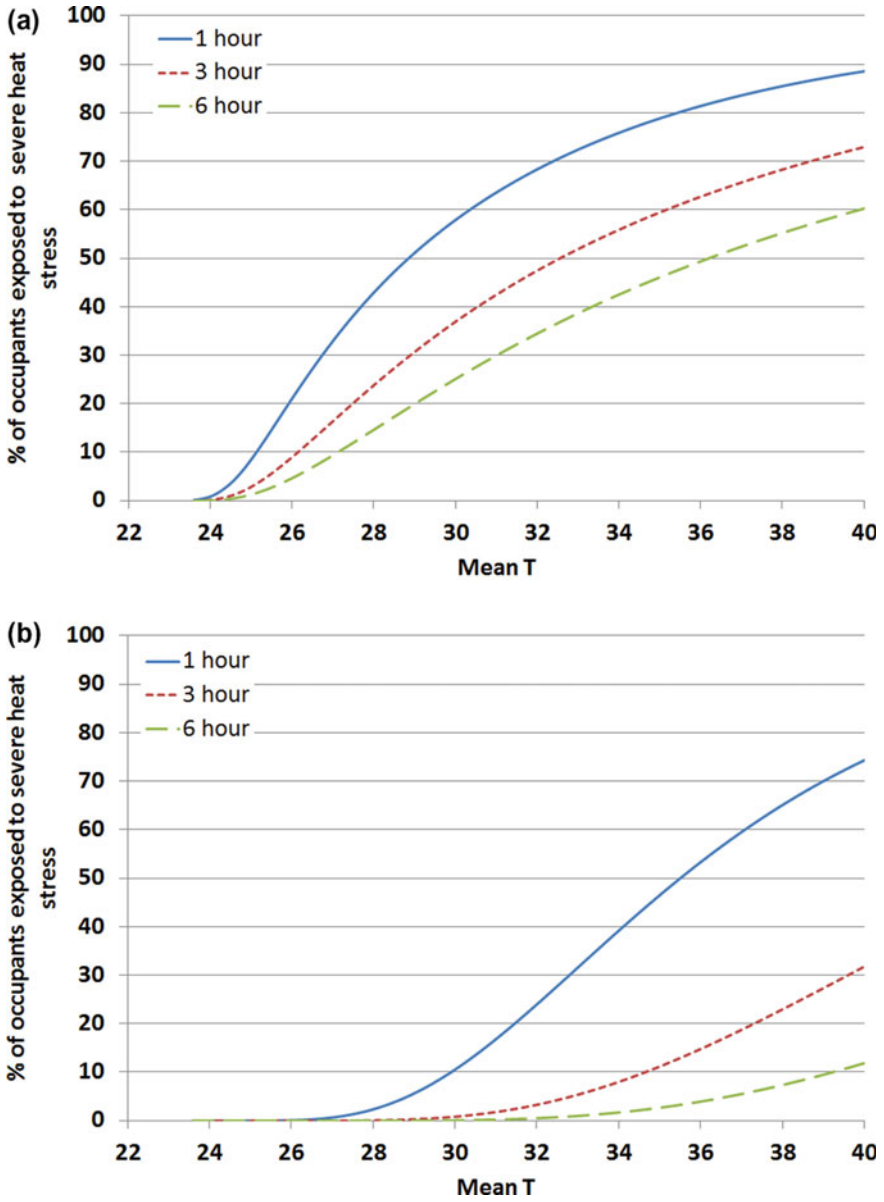


**Fig. 9.5** Percentage of occupants exposed to heat stress under **a** present conditions and **b** entire existing houses upgraded to 5.4 star [54]

**Table 9.2** Predicted health impacts of the Melbourne's 2009 heatwave in different star rated houses [59]

| | 0.9 star | 1.8 star | 2.3 star | 3.7 star | 4.5 star | 5.4 star |
|---|---|---|---|---|---|---|
| Deaths | 374 | 240 | 197 | 96 | 62 | 37 |
| Ambulance calls | 514 | 399 | 347 | 196 | 129 | 63 |
| Emergency department presentations | 1055 | 864 | 774 | 511 | 394 | 280 |
| After hour doctor consultations | 71 | 59 | 50 | 28 | 20 | 13 |

$$NetBenefit\ (non-airconditioned\ house) = \left( \sum_{t=2015}^{t=T} \left[ \Pr(heatwave\ in\ year\ t) \frac{\Delta R}{(1+r)^{t-2015}} + \frac{\Delta H}{(1+r)^{t-2015}} + \frac{\Delta E}{(1+r)^{t-2015}} \right] - \frac{U}{(1+r)^{t_{upgrade}-2015}} \right) \tag{9.3}$$

$$Net\ Benefit(Air\ conditioned\ house) = \left( \sum_{t=2015}^{t=T} \left[ \frac{\Delta C}{(1+r)^{t-2015}} + \frac{\Delta H}{(1+r)^{t-2015}} \right] - \frac{U}{(1+r)^{t_{upgrade}-2015}} \right) \tag{9.4}$$

where

Pr (heatwave in year t) = probability that a 2009 type heatwave will occur in year t.
$\Delta R$ = reduced cost of a 2009 type heatwave due to upgrading.
r = discount rate.
$\Delta$ H = reduced cost of heating.
$\Delta$ C = reduced cost of cooling.
$t_{upgrade}$ = year when upgrading takes place.
T = end of service life.
U = cost of upgrading house star rating.
$\Delta$ E = extended thermal comfort period during summer day in non-air-conditioned house.

### 9.5.1 Heatwave Cost

The mortality cost of heatwaves was approximated using "value of statistical life approach", as recommended for economic research by the environmental protection agency. A value of AUD $4.2 million was used according to "Best practice Regulation guidance note: value of statistical life" published by office of best practice regulation, department of prime minister and cabinet of Australian government [60]. The morbidity cost was calculated using an incident based "cost of illness" approach that included cost of ambulance attendance, cost of transportation to hospital, cost

**Table 9.3** Health impact cost of 2009 heatwave in Victoria

| Types of health impact | Number | Per unit cost | Total cost (All cost are in 2015 AUD) |
|---|---|---|---|
| Death | 374 | $4,200,000 [60] | $1,570,800,000 |
| Ambulance attendance | 514 | $481 [62] | $247,234 |
| Transport to hospital | 411 | $1115 [62] | $458,265 |
| Emergency department (ED) visit-non admitted patients | 1055 | $277 [63] | $292,235 |
| Hospitalization Followed by ED visit | 0–1055 | $3985 [63] | $0–$4,204,175 |
| After hour doctor consultation | 71 | $160 [64] | $11,360 |
| Loss of productivity | 570 | $276 [65] | $157,237–$786,186 |
| Total cost | | | $1,571,966,331 –$1,576,507,220 |

of emergency department visits and hospitalization, cost of after hour doctor consultation and the value of lost work productivity. Table 9.3 shows the types of health impact, per unit cost and total cost of the 2009 heatwave for Victoria. The source of per unit cost of different health impact can be found in the references mentioned next to it. All costs are reported in 2015 Australian dollars. Loss of productivity was calculated by multiplying the average daily income of Victorian people, number of people (below 75 years) admitted to hospital and average length of hospitalization. It was reported [61] that 46% of the patients arrived in emergency department were over 75 years old. In case of non-admitted patients the number of working days lost is one. In case of admitted patients, the loss of working days was assumed as five as it is the average length of stay. According to Australian bureau of statistics, the average income of Victorian people is $276 per day. It was assumed in the present study that heat related mortality and morbidity occurred in 0.9 energy star rated houses only. Hence, cost of heatwave mentioned in Table 9.3 is for 0.9 star rated houses. Using the similar approach, costs of heatwave were calculated for 1.8, 2.3, 3.7, 4.5 and 5.4 star houses. In those cases, number of deaths, ambulance calls, emergency presentations and after hour calls mentioned in Table 9.2 were used.

### *9.5.2 Heating Cost*

Table 9.4 shows the annual costs of heating different energy rated houses in Melbourne with different heating sources. According to Australian Bureau of Statistics, there are three different types of heating sources: natural gas (64.3%), electricity (20.9%) and wood (10.2%) [65]. Out of the 20.9% houses where electricity is used for heating, half of the houses are assumed to use direct electrical heating (fan heater, convection heater etc.) and the other half are assumed to use reverse cycle heating as

**Table 9.4** Annual heating costs of a typical house in Melbourne, Australia

| House energy star rating | Annual heating energy consumption ($MJ/m^2$) | Direct electrical heating cost (AUD 2015) | Reverse cycle electric heating cost (AUD 2015) | Gas heating cost (AUD 2015) | Wood heating cost (AUD 2015) |
|---|---|---|---|---|---|
| 0.9 | 526 | $5734 | $1764 | $1799 | $2234 |
| 1.8 | 387 | $4219 | $1298 | $1324 | $1644 |
| 2.3 | 319 | $3477 | $1070 | $1091 | $1355 |
| 3.7 | 197 | $2147 | $661 | $674 | $837 |
| 4.5 | 150 | $1635 | $503 | $513 | $637 |
| 5.4 | 118 | $1290 | $397 | $405 | $503 |

**Table 9.5** Annual costs of cooling a house using reverse cycle air conditioner

| House star rating | 0.9 | 1.8 | 2.3 | 3.7 | 4.5 | 5.4 |
|---|---|---|---|---|---|---|
| Annual cooling energy consumption ($MJ/m^2$) | 43 | 33 | 29 | 20.6 | 20.2 | 20.1 |
| Cost of cooling (AUD 2015) | $492 | $378 | $332 | $236 | $231 | $230 |

there was no data available. The unit cost of electricity, gas and wood were considered as 0.22 c/kWh, 1.9 c/MJ and $330/tonne after going through the price list from different sources.

### *9.5.3 Cooling Cost*

Table 9.5 shows the annual coolings costs of different star rated houses in Melbourne. In the cost calculation, it was assumed that reverse cycle air-conditioner is used for cooling because more than 50% of the air-conditioned houses in Victoria uses reverse cycle air conditioner. It was also assumed that the air conditioner has a COP value of 3.25 which is the minimum requirement for a 2 star air conditioner [66]. Electricity price in Victoria was taken as 0.22 c/kWh. The table shows that annual cost of cooling reduces by a factor of 2 if a 0.9 star house is upgraded to 5.4 star.

### *9.5.4 Cost of Upgrading House Star Rating*

Table 9.6 shows the modifications required to upgrade various energy star rated houses to 5.4 star ratings. Table 9.7 shows per unit cost of the required modifications.

**Table 9.6** Modifications required to upgrade to desired star ratings

| Existing star ratings | Modifications required to upgrade to 5.4 star |
|---|---|
| 0.9 | Add insulation R6.0 in ceiling, R 4.0 in wall, tight sealing the house |
| 1.8 | Add insulation R6.0 in 60% of ceiling and R5 in 40% ceiling, R 4.0 in wall, tight sealing the house |
| 2.3 | Add insulation R5.0 in ceiling, R 4.0 in wall, medium sealing the house |
| 3.7 | Add insulation R4.0 in ceiling, R 4.0 in wall, sealing minor gaps |
| 4.5 | Add insulation R2.0 in ceiling, R 2.0 in wall, sealing minor gaps |

**Table 9.7** Costs of modification per unit

| Modifications | Per unit cost |
|---|---|
| R 6.0 ceiling insulation | \$16.0 per $m^2$ |
| R 4.0 ceiling insulation | \$7.80 per $m^2$ |
| R 2.0 ceiling insulation | \$6.75 per $m^2$ |
| R 4.0 wall insulation | \$11.20per $m^2$ |
| R 2.0 wall insulation | \$5.60 per $m^2$ |
| Cost of tight sealing a house | \$1000 |
| Cost of medium sealing a house | \$500 |
| Sealing minor gaps | \$200 |

*All the costs are approximated from the quotations of* www.insulationaustralia.com.au

### *9.5.5 Net Benefits of Upgrade*

Net-benefit of upgrading different star rated non-air-conditioned and airconditioned house to 5.4 star was calculated using Eqs. (9.3) and (9.4) and presented in Fig. 9.6. In this calculation, discount rate r = 0.05 and probability of heatwave Pr = 0.01 was used. Due to the difficulties associated with the reliable cost calculation, the term $\Delta$ E in Eq. (9.3) was set to zero in this study. The figure shows that upgrading a 0.9 star house to 5.4 star is highly beneficial compared to other cases for both air-conditioned and non-airconditioined case. For 0.9 star house, net-benefit becomes positive in less than 3 and 2 years for non-airconditioned and air conditioned houses, respectively. In case of upgrading 1.8 and 2.3 star house to 5.4 star, the net-benefit becomes positive in less than 5 years for non-airconditioned house and less than 4 years for air-conditioned house. Upgrading a 4.5 star house to 5.4 star was found to be least beneficial with payback period of around 25 years.

It should be noted that the net benefit of upgrade will be lower than the calculated value if the discount rate is higher than 0.05. Similarly the benefit from reduced heatwave cost would increase by 50 times if the probability of a 2009 type heatwave is increased from 1 in 100 years (Pr = 0.01) to 1 in every 2 years. However, the cost savings due to a fifty times increase in the probability of heatwave is still much lower than the cost savings from reduced heating cost. Hence, it can be concluded

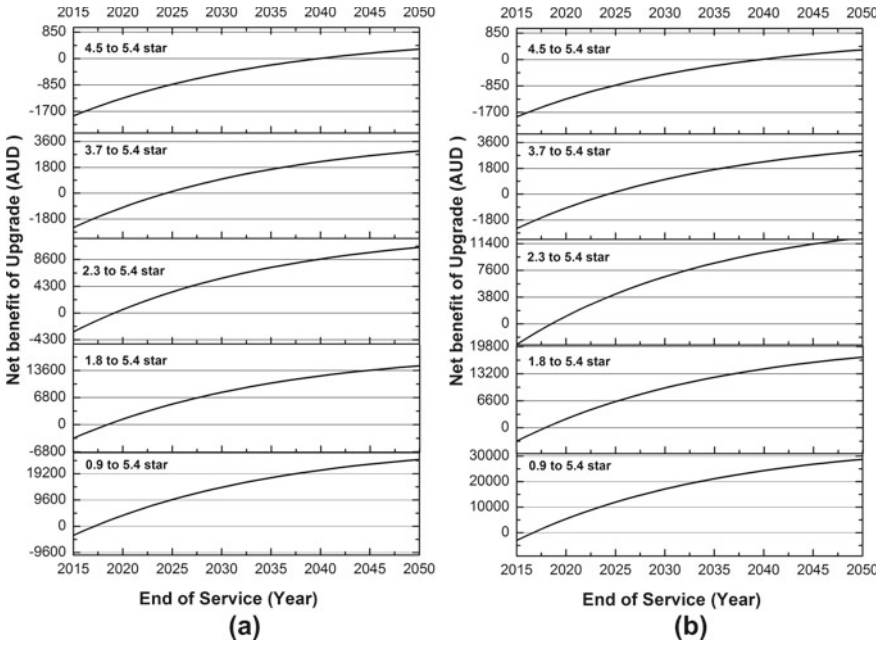


**Fig. 9.6** Net benefit of upgrading energy star rating of a **a** non-air-conditioned and **b** non-airconditioined house

that net benefit of upgrade in case of a non-air-conditioned house is more sensitive to reduction in heating cost than the reduction in heatwave cost. However, benefit from reduced heatwave cost is expected to increase as it is reported that heatwaves are becoming hotter, longer and more frequent in Melbourne [1].

## 9.6 Emerging Technology to Minimise Building Overheating

The effectiveness of some overheating mitigation measures during a heatwave is always positive, which means they always contribute to reducing overheating. For example, the measures to reduce solar heat gain using shading, reflecting coating, and low SHGC windows always reduces overheating. The use of green envelopes and vegetation also reduces the urban heat island impact and consequently helps to reduce overheating. On the other hand, mitigation measures such as insulation can have both positive and negative effects on building overheating depending on the indoor and outdoor thermal conditions.

During the daytime, a highly insulated envelope delays the heat transfer through the envelope and keeps the indoor environment comfortable for a longer period.

However, the indoor environment eventually heats up and in the evening when outdoor weather cools down, the indoor environment is overheated due to the trapped heat. In this scenario, natural ventilation is required to cool down the indoor environment. Fosas et al. [14] reported that insulation has a negligible impact on overheating unless there is no or very limited purge ventilation. Rather a high level of insulation is required to minimise climate change impact and deliver a better indoor environment. However, the strategy of natural ventilation through opening windows is not always available or desirable for a variety of reasons. Previous studies on window opening behaviour of dwellers indicated the following reasons for closing windows: noise, air pollution, crime, privacy, and insects. Moreover, the outdoor temperature may be too low to open windows in some climate zones at night, even in cooling seasons. Besides, natural ventilation cooling is only effective in a suburban and rural area, whilst it is avoided in cities due to urban heat island effects and noise.

In a house with low or no insulation and high infiltration, the indoor environment cools down very quickly at night, which makes it comfortable. However, those houses also heat up very quickly during the daytime. Therefore, there is a need to have a smart insulation material that can resist heat as much as possible when the outside temperature is higher than indoor and also facilitate in releasing trapped heat from indoor to outdoor without relying solely on natural ventilation. The emerging technology, known as Dynamic Insulation Materials (DIM) can serve this purpose. In case of a DIM, the thermal conductivity can be controlled depending on the external and internal thermal environment, which in turn alters the resistance level of the wall. Figure 9.7 shows the basic principle of one such DIM technology. In this case, DIM is a rigid, cellular panel that is placed within external wall cavities.

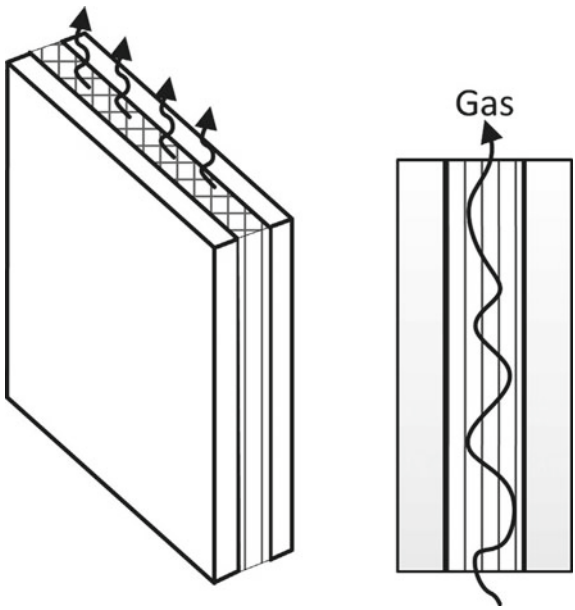


**Fig. 9.7** Schematic of a dynamic insulation material [68]

The thermal conductivity of this panel can be varied by the introduction of inert gases with variable conductivities. Other reported technologies to achieve variable insulation levels include varying gas pressure, using low and high conductivity fluid tanks and closed-loop forced convective dynamic insulation system [67].

During a cooling season, when the outside surface temperature is higher than the inside surface temperature, the insulation value switches to the maximum and prevents heat gain. In the evening, when the outside surface temperature is lower than the inside surface temperature, the R-value switches to minimum and enhances heat loss in the absence of natural ventilation through windows. DIM has the potential to reduce annual cooling demand in residential buildings by 15–39% in heating dominant US climate zones depending on the window sizes and internal heat gain [68]. In another study, savings between 7 and 42% were reported depending on the climate zones [69]. DIM is highly effective when the internal heat gains are high and the ambient temperatures are mild [70].

A numerical study was conducted for Melbourne climate to understand the effectiveness of DIM in reducing building overheating. A typical single-story brick veneer Australian house was simulated using building simulation software EnergyPlus v9.2. The simulation was carried out under the assumption that the windows are always closed. The objective was to investigate the effectiveness of DIM in cooling down the building in the absence of natural ventilation. The insulation value in the external walls and ceiling was switched between 0.4 $m^2$k/w and 4 $m^2$k/w according to the internal and external surface temperature of the walls. For the ceiling, the insulation value was switched between 0.6 $m^2$ k/w and 6 $m^2$ k/w. During the cooling season, when the wall surface temperature of the outside face is higher than the inside face, reducing heat gain is important to prevent building overheating. Hence, a higher insulation value is applied. When the wall surface temperature of the inside face is higher than the outside face, heat loss from indoor to outdoor is preferred to prevent overheating. In this case, a lower value of insulation is applied. In the case of static insulation materials, the value was fixed at 4 $m^2$ k/w for walls and 6 $m^2$ k/w for a ceiling.

Figure 9.8 shows that dynamic insulation results in lower indoor air temperature consistently both in bedroom and living room in January in Melbourne. On average, the indoor air temperature was 1.1 and 1.2 °C lower with the application of dynamic insulation in bedroom and living room, respectively. Predominantly, the dynamic insulation results in lower envelope resistance at night which accelerated heat loss and cooled down the indoor environment, it also cooled down the thermal mass of the building which helped to reduce the daytime heat gain. Figure 9.9 shows that dynamic insulation reduced the percentage of occupied hours over the comfort threshold in both living and bedroom. The comfort threshold for living and bedroom were 28 and 26 °C as per CIBSE standards. The living room was considered occupied from 7 am to 10 pm and the bedroom was considered occupied from 10 pm to 7 am. The CIBSE standard recommends that the indoor temperature should not be over the comfort threshold for 1% of the occupied hours annually to minimise overheating risk. Figure 9.9 shows that DIM is close to meeting this CIBSE standard in the bedroom. However, in the living room, the percentage of occupied hours over the

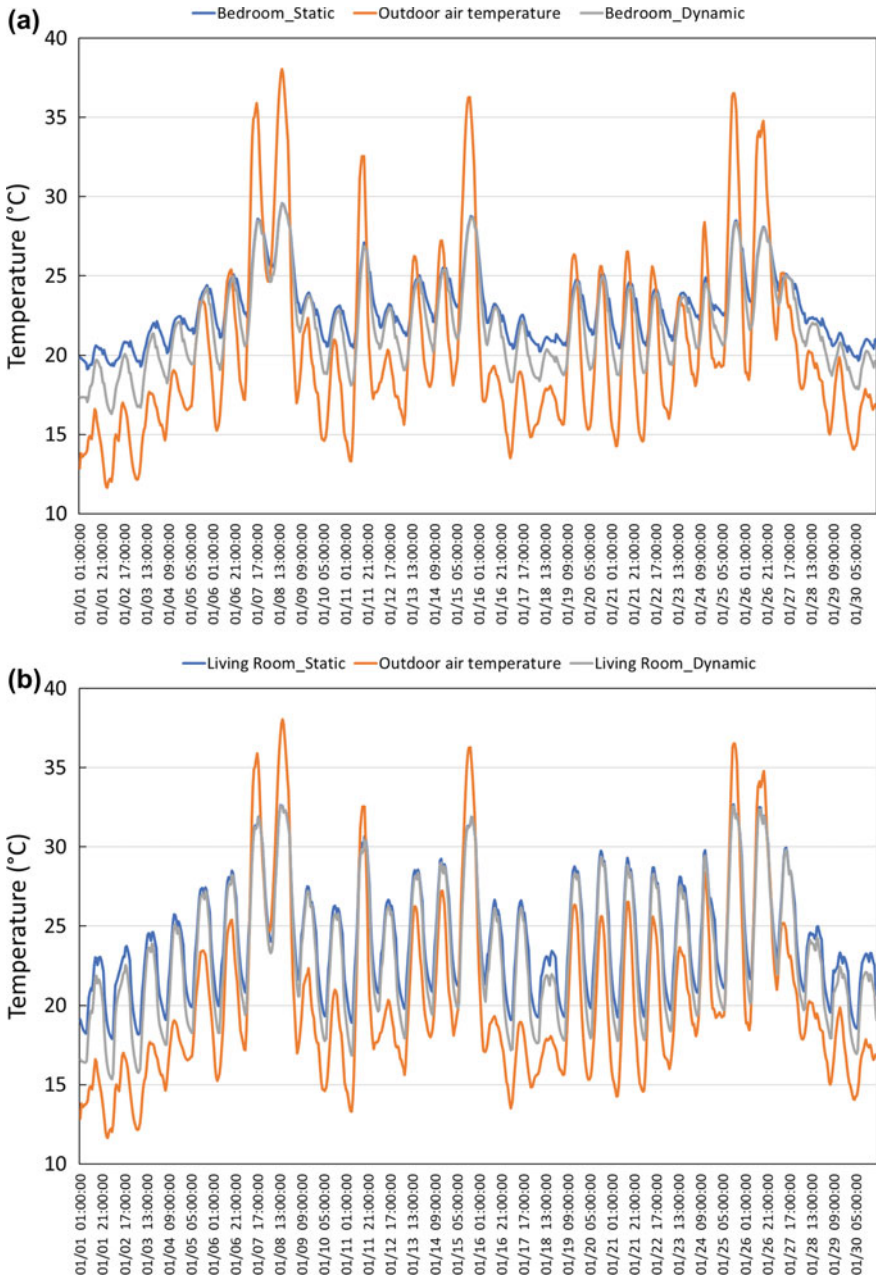


**Fig. 9.8** Indoor air temperature of **a** Bedroom and **b** Living zones with static and dynamic insulation materials

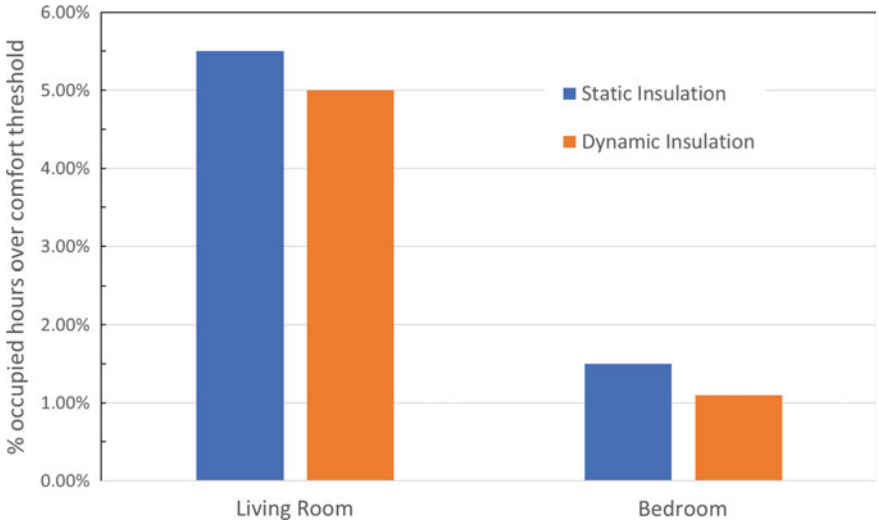


**Fig. 9.9** Percentage of occupied hours over a threshold in living and bedroom

threshold is still much higher than the recommendation, although the DIM resulted in some reduction. Further research is required to identify optimum thermal resistance switch ratio and control strategy considering the different building parameters, such as zone type, wall type, orientation, and window to wall ratio to maximise energy savings and prevent building overheating.

## 9.7 Summary

Building overheating poses significant risks to human health, and climate change is exacerbating this phenomenon. The major factors that contribute to building overheating are low energy building measures, lightweight construction materials, occupant behaviour, internal heat gain and urban heat island effects. In the heating-dominated region, retention of winter heat has been the principal focus of dwelling design and construction which results in overheating during the hot summer period due to reduced heat loss. The lightweight structural panels are also responsible for summer overheating in a high-rise apartment building in urban areas due to low thermal mass. In addition to that, in urban areas, occupants prefer to keep the window closed due to security, noise and pollution, which prohibits useful night ventilation. Finally, the urban heat island significantly influences the urban microclimate and results up to 10 °C ambient temperature compared to the rural area. This high outdoor temperature exacerbates summer overheating and reduces the natural ventilation cooling effect.

Risk of experiencing heat stress is higher in a lower energy rated house. The risk can be mitigated by retoriftting existing lower energy rated building to higher star through passive measures like insualiton, sealing, shading etc. The risk of experiencing 6 heat stress hours by Melbourne residents on a hot summer day with 36 °C mean temperature was found to reduce from 50% to only 4% by retrofitting the entire lower energy rated houses to 5.4 star. Net-benefit analysis showed that upgrading the lower energy rated houses to 5.4 star is highly beneficial with net-benefit becoming positive within 2–5 years. Upgrading a 4.5 star house to 5.4 star was found to be least beneficial with payback period of around 25 years.

Previous studies have investigated a number of measures to mitigate overheating risks in buildings. These measures can be divided into four categories (1) Modification of local microclimate, (2) resistance to heat transfer from outdoor to indoor (3) Absorption of transferred heat through thermal mass, and (4) Release of trapped heat from indoor to outdoor. The change in urban microclimate with the introduction of green infrastructure can lower the urban air temperature up to 3 °C due to transpiration cooling. Advanced thermochromatic paint with phase change materials can lower building envelope exterior surface temperature up to 8 °C by increasing the surface solar reflectivity, which can minimise the urban heat island phenomenon.

Improving envelope thermal resistance is an effective measure to minimise overheating as long as the outdoor temperature is lower than the indoor temperature. When the hot weather continues for some time, the heat slowly transfers through the building envelope and starts to increase the indoor air temperature. In this scenario, walls with high thermal mass can absorb the transferred heat and restrict the indoor temperature rise. Use of latent heat thermal energy storage, such as phase change materials has been shown to be effective in significantly reducing indoor temperature rise.

However, once the thermal mass is saturated, the indoor temperature starts to rise and may exceed the thermal comfort threshold. When the outdoor air temperature is lower than the indoor temperature, the focus is on releasing the heat from indoor to prevent overheating and cool down the thermal mass. In a highly insulated and airtight house, natural ventilation via opening windows is required to release the trapped heat. However, the strategy of natural ventilation through opening windows is not always available or desirable for a variety of reasons, including noise, air pollution, crime, privacy, and insects. New technology like DIM, which can change the thermal resistance of the wall as needed, can help to release the trapped heat from inside. The DIM with variable thermal conductivity is an ideal smart insulation material that reduces heat gain during the daytime and increases heat loss at night. The integration of dynamic insulation materials has averagely reduced the indoor air temperature by 1.1 °C and 1.2 °C in the living room and bedroom, respectively, in a typical Melbourne house.

## References


1. Steffen W, Hughes L, Perkins S (2014) Heatwaves: hotter, longer, more often. Climate council of Australia limited
2. Morey J, Beizaee A, Wright A (2020) An investigation into overheating in social housing dwellings in central England. Build Environ 176**:**106814
3. Coates L, Haynes K, O'Brien J, McAneney J, de Oliveira FD (2014) Exploring 167 years of vulnerability: an examination of extreme heat events in Australia 1844–2010. Environ Sci Policy 42:33–44
4. Victorian Government Department of Human Services (2014) The health impacts of the January 2014 heatwave in Victoria. Melbourne, Victoria
5. Ruud S, Lundin L (2004) Bostadshus utan traditionellt uppvärmningssytem-Resultat från två års mätningar. In: Ruud S (ed). Sweden: Klimatisering och installationsteknik
6. Wright AJ, Young AN, Natarajan S (2005) Dwelling temperatures and comfort during the August 2003 heat wave. Build Serv Eng Res Technol 26:285–300
7. Steffen W, Hughes L, Perkins S (2014) Heatwaves: hotter, longer, more often. Climate council of Australia
8. Hughes C, Natarajan S (2019) Summer thermal comfort and overheating in the elderly. Build Serv Eng Res Technol 40:426–445
9. Beizaee A, Lomas KJ, Firth SK (2013) National survey of summertime temperatures and overheating risk in English homes. Build Environ 65:1–17
10. Mitchell R, Natarajan S (2019) Overheating risk in Passivhaus dwellings. Build Serv Eng Res Technol 40:446–469
11. Gupta R, Barnfield L, Gregg M (2017) Overheating in care settings: magnitude, causes, preparedness and remedies. Build Res Inform 45:83–101
12. McGill G, Sharpe T, Robertson L, Gupta R, Mawditt I (2017) Meta-analysis of indoor temperatures in new-build housing. Build Res Inform 45:19–39
13. Schirmer J, Yabsley B (2018) Living well with a changing climate
14. Fosas D, Coley DA, Natarajan S, Herrera M, Fosas De Pando M, Ramallo-Gonzalez A (2018) Mitigation versus adaptation: does insulating dwellings increase overheating risk? Build Environ 143:740–759
15. Truong H, Garvie AM (2017) Chifley passive house: a case study in energy efficiency and comfort. Energy Procedia 121:214–221
16. Kumar D, Alam M, Zou PXW, Sanjayan JG, Memon RA (2020) Comparative analysis of building insulation material properties and performance. Renew Sustain Energy Rev 131**:**110038
17. Ascione F, Bianco N, De Masi RF, De' Rossi F, Vanoli GP (2014) Energy refurbishment of existing buildings through the use of phase change materials: energy savings and indoor comfort in the cooling season. Appl Energy 113**:**990–1007
18. CoCC, Committee on Climate Change (2013) Fourth carbon budget review–technical report: sectoral analysis of the cost-effective path to the 2050 target. Committee on climate change London.
19. Elsharkawy H, Zahiri S (2020) The significance of occupancy profiles in determining post retrofit indoor thermal comfort, overheating risk and building energy performance. Build Environ 172**:**106676
20. Ji Y, Webster PJJR (2012) Comparative thermal response of internally and externally insulated houses
21. Tink V, Porritt S, Allinson D, Loveday D (2018) Measuring and mitigating overheating risk in solid wall dwellings retrofitted with internal wall insulation. Build Environ 141:247–261
22. Lavaf Pour Y, Sharples S (2017) The Influence of façade design on the optimum window to wall ratio and overheating rate in UK Passivhaus dwellings for current and future climates: a Parametric Design Method
23. Ozel M (2012) The influence of exterior surface solar absorptivity on thermal characteristics and optimum insulation thickness. Renew Energy 39**:**347–355

24. Cheng V, Ng E, Givoni B (2005) Effect of envelope colour and thermal mass on indoor temperatures in hot humid climate. Sol Energy 78:528–534
25. Nabinger S, Persily A (2011) Impacts of airtightening retrofits on ventilation rates and energy consumption in a manufactured home. Energy Build 43:3059–3067
26. Mourkos K, Mcleod RS, Hopfe CJ, Goodier C, Swainson M (2020) Assessing the application and limitations of a standardised overheating risk-assessment methodology in a real-world context. Build Environ 181:107070
27. Adekunle TO, Nikolopoulou M (2016) Thermal comfort, summertime temperatures and overheating in prefabricated timber housing. Build Environ 103:21–35
28. Vellei M, Ramallo-González AP, Coley D, Lee J, Gabe-Thomas E, Lovett T, Natarajan S (2017) Overheating in vulnerable and non-vulnerable households. Build Res Inform 45:102–118
29. Lapinskiene V, Motuzienė V, Mikučionienė R (2017) Impact of internal heat gains on building's energy performance. Environmental engineering 10th international conference vilnius gediminas technical university, Lithuania
30. Oke TR (2002) Boundary layer climates, Routledge
31. Porritt SM, Cropper PC, Shao L, Goodier CI (2012) Ranking of interventions to reduce dwelling overheating during heat waves. Energy Build 55:16–27
32. Santamouris M, Haddad S, Fiorito F et al (2017) Urban heat island and overheating characteristics in Sydney, Australia. An analysis of multiyear measurements
33. Magli S, Lodi C, Lombroso L, Muscio A, Teggi S (2015) Analysis of the urban heat island effects on building energy consumption. Int J Energy Environ Eng 6:91–99
34. Palme M, Carrasco C, Ángel Gálvez M, Inostroza L (2017) Natural ventilation: a mitigation strategy to reduce overheating in buildings under urban heat island effect in South American cities. IOP Conf Ser: Mater Sci Eng 245**:**072046
35. Soudian S, Berardi U, Laschuk N (2020) Development and thermal-optical characterization of a cementitious plaster with phase change materials and thermochromic paint. Sol Energy 205:282–291
36. Zinzi M, Santamouris M (2019) Introducing urban overheating—progress on mitigation science and engineering applications. Climate 7
37. Karlessi T, Santamouris M, Synnefa A, Assimakopoulos D, Didaskalopoulos P, Apostolakis K (2011) Development and testing of PCM doped cool colored coatings to mitigate urban heat island and cool buildings. Build Environ 46:570–576
38. Santamouris M (2014) Cooling the cities—a review of reflective and green roof mitigation technologies to fight heat island and improve comfort in urban environments. Sol Energy 103:682–703
39. Barnett G, Beaty M, Chen D, Mcfallan S, Meyers J, Nguyen M, Ren Z, Spinks A, Wang X (2013) Pathways to climate adapted and healthy low income housing. National climate change adaptation research facility gold coast
40. van Hooff T, Blocken B, Hensen JLM, Timmermans HJP (2015) Reprint of: on the predicted effectiveness of climate adaptation measures for residential buildings. Build Environ 83:142–158
41. Tabares-Velasco PC, Srebric J (2011) Experimental quantification of heat and mass transfer process through vegetated roof samples in a new laboratory setup. Int J Heat Mass Transf 54:5149–5162
42. Hao X, Xing Q, Long, P, Lin Y, Hu J, Tan H (2020) Influence of vertical greenery systems and green roofs on the indoor operative temperature of air-conditioned rooms. J Build Eng 31**:**101373
43. Lesjak V, Pajek L, Košir M (2020) Indirect green façade as an overheating prevention measure. Gradevinar 72:569–583
44. Bansal NK, Garg SN, Kothari S (1992) Effect of exterior surface colour on the thermal performance of buildings. Build Environ 27:31–37
45. MALZ, S., KRENKEL, W. & STEFFENS, O. 2020. Infrared reflective wall paint in buildings: Energy saving potentials and thermal comfort. *Energy and Buildings,* 224**,** 110212.

46. Tillson A-A, Oreszczyn T, Palmer J (2013) Assessing impacts of summertime overheating: some adaptation strategies. Build Res Inform 41:652–661
47. Nedhal A-T, Qahtan A (2016) Influence of glazing types on the indoor thermal performance of tropical high-rise residential buildings. Key Eng Mater 692:27–37
48. Siddiqui O, Fung A (2009) Utilization of thermal mass in the Toronto net zero energy house for thermal comfort and energy savings. Proceedings Eleventh International IBPSA Conference, Glasgow, Scotland 27–30(2009):2131–2137
49. Rodrigues L, Sougkakis V, Gillott M (2016) Investigating the potential of adding thermal mass to mitigate overheating in a super-insulated low-energy timber house. Int J Low-Carbon Technol 11:305–316
50. Kuczyński T, Staszczuk A (2020) Experimental study of the influence of thermal mass on thermal comfort and cooling energy demand in residential buildings. Energy 195:116984
51. Ramakrishnan S, Wang X, Sanjayan J, Wilson J (2017) Thermal performance of buildings integrated with phase change materials to reduce heat stress risks during extreme heatwave events. Appl Energy 194:410–421
52. Auzeby M, Wei S, Underwood C, Chen C, Ling H, Pan S, Ng B, Tindall J, Buswell R (2017) Using phase change materials to reduce overheating issues in UK residential buildings. Energy Procedia 105:4072–4077
53. Jensen C, Chu A, Cadorel X, Hes DD (2017) Living well—apartments, comfort and resilience in climate change. University of Melbourne, Australia
54. Alam M, Rajeev P, Sanjayan J, Zou PXW, Wilson J (2018) Mitigation of heat stress risks through building energy efficiency upgrade: a case study of Melbourne, Australia. Aust J Civ Eng 16:64–78
55. Holmes SH, Phillips T, Wilson A (2015) Overheating and passive habitability: indoor health and heat indices. Build Res Inform:1–18
56. Lemke B, Kjellstrom T (2012) Calculating workplace WBGT from meteorological data: a tool for climate change assessment. Ind Health 50:267–278
57. Tesfamariam S, Sánchez-Silva M, Rajeev P (2013) Effect of topology irregularities and construction quality on life-cycle cost of reinforced concrete buildings. J Earthquake Eng 17:590–610
58. Sustainablity Victoria (2014) Victorian household energy reports. Melbourne: Sustainability Victoria
59. Alam M, Sanjayan J, Zou PXW, Stewart MG, Wilson J (2016) Modelling the correlation between building energy ratings and heat-related mortality and morbidity. Sustain Urban Areas 22:29–39
60. December (2014) Best practice regulation guidance note: value of statistical life. Office of best practice regulation, Department of prime minister and cabinet, Australian government
61. VGDHS (Victorian Government Department of Human Services) (2009) Heatwave in Victoria: an assessment of health impacts. Melbourne, Victoria
62. Fees-Ambulance victoria (2014a) [Online]. Available: http://www.ambulance.vic.gov.au/About-Us/Fees.html [Accessed]
63. Independent hospital pricing authority (2014) National hospital cost data collection Australian public hospitals cost report 2011–2012, Round 16
64. National home doctor service (2014b) [Online]. Available: http://www.mmds.com.au/ [Accessed]
65. ABS ABOS (2014) Australian bureau of statistics [Online]. Available: http://www.abs.gov.au [Accessed]
66. Appliance energy consumption in Australia: equations for appliance star ratings (2010) [Online]. Available: http://www.energyrating.gov.au/ [Accessed]
67. Koenders SJM, Loonen RCGM, Hensen JLM (2018) Investigating the potential of a closed-loop dynamic insulation system for opaque building elements. Energy Buildi 173:409–427
68. Park B, Srubar WV, Krarti M (2015) Energy performance analysis of variable thermal resistance envelopes in residential buildings. Energy Build 103:317–325

69. Menyhart K, Krarti M (2017) Potential energy savings from deployment of Dynamic Insulation Materials for US residential buildings. Build Environ 114:203–218
70. Shekar V, Krarti M (2017) Control strategies for dynamic insulation materials applied to commercial buildings. Energy Build 154:305–320

# Chapter 10
# Improving Regional Infrastructure Resilience to Earthquakes, Storms and Tsunami


**David Elms, Ian McCahon, and Rob Dewhirst**

**Abstract** This chapter addresses decision-making for improving the resilience of civil infrastructure to extreme events over a broad region. It shows how this was approached for the West Coast Region of New Zealand. The issues were complex and needed a systemic approach. The project's client required recommendations for improving infrastructure resilience. Our earlier risk-based work provided knowledge of the region and its natural hazards. A strategy for resilience improvement had to show both what interventions would be better value, and also, given a limited annual budget, how improvements could be prioritised over time. Both issues required an assessment of value, and we developed an appropriate resilience metric. Each infrastructure element was given two scores: its *vulnerability* or lack of resilience, and its *significance* or the effect of a failure on community resilience. This in turn was measured by community income. An underlying idea was the concept of a *virtual pipeline*, arising from the fact that infrastructure is mainly concerned with flows—of energy, goods, people, waste and so on.

**Keywords** Resilience · Infrastructure · Systems · Value · Vulnerability · Significance

## 10.1 Introduction

A functioning society in any country or region depends on a number of flows—movements of people, produce and supplies, of, for instance, electrical power, finance,

D. Elms (✉)
Department of Civil and Natural Resources Engineering, University of Canterbury, Christchurch, New Zealand
e-mail: david.elms@canterbury.ac.nz

I. McCahon
Geotech Consulting Ltd., PO Box 130 122, Christchurch 8141, New Zealand
e-mail: mccahon@geotech.co.nz

R. Dewhirst
Rob Dewhirst Consulting Ltd., 38A Penruddock Rise, Christchurch 8025, New Zealand
e-mail: radewhirst@snap.net.nz



M. G. Stewart and D. V. Rosowsky (eds.), *Engineering for Extremes*, Springer Tracts in Civil Engineering, https://doi.org/10.1007/978-3-030-85018-0_10

information or waste. They hold together the lifeblood of society within the region and dictate its interaction with the outside world. They are not independent but interact as a complex system of systems. The flows depend on a complex interacting infrastructure of roads, rail, channels, wires and enabling controls—the region's lifelines. They also depend on the end points of the lifelines, on origins and destinations such as homes, businesses, townships, reservoirs, treatment facilities, stores and so on which are all part of an overall system of links and nodes. We'll call it the region's lifeline system.

Extreme events impact the lifeline system. Bridges can fail in floods, power lines can be wrecked in storms, transportation links and nodal structures (stores, pumping stations) can be demolished by earthquakes and a tsunami could devastate an area. A major decision issue is, how can a lifeline system be made more resilient in the face of largely unanticipated extreme events? What would be the most cost-effective interventions to improve overall infrastructure performance? In what follows we outline how we developed a prioritised list of interventions for improving a region's infrastructure resilience within New Zealand.

In extensive earlier work we had used risk approaches, but now the client wanted us to shift the focus to resilience. There was good reason for this, as we explain below. "Resilience" is currently used in many different contexts—ecology, sociology, psychology and so on as well as engineering—with a variety of meanings, so we'll summarise our own understanding and its implications. First, though, we'll show how the reason for moving to a resilience framework arises from some inherent limitations in risk approaches.

## 10.2 Some Limitations of Risk

Risk management is a mature and widely accepted discipline. Its use is essential when making decisions under uncertainty as well as in rational approaches to safety. Its power and its wide acceptance give confidence. However, confidence could in some cases lead to a problem in that practitioners' very familiarity with risk methods could hide serious limitations [1, 2], though "limitations" should not be read as implying criticisms. Here are three:

a. Major issues are sometimes omitted from a risk analysis either because of ignorance or in order to simplify the analysis. In structural engineering, the analysis will typically leave out consideration of human error, leading [3] to write that the observed failure rates of major structures such as bridges "are three or more orders of magnitude greater than the calculated values".
b. Engineering risk analyses are often so complex that the relevant system is represented for the purposes of analysis by a severely simplified underlying model so that many perhaps serious matters are not taken into account.
c. A risk assessment will normally consider the likelihood and consequence of a single assumed event—one specific earthquake for example—whereas what is

> really required is the knowledge that, say, an infrastructure system will respond adequately no matter what event actually occurs, even to the extent that the designers had neither expected nor anticipated it.

Carmichael [1] went as far as to say that incompleteness—point (a) above—is the Achilles heel of risk management.

This is not at all to say that risk approaches are bad and should be abandoned. After many years of working separately and together on risk related projects, we are convinced of the power of risk methods in addressing uncertainty and underpinning engineering decisions. However, we have also come to believe that risk should be used carefully and with mature understanding and that the user should be aware of its limitations, such as those noted above. Some of the difficulties can be dealt with by considering resilience. Risk and resilience can be thought of as complementary, rather than alternatives. Both deal with uncertainty, but the essential difference is that resilience proceeds by focussing on an artefact or system itself—a bridge, say—as opposed to the focus of risk, which is not on the system so much as on a specific event that might attack it. In a way, it is a fundamental difference in outlook. It relates to the distinction between extrinsic and intrinsic points of view discussed elsewhere [4] and elaborated in the next section.

## 10.3 Resilience

Resilience is not an easy concept to pin down—one report referred to a claim that "well over 100 unique definitions of resilience have appeared" [5]. Hosseini et al. [6] review a number of definitions and show that different disciplines can have significantly different understandings of the nature of resilience. Agarwal [7–10] give useful discussions generally related to infrastructure. The underlying idea is that a functioning system is resilient if it can survive a major perturbation or shock and regain its functionality. The emphasis is on survival, and it deals with restoration of function rather than the continued existence of a specific thing or artefact. We might consider the resilience of a bridge: if it is destroyed then there may be alternative means of crossing the river so that the ability to cross—the function—continues. A more subtle point is that of one's personal viewpoint or stance. There are usually two ways of looking at an engineering problem: from within, or from without: intrinsic and extrinsic approaches. Most engineering, and perhaps most science, takes an extrinsic approach and looks at a problem from outside. Risk analysis typically takes this stance. But a resilience assessment needs the point of view of what is being considered, rather than that of an outside observer. This is because the quality of resilience is something inherent in the system and is independent of whatever external shock might test it. Consider a community. One might consider the *risk*, say, of a community being damaged by a hundred-year flood, and one concentrates on the occurrence of that event. However, the *resilience* of the community is to do with the community's underlying nature and not with any particular event that might threaten it.

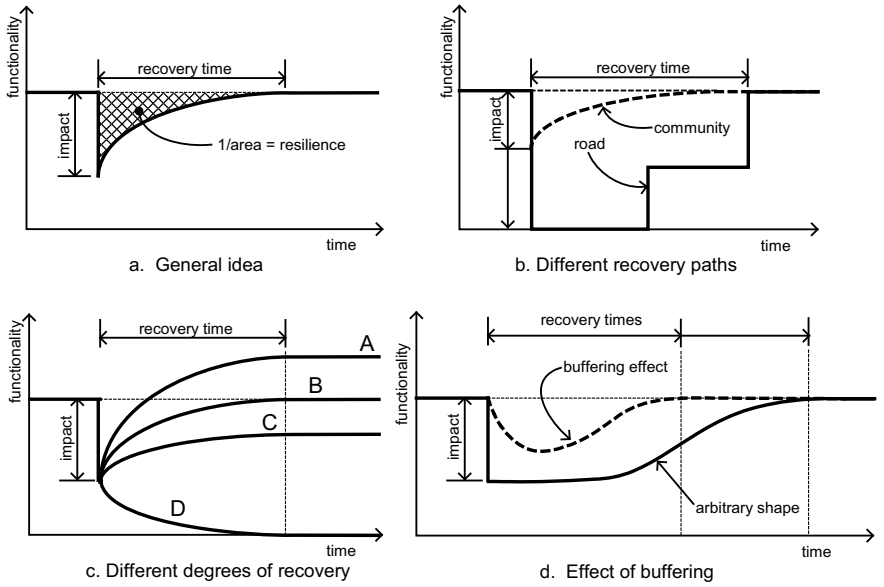


**Fig. 10.1** Resilience concepts: system response to a perturbation

The intrinsic stance requires the engineer to engage with the object, rather than with what might happen to any single specific scenario. Elms [4] considers the need for intrinsic engagement as part of a more general approach to complex system work. The underlying point is that risk and resilience should be thought of as complementary.

Figure 1a shows some resilience concepts. A system, say a community, has a steady level of functionality (some might say "stable", but we choose not to use that word as stability is a tricky concept—is a candle flame stable?). At some point in time the system is hit by a disaster and there is an immediate impact on its functionality which drops to a lower level, perhaps zero. There is then a time of recovery until normal functionality is restored. The cross-hatched area is seen by some as a possible measure of resilience [11] though this measure is limited in practice because the costs of initial damage and limited functionality during recovery typically lie with different parties. We discuss resilience measures below. Figure 1a contains three basic resilience concepts: degree of impact, recovery time and recovery trajectory. However, its vertical axis shows only one variable, "functionality", whereas in practice there could be many where larger systems are considered: various parts of a road system, for instance, could receive different types of impact and have different paths to recovery. The shape of the recovery curve for a road is more likely to be that shown in Fig. 1b, with an initial complete loss of functionality changing first to partial and later to complete recovery.

Nor is the steady-state final recovery level always a return to the original. Figure 1c shows that the system might not return to its original state. It might be permanently impaired and return to a lower level of functionality (curve C). There could also be

cases where the final result is better than before. More importantly, there might be situations where the impact is such that recovery is never achieved and functionality sinks to zero (curve D): the impact is too great, a tipping point is reached, and recovery is impossible. Although some situations, processes, companies or industries are sensitive and a minor impact could push them over the edge with serious consequences, a resilient system would rarely reach a tipping point.

Finally, Fig. 1d illustrates that a recovery path could take many shapes. There might, for instance, be an initial delay before recovery could start. The figure also shows the effect of buffering, a useful strategy for improving resilience. Both initial impact and recovery path can be improved by introducing a buffer, which typically could be the availability of supplies for a community when their normal source is cut off, or perhaps a reservoir as a temporary source of water. A buffer acts to both delay and reduce the immediate effect of an impact.

A fundamental difficulty with resilience is its metric—how it could be measured. Risk has no problem with this, as likelihood and consequence can be combined to give a clear metric—a value—which can be the basis of decision-making. For resilience, there is no obvious value despite many attempts to define one. Yet we need a value to be able to include resilience into a decision process, to know whether one strategy for resilience is better than another. Or, as in the example discussed below, a client might be faced with a number of possibilities for increasing the resilience of individual elements of an infrastructure system with the aim of increasing the resilience of the whole. With a limited budget, not all interventions could be carried out at once. Prioritising them would need a measure.

One possibility for a metric that is often mentioned is the inverse of the area above the recovery curve (Fig. 1a) noted earlier. Hosseini et al. [6] give a useful review of the general issue. SEBoK [5] gives 12 possible measures. The variety of measures reflects the different contexts in which resilience occurs as well as implying different underlying definitions.Hollnagel and Woods [12] maintains that "We can only measure the *potential* for resilience but not resilience itself." We develop our own measure below. However, considering the problem from an intrinsic rather than extrinsic point of view, we can see that the value of a system's resilience might well involve more than one measure. For example, consider a bridge failure where the bridge is part of a community's infrastructure. There would be a direct cost involved in repairing or replacing the bridge, presumably carried by local government and its insurers. Far more significant to the community would be the cost arising from lack of functionality. This would be time-dependent in different ways for different community sectors. For example, a dairy farm might lose an entire season's income if cows could not be milked and had to be dried off, and it would be critical that functionality resumed before that critical point was reached. In contrast, the costs to some other business might increase more gradually with time to functionality (Fig. 10.2).

In any case, community costs increase with recovery time, and they may well be significantly greater than direct repair costs. Restoration time is central to resilience thinking. Time is not usually an issue with risk-based approaches, which is why most disaster planning work, which tends to be risk-focussed, emphasises immediate

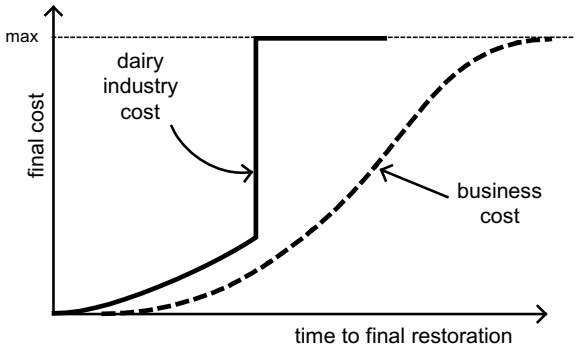


**Fig. 10.2** Community costs for different sectors depend on length of time to final restoration. The costs follow different paths to their maximum

response rather than restoration and recovery. Given the immense recovery costs of some recent natural disasters, this thinking has to change, and must include resilience considerations. Response and recovery are equally important from the community point of view.

In many situations where resilience is used, quantitative measures might not be relevant. Resilience can be more a way of looking at the situation and seeing how things could be done better in broad terms, and indeed this is also true of risk. A detailed numerical analysis could be inappropriate because of the uncertainty and quality-limitations of much of the information to hand as well as limitations imposed by simplifications and assumptions. It is the logic implied by a resilience approach that is important, not the fine detail: ideas usually count more than numbers. For instance, there is a fundamental difference between a brittle and a resilient structure, even though precise numbers might be unimportant.

There are different strategies for improving resilience. SEBoK [5] states that it can be helpful to understand that a resilient system possesses four attributes: *capacity*, *flexibility*, *tolerance* and *cohesion.* Here, *capacity* is "the attribute of a system that allows it to withstand a threat", and it can be achieved through absorption, redundancy and layered defence. *Flexibility* is "the attribute of a system that allows it to restructure itself", which could be achieved by reorganisation, complexity avoidance and backup availability. *Tolerance* is "the attribute of a system that allows it to degrade gracefully following an encounter with a threat." It is the opposite of brittleness, and can be provided by localised capacity, loose coupling, reparability and buffering. *Cohesion* is "the attribute of a system that allows it to operate before, during and after a threat." System nodes need to be able to communicate and cooperate with each other. All four attributes are relevant to infrastructure resilience. A report by Bodeau et al. [13] gives an interestingly different set of strategies, while [14] gives a broader systems-oriented review.

Working with resilience in mind requires more than knowledge and a set of techniques. As mentioned earlier, it also requires a particular attitude, a mind-set, and this can be different from many people's normal way of going about things. Woods and Hollnagel [15] even suggest that "it may be compared to a paradigm shift in the Kuhnian sense [16]."

A significant issue is that resilience deals with the unexpected. Taleb [17] warns against "black swans", those sometimes-devastating impacts which are not anticipated. Thus a resilience approach means being prepared for anything—for the unexpected. There are two implications here. The first is a need for awareness, for expecting the unexpected and therefore looking for it. There is a creative element to it: we could call it *creative awareness.* The second implication is that there will be a need to move quickly to deal with whatever is the problem. One needs *fleetness of foot*. These two ideas can be used to underpin and suggest practical engineering approaches. A third is *adaptability.*

Practical engineering tends to be more demanding than the more well-ordered world of theory—demanding in the sense that theory tends to follow well-groomed paths while so much of the problem in practice is to form clear paths through an unruly tangle of ill-defined undergrowth. Such was the case in the project outlined in the next section.

## 10.4 Improving Infrastructure Resilience to Extreme Natural Events

A client asked us to report on improving infrastructure resilience to extreme natural events in the West Coast of New Zealand's South Island. The scope was daunting. The island is divided by a chain of high mountains, the Southern Alps, running from north to south. The region on the west, the West Coast, is long, narrow and rugged (Fig. 10.3), and its only connection with the more populated east is by three high mountain passes and a roundabout route in the north. The region is particularly vulnerable to natural disasters. It is geologically active—the highest mountains rise by about a centimetre a year. Its geology and topology mean that not only is there a high risk of earthquake and storm events, but also that its communities are scattered and held together physically by a far-flung network of fragile connections. It is also a region of great natural beauty, attractive to tourists.

A large and active fault—the Alpine Fault—runs along the region and follows the boundary between the Indo-Australian and Pacific tectonic plates (Fig. 10.3). The risk of a major earthquake resulting from rupture of this fault is well understood, but significant earthquakes could also stem from other sources. Predicting the extent, locality and nature of an earthquake—even an Alpine Fault event—is impossible. All that can be said is that a major event will happen, and that because its nature and location are unknown beforehand, the region must expect the unexpected. This is also true of storms. Major storm events generally occur because of the interaction between the predominantly westerly winds and the high Southern Alps, and from the remains of tropical cyclones tracking down from the north. Some storms are particularly severe either because of their immediate intensity or because they cover an unusually wide area, making recovery harder. Again, what exactly might happen cannot be predicted. A third type of natural event—a tsunami—is a rare but regular occurrence. It could be devastating to coastal areas.

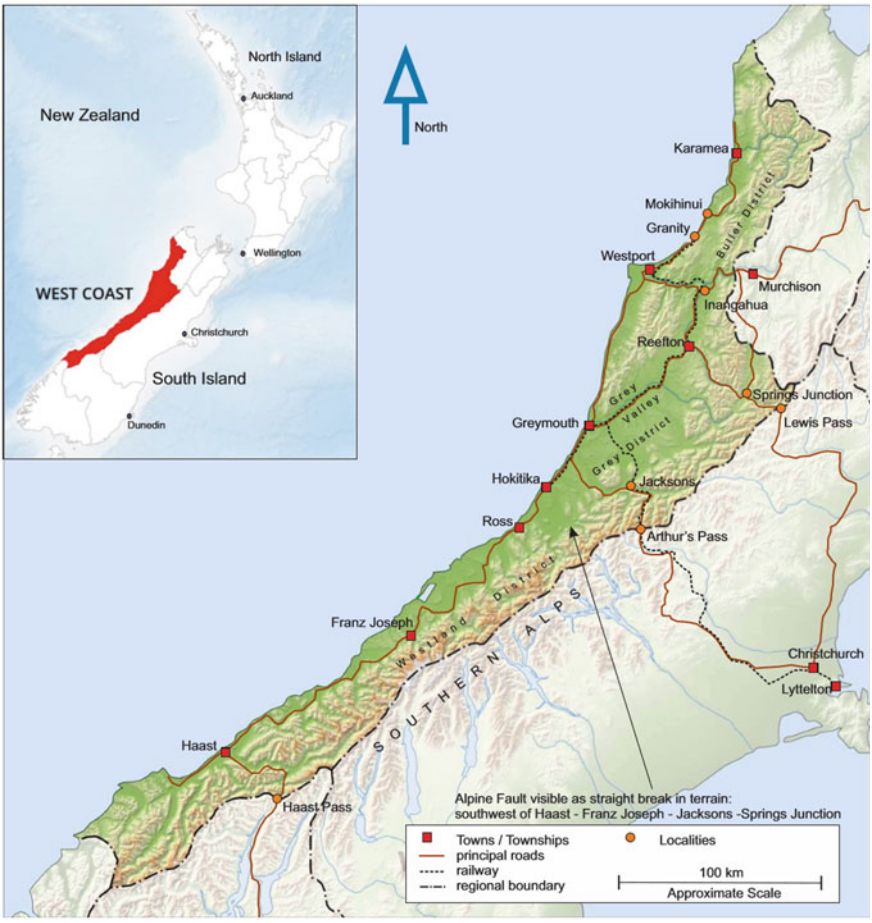


**Fig. 10.3** The West Coast of the South Island, showing major transport links

The Coast's infrastructure consists of many subsystems: roading, rail, communications, power distribution, flood control, sewerage, fuel supply and so forth. Any one of these is complex in its own right. Roading, for instance, is an extended network of roads, sometimes with and elsewhere without redundancy, stretching over the region's 700 km length, with many flood-vulnerable bridges, and in places with roads clinging to earthquake- and slip-threatened slopes. Reducing the infrastructure to a system model was no easy task. It was helped by thinking of most components as flow-enabling lifelines. Lifelines can be categorised into.

Transport—roading, rail, ports, airports
Telecommunications and broadcasting
Energy—electric power and fuel
Protection—river and coastal protection works

Water and wastewater.

Also essential for community functioning are supply chains and services maintaining food supplies, medical services and supplies, building supplies, goods, fuel, financial services, insurance, governance, emergency services and education among others.

In earlier work in the region we had used risk-based approaches to look at the more limited problems of emergency response and infrastructure vulnerability to earthquakes, and we considered single-earthquake scenarios. In contrast, we now had to deal with all possible natural-hazard threats, requiring a shift from risk to resilience. We were also asked to change the focus from immediate response to longer term recovery because a major lesson from the two Christchurch earthquakes of 2010 and 2011 was the critical importance of dealing well with the recovery phase. As the clients could not be expected to address all recommended improvements immediately, our recommendations had to be prioritised in order of importance. The resulting report is available on the Internet [18].

## 10.5 Strategy and Structure

Extensive earlier risk-based experience in the region [19] meant that we began with a good understanding of the area as a whole. The next step was to define the overall system with which we would be working. We realised that besides the physical aspects of topology, geology and infrastructure we also needed to include the social system – the West Coast community and what contributed to its resilience.

Clearly, we required a systems model of the infrastructure. The distinction between a *system* and a *system model* is discussed elsewhere [4].[1] The elements of the infrastructure system model, such as a bridge, for example, or a stretch of road, had to be categorised in terms of their *vulnerability* and their *significance*. Here, "vulnerability" is used in the sense of the reverse of resilience and refers to the potential for the infrastructure element to be damaged (though we don't know by what) and "significance" means the degree of influence that damage to the element will have on the normal function of the community. Vulnerability and significance would be combined to give a measure of the relative importance of any intervention to improve the resilience of an infrastructure element.

In defining the infrastructure model, we divided the infrastructure into a system of interacting elements (Fig. 10.4). The elements were of many different types. Some were individual points such as a bridge or a flood wall, while others could be, for instance, a considerable stretch of road. Most elements were themselves complex, such as a road element in steep country which could be affected by earthquakes or floods causing slips, washouts or bridge damage over a considerable length. The road element could also contain power lines and fibre-optic cable. There was often

[1] Essentially, a system is that part of the overall situation that you're dealing with, and the system model is the model you're using to analyse the system.

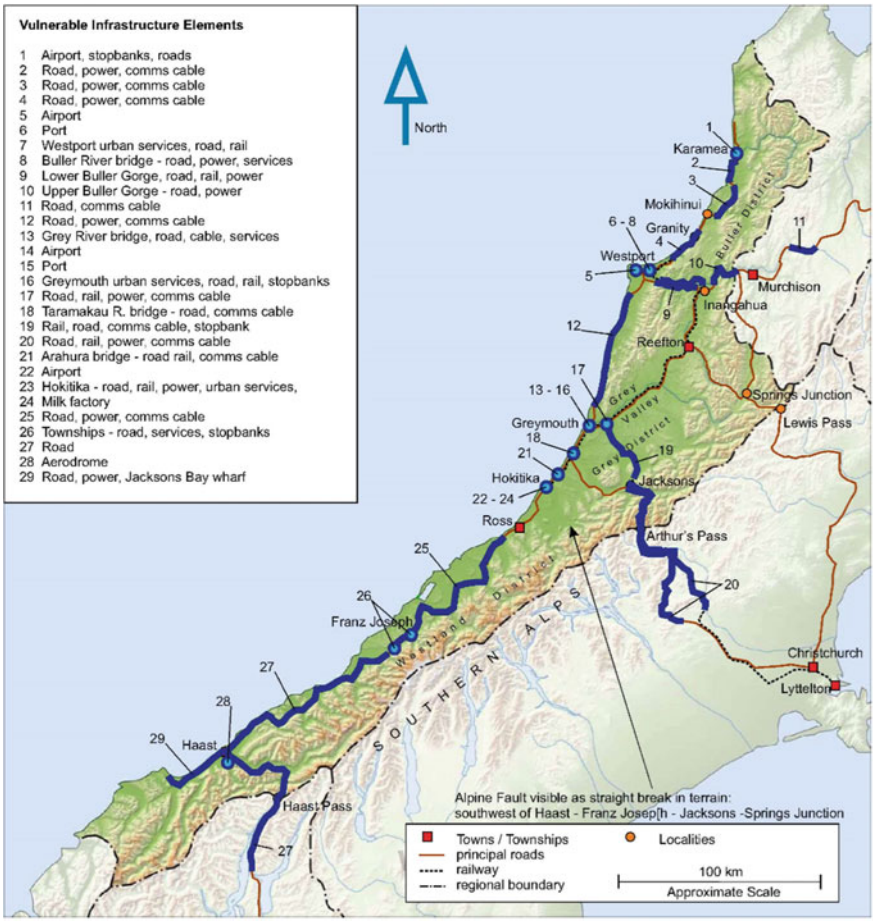


**Fig. 10.4** System model: vulnerable infrastructure elements in the West Coast Region

interdependency between elements. Functional failure in one could affect others—a bridge failure, for instance, could lead to delays in restoring other system elements such as power supplies. Choice of the elements was far from straightforward and a number of trials were required before we felt comfortable with the balance and sense of the whole. In the subsequent analysis, we had to both consider each element as a whole (there were 29) and keep our attention on the often-numerous relevant components within the element. It was no mean task.

As to "normal function of the community" and how infrastructure failure would affect it, we looked at the effect of a failure on community income. A simplified surrogate for this was the income resulting from the region's three main economic activities.

## 10.6 Vulnerability

Infrastructure vulnerability could be found by "probing" the infrastructure and its elements to determine system response—that is, to identify weaknesses. The probes we used were extreme natural events, and they had to be defined in a consistent way. We chose three: an earthquake, a storm and a tsunami. It was assumed that if the infrastructure could cope with these, applied locally, it would be sufficiently resilient to be able to cope with anything, however unexpected.

The earthquake scenario was based on the prediction of an event caused by rupture of the Alpine Fault, with the addition of the effects of a large historical earthquake in the region for determining vulnerability in areas not greatly affected by an Alpine Fault event [18] (*Supp. 2: Earthquakes*). We had to assume broad areas of high intensity shaking, aggregated from many possible earthquake events, though not all serious damage possibilities such as a major rock avalanche would happen for any single event.

The storm and tsunami scenarios assumed 500-year events in order to be comparable with the 500-year return period used for New Zealand seismic design. The definition of a 500-year storm is not straightforward. Does it refer to rainfall in a specific catchment, or is it also related to the extent of the area affected? Does it involve high winds as well as heavy rainfall, impacting infrastructure both through primary damage and also by preventing access for restoration and repair elsewhere? Hydrologists we approached found these questions difficult as they normally focus on rainfall in specific catchments for purposes of flood prediction and hydroelectric generation capacity. *Supplement 3: Storms* discusses these issues [18].

Tsunamis are fortunately infrequent. They are damaging not only because of flooding and direct flow of water but also because of debris impact. The damage from a distant-source tsunami could be widespread and affect different communities at the same time, straining available resources. Mapping data showed that a 500-year event would cause serious damage in coastal areas and towns [18] (*Supp. 4: Tsunami*).

## 10.7 Significance and Virtual Pipelines

"Significance" is the effect on the community of the failure of any infrastructure element. The question is, how should this effect be measured? This was no easy task as we could find no sensible precedent, and we had to develop our own approach. The way forward was to focus on community resilience and see how that would be impacted by infrastructure failure. How, then, could we assess the community's resilience? As noted above, we decided to use overall community income as a surrogate for its resilience, arguing that if there were no income, the community could not survive. A possible alternative would have been the community's GDP and we had figures for this, but GDP is a complex concept containing irrelevant features such

as service sector salaries, so we rejected it for the more straightforward measure of productive income. To simplify further, we chose to use only the income for the three main income earners: mining, tourism and the dairy industry.

It was not immediately obvious how we could obtain significance ratings. Original thinking was needed. We found a way forward when we realised that each of the three economic sectors could be thought of in terms of flow. The region is long and narrow. The spread-out nature of the Coast means that transportation and communication links are particularly important. Slowing or stopping the flow harms a sector's income. For mining, the flow is a flow of coal which is shipped by rail from mines north of Westport over the Alps to Christchurch's Port of Lyttelton. The dairy industry flow pattern is more complex. Milk is collected from farms throughout the region and brought to Hokitika for processing, and there are often alternative routes should a road be closed. The processed product—a thousand tonnes a week—is shipped from Hokitika to Christchurch by rail. Tourism is also a flow, with tourists travelling from Christchurch over the Alps to the West Coast and then south through the Haast Pass. To deal with all this we developed the concept of a *virtual pipeline.*

A virtual pipeline is a complex comprising all those things needed for maintaining the flow. Take tourism for example. Tourists obviously need roads to travel on, but in addition almost all need accommodation as the West Coast loop is too long to traverse in a single day. They need food and drink, electric power, telecommunication links, toilet facilities, tourist attractions and shops. All are part of the pipeline, and problems in any one of them would impinge on the flow. For instance, even if all the roads were passable the flow would stop if there were no accommodation, and it would also be affected if no tourist attractions were available.

We therefore considered the extent to which the mining, dairy and tourism pipelines, and hence community income, would be affected by failure of infrastructure elements. This gave the required significance levels which were finally combined with an element's vulnerability to determine its *importance.* A bridge, for example, might have a high degree of vulnerability, but if it led only to a single farm its significance would be low, and its importance—the weight to be given to upgrading it—would also be low. If, however, the bridge were a vital element in the tourist pipeline, then with high vulnerability and high significance, its importance rating would be high. (Note that we are not talking of *risk* here, because we are not specifying event scenarios and their likelihoods).

The mining pipeline is simple: coal is won and is then taken by rail over the mountains to the Port of Lyttelton. Rail is therefore critical. It is somewhat vulnerable to the slips and washouts caused by storm events but is generally back in operation within a week. A major tsunami would affect the line along the northern coast, but again it should not be closed for long. However, the effect of a major earthquake would be more serious. The whole length of the line through and to the west of the mountains is vulnerable. Many bridges had already been upgraded, but there is no obvious way to deal beforehand with the massive slips, debris flows and general land instability to be expected in a major event other than to be well-prepared to tackle the problems. Preparedness might entail a review of rail equipment and resources stationed on the West Coast.

As noted above, the dairying virtual pipeline is more complex. Milk is collected from farms spread over 700 km using a sparse network of roads. It is processed in Hokitika and the products are shipped out by rail. Major aspects of the pipeline are communication, roads, rail and power (for farms). Of these, communication and power are sufficiently flexible that they can usually be restored fairly quickly, though consideration should be given to improving the ability of local power generation to function in the absence of grid power. Many farmers have their own generators, but reserve fuel supplies are a significant issue. The most critical problem is transportation. Rail is discussed above, but roading needs thought. It is the most important issue both because of its vulnerabilities and because restoration takes longer.

As noted earlier, the tourism pipeline involves the road loop from Arthur's or the Lewis Pass down the Coast and then across the Haast Pass. It is far more than the roads alone and includes accommodation and other facilities as well. These also depend on roads for supply and repair. Roads and bridges are vulnerable to flooding, to tsunami and to slips and landslides due to either heavy rain or earthquakes. Some trouble spots are well known, but a major storm or earthquake would inevitably bring unexpected problems. In the mid-north of the region, alternative routes are available in some places and this redundancy improves the overall roading resilience. However, the road from Westport north to Karamea (Fig. 10.3) is a dead-end route, and the situation is particularly bad for the Karamea area because the road is through a wild and vulnerable area where a major earthquake could close the road for months. There is no obvious way round this problem because even if the Karamea Airport were made as robust as possible, it could not handle milk transport.

South of Hokitika there is only one route through South Westland to the Haast Pass and beyond. This is a critical route for tourism and a significant route for dairying. Beyond Ross the road traverses challenging countryside and powerful rivers as well as passing near to or along sections of the Alpine Fault rupture zone. It is particularly vulnerable to major earthquakes and storms, both of which could produce large slips and landslides—even rock avalanches—as well as bridge problems.

Essential parts of the dairying and tourist pipelines are communication and power supplies. These are more readily repaired or brought back into service than roading, but nevertheless they are vulnerable in some locations. A magnitude 8 earthquake would essentially close down dairying and tourism for many months. However, smaller events could also happen.

## 10.8 Results

Recommendations were made in three levels: general overarching issues; specific recommendations for defined infrastructure elements graded according to importance; and detailed and local recommendations too specific to be included here but which can be found in *Supplements 6 to 12* of the Report [18].

Regarding overarching matters, the first general issue was the urgency of communication. Looking at recovery from, say, a moderate earthquake, one of the first things

farmers, tourist operators and indeed almost anyone involved would need to do would be to plan ahead. For this they would want immediate and timely information, and this means high priority should be given to providing communication links as soon as possible after the event.

Beyond the immediate concerns of economic and social recovery, an immediate requirement after a major event would be road connections both within the West Coast and between the Coast and the rest of New Zealand. A major strategic recommendation was thus the establishment of a robust central spine of upgraded roads (including bridges, culverts, embankments and so on) either immediately useable after an event or easily and quickly reparable. Such a spine would run northwards from Ross to Greymouth (Fig. 10.5) and then up the Grey Valley to Reefton where it would divide, one arm going to Inangahua Junction then down the river gorge to

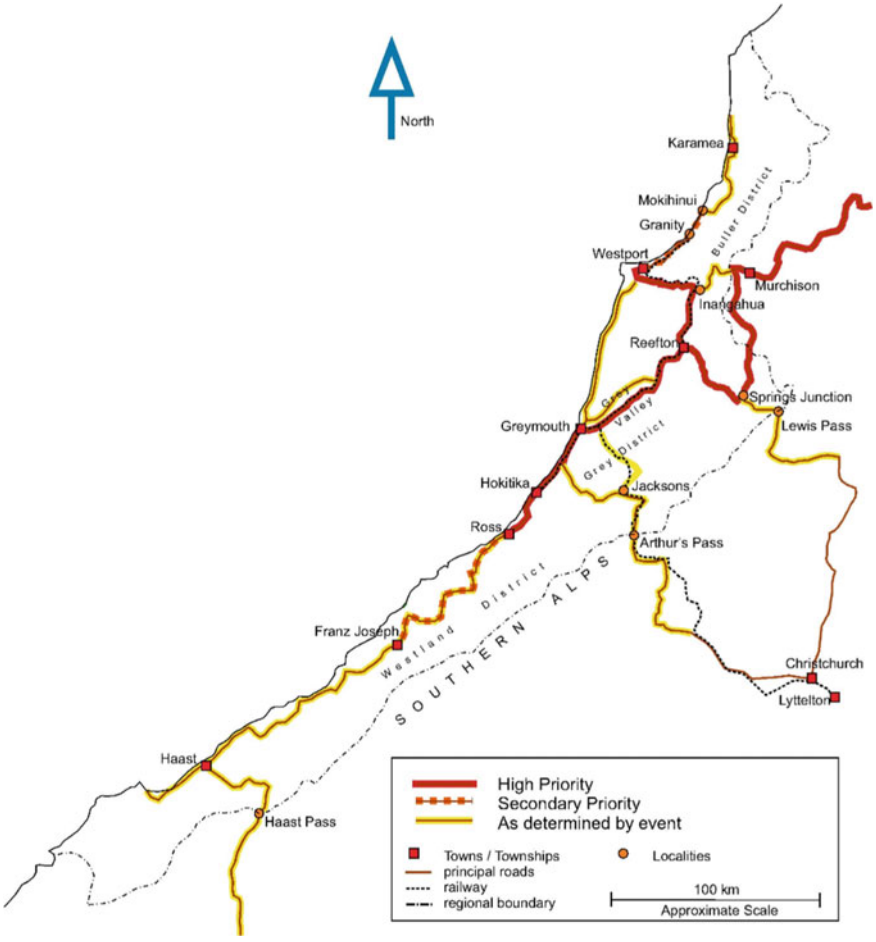


**Fig. 10.5** Recommended resilient roading system

Westport while the other would cross to Springs Junction before turning north past Maruia to Murchison and leaving the region. This road system would connect main centres of population (Greymouth, Westport, Hokitika and Reefton) while working towards possible connections to centres outside the region. These roads are key and should be made as robust as possible. Next in priority should be roads extending the spine south to Franz Josef and north to Mokihinui. Priority for restoring all other roads would be determined by the nature of the event and where restoration would be easiest: down through the Haast Pass, through Arthur's Pass or over the Lewis Pass as seemed most appropriate at the time.

Some infrastructure vulnerabilities could have widespread effects. For instance, a single stop bank near Jacksons (Fig. 10.3) guards against the possibility that a major river might entirely change its course. The stop bank is traversed by the Alpine Fault rupture zone, and a major earthquake could shear it across with widespread and devastating effects. The vulnerability here is moderate but the significance is extreme. Fortunately, there is a simple solution: double the width of the stop bank so that even if the two sides moved, there would still be sufficient overlap to prevent a breach.

Beyond the virtual pipelines, attention also had to be given to the resilience of individual communities, particularly the larger urban communities of Greymouth, Westport and Hokitika, with emphasis on lifeline infrastructure and its performance in the recovery phase. The effects of earthquakes are now becoming more widely understood, but all three main centres are vulnerable to serious flooding from either a major (500-year) storm or a major far-source tsunami.

Turning now to the main thrust of the work, which was to identify specific infrastructure vulnerabilities and rank them in order of importance, we assigned vulnerability and significance gradings to all the infrastructure elements identified for the infrastructure systems model (Fig. 10.4). Each element was given vulnerability and significance grades at three levels according to the definitions in Tables 10.1 and 10.2. The use of only three levels may seem rather crude, but further refinement was not justified given both the nature of the information to hand and the use to which the results would be put. We also kept the effects of the earthquake, storm and tsunami probes separate. As an example, Table 10.3 shows the earthquake-related output for

**Table 10.1** Vulnerability grading

| | | Lifeline stopped in 500 year event for: |
|---|---|---|
| Somewhat vulnerable | | 1 – 2 weeks |
| Vulnerable | | 2 – 4 weeks |
| Very vulnerable | | More than 1 month |

**Table 10.2** Significance Grading

| | | Mining | Dairy | Tourism |
|---|---|---|---|---|
| Significant | | Less than 4 weeks | < 4 weeks | < 2 weeks |
| More significant | | 4 to 8 weeks | 4 to 8 weeks | 2 to 8 weeks |
| Very significant | | More than 8 weeks | > 8 weeks | > 8 weeks |

some aspects of the Coast. The full report [18] contains many more such tables. Note the explanations of significance and the accompanying comments.

The third group of results was a detailed review of a number of specific and localised issues we had identified, pertinent only to the local authority in whose area they occurred. They are not dealt with here, but an interested reader could find them in *Supplements 6–12* of the main report [18].

## 10.9 Concluding Thoughts

The thinking in this chapter arose from a project in which we were asked to provide recommendations for improving the resilience of a region's infrastructure. For many years we had worked within a risk framework. Now, we had to understand resilience, and how it related to and differed from risk. We concluded that the two were related in that both dealt with uncertainty. They were complementary to one another while at the same time being fundamentally different. While risk looked at the probability or frequency of specific events impacting on systems together with the cost consequences of these events, resilience was best thought of as a property of the system itself, with no thought of specific impacting events or their consequences. Risk concerned itself with what happened to the system, while resilience was an inherent property of the system. How, then, could this property be measured? While risk could be computed as a value to be used directly in informing a decision, there was no obvious means of measuring resilience, despite many attempts at defining one. In the work we were required to do, we had to recommend, or decide, an ordering of interventions to improve resilience, and this meant we had to have a measure. Interestingly (we think) it was a measure necessarily going beyond immediate technical matters and instead relating to broader elements of the region, particularly human factors and the resilience of individual communities. We also came to see that resilience approaches could overcome some of the limitations of risk methods. Here again the two can be seen to be complementary.

In this chapter we have shown how our understanding of resilience developed, and also how we were able to find a measure appropriate to the task. Beyond that, we have

**Table 10.3** Typical result for lifeline asset vulnerability and significance, in this case for earthquake in some northern locations

| No. | Description | Lifeline Assets | Vulnerability | Significance | Comment |
|---|---|---|---|---|---|
| 1 | Karamea | • Airport<br>• Stop banks<br>• Roads | Liquefaction damage | Air travel would be the only transport route to the area if the road is not available. | Some damage to all lifelines expected from shaking, liquefaction and ground movement. |
| 2 | Karamea – Little Wanganui. | • Road<br>• Power<br>• Fibre | Liquefaction damage. | Lifelines important for the dairy farms to allow communications, production and regular export of milk from the area | Farmers have generators but fuel supply might be a limiting factor. |
| 3 | Karamea Bluffs & Mokihinui | • Road<br>• Power<br>• Fibre | Multiple slips and debris-flow damage due to earthquake | The only land link to the Karamea area | There is no alternative route available for all three assets. Failure of any for an extended time would have a severe impact on the community on the Karamea area. |
| 4 | Hector - Waimangaroa | • Road<br>• Power<br>• Fibre | Slips and structural damage | Loss of lifelines impacts on coal and dairy production and export. | Limited alternative power options particularly for the Stockton mine and in the Karamea area if the road (for fuel transport and milk export) is also affected. Loss of lifelines would isolate communities of Hector and Granity. |
| 5 | Westport Port | | Earthquake shaking damage | Used by fishing boats. No impact on mining, dairy and tourism | The port is only used by fishing boats. Vulnerable to lateral spreading of steep batter slopes and to liquefaction. |
| 6 | Westport Airport | | Earthquake shaking damage | Limited to no impact on mining, dairy and tourism | Impacts on the Buller District and may impact on Grey District also as it is the only airport on the Coast with regular direct flights to Wellington. |

shown how systems thinking is invaluable for complex projects of this nature. We have also suggested that civil infrastructure can helpfully be thought of and modelled as flows through virtual pipelines.

## References


1. Carmichael DG (2016) Risk—a commentary. Civ Eng Environ Syst 33(3):177–198. https://doi.org/10.1080/10286608.2016.1202932
2. Elms DG (2019) Limitations of risk approaches. Civ Eng Environ Syst 36(1):2–16. https://doi.org/10.1080/10286608.2019.1615474
3. Brown CB (1988) Errors in structural engineering. J Struct Eng (ASCE) 114(11):2575–2593
4. Elms DG (2020) The systems stance. Civ Eng Environ Syst 37(4):166–182. https://doi.org/10.1080/10286608.2020.1820722
5. SEBoK (2017) Resilience engineering. http://sebokwiki.org/wiki/resilience_engineering Accessed June 2017
6. Hosseini S, Barker K, Ramirez-Marquez JE (2016) A review of definitions and measures of system resilience. Reliab Eng Syst Saf 145:47–61
7. Agarwal J (2015) Improving resilience through vulnerability assessment and management. Civil Environ Syst 32(1–2):5–17. https://doi.org/10.1080/10286608.2015.1025065
8. Blockley DI (2015) Finding resilience through practical wisdom. Civil Environ Syst 32(1–2):18–30. https://doi.org/10.1080/10286608.2015.1022725
9. MacAskill K, Guthrie P (2015) A hierarchy of measures for infrastructure resilience—learning from post-disaster reconstruction in Christchurch New Zealand. . Civil Environ Syst 32(1–2):130–142. https://doi.org/10.1080/10286608.2015.1022728
10. Rosowsky DV (2019) Defining resilience. Sustain Resilient Infrastr. https://doi.org/10.1080/23789689.2019.1578166
11. Bruneau M, Chang SE, Eguchi RT, Lee GC, O'Rourke TD, Reinhorn AM, Shinozuka M, Tierney K, Wallace WA, von Winterfeldt D (2003) A framework to quantitatively assess and enhance the seismic resilience of communities. Earthq Spectra 109(4):733–752
12. Hollnagel E, Woods DD (2006) Epilogue: resilience engineering precepts. In: Hollnagel E, Woods DD, Leveson N (eds) Resilience engineering: concepts and precepts. Ashgate Publishing, Aldershot, UK, pp 347–358
13. Bodeau D, Brtis J, Graubert R, Salwen J (2013) Resiliency techniques for systems-of-systems. The MITRE Corporation Bedford, MA, USA
14. Brtis J, Jackson S, Squire A, Turner R (2020). System resilience. systems engineering body of knowledge (SEBoK). https://www.sebokwiki.org/w/index.php?title=System_Resilience&oldid=60257. Accessed 2 Oct 2020
15. Woods DD, Hollnagel E (2006) Prologue: resilience engineering concepts. In: Hollnagel E, Woods DD, Leveson N (eds) Resilience engineering: concepts and precepts. Ashgate Publishing, Aldershot, UK, pp 1–6
16. Kuhn TS (1970) The structure of scientific revolutions, 2nd edn. University of Chicago Press, Chicago
17. Taleb NN (2010) The Black Swan: The impact of the highly improbable, 2nd edn. Random House, New York
18. McCahon IA, Elms DG, Dewhirst RA (2017) Improving resilience to natural disasters: West Coast lifelines vulnerability and interdependency assessment. Report for the West Coast Civil Defence Emergency Management Group, New Zealand. https://westcoastemergency.govt.nz/west-coast-lifelines/. Accessed February 2021
19. Elms DG (2015) Improving community resilience to natural events. Civ Eng Environ Syst 32(1–2):77–89. https://doi.org/10.1080/10286608.2015.1011626

# Chapter 11
# Earthquake-Tsunami Risk Assessment and Critical Multi-hazard Loss Scenarios: A Case Study in Japan Under the Nankai-Tonankai Mega-Thrust


**Katsuichiro Goda, Raffaele De Risi, Flavia De Luca, Ario Muhammad, Tomohiro Yasuda, and Nobuhito Mori**

**Abstract** The Nankai-Tonankai Trough is the primary source region for mega-thrust subduction earthquakes in Japan. In this chapter, a case study for a coastal town in western Japan is presented to assess the earthquake-tsunami risks due to the future Nankai-Tonankai mega-thrust subduction event using a novel earthquake-tsunami risk model. The multi-hazard risk model incorporates stochastic rupture sources, spatially correlated ground motion fields, tsunami inundation simulations, detailed building portfolio data, seismic and tsunami fragility models, and building damage cost estimation. It produces the multi-hazard and single-hazard loss distributions, accompanied by detailed earthquake rupture scenarios, shaking-tsunami hazard intensity distributions, and building damage distributions. Importantly, the new multi-hazard tool facilitates the identification of critical multi-hazard loss scenarios and produces integrated hazard-risk maps that are particularly useful for disaster risk reduction and management purposes.

## 11.1 Introduction

Coastal communities in active seismic regions are exposed to significant risk due to mega-thrust subduction earthquakes and tsunamis. Such a risk is due to both

K. Goda (✉)
Department of Earth Sciences, Western University, London, ON, Canada
e-mail: kgoda2@uwo.ca

Department of Statistical & Actuarial Sciences, Western University, London, ON, Canada

R. De Risi · F. De Luca · A. Muhammad
Department of Civil Engineering, Bristol University, Bristol, UK

T. Yasuda
Kansai University, Suita, Osaka, Japan

N. Mori
Disaster Prevention Research Institute, Kyoto University, Kyoto, Japan



M. G. Stewart and D. V. Rosowsky (eds.), *Engineering for Extremes*, Springer Tracts in Civil Engineering, https://doi.org/10.1007/978-3-030-85018-0_11

shaking and tsunami. In the last two decades, moment magnitude (M) 9-class mega-thrust events caused catastrophic consequences in Indian Oceans and Japan (e.g. [1, 2]. Catastrophic events could strike other active subduction zones globally (e.g. Makran and Cascadia subduction zones) and hence, effective earthquake-tsunami risk management strategies are urgently needed. Therefore, a cascading multi-hazard assessment approach needs to be considered to develop effective earthquake-tsunami risk management strategies for coastal communities.

A probabilistic multi-hazard analysis quantifies the natural disaster risk and facilitates the evaluation of the cost–benefit effectiveness of available risk mitigation options [3, 4]. For earthquake-related hazards, recent advances in the fields of earthquake and tsunami engineering have led to the development of new multi-hazard risk assessment methods for earthquakes and tsunamis. For instance, Goda and De Risi [5] proposed a multi-hazard loss model for Japanese subduction earthquakes and tsunamis by simulating shaking and tsunami hazard processes sequentially and by applying seismic and tsunami fragility functions. Their work extended the performance-based earthquake engineering methodology for regional seismic risk assessment [6, 7] into the performance-based earthquake-tsunami engineering methodology. On the other hand, Attary et al. [8] proposed a physics-based approach to estimate the risk of structures subjected to a destructive tsunami following an earthquake. That study extended the analytical method of quantifying the seismic fragility of structures by considering a cascading sequence of seismic and tsunami loadings to structures.

Among the global active subduction zones, the Nankai-Tonankai Trough region of western and central Japan is anticipating a mega-thrust subduction event in the near future. Since 684 A.D., nine M8.0 + events occurred in the Nankai-Tonankai Trough region [9, 10] with a mean recurrence period ranging between 100 and 150 years. The most recent events were the 1944 Tonankai earthquake and the 1946 Nankai earthquake, rupturing the eastern and western parts of the Nankai-Tonankai Trough, respectively. When the Nankai-Tonankai Trough segments rupture separately, the earthquake magnitude tends to result in smaller magnitudes (typically less than M8.5). On the other hand, the Nankai and Tonankai segments can rupture synchronously as indicated by geological evidence from the past earthquakes, such as the 1361 Shohei and 1707 Hoei events [11], resulting in greater moment magnitudes (M8.6 and above). For preparing against future earthquake-tsunami disasters in western and central Japan, the Central Disaster Management Council (CDMC) of the Japanese Cabinet Office developed national tsunami source models (hereafter, 2012 CDMC models) by considering the synchronous M9 rupture scenarios of the Nankai-Tonankai Trough earthquake and produced tsunami inundation maps for tsunami disaster preparedness purposes. Recently, Goda et al. [12] generated a realistic set of 1000 stochastic earthquake source models of M8.7–M9.1 and performed Monte Carlo tsunami inundation simulations to quantify the uncertainty associated with regional and local tsunami hazard assessments.

This chapter presents a quantitative multi-hazard risk assessment for a coastal community in Kuroshio Town, Kochi Prefecture, Japan, due to future Nankai-Tonankai Trough mega-thrust events. It discusses the adequacy of the current

earthquake-tsunami preparedness from financial loss and life-safety viewpoints. To consider extreme scenarios relevant for planning disaster risk mitigation actions, 1000 stochastic earthquake rupture models of M8.7–M9.1 [12] are employed. Subsequently, joint assessment of shaking-tsunami intensity footprints in a coastal community is conducted by simulating spatially correlated ground motion fields and by conducting tsunami inundation simulations based on the stochastic earthquake source models. The hazard footprint results are then combined with empirical seismic and tsunami fragility functions that are applicable to conventional wooden buildings in Japan. The main outputs from the developed multi-hazard risk model of a building portfolio subjected to mega-thrust subduction earthquakes and tsunamis are the multi-hazard and single-hazard loss distributions, accompanied by detailed earthquake rupture scenarios, shaking-tsunami hazard intensity distributions, and building damage distributions. The new multi-hazard tool facilitates the identification of critical multi-hazard loss scenarios and leads to integrated hazard-risk maps that are particularly useful for disaster risk reduction and management purposes.

## 11.2 Case Study

### *11.2.1 Nankai-Tonankai Mega-Thrust Events*

The Nankai-Tonankai Trough is the primary source of major subduction earthquakes in western and central Japan, and their seismic activities are induced by tectonic moments of the Philippine Sea Plate and the Eurasian Plate with slip rates between 40 and 55 mm/year [13]. The rupture region can be broadly divided into the Nankai and Tonankai segments, as shown in Fig. 11.1a. The Nankai segment spans from Hyuga-nada, Shikoku Island, and Kii Peninsula and ruptured many times in the

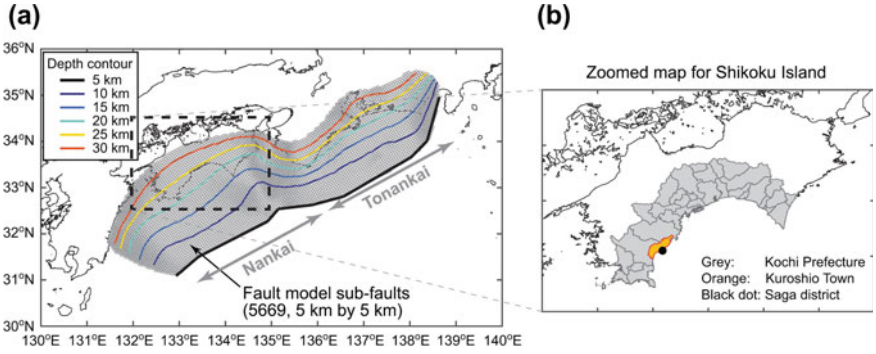


**Fig. 11.1** **a** Nankai-Tonankai Trough source region and **b** location of the target case-study site Saga district in Kuroshio Town, Kochi Prefecture. The fault plane geometry of the 2012 CDMC models is shown in panel **a** (Color figure online)

past. Abundant evidence indicates that earthquakes originating from the Nankai segment can produce intense ground shaking and large-scale coastal inundations due to tsunamis (e.g. [14]. The rupture history of the Tonankai segment, which spans from Kii Peninsula, Enshu-nada, and Tokai, is also well studied (e.g. [11]. The past Tonankai events caused widespread shaking and tsunami effects in the central Pacific region of Japan.

For tsunami hazard mapping of a future Nankai-Tonankai mega-thrust event, the CDMC developed eleven M9-class earthquake source models by considering that the synchronized rupture across both the Nankai and Tonankai segments is possible. The eleven source models reflect (a limited number of) different rupture scenarios in terms of locations of large slip concentrations (i.e. asperities) within the rupture plane (see [12] for more details). The main subduction interface of the 2012 CDMC models consists of a set of 5669 sub-faults, each sub-fault having a size of 5 km by 5 km, with the total fault plane area of $1.44 \times 10^5$ km$^2$ (Fig. 11.1a). The geometrical parameters (i.e. strike, dip, and rake) of the sub-faults are variable over the curved, steepening fault plane along the dip direction. The models are intended to represent extreme scenarios that can be used for improving regional and local tsunami disaster preparedness, such as the construction of coastal defense structures and planning of tsunami evacuation.

### *11.2.2 Kuroshio Town, Kochi Prefecture, Japan*

Kuroshio Town is a municipality in Kochi Prefecture (Fig. 11.1b) that faces severe hazards due to the Nankai-Tonankai subduction earthquakes. As of September 2020, the population and household number of Kuroshio Town are 10,905 and 5475, respectively. According to the 2012 national seismic-tsunami hazard assessments conducted by the Japanese Cabinet Office, shaking and tsunami hazard levels that need to be considered for Kuroshio's earthquake disaster risk reduction strategy and planning are the Japan Meteorological Agency Seismic Intensity scale VII (highest, equivalent to the Modified Mercalli Intensity of X–XII) and the assessed tsunami wave/run-up height of 34 m [15]. Therefore, it is critical to evaluate the seismic and tsunami risks to people and assets in Kuroshio Town.

The Saga district is one of the main populated areas in Kuroshio Town along the coast. Within the area shown in Fig. 11.2a, approximately 2200 people live in 900 households. Houses and facilities (see black polygons in Fig. 11.2a, c) are distributed on an alluvial plain along the Iyoki River. Sedimental deposits are prevalent in the low-lying river mouth areas, and thus larger ground shaking intensity is expected there. This can be seen in Fig. 11.2b showing the average shear-wave velocity in the upper 30 m (Vs30) obtained from J-SHIS (250-m mesh grids; https://www.j-shis.bosai.go.jp/en/). Values of Vs30 at locations of the houses and local facilities are typically less than 300 m/s (e.g. NEHRP site class D), indicating that local site conditions are relatively soft. The low-lying area of the district is surrounded by steep slopes/hills (Fig. 11.2c). In this zoomed area, a tsunami evacuation tower was

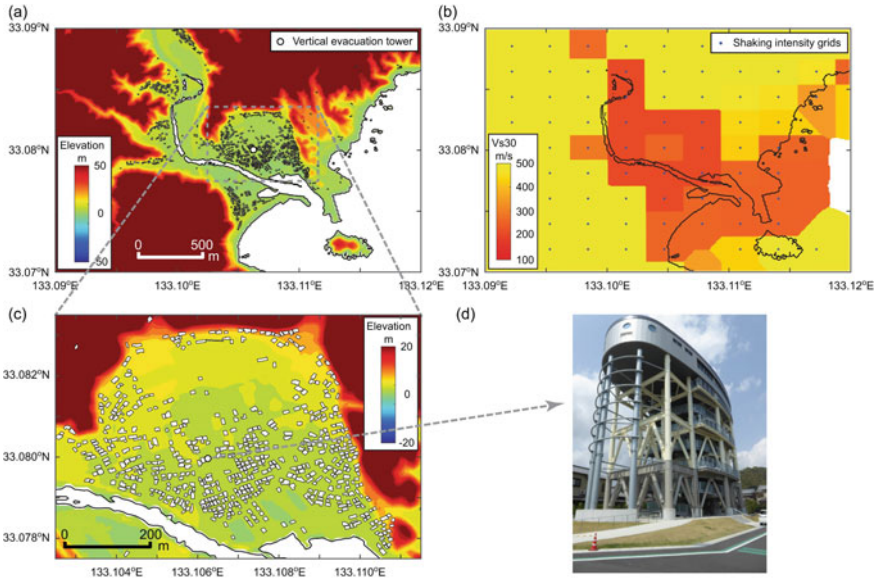


**Fig. 11.2** Building distribution in the Saga district of Kuroshio Town: **a** elevation, **b** average surface shear-wave velocity based on J-SHIS, **c** zoomed area near the vertical evacuation tower, and **d** photo of the vertical evacuation tower (Color figure online)

constructed for residents living in the low-lying areas (Fig. 11.2d). The evacuation space of the tower is 25.3 m from the mean sea level. By taking into the tower's land elevation of 3.4 m, the critical inundation depth for safe evacuation is 21.9 m. This critical depth can be used to evaluate the adequacy of the evacuation tower under extreme situations.

A national GIS database maintained by the Geospatial Information Authority of Japan (https://www.gsi.go.jp/kiban/) is utilized to develop a building exposure model for the Saga district. The dataset includes geographical coordinates and property plot boundary data of individual buildings, and thus building footprint areas of individual buildings can be calculated. By including buildings that have footprint areas between 50 and 200 $m^2$ and visually inspecting buildings using Google Earth image of the area, 942 buildings are selected for the multi-hazard risk assessment (see Sect. 11.3). The spatial distribution of the selected buildings is shown in Fig. 11.2a, c. For the risk assessment, the unit construction cost for typical wooden buildings is obtained from the Japanese building cost information handbook [16]. It is assumed to be lognormally distributed with mean = 1600 US$/$m^2$ and coefficient of variation = 0.32 (assuming 1 US$ = 100 yen). In calculating the total building replacement cost (= total footprint area times unit construction cost), the total footprint area is estimated by multiplying the building footprint area of each individual property (as in the original building database) by a factor of 1.3. Such a number is considered to be applicable based on the building/construction statistics from [16] and the Ministry

of Land, Infrastructure, Transport and Tourism (http://www.mlit.go.jp/toukeijouhou/chojou/stat-e.htm). Based on the above building cost information, the expected total cost of the 942 buildings in Saga is US$196 million.

## 11.3 Multi-hazard Risk Assessment for the Nankai-Tonankai Mega-Thrust

Building upon the stochastic source models and tsunami inundation analyses conducted by [12] for future Nankai-Tonankai mega-thrust events, an earthquake-tsunami loss model for the Nankai-Tonankai events is developed. The risk model accounts for the uncertainty associated with the rupture characterization in terms of fault geometry and earthquake slip distribution. Such earthquake source uncertainty is propagated through probabilistic calculations of seismic-tsunami damage and loss of a building portfolio. The multi-hazard loss estimation is based on the methodology proposed by [5], which was developed for the Tohoku region of Japan, and consists of three major modules: (i) earthquake source and seismic-tsunami footprint modeling, (ii) seismic-tsunami fragility modeling, and (iii) risk assessment. A computational procedure of the multi-hazard loss estimation is illustrated in Fig. 11.3. Since the multi-hazard risk assessment methodology implemented for the Nankai-Tonankai mega-thrust is mostly identical to the framework presented in [5], the computational modules are described succinctly in the following subsections. Furthermore, because detailed descriptions of the stochastic source modeling and tsunami inundation analyses for the Nankai-Tonankai earthquakes can be found in [12], explanations for this aspect are kept brief as well.

### *11.3.1 Hazard Characterization*

A stochastic source model captures the spatial uncertainty of earthquake rupture for a given earthquake magnitude. In generating the stochastic rupture models for the Nankai-Tonankai mega-thrust events, the 2012 CDMC fault plane (Fig. 11.1a) is adopted as a baseline. The source uncertainty is characterized by empirical prediction equations of earthquake source parameters and stochastic synthesis of earthquake slip [17]. For a magnitude value, eight source parameters, i.e. fault width, fault length, mean slip, maximum slip, Box-Cox power parameter, correlation length along dip, correlation length along strike, and Hurst number, are generated. Once the geometry and position of a stochastic source model are determined, a random heterogeneous slip distribution is generated using a Fourier integral method, where amplitude spectrum is represented by von Kármán spectrum and random phase [18]. To generate a slip distribution with realistic right-heavy tail features, the synthesized slip distribution is converted via Box-Cox power transformation. The transformed

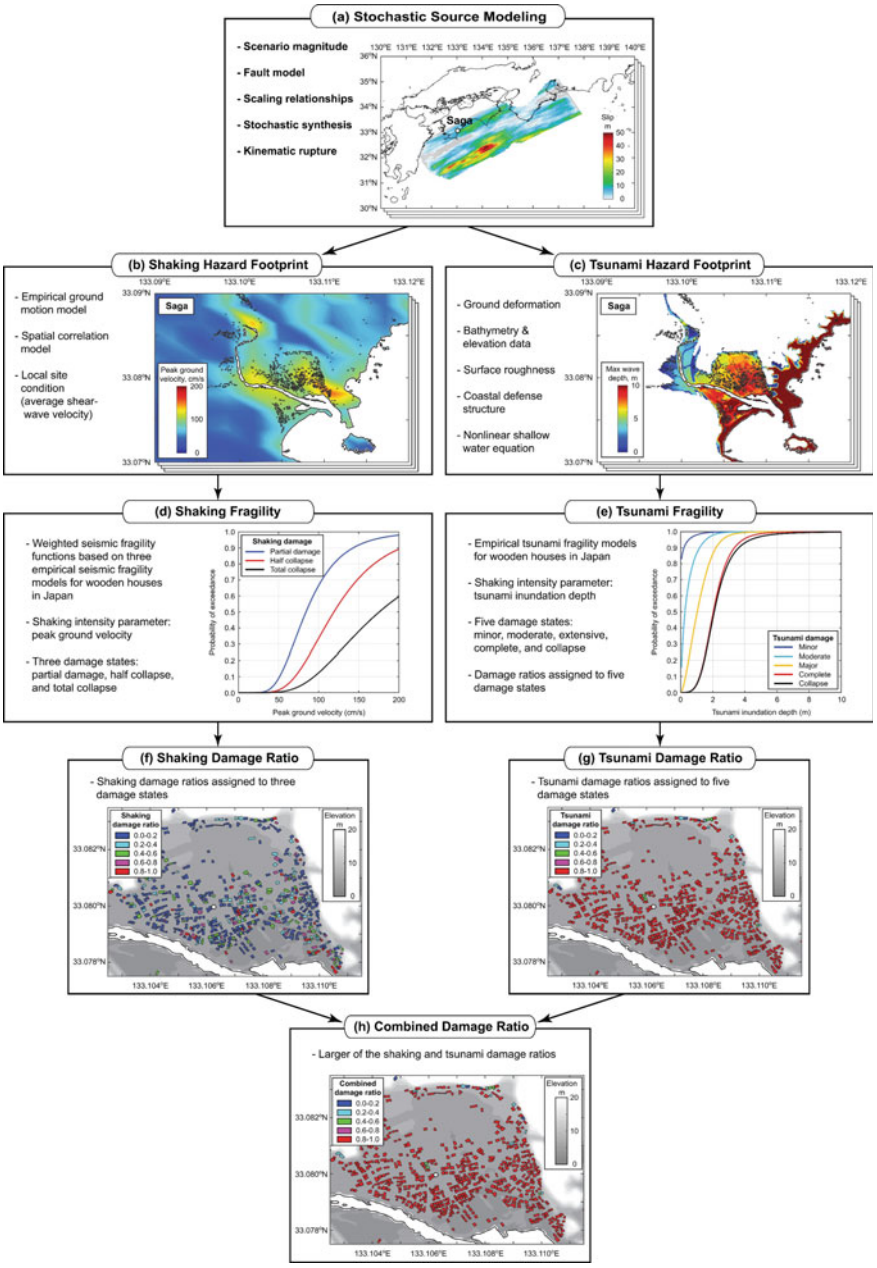


**Fig. 11.3** Multi-hazard loss estimation: **a** stochastic source modeling, **b** shaking hazard footprint, **c** tsunami hazard footprint, **d** shaking fragility, **e** tsunami fragility, **f** shaking damage ratio, **g** tsunami damage ratio, and **h** combined damage ratio (Color figure online)

slip distribution is then adjusted to achieve suitable slip characteristics, such as mean slip and maximum slip. In this study, stochastic synthesis of constrained random slip distributions is performed to generate 1000 stochastic source models having earthquake magnitudes in the range between M8.7 and M9.1 [12]. The synthesized earthquake source models reflect possible variability of tsunamigenic earthquakes from the Nankai-Tonankai Trough in terms of geometry, fault location, and slip distribution (Fig. 11.3a).

For a given earthquake source model, shaking and tsunami hazard intensities at building locations are evaluated by using a ground motion model and by solving non-linear shallow water equations for initial boundary conditions of sea surface caused by an earthquake rupture. In this study, the peak ground velocity (PGV) is selected as a shaking hazard parameter, and the maximum inundation depth is adopted as a tsunami hazard parameter. The choice of PGV as seismic hazard measure is owing to its compatibility with empirical seismic fragility functions in Japan. The local site conditions are based on the J-SHIS average shear-wave velocity database (Fig. 11.2b). The PGV ground motion model by [19] together with the intra-event spatial correlation model of [20] is used to generate spatially correlated ground motion fields for the 1000 stochastic sources (Fig. 11.3b).

On the other hand, tsunami propagation and inundation simulations are performed using a TUNAMI computer code by [21]. The computational domains are nested with 2430-m, 810-m, 270-m, 90-m, 30-m, and 10-m grids. High-resolution elevation data together with coastal/riverside structural data (e.g. breakwater and levees) and surface roughness data are taken into account to ensure the accuracy of local tsunami inundation analyses (note: the mentioned data are the same as the 2012 CDMC models). The maximum inundation depths at the building locations are determined by subtracting the land elevations from the maximum inundation heights. Tsunami simulations are conducted for all 1000 stochastic sources by considering a time step of 0.1 s to satisfy the Courant–Friedrichs–Lewy condition and tsunami simulation duration of 3 h. For each of the stochastic source models, a detailed local tsunami inundation map can be obtained (Fig. 11.3c).

### *11.3.2 Fragility and Damage Evaluation*

A vulnerability model relates the hazard intensity and the damage via an impact severity metric (e.g. damage ratio). In the developed multi-hazard risk model, damage ratios for shaking and tsunami are estimated by applying seismic and tsunami fragility functions. For shaking damage, the adopted seismic fragility models are three empirical functions for low-rise wooden buildings in Japan [22–24]. Those functions were developed based on shaking damage data from the 1995 Kobe earthquake, seven crustal earthquakes that occurred between 2003 and 2008, and the 2011 Tohoku earthquake, respectively. The three seismic fragility functions are combined by considering equal weights. The damage states for shaking are defined as: partial damage, half collapse, and complete collapse, and the corresponding damage ratios

are assigned as 0.03–0.2, 0.2–0.5, and 0.5–1.0, respectively [25]. The weighted seismic fragility functions for the partial damage, half collapse, and complete collapse damage states are shown in Fig. 11.3d.

For tsunami damage, the tsunami fragility model developed by [26] based on the tsunami damage data from the 2011 Tohoku event is adopted. The fragility model is expressed in terms of tsunami flow depth. The following five tsunami damage states are considered: minor, moderate, extensive, complete, and collapse, together with the damage ratio ranges of 0.03–0.1, 0.1–0.3, 0.3–0.5, 0.5–1.0, and 1.0, respectively (http://www.mlit.go.jp/toshi/toshi-hukkou-arkaibu.html). The tsunami fragility functions for the minor, moderate, extensive, complete, and collapse damage states are shown in Fig. 11.3e.

### *11.3.3 Risk Assessment*

A damage ratio of each building due to ground shaking is determined by identifying the shaking damage state for a given PGV value and then by simulating a uniform random variable within the lower and upper bounds of the respective damage state. The same procedure can be adopted for determining the tsunami damage ratio. The shaking and tsunami damage ratio maps of the buildings in the zoomed area of the Saga district (Fig. 11.2c) are illustrated in Fig. 11.3f, g, respectively. The shaking damage varies from building to building in the zoomed area; because the PGV intensity is variable and is relatively high (exceeding 100 cm/s; Fig. 11.3b), the half-collapse and collapse damage states can be induced in some buildings due to shaking alone (Fig. 11.3d). On the other hand, the tsunami damage is severe and is more uniform in the low-lying area of the Saga district, where flow depths exceeding 5 m are experienced for the event shown (Fig. 11.3c). With such high levels of flow depth, the majority of the low-rise wooden houses will be collapsed or washed away (Fig. 11.3e).

Subsequently, for each building, a greater of the estimated shaking and tsunami damage ratios is adopted as the final damage ratio of the building. A multi-hazard loss value is calculated by sampling a value of the building replacement cost and then by multiplying it by the final damage ratio. For the illustrative cases shown in Fig. 11.3e, f, the combined damage ratios of the buildings in the zoomed area of the Saga district are displayed in Fig. 11.3h. The final seismic-tsunami damage ratio map reflects the estimated damage patterns from both shaking and tsunami risk assessments. For the earthquake scenario shown in Fig. 11.3, the tsunami risk dominates. It is noteworthy that the above-mentioned approach of calculating the combined shaking-tsunami damage ratio does not account for the interaction between shaking and tsunami damage (including tsunami debris effects) explicitly. For the present study, this limitation is alleviated because the tsunami fragility model by [26] is based on the tsunami damage data from the 2011 Tohoku event that include the effects due to shaking damage. Nevertheless, when a multi-hazard loss model

is developed for a different region, it is desirable to consider such shaking-tsunami damage accumulation effects (e.g. [8]).

Finally, by repeating the risk assessments for all selected buildings and all earthquake scenarios, multi-hazard and single-hazard loss samples can be obtained for the building portfolio of interest. In the post-processing stage of the multi-hazard loss estimation, outputs, such as synthesized earthquake scenario, simulated PGV distribution, inundation depth distribution, and single-hazard as well as multi-hazard damage ratio distribution, can be associated with the corresponding loss estimates to develop critical multi-hazard scenario maps.

## 11.4 Multi-hazard Loss Estimation Results

### *11.4.1 Loss Distributions for Building Portfolio in Saga*

The building portfolio loss samples for the 1000 stochastic source models of the Nankai-Tonankai mega-thrust events are obtained from the developed multi-hazard risk model. Figure 11.4 shows a histogram of the combined shaking-tsunami loss for the building portfolio in the Saga district, whereas Fig. 11.5 shows a scatter plot and histograms of the shaking loss and tsunami loss for the building portfolio in Saga. In these two figures, the loss samples are distinguished for two magnitude ranges (M8.7–8.9 and M8.9–9.1). As shown in Fig. 11.4, the combined loss tends to increase with the earthquake magnitude. By inspecting single-hazard loss histograms shown in Fig. 11.5, the tsunami loss tends to increase with the magnitude more

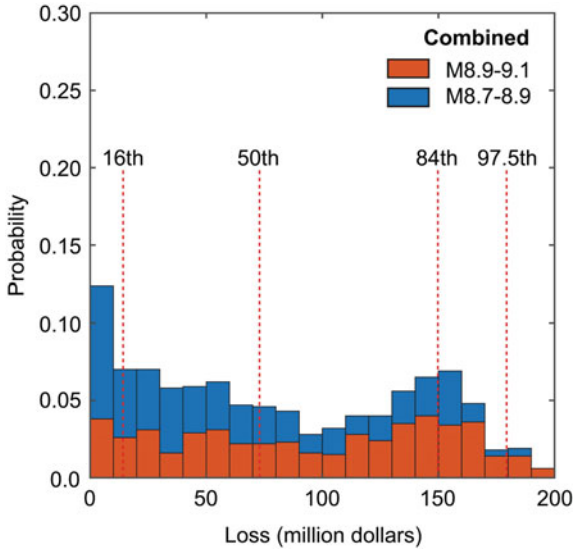


**Fig. 11.4** Histogram of the combined shaking-tsunami loss for the building portfolio in the Saga district (Color figure online)

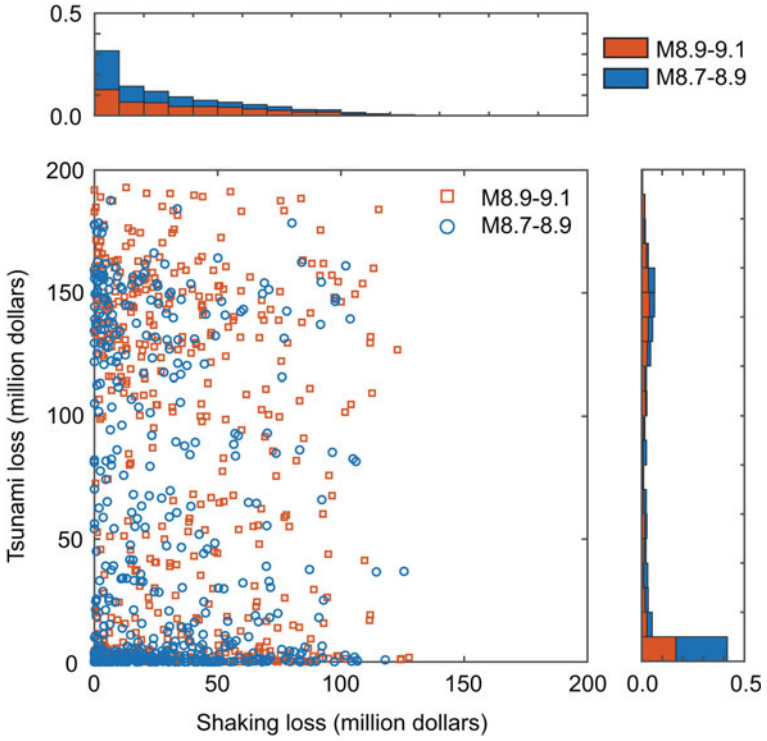


**Fig. 11.5** Scatter plot and histograms of the shaking loss (x-axis) and tsunami loss (y-axis) for the building portfolio in the Saga district (Color figure online)

significantly than the shaking loss. It thus contributes more towards the increase in the combined loss with the earthquake magnitude, as shown in Fig. 11.4. This observation is consistent with the results reported in [5] for the Tohoku region case where tsunami risk is more nonlinearly affected by the earthquake size than shaking risk.

Concerning the estimated shaking loss based on the developed multi-hazard catastrophe model, the increase in earthquake magnitude results in a larger earthquake rupture area (as per empirical scaling relationships), and hence there is a larger probability that the distance from the rupture plane to the building sites becomes shorter. On the other hand, the increase in earthquake magnitude itself does not result in the increased ground motion intensity due to the saturation of magnitude scaling [19]. This is the main reason that the magnitude effect on the shaking loss is limited, as seen on the top panel of Fig. 11.5.

In contrast, the tsunami loss is more influenced by the increase in tsunami potential energy due to larger earthquakes [12]. The tsunami potential energy is the sum of the squared sea surface elevations caused by an earthquake rupture and is strongly correlated with the inundation area, which is an accurate predictor for local tsunami

loss. Therefore, a more significant increase in the tsunami loss is expected with the increase in earthquake magnitude, as seen in the right panel of Fig. 11.5, than the shaking loss. It is also noticeable that the tsunami loss histograms exhibit bimodal loss distributions, i.e. a lower mode at tsunami losses less than US$20 million and a higher mode at tsunami losses greater than US$100 million. When a large loss occurs in Saga, the earthquake asperities tend to be located off Shikoku Island and thus massive tsunami waves generated by the ruptures are directed towards the target coastal areas.

Lastly, from the scatter plot shown in Fig. 11.5, it is not possible to identify an explicit dependency between the shaking loss and the tsunami loss. This is due to (at least) two reasons. One reason is that the current ground motion model does not account for locations of asperities in computing the ground shaking intensity (i.e. the site-to-source distance depends only on the overall fault model and does not reflect local features of the earthquake rupture) and its predicted intensity is saturated with respect to earthquake magnitude. In addition, the ground motion variability term, such as between-event variability, does not depend on the average earthquake slip. The other reason for the lack of explicit dependency between the shaking loss and the tsunami loss is the consideration of a local target area in this study. When the multi-hazard loss estimation is performed for a broader region (e.g. Shikoku or western Japan), the bimodal characteristics of the regional tsunami loss distribution will become less noticeable, and the regional shaking loss distribution depends more on the earthquake magnitude.

### *11.4.2 Multi-hazard Shaking-Tsunami Hazard Intensity at Vertical Evacuation Tower in Saga*

It is insightful to examine the shaking and tsunami hazard intensities at the vertical evacuation tower in Saga (Fig. 11.2d). For this purpose, information on PGV and inundation depth at the vertical evacuation tower is extracted and is shown as a scatter plot and histograms in Fig. 11.6. The PGV distributions (top panel) have similar unimodal shapes for the two magnitude ranges with the representative PGV values of 80 cm/s and the extreme PGV values exceeding 250 cm/s. The inundation depth distributions (right panel) exhibit the right-skewed distributions with large concentrations at inundation depth of 0 m (i.e. the site is not inundated, noting that the tower is at 3.4 m above the mean sea level). There is one case where tsunami depth becomes greater than the critical depth of 21.9 m; the chance of experiencing such incidence may be regarded as sufficiently small given that extreme rupture scenarios are simulated in this study [12]. Importantly, the multi-hazard risk model can produce useful outputs that feed into advanced engineering analyses. For instance, the joint multi-hazard intensity values are particularly useful for examining the structural integrity of the vertical evacuation tower under extreme seismic-tsunami loading conditions.

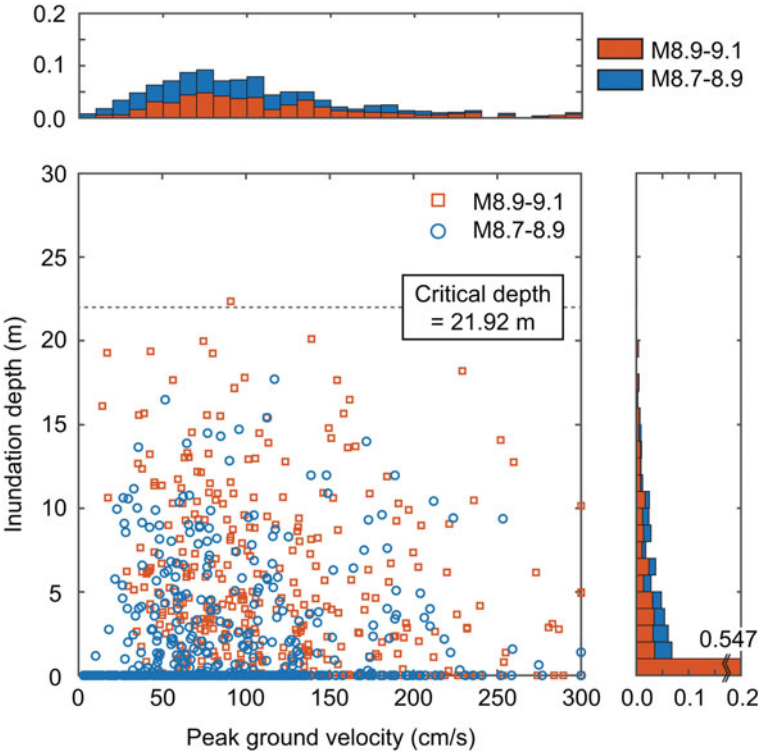


**Fig. 11.6** Scatter plot and histograms of peak ground velocity (x-axis) and inundation depth (y-axis) at the vertical evacuation tower in Saga (Fig. 2d) (Color figure online)

### *11.4.3 Critical Hazard-Risk Loss Scenario Maps*

Critical hazard-risk scenario maps that are directly linked with the estimated consequences of the events are useful for disaster risk mitigation and preparedness. Such integrated maps can be created by identifying a set of hazard scenarios that lead to a specified level of portfolio loss (e.g. Fig. 11.4). For these purposes, the average characteristics of the earthquake source, hazard intensity footprint, and damage severity that correspond to a range of loss levels are investigated in this section. In the following, the four representative multi-hazard loss levels, 16th, 50th, 84th, and 97.5th percentiles, are focused upon, and the percentile loss ranges are defined by considering the representative percentile loss levels plus/minus 2.5%. For instance, in developing the average critical multi-hazard scenario maps for the 84th percentile loss level, all loss events that cause the combined portfolio loss between 81.5th and 86.5th levels (51 cases for the 1000 stochastic source models) are consolidated to produce the average critical hazard-risk scenario maps. It includes the earthquake source model, initial vertical deformation profile, PGV distribution, inundation depth distribution, shaking damage ratio, tsunami damage ratio, and combined damage

ratio. Such integrated average critical hazard-risk scenario maps for the 16th, 50th, 84th, and 97.5th percentile loss levels are shown in Figs. 11.7, 11.8, 11.9, and 11.10, respectively.

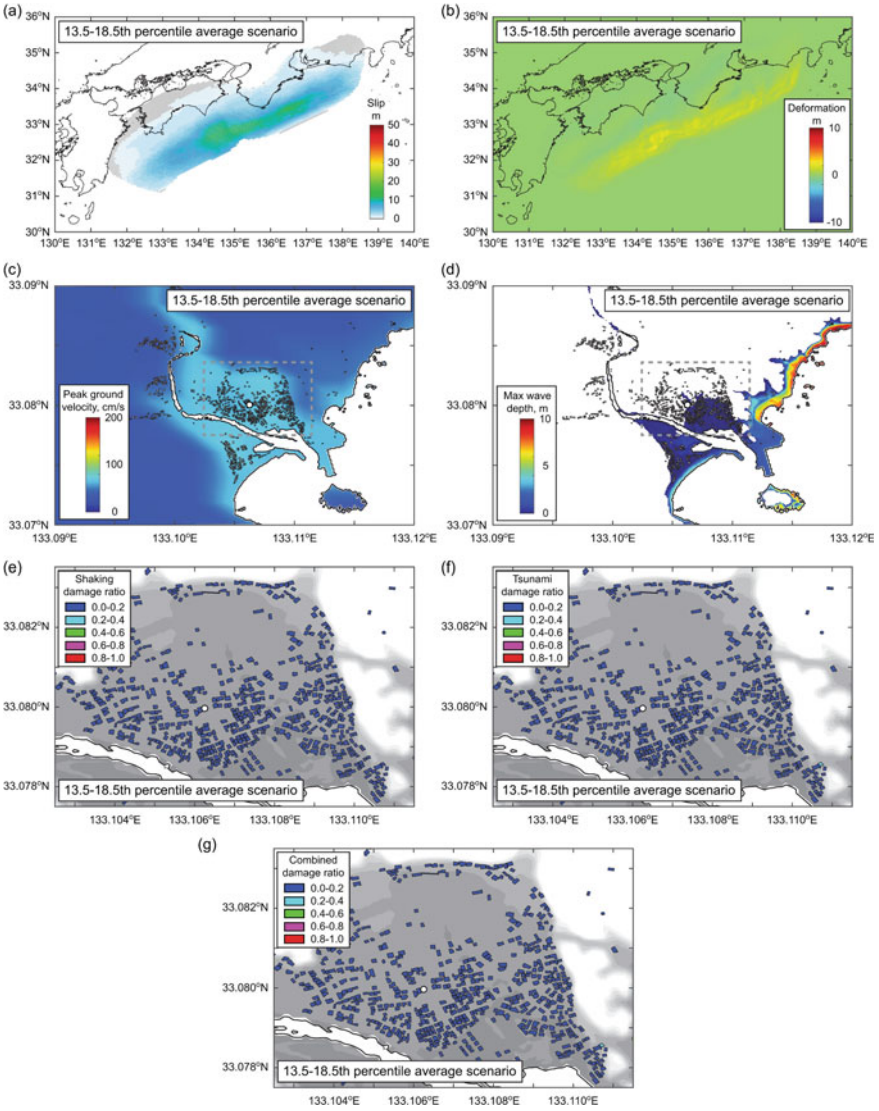


**Fig. 11.7** Average shaking-tsunami hazard-risk maps for the 16th (13.5–18.5th) percentile loss scenarios for the building portfolio in the Saga district. **a** Earthquake source model, **b** initial vertical deformation distribution, **c** peak ground velocity, **d** inundation depth, **e** shaking damage ratio, **f** tsunami damage ratio, and **g** combined damage ratio. The background color map in **e**, **f**, and **g** shows the elevation for the range of 0 m (gray) and 20 m (white) (Color figure online)

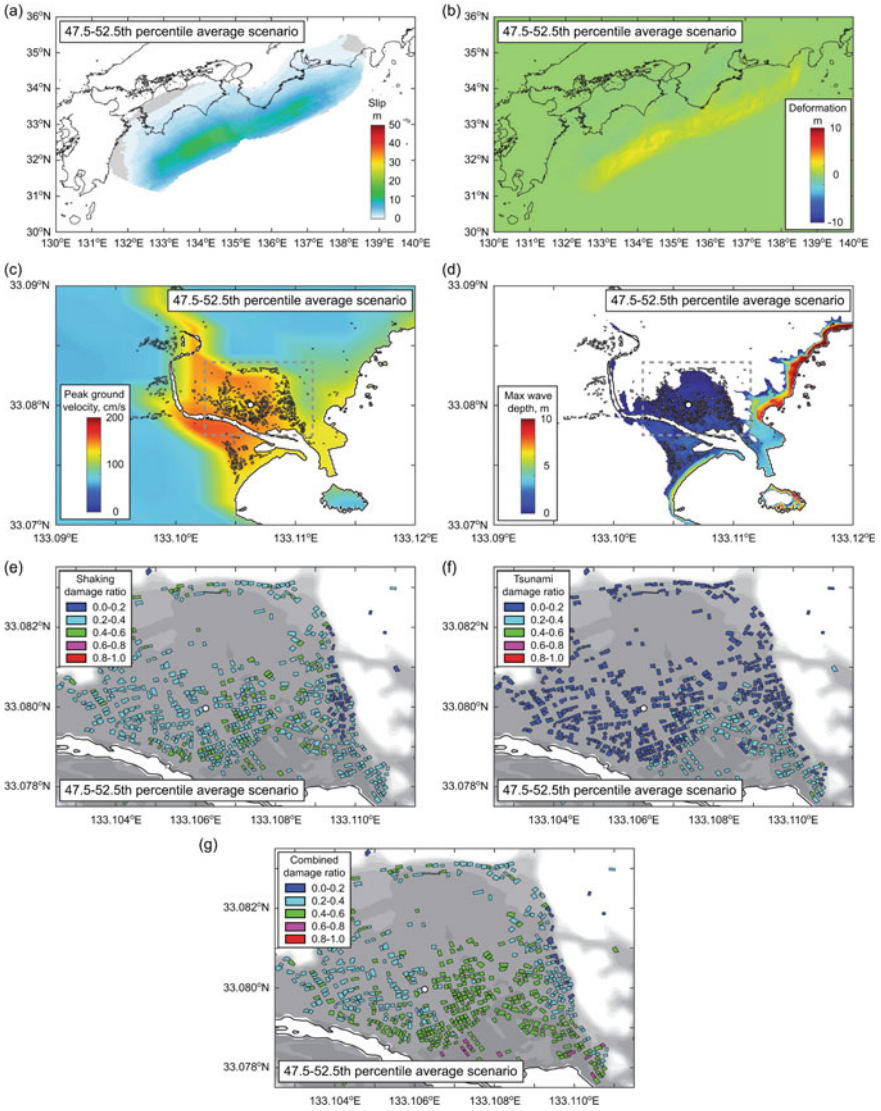


**Fig. 11.8** Average shaking-tsunami hazard-risk maps for the 50th (47.5–52.5th) percentile loss scenarios for the building portfolio in the Saga district. **a** Earthquake source model, **b** initial vertical deformation distribution, **c** peak ground velocity, **d** inundation depth, **e** shaking damage ratio, **f** tsunami damage ratio, and **g** combined damage ratio. The background color map in **e**, **f**, and **g** shows the elevation for the range of 0 m (gray) and 20 m (white) (Color figure online)

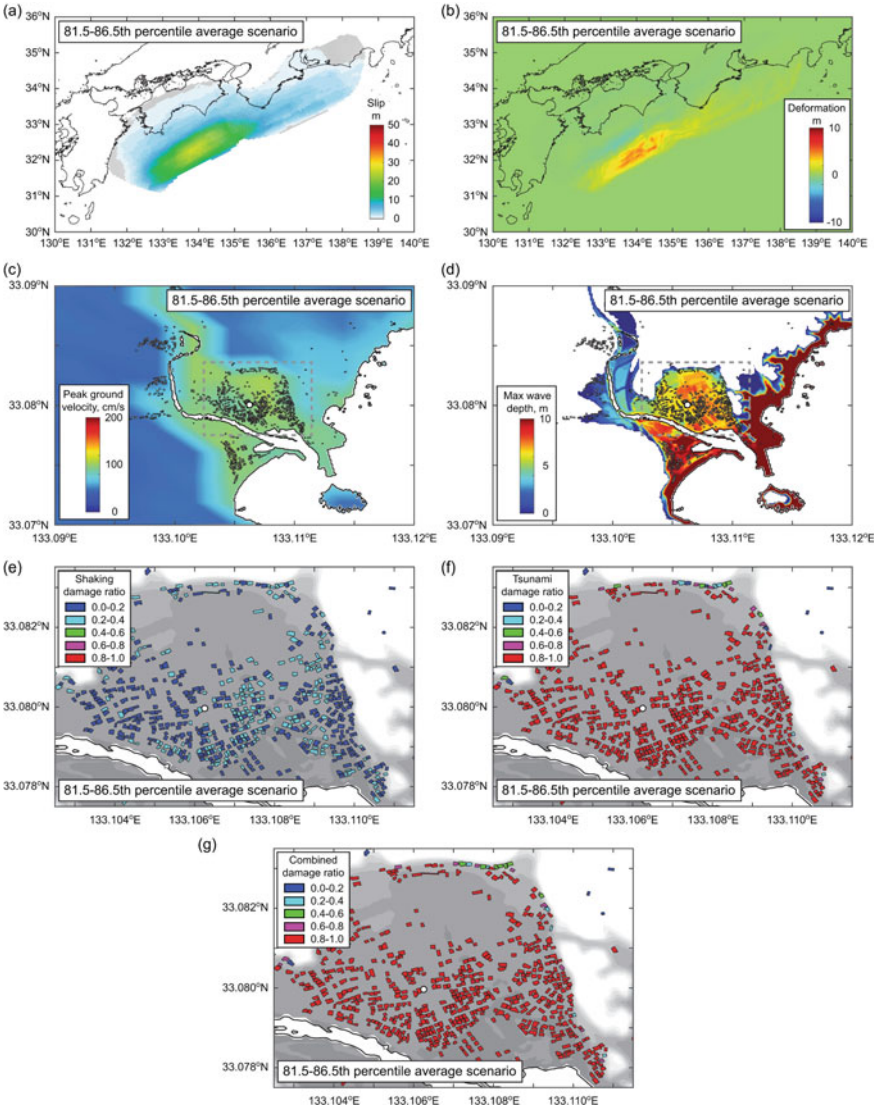


**Fig. 11.9** Average shaking-tsunami hazard-risk maps for the 84th (81.5–86.5th) percentile loss scenarios for the building portfolio in the Saga district. **a** Earthquake source model, **b** initial vertical deformation distribution, **c** peak ground velocity, **d** inundation depth, **e** shaking damage ratio, **f** tsunami damage ratio, and **g** combined damage ratio. The background color map in **e**, **f**, and **g** shows the elevation for the range of 0 m (gray) and 20 m (white) (Color figure online)

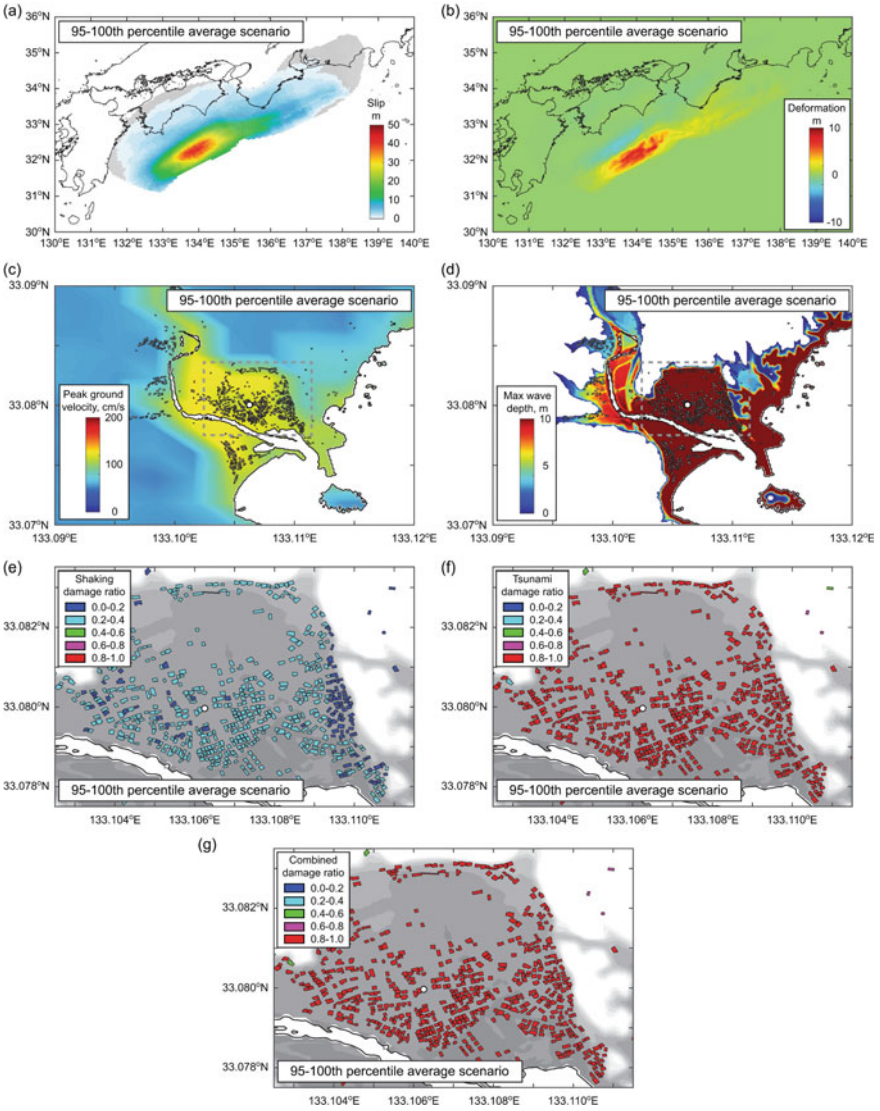


**Fig. 11.10** Average shaking-tsunami hazard-risk maps for the 97.5th (95–100th) percentile loss scenarios for the building portfolio in the Saga district. **a** Earthquake source model, **b** initial vertical deformation distribution, **c** peak ground velocity, **d** inundation depth, **e** shaking damage ratio, **f** tsunami damage ratio, and **g** combined damage ratio. The background color map in **e**, **f**, and **g** shows the elevation for the range of 0 m (gray) and 20 m (white) (Color figure online)

An important observation from all average critical hazard-risk scenario maps shown in Figs. 11.7, 11.8, 11.9, and 11.10 is that notable general trends of the earthquake sources, hazard intensity, and damage severity emerge. For instance, the earthquake source model for the representative 16th percentile loss scenario (Fig. 11.7a) shows a broad slip concentration spanning across the Nankai and Tonankai segments. This broad slip concentration is moved to the Nankai segment off Shikoku Island when the representative 50th percentile loss scenario is considered (Fig. 11.8a). With the increase of the representative loss level, the maximum value of the earthquake slip increases from 15–20 m for the 50th percentile (Fig. 11.8a), to 25–30 m for the 84th percentile (Fig. 11.9a), and to 40 m for the 97.5th percentile (Fig. 11.10a). Similar gradual increases of the initial deformation profile can be observed in Figs. 11.7b, 11.8b, 11.9b, and 11.10b.

The shaking and tsunami hazard intensities tend to increase with the percentile levels of portfolio loss. However, for shaking intensity and damage ratio, the 50th percentile scenario (Fig. 11.8c, e) results in greater hazard and risk values than those for the 84th percentile scenario (Fig. 11.9c, e). This is because, at the 50th percentile loss level (which is approximately US$70 million), the dominant loss contribution is originated from shaking, whereas the 84th percentile loss (which is approximately US$150 million) is mainly contributed by the tsunami. In other words, the significant loss nonlinearity due to tsunami causes different critical multi-hazard loss maps (i.e. Fig. 11.8 vs Fig. 11.9). These features need to be carefully considered in developing critical hazard-risk scenario maps. The hazard dominance depends on the local characteristics in terms of proximity to the earthquake rupture areas, topography, building exposure, and vulnerability, and thus these need to be captured by the multi-hazard risk model properly.

From earthquake-tsunami disaster risk management perspectives, using the average critical hazard-risk scenario maps is effective in conveying the uncertainty associated with the predictions of earthquake-tsunami consequences. It is because scenario-to-scenario variability of the hazard-risk maps can be largely smoothed out. Moreover, it should be emphasized that the average earthquake source models are different from national earthquake source models, such as the 2012 CDMC models [12]. The former has the connections to the multi-hazard loss distribution of the target building portfolio, whereas the latter does not have such linkage. In this regard, the critical earthquake scenarios and related hazard and risk maps are more relevant for disaster risk management purposes and can be utilized for other more advanced analyses, such as earthquake-tsunami evacuation planning.

## 11.5 Conclusions

A new multi-hazard risk model for a coastal building portfolio exposed to the future Nankai-Tonankai mega-thrust subduction earthquake and tsunami was developed. The earthquake-tsunami risk model incorporated the stochastic rupture sources, spatially correlated ground motion fields, tsunami inundation simulations, detailed

building data, seismic and tsunami fragility models, and damage cost estimation. The main results from the developed model were obtained as the multi-hazard and single-hazard loss distributions, accompanied by earthquake rupture scenarios, shaking-tsunami hazard intensity distributions, and building damage distributions.

The case study application of the new earthquake-tsunami risk model is conducted for the Saga district of Kuroshio Town, Kochi Prefecture. This area is one of the most exposed municipalities subject to the Nankai-Tonankai events in south-western Pacific region of Japan. The results highlighted the following conclusions. First, the multi-hazard loss distribution exhibits a large variation in the estimated loss values and thus, it is essential to consider a wide range of possible earthquake rupture scenarios to quantify this uncertainty. In particular, the tsunami loss tends to increase with the magnitude more significantly than the shaking loss and contributes more towards the increase in the multi-hazard total loss with the earthquake magnitude. Second, the multi-hazard risk model can produce useful input data for more advanced earthquake-tsunami engineering analyses, such as joint multi-hazard intensity values (peak ground velocity and maximum tsunami inundation depth) at the vertical evacuation tower in Saga. Third, critical hazard-risk scenario maps can be developed by linking the calculated portfolio loss percentiles with other multi-hazard characteristics, such as earthquake source, hazard intensity footprint, and damage severity. The average-scenario-based critical hazard-risk maps can capture notable general trends of the earthquake sources, hazard intensity, and damage severity that emerge at specified portfolio loss levels and are particularly useful for disaster risk management purposes.

**Acknowledgements** The work was supported by the Leverhulme Trust (RPG-2017-006), the Canada Research Chair program (950-232015), the NSERC Discovery Grant (RGPIN-2019-05898), and the Japan Society for the Promotion of Science Joint Research Project (19039901-000829). The tsunami simulations were performed using Blue Crystal Phase 3, which was supported by the Advanced Computing Research Centre of the University of Bristol.

## References

1. Fraser S, Pomonis A, Raby A, Goda K, Chian SC, Macabuag J, Offord M, Saito K, Sammonds P (2013) Tsunami damage to coastal defences and buildings in the March 11th 2011 Mw9.0 Great East Japan earthquake and tsunami. Bull Earthq Eng 11:205–239
2. Murata S, Imamura F, Katoh K, Kawata Y, Takahashi S, Takayama T (2010) Tsunami—to survive from tsunami. World Scientific, pp 302
3. Marzocchi W, Garcia-Aristizabal A, Gasparini P, Mastellone ML, Di Ruocco A (2012) Basic principles of multi-risk assessment: a case study in Italy. Nat Hazards 62:551–573
4. Mignan A, Wiemer S, Giardini D (2014) The quantification of low-probability–high-consequences events: part I a generic multi-risk approach. Nat Hazards 73:1999–2022
5. Goda K, De Risi R (2018) Multi-hazard loss estimation for shaking and tsunami using stochastic rupture sources. Int J Disaster Risk Reduction 28:539–554
6. Porter KA, Scawthorn CR, Beck JL (2006) Cost-effectiveness of stronger woodframe buildings. Earthq Spectra 22:239–266

7. Yoshikawa H, Goda K (2014) Financial seismic risk analysis of building portfolios. Nat Hazard Rev 15:112–120
8. Attary N, van De Lindt JW, Barbosa AR, Cox DT, Unnikrishnan VU (2019) Performance-based tsunami engineering for risk assessment of structures subjected to multi-hazards: tsunami following earthquake. J Earthq Eng. https://doi.org/10.1080/13632469.2019.1616335
9. Ando M (1975) Source mechanisms and tectonic significance of historical earthquakes along the Nankai Trough, Japan. Tectonophysics 27:119–140
10. Garrett E, Fujiwara O, Garrett P, Heyvaert VMA, Shishikura M, Yokoyama Y, Hubert-Ferrari A, Brückner H, Nakamura A, De Batist M, and the QuakeRecNankai team (2016) A systematic review of geological evidence for Holocene earthquakes and tsunamis along the Nankai-Suruga Trough, Japan. Earth-Sci Rev 159:337–357
11. Fujiwara O, Aoshima A, Irizuki T, Ono E, Obrochta SP, Sampei Y, Sato Y, Takahashi A (2020) Tsunami deposits refine great earthquake rupture extent and recurrence over the past 1300 years along the Nankai and Tokai fault segments of the Nankai Trough, Japan. Quat Sci Rev 227:105999
12. Goda K, Yasuda T, Mori N, Muhammad A, De Risi R, De Luca F (2020) Uncertainty quantification of tsunami inundation in Kuroshio Town, Kochi Prefecture, Japan using the Nankai-Tonankai megathrust rupture scenarios. Nat Hazards Earth Syst Sci 20:3039–3056
13. Yokota Y, Ishikawa T, Watanabe S, Tashiro T, Asada A (2016) Seafloor geodetic constraints on interplate coupling of the Nankai Trough megathrust zone. Nature 534:374–377
14. Tanigawa K, Shishikura M, Fujiwara O, Namegaya Y, Matsumoto D (2018) Mid- to late-Holocene marine inundations inferred from coastal deposits facing the Nankai Trough in Nankoku, Kochi Prefecture, southern Japan. The Holocene 28:867–878
15. Central Disaster Management Council (CDMC) (2012) Working group report on mega-thrust earthquake models for the Nankai Trough, Japan. Cabinet Office of the Japanese Government, Tokyo, http://www.bousai.go.jp/jishin/nankai/nankaitrough_info.html
16. Construction Research Institute (2011) Japan building cost information 2011, Tokyo, Japan, pp 547
17. Goda K, Yasuda T, Mori N, Maruyama T (2016) New scaling relationships of earthquake source parameters for stochastic tsunami simulation. Coast Eng J 58:1650010
18. Mai PM, Beroza GC (2002) A spatial random field model to characterize complexity in earthquake slip. J Geophys Res: Solid Earth 107. https://doi.org/10.1029/2001JB000588
19. Morikawa N, Fujiwara H (2013) A new ground motion prediction equation for Japan applicable up to M9 mega-earthquake. J Disaster Res 8:878–888
20. Goda K, Atkinson GM (2010) Intraevent spatial correlation of ground-motion parameters using SK-net data. Bull Seismol Soc Am 100:3055–3067
21. Goto C, Ogawa Y, Shuto N, Imamura F (1997) Numerical method of tsunami simulation with the leap-frog scheme. IOC Manual, UNESCO, No. 35, Paris, France
22. Midorikawa S, Ito Y, Miura H (2011) Vulnerability functions of buildings based on damage survey data of earthquakes after the 1995 Kobe earthquake. J Japan Assoc Earthq Eng 11:34–47
23. Wu H, Masaki K, Irikura K, Kurahashi S (2016) Empirical fragility curves of buildings in northern Miyagi Prefecture during the 2011 off the Pacific coast of Tohoku earthquake. J Disaster Res 11:1253–1270
24. Yamaguchi N, Yamazaki F (2001) Estimation of strong motion distribution in the 1995 Kobe earthquake based on building damage data. Earthq Eng Struct Dynam 30:787–801
25. Kusaka A, Ishida H, Torisawa K, Doi H, Yamada K (2015) Vulnerability functions in terms of ground motion characteristics for wooden houses evaluated by use of earthquake insurance experience. Architectural Inst Japan J Technol Design 21:527–532
26. De Risi R, Goda K, Yasuda T, Mori N (2017) Is flow velocity important in tsunami empirical fragility modeling? Earth-Sci Rev 166:64–82

# Chapter 12
# Building Resilience in Changing Cryosphere Services


**Bo Su, Xiaoming Wang, Cunde Xiao, Jinglin Zhang, and Bin Ma**

**Abstract** The cryosphere is a portion of the Earth system where water is in solid form, normally found in the polar and high-altitude regions. With the global warming, it experiences a rapid change and the change is accelerating. This would profoundly impact, not only on climate systems, but also its functions to support our societies, known as cryosphere services. To some extent, it is reflected by more extreme events in the cryosphere, and particularly by increasing slow-onset deterioration of the cryosphere service. In response to the impact, there is an urgent need to build resilience into both service suppliers and beneficiaries, ultimately towards the minimization of their vulnerability and underlying risks to the change. It is therefore of great importance to understand the key processes and attributions of the changing services in the cryosphere, and more importantly, to attain the knowledges on building resilience and advancing sustainable development in the cryosphere regions. In this chapter, we briefly introduce the cryosphere change and their impact on the services, as well as risks arising from the hazards in response to global warming. To adapt to the changing services and mitigate risks, we explore the approach to enhance society's resilience in the cryosphere, and illustrate by a case study to manage glacier water resources for sustainable agriculture in the Tarim River Basin.

**Keywords** Resilience · Cryosphere · Climate change · Sustainability · Social-ecological systems

B. Su · C. Xiao
State Key Laboratory of Earth Surface Processes and Resource Ecology, Beijing Normal University, Beijing 100875, China

X. Wang (✉) · J. Zhang
State Key Laboratory of Cryosphere Science, Northwest Institute of Eco-Environmental and Resources, Chinese Academy of Sciences, Lanzhou 730000, China
e-mail: xiaomingwang@lzb.ac.cn

B. Ma
State Key Laboratory of Tibetan Plateau Earth System, Resources and Environment, Institute of Tibetan Plateau Research, Chinese Academy of Sciences, Beijing 100101, China



M. G. Stewart and D. V. Rosowsky (eds.), *Engineering for Extremes*, Springer Tracts in Civil Engineering, https://doi.org/10.1007/978-3-030-85018-0_12

## 12.1 The Cryosphere and Their Services Under Changing Climate

Deriving from the Greek 'kryos', the term 'cryosphere' is collectively considered as a set of the Earth's surface systems where water is in the solid form [1]. In general, the cryosphere is composed of mountain glacier, ice sheet, permafrost and seasonally frozen ground, snow cover, river and lake ice, sea ice, ice shelf, iceberg, and frozen water in the atmosphere [2]. The cryosphere interacts with the lithosphere, hydrosphere, and atmosphere of the Earth system, and exists widely in polar regions and high mountains.

All components of the cryosphere are inherently sensitive to changing climate. Over the last decades, the Greenland and Antarctic ice sheets experienced a rapid mass loss as a result of global warming, and most glaciers continue to retreat globally. The shinkage in the cryosphere is observed not only from the sea ice in the Arctic, but also the spring snow cover in the regions at a low elevation in the northern hemisphere. The permafrost also deteriorated globally and its temperature increased to a record high level (1980s-present) [1]. It is projected that the cyrosphere would likely continue to shrink in the near-term (2031–2050) and beyond as global temperature increases, as indicated in both CMIP5 (Coupled Model Intercomparison Project 5) [3] and CMIP6.

The cryosphere plays a crucial role, not only in global weather and climate systems, but also in ecosystems as well as carbon and water cycles [4]. It exerts the influences by various of its functions, such as the provision of water, cold storage and latent heat exchange, regulation of water vapor and heat, high albedo to reflect solar radiation, low thermal conductivity for insulation, meltwater to affect thermohaline circulation and so on [3, 5]. Considering the functions that are all in a close interaction with other spheres, particularly, the anthroposphere, changes in the cryosphere would affect our societies (Fig. 12.1). On the one hand, it provides a wide array of benefits to human well-being, known as cryospheric services (CS) [6]. The CS can be grouped into five major categories (i.e., provisioning, regulating, cultural, bearing and supporting services) and 17 sub-categories based on the process of different CSs and their relationships with human well-being [4] However, it also produces cryospheric hazards, such as avalanches, glacial lake outburst floods, etc., which could cause serious damages and losses in societies [7, 8].

In response to global warming and consequent cyrosphere retreat, the cryosphere functions and their associated services have been deteriorating and would continue so or eventually disappear. The deterioration or loss of CSs can further create cascading risks in the socio-ecosystems (Fig. 12.2). These are highlighted by the following aspects.

The meltwater would decline once the mass of glaciers drops below a threshold following a warming climate, aggravating water scarcity and further threatening the ecological and food security [10]. The runoffs in the mountainous areas would become more variable and the risk of hydrological extremes (floods/droughts) would then increase [11]. It could also cause water conflicts in transboundary basins.

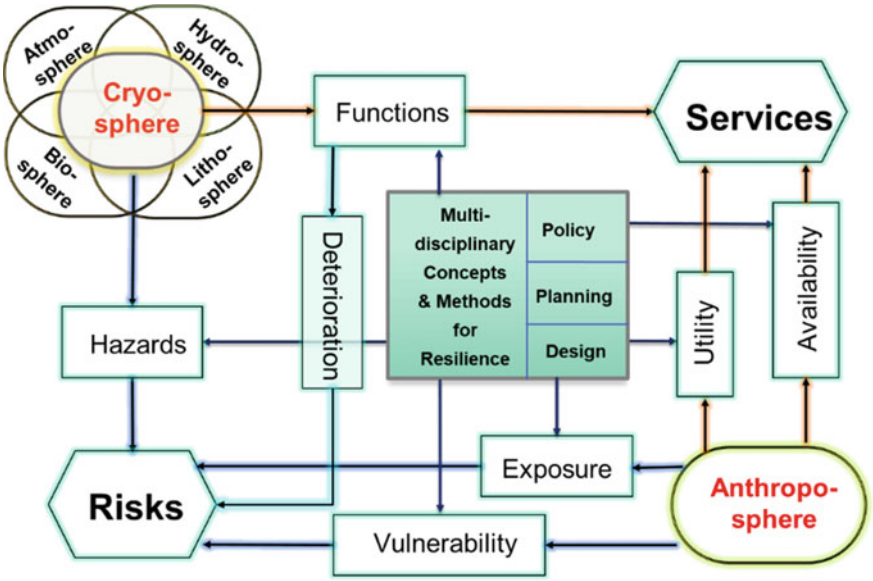


**Fig. 12.1** The relationship between cryosphere and anthroposphere with interaction with other spheres [9] (Color figure online)

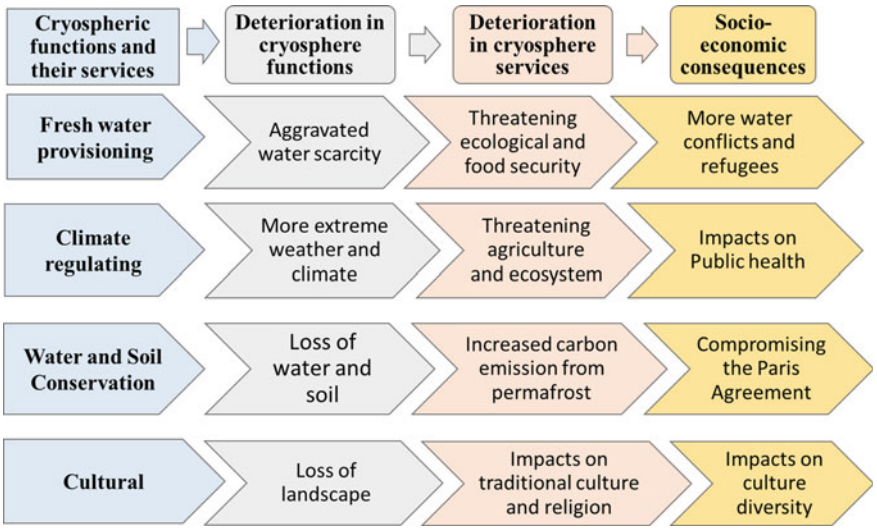


**Fig. 12.2** The cascading consequences resulting from the deterioration of cryospheric functions and their services [9] (Color figure online)

The reduction in the cryosphere and subsequent less cold storage and albedo may also increase the earth surface temperature. The ocean circulation could be impacted by increased melt freshwater and inhibiting sinking of upper ocean waters at the high-latitude [12]. The deterioration of climate regulation function would likely exacerbate climate extremes such as heat and cold waves [13], which inevitably increase the risks of both ecosystem and human health.

The loss of cryosphere changes the landcover that would have protected the earth surface from erosion and conserved water. For example, climate warming causes frozen ground to thaw, permafrost to collapse, and new thermokarst lakes [14]. The change eventually impacts on ecosystem and societies [15]. Meanwhile, the loss of carbon sinks due to permafrost deterioration would further increase the challenges during the implementation of the "Paris Agreement" [16].

The reduction in cryospheric landscapes would also affect the cultural services that support aesthetic, inspirational, tourism, traditional and religion needs. This would likely cause a loss of some unique cryospheric culture and further impact on global cultural diversity [17].

In addition, Climate change-induced instability of the cryosphere could greatly increase the frequency and intensity of cryospheric hazards, in particular, affecting the mountainous area relatively with lower adaptive capacity [3, 7, 8].

## 12.2 Pathways for Resilience Building in the Cryosphere

In response to the changes in cryosphere and their services, there is an urgent need to sustain the resilience in environment and build it into societies, ultimately towards the minimization of their vulnerability and risk to the change. In the IPCC Assessment Report (AR5), the WGII Contribution discusses the concept of climate-resilient pathways, which it defines as "sustainable-development trajectories that combine adaptation and mitigation to reduce climate change and its impacts" [18, 19]. This statement emphasizes on the role of adaptation and mitigation on actions to implement resilience. The essential pathways of developing resilience of our societies to addressing the challenges of cryosphere changes should be included the following option, as shown in Fig. 12.3.

Firstly, global mitigation actions for anthropogenic warming are considered to be the most fundamental approach for the reduction in adverse impacts of cryosphere changes [20, 21]. The IPCC Special Report on global warming of 1.5 °C concluded: "human activities are estimated to have caused approximately 1.0 °C of global warming above pre-industrial levels, with a likely range of 0.8 °C to 1.2 °C; global warming is likely to reach 1.5 °C between 2030 and 2052 if it continues to increase at the current rate" [21]. This would have a significant implication to the cryosphere changes, the functions and services that the cryosphere could offer.

There are urgent needs to implement adaptation to face the changes [17]. It needs a more systematic approach to advance our societies that could inherently capable of, not only absorbing the changes, but also capacity to recover. The strengthening

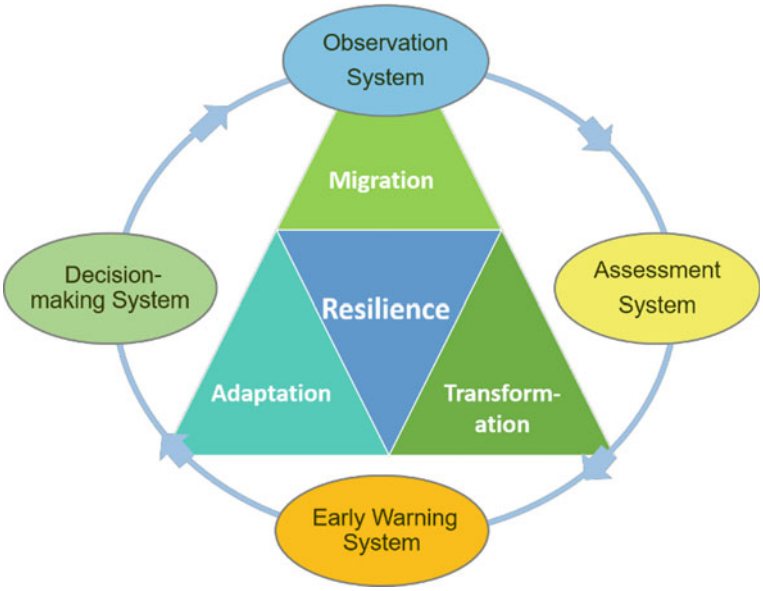


**Fig. 12.3** A general pathway for resilience building in the cryosphere [20] (Color figure online)

of adaptive capacity is indispensable due to the relatively lower socio-economic development and higher vulnerability to hazards in the most cryospheric-affected areas.

Due to the irreversible consequences of many cryospheric changes under the global warming, the transformation in socio-ecosystems may be an important way to cope with the deterioration or loss of cryosphere functions and their services at local, regional, and global scales. Transformation leads to a fundamental change in existing policies, systems, decision-making procedures, human behavior, and even cultural values [22]. To this end, there is an increasing demand for different stakeholders in the cryosphere-affected area (including government departments, scientific research institutions, non-governmental organizations, etc.) to actively have more dialogues and consultations, strengthen social mobilization and improve actions with more focus on the leapfrog in new technology, land use planning, coherent socioeconomic development, and environment conservation.

Finally, robust systems including monitoring, assessing, early warning and decision-making should be established consistently towards more resilient and sustainable pathway [20]. Specifically, the procedure should include: (1) determine the key driving, state and parameter variables of the socio-ecological systems (SESs) in the cryosphere-affected area, diagnose the current status and anticipated future changes of SESs based on positioning and remote sensing observations, model simulations, socioeconomic statistics, field and participatory survey. (2) build the coupled climate-cryosphere-SESs models to understand the system' dynamics and feedbacks, further find the problems and provide more accurate early warning. (3) list and discuss

potential solutions for sustainability of SESs based on the relevant science basis and the participatory dialogue among different stakeholders. (4) evaluate the consequences of implementing the solutions comprehensively, including costs, benefits, and risks so as to make reasonable decision and planning. (5) monitor and assess the system's dynamics continuously, including the implementation progress of existing solutions, and adjust the initial schedule if a better solution occurs.

## 12.3 Building Resilience for the Changing Glacier Meltwater Services in the Tarim River Basin, Northwestern China

Mountain glacier is indispensable supplier of freshwater in broad cold and arid areas of the world. The freshwater resource can be widely used for ecosystem conservation, hydropower, domestic, agricultural, and industrial activities, etc. Moreover, the glacier has a unique regulating function of "peak shaving and valley filling" through the accumulation of large volumes of frozen water during cold or/and humid periods and their ablation during warm seasons or/and droughts. This can maintain the relative stability of river runoff at annual or seasonal scales. In the past several decades, the functions of both provision and regulation have significantly changed with their profound impacts on the streamflow regimes and SESs of downstream areas. In this case study, we take the Tarim River Basin (TRB) as an example, to (1) analyze the changes and uncertainty of glacier meltwater under changing climate; (2) investigate the importance of glacier meltwater in drought impact mitigation in terms of the avoidance of agricultural damage, and (3) explore how to build resilience into societies to response to the changing glacier meltwater services, so as to maximize the utilization of glacier meltwater resources and minimize their vulnerability and risk to the change.

### *12.3.1 Study Area*

The TRB is the biggest inland river basin in China, with an area of $1.02\times10^6$ km$^2$. Located in the central Eurasia and bounded by the Tianshan Mountain in the north, the Kunlun Mountains in the south, the TRB exhibits a unique landscape pattern of mountain-oasis-desert system (Fig. 12.4). The upstream mountainous areas are acted as a water tower, due to their huge water storage and supply roles. It was estimated that the annual mean precipitation in the mountainous areas can reach to 400 mm and the total glacier area is 24,645.4 km$^2$ [23]. The oasis region is characterized as the warm continental arid zone with scarce precipitation and high potential evaporation, where the vast majority of socioeconomic activities concentrate. TRB is one of vital basins for the production of grain and cotton in China, and its development is

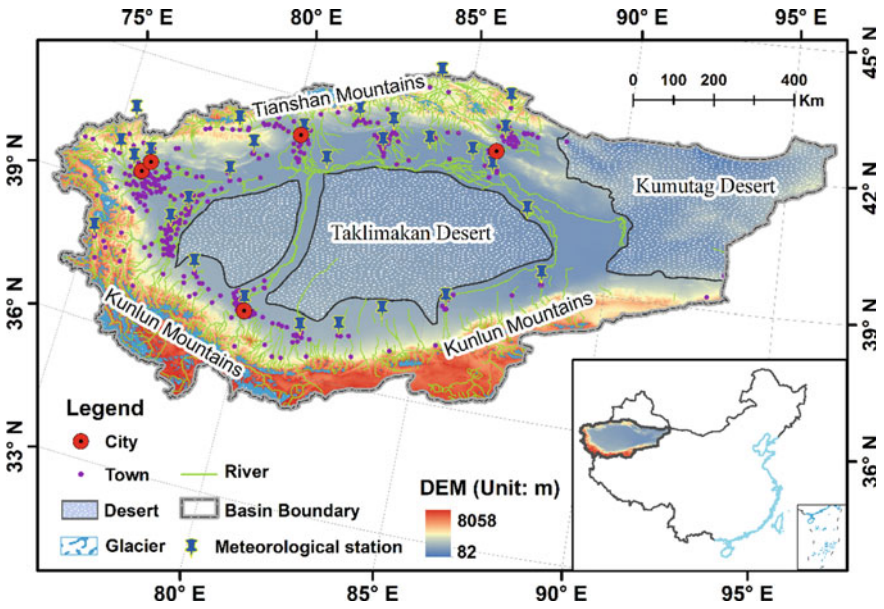


**Fig. 12.4** Study area (Color figure online)

heavily dependent on precipitation and cyrosphere meltwater in high mountains [24]. Deserts and endorheic lakes are often a part of the downstream areas. The second largest desert in the world, i.e., the Taklimakan Desert, is located in the central part of the Tarim river Basin. In addition, the Kumutag Desert is situated in the east.

### *12.3.2 Changes in the Glacier Meltwater Under Changing Climate*

Glacier mass loss and associated changes in runoffs and water resources are a global concern and have received an increasing attention. A wealth of studies has investigated the responses of glacier runoff to climate change and their impacts on streamflow using in-situ observations, model simulations and scenario projections at different scales [4, 10, 11]. The glacier runoff is generally expected to continue to increases for a certain period of time as the climate changes and glaciers mass declines, but after the "peak water", the runoff will then steadily decrease. Continuous in-situ monitoring of glacier mass and runoff changes can provide detailed and accurate information for a deeper understanding of glacio-hydrology. However, only a very few glacier runoffs have been observed due to the inaccessibility of most glacierized areas. With the development of remote sensing and glaciological modelling, the assessment of glacier mass and runoff changes in a larger scale, such

as glacierized mountain ranges, basin, national, and even global scales, gradually becomes possible. Huss and Hock [10] found that about a half of the global large-scale glacierized basins have already passed the water peak and the glacial runoff in the remaining basins would continue to rise in the near future because of their higher glacier coverages, and by 2100, one-third of these basins might experience runoff decreases greater than 10% due to glacial mass loss during at least one month of the melt seasons.

To investigated the past and future changes in glacier meltwater and their uncertainty across the TRB, here we directly adopt the existing simulation data of global glacier runoff changes from 1980 to 2100, which were provided by [10]. They used the Global Glacier Evolution Model (GloGEM) to compute the monthly changes in the glacier mass (including snow accumulation, snow and ice ablation, and refreezing) and associated runoff for each glacier individually in each basin. The GloGEM is driven by a near-surface air temperature and precipitation dataset with a monthly resolution (derived from the ERA-Interim Reanalysis, 1980–2012) for the past. The future changes were projected using 14 Global Circulation Models of the fifth phase of the Coupled Model Intercomparison Project (CMIP5, 2013–2100) and three RCP scenarios (RCP2.6, RCP4.5 and RCP8.5). A more detailed description of the model is given by Huss and Hock [10]. The uncertainties of glacier runoff modelling include: (1) the climate projections, (2) initial ice thickness data; and (3) model parameterization. The uncertainties of climate projections are described by the standard deviations of 14 GCMs. For (2) and (3), the uncertainty is considered as the arithmetic mean of the absolute deviation of each sensitivity experiment from the reference run [10].

The annual glacier runoff across the TRB is projected to rise from 31.8 $km^3$ in the 1980s until the peak water occurred in roughly the 2030s for RCP2.6 and 2050s for RCP4.5 and RCP8.5, followed by steadily decline thereafter. Due to a strong warming and large ice loss, Peak water is generally reached later under a high emission scenario, and the glacier runoff in the water peak is larger than that of high emission scenario (Fig. 12.5). Figure 12.6 presents the evolution of monthly mean glacier runoff across the Tarim river basin from 1980 to 2100 at the decade scale, with the multi-GCM mean and RCP4.5 for the future projection. The results shown that the glacier runoff in the TRB is concentrated in the period from May to September, and the meltwater always peaks in July and August. In addition, the glacier runoff is projected to consistently rise in May and June, and initially increase and then decline in August and September, and glaciers into melting season would generally become earlier.

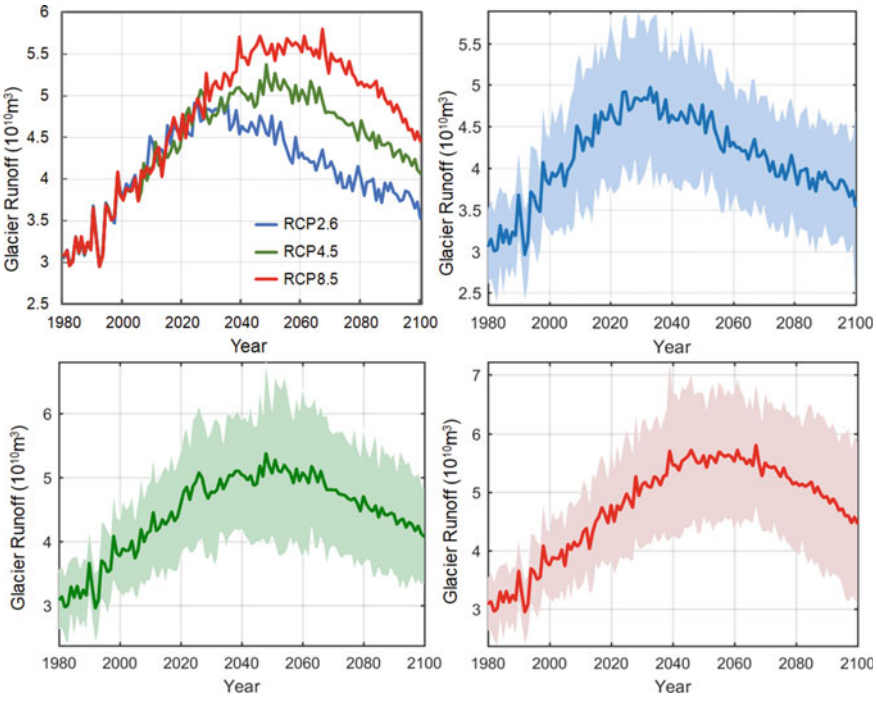


**Fig. 12.5** Time series of modelled annual glacier runoff across the Tarim river basin between 1980 and 2100. The future changes (2013–2100) were projected using 14 Global Circulation Models of the fifth phase of the Coupled Model Intercomparison Project (CMIP5) and three RCP scenarios (RCP2.6, RCP4.5 and RCP8.5). The ensemble mean is the solidline and shadow area refers to the 1 standard deviation of the results from 14 GCMs (Color figure online). *Data source* [10]

### *12.3.3 Importance of Glacier Meltwater to Agricultural Drought Risk Mitigation*

We investigate the climatology and drought characteristics in the TRB (excluding the desert areas) in terms of precipitation and potential evapotranspiration as main indicators based on 23 meteorological stations. Potential evapotranspiration is estimated based on the Penman–Monteith method proposed by [25] using surface temperature, surface net radiation, surface pressure, and surface specific humidity as inputs. The results show that the regionally-averaged annual precipitation and potential evapotranspiration were respectively 93.1 mm and 1196.0 mm during 1961–2017 (Fig. 12.7). The region-wide precipitation exhibited an increasing trend, while potential evapotranspiration decreased during 1961–1996 decreased in 1997–2017. The difference between precipitation and potential evapotranspiration are considered as the aridity index to measure the regional drought. The drought is the most influential hazard in the TRB, and cause serious threats to the regional socio-ecological

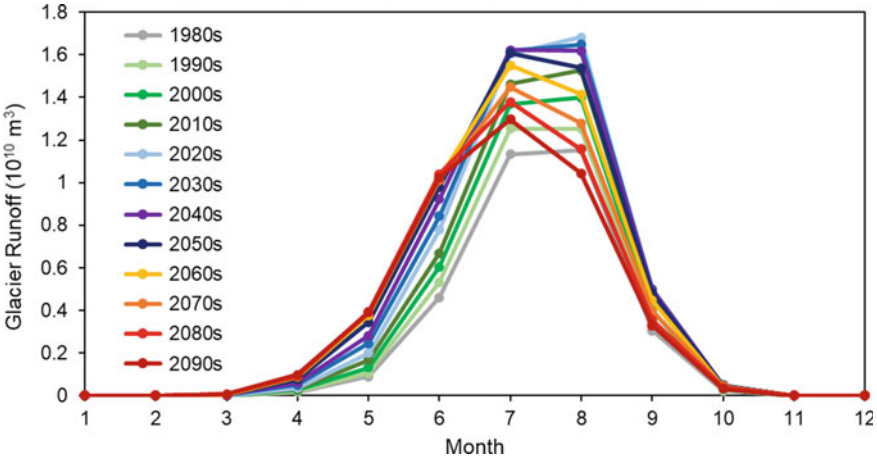


**Fig. 12.6** Modelled monthly mean glacier runoff across the Tarim river basin at the decade scale. The changes during 2013–2100 were projected under the multi-GCM mean and RCP4.5 (Color figure online). *Data source* [10]

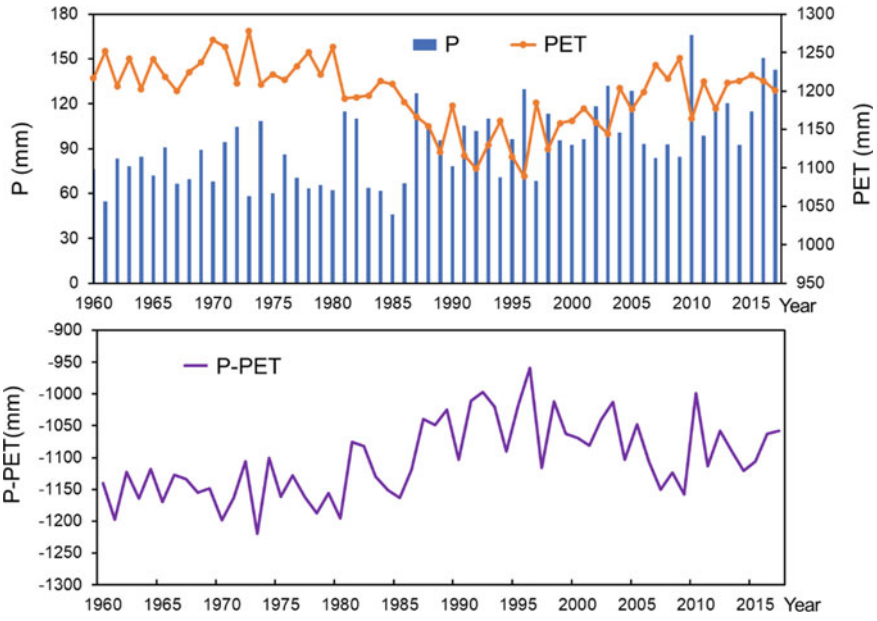


**Fig. 12.7** Region-wide precipitation (P) and potential evapotranspiration (PET) over the Tarim river basin during 1960–2017 (Color figure online)

development. In addition, the aridity exhibited increasing trend during 1961–1996 but decreased trend after 1996.

To estimate the role of glacier meltwater in enhancing drought resilience, we further apply the equivalent precipitation in the aridity calculation,

$$P = P_0 + \frac{G}{A}$$

where $P$ is the equivalent precipitation in the river basin, $P_0$ is the initial total precipitation, $G$ is the total glacier runoff, $A$ is the total affected area. We here consider two scenarios: (1) Scenario A1: the meltwater is averagely distributed to the entire TRB region (excluding the desert areas), i.e., a total area of 680,332.3 km$^2$; (2) Scenario A2: all of the meltwater is averagely distributed to only the entire crop planting area, taking 20,000 km$^2$ here. For Scenario A1, it means that only 3% of the meltwater is used by the agriculture irrigation in the TRB. The actual meltwater utilization rate should be in-between.

Figure 12.8 shows the probability density of aridity (P-PET) with glacial meltwater

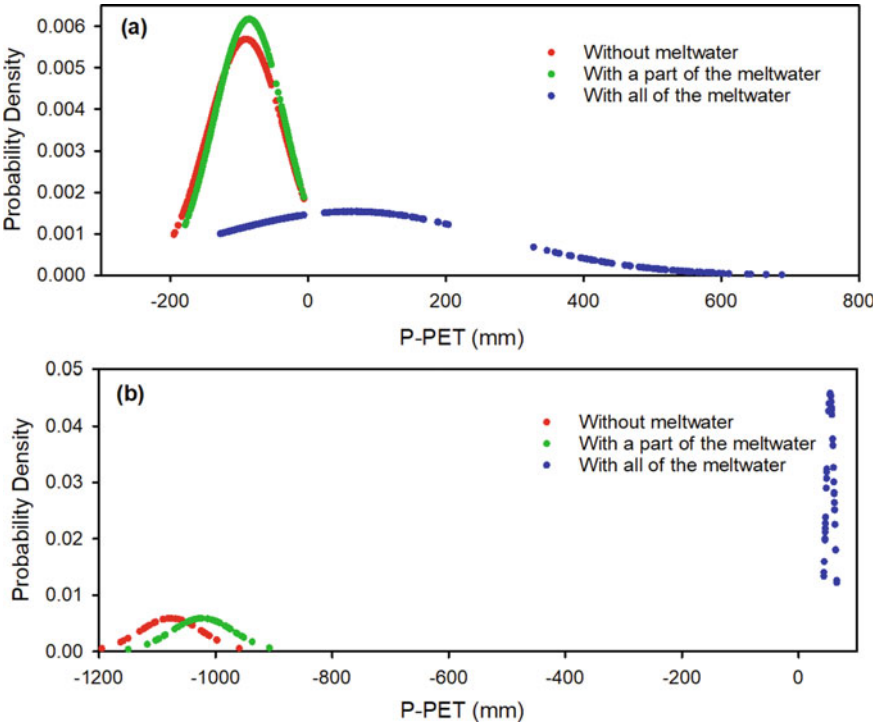


**Fig. 12.8** The probability density of aridity (precipitation minus potential evapotranspiration, P-PET) with all of the glacial meltwater (blue line) and a part of that (green line) as well as without meltwater (red line) in the Tarim river basin at the **a** month and **b** annual scales (Color figure online)

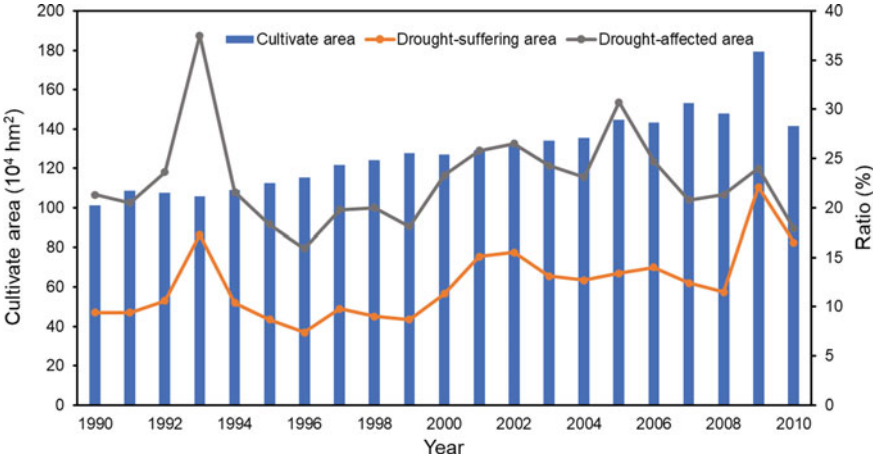


**Fig. 12.9** Region-wide cultivate area and the ratios of drought-affected area and drought-suffering area over the Tarim river basin during 1990–2010 (Color figure online)

(including two scenarios) and without consideration of meltwater in the TRB at (a) monthly and (b) annual scales. The results indicate that the glacial meltwater in the TRB tends to reduce the aridity significantly at both the annual and monthly scales, especially in the extreme drought periods. Furthermore, the agriculture drought can be thoroughly mitigated if all of the glacial meltwater is used for irrigation.

The TRB is one of major basins for the production of grain and cotton in China. As the increasing demand for crops with growing socio-economic development, the irrigation areas have expanded rapidly in the past several decades as shown in the Fig. 12.9. This indicates more and more crops are exposed to the drought. To estimate the agriculture drought risk, we further develop a drought vulnerability curve by taking agriculture loss as a function of drought index based on the available data. As shown in Fig. 12.10, the annual agriculture drought loss has a significant negative correlation with P-PET value in the whole TRB. The agricultural drought risk could therefore be greatly reduced if we could effectively use meltwater, especially in the extreme drought year, such as by developing meltwater storage infrastructure.

### *12.3.4 Resilience Strategies for the Changing Glacier Meltwater Services*

Glacier meltwater is crucial to agricultural drought risk mitigation in arid regions, and the maximization of glacier water resources utilization is therefore poised to be capable of enhancing the drought resilience under the changing glacier meltwater. In this regard, well-planned development and management of reservoirs are likely the most effective approach to mitigate the drought and associated agricultural risk in

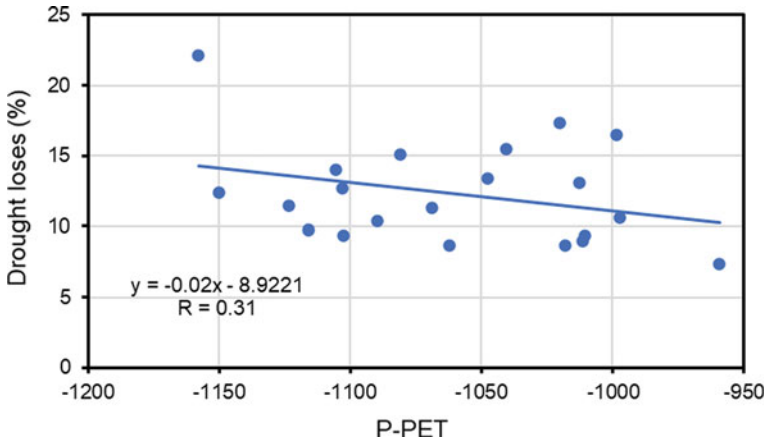


**Fig. 12.10** Drought vulnerability curve (Color figure online)

arid regions. They could also potentially mitigate the risks of hydrological extreme events. In addition, it is necessary to strengthen the monitoring of water resources utilization and improve the water use efficiency. Improvement of crop varieties may also be an effective way to reduce the drought vulnerability.

Having said that, the associated costs and cost-effectiveness of these adaptation measures still to be contested in the future, which should drive the decision-making, i.e., towards the maximization of glacier water resources utilization, the minimization of the risk to the change, and high cost-effectiveness ratio. Two important aspects should be considered as to when the adaptation strategies become economically viable, and where the adaptation measures taken into practice is the best choice [26]. Especially, in the medium term, the increase in glacier runoff can provide opportunities not only for the alleviation of water pressure, but also meet the increasing water needs for the socio-economic development. However, it should be awarded that more profound water shortage risk may emerge once the glacier runoff eventually declines after the peak. This implies that more robust or resilient measures should be taken into account by relevant stakeholders in the future in a long term [27].

## 12.4 Summary

The cryosphere is highly sensitive to changing climate, and its change would further impacts on our societies. In this chapter, we not only illustrate the changing cryosphere, but also demonstrate the changes of the service that our societies benefits from. We explored the pathways to build resilience in the cryosphere to mitigate the risks of changing cryosphere services. It is understood that the resilience building in the cryosphere should take a more integrated approaches in mitigation, adaptation and transformation. More specifically, it is required to establish series of robust

systems including monitoring, assessing, early warning and decision-making, so as to navigate the development in the changimg cryosphere service towards more resilient and sustainable pathway. Finally, by taking a case study of the TRB, we further illustrated: (1) the changes and uncertianty of the glacier meltwater under changing climate, (2) the importance of meltwater in the drought mitigation and agricultural risk reduction, and (3) potential agricuture resilience strategies under the changing glacier meltwater. Our results showed the glacial meltwater in the TRB tends to reduce the aridity significantly, especially in the extreme drought periods. The agricultural drought risk could therefore be greatly reduced if we could effectively use meltwater, such as well-planned development and management of reservoirs. The other petental resilent masures also include the improvement of the meltwater use efficiency and the improvement of crop varieties, etc. However, the robust or resilient decision making should still be considered in the future based on the assessment of the associated costs and cost-effectiveness of these adaptation measures.

## References

1. Climate Change IPCC (2013) The physical science basis; the contribution of working Group I to the fifth assessment report of the intergovernmental panel on climate change. Cambridge University Press, Cambridge, UK, p 2013
2. Qin DH, Ding YJ, Xiao CD et al (2018) Cryospheric science: research framework and disciplinary system. Natl Sci Rev 5(2):255–268
3. IPCC (2019) Special report on the ocean and cryosphere in a changing climate. [2019–09–20]. https://archive.ipcc.ch/srocc/
4. Su B, Xiao C, Chen D et al (2019) Cryosphere services and human well-being. Sustainability 11(16):4365
5. Wang X, Liu SW, Zhang JL (2019) A new look at roles of the cryosphere in sustainable development. Adv Clim Chang Res 10(2):124–131
6. Xiao CD, Wang SJ, Qin DH (2015) A preliminary study of cryosphere service function and value evaluation. Adv Clim Chang Res 6(3–4):181–187
7. Ding YJ, Mu CC, Wu TH et al (2020) Increasing cryospheric hazards in a warming climate. Earth-Sci Rev:103500
8. Wang SJ, Xiao CD (2019) Global cryospheric disaster at high risk areas: Impacts and trend. Chin Sci Bull 64(9):891–901
9. Xiao CD, Su B, Wang XM et al (2019) Cascading risks to the deterioration in cryospheric functions and services. Chin Sci Bull 64(19):1975–1984
10. Huss M, Hock R (2018) Global-scale hydrological response to future glacier mass loss. Nat Clim Chang 8(2):135–140
11. Huss M, Bookhagen B, Huggel C et al (2017) Toward mountains without permanent snow and ice. Earth's Future 5(5):418–435
12. Rahmstorf S, Box JE, Feulner G et al (2015) Exceptional twentieth-century slowdown in Atlantic Ocean overturning circulation. Nat Clim Chang 5(5):475–480
13. Coumou D, Lehmann J, Beckmann J (2015) The weakening summer circulation in the Northern Hemisphere mid-latitudes. Science 348(6232):324–327
14. Niu FJ, Luo J, Lin ZJ et al (2016) Thaw-induced slope failures and stability analyses in permafrost regions of the Qinghai-Tibet Plateau China. Landslides 13(1):55–65
15. Melvin AM, Larsen P, Boehlert B et al (2017) Climate change damages to Alaska public infrastructure and the economics of proactive adaptation. Proc Natl Acad Sci 114(2):E122–E131

16. Schuur E, McGuire A, Schädel C et al (2015) Climate change and the permafrost carbon feedback. Nature 520:171–179. https://doi.org/10.1038/nature14338
17. Arctic Council (2016) Arctic resilience report. Stockholm: Stockholm Environment Institute and Stockholm Resilience Centre
18. IPCC (2014) Climate change 2014: impacts, adaptation, and vulnerability. Cambridge: Cambridge University Press
19. Chen DL, Qin DH, Xiao CD et al (2019) Climate resilience and its implications for China. Climate Change Research 15(2):167–177 (in Chinese)
20. Su B, Xiao CD (2020) Research and practice on socio-ecological systems resilience over cryosphere affected areas: progress and prospects. Climate Change Research 16(5):579–590 (in Chinese)
21. IPCC (2018) Special report on global warming of 1.5°C. UK: Cambridge University Press
22. Folke C, Carpenter S, Walker B et al (2010) Resilience thinking: integrating resilience, adaptability and transformability. Ecol Soc 15(4). https://doi.org/10.5751/ES-03610-150420
23. Ling H, Xu H, Fu J (2013) High-and low-flow variations in annual runoff and their response to climate change in the headstreams of the Tarim River, Xinjiang, China. Hydrological Processes
24. Ruzi M (2013) Tarim river basin drought disaster characteristics and genetic analysis. Xinjiang Agriculture University (In Chinese)
25. Allen RG, Pereira LS, Raes D, Smith M (1998) Crop evapotranspiration—guidelines for computing crop water requirements. In: FAO Irrigation and drainage paper, Vol 56. United Nations Food and Agriculture Organization
26. Stewart MG, Val DV, Bastidas-Arteaga E et al (2014) Climate adaptation engineering and risk-based design and management of infrastructure. Dan M
27. Su B, Xiao C D, Chen D, et al (2021) Mismatch between the population and meltwater changes creates opportunities and risks for global glacier-fed basins. Sci Bull

# Chapter 13
# Extreme Vehicles and Bridge Safety


**Colin Caprani and Mayer Melhem**

**Abstract** Besides natural hazards, one of the leading causes of bridge collapse is overloading. So for bridge owners, making decisions about heavy vehicle access to the road network is one of their main concerns. On one hand, it is imperative that the public be kept safe through low levels of loading, but on the other, the efficiency of the road network and freight increasingly depend on heavier and longer trucks. This problem is particularly acute when considering massive indivisible loads such as transformers and wind turbine nacelles, for example, which can even be socially and politically sensitive. In this chapter, we review the tiered approaches used for making bridge network access decisions; from the use of basic bridge formulae to advanced probabilistic assessment methods. Broader, we briefly touch on the use of reliability assessment as a basis for making decisions on network-level access, and the change in risk profile in aggregate as a result. Of course, increasingly owners are turning towards gaining more data from their assets using Structural Health Monitoring to support decision-making. Therefore we discuss how its benefits as a decision-making support tool can be assessed using the Value of Information framework. Finally, we discuss why the low probability-high consequence problem of heavy vehicle network access is particularly challenging for human decision-makers, by exploring the cognitive biases that can make for sub-optimal decisions. From this, recommendations are given for some strategies to overcome these biases in the context of heavy vehicle bridge access. In summary, this chapter explores the guidelines, technological, theoretical, and psychological factors that make heavy vehicle network access a challenging topic in engineering systems safety.

The original version of this chapter was revised: The errors inadvertently inserted have been corrected. The correction to this chapter is available at
https://doi.org/10.1007/978-3-030-85018-0_23

C. Caprani (✉) · M. Melhem
Monash University, Melbourne, Australia
e-mail: colin.caprani@monash.edu

M. Melhem
e-mail: mayer.melhem@monash.edu



M. G. Stewart and D. V. Rosowsky (eds.), *Engineering for Extremes*, Springer Tracts in Civil Engineering, https://doi.org/10.1007/978-3-030-85018-0_13

## 13.1 Introduction

Bridges are inherently exposed to a wide range of risks. Once constructed, bridges are exposed to environmental degradation, traffic and environmental loading, earthquakes, flooding, fire, impact loads, explosions, and storm surges. Certainly a specific site will have some or other of these as accentuated risks, and others will be inapplicable. Management of the ongoing safety of the constructed bridge stock is a vital role of the asset owner; typically, a state road authority, a local council, or rail line owner. The success of the current management of bridge safety can be empirically evaluated through retrospective analysis of the frequency and cause of bridge failures.

The MRGenCi database [7] includes over 960 structural failures, including 282 bridges. The Imhof database [31] includes data on 382 bridge collapses. Both databases (which include some overlaps in data), conclude that overloading and natural hazards are the leading causes of bridge failures. Other less frequent causes of collapse include design or construction errors, impact, vandalism, and deterioration. Of course, natural hazards is a broad term including, most notably, scour, but also earthquakes and storm surges.

The MRGenCI database is particularly useful as the level of safety achieved by bridges can be seen against that of other structural forms, such as buildings and dams. Indeed, bridges are the safest of civil engineering structures according to this database, with an annual probability of fatality of approximately, $p_f = 1 \times 10^{-8}$. A frequently used measure of safety, the reliability index, $\beta$, rescales this probability using the standard normal distribution as $\beta = -\Phi^{-1}(p_f)$ which in this instance gives $\beta = 5.61$ and this can be compared to a fairly typical annual acceptable level of safety of $\beta = 4.2$ ($\approx 10^{-5}$) (Annex G, ISO 2394 2015). From this it can be ascertained that bridges are performing well, and by extension, that current bridge management practices are adequate. However, the key problem with such a retrospective evaluative approach is it can only be used to predict future performance when the underlying phenomenon is stationary (i.e. no change in the condition of the population of bridges over time).

In most developed countries, a significant proportion of the existing bridges were built in the decades immediately following the Second World War. These bridges are between 50 and 70 years old now, and are certainly at the end of their anticipated lifetime. For example, in Europe over 50% of the continent's 1 million bridges are older than 50 years [58], and in the US around 26% of the ~650,000 bridges are of concern (ASCE Infrastructure Card). While age is not necessarily a direct cause of problems, it is a good predictor of a reduction in capacity. For example, Wang et al. [68] showed that the 22% of bridges with a load limit (i.e. "posted") in Georgia are correlated strongly with age: older bridges are far more likely to be posted.

So although existing bridge management practices have performed well, there is a substantial number of aged bridge structures that render past performance a poor indicator of future needs. Further, as noted, one of the leading causes of bridge risks is overloading, and so this chapter reviews the current approaches to managing bridge overloading risk, and examines the role of policy and structural health monitoring in

adjusting current decision-making practices. Whilst this chapter focuses on highway bridges, many of the discussed points extend to the management of bridges servicing rail, pedestrians, or other forms of traffic.

## 13.2 Bridge Overloading Risks

### *13.2.1 Normal Traffic*

For highway bridges, cars and trucks are clearly the main concern for traffic loading. Truck weight is certainly the most important factor in considering bridge overloading. The weight of cars is not significant, but the role cars play in the spatial distribution of trucks on the road is significant for bridge loading. Truck weight is strongly related to the configuration of the truck: whether two-axle rigid-body, 5-axle articulated, or a tractor-trailer-trailer combination vehicle. The right of access to the road network for a specific vehicle configuration is determined by some access policy rule, which is explained in the next section. Vehicles that can access the entire road network without limitation are often termed General Mass Limit vehicles. Thus, a given road network with given access policy (i.e. truck types and weights) could expect to have some reasonable certainty on the maximum possible amount of load that could be expected on a given length of bridge, given the number of lanes, traffic volume, and traffic composition. Unfortunately, although this computation is feasible, it is not particularly accurate because the main random variable, truck weight, is highly uncertain.

The degree to which trucks are loaded, relative to their legal limit, depends critically on two factors: the economics of running a vehicle fleet and the level of legal enforcement that operators expect. In terms of the economics, operators try as much as possible to limit the number of journeys in which the truck has no payload. Beyond that, there is an incentive to illegally overload the vehicle as operators can then charge a lower price per unit weight for the same journey. Illegal overloading has a number of significant deleterious effects including pavement damage [12], increased environmental impact [54], and reduced road safety [67]. As a consequence, legal weight limits are enforced in most jurisdictions. However, this enforcement is undertaken using a range of means, the most common of which is static weight stations. Of course, once constructed, the locations of these weigh stations are known, and so their effectiveness on the drivers of illegally overloaded vehicles is limited, as long as there are alternative routes available. Other means of effecting enforcement include random roadside inspections using weigh mats, for example.

Disregarding the means of enforcing legal limits, it is the expectation of the level of enforcement that has most effect on the number of illegally overloaded vehicles on a road network. Indeed, both OBrien et al. [50] and Enright [18] consider the histograms of gross-vehicle weight from western and eastern European countries finding that the tails of the distributions are quite different depending on both permits

(Permit Vehicles—see below), and the level of enforcement in the different jurisdictions. In a region with high compliance, less than 1% of vehicles can be expected to be overloaded, whereas in a region with lower compliance this number can be considerably higher. Consequently, for good evaluation of the compliance rate in a region, and hence the true level of bridge loading due to truck traffic, an unbiased source of detailed vehicle data is required. As a result, Weigh-In-Motion (WIM) systems, which are almost undetectable by drivers, and hence yield an unbiased sample, are a key requirement to accurately determine regional highway bridge loading, which in turn aids rational and informed decision-making.

### *13.2.2 Permit Vehicles*

The convenience and economic benefits of road transport has incentivized more frequent larger and heavier vehicles to access the network, with weights and dimensions beyond the General Mass Limits [52]. Furthermore, it is typical for some existing bridges in the road network to have been designed to notional traffic loads that are lower than modern standards and thus cannot accommodate such heavier vehicles. Consequently, heavy vehicle classifications exceeding General Mass Limits are permitted for routine (ongoing) access only for a subset of the road network.

Examples of dedicated routes for the routine access of permit vehicles include the Higher Mass Limit (HML) network in Australia [61], the Blue Route passing through Denmark linking Hamburg, Germany to Malmo, Sweden, and in Mexico [71]. Permit vehicles in these restricted networks are not allowed access to the general road network. Permit vehicle types include higher capacity/long combination freight vehicles, mobile cranes, and oversize/overmass vehicles. Indeed the significance of these forms of vehicles to a region's economy can mean that the bridges on the intended restricted route may be strengthened to meet the permit specification.

The decision to allow a particular vehicle configuration routine access to the restricted network is mostly made in a similar manner to that of the general network as explained later. However, in recent decades there has been an increasing move in some countries towards performance-based standards (PBS) of heavy vehicles, including Canada [65] and Australia [49]. These PBS schemes are not prescriptive in the manner which bridge and road access is assessed, but instead specify outcomes-based requirements. For bridges, this may take the form of a requirement that the proposed vehicle does not cause load effects (e.g. bending moment, shear force) more onerous than those caused by vehicles already on the network. Indeed, the PBS scheme itself can have more nuanced rules for granting access on the basis of bridges, and the Australian PBS scheme has three tiers of verification increasing in sophistication.

In addition to the generic requirements under a performance-based scheme for permit vehicles, some states in Australia have adopted an Intelligent Access Program. In this program, permit vehicles are equipped with an on-board unit that monitors the weight of each axle, and tracks the vehicle movement. This data ensures certainty

in both the load and location of the vehicle. The increased certainty in the bridge loading caused by this vehicle means that the road owner (typically the state road authority) does not need to account for illegal overloading of these vehicle types in assessing bridge safety. The benefit of the scheme to the vehicle operator is increased network access over that which could be offered if safety factors that allow for illegal overloading had to be adopted.

### *13.2.3 Superloads*

Separate to the permit vehicles that can be granted routine access to a special subset of the road network, are those extraordinary vehicles that typically require one-off access on a single route. These vehicles are typically substantial in weight and length (e.g. 600 tonnes, 90 m long), and require special transport logistical arrangements, including road closures, movement of overhead power lines, street furniture, and so on. These vehicles typically carry special bulk indivisible payloads such as generators, transformers, wind turbine nacelles, and smelters. As such, these movements are usually of critical importance to a region's industry and employment, and so may be politically sensitive, adding another layer of consideration for the decision to grant a permit to travel. The societal importance of superload transports, means that road owners will typically move through the full hierarchy of options available to them to consider and justify (or not) the safe access of such vehicles to the bridge on the requested route. Indeed, both bridge strengthening and bridge monitoring can be considered to facilitate the movement of these vehicles, along with restrictions on speed and the presence of other vehicles on the road concurrently.

The risk that superload transports pose to a bridge are difficult to evaluate qualitatively. On one hand it is certain that the axle loads will be significant. For example, platforms of 10 axles may have line loads of 20 tonnes per axle, spread over 8 tyres, spaced about 1.3 m apart and with a width of around 4.8 m. Contrast this with very heavy tri-axle group loads (about 2.4 m transverse width, 1.4 m axle-spacing) of about 30 tonnes for a 5-axle semi trailer in a single lane normal traffic. On the other hand, the axle loads for a superload vehicle are quite well known, and are well controlled during transit, usually including a 5 km/h speed limit during bridge traverses to limit dynamic interaction. Contrast this with the potential for illegal overloading in normal traffic, the potential for multiple very heavy truck presence events on the bridge, and the existence of dynamic interaction at full highway speeds. From this then, it is clear that although heavier, the risks caused by normal traffic, permit traffic, and superloads must all be managed through quantitative structural and risk analysis calculations.

## 13.3 Bridge Access Decision-Making

### *13.3.1 Background*

The capacity of existing highway bridges is most commonly the decisive factor in allowing access for vehicles. Indeed, many transport jurisdictions are confronted with an "ageing bridge stock—increasing road freight" challenge in the management of their bridge networks. Consequently, rational approaches for deciding vehicle access to the network are necessary, which ensures public safety and achieves full bridge utilisation [26].

In this section we review the tiers of analysis that are typically used in making decisions on bridge access for vehicles. These tiers of analysis either focus on the risk to individual bridges (bottom-up) or the entire network (top-down) [52, 66]. Moreover, these tiers of analysis increase in complexity, and therefore the cost of analysis also increases. In turn, this induces another decision: whether it is worth the additional cost of a more complex analysis. However, the lower tiers (bridge formula and line models) are often tasked to the applicant to demonstrate adherence with jurisdictional requirements where access is sought. As such, these decisions tend not to cost the road owner, other than marginal costs associated with increased maintenance costs. Higher tier assessments on the other hand are typically undertaken by the road owner due to specific needs to facilitate a new vehicle configuration or a one-off superload. As these can be politically- or socially-important decisions, they are often borne by the asset owner, though in some cases the costs can be passed on to the direct beneficiary. Regardless of who pays for the analysis, the next tier will usually only be undertaken where it is likely to be beneficial.

### *13.3.2 Bridge Formulae*

Bridge formulae are a convenient practical top-down approach, commonly adopted in many countries as a first-tier in permitting vehicle access [40, 52, 71]. These formulae provide limits on the mass of a vehicle as a function of its length and/or number of axles. They are calibrated so as not to overload the existing bridge structures on the network. For example, in the United States:

$$W = 500(L \times N/(N-1) + 12n + 36) \tag{13.1}$$

where $W$ is the maximum allowable vehicle mass in pounds, $L$ is spacing in feet between the outer axles of any two or more consecutive axles, and $n$ is the number of axles. Interestingly, the Australian bridge formulae for general vehicle access (the GML network) does not consider the number of axles:

$$M = 3L + 12.5 \text{ for } M < 42.5\,\text{t} \tag{13.2}$$

$$M = L + 32.5 \text{ for } 42.5 < M < 50\,\text{t} \tag{13.3}$$

in which $M$ is the maximum allowable mass of the vehicle in tonnes and $L$ is the distance between the first and last axle in meters. As noted previously, the HML network in Australia permits access to vehicle combinations not given GML access, and the corresponding bridge formulae are:

$$M = 3L + 12.5 \text{ for } M < 42.5\,\text{t} \tag{13.4}$$

$$M = 1.5L + 29.5 \text{ for } 42.5 < M < 62.5\,\text{t} \tag{13.5}$$

Bridge formulas are not derived directly from bridge capacities, but are instead based on the notional load models to which the bridges on the relevant network were originally designed. The central idea here is that once the bridges are inspected and maintained in a condition that renders applicable the original bridge capacity, then it is known that (neglecting design or construction errors) the lower bound of that capacity is implied by the envelope of load effects caused by the load model to which it was designed. Since bridge formulas based on this principle are necessarily general, they tend to be governed by the lowest capacity bridges on the network, which most often are the oldest, as load models have tended to increase in weight over time [30]. Further, these formulas do not account for unique vehicle combinations and are examined for a range of common vehicle configurations. Indeed, bridge formulas have been found to be unconservative beyond certain bridge spans [39]. As a result, bridge formulas are becoming seldomly used for permit vehicle network access, being replaced by the PBS schemes noted previously, with explicit calculations of adherence to capacity envelopes, as calculated by simplified line models: the next tier of assessment.

### *13.3.3 Line-Models*

This method of analysis for vehicle access represents the bridge as a one-dimensional line model. Similar to bridge formulae, it is based on the idea that the bridge capacity can (at worst) be implied by the load model to which it was designed (relying on maintenance and inspection to assure its original capacity has not degraded). Representing the width of a single notional lane as a one-dimensional beam model neglects the influence of the transverse distribution of load. However, it is not the absolute values of the load effects that are of interest, but the relative values between the proposed access vehicle and the design load model. And so this assumption is valid, as long as both vehicles occupy the same notional lane width. Where the proposed vehicle is

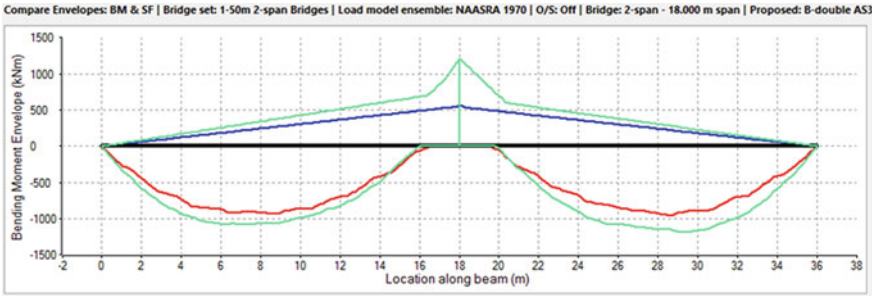


**Fig. 13.1** Comparison of the bending moment envelopes for a continuous 36 m long two-span (18 m) bridge from the design load model (blue and red lines: NAASRA 1970) and a proposed B-double vehicle (green line) (Color figure online)

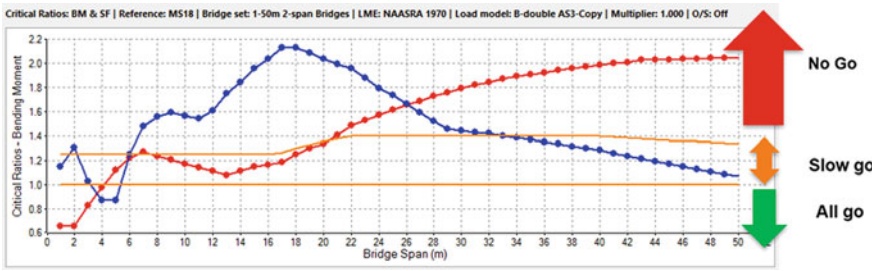


**Fig. 13.2** The ratio of load effects from the proposed-to-design load model for a range of two-span bridge spans, 1–50 m: sagging moment (red), hogging moment (blue) (Color figure online)

wider than a single notional lane, as can happen with special platform transports, a reduction factor to convert the proposed vehicle to an equivalent single-lane vehicle can be used to maintain the equivalency. Finally, although the line model analysis is static, the allowance for dynamic effects can be readily included, and where it is possible to transit the proposed vehicle at walking speed, then the dynamic allowance for the load model can be used to increase the allowable permit vehicle load.

As an example of the use of line models, Fig. 13.1 shows the bending moment envelopes from the design load model and a proposed vehicle for a two-span bridge. In this instance, the proposed vehicle offers a significantly greater hogging moment to the bridge than the design load model. While it is also too big for sagging moments, the difference is not as large. As noted above, it is not the absolute values that are relevant, and so the ratios between the proposed and design load models can be plotted, covering a range of bridge lengths, as shown in Fig. 13.2. In this figure, both the sagging and hogging ratios are shown, and where the ratios are less than unity, access can be permitted (i.e. the proposed vehicle does not offer load effects greater than the capacity implied by the design load model). The region indicated "Slow go" is where the proposed vehicle cannot operate at full highway speed, but by travelling at 5 km/h can utilize the bridge capacity otherwise used by the dynamic

allowance. Nevertheless, beyond this ratio, and regardless of the vehicle speed, the proposed vehicle offers load effects beyond the bridge capacity and so these spans are designated "No go".

In pursuing analysis approaches such as this, there are clearly a number of assumptions in the method, but it can cater for a wide range of bridge configurations, codes of practice from different eras, and arbitrary configurations of proposed vehicles. The method is quick to apply to a large number of existing bridges, and indeed many results can be pre-computed for quick decision-making. Nevertheless, the method is generic, assumes bridges are in pristine condition, and does not consider any bridge-specific attributes. For example, the assumption that a bridge's capacity is precisely the same as that of the load effects induced by its design load model is known to be quite conservative, and so there is a reserve of capacity that this method cannot utilize. Therefore, a more refined bridge-specific approach, based on more usual structural engineering design principles is used for the next tier of access decision-making.

### *13.3.4 Rating Factors*

The capacity of a bridge to carry a proposed vehicle is commonly conducted globally as a means to make decisions on vehicle access to individual bridges in the network [24, 32]. It is based on the basic formulation of a structural engineering safety check:

$$\phi R \geq \gamma S \tag{13.6}$$

where $R$ is the resistance, $\phi$ is the partial factor of safety for resistance, $S$ is the load effect, $\gamma$ is the partial factor of safety for load effect. Expanding this to cover the range of sources of loading, and then re-arranging to express the allowable live load yields the basic Rating Factor (RF) equation:

$$\text{RF} = (\phi R - \gamma S_D)/\gamma S_L \tag{13.7}$$

where $S_L$ is the load effects from a nominated rating vehicles and $S_D$ are other non-traffic sources of loading (e.g. self-weight, temperature effects, creep and shrinkage, etc.). Clearly then when RF < 1 there is insufficient capacity for the proposed traffic loading (e.g. permit vehicle) and a higher tier of analysis may be beneficial.

The Rating Factor approach has many refinements over lower-tier methods. It is a semi-probabilistic method in which the partial factors are calibrated to achieve some predefined target reliability, and it considers the true capacity (even if degraded to some extent) of the bridge components for different limit states (e.g. shear, moment). Furthermore, the bridge deck can be modelled such that the transverse behaviour is considered (e.g. grillage modelling). Due to these refinements, a Rating Factor calculation must be done by a suitably qualified and experienced bridge engineer.

Although the use of Rating Factors is the most prevalent of the higher tiers of assessment, it has some drawbacks. Firstly, in some countries, the partial factors for load and resistance are the same as those adopted in design, and are thus calibrated to a longer design-life than the remaining service life of the existing structure. Secondly, these partial factors are calibrated for the worst case situation across the region and so for the vast majority of cases there is a reserve of capacity that is ignored. Thirdly, it is also common that contemporary design provisions are applied to estimate bridge capacity. Indeed, Bruhwhiler et al. [8] states that the application of design standards to existing structures is "a problematic approach as standards for new structures are in principle not, or only, analogously applicable to existing structures". As a result of these aspects, rating factors give conservative capacity assessments and decisions on bridge network access, thereby not achieving full bridge utilization. Whilst some inputs to the Rating Factor may be made more accurate through higher-tier assessments (detailed in the next section), the decision to allow a new heavy freight vehicle network access can require detailed analysis of many highway bridges, making the use of refined Rating Factor calculations costly. As such, refined rating factors are typically better suited for one-off permit vehicles such as superloads.

### *13.3.5 Higher Tier Assessments*

The standards of many countries including Australia, Canada, Denmark, Switzerland, United Kingdom, and United States allow the use of higher-tier bridge assessment when the rating factor or other conservative assessments conclude bridge capacity is inadequate [42, 69]. Examples include field investigations, advanced analysis methods, and bridge-specific calibration of partial safety factors [38]. Broadly, these higher-tier methods either implicitly or explicitly seek to manage bridge reliability and risk. When the calculation of reliability is explicit, a more descriptive term is probability-based bridge assessment (PBBA).

Field investigations include in-situ material testing, load testing, and structural health monitoring (SHM—discussed later). For concrete structures, testing includes concrete cores and non-destructive tests like the rebound hammer and ultrasonic techniques [38]. Load testing includes both static service or proof loading, or dynamic load response testing. Advanced analysis methods are applicable for accurate estimations of capacity and load effects, potentially refining the conservative rating factor. An example for capacity is the use of modified compression field theory (MCFT) rather than codified design provisions for shear capacity in shear-critical concrete bridge elements [14, 42]. Meanwhile, sophisticated non-linear finite element models may be used to obtain more accurate load effects. In addition, traffic loading data collected from weigh-in-motion (WIM) sites or other sensors near or on a bridge structure can be used directly or in simulations to obtain more realistic estimates of bridge loading conditions [42]. Structural reliability concepts may be used to calibrate partial factors of safety to appropriate target levels of safety for assessment. However, reliability-calibration achieves uniform notional levels of safety across a

jurisdiction or network. Instead, the direct use of structural reliability theory on the highway bridge structures through PBBA is more beneficial, expressing safety as a continuum (O'Connor and Enevoldsen 2007).

PBBA use in the assessments of bridge load ratings has provided significant benefits to bridge asset owners over traditional deterministic (factor of safety) or semi-probabilistic approaches. In one Danish study, the savings ranged from €300 to 1800 k [17]. Another practical example is O'Connor and Enevoldsen [51] who study a 50-year old Danish post-tensioned concrete slab bridge. The bridge was originally deemed inadequate for ultimate limit state hogging moment of the section over the support. However, PBBA showed that the structure was adequate with sufficient load-carrying capacity. Similarly, Wisniewski et al. [70] conducted an assessment for critical sections of bending (mid-span) and shear (1 m from support) for an existing Portuguese simply-supported prestressed concrete girder bridge. Again, the critical sections were deemed inadequate by the traditional approach, but showed to be adequate through PBBA.

There are several published guidelines on PBBA for bridge load capacity assessments. Examples include the Danish Road Directorate [15], COST345 [6], and NCHRP Report 301 [46]. These guidelines present appropriate probabilistic models for the random variables of resistance and loading, discuss structural reliability methods, and stipulate target reliability indices for use in load capacity assessments of existing highway bridges. Nowadays, international bridge standards such as the American, Canadian, Danish, Swiss and British codes have allowed the use of structural reliability theory as a higher-tier assessment of highway bridges [38, 69]. Probability-based bridge assessment is also now entering Australian practice [42].

From the continuum measure of safety that PBBA offers, it is possible to quantify individual bridge risk. Cesare et al. [10], Stewart [63], and Fiorillo and Nassif [20] have demonstrated how risk-based bridge management approaches can be adopted in the assessment of individual highway bridges, and in the decision-making process that follows.

## 13.4 Network Assessments

### *13.4.1 Introduction*

Current practice in whole-of-bridge network assessment focuses on quantifying individual bridge performance, rather than the overall network performance [10, 20, 25, 52]. In practice, these assessments often adopt subjective and qualitative notions of safety and risk using engineering judgment rather than quantitative methods [28, 45]. These approaches fail to recognize that network-wide access decisions (e.g. introduction of a new permit vehicle) have network-wide risk implications. Furthermore, network-wide access decisions should not be made solely using individual bridge risk assessments since there are normally highway bridges of similar era,

materials, and degradation (for example), causing network-wide correlations which strongly influence network-wide risk. Instead, top-down bridge network-level performance assessments should be used for network access policy decision-making, using information from individual bridges.

As the problem of network-wide risk has been recognized over the last decade or so, the performance of a bridge network has been expressed by a variety of probability-based performance indicators [29]. The most common network performance indicators adopted in the literature are bridge network reliability and bridge network risk [21].

### *13.4.2 Reliability as the Performance Indicator*

Following Frangopol and Liu [23], bridge network reliability can be divided into:

- Connectivity reliability: the probability that single or multiple locations in the transportation network remain accessible after bridge failure(s) from a hazard;
- Travel time or capacity reliability: the probability that the network travel time or capacity remains less than a set threshold such as the original travel time or original capacity after the bridge failure(s) from a hazard.

Examples of connectivity reliability include Liu and Frangopol's [41] use of series–parallel system reliability methods, whereas Kang and colleagues use a matrix-based system reliability approach [33, 35]. For large networks, Zuev et al. [77] recommends the use of subset simulation for network reliability problems. For earthquake hazards, Zuev et al. [57] adopted Markov-chain Monte Carlo (MCMC) simulation. However, in these prior approaches the individual bridge failure events from the investigated hazard are assumed to be independent. Indeed, the interconnected nature of highway networks and similarity in attributes between bridges is well recognized to result in correlations in bridge service states across the network [21].

Bridges of the same era, structural form, and design traffic load models will have correlated capacities. Likewise, similarities in traffic across the network give rise to correlated loading. Through a number of studies, Bocchini and Frangopol have illustrated the importance correlation plays on bridge network connectivity and travel time reliability with seismic loading as the network hazard [2–5]. In these studies, two-dimension random fields were adopted to describe the spatial correlation in bridge service states. These correlations are inferred through the correlations in the expected bridge damage states, obtained from individual bridge fragility curves from the computer software HAZUS [3]. In a similar study, Rokneddin and colleagues [27, 56] adopted their previously MCMC methodology [57] but for a correlated bridge network subjected to seismic loading. The correlation in bridge service states is assumed as an agglomeration of three factors, bridge condition ratings, network access level, and degree assortativity. Bridge service states are then simulated from the correlations in the same manner as Bocchini and Frangopol.

Notice, the correlation of bridge service states (failure events) are inferred by some predefined network correlations assumption rather than directly established from the correlations in the random variable that define the bridge failure. The capacity and loading bridge network correlations should be considered in any network-level assessments to provide rational decision-making for any hazard including new heavy vehicle access.

### *13.4.3 Risk as the Performance Indicator*

Expressing the outcomes associated with bridge failure events in economic terms greatly assists decision-making in bridge networks [22]. Previously, vehicle access has been granted through network economic studies, concluding that the benefits of introducing the permit vehicle outweigh the costs to repair or replace the servicing bridges in the network [11, 30, 47]. However, this comparison assumes the necessary bridge funding is available, ignoring the increased risk profile over the entire network under the hazard. As such, risk-based approaches, expressed through economic terms, are a more suitable tool to make informed network access decisions [66].

Although current practice tends to adopt qualitative measures for risk [28, 72], several recent studies have investigated quantifying bridge network risk from a range of hazards including seismic loads [16, 43, 76], structural deterioration, Saydam et al. [59, 75], and overloading [16, 19, 74].

In these earlier studies, the correlations in bridge failure events due to the interconnected nature of the network have not been considered. More recent studies have considered this correlation in the network risk quantification. For most of these works life-cycle assessments are conducted. The risk-based approach allows for the analysis and calibration of importance factors for bridges in the network, assisting in determining the best allocation of funds to prevent such hazards. Indeed, these are demonstrated by Fiorillo and Ghosn [19], Yang and Frangopol [75], Yang and Frangopol [73], and Messore et al. [43].

In general, these bridge network risk studies have different approaches to represent the network topology. Both direct and indirect costs are considered as consequences associated with network disruptions to certain hazards. These consequences are typically established considering the interconnected nature of a bridge network by adopting sophisticated transportation analysis methods. In most previous studies on bridge network risk assessment, these consequences are taken as deterministic values. However, a few studies have recognized the epistemic uncertainties in cost variables [16, 76]. Further, where correlations are considered, they generally have been at the failure event, rather than the individual network variables. Finally, the selected risk metric in previous studies has almost always been the expectation of average risk. For risk-adverse situations, including decision-making of permit vehicle access, alternative measures such the value-at-risk and conditional value-at-risk (also known as the expected shortfall) may be better suited [1, 55]. Indeed, these alternative risk metrics have been used for applications outside bridge networks [53, 62].

## 13.5 Structural Health Monitoring

Structural Health Monitoring (SHM) is nowadays a fairly generic name given to the measurement and evaluation of structural performance, especially for structures that are currently in service. Although the name implies the detection of mal-health, in other words damage to a structure, practical methods of damage detection for field deployment have proved fairly elusive. Nevertheless, the field monitoring of a critical structure can yield much information of great value; most notably allowing the tuning of the associated structural model to properly reflect real-world behaviour, which allows more authentic assessment. Indeed, monitoring can assist bridge owners diagnose changes in bridge performance and condition and reduce the subjectivity of visual inspections. In this section we briefly review some of the SHM technologies that can be used to inform access decisions, and also indicate the means of evaluating the decision to use SHM itself for this purpose, through Value of Information estimation.

### *13.5.1 Monitoring Technologies*

SHM systems are mainly composed of sensors and data acquisition units. Although there are a wide range of sensor types available, practical applications tend to focus on a much smaller subset. Strain measurements are a very useful direct means of determining localized deformations and can be made using traditional means like strain transducers (enclosed full-bridge strain gauges) and strain gauges (e.g. directly on reinforcement), or alternatives such as optical fibre sensors (fibre-bragg grating), or vibrating wire gauges. On the other hand, more global estimates of structural behaviour can be found from measuring bridge vibrations and bridge deflections. Accelerometers give critical information to determine the natural frequencies, damping, and mode shape of bridges, which are directly related to the global mass, stiffness, and energy dissipation in the bridge system [48]. Similarly, displacements such as deflection (linear variable displacement transducers) and rotation (tilt sensor) provide an aggregated measure of the stiffness of the structure. Now while these global measures tend to estimate stiffness and not strength, knowledge of the system stiffness can be used to update the material properties and structural model so that more accurate estimates of the system strength can be made.

An important decision for SHM systems is the connection between the sensor and the data acquisition system. Wired solutions are the traditional means of both supplying power to the sensor and reading the data, and have high bandwidth, sample rate, and usually low signal loss. However, wiring, especially for large structures, can be an onerous and expensive undertaking. Wiring can also be subject to vandalism. Increasingly, wireless options are becoming available to mitigate against the shortcomings of wired systems. However, the provision of power to sensors, sample rates, and data bandwidth remain challenges for wireless systems. The choice between a

wired and wireless system then depends on the desired duration of the monitoring, the ease of access, the required accuracy and sample rates of the data, and the cost of the system itself, and its installation.

### *13.5.2 Value of Information*

Although the choice of which SHM system can be made on the basis of cost and not risk, the decision to utilise a monitoring system on a bridge in the first place should depend on the increased knowledge (and consequent increased confidence) that can be expected, and its impact on the management of the overloading risks to which the bridge is exposed. In other words, the decision to use SHM should be based on the expected value of information to be gained. Further, in determining this value, the change in risk should be included, and both the measurement and system uncertainties should be captured in the analysis.

In recent years, the Value of Information (VoI) statistical decision theory, first developed by Schlaifer and Raiffa [60], has been increasingly applied to the utilization of SHM. This approach is founded on the idea that the value of the SHM system is reflected by the difference in decisions and their outcomes that can be expected with and without the monitoring data. For bridges, the outcomes are ideally measured in monetary terms, based on changes in risk.

The general VoI framework is explained as follows. Consider the prior situation in which a decision must be made in the absence of SHM data. We have some possible decisions available from the set of all decisions, $a \in A$, which can influence (e.g. through permit vehicle access) the uncertain parameters of the system, $\theta$ (e.g. reliability index). We seek the most benefit from these decisions, $b\,(a, \theta)$, typically measured in risk reduction. The best decision is that giving the most benefit on average:

$$a_{\text{opt}} = \arg\max_{a \in A} \mathrm{E}_{\theta}[b(a, \theta)], \tag{13.8}$$

for which the benefit is:

$$B = \mathrm{E}_{\theta}\big[b\big(a_{\text{opt}}, \theta\big)\big]. \tag{13.9}$$

Next we consider the posterior situation if we had new data, $x$. Then we can anticipate updating our knowledge of the system parameters based on this data, $\theta|x$. Now, the best decision, giving the most benefit on average is then:

$$a^{*}_{\text{opt}} = \arg\max_{a \in A} \mathrm{E}_{\theta|x}[b(a, \theta|x)], \tag{13.10}$$

which is not necessarily the same as the optimum decision without the data, and this decision has the associated expected benefit:

$$B^*(x) = \mathrm{E}_{\theta|x}\left[b\left(a^*_{\mathrm{opt}}, \theta|x\right)\right] \tag{13.11}$$

where the functional dependence on the data is made clear. With these two possible benefits the Conditional Value of Information (CVoI), that is, conditional on the data, is then:

$$\mathrm{CVoI}(x) = B^*(x) - B \tag{13.12}$$

which is always non-negative [36]. Of course, the issue now is that before making the decision to install the SHM system and obtain the data, $x$, we cannot determine what the CVoI will be, as the data is uncertain—realizations of the random variable $X$. Hence we conduct a preposterior analysis in which we average over each possible $\mathrm{CVoI}(x)$ given our prior beliefs on what the data may be. This then yields the Expected Value of Information:

$$\mathrm{EVI} = \mathrm{E}_X[\mathrm{CVoI}(x)] = \mathrm{E}_X\left[B^*(x)\right] - B \tag{13.13}$$

Finally, if the cost of the SHM system is $C_{\mathrm{SHM}}$, then the net benefit from the data is EVI–$C_{\mathrm{SHM}}$, which, if positive, gives a net gain warranting the installation of the system.

Khan et al. [34] apply the general VoI framework to consideration of a superload vehicle for which a permit is sought to traverse a bridge. The shear capacity of a pier crosshead is used for illustration. In this widely applicable study for access decision-making, the benefits are taken as reductions in risk, which are evaluated as the probability of an event times its monetary consequences. The probability of breaching several limits states including cracking, yield, and failure of the section are found using structural reliability as the higher tier assessment. Further, the costs considered are the cost of bridge failure, consulting and delay costs (should access not be immediately granted), and the costs of major and minor repairs. The decision space includes options such as:

- Do Nothing, following the Rating Factor evaluation, for which the failure risk is the cost of failure times its probability assuming $\beta = 5.0$.
- Major repair, for when the reliability index at failure is less than the target reliability index, and for which the risks are the cost of analysis, major repair, and the failure risk based on an enhanced strength for which $\beta = 5.4$.
- Minor repair, for when the reliability index is lower than that acceptable for cracking of the section, for which the risks are the cost of analysis, minor repair, and the failure risk using $\beta = 4.3$.

- Do Nothing, following a reliability assessment which indicates an adequate level of safety, for which the risks are the cost of analysis and the failure risk, based on the actual calculated probability of failure.

The results of this analysis conclude that SHM does not offer good value when the decisions are clear, such as when the bridge capacity is clearly adequate, or is clearly inadequate. However, for a wide range in between these extremes, the VoI is shown to be worth up to A$1 million, substantially more than the cost of a monitoring system, rendering SHM a valuable investment in these scenarios.

## 13.6 Discussion and Conclusions

The failure of a bridge is a classical low probability-high consequence (LP-HC) problem in risk management. Unfortunately as we have seen too often in recent years, we appear to be failing to prepare for these disasters [9]. Meyer and Kunreuther [44] examine the causes behind why people fail to prepare for disasters, describing the cognitive biases that can be at play. It is instructive to examine these from the point of view of managing structural risks due to bridge overloading:

- Myopia can mean that the decision-maker's planning horizon does not extend sufficiently far out in time to derive long term value from the necessary present-day investment costs. This is further understandable when competing demands for resources have more immediate and tangible impact, even if of lesser objective value.
- Amnesia means that the lessons and real impact of past disasters are forgotten; not in a factual sense, but in the sense that the natural visceral and emotional impacts dissipate as memories fade. The difficulty here is that we cannot rationalize an emotional response to a hypothetical event, thereby somewhat devaluing it as a human experience (rather than a pure objective monetary decision).
- Optimism leads people, and by extension decision makers and hence countries, to rationalize that although rare events happen elsewhere, they cannot happen 'here' (wherever that may be). This is further exacerbated by the amnesia bias in that the instinctive response to years of disaster-free experience 'here' conflict with the intellectual analysis based on quantified risk: our hopes for the future can override what reason says about it.
- Inertia causes us to maintain the status quo; after all, the established methodologies have worked 'here' for a long time, and so should a disaster occur just as some new decision or way or working was introduced, that decision-maker would be readily blamed (e.g. the precedence set by the jailing of six Italian seismologists following the 2009 L'Aquila earthquake).
- Simplification relates to low probability events and how people discount them entirely once below their threshold for concern. This bias leads people to make complex decisions based on a small number of factors that come most readily to

mind. Indeed, this bias can also mean that concern for the extreme event dissipates when any (even ineffective) measure is taken to mitigate it.
- Herding bias means that people find comfort in the knowledge that others are making the same decisions. While this bias is somewhat apparent in the commonalities across many vehicle access methodologies internationally, it is hard to separate from the agreed science. Nevertheless, in discussing various approaches with decision-makers, successful precedence case studies are highly valued.

Against the biases intrinsic to human decision-makers, Kunreuther [37] proposes a checklist for developing a risk management strategy. While developed for climate-change induced disasters, many of the points are relevant to structural risk:

- Listen to experts: policy-makers should seek the advice of domain experts in determining suitable protective measures.
- Involve stakeholders: industry and government can act as partners in meeting each other's needs for efficient freight transport solutions and safe infrastructure (the Australian Intelligent Access Program is a good example of this).
- Bias awareness: recognize that the LP-HC problem inherently poses difficulties for human decision makers due to the biases listed above.
- Communicate risks: by making the risks relatable and encouraging visceral reaction to potential calamities, some of the intrinsic biases can be overcome.
- Short-term incentives: convert the long-term benefits of protective measures into short term measurable goals.
- Value regulations: communicate to stakeholders and the public the value in terms of avoided losses or damage reduction resulting from strong and enforced regulations.

The lower tier methods of vehicle access decision making are clearly mechanistic, and so less influenced by some of the factors outlined here. However, as described these lower-tier methods are conservative and so the risk is reasonably well managed through their use. In contrast, the biases are clearly significant when we enter the space of higher-tier and specialized assessment methods, for individual bridges, or a network of bridges, especially when coupled with the vast array of SHM solutions on offer. And of course this is the space where the risks are higher. As research has progressed in the last few decades, we have arrived at a previously almost unimaginable range of advanced techniques to quantify structural engineering risk. However, decisions are often eventually made by senior engineers who may not be technical experts in these techniques, but who are skilled at intuitively reflecting the organizational preference on the balance between benefits and risk aversion. In this context, given the substantial technical evidence that can be provided to the senior engineer, researchers and others involved in decision-making support should ask the question: how can we best support this person to make optimal decisions?

## References


1. Artzner P, Delbaen F, Eber J, Heath D (1999) Coherent measures of risk. Math Financ 9:203–228. https://doi.org/10.1111/1467-9965.00068
2. Bocchini P, Frangopol DM (2011) A probabilistic computational framework for bridge network optimal maintenance scheduling. Reliab Eng Syst Saf 96(2):332–349. https://doi.org/10.1016/j.ress.2010.09.001
3. Bocchini P, Frangopol DM (2011) A stochastic computational framework for the joint transportation network fragility analysis and traffic flow distribution under extreme events. Probab Eng Mech 26(2):182–193. https://doi.org/10.1016/j.probengmech.2010.11.007
4. Bocchini P, Frangopol DM (2011) Generalized bridge network performance analysis with correlation and time-variant reliability. Struct Saf 33(2):155–164. https://doi.org/10.1016/j.strusafe.2011.02.002
5. Bocchini P, Frangopol DM (2013) Connectivity-based optimal scheduling for maintenance of bridge networks. J Eng Mech 139(6):760–769. https://doi.org/10.1061/(ASCE)EM.1943-7889.0000271
6. Brady KC, O'Reilly M, Bevc L, Znidaric A, O'Brien EJ, Jordan R (2004) COST 345, procedures required for the assessment of highway structures. European Commission Directorate General Transport and Energy
7. Breysse D, Ndiaye A (2014) Failure case databases related to risk in civil engineering. In: Proceedings of the Institution of Civil Engineers - Forensic Engineering, Vol 167 Issue 1, February 2014, pp 27–37. https://doi.org/10.1680/feng.13.00021
8. Brühwiler E et al (2012) Swiss standards for existing structures. Struct Eng Int 275–280. https://doi.org/10.2749/101686612X13291382991209
9. Caprani C (2018) Genoa bridge collapse a sign of things to come if infrastructure maintenance ignored. https://www.abc.net.au/news/2018-08-17/genoa-bridge-collapse-road-safety-ponte-morandi-west-gate/10131098
10. Cesare M, Santamarina JC, Turkstra CJ, Vanmarcke E (1993) Risk-based bridge management. J Transp Eng 119(5):742–750
11. Christidis P, Leduc G (2009) Introducing mega-trucks: a review for policy makers. Institute for Prospective Technological Studies, Seville
12. Cole DJ, Cebon D (1992) Spatial repeatability of dynamic tyre forces generated by heavy vehicles. J Automobile Eng I Mech E Part D 206:17–27
13. Colin CC, Melhem MM (2020) On the use of MCFT per AS 5100.5 for the assessment of shear capacities of existing structures. Australian J Struct Eng 21(1):53–63. https://doi.org/10.1080/13287982.2019.1664207
14. Collins MP, Bentz EC, Sherwood EG, Xie L (2008) An adequate theory for the shear strength of reinforced concrete structures. Mag Concr Res 60(9):635–650. https://doi.org/10.1680/macr.2008.60.9.635
15. Danish Roads Directorate (2004) Guideline for probability-based assessment of bridges
16. Deco A, Frangopol D (2013) Life-Cycle Risk Assess Spatially Distrib Aging Bridges Seismic Traffic Hazards 29(1):127–153
17. Enevoldsen I (2011) Practical implementation of probability based assessment methods for bridges. Struct Infrastruct Eng 7(7–8):535–549. https://doi.org/10.1080/15732479.2010.496992
18. Enright B (2011) Simulation of traffic loading on highway bridges, PhD Dissertation, University Colelge Dublin, Ireland
19. Fiorillo G, Ghosn M (2019) Risk-based importance factors for bridge networks under highway traffic loads. Struct Infrastruct Eng 15:113–126. https://doi.org/10.1080/15732479.2018.1496119
20. Fiorillo G, Nassif H (2020) Development of a risk assessment module for bridge management systems in New Jersey. Transp Res Rec 2674(9):324–337

21. Frangopol DM, Bocchini P (2012) Bridge network performance, maintenance and optimisation under uncertainty: accomplishments and challenges. Struct Infrastruct Eng 8(4):341–356. https://doi.org/10.1080/15732479.2011.563089
22. Frangopol DM, Dong Y, Sabatino S (2017) Bridge life-cycle performance and cost: analysis, prediction, optimisation and decision-making. Struct Infrastruct Eng 13(10):1239–1257. https://doi.org/10.1080/15732479.2016.1267772
23. Frangopol DM, Liu M (2007) Maintenance and management of civil infrastructure based on condition, safety, optimization, and life-cycle cost. Struct Infrastruct Eng 3(1):29–41. https://doi.org/10.1080/15732470500253164
24. Fu G, Fu C (2006) NCHRP synthesis 359: bridge rating practice and policies for overweight vehicles. Transportation Research Board, Washington, DC.https://doi.org/10.17226/13954
25. Gaynor D, Chin C, McMaster H (2020) Framework and tools for road freight access decisions. Austroads Publications, Sydney
26. Geiger D et al (2005) Transportation asset management in Australia, Canada, England, and New Zealand. Alexandria
27. Ghosh J et al (2014) Seismic reliability assessment of aging highway bridge networks with field instrumentation data and correlated failures, I: methodology. Earthq Spectra 30(2):795–817. https://doi.org/10.1193/040512EQS155M
28. Ghosn M, Fiorillo G, Liu M, Ellingwood BR (2019) Risk-based structural evaluation methods. Am Soc Civil Eng. https://doi.org/10.1061/9780784415474
29. Ghosn M et al (2016) Performance indicators for structural systems and infrastructure networks. J Struct Eng 142(Technical Papers):1–18. https://doi.org/10.1061/(ASCE)ST.1943-541X.0001542
30. Heywood R, Pearson R (1997) Adequacy of Australian bridges. Department of Transport and Regional Development
31. Imhof D (2004) Risk assessment of existing bridge structures. Cambridge, UK: University of Cambridge; PhD thesis
32. Johannessen D, Lake N, Heldt T, Meiklejohn R, Seskis J (2020) ARRB: bridge management best practice guide. Australian Road Research Board
33. Kang WH, Song J, Gardoni P (2008) Matrix-based system reliability method and applications to bridge networks. Reliab Eng Syst Saf 93(11):1584–1593. https://doi.org/10.1016/j.ress.2008.02.011
34. Khan MS, Caprani CC, Ghosh S, Ghosh J (2020) Value of strain-based structural health monitoring as decision support for heavy load access to bridges. Struct Infrastruct Eng. in press, accepted 5 November
35. Kim Y, Kang W-H (2013) Network reliability analysis of complex systems using a non-simulation-based method. Reliab Eng Syst Saf 110:80–88. https://doi.org/10.1016/j.ress.2012.09.012
36. Konakli K, Sudret B, Faber MH (2016) Numerical investigations into the value of information in lifecycle analysis of structural systems. ASCE-ASME J Risk Uncertainty Eng Syst Part A Civil Eng 2(3):B4015007
37. Kunreuther H (2020) Risk management solutions for climate change-induced disasters. Risk Anal 40:2263–2271. https://doi.org/10.1111/risa.13616
38. Lake N et al (2018) Higher order bridge assessment in Australia. Austroads Publication, Sydney
39. Lake N, Johannessen D, Bereni M, Heldt T (2020) Investigation and development of bridge formulae for inclusion in the performance-based standards. Austroads Publications, Sydney
40. Lake N, Seskis J, Ngo H, Kotze R (2014) Review of axle spacing mass schedules and future framework for assessment of heavy vehicle access applications. Austroads Publications, Sydney
41. Liu M, Frangopol DM (2005) Time-dependent bridge network reliability: novel approach. J Struct Eng 131(2):329–337. https://doi.org/10.1061/(ASCE)0733-9445(2005)131:2(329)
42. Melhem MM, Caprani C, Stewart MG, Zhang S (2020) Bridge assessment beyond the AS 5100 deterministic methodology. Austroads Publications, Sydney
43. Messore M, Capacci L, Biondini F (2021) Life-cycle cost-based risk assessment of aging bridge networks. Struct Infrastruct Eng 17(4):515–533

44. Meyer R, Kunreuther H (2017) The ostrich paradox: why we underprepare for disasters. Wharton Press, Philadelphia, PA
45. Milling D, Germanchev A, Ngo H, Noya L, Latter L (2020) Local government heavy vehicle route assessment guidelines. National Asset Centre of Excellence
46. Moses F, Verma D (December 1987) Load capacity evaluation of existing bridges. NCHRP Report 301, NCHRP 12–28(1) Final Report, Transportation Research Board, Washington, DC
47. MTO (1997) Impact of the highway infrastructure of existing and alternative vehicle configurations and weight limits. Ministry of Transportation of Ontario
48. Ngan JW, Caprani CC, Bai Y (2019) Full-field finite element model updating using Zernike moment descriptors for structures exhibiting localized mode shapes. Mech Syst Sig Process 121:373–388. https://doi.org/10.1016/j.ymssp.2018.11.027
49. NHVR (2020) Performance-based standards scheme: the standards and vehicle assessment rules. National Heavy Vehicle Regulator
50. OBrien EJ, Caprani CC, O'Connell G (March, 2006) Bridge assessment loading: a comparison of west and central/east Europe. J Bridge Struct 2(1):25–33
51. O' Connor A, Enevoldsen I (2008) Probability based modelling and assessment of an existing post-tensioned concrete slab bridge. Eng Struct 30(5):1408–1416. https://doi.org/10.1016/j.engstruct.2007.07.023
52. OECD (2011) Moving freight with better trucks: improving safety, productivity and sustainability. OECD Publishing. https://doi.org/10.1787/9789282102961-en
53. Osawa R, Honda R (2021) Quantification of tail risk to evaluate infrastructure maintenance policies considering time-consistency. Struct Infrastruct Eng 17(4):471–480
54. Poulikakos LD, Heutschi K, Arraigada M, Anderegg P, Soltic P (2010) Environmental footprint of road freight: case studies from Switzerland. Transp Res Part A Policy Prac 17:342–348. https://doi.org/10.1016/j.transpol.2010.03.002
55. Rockfellar R, Uryasev S (2002) Conditional value-at-risk for general loss distributions. J Bank Finan 26(7):1443–1471
56. Rokneddin K et al (2014) Seismic reliability assessment of aging highway bridge networks with field instrumentation data and correlated failures, II: application. Earthq Spectra 30(2):819–843. https://doi.org/10.1193/040612EQS160M
57. Rokneddin K, Ghosh J (2013) Bridge retrofit prioritisation for ageing transportation networks subject to seismic hazards. Struct Infrastruct Eng 9(10):1050–1066. https://doi.org/10.1080/15732479.2011.654230
58. SAMARIS (2006) Guideline for the optimal assessment of highway structures, FP6 SAMARIS Project Final Report, Office for Official Publications of the European Communities
59. Saydam D, Bocchini P, Frangopol DM (2013) Time-dependent risk associated with deterioration of highway bridge networks. Eng Struct 54:221–233. https://doi.org/10.1016/j.engstruct.2013.04.009
60. Schlaifer and Raiffa (1961) Applied statistical decision theory. Harvard University, Boston
61. Seskis J, Lake N, Ngo H (2018) Implementation of a nationally consistent framework for the assessment of bridge in Australia. Austroads Publications, Sydney
62. Seyedshohadaie SR, Damnjanovic I, Butenko S (2010) Risk-based maintenance and rehabilitation decisions for transportation infrastructure networks. Transp Res Part A Policy Prac 44(4):236–248
63. Stewart MG (1998) A risk-based approach to the assessment of existing bridges. In: 19th ARRB transport research conference, Sydney
64. Sun Y, Carmichael DG (2018) Uncertainties related to financial variables within infrastructure life cycle costing: a literature review. Struct Infrastruct Eng 14:1233–1243. https://doi.org/10.1080/15732479.2017.1418008
65. TAC (1994) Impacts of Canada's heavy vehicle weights and dimensions research and interprovincial agreement. Transport Association of Canada, Ottawa
66. TRB (2019) Transportation research board special report 328: research to support evaluation of truck size and weight regulations. The National Academies Press, Washington, DC.https://doi.org/10.17226/25321

67. VC-COMPAT (2006) Improvement of vehicle crash compatibility through the development of crash test procedures, EU sixth framework project, public deliverables. Available at http://vc-compat.rtdproject.net/
68. Wang N, O'Malley C, Ellingwood B, Zureick A (2011) Bridge rating using system reliability assessment. I: assessment and verification by load testing. J Bridge Eng 16:854–862, Special Issue: AASHTO-LRFD Bridge Design and Guide Specifications: Recent, Ongoing, and Future Refinements
69. Wisniewski DF, Cruz PJ, Henriques AAR, Simoes RA (2012) Probabilistic models for mechanical properties of concrete, reinforcing steel and pre-stressing steel. Struct Infrastruct Eng 8:111–123
70. Wisniewski D, et al (2009) Probability-based assessment of existing concrete bridges-stochastic resistance models and applications. Struct Eng Int: J Int Assoc Bridge Struct Eng (IABSE) 19(2):203–210. https://doi.org/10.2749/101686609788220268
71. Woodrooffe J, Middleton D, Villa J, Terra MS (2011) NCHRP research results digest 362: review of mexican experience with the regulation of large commercial motor vehicles. Transportation Research Board, Washington, DC.https://doi.org/10.17226/14677
72. Wright BP, Tl SP (2021) Engineering guideline to bridge asset management. Austroads Publication, Sydney
73. Yang DY, Frangopol DM (2018) Risk-informed bridge ranking at project and network levels. J Infrastruct Syst 24(3):04018018
74. Yang DY, Frangopol DM (2019) Societal risk assessment of transportation networks under uncertainties due to climate change and population growth. Struct Saf 78:33–47. https://doi.org/10.1016/j.strusafe.2018.12.005
75. Yang DY, Frangopol DM (2020) Life-cycle management of deteriorating bridge networks with network-level risk bounds and system reliability analysis. Struct Saf 83:101911. https://doi.org/10.1016/j.strusafe.2019.101911
76. Yazdi-Samadi MR, Mahsuli M (2020) Time-variant seismic risk analysis of transportation networks considering economic and socioeconomic impacts. J Earthquake Eng 24:745–773. https://doi.org/10.1080/13632469.2018.1453401
77. Zuev KM, Wu S, Beck JL (2015) General network reliability problem and its efficient solution by Subset Simulation. Probab Eng Mech 40:25–35. https://doi.org/10.1016/j.probengmech.2015.02.002

# Chapter 14
# Fire Safety in Road Tunnels


**T. D. Gerard Canisius, Dimitris Diamantidis, and Suresh Kumar**

**Abstract** Modern industrial societies need efficient and safe transportation systems for their existence and progress. Tunnels form an important component of road transportation systems in many countries. However, significant fire incidents within them have highlighted human safety as a major concern, resulting in considerable changes to the safety requirements to be satisfied during the design and assessment of new and existing tunnels, respectively. This chapter discusses state-of-practice related to the implementation of risk analysis methods in road tunnel projects. It reviews relevant safety criteria in standards and describes basic aspects on risk acceptance and decision-making with respect to the choice of the safety measures to be implemented. This contribution presents the determination of human safety consequences for use in risk analysis by considering design fires, the development and spread of effects of such fires and emergency evacuation of people. The methodology is illustrated via a case study that deals with the re-qualification of an existing road tunnel in Wales.

## 14.1 Introduction

The worldwide road network has grown steadily over the last century due to the increase of traffic volumes. There are many tunnels longer than 10 km. The longest road tunnel worldwide is currently the Laerdal Tunnel in Norway; with bidirectional traffic and a total length of 24.5 km.

Life safety is a major issue in the design of a new tunnel and in the assessment of an existing tunnel, especially for those with a considerable length (e.g. greater

T. D. Gerard Canisius (✉)
Fire and Structural Safety Risk Consultant, Canisius Ltd, Watford, UK
e-mail: gerard@canisius.co.uk

D. Diamantidis
Professor, Faculty of Civil Engineering, Ostbayerische Technische Hochschule Regensburg, Regensburg, Germany

S. Kumar
Fire Safety Consultant, London, UK



M. G. Stewart and D. V. Rosowsky (eds.), *Engineering for Extremes*, Springer Tracts in Civil Engineering, https://doi.org/10.1007/978-3-030-85018-0_14

than 1500 m). Past incidents such as the fire in the Mont-Blanc Tunnel in France, the accident in the Tauern Tunnel in Austria and the fire in the Gotthard Tunnel in Switzerland have led to significant changes in safety requirements in applicable regulations and standards.

The difference between safety in a tunnel and an open road is related to the rarity of intersections, the smaller influence from climatic conditions such as fog, rain, ice, or snow, the more difficult conditions for rescue and clearance in the tunnel and the potentially more severe consequences of fire incidents due to the significantly confined environment. Some important factors influencing tunnel safety in general are for example traffic type and volume, tunnel configuration, dimensions and alignment.

Additional factors affect fire safety within a tunnel: for example the fire safety measures provided within it, including means of escape, detection and warning systems, fire and smoke control measures and facilities for emergency services personnel. Also the tunnel lining material, the shape and dimensions of the tunnel cross section, the exposure of portals to high winds, air/smoke flow through cross passages in twin-bore tunnels and the altitude of the tunnel are important factors.

The scope of this contribution is to illustrate how risk and decision-making methodologies can be applied to fire safety in road tunnels. Safety criteria in standards and regulations are reviewed in Sect. 14.2. The analysis of the human consequences in case of a tunnel fire are presented in Sect. 14.3. A case study dealing with the re-qualification of an existing road tunnel in Wales is discussed in Sect. 14.4. Concluding remarks are provided in Sect. 14.5.

## 14.2 Safety Criteria in Regulations and Standards

### *14.2.1 General*

As mentioned above, incidents involving fire can lead to significant life safety consequences. Fires in tunnels have been discussed in various publications (e.g. [2, 11, 18, 29]) and have been considered in the development of the standards, guidelines and recommendations (e.g. [8, 19, 24–26]).

Owing to the issues described in the previous section, there has been considerable activities to improve tunnel safety, including:

- The development of tunnel fire safety standards such as that of the UK [3];
- The development of risk-informed methods and associated computation tools (e.g. [16, 21])
- Research projects related to tunnel safety, especially with respect to the fire hazard (e.g. [10, 29]); and
- The development of a European regulation in terms of EU Directive [8] on the minimum requirements for tunnels longer than 500 m on the Trans European

Road Network and their local implementations such as the Road Tunnel Safety Regulations [25] of the UK.

### *14.2.2 Prescriptive Versus Risk-Informed Approach*

Two approaches to tunnel safety can be distinguished as summarised below.

(a) **prescriptive approach**
The traditional approach to design of the built environment is based on prescriptive standards. They usually are developed over many years and represent a rich seam of knowledge. In a prescriptive approach a tunnel is considered sufficiently safe if it is designed in line with the standards; which means that the tunnel and its safety devices fulfil the minimum requirements given in the regulations. The standards specify particular safety features, actions etc. to be implemented. Such minimum requirements were provided, for example, in British Guidance of 1999 [3], European Directive [8] and German Standard [24].

The safety checks in this approach can be performed based on the code requirements, with tunnels classified on the basis of their configuration and length, traffic volume and direction(s) and type of goods allowed. For each category a set of safety measures is recommended; with their technical specifications also provided in some standards. This approach is simple but not fully transparent since the fire risk in the tunnel is not determined. The prescriptive methods encompass tunnel safety management during maintenance periods when, for example, traffic can be restricted and potentially on contraflow.

(b) **risk-informed approach**
Risk-informed approaches to the design and assessment of structures and infrastructures have been in use since the 1970s, starting with the nuclear industry. Such methods were later applied to assess risks in both new and existing tunnels. In this approach a tunnel is considered sufficiently safe if predefined risk acceptance criteria are satisfied (e.g. [6, 16, 20]).

The application of a risk analysis requires appropriate methods and tools and input data on accident frequencies and consequences. The analysis allows a structured, harmonised and transparent risk assessment also in the case of fire. The approach can be used for the comparison of alternative tunnel solutions, hence also to demonstrate the safety of a tunnel in case of its deviation from prescribed requirements, and for the cost-optimal selection of safety measures.

Generally, the risk-informed approach includes hazard identification, risk analysis and risk evaluation (risk appraisal) and risk mitigation. It requires users to posses specific knowledge related to the safety hazards, risk analysis methods and tools and many input data for which in some cases only limited information may be available. Typical examples of the last item are branch probabilities in the development of an

accident, effectiveness (risk reduction) of modern safety measures, development of fires and consequences in case of fire in a partially confined environment, effects of applied active safety measures and behaviour of users in emergency situations. Therefore, it appears necessary to consider uncertainties in risk analyses by using appropriate statistical models and/or by performing sensitivity analyses. EU Directive [8] recommends the use of risk analyses where necessary and the World Road Association [21] provides tools for such purposes (also see [17]).

Risk analyses for tunnels have been performed for road tunnels in the last decade and results are reflected in the literature [e.g. 13, 27, 31], and in unpublished studies not available to the wider community. The studies deal with different types of tunnels and with different hazards. Since fires in tunnels are particularly hazardous to life due to the potential concentration of smoke and heat radiation, the human risk for a group of persons (societal risk) is thereby applied as the main criterion. For this, different fire sizes are considered, e.g. from fire in a passenger car, a bus, a heavy goods vehicle (HGV) with combustible goods and even a petrol tanker, in order to assess the risk. Risk analysis procedures and associated tools have been analytically described by the World Road Association [21–23].

### *14.2.3 European Directive 2004/54/EC*

The European Directive 2004/54/EC [8] is a current major legislative text that sets a minimum fire safety level for road tunnels in the Trans-European Road Network. Utilising results of recent investigations, it specifies safety measures based on a classification of tunnels according to their.

1. annual average daily traffic (AADT) volume given in terms of vehicles per lane:
   (a) $\leq$2000 vehicles per lane
   (b) >2000 vehicles per lane; and
2. length:
   (a1) 500–1000 m and (a2) >1000 m for traffic volume of case (a)
   (a2) 500–1000 m, (b2) 1000–3000 m and (b3) >3000 m for traffic volume of case (b).

On this basis different fire safety measures such as emergency walkways, distance between emergency exits, fire resistance of structures, natural and mechanical ventilation, firefighting water supply, monitoring systems etc. are specified as minimum requirements for each tunnel class. Where the prescribed requirements cannot be satisfied or where it is desired to achieve a more economical facility, a fire risk assessment can be carried out to asses and demonstrate sufficient safety. The latter is undertaken when, for example, specified requirements can be achieved only at a disproportionately high cost and it is necessary to examine and demonstrate the suitability of more economical alternative risk reduction measures. The assessment

of risk and the evaluation of possible safety measures should be accomplished based on quantitative acceptance criteria.

Neither specific risk analysis methods nor quantitative risk acceptance criteria are described in the EU Directive. Hence, the member states of the European Union shall ensure that, at national level, a detailed and well-defined methodology, corresponding to the best available practices is used. The risk analyses shall be carried out by a body which is functionally independent from the tunnel manager, i.e. from the public or private body responsible for the management of the tunnel.

### *14.2.4 Human Risk Criteria*

The calculated risk needs to be compared to well defined risk tolerability criteria. Although there are no universally accepted risk criteria for road tunnels, there are established criteria in use in some countries for specific applications [22].

In case of fire risk in tunnels, the potential harm to people (fatalities and/or injuries) is a risk with two important points of view [5, 14, 22]:

- The point of view of the individual who decides to undertake an activity, weighing the direct and indirect personal costs against benefits (*individual risk*).
- The point of view of the society, which considers whether an activity is acceptable in terms of the cost–benefit trade-off for the affected population (*societal risk*).

In case of societal risk, two types of criteria are applied to tunnel fire safety [22]: (a) the expected value (EV) and (b) the frequency versus number of fatalities (F-N) curves. Both these criteria are briefly described below.

(a) **Expected value (EV) or risk value**
A simple measure of societal risk is the risk value or expected value EV i.e. the expected value of all consequences caused by considered accidental events. It is the long-term average number of statistically expected fatalities per year for a tunnel. For the particular event of a fire, it is equal to the sum of the expected consequences of $n$ different fire hazard scenarios $i$:

$$EV = \sum_{1}^{n} (p_i C_i) \tag{14.1}$$

where $p_i$ is the probability of a specific fire hazard scenario and $C_i$ are the associated human consequences (fatalities, injuries or weighted fatalities by representing a particular type of injury as equivalent to a fraction of a fatality). [Note: The probability of hazard scenarios can be obtained using Bayesian methods, Apostolakis [1]]. Expressing risk in terms of the $EV$ has the advantage of allowing the total risk of the tunnel to be expressed as a single number which treats all consequences, i.e. fatalities, as equally important irrespective of the number of lives that maybe lost simultaneously in a major accident such as

fire [21]. The application of absolute criteria is simple, but the determination of thresholds as a basis for decision making is not straightforward. In some countries a limit value for EV of $10^{-3}$ fatalities per year is recommended for the transportation of dangerous goods [22]. In many cases relative criteria are used by comparing results of the investigated tunnel to the results based on the same methodology for a reference tunnel that complies with all requirements of the guidelines. The result of the comparison of two singular values is clear and easy to interpret and communicate.

(b) **Frequency versus number of fatalities (F-N) curves**
In this criterion graphical information is provided by relating the number of fatalities $N$ and the frequency of accidents $F$ with more than $N$ fatalities (see, for example, [5, 12, 15, 22, 32]). The cumulative frequency $F$ is commonly compared with a target value $F_t$ [5, 28]. Thus the risk criterion may be expressed as an inequality:

$$F \leq F_t = AN^{-k} \tag{14.2}$$

The criterion of societal risk is usually shown in a graph with logarithmic scale for both the number $N$ (within the interval from 1 to 1000) on horizontal axis and the cumulative frequency $F$ on the vertical axis (within the interval from $10^{-8}$ to 1). Then the frequency curve is represented by a straight line having the slope $-k$ ($k$ is commonly given by the values within the interval from 1 to 2 [5, 28]. The parameter $A$ reflects the intercept of the line (on the vertical axis). Example bounds for tunnel human risk in the F-N space are provided in [12]. Based on the $F$-$N$ curves, the so-called ALARP—as low as reasonably practicable—region can be defined by implementing two limits (i.e. lines) [5]. The area above the upper limit represents conditions not tolerable under any circumstance, while the safety region below the lower limit is considered sufficiently safe and, thus, of no practical interest. In the domain between upper and lower bound, various extra safety measures are to be considered and selected to provide a set of available options for risk treatment. The selected risk treatment will be so as to optimise the expected utility that has to be achieved, as shown in the next Sect. 14.2.5.

Acceptability curves such as the above have been also developed and applied in various industrial fields, including the chemical and the transportation industries. It is to be noted that $F$-$N$ risk acceptance criteria can be obtained also from $F$-$N$ curves calculated for a compliant tunnel that can be considered as a reference tunnel.

### *14.2.5 Decision Criteria*

Total safety related costs can be optimised via a cost–benefit approach which either is constrained by limits on human consequences given in regulations or, where it is not considered unethical, incorporates a valuing of human life in the optimisation. Once

the optimum solution is obtained, risk treatment is implemented through appropriate prevention and mitigation measures.

In a cost–benefit analysis for human consequences, for each possible safety measure *i*, the related costs are considered. In the first step all costs are related to the decision point using the net present value method. This implies that either the net present value or the net value at the time of the optimisation is calculated. If an interest rate $\gamma$ and an inflation rate $\delta$ are considered, the annuity factors $A$ and $T$ can be derived. Then the cost–benefit information for each individual safety measure can be evaluated based on the utility reflected in the risk reduction due to the safety measure *i* and using the following inequality:

$$A(n, \gamma, \delta)C_{Ii} + T(n, \gamma, \delta)C_{Mi} < SWTP\Delta R_{Hi} \tag{14.3}$$

where:

| | |
|---|---|
| $C_{Ii}$ | investment costs for the safety measure i |
| $C_{Mi}$ | annual maintenance/operation costs for the safety measure i<br>[Note: The use of an annual maintenance cost here is a simplification as a safety measure is likely to require more involved additional maintenance activities over longer intervals during its service life]. |
| $n$ | service life in years of the potential safety measure including the effect of obsolescence |
| $\Delta R_{Hi}$ | reduction related to human risk in terms of weighted fatalities |
| $SWTP$ | societal willingness to pay (to save a human life, see for example [14]). |

## 14.3 Consequence Analysis Methods

### *14.3.1 General*

The following description is limited to the determination of human safety risks as a direct effect of flames, heat and smoke within a tunnel and does not consider risks due to structural failure and traffic disruption.

The usual analysis methods and related computer modelling to assess tunnel fire safety risk has three stages:

- Modelling of the fire and smoke conditions within the tunnel, usually using computer-based methods such as Computational Fluid Dynamics (CFD);
- Modelling of evacuation during a fire emergency; and
- Determination of potential casualty numbers.

### *14.3.2 Fire Propagation: CFD Analysis*

CFD analysis is carried out to simulate fire and smoke propagation within a tunnel and determine how that could detrimentally affect the evacuees. The results of an analysis, here carried out using the computer program [9], are used to estimate boundaries of the tenable regions within a tunnel under various adverse heat and smoke conditions.

A CFD analysis, to be carried out by specialists, consists of steps such as the geometrical modelling of the tunnel, the thermal modelling of boundaries, the determination of the fire size and its growth model, the consideration of adverse wind pressure between portals, the presence of active control measures such as mechanical ventilation via jet fans, etc. The output from a CFD analysis includes prediction of flame temperatures, hot gas temperatures characterising radiative and convective heat fluxes, surface temperatures of the tunnel walls and soffit, temperatures at jet fans, smoke visibility etc.

For ventilation design to cope with a fire emergency, design fire sizes (given in terms of the heat release rate HRR) for common vehicles are recommended for example by Highways Agency of the UK in its guide [3]. According to this guidance:

- A car produces an HRR of 10 MW;
- A bus, a coach or an HGV produces an HRR of 30 MW; and
- An HGV that contains highly combustible goods is able to produce an HRR of 100 MW.

[Note: For structural fire design of a tunnel, a higher HRR such as 300 MW from a petroleum tanker is used.]

The CFD analysis of smoke and heat conditions within a tunnel is carried out under a given differential pressure between its portals. This difference in pressure occurs due to environmental conditions: mainly wind that usually predominates. The probability of various pressure differentials can be determined using either raw wind data or a wind rose for the site.

An example set of results from a CFD analysis of a curved tunnel is shown graphically in Figs. 14.1 and 14.2. The fire is assumed to occur at the location shown in Fig. 14.1 that also illustrates the vehicle entry/inlet and exit/outlet portals of this tunnel with uni-directional traffic. The horizontal contour plots of ambient temperature along the tunnel at a particular height above the road level are shown in Fig. 14.2 for three occasions since the ignition of the fire. The shown plots in the example are for conditions after jet fans, acting in the direction of the exit portal, have been started to ventilate the tunnel. In the contours blue colour is used to represent


**Fig. 14.1** The assumed location of a fire, shown in a plan view of the computer model of a tunnel

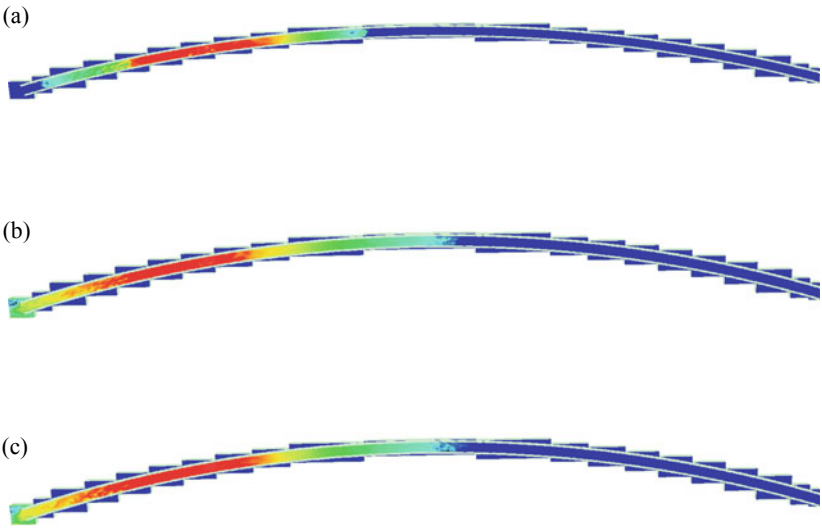


**Fig. 14.2** Example of how jet fans help to control smoke and heat during a 30 MW fire with no pressure differential between portals. Blue colour denotes smoke at 20 °C. Smoke is hotter as the colour becomes redder. **a** At 70 s from ignition and 10 s since the four considered banks of fans reached full power. Hot smoke has spread both upstream (i.e. to the right) and downstream of the location of the fire indicated by an arrow in Fig. 14.1. **b** At 190 s from ignition and 130 s since the four considered banks of fans reached full power. The fans have pushed the hot smoke towards the location of the fire, making the region upstream of it to be of lower temperature. **c** At 280 s from ignition and 220 s since the four considered banks of fans reached full power. The fans that earlier pushed the hot smoke towards the location of the fire maintain this condition (i.e. back-layering is controlled)

colder temperatures while the red colour is used for hotter temperatures, with colours in-between representing temperatures in between. Such information, when expressed digitally, can be used to determine tenability conditions within the tunnel for use in casualty analysis.

### *14.3.3 Evacuation Analysis*

On having determined temporal information on fire conditions within the tunnel for different fire loads, subject to the considered portal wind pressures and necessary assumptions, the next step is to determine the exposure of individuals to heat and smoke as they evacuate. For this Monte Carlo simulations are carried out based on information available from the European Research Project UPTUN on cost-effective, sustainable and innovative upgrading methods for fire safety in existing tunnels [30].

In accordance with the UPTUN method, it is considered that a set of people (group a) would start to evacuate immediately after the ignition of a fire, before an evacuation

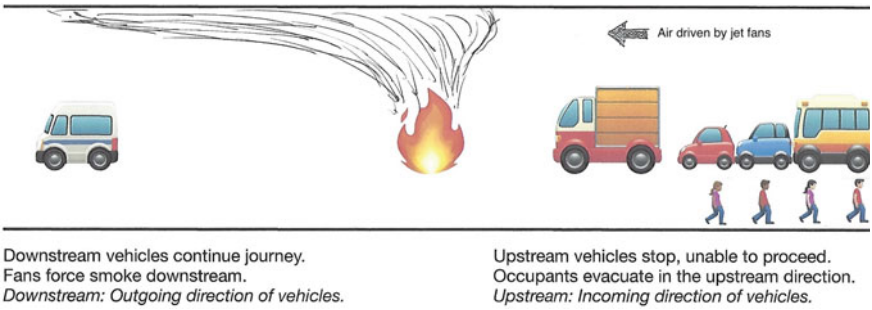


**Fig. 14.3** The movement of evacuees during a fire in a tunnel with single direction traffic, as assumed in the UPTUN model [30] and used in this work

order is issued. Another set (group b) also would evacuate before an evacuation order has been received (for example, via a public address system available within the tunnel), but they would do so only after the first set of people. A third set (group c) would wait until an evacuation order is received. The time evacuees take to come out of a vehicle is considered random with a prescribed probability distribution. The evacuees who come out vehicles are considered to hesitate and wait for another short period before starting to walk towards safety. This hesitation time also is considered as a random parameter.

The speed with which the evacuees walk has a random probability distribution. The people are considered to be safe once they reach an emergency exit (e.g. a cross-passage door) or the upstream (i.e. entrance) portal. (Here upstream and downstream refer to the flow of traffic.) It is assumed that nobody walks downstream past a fire as shown in Fig. 14.3 for a tunnel with one traffic direction; however, it may happen in real life during the initial stages of a fire if the exit portal or any other downstream emergency exit is only a short distance away from the evacuee and the path to it is not considered hazardous.

In evacuation and casualty analyses, all vehicles downstream of a fire are assumed to move away leaving the fire behind. This is a valid assumption for tunnels where no traffic congestions can be expected beyond its exit portal. However, congestion may occur during a period of heavy traffic, for example if there are traffic control lights downstream of the exit portal, and this should be given consideration.

It is assumed that a fire event will be always detected via a video surveillance system (either manual or automatic), supplemented potentially by other means such as linear heat detectors. It is also assumed that an announcement ordering evacuation will be made always on detection of a fire (or the likelihood of a potential fire). Provision can be made in the evacuation model to consider situations where there is no non-video based fire detection, or where such detection has failed.

The time to detect a fire is determined as the lesser of that by video surveillance and, if provided, linear heat detectors. The probability distribution of the video based detection times can be based on information provided by the tunnel manager/operator because it is very much dependent on the local systems. The detection and alarm

**Table 14.1** Tolerability limits for various tenability conditions

| Mode of heat transfer | Source | Tolerance time |
|---|---|---|
| Radiation | Smoke layer at 160 °C<br>4 m above person's head | 6 min |
| | Smoke layer at 160 °C<br>0.5 m near person's head | 5 min |
| | Smoke layer at 200 °C | 30 s |
| | Flame surface at 370 °C<br>Emissivity assumed 0.9 | 6.5 s |
| Convection | Smoke layer 0.5 m above person's nose at 1.5 m | 1–30 min |

times for linear heat detectors are available in [2], given as to be in the range of 30–60 s from ignition. Accordingly, a probabilistic distribution of detection and alarm time for linear heat detectors can be considered as a uniform distribution between these two limits.

At the start of a fire, the evacuees are considered to be uniformly spread in the tunnel length upstream of the fire, between it and the last vehicle in the stranded queue of traffic. The location of the last vehicle can be determined based on the average number of vehicles and their average length, together with, for example, a uniform gap of 2 m assumed between vehicles in the example presented here.

### *14.3.4 Determination of Casualty Numbers*

On having determined the evacuation conditions for each evacuee during his evacuation as simulated by a Monte Carlo simulation, it is necessary to determine how that person can be affected by heat and smoke within the tunnel. This requires tenability criteria beyond which a person may be adversely affected by such products of a fire.

The human body tenability criteria related to the effects of heat of flames and smoke are for example provided in British Standard [4] and reported here in Table 14.1. Based on these values and the exposure of each person, the number of casualties can be calculated.

## 14.4 Case Study

### *14.4.1 General Description*

The case study presented here is with respect to the Penmaenbach Westbound Tunnel on A55 in North Wales, which is a 658 m long two-lane existing highway tunnel with uni-directional traffic and a speed limit of 70 mph. This tunnel did not comply with a

prescriptive safety measure required by an EU Directive [8] which was implemented in the UK as Road Tunnel Safety Regulations [25], specifically the requirement for emergency exits along the tunnel at a spacing of 500 m. Providing an emergency exit retrospectively had to be discounted because of its complexity and the consequential impact the work would have upon the road network availability, reliability, delays and environmental issues. However, this tunnel had jet fans for providing mechanical ventilation during a fire; which was not required by the EU Directive because the tunnel was shorter than 1000 m. As the regulations allowed an equivalent level safety to be provided by alternative means, with their effectiveness demonstrated via a risk assessment, the tunnel's owners (the Welsh Government) decided to examine the sufficiency of the available provisions against an equivalent compliant tunnel (which is the 'relative' or 'comparative' method indicated in Sect. 14.2 and used in [17]).

The tunnel has a curved soffit and also is curved in the horizontal plane. It has slight gradients that were too low to affect the walking speed of evacuees [30]. The tunnel portals are open to significant variations in wind conditions, making its consideration in CFD analysis important. Depending on the direction of the wind, it would aid or (mostly) tend to counter the performance of the jet fans. There were six banks of jet fans, with two fans in each. These fans were started in a particular order, instead of simultaneously, to prevent significant electrical surges during the process.

A commonly accepted procedure to determine the fire incident rate, or an annual probability of fire, within a tunnel is to use the average rate of incidents per vehicle-mile in similar open roads in the country as the basis for calculations. The open-road value is converted to a tunnel value based on its length and the traffic volume (i.e. AADT). The particular tunnel's predicted fire accident rates, in terms of the fire return periods, derived from available statistics of the road network were 400 and 3400 years for 30 and 100 MW fires, respectively.

The AADT of the tunnel is 22,000 and a factor of 1.25 was considered to account for future increase in traffic. The vehicle population consists of 75% cars, 23% HGVs and 2% buses. Although this can be considered as random, here it is considered as deterministic and fixed. Vehicles lengths were considered as deterministic with values of 4.12 m for cars, 12 m for buses and 16.5 m for HGVs, respectively. The average number of occupants is 1.6 for cars, 50 for buses and one for HGV.

### *14.4.2 CFD Analysis*

The CFD analysis of fire conditions within the tunnel was carried out using the software (FDS 2014). Design fire sizes, in terms of the peak heat release rate (HRR), were 30 and 100 MW (see Sect. 14.3.2). The fires of cars (10 MW) were not considered as was the 300 MW for a petrol tanker. The former was small enough to be easily controlled by the existing jet fans and the latter is considered unrealistically severe for ventilation/life safety design.

Statistics for adverse wind pressure at the tunnel portals were determined from wind data for the site. The pressure difference between the two portals is considered

positive when opposing the movement of traffic and the fan blast. The CFD analyses were carried out with different adverse pressures between portals, ranging from zero to 30 Pa, with the upper limit being advised as the most credible for the location when under high winds. The results from such analyses contributed to the determination of weighted averages of casualties that reflected the probability of various wind conditions. The CFD analyses included situations where no fans operated (in the 'compliant' solutions). In analyses where mechanical ventilation was provided, two banks of fans were considered unavailable due to breakdown and fire damage (see [3]), resulting in the use of only four of the six banks.

### *14.4.3 Evacuation Simulation*

The evacuation simulation was based on information available in [30], supplemented with local information available from the tunnel manager, as reported in Table 14.2. During evacuation simulation, a fire is considered equally probable to occur anywhere along the tunnel and the fire location for each simulation is randomly generated based on a uniform distribution. The evacuees are considered to be in place of relative safety once they reach an emergency exit (e.g. a cross-passage door) or the upstream (i.e. entry) portal.

The UPTUN information were supplemented, for example as follows in relation to the particular analysis:

- The fire detection method available (initially) was video cameras (CCTV) installed throughout the tunnel and monitored by staff. Provision has been made in the model to consider situations where there is no fire detection, or where detection has failed.

**Table 14.2** Input data, including probabilistic data, for the evacuation analysis

| Parameter | Standard | Conservative |
|---|---|---|
| Heat detection time [s] | Uniform (30, 60) | Uniform (30, 60) |
| Video detection time [s] | Uniform (17, 40) | Uniform (17, 40) |
| Tunnel closure time after detection [s] | Uniform (30, 60) | Uniform (30, 60) |
| Time to announce evacuation | Uniform (5, 10) | Uniform (30, 60) |
| Walking speed [m/s] | Uniform (0.44, 1.12) | Uniform (0.30, 0.75) |
| Limit on distance to fire group a [m] | 15 | 1 |
| Limit on distance to fire group b [m] | 30 | 1.5 |
| Hesitation time for group a [s] | 1 | 5 |
| Hesitation time for group b [s] | 5 | 10 |
| Maximum time to evacuate vehicle group a [s] | 10 | 20 |
| Maximum time to evacuate vehicle group b [s] | 30 | 60 |

- The order from the public address system (PAVA) to evacuate the single bore tunnel is (always) made following the detection of a fire (or the potential for a fire) and receipt of authorisation from the relevant manager.
- The walking speeds of evacuees are random, with a probability distribution as reflected by UPTUN. However, in some cases, all generated UPTUN-based evacuee speeds were reduced to 2/3 of the corresponding value of to reflect unforeseen difficult conditions, for example in the absence of mechanical ventilation and the presence of less mobile people.

The described method for assessing types of casualties is efficient and quick as desired by a study that uses a large number of computer simulations. However, it is unable to determine the situations where an evacuee is subject to significantly higher radiation or temperatures than the tenability criteria and, consequently, could have only a shorter tolerance of hazardous exposure. Nevertheless, sensitivity studies conducted using very high safety factors and, consequently, very short tolerance limits, indicated that the analyses are sufficiently robust to allow a comparison of risks in compliant and non-compliant tunnels. It can be also considered robust to a certain extent for absolute risk studies because of the significant dominance of the flame tolerance limit of 6.5 s when determining the casualties.

The methodology described so far determines the expected indicative number of casualties from each simulation for a particular fire location, fire load and an adverse wind pressure, which are the major random variables considered. These individual values were probabilistically combined to determine the expected number of casualties for a one-year period. However, in the following, the annual results for each fire size are presented separately because they provide insights into the differences between them unlike when they are summed probabilistically to obtain overall annual casualty figures.

### *14.4.4 Results*

Representative results for indicative life safety consequences in the considered existing tunnel and a compliant equivalent tunnel, given a 100 MW fire and a 30 MW fire under particular wind conditions, are shown in Figs. 14.4 and 14.5, respectively. These results are for two sets of simulation parameters, viz. a '*standard*' set which are considered to reflect a normal situation and a '*conservative*' set that reflect a situation with much longer evacuation times (and, hence, potentially higher life safety risks). The results are for the existing tunnel with two jet fans in each of the four banks of fans and for an equivalent compliant tunnel with no mechanical ventilation but possessing an additional exit from it. The casualty numbers shown in the figures are the expected values under either 30 or 100 MW fires anywhere within the tunnel, with the probability of occurrence of a fire considered uniform along the tunnel. In addition to the above, the results from analyses that investigated the benefit of replacing the two existing jet fans of each bank with three more powerful fans are

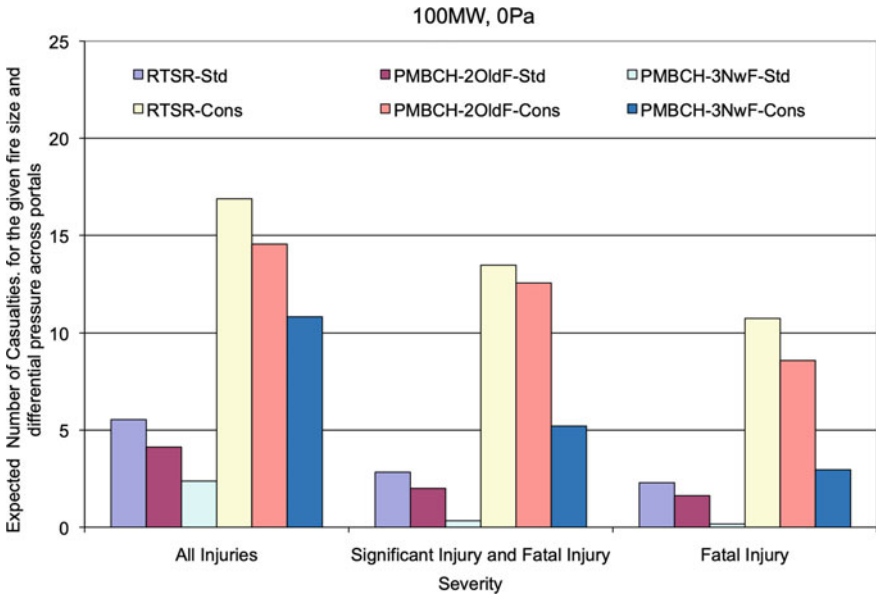


**Fig. 14.4** Expected human consequences given a 100 MW fire with equal occurrence probability along the tunnel and with no adverse pressure differential across the portals. See Sect. 14.4.4 for details on abbreviations used in the legend

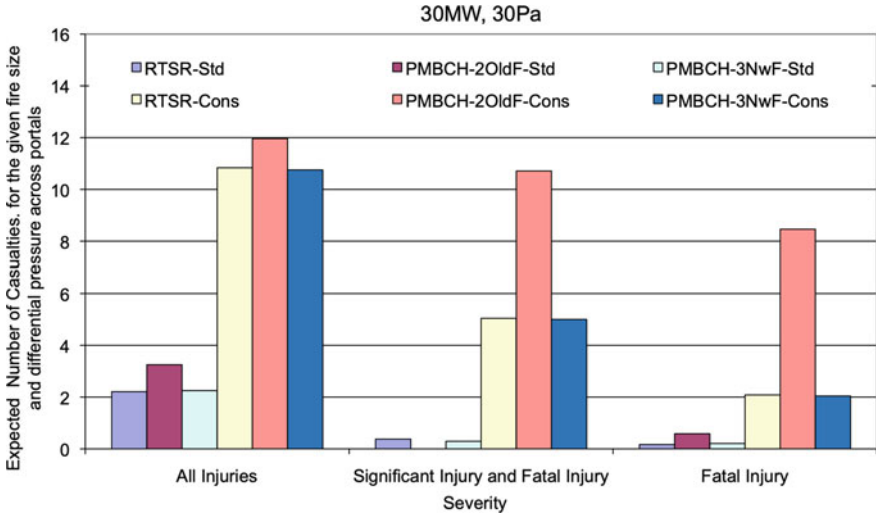


**Fig. 14.5** Expected human consequences given a 30 MW fire with equal occurrence probability along the tunnel and with an adverse pressure differential of 30 Pa across the portals. See Sect. 14.4.4 for details on abbreviations used in the legend

presented in the Figs. 14.4 and 14.5. The following abbreviations have been used in Figs. 14.4 and 14.5 in order to distinguish the different results in them.

- Std = Standard Parameter Case
- Cons = "Conservative" Parameter Case
- 3NwF = With three new more powerful jet fans per bank
- PMBCH = The existing tunnel
- RTSR = Equivalent [25] compliant tunnel, with a new exit and without jet fans.

In the presence of existing jet fans the expected casualty numbers for a 30 MW fire under a 30 Pa pressure differential are higher in the existing tunnel than in the considered equivalent compliant tunnel with no mechanical ventilation (Fig. 14.5). The opposite behaviour is seen for a 100 MW fire with no adverse pressure differential (Fig. 14.4). However, the existing tunnel was seen to pose a lower risk than the compliant tunnel when the results for each fire size under all different wind conditions were probabilistically combined to determine the expected casualties under a particular fire size.

Notwithstanding the above positive results, in order to improve the margin of safety between the two considered tunnel configurations, the effect of replacing the existing two jet fans in each bank with a set of three more powerful fans was additionally investigated. Also the results of this new design condition are presented in Figs. 14.4 and 14.5 and 14.6. The following observations and conclusions can be made with respect to the results shown in these three figures:

- With three new more powerful fans per bank, under the 30 MW fire and a very high and extreme adverse wind pressure differential of 30 Pa, the risks in the existing tunnel are similar to that of the considered compliant tunnel. Therefore, when upgraded, the overall risks in the existing tunnel over all wind conditions will be lower than in the considered compliant tunnel (see Fig. 14.6). This is because the jet fans are more effective against the more common lower adverse pressure differentials across portals.
- With the upgraded tunnel showing lower overall conditional risks (under all adverse pressure differentials) for each of the two fire sizes considered, also the annual risk obtained by probabilistically combining these results as given in expression (14.1) will be lower for it than for the considered compliant tunnel.

Following this work the Welsh Government chose to implement a variation of the suggested solution by providing two extra fans at each of the six banks of fans, to give a total of four fans per bank, to similarly improve the performance. In this way, using the alternative safety measure of mechanical ventilation, the existing tunnel satisfied the requirements of [25] to a higher level than the considered equivalent compliant tunnel.

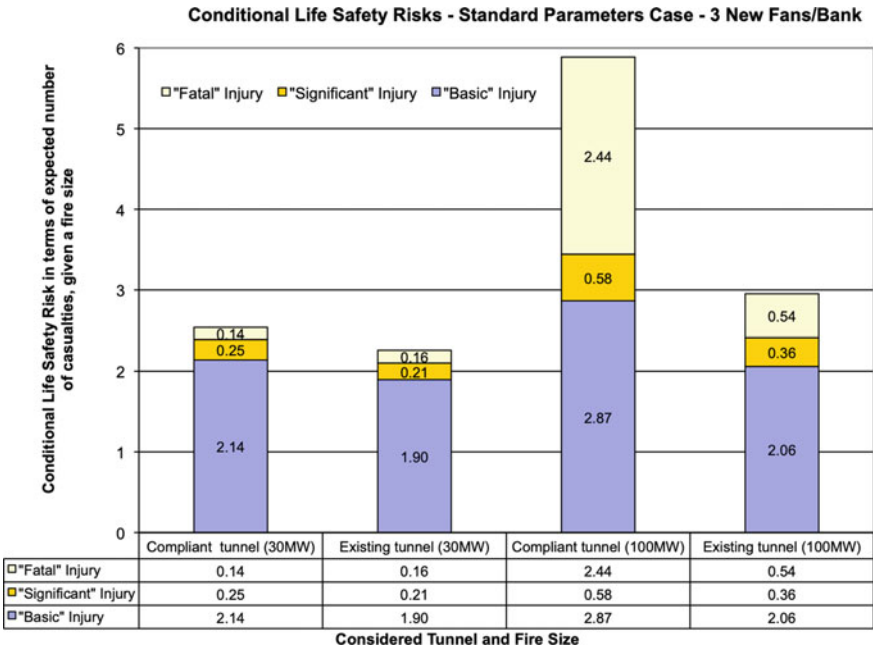


**Fig. 14.6** Conditional life safety risks in terms of the expected number of different types of casualties, given a 30 MW fire and a 100 MW fire. Fires considered here are within a compliant tunnel and the existing tunnel with three new and more powerful fans per bank. Standard parameter case

## 14.5 Concluding Remarks

Vehicle fires in road tunnels represent an extreme hazard to the users, manifested through significant accidents in the past. This chapter provides a critical review of provisions in standards and regulations and summarises state-of-the art methodologies to assess related human risk. It also examines and discusses decisions related to respective safety measures in the light of uncertainties.

The analysis of fire life safety in a tunnel is a complex process involving several parties. The results of the case study of an existing tunnel show the practical usefulness of the presented methodologies that involved computer simulations comprising CFD analysis, evacuation modelling, casualty analysis and statistical analysis.

**Acknowledgements** The work reported here was funded by the Government of Wales via its subsidiary organisation WTTC. Much support was received from staff of WTTC and North and Mid-Wales Trunk Road Agent (NMWTRA), especially Geraint Jones and Andrew Roberts.

## References


1. Apostolakis G (1981) Bayesian methods in risk assessment, advances in nuclear science and technology, vol 13. NY, USA, pp 415–465
2. Baird A, Carvel R (2011) Handbook of tunnel fire safety, 2nd edn. Thomas Telford, London
3. BD 78/99 (1999) Design manual for roads and bridges, volume 2, section 14.2, part 9: design of road tunnels. HMSO, UK
4. BS 7899-2 (1999) Code of practice for assessment of hazard to life and health from fire—part 2: guidance on methods for the quantification of hazards to life and health and estimation of time to incapacitation and death in fires. BSI, London
5. CIB (2001) Risk assessment and risk communication in civil engineering. CIB Report 259. CIB Secretariat, The Netherlands
6. Diamantidis D (2005) Risk analysis versus risk acceptability in major European tunnel projects. In: Proceedings 1st Asia Pacific conference on risk management and safety, Hong Kong
7. Diamantidis D, Holicky M, Sykora M (2017) Target reliability levels based on societal, economic and environmental consequences of structural failure. In: Proceedings ICOSSAR, Vienna, Austria
8. European Union (2004) Minimum safety requirements for tunnels in the trans-European road network. Directive 2004/54/EC of the European Parliament and of the Council, 29 April 2004; Official Journal of the European Union L, pp 56–76, 7 June 2004
9. FDS (2014) Fire dynamics simulator. NIST, Gaithersburg, Maryland, USA
10. Haack A (2006) Overview of European tunnel research and ITA committee on operational safety of underground facilities. In: Workshop on safety in tunnels and underground structures, Riyadh, Saudi Arabia
11. Hoj NP (2004) Guidelines for fire safety design compared fire safety features for road tunnels. In: First international symposium safe and reliable tunnels, Prague, Czech Republic
12. Holicky M (2007) Risk criteria for road tunnels. In: Special workshop on risk acceptance and risk communication, March 26–27, Stanford University, USA
13. Holicky M, Diamantidis D (2008) Optimisation of road tunnel safety, vol 103. Beton und Stahlbetonbau
14. ISO 2394 (2015) General principles on reliability for structures. Geneve, Switzerland
15. Jonkman SN, Van Gelder PHAJM, Vrijling JK (2003) An overview of quantitative risk measures for loss of life and economic damage. J Hazard Mater 99(1):1–30. ISSN 0304-3894. https://doi.org/10.1016/S0304-3894(02)00283-2
16. Kohl B, Botschek K, Hörhan R (2006) Austrian risk analysis for road tunnels. In: 3rd International conference, tunnel safety and ventilation, Graz, Austria
17. Kohl B, Wiersma T, Serrano GL (2014) Application of risk assessment as tool for road tunnel safety management. Routes/Road Issue No. 364, PIARC, pp 62–69
18. Kordina K (2003) Brände in unterirdischen Verkehrsanlagen, Bautechnik 80, Heft 3
19. Mashimo H (2002) State of the road tunnel safety technology in Japan. Public Works Research Institute, Tsukuba, Japan
20. Neumann C, Sistenich C (2011) Results of a comparative application of QRA methodology for road tunnels in Germany. In: 6th International conference on traffic and safety in road tunnels, Hamburg, Germany
21. PIARC (2008) Risk analysis for road tunnels. PIARC Technical Committee C3.3: Working Group 2; Management of Road Tunnel Safety, World Road Association (PIARC), France, ISBN 2-84060-202-4
22. PIARC (2012) Current practice for risk evaluation of road tunnels. Technical Committee C4, Road Tunnel Operation. World Road Association (PIARC), France, ISBN 978-2-84060-290-3
23. PIARC (2016) Fixed fire fighting systems in road tunnels: current practices and recommendations. Technical Committee C.3.3 Road Tunnel Operations, World Road Association (PIARC), France, ISBN 978-2-84060-375-7

24. RABT (2006) (German Tunneling Guidelines) Richtlinien für die Ausstattung und den Betrieb von Straßentunneln, Forschungsgesellschaft für das Straßenwesen, Technische Regelwerke. FGSV-Nr.: 339. ISBN: 3-937356-87-8
25. RTSR (2007/2009) Road tunnel safety regulations 2007 (UK SI 2007 No. 1520), Amended 2009 (UK SI 2009 No. 64). UK Government
26. RVS—09.03.11 (Austrian Tunneling Guidelines) (2008) Tunnel risk model TuRisMo. Vienna, FSV
27. Scott P (2001) Risk based methods in tunnel design and operation. J Constr Manag Eng JSCE 693(V1–53):1–12
28. Trbojevic VM (2003) Development of risk criteria for road tunnels. In: 5th International conference—safety in road and rail tunnels. Marseille, France
29. UPTUN (2008a) Cost-effective, sustainable and innovative upgrading methods for fire safety in existing tunnels. Joint European Research Project. Various Reports. Brussels, Belgium
30. UPTUN (2008b) Human factors aspects in tunnels: tunnel user behaviour and tunnel operators. WP3 Human Response D33. Brussels Belgium
31. Vrouwenvelder ACWM, Krom AHM (2004) Hazard and the consequences for tunnels structures and human life. In: 1st International symposium safe and reliable tunnels in Prague, CUR, Gouda, The Netherlands
32. Vrouwenvelder T, Lovegrove R, Holicky M, Tanner P, Canisius G (2001) Risk assessment and communication in civil engineering. In: Safety, risk, reliability—trends in engineering, IABSE Conference, Malta

# Chapter 15
# Cost-Benefit Analysis of Design for Progressive Collapse Under Accidental or Malevolent Extreme Events


**André Teófilo Beck, Lucas da Rosa Ribeiro, and Marcos Valdebenito**

**Abstract** Engineering structures are sometimes subject to extreme loading events like vehicle impact, gas explosions, fire or terrorist bombing. These events are characterized by very small probabilities of occurrence, but large effects on design loads. Extreme loading events are also characterized by large uncertainty: impact load changes significantly with vehicle mass and speed, explosion pressure waves depend on charge distance and size, etc. Due to large uncertainty in possible loading scenarios, it is often considered that such extreme events may lead to complete loss of load-bearing elements like walls, beams or columns. In this context, the decision to design or strengthen a structure to support eventual loss of a load-bearing element is a typical example of decision making in presence of uncertainty, with obvious impacts on construction costs. In this chapter, we address the cost-benefit of strengthening structures to withstand loss of load-bearing elements. We show how this decision is rooted on the probability of losing the load-bearing element, which should be the result of a risk analysis addressing a structure's adjacency, ownership and intended use. We also discuss how this decision depends on the aspect ratio of buildings, on strengthening costs, and on the extent of strengthening measures.

## 15.1 Introduction

The decision to design or strengthen a structure to support eventual loss of a load-bearing element, due to abnormal actions, has obvious impacts on construction costs. Such decision must take into account whether the designed structure is a potential target for abnormal accidental or malevolent action. This is clearly a problem of decision making in presence of uncertainty, as even a potential target structure may,

A. T. Beck (✉) · L. da Rosa Ribeiro
Department of Structural Engineering, University of São Paulo, Av. Trabalhador São-carlense, 400, São Carlos, SP 13566-590, Brazil
e-mail: atbeck@sc.usp.br

M. Valdebenito
Faculty of Engineering and Sciences, Universidad Adolfo Ibáñez, Av. Padre Hurtado 750, 2562340 Viña del Mar, Chile



M. G. Stewart and D. V. Rosowsky (eds.), *Engineering for Extremes*, Springer Tracts in Civil Engineering, https://doi.org/10.1007/978-3-030-85018-0_15

or may not, be subject to loss of load bearing elements within its design life. If one makes the decision to strengthen a beam or slab, to make it able to bridge over failed columns, construction cost goes up significantly. Yet, if the decision is for a conventional design, but the building eventually suffers a column loss event, one pays for the consequences of local collapse and, eventually, progressive failure leading to global collapse.

Column loss in a building or bridge is an extreme loading event: it has small probability of occurrence, but large impacts in overloading the structure, and potentially catastrophic consequences in case of progressive failure and global collapse. Hence, it is important to comprehensively identify the hazards, and use good engineering judgment to estimate the resulting loading events. Identification of hazards and loading events is typically done by risk analysis, considering the buildings ownership and intended use, as well as the surrounding environment.

Under multiple hazards, the probability of structural collapse can be evaluated as (Chaps. 1, 3, [10, 11, 14]):

$$p_C = P[C] = \sum_H \sum_{LD} P[C|LD, H]P[LD|H]P[H] \tag{15.1}$$

where $C$ stands for collapse, $P[H]$ is the probability of hazard occurrence; $P[LD|H]$ is the conditional probability of local damage, given hazard $H$; $P[C|LD, H]$ is the conditional probability of collapse, given local damage $LD$ and hazard $H$. In this text, we address local damage leading to Column Loss ($CL$) events.

The potential hazards in Eq. (15.1) are of accidental or malevolent nature: vehicular collisions, fire, explosion; the modelling of such actions is addressed elsewhere in this book (Chap. 5). The probability of column loss, given the above hazards, $P[CL|H]$, depends on:

(a) the abnormal loading events, originated by the above hazards;
(b) measures to locally strengthening the target columns.

Typically, these loading events are characterized by large uncertainty: impact loads depend on mass and velocity of impacting vehicle; explosion load varies significantly with size and distance of the charge. As a result, column loss probabilities are strongly dependent on hazard modelling, as shown elsewhere for steel [26] and for RC columns [25].

Due to the large uncertainties above, design for discretionary column removal is advocated in modern design codes [2, 8, 15]:

> localized damage due to extreme accidental or malevolent actions may be acceptable, provided the structural system has enough capacity to bridge over damaged elements.

This approach is considered herein, with one important amendment: we consider the column loss probability, given notionally as $p_{CL} = \sum_H P[CL|H]P[H]$, as an independent parameter, which separates the structural systems analysis from the hazard-dependent risk analysis. More specifically: we understand that a risk analysis can be performed, taking into account all hazards, as well as buildings ownership,

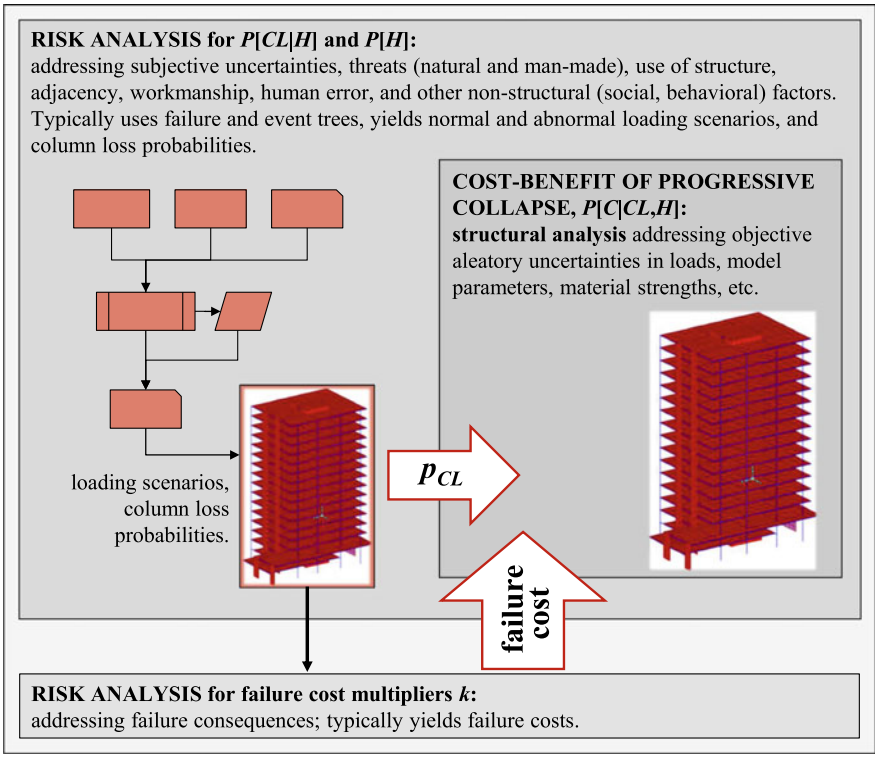


**Fig. 15.1** Separation of risk and cost-benefit structural reliability analyses

intended use and adjacency, and yielding the probability of column loss, $p_{CL}$, for specific buildings. The risk analysis should include an estimation of the expected costs of failure, in terms of local damage, progressive failure and global collapse, as illustrated in Fig. 15.1 and further discussed in the sequence. With these preliminaries, the optimal cost-benefit analysis for load bridging design becomes threat-independent: it can be made looking only at structural behavior, and independent of hazards, building use or environment. Considering $p_{CL}$ as an independent parameter complies with the *latent failure probability* concept, introduced by Beck [3] in the context of structural optimization.

This text focuses on the conceptual decision as whether to strengthen a building structure for load bridging under discretionary column removal, or not. The text does not address practical design measures such as binding, ductility, structural fuses, compressive arch and catenary actions, which are important for any comprehensive building design.

## 15.2 Problem Formulation

### *15.2.1 Design Under Conventional and Abnormal Loads*

Under normal gravity loads, usual design of steel and RC buildings is given by ASCE [2]:

$$\phi R_n \geq 1.2D_n + 1.6L_n. \tag{15.2}$$

where $R$ is resistance or strength, $D$ is dead load, $L$ is live load, subscript $()_n$ is for nominal value. In Eq. (15.2), $\phi$ is the strength design factor, and the values 1.2 and 1.6 are the usual load factors for conventional codified design.

Under extraordinary or abnormal loading events, such as loss of a load bearing element, the term $P[C|CL, H]$ in Eq. (15.1) is evaluated considering specific requirements, like [2, 13]:

$$\phi R_m \geq 1.2D_n + 0.5L_n. \tag{15.3}$$

where subscript $()_m$ indicates mean strength. Note that the live load factor is reduced in Eq. (15.3), in comparison to Eq. (15.2), as under the abnormal loading event the structure is only expected to carry the sustained component of live load, instead of the fifty-year extreme live load.

To address optimal cost benefit design under discretionary column removal, we insert an additional design factor $\lambda_{PC}$ in Eq. (15.3):

$$\phi R_m \geq \lambda_{PC}(1.2D_n + 0.5L_n). \tag{15.4}$$

where subscript $()_{PC}$ is for Progressive Collapse. The structural cost-benefit analysis is performed with $\lambda_{PC}$ as the design parameter, and with mean required strength given by $R_m(\lambda_{PC}) = \lambda_{PC}(1.2D_n + 0.5L_n)/\phi$. We consider $\phi = 1$ in alternate path analysis, following ASCE 41 [1]. Note that $\lambda_{PC}$ has the same effect as $1/\phi$; hence, optimal $\lambda^*_{PC}$ values presented herein can be easily related to specific code-recommended values for $\phi$.

Design for progressive collapse is of secondary nature [16]. Usually, the main structural characteristics are defined under normal loading conditions (Eq. 15.2), and the structure is verified and strengthened to be able to withstand local damage. This may result, for instance, in increasing reinforcement ratios, to allow a beam or slab to bridge over a lost column. This should be considered when interpreting results presented herein, as we address progressive collapse in a more direct manner. The simplified examples considered herein only address gravity loads. Hence, as a limitation of results discussed herein, wind loads and lateral stability are not considered.

### 15.2.2 Reliability Analysis

The existence of uncertainties implies in a possibility of undesirable structural responses. For the problem considered herein, for instance, uncertainty implies that we may design for load bridging over a single failed column, but an abnormal loading event may result in two adjacent failed columns. Uncertainties also relate to the actual abnormal loadings the structure may be subject to, and to the extent of initial damage. Uncertainties in conventional design relate to the actual values of strength variables; the future values of dead and life load actions; and to the imprecision of engineering models. For the purpose of problem formulation, uncertain structural parameters are grouped in random variable vector $\mathbf{X}$.

We write limit state equations to divide the random variable space in failure and survival domains. For the usual design condition (Eq. 15.2), the corresponding limit state equation is:

$$g_{NLC}(\lambda_{PC},\mathbf{X}) = M_I R_I\left(\lambda_{PC}, f_c, f_y, \ldots\right) - D - L_{50}, \tag{15.5}$$

where $R_I(.)$ is the strength function for the intact structure, $M_I$ is a non-dimensional strength model error variable, $D$ is the dead load, and $L_{50}$ is the fifty-year extreme live load. In Eq. (15.5), $()_{NLC}$ refers to Normal Loading Condition. Usually, Eq. (15.5) is not a function of the progressive collapse design factor $\lambda_{PC}$. However, as the structural elements are strengthened for load bridging using Eq. (15.4), the reliability index under normal loading condition, $\beta_{NLC}$, also varies with $\lambda_{PC}$.

The limit state equation for abnormal loading (column loss) condition is:

$$g_{CL}(\lambda_{PC},\mathbf{X}) = M_{CL} R_{CL}\left(\lambda_{PC}, f_c, f_y, \ldots\right) - D - L_{APT}, \tag{15.6}$$

where $M_{CL}$ is a non-dimensional strength model error variable, for the damaged structure, and $R_{CL}(.)$ is the strength function under column loss condition. In Eq. (15.6), $L_{APT}$ is the sustained component of live load.

For each conditional loading event, the collapse failure probability is:

$$P[C|CL, H] = \int\limits_{g(\lambda_{PC},\mathbf{X})\leq 0} f_{\mathbf{X}}(\mathbf{x})\mathrm{d}\mathbf{x}, \tag{15.7}$$

where $f_{\mathbf{X}}(\mathbf{x})$ is the joint density function of random variable vector $\mathbf{X}$. When computing Eq. (15.7) under normal loading condition, $g(\lambda_{PC},\mathbf{X})$ is given in Eq. (15.5). Under column loss scenarios, the limit state equation is given in Eq. (15.6).

In this text, simple academic problems are addressed, and conditional collapse probabilities are evaluated using First Order Second Moment (FOSM) analysis. The results are checked elsewhere [6] using full distributions and the First Order Reliability Method (FORM), where it is shown that the main aspects of the problem can be illustrated with FOSM. First order analysis yields the relationship:

$$P[C|LD, H] = \Phi[-\beta], \tag{15.8}$$

where $\Phi[.]$ is the standard Gaussian cumulative distribution function, and $\beta$ is the Cornell (FOSM) or Hasofer-Lind (FORM) reliability index [20]. Using limit state Eqs. (15.5) and (15.6) when solving Eq. (15.7) leads to the reliability index for normal loading ($\beta_{NLC}$) and for column loss ($\beta_{CL}$) conditions.

### *15.2.3 Quantifying Consequences of Failure*

In order to address the optimal cost-benefit of design alternatives, we need to quantify the costs of construction, including the cost of strengthening for load bridging, as well as the consequences of local damage, progressive failure and global collapse. Failure consequences are strongly dependent on non-structural factors, such as structural adjacency and intended use. Consequences of structural failure involve the costs of shutdown for rehabilitation and repair (lost revenue), costs for removing debris and rebuilding, damage to building contents and neighboring facilities, injury, death, and environmental damage. Out of these, only the cost of reconstruction depends on design safety margins. Hence, to separate non-structural consequence factors from the structural reliability analysis, as illustrated in Fig. 15.1, failure consequences are considered via an independent cost parameter $k$.

The initial construction cost is directly proportional to $\lambda_{PC}$, and is made non-dimensional by dividing by a reference construction cost, $R_m(\lambda_{PC} = 1)$:

$$C_{construction}(\lambda_{PC}) = \frac{R_m(\lambda_{PC})}{R_m(\lambda_{PC} = 1)} = \lambda_{PC}. \tag{15.9}$$

Monetary consequences of failure are given by non-dimensional cost multiplier $k$, as $k$ times the reference cost. This cost term is also made non-dimensional by dividing by the reference cost, yielding:

$$C_{collapse} = k\frac{R_m(\lambda_{PC} = 1)}{R_m(\lambda_{PC} = 1)} = k. \tag{15.10}$$

Costs of failure are only paid for in the future, when and if failure occurs. The so-called expected cost of failure, $C_{EF}$, is obtained by multiplying the failure cost by the estimated failure probability, which complies with the definition of risk. The expected costs of collapse, under normal loading and column loss conditions, respectively, are:

$$(C_{EF})_{NLC} = k\Phi[-\beta_{NLC}(\lambda_{PC})], \tag{15.11}$$

$$(C_{EF})_{CL} = p_{CL}k\Phi[-\beta_{CL}(\lambda_{PC})]. \tag{15.12}$$

Different cost multipliers can be considered for normal loading and column loss conditions, as partial collapse is more acceptable under severe initial damage. In this text, for simplicity, the same cost multiplier is used. One important difference between the expected cost terms in Eqs. (15.11) and (15.12) is that the column loss term is multiplied by the column loss probability, $p_{CL}$.

Herein, cost of construction (Eq. 15.9) is the cost of the structural frame. Marchand and Stevens [18] studied the ratios between construction costs for the structural frame and for the entire building. These ratios were found as 6.8 for RC frames, 16.7 for steel frames, 4.4 for cold-formed steel and 10.5 for wood structures. Collapse failure costs could be at least equal, but easily higher than the costs for reconstructing the whole structure, and not just the structural frame. Hence, collapse failure cost multipliers can be significantly higher than the figures above, and should be considered constant (as in Eq. 15.10), instead of functions of $\lambda_{PC}$.

Following the Joint Committee on Structural Safety [17, 30], for civil engineering structures a full cost-benefit analysis is recommended for $k \geq 10$. In this paper, we consider $k = 10$ for ductile bending failures and $k = 20$ for brittle crushing failures, unless otherwise stated.

Equations (15.9) and (15.10) have to be adapted for particular applications. In the design of regular frames, for instance, consequences of partial collapse failures should take into account the extension of damaged areas, as shown in [7].

### *15.2.4 Optimal Design Under Conventional and Abnormal Loads*

The total expected cost, $C_{TE}$, is obtained by collecting and adding the cost terms in Eqs. (15.9)–(15.12), following [6]:

$$C_{TE}(\lambda_{PC}) = \lambda_{PC} + k\Phi[-\beta_{NLC}(\lambda_{PC})] + kp_{CL}\Phi[-\beta_{CL}(\lambda_{PC})]. \tag{15.13}$$

Note that other cost terms could be incorporated, following the multi-hazard formulation (Eq. 15.1). The cost-benefit analysis is done by solving the following risk optimization problem [4, 5, 28]:

$$\begin{aligned} &\text{Find} : \lambda^*_{PC} \\ &\text{which minimizes} : C_{TE}(\lambda_{PC}) \\ &\text{subject to} : \lambda_{PC} > 0. \end{aligned} \tag{15.14}$$

One central aspect of the optimization problem in Eq. (15.14) is the objective function in Eq. (15.13) which combines, in a single equation, design under normal loading condition, and design under abnormal (column loss) condition. Usually, the probability of collapse under normal loading condition, term $\Phi[-\beta_{NLC}(\lambda_{PC})]$

in Eq. (15.13), is one or two orders of magnitude smaller than the probability of collapse under column loss condition, term $\Phi[-\beta_{CL}(\lambda_{PC})]$ in Eq. (15.13). However, as this last term is multiplied by a (generally small) column loss probability $p_{CL}$, and as $p_{CL}$ is considered an independent parameter, one can find the $p_{CL}$ value above which there is economic gain, or positive cost-benefit, in designing a beam or slab for bridging over a failed column.

The column loss probability $p_{CL}$ in Eq. (15.13) is the lifetime probability per building. Herein, a 50-year design life is considered. Hence, the 50-year $p_{CL}$ value can be related to yearly threat probabilities $h$ by making: $h = -\ln[1 - p_{CL}]/50$.

## 15.3 Plastic Design of a Continuous Steel Beam

As a first example, we recall and discuss a variant of the continuous steel beam example of [6]. This is a *toy* problem, which has semi-analytical solution, but reveals the main aspects of the formulation in Eqs. (15.13) and (15.14).

Design of the six-span continuous steel beam illustrated in Fig. 15.2 is considered. The outer span lengths ($L_{ext}$) are such that the maximum bending moment, given internal or external column loss, are the same. This is achieved by considering

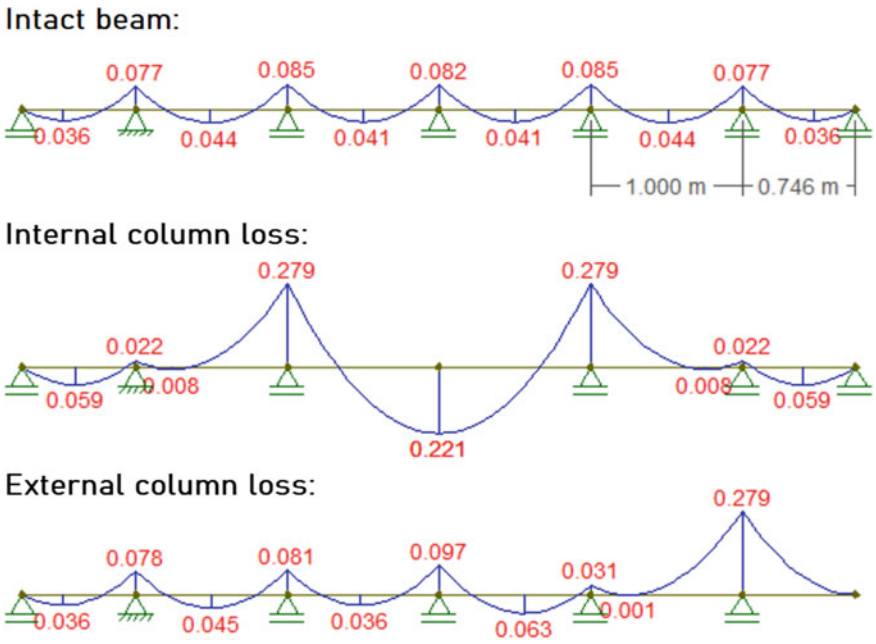


**Fig. 15.2** Bending moments on six span continuous beam. Normal loading condition (top), internal column loss (middle) and external column loss (bottom)

**Table 15.1** Random variable statistics for the continuous beam problem [6, 12]

| Variable | Mean (μ) | C.O.V. (σ/μ) | Distribution |
|---|---|---|---|
| Plastic moment strength of steel beams ($Z$)—nondimensional | 1.30 | 0.12 | Normal |
| Dead load ($D$) | 1.05 $L_n$ | 0.10 | Normal |
| Live load, arbitrary point in time value ($L_{APT}$) | 0.25 $L_n$ | 0.55 | Gamma |
| Live load, 50 year extreme ($L_{50}$) | 1.0 $L_n$ | 0.25 | Gumbel |

$L_{ext} = 0.7464 L_{int}$, where $L_{int}$ is the internal span length. The design variable is the plastic section modulus, $z_P$. The problem is solved for unitary nominal live and dead loads: $L_n = D_n = 1$. Similar solution for $L_n = 3D_n$ is shown in [6]. Solutions are non-dimensional in terms of nominal material strength.

Simple static analysis yields the maximum bending moment factors for the normal loading and column loss conditions:

$$\begin{aligned} m_{NLC} &= 0.085; \\ m_{CL} &= 0.279. \end{aligned} \tag{15.15}$$

A closed form solution for reliability index is obtained by considering resistance as the non-dimensional plastic modulus (variable $Z$, Table 15.1), multiplied by plastic moment $z_P$, and by approximating load distributions as Gaussian. This makes the limit state linear in Gaussian random variables. The reliability index $\beta(\lambda_{PC}, m)$ is given in terms of bending moment factors ($m$):

$$\beta(\lambda_{PC}, m) = \frac{E[g(\lambda_{PC}, \mathbf{X})]}{\sqrt{Var[g(\lambda_{PC}, \mathbf{X})]}} = \frac{z_P \mu_Z \lambda_{PC} - m(\mu_D + \mu_L)}{\sqrt{z_P^2 \sigma_Z^2 \lambda_{PC}^2 + m^2 \left(\sigma_D^2 + \sigma_L^2\right)}}, \tag{15.16}$$

where $\mu$ is for mean value, and $\sigma$ is for standard deviation. For normal loading condition ($\beta_{NLC}$), the fifty-year extreme load ($L_{50}$) is considered in Eq. (15.16). For column loss conditions, $\beta_{CL}$ is obtained using $L_{APT}$. The FORM solution is obtained considering actual probability distributions (Table 15.1), as shown in [6].

Plastic design of the continuous beam under normal loading conditions [2, 9] and using Eq. (15.2) with $\phi = 0.9$, $L_n = D_n = 1$ and for unitary nominal strength, leads to a required plastic section modulus of $z_{NLC} = 0.264$. In the sequence, this design is compared with the design for discretionary column (or support) removal.

The usual design with $z_{NLC} = 0.264$ does not comply with Eq. (15.3), as the reader can verify. Plastic (re-)design using Eq. (15.3) with $\phi = 1.0$, and mean resistance $\mu_Z = 1.3$, results in $z_{PC} = 0.365$, which is the reference progressive collapse design, corresponding to $\lambda_{PC} = 1$. Reliability indexes for the strengthened beam are $\beta_{NLC} = 4.89$, $\beta_{CL} = 1.50$.

Figure 15.3 shows the objective functions (Eq. 15.13), in terms of design factor

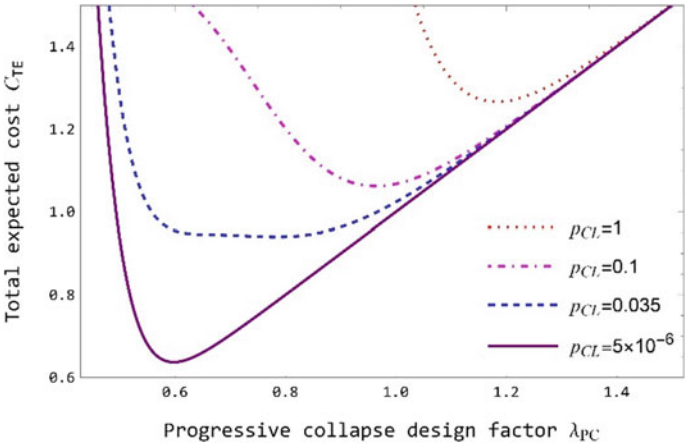


**Fig. 15.3** Total expected cost functions for different fifty-year column loss probabilities ($p_{CL}$)

$\lambda_{PC}$, for specific values of the fifty-year column loss probability ($p_{CL}$). Total expected costs grow for large $\lambda_{PC}$ (right) due to over-conservative design. The curves grow very fast for small $\lambda_{PC}$ (left) as one pays for expected consequences of failure. It can be observed in Fig. 15.3 that $p_{CL}$ plays a major role in controlling the objective function, and this justifies using Eq. (15.13) as a guide for optimal design under progressive collapse, in general, or discretionary column removal, as addressed herein.

As observed in Fig. 15.3, for $p_{CL} = 0.1$ the optimal design factor is nearly unitary ($\lambda^*_{PC} \approx 1$). For larger column loss probability, optimal $\lambda^*_{PC}$ is larger; for $p_{CL} < 0.1$, the optimum design factor $\lambda^*_{PC}$ is significantly smaller than unity. For $p_{CL} = 0.035$, we observe that the optimal design becomes indifferent to $\lambda^*_{PC}$ in the range $0.6 \lesssim \lambda^*_{PC} \lesssim 0.8$, as the objective function displays a flat bottom. The smallest column loss probability considered herein, $p_{CL} = 5 \times 10^{-6}$, is the fifty-year value corresponding to the *de minimis* risk of $10^{-7}$ per year [21], below which any threats can be neglected.

The first general result that can be derived from Fig. 15.3 is that design factors for discretionary column removal could be differentiated w.r.t. column loss probability. This possibility is discussed in [6], where a broader range of problems is addressed.

Usual design, under normal loading condition (Eq. 15.2), is compared in Fig. 15.4 with progressive collapse design using Eq. (15.3), and with optimal progressive collapse design using Eqs. (15.4) and (15.14). The figure compares total expected costs (Eq. 15.13) obtained with the three formulations, by considering the designs $z_{NLC}$, $z_{PC}$ and $z^*_{PC}$ (the last one, obtained from $\lambda^*_{PC}$). Total expected costs grow significantly for large $p_{CL}$, as could be expected, but especially for usual design, which ignores the impacts of column loss. For large $p_{CL}$ (or $p_{CL} > 0.05$ in figure), the progressive collapse design is clearly more economical, for obvious reasons. For $p_{CL} < 0.05$, usual design is more economical than progressive collapse design with

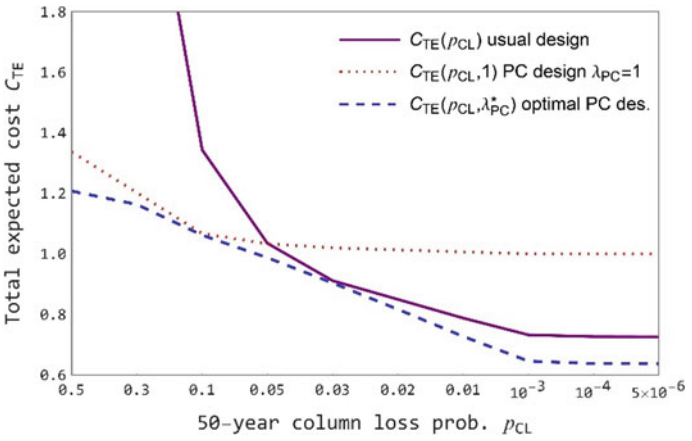


**Fig. 15.4** Total expected costs as function of $p_{CL}$, for usual design under normal loading conditions, and for optimal design under column loss; non-linear horizontal scale

$\lambda^*_{PC} = 1$. For $p_{CL} < 0.05$, the optimal progressive collapse design with $\lambda^*_{PC}$ is cheaper than usual design, but for a particular reason: it is the result of a problem-specific optimization, whereas conventional design reflects a code addressing whole classes of structures.

It is also observed in Fig. 15.4 that, for column loss probabilities in the range $0.05 \lesssim p_{CL} \lesssim 0.02$, the optimal progressive collapse and usual design yield similar results. This corresponds to the region of flat bottom objective function observed in Fig. 15.3, for $p_{CL} = 0.035$. In this region, the optimal design becomes indifferent to considering column loss, or not; the optimal $\lambda^*_{PC}$ becomes smaller than one, and the conditional reliability index $\beta_{CL}$ goes from positive to negative, as illustrated in Fig. 15.5. A conditional reliability index $\beta_{CL} = 0$ means a fifty-fifty chance of beam collapse in case of column loss, since $P[C|CL, H] = \Phi[0] = 0.5$.

As stated by Beck et al. [6], it does not make practical sense to design a beam or slab for load bridging over a failed column with zero or negative reliability index, or with $\lambda^*_{PC} \ll 1$. If the design factor is limited to $\lambda^*_{PC} \geq 1$, it becomes clear (see Fig. 15.4) that usual design is more economical than progressive collapse design, for small column loss probabilities. For the continuous beam addressed herein, progressive collapse design is more economical only for $p_{CL} > 0.05$ (Fig. 15.4).

## 15.4 The Column Loss Probability Threshold Concept

The observations above, and similar results presented in [6], covering typical RC floors and regular plane frames, led the authors to postulate the existence of a threshold column loss probability, $p^{th}_{CL}$, tentatively defined as:

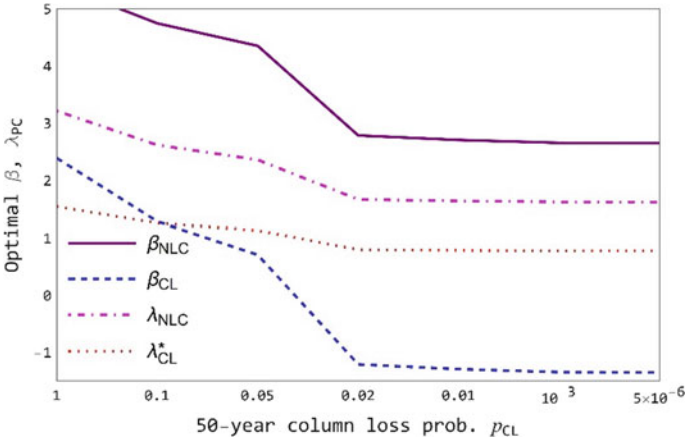


**Fig. 15.5** Optimal values of reliability indexes $\beta_{NLC}$ and $\beta_{CL}$, central safety factor under normal loading condition ($\lambda_{NLC}$) and optimal design factor for progressive collapse ($\lambda^*_{PC}$), as function of fifty-year column loss probability

> Column loss probability threshold $p^{th}_{CL}$ is the value above which design for load bridging under discretionary column removal has positive cost-benefit, in comparison to usual design.

Still citing [6]:

> The column loss probability threshold $p^{th}_{CL}$ varies for different structures, for different initial damage scenarios, for different strengthening actions and as a function of failure cost multiplier $k$. It may also vary w.r.t. loading and failure modes considered.

This remark is further analyzed herein, by looking into optimal design of regular plane frame buildings with different aspect ratios (number of stories $\times$ number of bays) and by considering different initial damage scenarios and strengthening actions. For the various problems addressed in [6], threshold column loss probabilities were found to be around $p^{th}_{CL} = 0.01$, or of this order of magnitude. As shown by Beck et al. [7], this value can change significantly with frame aspect ratio, initial damage and strengthening action.

## 15.5 Design of Regular Plane Frames

This example is based on and discusses results from Beck et al. [7]. Design of regular two-dimensional multi-storey multi-bay frames is considered, following the simple analytical model of [19]. The model considers bending failure of beams and crushing failure of columns. The collapse mechanisms are local bending, local crushing, and global pancake failures. The model considers possible transition of local crushing turning into bending collapse. In this context, Eq. (15.14) allows one

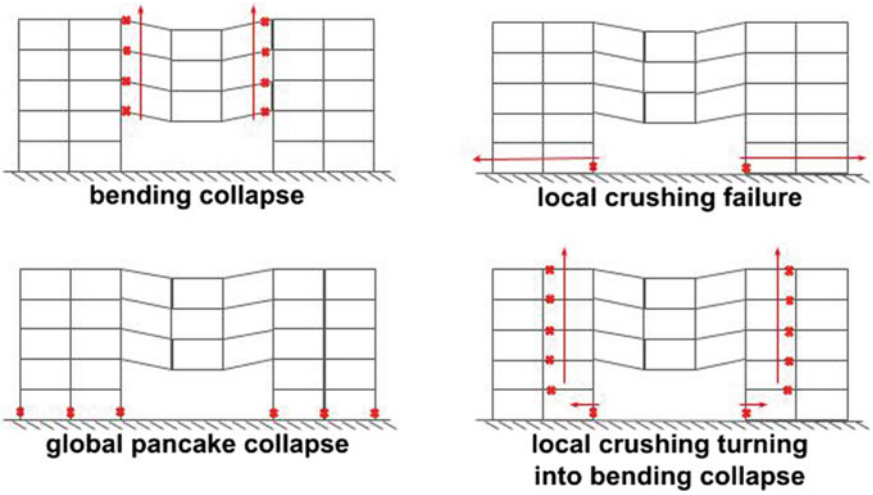


**Fig. 15.6** Sketch of regular plane frame collapse mechanisms

to obtain optimal or cost-effective compromise solutions between competing collapse modes. The problem is illustrated in Fig. 15.6.

The model considers regular frames with $n_c$ columns and $n_s$ stories, and an initial damage event leading to failure of $n_{r,c}$ columns and $n_{r,s}$ stories, where subscript $r$ is for 'removed'. Beam length is $L$ for all spans, and column height is $H$ for all stories. Ultimate strengths of beams and columns are evaluated considering brittle elastic and fully plastic material behaviors. Collapse of beams is by formation of plastic mechanism; local and global collapse of columns is by brittle elastic crushing. The complete model is presented in [19, 7]. Formulation of the design, reliability, cost and optimization problems is similar to Eqs. (15.2)–(15.14), with few significant differences:

(a) two design variables are considered, for the independent dimensioning (and strengthening) of beams and columns, $\lambda_{PC} = \{\lambda_B, \lambda_C\}$;
(b) strengthening involves increasing the steel reinforcement ratio of beam and columns; cost of steel is assumed as 70% of the cost of beams and columns;
(c) the strengthening action covers all columns and all beams of $n_{st} = 2$ stories; beams and columns are strengthened considering Eq. (15.4); columns are strengthened considering local load re-distribution;
(d) initial cost is given by total length of beam and column elements; failure costs are given by the area (total length of elements) affected by initial damage and by progressive collapse;
(e) Equation (15.13) is adapted to reflect the cascading failure events which may initiate with $n_{r,c}$ column failures: if local crushing failure occurs, bending failure may follow with $n_{r,c} + 2$, and so on, progressively, until crushing failure is naturally arrested, or until global pancake collapse.

**Table 15.2** Description of reference case and main problem variants, regular plane frame design

| Main problem variants | Aspect ratio $(n_s \times (n_c - 1))$ | Initial damage $(n_{r,c} \times n_{r,s})$ | $p_{CL}^{th}$ |
|---|---|---|---|
| *Reference* case: "square" frame | $(8 \times 8)$ | $(1 \times 1)$ | $1.0 \times 10^{-2}$ |
| Design for increased damaged area[a] | $(8 \times 8)$ | $(3 \times 2)$ | $3.0 \times 10^{-2}$ |
| Tall frame | $(16 \times 4)$ | $(1 \times 1)$ | $1.6 \times 10^{-3}$ |
| Low frame | $(4 \times 16)$ | $(1 \times 1)$ | $5.0 \times 10^{-2}$ |

[a]This is similar to the case considered in [6]

Herein, we start by considering a building similar to that addressed in [6]: the number of stories and columns is $(n_s \times n_c) = (8 \times 9)$; aspect ratio of the regular bays is $(L \times H) = (6 \times 3)$ meters; the live-to-dead load ratio is $L_n/D_n = 1$; failure cost multipliers are $k = 10$ for ductile beam bending failures, and $k = 20$ for column brittle elastic crushing failures.

The frame is subjected to different magnitudes of initial damage, given by numbers of removed columns $(n_{r,c})$ and number of removed stories $(n_{r,s})$, as detailed in Table 15.2. In this problem, the column loss probability $p_{CL}$ actually refers to this initial damage event. We start by considering the progressive collapse design for a single removed column: using Eq. (15.4), we design beams and columns of the first two stories $(n_{st} = 2)$ to bridge over a single removed column $(n_{r,c} = n_{r,s} = 1)$. This is the *reference* case in Table 15.2.

In the second main case, we consider increased initial damage, with $(n_{r,c} \times n_{r,s} = 3 \times 2)$; strengthening of the first two floors $(n_{st} = 2)$.

Finally, we consider seven different frame configurations, by keeping the approximate same tributary area $(n_s \times (n_c - 1))$, and proportionally increasing/reducing the number of stories/bays. The limiting cases are a tall building with 16 stories by 4 bays, and a low building with 4 stories and 16 bays.

### 15.5.1 Results: Comparison of Total Expected Costs

We start by comparing results in terms of total expected cost of the alternative designs. Figure 15.7 illustrates the total expected cost functions for the *reference* case, considering usual design under normal loading conditions (Eq. 15.2), progressive collapse design using the ASCE formula (Eq. 15.3) and optimal progressive collapse design using Eqs. (15.4) and (15.14). The general trend is the same observed for the continuous beam problem (Fig. 15.4), and the threshold column loss probability is around $p_{CL}^{th} \approx 0.01$. The optimal design has a larger margin *w.r.t.* the two design alternatives, as observed in Fig. 15.7.

Figure 15.8 shows similar results for the case with larger initial damage, for which

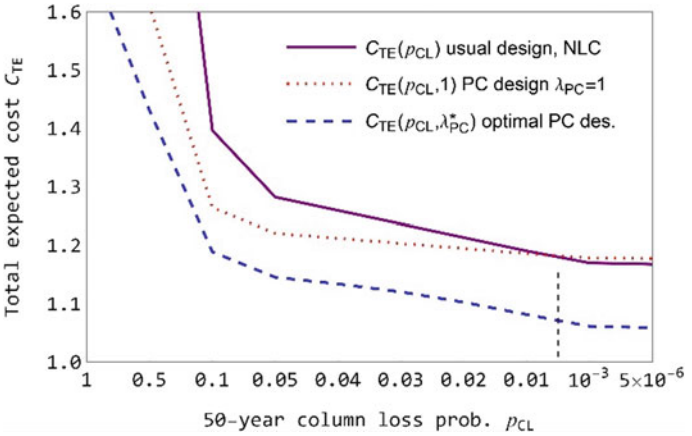


**Fig. 15.7** Total expected costs as function of $p_{CL}$, for *reference* case ((8 × 8) frame, (1 × 1) initial damage); non-linear horizontal scale

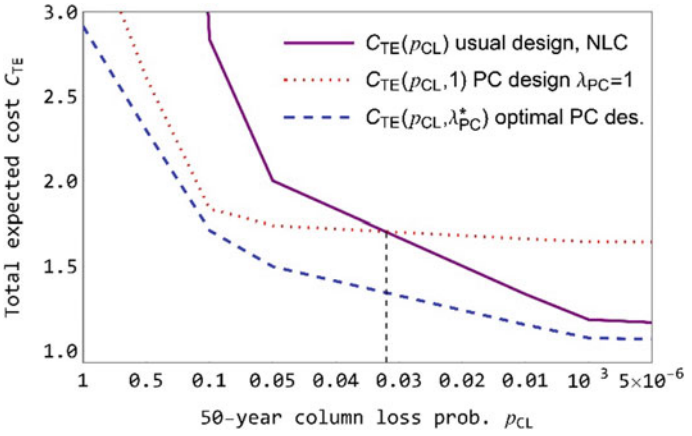


**Fig. 15.8** Total expected costs as function of $p_{CL}$, for increased initial damage ((8 × 8) frame, (3 × 2) initial damage); non-linear horizontal scale

$p_{CL}^{th} \approx 0.03$ is obtained. As observed, designing the same (8 × 8) frame to sustain loss of three columns of two floors is cost-effective only for a larger column loss probability value, because the strengthening cost is significantly higher. Hence, the impact in construction cost is justified only for larger threat probabilities.

Threshold column loss probabilities in Figs. 15.7 and 15.8 were determined by comparing total expected costs for usual design condition, with those for progressive collapse design using recommended design factors ($\lambda_{PC} = 1$). This is convenient, as it relates the threshold probability with familiar design concepts. However, when the optimization problem in Eq. (15.14) is solved, the threshold probability appears as a

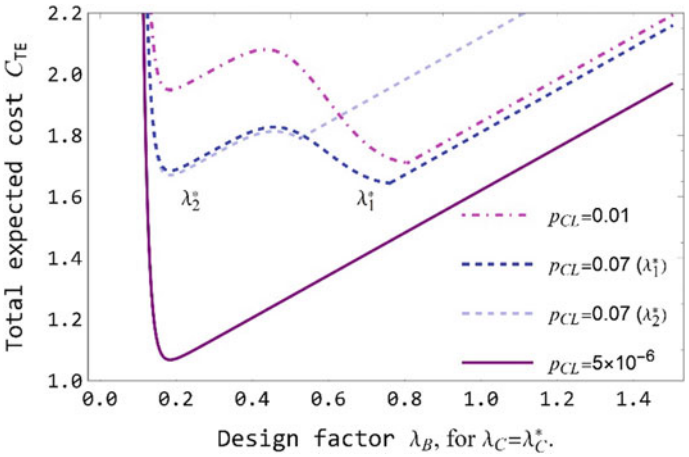


**Fig. 15.9** Total expected costs as function of $\lambda_B$, for specific values of $p_{CL}$. For $p_{CL} = 0.07$, two local minima can be observed

point of indifference, where design for load bridging and usual design have similar total expected costs [6]. This was illustrated in Fig. 15.3, for the continuous beam problem. Similar results are presented in Fig. 15.9 for the regular frame, with large initial damage ($n_{r,c} \times n_{r,s} = 3 \times 2$). In this figure, two local minima can be observed: $\lambda_1^* = \{\lambda_B^*, \lambda_C^*\} = \{0.76, 0.93\}$; and $\lambda_2^* = \{0.18, 0.74\}$; with similar objective function values: $C_{TE}(\lambda_1^*) = 1.64$; $C_{TE}(\lambda_2^*) = 1.67$. Clearly, $\lambda_1^*$ corresponds to load bridging design with reduced design factors (as strengthening costs are significant), whereas $\lambda_2^*$ corresponds to usual design. Note that the reference value $\lambda_{PC} = 1$ corresponds to progressive collapse design (Eq. 15.4). Design of the beams to bridge over three failed columns requires 6.19 times greater strength, w.r.t. usual design, hence $6.19 \times 0.18 = 1.11$ corresponds approximately to usual design. Finally, it is observed that the load bridging design with $\lambda_1^*$ is more robust than the design with $\lambda_2^*$, as near $\lambda_2^*$ expected costs of failure rise sharply (Fig. 15.9).

As observed in Figs. 15.8 and 15.9, as well as in Figs. 15.3 and 15.4, the threshold column loss probability obtained by comparing total expected costs ($p_{CL}^{th} \approx 0.03$), for usual versus progressive collapse design, is close to the value for which optimal design is indifferent to strengthening for load bridging ($p_{CL}^{th} \approx 0.07$).

### 15.5.2 *Results: Probability Threshold $p_{CL}^{th}$ for Other Frame Aspect Ratios*

We now consider frame structures with different aspect ratios, as described in Table 15.2. The tall frame has 16 stories by 4 bays: $(n_s \times (n_c - 1)) = (16 \times 4)$; the low frame is $(4 \times 16)$. Intermediate cases, with similar tributary area, are shown in

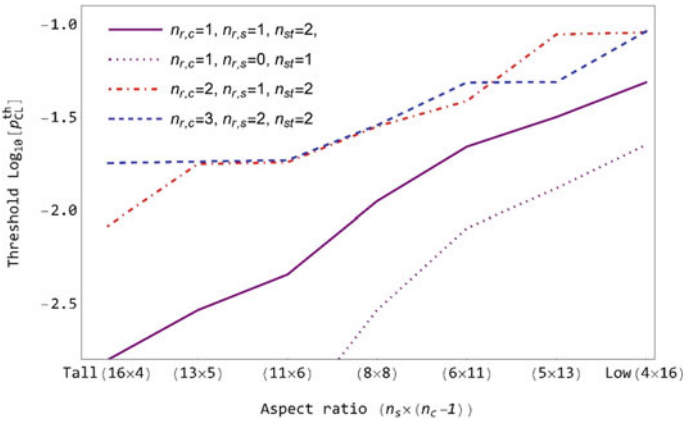


**Fig. 15.10** Threshold column loss probabilities, as function of frame aspect ratio, and for different number of removed columns ($n_{r,c}$), removed stories ($n_{r,s}$) and strengthened stories ($n_{st}$). With data from Beck et al. [7]: $k = 20$ for ductile bending failure, $k = 40$ for brittle column crushing failure

Fig. 15.10, which illustrates change in column loss probability thresholds in terms of frame aspect ratio. These results are taken from Beck et al. [7], and $p_{CL}^{th}$ values refer to the point of indifference in optimal design, or to the root for which the bending reliability index is zero ($\beta_B = 0$). As observed, the taller the building, the smaller the value of $p_{CL}^{th}$. Hence, for taller frames, smaller threat probabilities justify the strengthening action, since failure consequences are proportional to building height (bending collapse propagates upwards). Figure 15.10 shows results for a single column removed from one story, up to three columns removed from two stories.

The strengthening action involves all columns and beams of either one or two stories. As observed, strengthening of a single story to sustain loss of a single column is justified for a larger number of frames, as $p_{CL}^{th}$ is minimal. The strengthening of two stories (as one cannot exactly anticipate what the initial damage extend may be) is justified only for larger threat probabilities (larger $p_{CL}^{th}$). The decision to strengthen two stories to sustain loss of two or three columns is justified only for even higher column loss probabilities.

As observed, the threshold column loss probability $p_{CL}^{th}$ depends on the magnitude of potential consequences (number of building stories), on the possible extent of initial damage, and on the strengthening decision. Table 15.3 summarizes the above results, also including results shown elsewhere (as stated in Table).

Threshold column loss probabilities were evaluated in Beck et al. [7] for an extensive range of frames of different aspect ratios, considering also different bay aspect ratios, failure cost multipliers, strengthening extents and extents of initial damage. Results of threshold column loss probabilities obtained in Beck et al. [7] are summarized in Fig. 15.11, where they are also compared with threshold values by different authors, and to threat probabilities for common structural threats. As observed, threshold probabilities for small and medium buildings agree with values

**Table 15.3** Summary of column loss probability threshold effects

| Factors which reduce $p_{CL}^{th}$, making PC design more economical over a wider range of $p_{CL}$ values | Factors which increase $p_{CL}^{th}$ |
|---|---|
| Increased failure consequences: larger $n_s$, larger failure cost factors $k$[a] | Reduced failure consequences: smaller $n_s$ and failure cost factors $k$[a] |
| Reduced strengthening decision: design for smaller damaged areas, or for smaller $n_{r,c}$,$n_{r,s}$ | Increased reinf. decision: design for larger damaged areas, reinforce greater number of floors |
| Increased relative weight of brittle column failure, or smaller number of bays $(n_c - 1)$ | Reduced relative weight of brittle column failure, or larger number of bays |
| Smaller uncertainty in load and strength variables[a] | Larger uncertainty in load and strength variables[a] |

[a]As shown in [6]

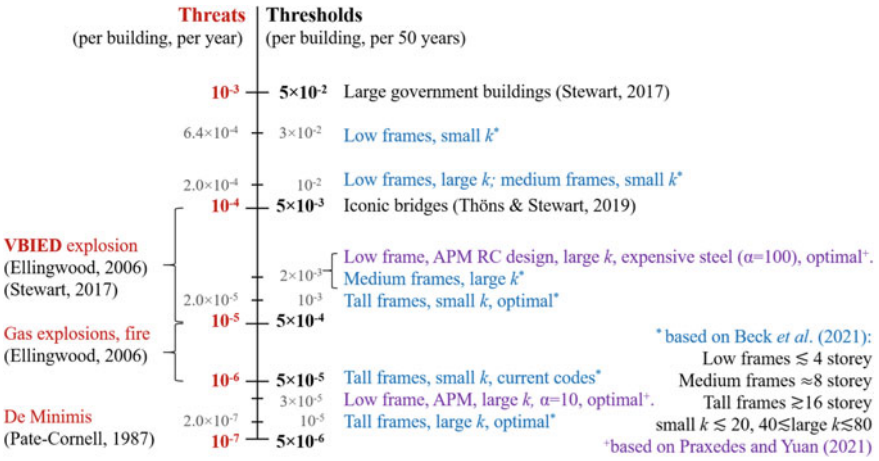


**Fig. 15.11** Comparison of threat and threshold probabilities (not to scale, $k$ = consequence cost factor, frame results for limited strengthening extent)

found in the literature [20–24, 27, 29]. However, threshold probabilities for high buildings can be significantly smaller, justifying progressive collapse design and strengthening for taller buildings.

### *15.5.3 Results: Comparison of Optimal Design Factors*

Figure 15.12 illustrates the optimal beam bending ($\lambda_B^*$). and column crushing ($\lambda_C^*$) design factors obtained by solving the optimization problem (Eq. 15.14), for the *reference* case, and for increased initial damage. These optimal factors correspond

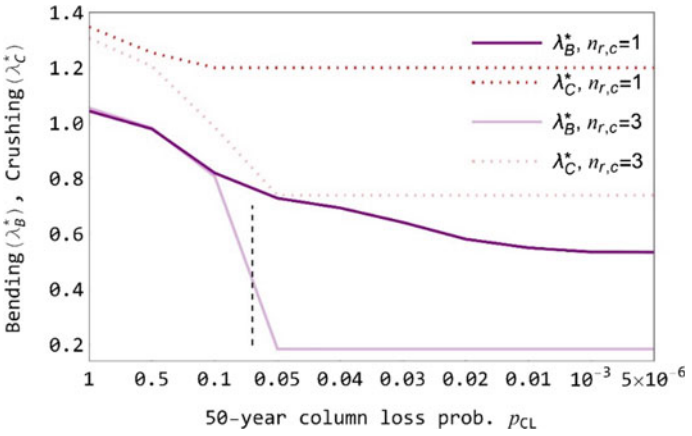


**Fig. 15.12** Optimal values of design factors for *reference* frame (8 × 8), for small ($n_{r,c} \times n_{r,s} = 1 \times 1$) and large ($n_{r,c} \times n_{r,s} = 3 \times 2$) initial damage; both with $n_{st} = 2$

to the $C_{TE}\left(p_{CL}, \lambda_{PC}^*\right)$ results in Figs. 15.7 and 15.8, with $\lambda_{PC}^* = \left\{\lambda_B^*, \lambda_C^*\right\}$. As observed in Fig. 15.12, the column loss probability is indeed a relevant problem parameter, as the optimal design factors $\lambda_B^*$ and $\lambda_C^*$ vary significantly with $p_{CL}$.

The optimal design factor for bending is smaller than unitary for most values of $p_{CL}$, and slightly larger than one just for $p_{CL} > 0.5$. This shows that the design factors of Eq. (15.3) could perhaps be adjusted to reflect column loss probabilities, as discussed in [6]. The optimal column crushing design factor is larger than one[1], and nearly constant, for $n_{r,c} = 1$. Yet, $\lambda_B^*$ and $\lambda_C^*$ change significantly with $p_{CL}$ for $n_{r,c} = 3$. The large drop in $\lambda_B^*$ and $\lambda_C^*$ occurs for $p_{CL} \approx 0.07$; it was shown in Fig. 15.9 that this corresponds to a transition, where optimal design goes from load bridging, with reduced design factors, to usual design under normal loading condition.

These results, and the differences observed in cost functions in Figs. 15.7 and 15.8, justify employing a risk-optimization approach in building design for discretionary column removal, especially for threats leading to $p_{CL} > p_{CL}^{th}$, as illustrated herein.

Figure 15.13 compares the optimal design factors in terms of frame aspect ratio, for initial damage equal to $(n_{r,c} \times n_{r,s}) = (1 \times 1)$. Following the trend of Fig. 15.12, optimal values of $\lambda_B^*$ vary significantly with column loss probability. Larger values of $\lambda_B^*$ are justified for taller buildings, as the consequences of local bending collapse propagate upwards.

For the low frames illustrated in Fig. 15.13, threshold column loss probabilities are $p_{CL}^{th} \approx 0.05$. Hence, optimal $\lambda_B^*$ values increase rapidly for $p_{CL} > p_{CL}^{th}$. Optimal values of $\lambda_C^*$ are insensitive to $p_{CL}$ for low frames, but significantly larger than one. As shown by Beck et al. [7], this is to avoid horizontal propagation of local

[1] For simplicity, columns were designed using the same 0.85 design factor of beams. Hence, $\lambda_C = 0.85/0.65 = 1.3$ is close to the ACI recommended design value for compression-controled elements.

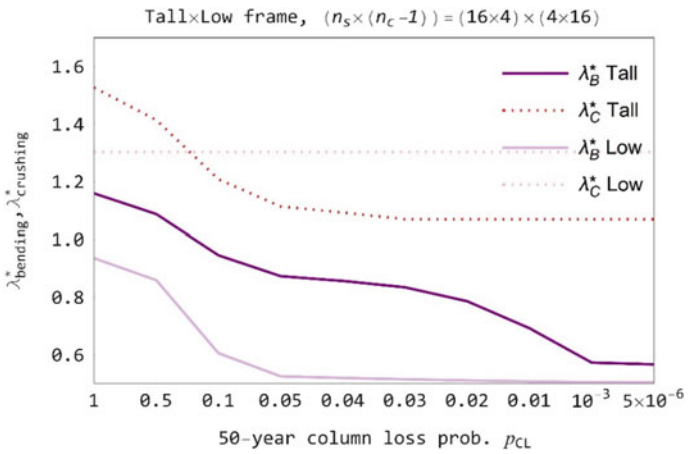


**Fig. 15.13** Optimal values of design factors for tall and low frames, initial damage $(n_{r,c} \times n_{r,s}) = (1 \times 1)$, $n_{st} = 2$, non-linear horizontal scale.

crushing failures, which could eventually propagate to the full horizontal extent of the frame. For the taller frames, most $p_{CL}$ values shown in Fig. 15.13 are above $p_{CL}^{th} \approx 1.6 \times 10^{-3}$. Hence, optimal values of $\lambda_B^*$ and $\lambda_C^*$ are more sensitive to changes in $p_{CL}$. Optimal $\lambda_C^*$'s increase rapidly from 1.1 to 1.55, as $p_{CL}$ increases from 0.05 to 1. This is perhaps justified by the extensive potential damage, caused by losing one column of a building with only five.

## 15.6 Conclusions

In this chapter, we discussed optimal cost-benefit design for progressive collapse, given abnormal accidental or malevolent actions. This problem of decision making in presence of uncertainty was formulated by considering the probability of losing a load-bearing element as an independent parameter, and by combining normal loading and abnormal loading conditions in the same objective function. This allowed us to demonstrate existence of a threshold column loss probability: above this value, strengthening beams or slabs for load bridging over failed columns has positive cost-benefit, in comparison to usual design. It is understood that column loss probabilities are evaluated from an encompassing risk analysis addressing structural use, ownership, and building adjacency.

Design for progressive collapse, considering discretionary column removal, is more cost-effective for larger threat probabilities, and when failure consequences are large, such as for taller buildings, and for larger failure cost multipliers. Cost-effectiveness of design for progressive collapse is strongly dependent on the strengthening decision, which includes the size of the initial damage considered, and the

decision on the numbers of stories/bays to be strengthened. The strengthening is more cost-effective when it has smaller impacts on construction costs.

For the regular plane frame example, interesting behavior was observed in terms of optimal design factors for beam bending and column crushing, for different structural configurations. The observed behavior is related to competition between local bending, local crushing, and global pancake collapse failures modes. As shown by Beck et al. [7], the strengthening budget needs to be optimally allocated to keep a good balance between these competing failure modes. The optimal balance changes as a function of building aspect ratio, and according to the probability of a column loss event.

**Acknowledgements** Funding of this research by joint project FAPESP-ANID (São Paulo State Foundation for Research—Chilean National Agency for Research and Development, grant n. 2019/13080-9) is gratefully acknowledged.

## References

1. ASCE/SEI 41-13 (American Society of Civil Engineers) (2017) Seismic evaluation and retrofit of existing buildings, ISBN: 9780784477915
2. ASCE 7 (American Society of Civil Engineers) (2010) Minimum design loads for buildings and other structures
3. Beck AT (2020) Optimal design of hyperstatic redundant structural systems: fundamentals. Eng Struct 219:110542. https://doi.org/10.1016/j.engstruct.2020.110542
4. Beck AT, Gomes WJS (2012) A comparison of deterministic, reliability-based and risk-based structural optimization under uncertainty. Probab Eng Mech 28:18–29. https://doi.org/10.1016/j.probengmech.2011.08.007
5. Beck AT, Gomes WJS, Lopez RH, Miguel LFF (2015) A comparison between robust and risk-based optimization under uncertainty. Struct Multidisc Optim 52:479–492. https://doi.org/10.1007/s00158-015-1253-9
6. Beck AT, Ribeiro LR, Valdebenito M (2020) Risk-based cost-benefit analysis of frame structures considering progressive collapse under column removal scenarios. Eng Struct 225.https://doi.org/10.1016/j.engstruct.2020.111295
7. Beck AT, Ribeiro LR, Valdebenito M, Jensen H (2022) Optimal design of regular frame structures subject to column loss events: a conceptual study. ASCE J Struct Eng 2022, 148(1). https://doi.org/10.1061/(ASCE)ST.1943-541X.0003196
8. DoD (Department of Defense) (2013) Design of buildings to resist progressive collapse. UFC 4–023–03, Washington, DC
9. EN 1990 (2002) Basis of structural design. European Committee for Standardization, Brussels
10. Ellingwood B (2006) Mitigating risk from abnormal loads and progressive collapse. J Perform Constr Facil 20(4):315–323. https://doi.org/10.1061/(ASCE)0887-3828(2006)20:4(315)
11. Ellingwood B (2007) Strategies for mitigating risk to buildings from abnormal load events. Int J Risk Assess Manage 7(6):828–845. https://doi.org/10.1504/IJRAM.2007.014662
12. Ellingwood B, Galambos TV (1982) Probability-based criteria for structural design. Struct Saf 1:15–26
13. Ellingwood B, Leyendecker EV (1978) Approaches for design against progressive collapse. J Struct Div (ASCE) 104(ST3):413–423
14. Ellingwood B, Dusenberry D (2005) Building design for abnormal loads and progressive collapse. Comput Aided Civ Infrastruct Eng 20(3):194–205. https://doi.org/10.1111/j.1467-8667.2005.00387.x

15. GSA (General Services Administration) (2013) Alternate path analysis and design guidelines for progressive collapse resistance. Washington, DC
16. He XHC, Yuan XX, Yi WJ (2019) A non-iterative progressive collapse design method for RC structures based on virtual thermal pushdown analysis. 189:484–496. https://doi.org/10.1016/j.engstruct.2019.03.102
17. JCSS (2001) Probabilistic model code. Joint Committee on Structural Safety, published online. http://www.jcss.byg.dtu.dk/Publications/Probabilistic_Model_Code. Accessed on 27 July 2017
18. Marchand KE, Stevens DJ (2015) Progressive collapse criteria and design approaches improvement. J Perform Constr Facil (ASCE) 29(5):B4015004. https://doi.org/10.1061/(ASCE)CF.1943-5509.0000706
19. Masoero E, Darò P, Chiaia BM (2013) Progressive collapse of 2D framed structures: an analytical model. Eng Struct 54:94–102. https://doi.org/10.1016/j.engstruct.2013.03.053
20. Melchers RE, Beck AT (2018) Structural reliability analysis and prediction. 3rd edn. Wiley, ISBN: 978-1-119-26599-3
21. Pate-Cornell E (1987) Quantitative safety goals for risk management of industrial facilities. Struct Saf 13(3):145–157. https://doi.org/10.1016/0167-4730(94)90023-X
22. Praxedes C (2020) Robustness-based optimal progressive collapse design of RC frame structures. Ph.D. Thesis, Ryerson University, Toronto, Ontario, Canada
23. Praxedes C, Yuan X-X (2021) A novel robustness assessment methodology for reinforced concrete frames under progressive collapse threats. J Struct Eng 147(8):04021119. https://doi.org/10.1061/(ASCE)ST.1943-541X.0003075
24. Praxedes C, Yuan X-X (2022) Robustness-oriented optimal design for reinforced concrete frames considering the large uncertainty of progressive collapse threats. Struct Saf 94:102139. https://doi.org/10.1016/j.strusafe.2021.102139
25. Shi Y, Stewart MG (2015) Spatial reliability analysis of explosive blast load damage to reinforced concrete columns. Struct Saf 53:13–25. https://doi.org/10.1016/j.strusafe.2014.07.003
26. Singh K, Gardoni P, Stochino F (2020) Probabilistic models for blast parameters and fragility estimates of steel columns subject to blast loads. Eng Struct 222:110944. https://doi.org/10.1016/j.engstruct.2020.110944
27. Stewart MG (2017) Risk of progressive collapse of buildings from terrorist attacks: are the benefits of protection worth the cost? J Perform Constr Facil 31(2):04016093
28. Tessari RK, Kroetz HM, Beck AT (2019) System reliability-based design optimization and risk-based optimization: a benchmark example considering progressive collapse. Eng Optim 51:1000–1012. https://doi.org/10.1080/0305215X.2018.1502760
29. Thöns S, Stewart MG (2019) On decision optimality of terrorism risk mitigation measures for iconic bridges. Reliab Eng Syst Saf 188:574–583. https://doi.org/10.1016/j.ress.2019.03.049
30. Vrouwenvelder T (1997) Probabilistic model code—part 1. Struct Saf 19:245–251

# Chapter 16
# Durability and Performance of Wind Turbines Under Climate Extremes


**Rui Teixeira, Alan O'Connor, and Dimitri V. Val**

**Abstract** This chapter discusses the impact which durability considerations and climate extremes play on the performance of wind turbine structures. An overview of the technological developments in wind energy production, both onshore and offshore, is provided. The rigorous design requirements and specifications, guidelines and codes of practice prescribed for design are discussed. The basis for computational simulations, necessary to model and assess performance is outlined. Characterization of extreme values is discussed and the impact of climate extremes on environmental loads is demonstrated. The impact of deterioration, in the context of the durability of wind turbine towers is evaluated in terms of the probability of exceedance of specified limit states. Finally, discussion is provided around optimal decision-making regarding design, operation and maintenance.

## 16.1 Introduction

The demand for renewable energy is unquestionable. Global climate trends have highlighted the need for renewable, low carbon-footprint technologies, and wind energy is one of the most prominent alternatives to conventional fossil fuel energy conversion. The fact that wind depends on the Sun, makes it a virtually infinite source of energy.

According to Frick et al. [17], approximately 2.5% of the total solar energy incident on the outer layer of the earth's atmosphere is transformed into wind energy. This equates to an overall wind power of approximately $4.3 \times 10^{15}$ Watts or an

R. Teixeira
School of Civil Engineering, University College Dublin, Dublin, Ireland

A. O'Connor (✉)
Department of Civil, Structural & Environmental Engineering, Trinity College Dublin, Dublin, Ireland
e-mail: OCONNOAJ@tcd.ie

D. V. Val
Institute for Infrastructure and Environment, Heriot-Watt University, Edinburgh, UK



M. G. Stewart and D. V. Rosowsky (eds.), *Engineering for Extremes*, Springer Tracts in Civil Engineering, https://doi.org/10.1007/978-3-030-85018-0_16

equivalent annual energy resource of $3.8 \times 10^7$ Terrawatt hours (TWh). Technically, there is more energy provided by the wind than could ever possibly be required. As a result, wind energy has experienced an exponential growth in installed power since the beginning of the current century. In particular during the last decade, the increase in the development of wind energy has been substantial. While this growing trend is expected to continue, further growth of the sector imposes more demanding, complex and accurate engineering analyses that need to enclose not only considerations of the in-service performance of turbines, but also of the impact of climate change on these.

Although various types of wind turbines have been tried and tested over the years, the wind energy industry appears to have settled on one particular design, the horizontal axis wind turbine (HAWT). This was determined as the most reliable, cost effective and straightforward solution, which currently accounts for practically every megawatt of global installed capacity. Figure 16.1a illustrates a basic outline of these machines. An electric generator, located inside the nacelle, is driven by a rotor shaft connected to a set of aerofoil blades. While some designs have been known to operate with one or two blades, the current standard is predominantly a three-blade design. The rotational kinetic energy of the rotor shaft is generated by harnessing the aerodynamic lift force as the airflow interacts with the aerofoil profile of the blades. This is the same principle which allows aircrafts to fly. In order for the blades to be positioned within the airflow the turbine must be elevated into the air by a support structure, a tower. The height of the tower is dependent on the particular turbine design (mainly, on the length of the blades), and the advantages of an increased blade length and elevation off the ground surface are well documented. In the present, blades that span longer than 100 m are being produced and towers for wind turbines with such blades are typically over 150 m. Hub heights that can surpass 250 m may be reached in some offshore wind installations.

By their nature, wind turbines are machines that exhibit particularly complex dynamic behavior. The continuous rotation of the blades within turbulent aerodynamic loading induces a variable reaction from the system. This is further accentuated by the flexibility of the blades, tower and other components. As the size of these machines increases, the magnitude of the dynamic response increases as well.

The primary dynamic effects observed in wind turbines are illustrated in Fig. 16.1b, c. In-plane bending of wind turbine blades is shown in Fig. 16.1b. This motion can be referred to as "edgewise" vibration, although some authors may use the term "lead-lag" vibration. Out-of-plane blade bending can be seen in Fig. 16.1c. This can be referred to as "flapwise" vibration, although the term "pitching" vibration is sometimes used in the literature. As blades extend to considerable lengths, the effect of blade torsion is also an important consideration in the blade design. The lateral and longitudinal vibration of the tower is also displayed in Fig. 16.1. Further dynamic effects include nacelle tilt, roll and yaw.

In recent years progressively more wind turbines have been installed offshore. As a reference, the European Union (EU) plans to reach 70 GW of installed capacity for offshore wind by 2030. In the case of offshore wind turbines (OWT), the contribution and role of engineering practices and procedures for cost reduction and reliability

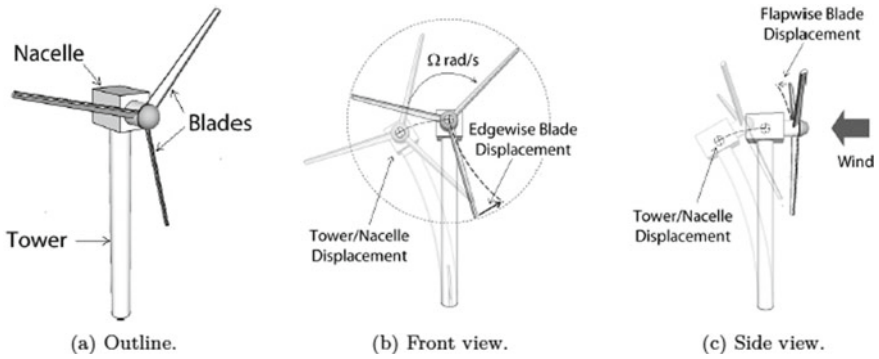


**Fig. 16.1** Outline of wind turbine components and dynamics [47]

enhancement is significant. In fact, IRENA [28] highlights that innovation in wind turbine design and operation has been a key driver for competitiveness in the wind energy sector. Iván et al. [30] identifies that research, along with a regulatory framework, are expected to be the key drivers of development for offshore wind up to 2050. In this context, while improvement of the techniques applied in the wind energy sector are in high demand, the development of innovative practices is no less important to enable the sector to become progressively more competitive.

Figure 16.2 shows that despite the significant developments in the two last decades, the Levelized Cost of Energy (LCOE), i.e., a ratio that includes the operational lifetime costs and divides it by the benefit of energy production, for OWT installations is just now achieving the level of economic competitiveness of conventional alternatives used for electricity production (e.g., fossil fuels). Wind, nevertheless, is one of the most powerful energy resources available on earth.

In the last decade, scale-up of wind turbines has been a major driver of economic competitiveness for the sector. Larger turbines mean more installed capacity and access to a larger resource, which contributes to amortize the project development costs faster. In this context, increases in the size of blades and tower height have been a major driver to decrease the LCOE for wind turbines [28]. The fact that the technological solution to harness the wind power is well established enables the sector to improve competitiveness through scale-up. Larger turbines, however, present increased challenges in engineering design.

An area of particular focus is the need to address uncertainty in the analysis and design of wind turbines. By enhancing the characterization and understanding of uncertainties, the sector can move towards more robust and optimized designs. Uncertainty characterization unlocks a new dimension of comprehension in design. Perception of the potential deviations experienced by the design variables enables a more complete understating of the risks associated with the operation of wind turbines [52].

Taking into account uncertainty in the design process is usually facilitated by probabilistic analyses. A brief evaluation of the standards for designing wind

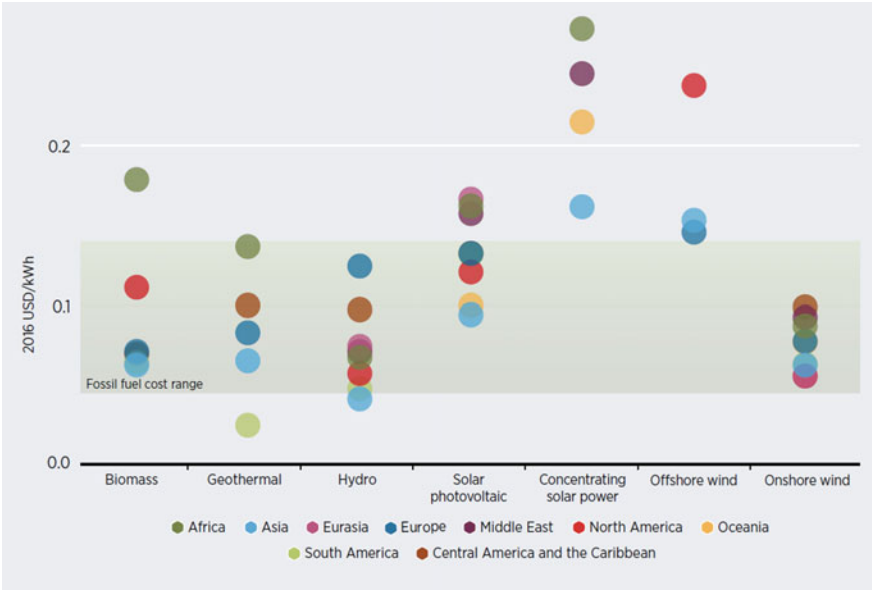


**Fig. 16.2** Levelized Cost of Energy (LCOE) for different sources of renewable energy divided by region, IRENA [28]

turbines (IEC 61400 class) or other recommended guidelines, such as DNV GL guidelines [12–15], shows that assessing uncertainty is a recurrent procedure inside the design chain. Nonetheless, only limited research has been developed so far in addressing some important future sources of uncertainty, such as climate change.

With regard to the wind turbine structural performance, some components are not allowed to fail; or more exactly, in the context of the probabilistic approach, the target annual probability of failure for such components is low $-10^{-4}$ (or $10^{-5}$ when failure can endanger personnel) [14]. For other components, which are less important to maintain a functioning a wind turbine (i.e., their failure does not cause the loss of the turbine or its inability to operate for a long period of time), the target probability of failure may be higher. In principle, when failure of a component does not represent danger to personnel and/or the environment, the target safety level of the component can be determined from purely economic considerations. This distinguishes two levels of relevance for the system's survivability per component—critical and non-critical.

The critical components account for most of the turbine cost breakdown. These are key structural elements of large dimensions, such as blades and tower. Failure of one of these elements usually results in either total loss of the system or prolonged disruption of its operation. The blades and tower alone account for more than 40% of the cost for a 6-MW wind turbine [5]. At the same time, according to IRENA [28], turbines comprise 64 to 84% of onshore, and 30 to 50% of offshore, wind energy projects costs. Foundations alone may account for 20% of the project total

cost. Therefore, design optimization and improvement of these critical components is essential for further reduction of the LCOE for wind energy. This should be done by taking into account impacts of climate change, in particular its extremes, which may affect both durability and performance of wind turbines.

## 16.2 Design Requirements

Design of wind turbines is regulated by different standards and support documents, which specify a set of requirements for the design. The most widely accepted standards are those of the International Electrotechnical Commission (IEC) series 61400, which are complemented by other standards, such as Det Norske Veritas—Germanischer Lloyd (DNV GL) standards and recommendations, and the International Organization for Standardization (ISO) standards.

The IEC [26] sets the requirements for the design of onshore wind turbines, while IEC [27] does so for offshore wind turbines. There are overlaps between these standards. There are also many references in IEC [26, 27]. Furthermore, it is also common for IEC [26] to direct some of more detailed requirements regarding the design to other standards such as the ones published by the ISO. Due to the inherent complexity of the design, the terms such as appropriate, reliable, or adequate are also frequently used in the standards. This implies that different techniques may be used in the design process if these are ensured as appropriate.

Regarding the design for operational conditions, two major issues can be highlighted: the loading and the response. In the scope of the loading are included the variables which are going to induce loading on a wind turbine, including their interaction with the system. Furthermore, changes in the loading profiles as a result of factors such as climate change should be considered. All aspects of the analysis which concern the response of a wind turbine to the loading variables, including durability-related effects, are in the scope of the response.

Figure 16.3 shows a simplified representation of the loading, response, some pivotal engineering concepts, and their interaction [52]. Within the loading scope are also different environmental conditions that will interact with the system. These manifest in loading through hydrodynamics (for sea conditions—OWTs only), aerodynamics (for wind conditions), and other external environmental or non-environmental conditions which generate additional types of physical interactions (e.g., ice loading, vessel loading), and their coupled behaviour.

The response tackles the analysis, as the name indicates, of the system's response and its dynamics. Most of the analysis addresses the response of the system and its reliability. For design purposes, structural response is usually assessed in the context of two types of ultimate limit states: ultimate strength and fatigue. The "feedback" from the structural response is what affects the electrical response, e.g., production of energy. The control and protection system overlaps both knowledge areas and their interactions.

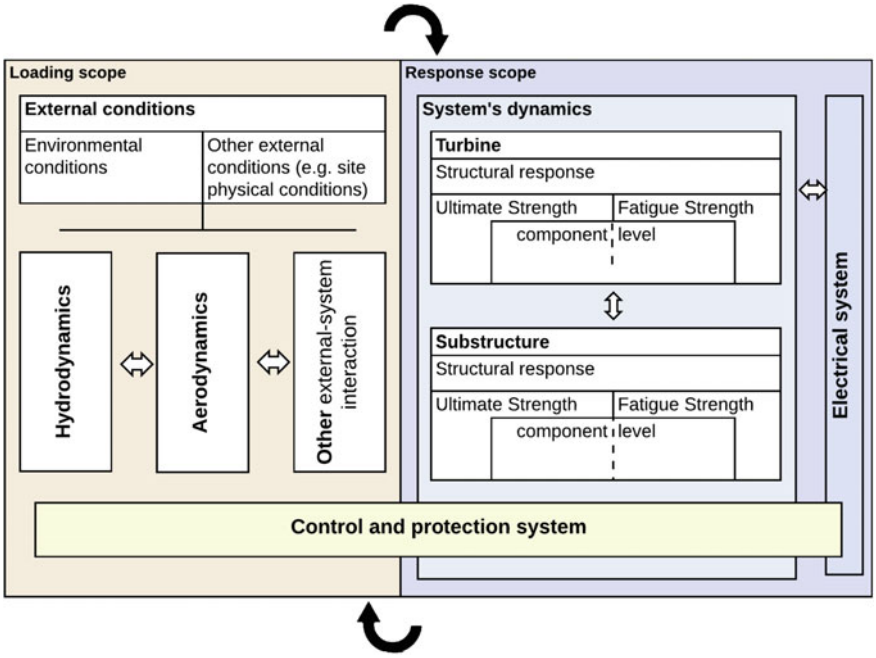


**Fig. 16.3** Design interaction of the loading and response for OWT operation regimes [52]

IEC [26, 27] recommends to base the structural analysis of wind turbines on ISO [29], indeed, many wind turbine design standards are built upon relevant ISO standards. DNV [14] presents an organized structure of assumptions for the design of OWTs, but also with many references to the ISO standards. DNV GL also offers a range of guidelines such as DNV [13, 15] for the design of offshore structures, which are of relevance to OWTs.

In order to produce robust designs, the IEC 61400 defines a set of Design Load Cases (DLCs), which represent various operational scenarios for the purpose of design. Each DLC is a set of operational conditions, which may occur during the lifetime of a wind turbine.

Among the DLC events, which must be analyzed, are environmental conditions represented by Normal Wind Profile (NWP), Normal Turbulence Model (NTM), Extreme Wind Model (EWM), Extreme Turbulence Model (ETM), Extreme Coherent Gust With Direction Change (ECD), Extreme Wind Shear (EWS), Extreme Operating Gust (EOG), and Extreme Direction Change (EDC). The DLCs are configured to simulate a variety of situations including normal power production, power production with a fault occurrence, a startup event, normal shut down, emergency shut down, parked conditions, parked with a fault, and transportation. Some of the faults, which are common to wind turbines, include a control system failure, electrical faults, and the loss of the electrical network connection. Within the load cases, both ultimate

and fatigue loads are included. Furthermore, it is clear that climate change may affect the probabilities and, thereby, return periods associated with environmental loads.

While a wind turbine must be capable of resisting the most extreme wind conditions for the ultimate limit-state (ULS), it is often the fatigue loading of the turbine which dictates the design. Hau [22] states that wind turbines are the perfect fatigue machines, owing to the considerable variability of the wind loads and the necessity for a highly elastic structure due to their size. Pedersen et al. [42] notes that turbulence in the inflow has the primary influence on fatigue damage accumulation in upwind turbines. Thomsen and Sørensen [55] investigated the fatigue effects on a wind turbine operating in wakes. Since wind turbines are generally located in clusters or wind farms, this is an important consideration in the design. It was shown that the increase in the fatigue loading in a wind farm could vary between 5 and 15% compared to free flow conditions, depending on the wind farm layout. It was also found that the increase of fatigue loads caused by wake effects was the same for both offshore and onshore sites. Wind turbine interaction within a wind farm has become one of the most relevant topics in the research of wind energy. It is noted that despite always being a recurrent concern in the design, just recently, the paradigm of the sector has started to move from individual machine analysis to coupled interaction assessment in windfarms.

As noted previously, OWTs are subjected to additional loading conditions which must be considered in the design, i.e., hydrodynamic loading. These additional marine induced effects such as, loads due to waves, sea and tidal currents, tidal fluctuation of the water level, sea ice, marine growth, seabed movement and scour, must be considered in the design. Given the random nature of waves, it has been suggested that their state is the best described by stochastic models. Considerable research has been conducted on the topic of stochastic wave modelling for OWTs [2, 8, 32, 35, 36]. BS EN 61400-3-1 [4] and DNV-OS-J101 [12] recommend to use spectral models for the simulation of wave states. One of such models, the Pierson-Moskowitz spectrum, is applicable to a fully developed sea state, while the JONSWAP spectrum is more suitable for a developing sea state, e.g., events such as storms. The correlation between wind and wave conditions must be also addressed [11]. As these conditions are affected by local site factors such as fetch, water depth and bathymetry, the determination of the parameters of the stochastic wave models must be made from suitable long-term measurements and allow for consideration of the effects of climate change, which may require the use of non-stationary stochastic models.

As a result of all the complexities that merge in the analysis of OWTs, the design standards for these need to be treated as dynamic documents, which build upon cumulated knowledge in the field. Often, new contributions to the standard improvement come from research. A representative example of that can be found in Cheng [9], where the author investigated extreme loads and concluded that the most significant operational loads for a pitch-controlled wind turbine occurred at mean wind speed values, slightly larger than the turbine's rated wind speed. To address this problem a methodology for robust design of such turbines accounting for extreme loading was introduced.

## 16.3 Computational Simulations

In wind turbines there is continuous movement of one main component of the system (the rotor) relative to the rest of its structure. The required flexibility of the turbine's blade and tower components coupled with strongly variable loading conditions (i.e., wind) makes dynamic analysis of such systems a complex problem, which still needs to be further investigated. Accurate dynamic analysis is essential for the design of wind turbines since it provides information about the interaction between the environmental loads and the structure and resulting internal dynamic forces within the structure. This information is obviously needed to design the structure, ensuring that it will be capable to withstand variable dynamic loads and operate effectively for the duration of its design life.

The behavior of wind turbine structures as they respond to the aerodynamic loads is termed aeroelasticity. This implies that the aerodynamic loads applied to the structure induce deflections, which in turn cause a change in the aerodynamic loads acting on the structure creating an iterative loop of varying loads and deflections. Since wind turbines generally have low structural damping they can suffer from aeroelastic instabilities under certain conditions. Aeroelastic phenomena such as, stall and flutter in wind turbines, are well documented [6, 18, 20, 21, 31].

The computational codes that analyze wind turbines are commonly referred to as aero-hydro-servo-elastic codes. The demand for these to be accurate is to some extent related to the fact that they show the potential to be significant enablers of further developments in the sector of wind energy. Major efforts to develop accurate aero-hydro-servo-elastic codes have been made since the establishment of the wind energy sector and resulted in the emergence of different codes to satisfy the necessity for simulation models. Current reference computational codes in the field of wind turbine simulation are FAST, HAWC2, GH Bladed, ADAMS and FLEX5. A brief overview of one these codes, FAST, developed by the National Renewable Energy Laboratory (NREL), is shown in Fig. 16.4.

One of the identified trends in the numerical simulation of wind turbines is the application of more complex computational fluid dynamics (CFD) and Finite Element (FE) techniques to the analysis the turbine's dynamic behavior. The application of both is expected to further increase the computational cost of the analysis of wind turbines, which is already rather high. Furthermore, the increasing size of wind turbines may also introduce significant non-linearities in the structural response due to larger deflections, which in turn may increase the demand for more complex modelling techniques such as the ones mentioned above. Furthermore, variation of the structural performance with time due to durability-related issues will add further complexity to the analysis.

Several publications have addressed the issue of the continuous drive to increase the complexity and, subsequently, computational demand associated with dynamic analysis of wind turbines [37, 41, 51, 53]. Keeping the computational efforts within reasonable bounds for the purpose of the wind turbine's design is important not only

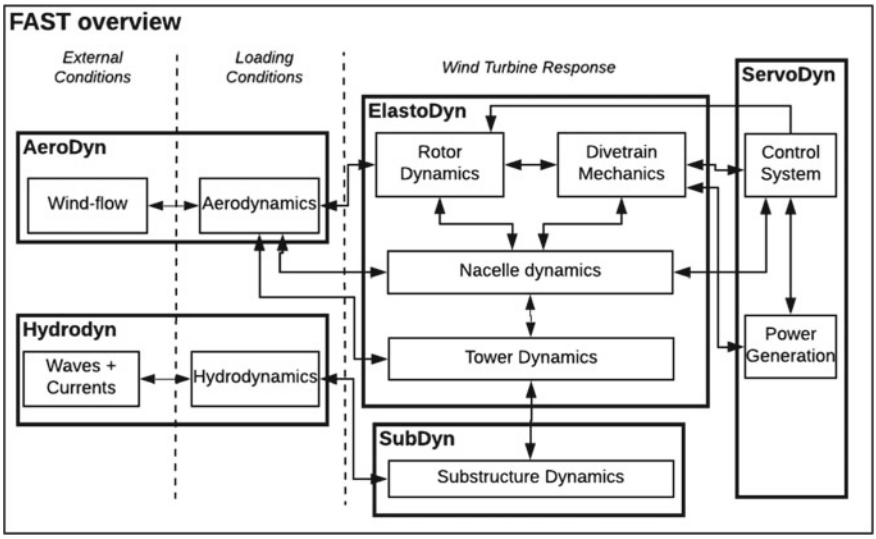


**Fig. 16.4** NREL's FAST (v8) software overview [33]

for foreseeable future but at present as well. The design process often requires repetitive analyses of a wind turbine for the same operational conditions. For example, Moriarty et al. [40] performed 2 × 4725 computational simulations to achieve an accurate assessment of the response for two wind turbine configurations—stall and pitched controlled (i.e., 4725 simulations for each configuration)—in order to analyse extreme and fatigue loading in the context of a probabilistic approach. Despite the high number of total simulations, only 9 simulations were performed per wind condition, which was defined by the mean wind speed (between 5–25 in 1 m/s increments) and turbulence level (between 0.2–5 in 0.2 increments). Further refinement of the considered wind conditions may increase the number of simulations to be performed exponentially.

## 16.4 Climate Change Consideration for Environmental Variables

Consideration of environmental loads plays a major role in the design of wind turbines. It is well known that our environment is changing and along with it the frequency and severity of environmental loads to which wind turbines are subjected. In this context, two aspects of environmental loading, namely, wind fields and hydrodynamic loading are considered.

An important component of dynamic modelling is accurate representation of the turbulent wind field. This is a topic which had been addressed in publications long before wind turbines became prominent with applications for bridges and building structures [24, 50, 59]. The emergence of wind turbines and the direct influence of accurate wind modelling on structural, aerodynamic and power production calculations have inspired further research on the topic.

The wind inflow, $V_0$, may be represented by a stochastic wind model with a fluctuating component, $V'(t)$, and a mean component, $\overline{V}$, which includes the effects of wind shear, i.e., $V_0 = \overline{V} + V'(t)$. The effect of wind shear is accounted for in this case by the log law:

$$\overline{V}(Z) = \frac{1}{k} v_* ln \frac{z_s}{z_0}$$

where $z_s$ is the height above the ground surface, $\overline{V}(z_s)$ is the mean wind velocity at height $z_s$, $v_*$ is the friction velocity, $k$ is the Von-Karman constant, and $z_0$ is the roughness length.

The fluctuating, or turbulent, wind velocity time-histories, $V'(t)$, can be generated using the Discrete Fourier Transform (DFT) method. Fourier coefficients are established from a specific Power Spectral Density Function (PSDF) as normally distributed random numbers with zero mean and standard deviation $\sigma_i$, where $\sigma_i$ is equal to the area under the PSDF between the frequency limits $f_i$ and $f_i + df$. The Kaimal spectrum as specified in Annex of IEC or BS EN 61400-1 [3] is used to generate a wind velocity time-history with a prescribed mean value of zero and standard deviation of 2.29 m/s (Fig. 16.5). This is a typical value for mean wind speeds of 18 m/s with low turbulence characteristics [3]. It is obvious that climate change will influence the statistical parameters associated with wind field modeling and that these should be considered in design, while the currently used values of the parameters are shown in Table 16.1 [47]. However, at present, there is still not enough

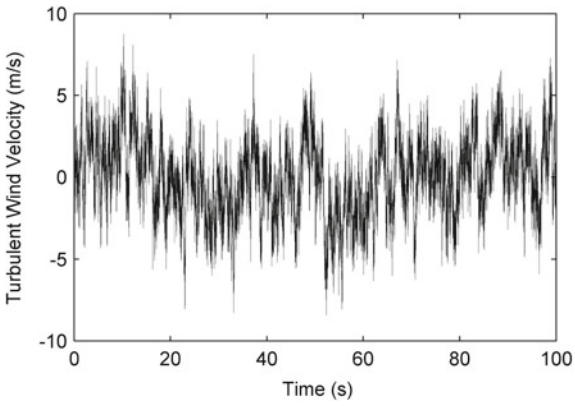


**Fig. 16.5** Wind turbulence time history [33]

**Table 16.1** Turbulence standard deviation at mean hub height wind speeds [47]

| | Mean hub height wind speed, $V$ (m/s) | | | | | |
|---|---|---|---|---|---|---|
| $\sigma_1$(m/s) | 16 | 18 | 20 | 22 | 24 | 25 |
| Low turbulence | 2.11 | 2.29 | 2.47 | 2.65 | 2.83 | 2.92 |
| Medium turbulence | 2.46 | 2.67 | 2.88 | 3.09 | 3.30 | 3.41 |
| High turbulence | 2.82 | 3.06 | 3.30 | 3.54 | 3.78 | 3.90 |

evidence to properly predict the impact of a changing climate on wind characteristics in different regions of the world [57]. Prediction of climate change influence on wind speeds is a recurrent research topic and, due to the large uncertainty that is inherent to climate change, has generated significant discussion in the literature [19, 25, 34, 45]. A common trend that has been identified is for changes in the annual mean wind speed to be less pronounced, while inter annual variability is expected to increase. Effects of climate change are also expected to be highly local and provisions for such local dependence are needed for future wind turbine analysis and design considerations. Regardless, at the present, there is still not enough evidence to properly predict the impact of a changing climate on wind characteristics in different world regions [57].

Nonetheless, several studies sought to characterize the explicit evaluation of potential impacts of climate change on wind energy and wind turbines before. Pryor and Barthelmie [44] predicted that it would have limited influence in the sector, however, they did not explicitly discuss the sector-specific technical considerations related to the turbines. Recent research efforts have been directed to address this issue in more detail. Hdidouan and Staffell [23] highlighted the need for conducting further research related to climate change effects on the wind energy sector when they evaluated the LCOE for windfarms. Wilke and Galasso [58] also tackled this issue by studying structural components of wind turbines. They concluded that the effects of climate change were expected to be small for the structural components because these are highly reliable, i.e., having very low probability of failure. Moreover, being the long-term operation costs of wind turbines mostly driven by non-structural elements. Nonetheless, the authors showed that environmental parameters influenced the loading on wind turbines. In this regard, only a limited number of studies have been found that tried to infer explicitly on how climate change scenarios may impact wind turbines at the system and component levels (in the response side as described previously), such as the influence on the Design Load Cases (DLCs), or other structural considerations. There is some agreement in the literature that regarding the environmental parameters, climate change will mainly affect the intensity and frequency of the extremes. Thus, further research may be required to investigate the extent of the climate change influence on the wind turbine durability and performance. This is particularly relevant for structural components that are highly influenced by extreme loading. An example of such can be identified in extreme loading and its large influence in the fatigue of composite material structural components [51, 53].

For the case of wave height, the need to characterize extreme waves using field data dates back to the 1960s, where a "design wave" was characterized using full records of data. Since then, the topic of extreme wave or "design waves" has been under discussion and possibly will remain so for decades to come. In the present it is common to use only exceedance data for this.

Currently, several standards and practices are found to guide the design of offshore structures. While some of them present generic considerations related to the definition of the significant wave height ($H_s$) occurrences, e.g. emphasizing the need for reliable and robust estimations, other standards/guidelines provide specific recommendations about the techniques for modeling $H_s$. DNV GL recommended practice on environmental conditions and loads, DNV [15], accepts the use of different approaches.

If $H_s$ is a random variable with maxima $m_{H_s}$, then for all $u < m_{H_s}$, the function

$$F_{x_{Hs},u}\left(x_{H_s}\right) = Pr\left[(H_s - u) \leq x_{H_s} \middle| H_s > u\right], x_{H_s} > 0$$

can be used to model exceedances of $H_s$, $x_{H_s}$, over a certain threshold $u$. This function represents the cumulative function over values exceeding the threshold $u$, which can also be defined as:

$$F_{x_{Hs},u}\left(x_{H_s}\right) = \begin{cases} \frac{F\left(x_{H_s}+u\right)-F(u)}{1-F(u)}, if\, x_{H_s+u} > u \\ 0, if\, x_{H_s} \leq u \end{cases}$$

a normalised representation of $F_{x_{Hs},u}\left(x_{H_s}\right)$. Analysis of $x_{H_s}$ comprises the definition of a subset of $H_s > u$. Pickands III [43] showed that the limit probability distribution of this subset approached a Generalized Pareto (GP) distribution [52], and an application of this approach to modelling of exceedance of wave data and characterization of extremes is now discussed.

It considers wave data recorded by Met Éireann at four different buoy locations around the Irish Coast, Fig. 16.6. The records started in 2000 and ended in the year 2015. These are then used to extrapolate data using only exceedances. Usage of exceedances allows to increase the accuracy of the extrapolation in the region of interest (the tail region, where extremes are located) and definition of a cumulative density function to define extreme waves.

Different values of $H_s$ with return period level $T_r$ depending on $u$ (=5.0 m) are shown in Table 16.2. The appropriateness of the threshold value as well as the return period estimation of $H_s$ in the context of expected sea states considering the effects of climate change should be reflected upon in assessing appropriate design values for OWTs. The interested reader is directed to the referred work where further discussion and insight on approximation of extreme using exceedance data and other extreme value analysis is provided.

In design is important to emphasize the large uncertainties associated with extreme predictions. For future climate change prediction, as well as for present extrapolation

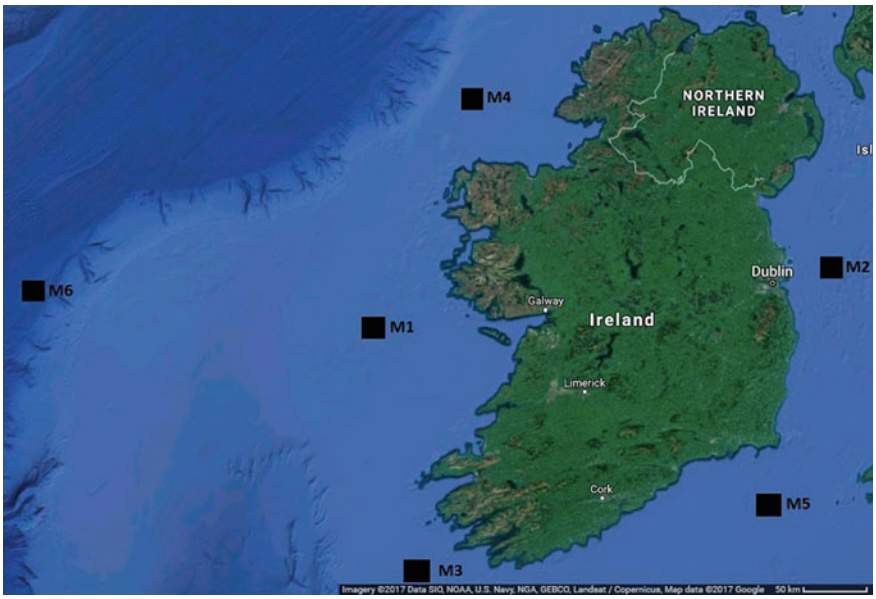


**Fig. 16.6** Map with Approximate Location of Met Éireann Oceanographic Buoys [54]

**Table 16.2** 20-year and 50-year return levels of $H_s$ [54]

| Buoy reference | $H_s$ | |
|---|---|---|
| | $T_{r\_20}$ | $T_{r\_50}$ |
| M1 | 15.58 | 16.73 |
| M4 | 19.65 | 22.22 |
| M5 | 12.42 | 13.75 |
| M6 | 20.25 | 22.63 |

of climate variables, the designer should be aware that complex modelling techniques do not suffice for lower uncertainty in the estimations, and hence, any extreme value prediction should be accompanied by an appropriate uncertainty assessment.

## 16.5 Modelling Impact of Durability on Performance

As a means of considering the impact of durability on the performance of wind turbines it is proposed that fragility curves to be employed, relating wind hazard intensity to a considered limit-state, as a method for comparing the relative structural performance of the turbines. A displacement-based fragility curve generation procedure may be utilized, based upon performance metrics related, e.g., to nacelle (tower tip) displacement. The choice of the displacement limit-state reflects the stability of

the tower structure and its ability to resist the prescribed loading conditions. Mean hub-height wind speed can be chosen as the fragility hazard parameter as it is quite straightforward and it dictates the underlying turbulent parameters of the wind speed.

The fragility term employed in the analysis may be represented as:

$$Pr\left[d_{tip} > LS \middle| \overline{V}_{hub} = \overline{V}\right]$$

where $d_{tip}$ is the maximum nacelle displacement, $LS$ is the tower limit-state, and $\overline{V}_{hub}$ is the mean wind speed at the hub height.

The proposed methodology has been employed to consider the performance of turbine structures manufactured from steel and pre-stressed concrete. The specific parameters of the modeled towers may be found in Quilligan et al. [46]. This methodology can also be applied to present the effect of the soil stiffness degradation around the pile foundations of wind turbines, which occur due cyclic lateral loading. This is relevant for both offshore and onshore wind turbines (e.g., [1, 60]). This phenomenon may have a major influence on the dynamic response of the turbines and also lead to an increase in their tilt and, subsequently, the maximum nacelle displacement.

One of the main factors affecting the durability of wind turbines, especially of those located offshore, is corrosion. Corrosion may have a detrimental effect on both steel and reinforced/pre-stressed concrete, i.e., the materials used for the turbines' towers. Corrosion of steelwork is relatively easily detected and protection against it is well developed (e.g., Bayliss and Deacon [7]). While it can be controlled it is still has high impact on the costs of the structure maintenance. The same extends to the corrosion of reinforcing steel in concrete. The latter can be caused either by carbonation, which is a slow process that poses a very low risk to wind turbine concrete structures due to their relatively short design life (typically, 20–25 years), or chloride ingress. Since sea-water contains salt, chloride-induced corrosion is a major danger to the durability of concrete structures of OWTs. A large amount of research has been done on modeling the chloride-induced corrosion and risk associated with it (e.g., [56]). In the context of climate change, both corrosion initiation and propagation depend on ambient temperature and humidity. The effect of a change in the ambient temperature on the rate of chloride ingress and corrosion propagation is usually taken into account by introducing a correction factor, $k_T$, which value is estimated based on the Arrhenius equation:

$$k_T = \exp\left[b_T\left(\frac{1}{T_{\text{ref}}} - \frac{1}{T}\right)\right]$$

where $b_T$ is a regression parameter, $T_{ref}$ the reference temperature (293 K), and $T$ the ambient temperature.

Any pre-stressed concrete towers of wind turbines would be also subjected to a number of effects, which can affect their performance and, subsequently, durability over time. Creep and shrinkage are two processes which must be considered in the long-term design of pre-stressed concrete structures and, therefore, of pre-stressed

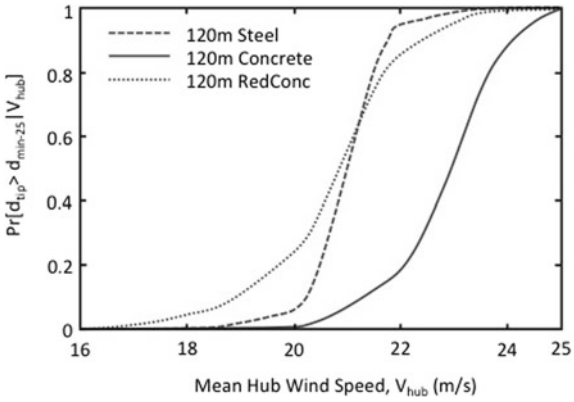


**Fig. 16.7** Fragility curves for 120 m steel and concrete towers [46]

concrete wind turbine towers. Both of these processes have the ability to induce tensile stresses, which may lead to cracking of the concrete and a reduction in the overall strength of the structure. Numerous efforts have been made by researchers, e.g., Cluley and Shepherd [10] and Mazloom [39], to quantify the effects of creep and shrinkage on the strength of pre-stressed concrete structures. Taking the approach outlined by Mayfield [38] and utilizing the formula:

$$J(t,t') = \frac{1+\phi(t,t')}{E(t')}$$

where $J(t,t')$ is the creep function, $\phi(t,t')$ is the creep coefficient, and $E(t')$ is the modulus of elasticity at age $t'$, it is possible to get an estimate of the reduced modulus of elasticity of the concrete after loading for time $t$. Considering that $J(t,t')$ is the strain at time $t$ due to a unit constant stress that has been acting since time $t'$, it can be shown that $1/J(t,t')$ is an approximation of the modulus of elasticity at time $t$.

Figure 16.7 presents the computed fragility curves for 120 m high wind turbine towers constructed from steel (120 m Steel) and pre-stressed concrete (120 m Conc) [46]. The figure also shows the revised fragility curve for the pre-stressed concrete tower, which indicates a reduction in the strength due to long term effects associated with creep and shrinkage (120 m RedConc). Generally, the results indicate a higher probability of the limit state exceedance when the durability aspects and the impact for long-term performance are considered. Similar conclusions regarding the performance of steel towers as a function of variation in durability characteristics can be drawn.

Furthermore, the impact of durability on the fatigue performance of turbines may need to be considered, since in many cases fatigue is the controlling limit state.

## 16.6 Decision Making Regarding Design, Operation and Maintenance

As should be clear from above, reductions in the LCOE of wind energy can be achieved through innovations, more efficient, reliable and durable design solutions, and optimal planning of operation and maintenance (O&M). To implement this in practice, rational and consistent procedures for decision making regarding the design, installation and O&M of wind turbines are required. These procedures should take into account currently available information, data which can be collected during the operational life of wind turbines, and also uncertainties associated with this data. Bayesian statistical decision theory provides a solid theoretical basis for such procedures [48].

Based on this theory, a comprehensive decision procedure can be represented by a decision tree shown in Fig. 16.8. Possible design decisions/solutions are represented by the set $\boldsymbol{Z} = \{z_1, z_2, \ldots\}$ which, in order not to overcomplicate the decision tree, encompasses all decisions related to the initial design and installation. In principle, the design solutions can be optimized to eventually maximize an expected 'utility' $u$ (z, $e$, $s$, $a$, $\theta$) associated with the operational life a wind turbine or, more generally, wind farm. The utilities are usually expressed in monetary terms as the difference between the total benefits and costs and depend on other factors, as should be clear from Fig. 16.8, which will be considered later. In practice, the design solutions are usually controlled by standards, e.g., IEC 61400, available resources and technologies. This emphasises the importance of continuous review and updating of the design standards, in particular, in light of climate change, since the optimality of the design solutions of wind turbines, to a large extent, depends on these documents. By the same reason, the search for optimal design solutions is often not included in the optimization process, which concentrates on optimizing the O&M strategies.

During their operational life, components of wind turbines deteriorate due to environmental loads and effects; possible deterioration processes include fatigue, corrosion, wear and erosion. In addition to uncertainties in load- and resistance-related parameters, there are large uncertainties associated with these deterioration processes. This means that possible states/conditions of wind turbines represented in the decision tree by the set $\boldsymbol{\theta}$, which include states of the turbine failure, are random

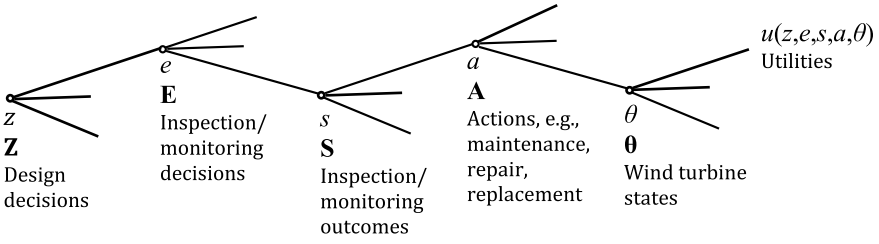


**Fig. 16.8** Decision tree for optimal design and O&M of wind farms

in their nature. In order to reduce the probability of turbine failure, certain actions **A** (e.g., preventive maintenance, repair, component replacement) may be required. Such actions may be planned using only previously available information, which is employed to predict the effects of deterioration processes on the condition of wind turbine components. The probabilities assigned to the possible states in $\boldsymbol{\theta}$ are then called prior probabilities; $P'[\theta_j]$ is the prior probability of the $j$-th state. After setting utilities of all possible action-state combinations, $u$ (z, $a_i$, $\theta_j$), the expected utilities corresponding to different actions can be calculated as $E[u(z, a_i, \theta)] = \sum_j u(z, a_i, \theta_j) P'[\theta_j]$. The action, which results in the maximum expected utility, can then be identified. In Bayesian decision theory, this is referred to as prior analysis.

The prior analysis is not efficient, especially over a relatively long time horizon (e.g., over 5 years), since the prediction of the state probabilities becomes very inaccurate. To reduce this uncertainty, inspections of wind turbines should periodically be conducted. The outcome of an inspection, $s$, i.e., new information about the condition of the turbine components, is then employed to update the prior probabilities assigned to the turbine states based on Bayes' theorem. The updated probabilities, $P''[\theta_j|s]$, are called posterior probabilities. The decision making process is similar to that described above in the context of prior analysis except that the expected utilities are calculated using the posterior probabilities and the utilities also depend on the inspection outcome $s$. This is referred to as posterior analysis. It is important to note that in this case a decision whether or not to conduct the inspection is not included in the decision procedure.

The most advanced type of analysis that enables optimal planning of inspection/monitoring activities, which are represented in the decision tree by the set **E**, is the so-called pre-posterior analysis. This analysis involves simulation of the inspection/monitoring outcomes and then updating the prior probabilities of the wind turbine states based on these outcomes. The utilities are then also depend on possible combinations of $(e, s)$. A framework for optimal planning of O&M activities for OWTs using pre-posterior analysis was proposed by Sorensen [49] and then extended by Florian and Sorensen [16] for offshore wind farms.

## 16.7 Conclusions

In this chapter, potential impacts of a changing climate on the performance, durability and, subsequently, analysis and design of wind turbines have been considered. It has been demonstrated that these impacts may be substantial and, therefore, need to be properly addressed. It is believed that this mainly should be done via updating relevant design standards and guidelines, in particular that concerns environmental loads (e.g., wind, waves) and conditions (e.g., temperature, humidity), as sufficiently reliable information on the impacts of climate change on these parameters become available. Since the design life of wind turbines is relatively short, usually 20–25 years, it is also believed that stochastic models of environmental loads and other climate-related variables (i.e., wind, waves, temperature, etc.) employed for their analysis and design

can be treated as stationary. This means that relevant parameters of the models should be adjusted in accordance to expected effects of climate change averaged over the intended period of the turbine's design life, but to be considered as time-invariant in the analysis/design. Such a simplification seems well justified, since based on available evidence changes in climate-related variables over 20–25 years are usually not significant. The importance of consideration of aspects related to durability and deterioration in the context of assessing the probability of limit state exceedance has been demonstrated. Finally a basis for determining optimal decisions regarding design, operation and maintenance is provided. It is clear from the chapter that such a basis would be incomplete without adequate consideration of durability and the influence of climate extremes.

## References

1. Abhinav KA, Saha N (2015) Dynamic analysis of an offshore wind turbine including soil effects. Procedia Eng 116(1):32–39
2. Agarwal P, Manuel L (2011) Incorporating irregular nonlinear waves in coupled simulation and reliability studies of offshore wind turbines. Appl Ocean Res 33(3):215–227
3. BS EN 61400-1 (2019) Wind energy generation systems. Design requirements. British Standards Institution
4. BS EN 61400-3-1(2019) Wind energy generation systems. Design requirements for fixed offshore wind turbines British Standards Institution
5. BVG (2014) UK offshore wind supply chain: capabilities and opportunities. Technical report, BVG Associates
6. Baxevanou C, Chaviaropoulos P, Voutsinas S, Vlachos N (2008) Evaluation study of a Navier-Stokes CFD aeroelastic model of wind turbine airfoils in classical flutter. J Wind Eng Ind Aerodyn 96(8–9):1425–1443
7. Bayliss D, Deacon D (2002) Steelwork corrosion control: from the middle ages to the renaissance. Edn 2:7–305
8. Chella MA, Tørum A, Myrhaug D (2012) An overview of wave impact forces on offshore wind turbine substructures. Energy Procedia 20:217–226
9. Cheng PW (2002) A reliability based design methodology for extreme responses of offshore wind turbines
10. Cluley N, Shepherd R (1996) Analysis of concrete cable-stayed bridges for creep, shrinkage and relaxation effects. Comput Struct 58(2):337–350
11. Colwell S, Basu B (2009) Tuned liquid column dampers in offshore wind turbines for structural control. Eng Struct 31(2):358–368
12. DNV-OS-J101 (2010) Design of offshore wind turbine structures. DNV
13. DNV (2011) Fatigue design of offshore steel structures. Recommended Practice DNV-RP-C2013, DNV GL AS
14. DNV (2014a) Design of offshore wind turbine structures. Offshore Standard DNV-OS-J101, DNV GL AS
15. DNV (2014b) Environmental condition and environmental loads. Recommended Practice DNVRP-C205, DNV GL AS
16. Florian M, Sorensen JD (2017) Risk-based planning of operation and maintenance for offshore wind farms. Energy Procedia 137:261–272
17. Frick S, Huenges E, Jorde K, Jung R, Kabus F, Kaltschmitt M, Kehl K, Laing D, Lewandowski I, Ortmanns W, Rau U, Sanner B, Sauer DU, Schneider S, Schröder G, Seibt P, Skiba M, Streicher W, Weinrebe G, Wiese A (2007) Renewable energy: technology economics and environment. Springer

18. Friedmann PP (1980) Aeroelastic stability and response analysis of large horizontal axis wind turbines. J Wind Eng Ind Aerodyn 5(3–4):373–401
19. Garreaud RD, Falvey M (2009) The coastal winds off western subtropical south america in future climate scenarios. Int J Climatology 29(4):543–554
20. Hansen MH (2003) Improved modal dynamics of wind turbines to avoid stall induced vibrations. Wind Energy 6(2):179–195
21. Hansen MOL (2008) Aerodynamics of Wind Turbines, 2nd edn. Earthscan, Camden High Street, London, NW1 0JH, UK, pp 8–12
22. Hau E (2006) Wind turbines: fundamentals, technologies, applications, economics, 2nd edn. Springer, Berlin
23. Hdidouan D, Staffell I (2017) The impact of climate change on the levelised cost of wind energy. Renew Energy 101:575–592
24. Higson H, Griffiths R, Jones C, Hall D (1994) Concentration measurements around an isolated building: a comparison between wind tunnel and field data. Atmos Environ 28(11):1827–1836
25. Hosking JS, MacLeod D, Phillips T, Holmes CR, Watson P, Shuckburgh EF, Mitchell D (2018) Changes in european wind energy generation potential within a 1.5 C warmer world. Environ Res Lett 13(5):054032
26. IEC (2019a) Wind energy generation systems—Part 1: Design requirements. Technical Report 61400-1. International Electrotechnical Commission, Geneva, Switzerland
27. IEC (2019b) Wind energy generation systems—Part 3–1: Design requirements for fixed offshore wind turbines. Technical Report 61400-3. International Electrotechnical Commission, Geneva, Switzerland
28. IRENA (2017) Renewable power generation costs in 2017. Technical report, International Renewable Energy Agency
29. ISO (2015) General principles on reliability for structures. Technical Report 2394, International Organization for Standardization
30. Iván P, Tom R, Ariola M (2017) Offshore wind in Europe: Key trends and statsitics 2017. Technical report, Wind Europe
31. Janetzke DC, Kaza KR (1983) Whirl flutter analysis of a horizontal-axis wind turbine with a two-bladed teetering rotor. Sol Energy 31(2):173–182
32. Jensen JJ, Olsen AS, Mansour AE (2011) Extreme wave and wind response predictions. Ocean Eng 38(17–18):2244–2253
33. Jonkman J (2013) The new modularization framework for the fast wind turbine cae tool. In: 51st AIAA Aerospace Sciences Meeting including the New Horizons Forum and Aerospace Exposition, p 202
34. Makkonen L, Ruokolainen L, Raisanen J, Tikanmaki M (2007) Regional climate model estimates for changes in nordic extreme events. Geophysica 43(1–2):19–42
35. Marino E, Borri C, Lugni C (2011) Influence of wind-waves energy transfer on the impulsive hydrodynamic loads acting on offshore wind turbines. J Wind Eng Ind Aerodyn 99(6–7):767–775
36. Marino E, Borri C, Peil U (2011) A fully nonlinear wave model to account for breaking wave impact loads on offshore wind turbines. J Wind Eng Ind Aerodyn 99(4):483–490
37. Marino E, Giusti A, Manuel L (2017) Offshore wind turbine fatigue loads: the influence of alternative wave modeling for different turbulent and mean winds. Renew Energy 102:157–169
38. Mayfield B (1982) Creep and shrinkage in concrete structures. Wiley, Chichester
39. Mazloom M (2008) Estimating long-term creep and shrinkage of high-strength concrete. Cement Concr Compos 30(4):316–326
40. Moriarty PJ, Holley W, Butterfield SP (2004) Extrapolation of extreme and fatigue loads using probabilistic methods. Technical report, National Renewable Energy Lab., Golden, CO (US)
41. Murcia JP, Réthoré PE, Dimitrov N, Natarajan A, Soørensen JD, Graf P, Kim T (2018) Uncertainty propagation through an aeroelastic wind turbine model using polynomial surrogates. Renew Energy 119:910–922
42. Pedersen R, Nielsen S, Thoft-Christensen P (2012) Stochastic analysis of the influence of tower shadow on fatigue life of wind turbine blade. Struct Saf 35:63–71

43. Pickands III J (1975) Statistical inference using extreme order statistics. The Annals of Statistics pp 119–131
44. Pryor SC, Barthelmie RJ (2010) Climate change impacts on wind energy: a review. Renew Sustain Energy Rev 14(1):430–437
45. Pryor SC, Barthelmie JB, Clausen NE, Drews M, MacKellar N, Kjellstrom E (2012) Analyses of possible changes in intense and extreme wind speeds over northern europe under climate change scenarios. Clim Dyn 38(1–2):189–208
46. Quilligan A, O'Connor A, Pakrashi V (2012) Fragility analysis of steel and concrete wind turbine towers. Eng Struct 36:270–282
47. Quilligan A (2012) Fragility analysis of steel and concrete wind turbine towers. PhD Thesis. Trinity College Dublin
48. Raiffa H, Schlaifer R (1961) Applied statistical decision theory, Boston (Mass.). Harvard university press
49. Sorensen JD (2009) Framework for risk-based planning of operation and maintenance for offshore wind turbines. Wind Energy 12:493–506
50. Suh SH, Roh HW, Kim HR, Lee KY, Kim KS (1997) Application of computational techniques for studies of wind pressure coefficients around an oddgeometrical building. J Wind Eng Ind Aerodyn 67–68:659–670
51. Teixeira R, Nogal M, O'Connor A (2019) Analysis of long-term loading characterization for stress-cycle fatigue design. Wind Energy 22(11):1563–1580
52. Teixeira R (2018) Analysis of offshore wind turbines: probabilistic assessment of operational design. PhD Thesis. Trinity College Dublin
53. Teixeira R, O'Connor A, Nogal M (2019) Fatigue reliability using a multiple surface approach. In: 13th international conference on applications of statistics and probability in civil engineering (ICASP13). Seoul, South Korea, 26–30 May 2019
54. Teixeira R, Nogal M, O'Connor A (2018) On the suitability of the generalized Pareto to model extreme waves. J Hydraul Res 56(6):755–770. https://doi.org/10.1080/00221686.2017.1402829
55. Thomsen K, Sørensen P (1999) Fatigue loads for wind turbines operating in wakes. J Wind Eng Ind Aerodyn 80(1–2):121–136
56. Val DV, Stewart MG (2009) Reliability assessment of ageing reinforced concrete structures—current situation and future challenges. Struct Eng Int 19(2):211–219
57. Val DV, Yurchenko D, Nogal M, O'Connor A (2019) Climate change-related risks and adaptation of interdependent infrastructure systems. In: Bastidas-Arteaga E, Stewart MG (eds) Climate adaptation engineering—risk and economics for infrastructure decision-making. Butterworth-Heinemann, Oxford OX5 1GB, UK, pp 207–242
58. Wilkie D, Galasso C (2020) Impact of climate-change scenarios on offshore wind turbine structural performance. Renew Sustain Energy Rev 134:110323
59. Yang WW, Chang TYP, Chang CC (1997) An efficient wind field simulation technique for bridges. J Wind Eng Ind Aerodyn 67–68:697–708
60. Yu H, Guzman C, Ntambakwa E (2016) Consideration of the cyclic degradation of cohesive soils in pile foundation design for offshore wind turbines, Geo-Chicago 2016. ASCE, Chicago, IL, pp 195–206

# Chapter 17
# Extreme Value Analysis for Offshore Pipeline Risk Estimation


**Robert E. Melchers**

**Abstract** Low alloy or mild steel pipelines operating under high pressures are widely used as economic solutions for oil and gas conveyance in the offshore industry. Protected externally with coatings or concrete, they are prone to corrosion of the internal surfaces. Such corrosion may affect pipeline safety and ability to contain the oil or gas being transported. Herein an overview is given of the principal factors affecting risk and a summary is given of the use of so-called Extreme Value Analysis to quantify the probability of failure of pipe-wall perforation, including prediction of future risk. Attention is given to provide understanding of the corrosion mechanisms involved to ensure risk analysis and prediction are based on sound principles.

## 17.1 Introduction

Steel pipelines play a major role in offshore oil and gas exploitation with most offshore facilities being surrounded by many miles of pipelines with various purposes, or in some cases, no purpose at all. These pipelines almost invariably are mild or high strength low alloy (HSLA) steel, with welded joints and those in active use are most of the time operating under considerable internal pressure, not necessarily constant in time. Many are production pipelines conveying crude oil or (wet) gas from a well to some type of facility. Depending on the crude, they may be under 'sweet' (low sulphur) or 'sour' (high sulphur) conditions. Other pipelines are mainly the so-called water injection pipelines (WIPs) used to inject water at high pressure into oil or gas wells to force as much as possible of the remain product from the aquifer. While pipelines have been used for many years for overland conveyance of oil and gas over very long distances, their use for long distances offshore is more recent. One example is the two 1200 km long Nord Stream pipelines in northern European waters to convey Russian natural gas through the Baltic Sea to Germany [48].

R. E. Melchers (✉)
Centre for Infrastructure Performance and Reliability, The University of Newcastle, Callaghan, NSW 2308, Australia
e-mail: rob.melchers@newcastle.edu.au



M. G. Stewart and D. V. Rosowsky (eds.), *Engineering for Extremes*, Springer Tracts in Civil Engineering, https://doi.org/10.1007/978-3-030-85018-0_17

The present chapter reviews, briefly, the main risks and potential consequences associated with offshore pipelines. A major aspect is the potential for wall perforation of the pipelines as a result of corrosion, primarily *internal* corrosion. The conventional industry practice monitoring techniques for this are outlined. The discussion then moves to the use of extreme value analysis for predicting the probability of pipe-wall penetration by localized corrosion, principally pitting but may also include crevice corrosion. Recent new approaches for using extreme value analysis for interpreting the usual corrosion field data such as obtained from intelligent pigging are then outlined. Theoretical justification is then given for the usually entirely empirical notion of using only the extreme depth pit depths for extrapolation to estimate the probability of occurrence of even deeper pits. The issue of estimating the depth of pitting at some time in the future is considered. In this context growth laws are very briefly reviewed and the usual approach applied in practice justified.

## 17.2 Some Background

As oil and gas exploration moves increasingly to deeper and perhaps more hostile waters or both, the critical assessment of the risk of failure, such as from a leak of oil or gas, or worse from a major rupture of the pipelines or failure of the associated facilities including platforms has become more important. Risk assessment procedures and criteria for fixed platforms such as those used in the shallower waters of the Gulf of Mexico and the North Sea are well developed and rely on well-established structural reliability theory. The performance criteria for use in such risk assessments are available in the extensive rules laid down by the relevant national agencies with sovereign control over the operational area, usually with the assistance of, or with delegated authority passed to, classification societies with specialized expertise in the offshore oil and gas sector.

With the need to move to deeper waters for new oil and gas sources the risks have, in general, become greater and alternatives to fixed 'jacket'-type platforms such as floating 'platforms' with a variety of structural configurations have been explored for many years [3]. However, more recently the trend has tended to focus on simplicity and vessels that are similar to ships (or are actually converted ships, such as oil tankers, suitably reinforced and adapted). These have the advantage that they can with-stand considerable wind and wave loadings such as occur in open sea conditions and in foul weather have greater stability and 'seaworthiness' than other configurations. Further, in advance of really foul weather they could be disconnected from risers and pipelines and towed to safer waters. Such vessels go by a variety of names, depending on their operational role—the most comprehensive are known as 'floating production storage and offloading' (FPSO) facilities. Typically these are packed on deck with closely spaced and highly complex facilities, and operational and crew quarters, using the tanks in the hull for product storage as required.

FPSOs are moored to the seafloor, usually with 8–12 mooring lines from a turret, usually mounted on the bow but sometimes amid-ships. Each mooring line typically

consists of steel chain at the top (permitting fastening to the vessel at the turret), wire rope for most of the mooring length and, near the seafloor reverting back to a long chain most of which rests in the seafloor and acts as an adaptable hold-fast [21, 37]. These types of vessels can be used in shallower waters but also for very deep waters—currently up to about 3 km deep—and are relatively easily relocated to a new field or to refurbishing facilities. Typically they are owned and operated by specialist contractors. They are subject to classification society rules and have an active research and development network (the FPSO Research Forum) that considers all aspects of design and operations.

Irrespective of the type of platform, the oil and gas must be extracted from the wells and this requires pipelines (Fig. 17.1). Most platforms serve a number of wells and extensive pipework is required, sometimes many miles (10–20 km) in length. Similarly, once extracted the oil or gas must be pumped ashore or to storage facilities. The crude oil these pipelines convey is a complex mixture of hydrocarbon gas, hydrocarbon condensate or oil, water with dissolved minerals, usually with a high salt content, and gasses including nitrogen ($N_2$), carbon dioxide ($CO_2$) and often hydrogen sulphide ($H_2S$). The mixture usually also contains various solids, including sand, scale and corrosion products from the pipelines themselves [3, 34].

For older oil and gas fields it is common practice to use a process called 'water-injection' to try to drive out as much as possible of the remaining oil or gas from the well, using seawater, production water (derived from the water cut of crude oil), aquifer waters or, perhaps contaminated, water from shore based facilities, pumped at high pressure (typically 600–800 bar) through water-injection pipelines (WIPs) into the well (Fig. 17.1). To control erosion, these injected waters are all treated to remove particular material such as sands. Usually they also are 'de-aerated' at the up-stream end, to remove as much oxygen as technically and economically feasible (usually not possible lower than 20 ppb oxygen) in a bid to control internal corrosion. For

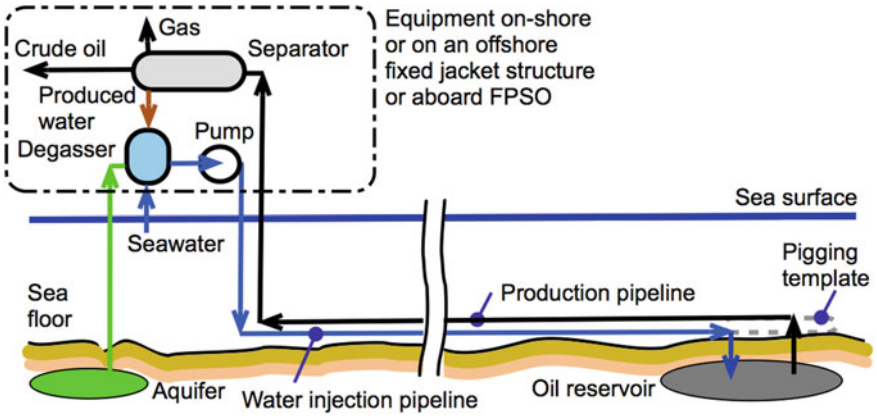


**Fig. 17.1** Schematic of production and water injection pipelines in relation to oil reservoir and sources of injection water

the same reason, chemical oxygen scavengers are sometimes added. In some cases the WIPs are also dosed with chemicals (mainly nitrates) meant to control hydrogen gas production within the oil remaining in the well by encouraging nitrate-reducing bacteria to out-compete the hydrogen-gas-producing sulphate-reducing bacteria [45]. To try to control microbiologically influenced corrosion (MIC) within the pipe, periodic or occasional pigging is used to try to remove surface deposits favoured by microorganisms [39]. However, the brushes on the pigs are unable to remove any rusts that are inside corrosion pits or crevices, thereby leaving conditions suitable for further corrosion.

In practice the only economic material for offshore pipelines is steel, and in particular mild (or carbon) steel (e.g. grades X52, X50 and X65) or high strength low alloy (HSLA) steels. Highly alloyed steels and alloys usually considered corrosion resistant are not economic and in the case of stainless steel (e.g. S31600) not even very effective for the constantly wet, low or zero oxygen conditions in water injection and oil production pipelines respectively. Because of corrosion and erosion the mild steel pipelines have a limited life. Those considered no longer serviceable are duplicated into the system, by-passed and purged to remove deleterious matters and then disconnected and, in many cases, then abandoned [35]. Sometimes they are salvaged. The latter practices are increasingly under considered undesirable because of environmental concerns. Several projects are underway to determine what to do with already abandoned pipelines. Evidently, a critical issue for operators is when a pipeline is considered no longer serviceable. Determining when this occurs depends on the structural integrity of the pipe, in particular its ability to contain the fluid being conveyed. This depends on the probability of pipe-wall penetration. As will be seen, in practice for offshore pipelines this is primarily related to corrosion. Prediction of the depth of corrosion is considered next together with probabilistic methods as currently used to make the assessment, and new interpretations for the same data.

## 17.3 Pipeline Risk Assessment

The primary hazard for oil production pipelines is leakage of crude oil from the pipe. Apart from loss of product, the main issue is the environmental impact of crude oil floating on seawater, causing various environmental problems including to fauna and flora, particularly for operations close to shore. For gas there is also the potential for explosions, even though this usually requires the occurrence of a narrow range of gas-oxygen mix such that the potential for (and probability of) initiation is low. For WIPs the main hazard is leakage of the water conveyed by the pipeline and the possibility of subsequent local environmental pollution.

Leakage caused by deterioration of the steel pipelines is mainly the result of corrosion, and specifically through *internal* corrosion. It is considered to account for more than 50% of the threat to pipelines, with external corrosion around 15% and overpressure, weld, flange and pipe damage, construction damage and 3rd party damage sharing the remainder [42]. Internal corrosion affects the pipe wall, the longitudinal

seam weld and the welds connecting one pipe spool to the next (Fig. 17.2). Where flanges are used to bolt one spool to the next or to other equipment, crevice corrosion within the joint may be an issue [15]. For both WIPs and production pipes so-called 'channelling corrosion' is sometimes observed [16]. This is the more severe loss of metal along the bottom of (near-)horizontal pipes (Fig. 17.3). For production pipes that normally is attributed to the interaction of erosion by the sands in crude oils with corrosion [41]. Perhaps surprisingly, the oil content in crude oils is seldom sufficient to stifle corrosion. The main cause for corrosion is the water that inevitable is part of crude oils. For WIPs it has been argued that the prime driver is MIC enhanced by the addition of nitrate to the water and settlement of rust and other particulate matter during periods of no-flow (such as for maintenance) [8] This is also part of the practice for production pipelines [18]. It follows from these remarks that neither

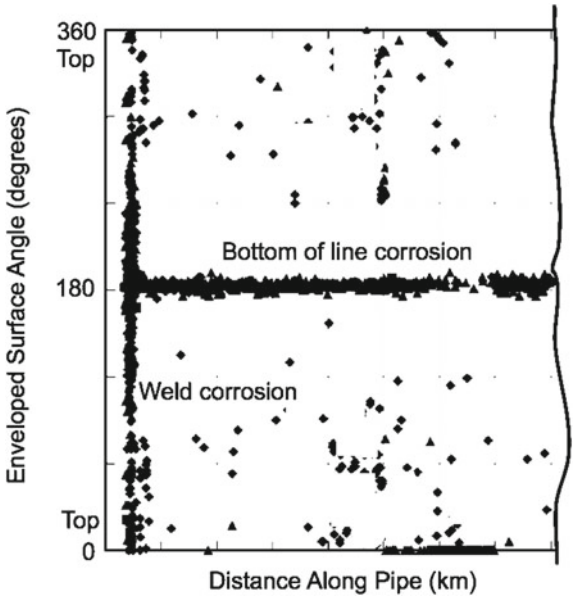


**Fig. 17.2** Short length of the interior surface of an enveloped WIP showing locations of predominantly localized corrosion, relatively much more severe at circumferential welds and around the 6 o'clock position (channelling or 'bottom of the line' corrosion) (after Comanescu et al [8]

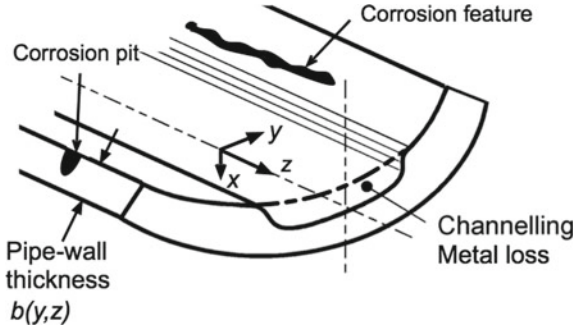


**Fig. 17.3** Schematic view of corrosion features, pitting corrosion and channelling corrosion (known also as 6 o'clock corrosion, bottom of the line corrosion, river-bottom corrosion or grooving corrosion)

in production pipelines nor in WIPs the corrosion process is isolated from other influences. As will be seen below, there is a further complication, and that is that a population of pits depths selected at random may not form a homogeneous population, which is one of the standard requirements in all techniques for fitting data to a probability distribution. This is irrespective of whatever distribution is considered.

The external surfaces of offshore pipes are protected with coatings or uPVC or similar high density plastics to control exterior corrosion [47]. Cathodic protection, widely used on-shore and often mandated there by regulatory authorities, is feasible for off-shore pipelines but in most cases is considered uneconomic owing the considerable depth at which these pipelines are located. Because of the high pressures at depth, operations such as inspection and repairs require remotely operated vehicles (ROVs), adding considerably to the cost. For this reason cathodic protection is seldom used off-shore [3, 34]. The interiors of the pipes conventionally are left as bare steel. Interior coatings are impractical and would have only very short lives, largely as a result of erosion and damage caused by the particulate matter carried by the crude oil or the injected water, typically with velocities up to 5 m/s.

For production pipelines the long-standing approach to predicting the likely amount of interior corrosion is based on damage to the metal surface that can be caused by gasses released from the oil. These are $CO_2$ and $H_2S$ for aerobic (sweet) and anaerobic (sour) conditions respectively. A number of semi-empirical formulae are available, mostly derived or adapted from the original de Waard and Milliams model [32, 33, 36]. They are based on fundamental electrochemistry and the reactions involved in $CO_2$ and $H_2S$ corrosion of steels in wet conditions, but deal, essentially, only with average or 'uniform' corrosion. To bring the model predictions more in line with physical observations empirical adjustment factors have been introduced, applicable for specific areas of operations. The depth of pitting or crevice corrosion is then estimated from the estimated uniform corrosion using further empirical formulae. For example, it is often considered that the pit depth is 4–8 times the depth of uniform corrosion. Clearly, the prediction accuracy is not high. There are at present no models for predicting pit depth for production pipelines [36].

For WIPs, prediction of maximum pit depth or wall penetration is even less well-developed, in part because MIC may play a role [44]. From a practical perspective there has been some progress [8] through building on models and understanding available from detailed investigations and the modelling of the progression of corrosion of steels in seawater [25]. Nevertheless considerable calibration and cross-correlation remains to be done to produce robust models for pit depth prediction as a function of exposure time.

The practical approach in the oil and gas sector relies mainly on (linear) extrapolation from existing conditions. For the latter, one technique to assess current conditions is to use sampling coupons mounted at an accessible location of a pipeline (e.g. upstream end for WIPs) such that they are flush with the internal pipe wall surface [38]. These are then sampled periodically for rust products, biofilms and bacterial consortia. For WIPs water quality samples also are taken. Together these observations provide a degree of on-going monitoring and may, for example, provide an

indication, for WIPs, whether MIC is involved in the corrosion process [44]. They may also provide some guidance as to the likely development of future corrosion.

The technique most widely used in practice to obtain information about the degree of interior corrosion at a given point in time is the use of 'intelligent pigging'. This employs a conventional pigging train with an extra module on which are mounted an array of magnetic flux leakage (MFL) sensors [46]. As the pigging train runs through the pipe, it transmits data about the distance along the pipe (typically fixed using GPS) and the length and depth of 'features'. Based on experience algorithms exist to translate the information about features to the extent and depth of pitting and grooving corrosion along the pipe and around its circumference. This is not a straightforward exercise and involves some interpretation and error although typically the pit depths are reported in intervals of 1 mm. This approach is used for both production pipelines and WIPs and sometimes going down the WIP and, via a 'template', essentially a U-turn mechanism, routed to travel back via the production pipeline. In practice also, the functions of pipelines may be inter-changed between production and WI.

For most applications the depth of the deepest penetrations are of most interest for predicting the probability of wall perforation. This information is also of interest because once serious corrosion has set in, the usual control strategies (biocides, pigging) become less efficient [31]. Conventionally, the data from pigging runs are analysed using Extreme Value statistics. How this is mostly done in practice, and potential improvements are considered in the next section.

## 17.4 Data Analysis

Because only the deepest pits are of practical interest, it is customary to extract from the very extensive data generated by the pigging runs only the deepest pit depth for, say, every 25 or 50 m of pipe and then to use these values in an extreme value analysis. Because of the usually wide separation between the points so selected, the pit depths may be assumed, asymptotically at least, as independent values [20]. Importantly, they should follow a Gumbel extreme value distribution. It is the theoretical and asymptotic distribution for the maximum of maxima and has been considered the 'arch-typical' EV distribution for pit depths [12]. In passing it is noted that this fundamental point is sometimes forgotten and other extreme value distributions have been used instead, including the generalized extreme value (GEV) distribution, an entirely empirical distribution constructed from the three original (i.e. classical) extreme value distributions that at least have a fundamental basis in their derivation [7]. The GEV distribution has three parameters rather than two and these can be determined only from the data. This means application of the GEV distribution not only lacks a solid theoretical foundation, it also requires more data [11].

Pit depth data that are entirely consistent with the Gumbel EV distribution plot as a straight line on so-called 'Gumbel paper', a plot in which the vertical, cumulative probability, axis is suitably distorted [12]. The procedures for putting the data into such a plot are well-known [7, 12]. The simplest is the rank-order method in which

the n pit depths ($x$) are ranked from minimum to maximum and each assigned a cumulative probability that starts from $1/(n+1)$ and increases by this amount for each increasing value of $y$:

$$F_X(x_i) = P_i(X < x_i) = i/(n+1) \quad i = 1, 2, ..., n \tag{17.1}$$

This provides an unbiased estimator for the cumulative probability for each value of the random variable $X = x_i$. The values of the pit depths $x_i$ are then plotted against the corresponding cumulative probability $F_X(y_i)$. For pipelines this has been described previously (e.g. [28, 29]). Figure 17.4 shows an example for a production pipeline divided into 25 m lengths for each of which the deepest feature (pit) was extracted and considered an independent random variable ($X$). In Figure 17.4, the right vertical axis shows the probability of a pit depth less than the given value, while the left vertical axis is given as the corresponding standardized or Gumbel variate $w$ defined, as usual, by Benjamin and Cornell [4]:

$$w = (X - u)\alpha \tag{17.2}$$

where the mode $u$ and the slope α are parameters of the distribution. This transformation results in the non-linear Gumbel cumulative probability function transforming to a straight (inclined) line on the Gumbel plot. That line has slope α and intercept $u$.

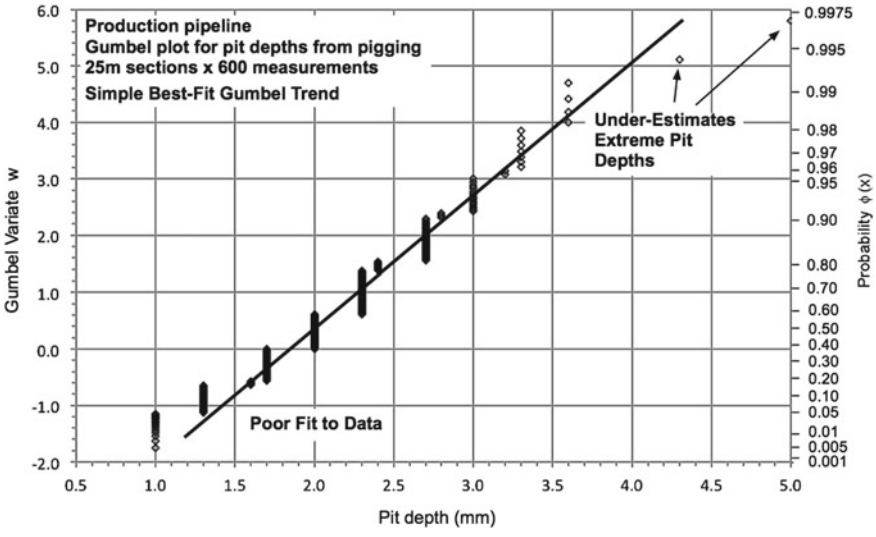


**Fig. 17.4** Maximum pit depth data, for each 25 m length, as extracted from the data stream obtained from a pigging run. The left vertical axis is given in terms of the Gumbel or reduced variate $w$ for which the right vertical axis shows the correspondence probability of the pit depth being less than a given value. The best fit 'Gumbel' trend line has been added

According to Fig. 17.4, for the data cohort used, there is a 95% probability that the maximum depth pit will be less than $x = 3$ mm deep [i.e. $P(X < x_i) = 0.95$], or, in terms of exceedence probabilities, a 5% probability that the depth will be greater than $x = 3$ mm [i.e. $P(X > x_i) = 0.05$]. Assuming all the data can be fitted by this Gumbel distribution, it is possible, in principle, to estimate the probability of a much deeper occurring. For example, the probability of occurrence of a pit deeper than say 4.5 mm would be $1 - 0.9975 = 0.0025$. However, the actual data show that a pit of around 5 mm depth was observed for a similar probability of occurrence. The problem is, as evident in Fig. 17.4, that the overall Gumbel distribution for the whole range of maximum observed pit depths does not fit the extremes (i.e. the higher values) very well, even though these are the pit depths of most practical interest.

For this reason, for extrapolation to ascertain the probability of occurrence of very deep pits in practical applications, only the upper right (partial) trend is considered, the data for shallower pits ignored and extrapolation confined to the deepest pits, as shown in Fig. 17.5. It shows that the data can be considered as composed of a set of piece-wise linear, partial, trends, and that only the upper right (partial) trend is relevant for extrapolation. For this reason, in practical applications most of the data are ignored and extrapolation confined to the deepest pits (Fig. 17.5). Thus, only the upper right (partial) trend is considered relevant. It is only this subset of the extreme data that should be considered as being in the 'domain of attraction' for the most relevant Gumbel EV distribution [6]. The fact that there is a considerable change in slope of the data for that sub-set and the rest on a Gumbel plot indicates that the choice of the data to use for this domain of attraction is not entirely empirical.

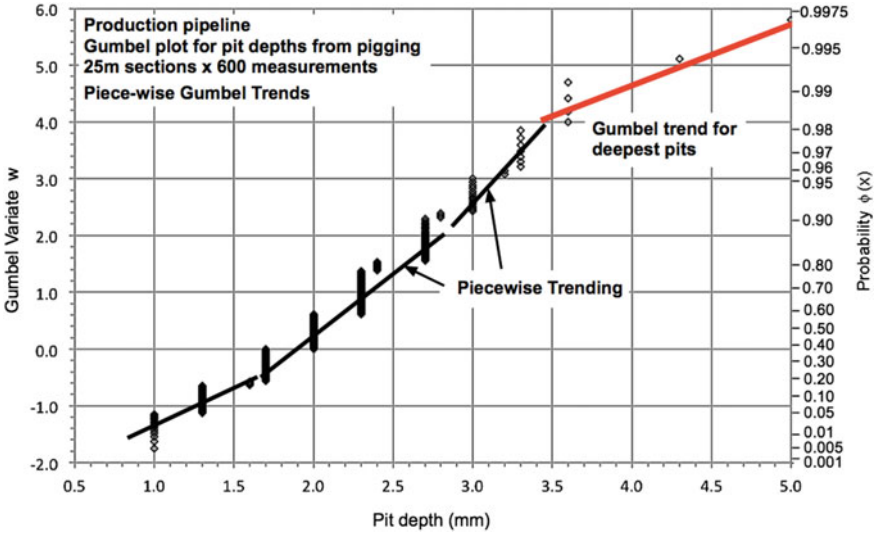


**Fig. 17.5** Data as in Fig. 17.4 reinterpreted as represented by a piecewise trend for which only the trend for the deepest pits is relevant in practice

Figure 17.5 also shows that on this Gumbel plot the data overall show piece-wise linear trending. This indicates that overall the data are not homogeneous. However, since each of these partial trends fit the data in the subset reasonably well, each partial trend may be considered Gumbel EV distributed in its own right, valid over a restricted range of values and, within that range either homogeneous or closely so. The piece-wise trend in Fig. 17.5 can therefore be interpreted as representing a multi-modal probability distribution in which each mode represents a (somewhat) different underlying population and thus, in this case, a (somewhat) different corrosion process. The latter will be discussed further below. Here it is noted simply that the multi-modal probability concept is not new.

As the extreme value distribution of independent maxima, the Gumbel EV distribution has long been applied for representing the probability distribution for maximum wind speeds. It is now known, from observations generally similar to those noted above, that wind speed data over a sufficiently large range of wind speeds plotted on a Gumbel plot show a different trend line for lower wind speeds as compared with higher wind speeds—in other words the Gumbel trend is piece-wise. Re-examination of the data and the sources of the data showed that there is a different trend line for wind speeds generated under normal conditions and those generated under thunderstorm conditions [13].

The implications of the piecewise trending in Figs. 17.4 and 17.5 follow directly from the observations of Gomes and Vickery [13] but now interpreted in terms of maximum pit depth rather than wind speeds. Each trend in Figs. 17.4 and 17.5 represents a (perhaps slightly) different pitting corrosion mechanism, or pitting corrosion under somewhat different conditions, and these change as pit depth increases. This can be seen in data considering the development of pit depth [27, 29]. The development of corrosion occurs in phases, each of which has its own degree of statistical uncertainty [23]. For extended exposures, such as for the data in Fig. 17.4, the corrosion of a surface will consist of some pitting in an early of development (Fig. 17.6), some developed further and some in the long-term pit progression process (phase 4). Each has associated with it a degree of uncertainty related to the pitting process as shown schematically in Fig. 17.6.

For the extended exposures of interest here the uncertainty in pit depth for all the pits on a corroded surface is considerable, as shown by the ‘underlying distribution’. Of these, only the deepest pits are of interest, represented by the extreme value distribution. For these extreme pit depths there remains considerable uncertainty, as shown schematically by the Extreme Value Distributions in Fig. 17.6. This implies a rather flat trend on a Gumbel plot, as indeed is seen in Fig. 17.5 for the deepest pits.

## 17.5 Estimation of the Probability of Failure

In structural theory an estimate of the nominal probability of failure requires consideration of all the variables that are likely to be of importance and to treat those as either ransom variables, or for those that are functions of time or influenced by time,

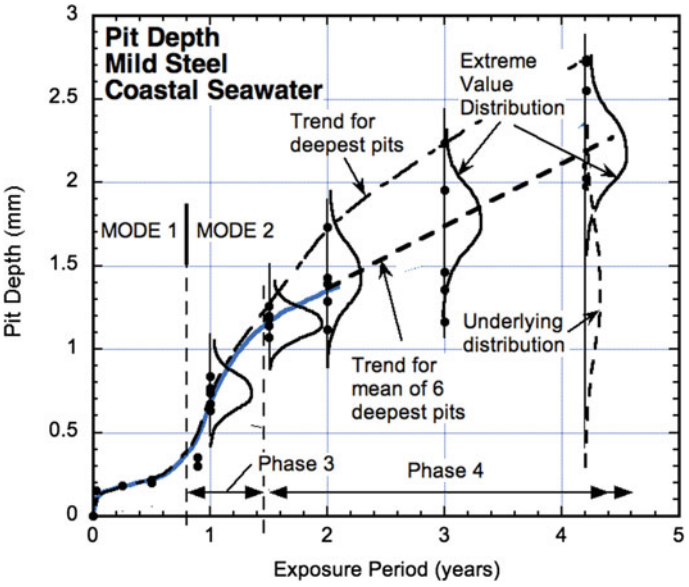


**Fig. 17.6** Development of maximum pit depth ($d_{max}$) (and the average of the 6 deepest pits) with increasing exposure time $t$. Schematic probability density functions for the underlying distribution of all pit depths and the EV distribution for the deepest pit depths are shown, the latter at various times, to indicate the changing variability in the data (based on Melchers [23])

as stochastic variables. For the probability of failure resulting from pipe-wall perforation by pitting, the problem can be much simplified [1]. In particular, that earlier work has shown that for pressure pipes, unlike most structural reliability problems, the loading (internal or external pressure) is well-defined and expressed as a random variable does not have a large variance (i.e. degree of uncertainty). The material parameters also are relatively well defined, with even smaller variances [30]. The most uncertain parameter is the rate of progression of corrosion [1]. In its simplest form, the structural reliability formulation is defined by the limit state G(·), being the perforation of the pipe-wall thickness $b$ ($y$, $z$, $t$) by the depth $d$ ($y$, $z$, $t$) (Fig. 17.3). Both can be considered as random variables. As indicated, both are dependent on location ($y$, $z$) and time $t$. For the wall-thickness the variability over ($y$, $z$) can be included in the variability of the wall thickness itself. For pit depth, however, there is much greater variability. One way of handling this is to invoke the notion of the extreme value of pit depth at time $t$. This extreme value can, in the case of pitting that potentially can occur over extended surface areas, be based on the deepest pit for likely to occur over a defined area, as was done in Figs. 17.4 and 17.5 for the maximum pit depth for each 25 m length of pipe. Then the area effect becomes subsumed in the extreme value distribution. The analogy to the notion of maximum wind speed per year being modelled as an extreme value distribution [13] should be clear. Confining attention now to a defined time $t$, the limit state becomes G [$b$ $d_{max}$] = 0 with the probability of failure at time $t$ defined as $P$ [G < 0]. On the extreme

value plots (Figs. 17.4 and 17.5), this is simply $P = 1 - \Phi(d < y)$, for which $\Phi(d < y)$ can be read from the plots.

## 17.6 Extrapolation in Time

The above analysis will allow, as indicated, an estimate of probability of occurrence of a pit of a given (deep) depth based on the data that was measured during an intelligent pigging operation. This helps decide the relative safety of a pipeline at the present time, and by implication, for the near future. Thus it is a tool for a point-in-time assessment of the condition of the pipeline.

In practice there is also interest in the likely condition of a pipeline into the future. This implies the ability to estimate the probability of occurrence (or exceedence) of a given depth of pitting at a *future* point in time. To make such estimates two potential approaches are available, at least in principle. One relies on the capacity to make predictions of pit growth based on past experience and understanding (empirical or theoretical or both) of the pitting process and the effect of various factors that influence such pit growth. The only possibility to date is to invoke an empirical pit depth growth model, such as a power law based on multiple observations for the time dependence of mean pit depths (e.g. [19]), even though observations for longer term pit depth development indicate that a bi-modal model is more likely appropriate, as shown for example in Fig. 17.6 after the exposure period exceeds about 0.8 years [23]. However, the underlying physical–chemical basis for such behaviour remains unclear. Nevertheless, that model could be useful for extrapolation of pit depths on steels in seawater. The long-term rate so obtained could be relevant for steel water injection pipelines with clean seawater as the injected water and without additives for corrosion suppression or for nitrate addition into the wells. Some understanding of the effects of these is available [8]. However, understanding of the effects of other conditions remains unclear. The net result is that for operating water injection pipelines reliance is often placed on the use of 'experience' for shorter-term extrapolation, essentially using linear projection from the current data at a constant rate. A more refined approach is to extrapolate pit depth data as obtained from successive intelligent pigging runs, usually taken some years apart. An example of the latter is shown in Fig. 17.7 for the longer-term corrosion, pit depth and channelling data trends in Fig. 17.7. A similar approach applies for production pipelines [9].

That the extrapolation is much dependent on the type of corrosion being considered (general wall corrosion, pitting or channelling corrosion) and that it also depends on the proprietary additives added for corrosion inhibition or nitrates added for inhibition of sulphate reducing bacteria in the well. The effect of adding nitrates is shown as the addition affect of microbiological corrosion, shown schematically in Fig. 17.7 for water injection pipelines, both for corrosion and for the depth of pitting. This effect of nitrates on microbial corrosion is consistent with other observations of the corrosion of steels in polluted waters [24]. Other factors, such as changes in the use

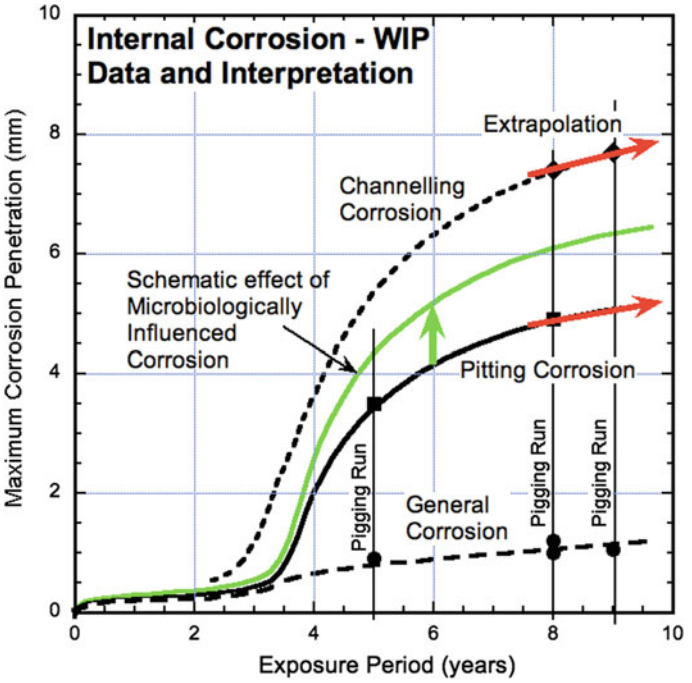


**Fig. 17.7** Example of general, pitting and channelling corrosion data for successive intelligent pigging runs, extrapolation of longer-term data trends and effect of microbiologically influenced corrosion, shown only for pitting depth (based on data in Comanescu et al. [8]. The trends shown are based in the trends shown in Fig. 17.6

and operation of pipelines such as extra injection of nitrates for reasons not associated with durability, can affect corrosion and pit depths [8]. This will be reflected in any extreme value analysis of maximum pit depths.

## 17.7 Clustering of Pit Locations and of Pit Depths

The use of extreme value analysis as reviewed above is based on the assumption of each of the extreme value observations (i.e. the maximum pit depth values) being statistically independent of the others. This is a long-held prior assumption for pitting. It may be considered reasonable, asymptotically [20] for the deepest pits that are a considerable distance apart. But it is certainly not true for all pitting. Figure 17.8 shows several microscope photographs of steel pitted by exposure to seawater for many months, similar to images reported earlier [23]. Many of the pits are clustered with others, and most show similar pit depths. However, there also are areas with quite different corrosion patterns. It has been observed that pits grow in increments with

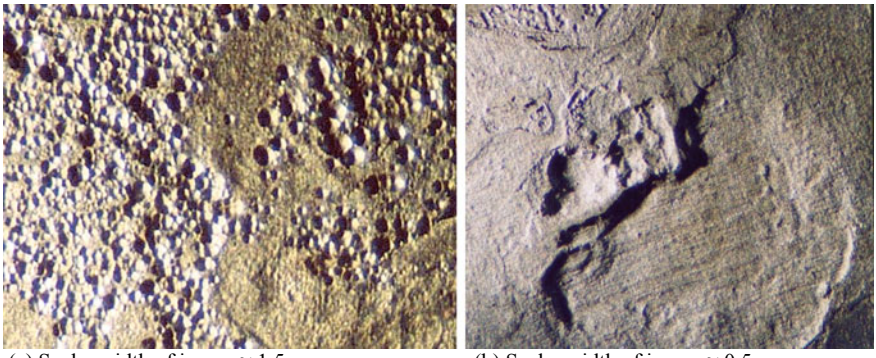

(a) Scale: width of image ≈ 1.5 mm. (b) Scale: width of image ≈ 0.5 mm.

**Fig. 17.8** Examples of, **a** clustering of corrosion pits of similar depths on a steel surface in seawater, and **b** plateau approximating uniform corrosion resulting from lateral amalgamations of multiple pits

formation of plateaus [17], consistent with theoretical predictions of sideways growth of pits once the pitting potential is exhausted [40] and this has been hypothesized as creating the complex corrosion morphology usually observed [25] (Fig. 17.8). It follows that pit propagation and the growth in pit depth over extended periods of time (months, years) follow a more complex pattern than typically observed in laboratory for shorter term exposures (e.g. [5]). An isolated roughly circular pit surrounded by a roughly circular cathodic zone as reported in the classic literature [10] is only seldom observed. In practice, a low degree of dependence between isolated maximum pits is likely, mainly because neither the environment nor the metal surface is spatially homogeneous and uniform. Pit initiation depends much on the local conditions of the metal surface, including imperfections and inclusions [5, 14], while pit depth development, particularly in phases 3 and 4 (Fig. 17.6) occurs almost entirely under rusts that have built-up from earlier corrosion [49]. Again, in practice there is much evidence of the spatial inhomogeneity of pitting over a surface, as can be seen in Fig. 17.2 for water injection pipelines.

Finally, it might be mentioned that the use of extreme value analysis for maximum pit depths has revealed that there is a pattern in the data for the extreme pits (such as the maximum pit depths for every 25 m length of pipeline). This pattern can be seen in Fig. 17.4 (and 5) with these extreme pit depths occurring predominantly in groups, for example at pit depths 2.0, 2.34, 2.67, 3.0 mm etc. It is not something that has been observed or predicted in the classical or the more modern literature. However, it is not confined to the cases mentioned but has been observed also for pitting of cast iron pipes buried in soils [2] and for aluminium alloys exposed to seawater [22], in each case with the application of extreme value analysis. While this is ultimately a feature of the step-wise pitting corrosion process (see above), it also highlights why earlier applications often were able to fit linear functions (i.e. Gumbel lines) through the data—there were essentially only a few points, and scatter was assumed to be an influence. The use of modern scanning tools in the laboratory and also availability

of tools such as intelligent pigging has enabled much larger data sets to be obtained and, in consequence has allowed the observation of piece-wise trends (Fig. 17.5) and rational explanations to be offered for the domain of attraction being very much limited to the most extreme of the extreme pit depths—an approach long used in industry on an entirely heuristic basis.

## 17.8 Conclusion

The present chapter has focussed on a major ingredient for the risk assessment of oil (and gas) production pipelines and for water injection pipelines, namely the probability of pipe-wall perforation due to internal corrosion. Once this has been established the probabilities from other events such as overpressure and physical damage to the welds, flanges and the pipe itself, as well as construction and 3rd party damage can be added in through the usual systems risk assessment processes [43]. As explained, pipe-wall perforation is essentially the result of internal corrosion, and in particular pitting corrosion and in some cases channelling corrosion. The latter is actually localize corrosion with physical–chemical characteristics similar to pitting, and thus could have been considered for extreme value analysis. Importantly, the more detailed analysis reviewed herein has shown the importance of careful consideration of probabilities in the upper tail, and that it is not from exactly the same statistical distribution as the remaining cohort (s) of extreme depth pits. The reason for this to be the case was explained in terms of the changing conditions (and physico-chemical mechanisms) under which pitting corrosion occurs in practice under extended exposures. This also is the reason why efforts to obtain the complete (continuous) probability distribution for pit depths from pit depth observations are unlikely to be useful—invariably those effects do not distinguish sufficiently between most of the data and the data in the tail of interest (i.e. the upper tail).

**Acknowledgements** The author acknowledges the support of the Australian Research Council (Grants DP14103388 and DP160101908), the funding and information provided through the FPSO Research Forum and AMOG Consulting, Melbourne and Houston. The data in Figs. 17.4 and 17.5 were provided by an anonymous source and processed into the basic Gumbel plot by Dr M Ahammed whose continued support is gratefully acknowledged.

## References

1. Ahammed M (1998) Probabilistic estimation of remaining life of a pipeline in the presence of active corrosion defects. Int J Press Vessels Piping 75:321–329
2. Asadi ZS, Melchers RE (2018) Clustering of corrosion pit depths for buried cast iron pipes. Corros Sci 140:92–98
3. Bai Y, Bai Q (2005) Subsea pipelines and risers. Elsevier, Oxford

4. Benjamin JR, Cornell CA (1970) Probability, Statistics, and Decision for Civil Engineers. McGraw-Hill Book Co., New York, 275, 666
5. Butler G, Stretton P, Beynon JG (1972) Initiation and growth of pits on high-purity iron and its alloys with chromium and copper in neutral chloride solutions. Brit Corros J 7(7):168–173
6. Castillo E, Sarabia JM (1992) Engineering analysis of extreme value data: selection of models. J Waterways, Port, Coastal Ocean Eng 118(2):129–146
7. Coles S (2001) An introduction to the modelling of extreme values. Springer, New York
8. Comanescu I, Melchers RE, Taxén C (2015) Corrosion and durability of offshore steel water injection pipelines. Ships Offshore Struct 11(4):424–437
9. Dawson J (2019) Predicting the future: applying corrosion growth rates from in-line inspections. Pipeline Technol J 1:30–35
10. Evans UR (1960) The corrosion and oxidation of metal: scientific principles and practical applications. Edward Arnold, London
11. Fougeres A-L, Nolan J, Rootzen H (2009) Models for dependent extremes using stable mixtures. Scand J Stat 36:42–59
12. Galambos J (1987) The asymptotic theory of extreme order statistics, 2nd edn. Krieger, Malabar, FL
13. Gomes L, Vickery BJ (1976) Tropical cyclone gust speeds along the northern Australian coast. Civ Engg Trans Inst Engrs Aust CE18(2):40–48
14. Greene ND, Fontana MG (1959) A critical analysis of pitting corrosion. Corrosion 15(1):41–47
15. Harro HH, Port RD (1993) The Nalco guide to cooling water systems failure analysis. McGraw Hill, New York
16. Heidersbach KL, van Roodselaar AC (2012) Understanding, preventing, and identification of microbial induced erosion-corrosion (channelling) in water injection pipelines. In: Proc. NACE international corrosion conference and expo 2012, Salt lake City, UT, paper no: C2012-0001221
17. Jeffrey R, Melchers RE (2007) The changing topography of corroding mild steel surfaces in seawater. Corros Sci 49:2270–2288
18. Larsen KR (2013) Managing corrosion of pipelines that transport crude oils. Mater Perform, NACE Int 52(5):28–35
19. Laycock PJ, Cottis RA, Scarf PA (1990) Extrapolation of extreme pit depths in space and time. J Electrochem Soc 137(1):64–69
20. Leadbetter MR, Lindgren G, Rootzen H (1983) Extremes and related properties of random sequences and processes. Springer, New York
21. Lee TM, Melchers RE, Beech IB, Potts AE, Kilner AA (2015) Microbiologically influenced corrosion (MIC) of mooring systems: diagnostic techniques to improve mooring integrity. In: Proceeding of the 20th offshore symposium, Feb. 2015. Houston, TX, Soc. Naval Arch. and Marine Engs
22. Llang M., Melchers RE (2021) Two years pitting corrosion of AA5005-H34 aluminium alloy immersed in natural seawater: data interpretation. Corrosion Engineering, Science and Technology 56(2): 126–136
23. Melchers RE (2004) Pitting corrosion of mild steel in marine immersion environment—1: maximum pit depth. Corrosion 60(9):824–836
24. Melchers RE (2014) Long-term immersion corrosion of steels in seawaters with elevated nutrient concentration. Corros Sci 81:110–116
25. Melchers RE (2015) On the bi-modal long-term characteristic for metallic corrosion. In: Proceedings conference corrosion & prevention, Adelaide, 15–18 Nov., Aust. Corrn. Assn., Melbourne, paper 041
26. Melchers RE (2018) A review of trends for corrosion loss and pit depth in longer-term exposures. Corros Mater Degrad 2018(1):4. https://doi.org/10.3390/cmd1010004
27. Melchers RE (2020) New insights from probabilistic modelling of corrosion in structural reliability analysis. Structural Safety 88(1), 102034
28. Melchers RE, Ahammed M (2017) New interpretation of maximum corrosion pit depths and implications for extreme value representation. In: Proceeding ICOSSAR, international conference on structural safety and reliability. Vienna

29. Melchers RE, Ahammed M (2018) Maximum pit depth variability in water injection pipelines. In: Proceeding 28th international ocean and polar engineering conference. Sapporo, Japan, June 10–15, pp 289–294
30. Melchers RE, Beck AT (2018) Structural reliability analysis and prediction, 3rd Edn. John Wiley, Chichester. https://doi.org/10.1002/9781119266105
31. Mitchell AF, Liengen T, Anfindsen H, Molid S (2012) Experience of molecular monitoring techniques in upstream oil and gas operations, Corrosion 2012. NACE International, Houston
32. Nesic S (2007) Key issues related to modelling of internal corrosion of oil and gas pipelines—a review. Corros Sci 49(2007):4308–4338
33. Nesic S, Kahyayian A, Choi YS (2019) Implementation of a comprehensive mechnaistic prediction model of mild steel corrosion in multiphase oil and gas pipelines. Corrosion 75(3):274–291
34. Palmer AC, King RA (2008) Subsea pipeline engineering, 2nd edn. Pennwell Corp, Tulsa
35. Pentney A, Carnes D (2015) Pipeline abandonment. In: Revie RW (ed) Oil and gas pipelines: integrity and safety handbook. Wiley, Hoboken, pp 689–696
36. Pessu F, Hua Y, Barker R, Neville A (2018) A study of the pitting and uniform corrosion characteristics of X65 carbon steel in different $H_2S$-$CO_2$-containing environments. Corrosion 74(8):886–902
37. Potts AE, Jayasinghe K, Kilner A, Melchers RE, Chaplin CR (2018) Advancements in Guidance for the Specification and Assessment of Mooring Steel Wire Rope. In: Offshore technology conference, Houston, TX, OTC-2881228812
38. Powell DE (2015) Internal corrosion monitoring using coupons and ER probes. In: Revie RW (ed) Oil and gas pipelines: integrity and safety handbook. Wiley, Hoboken, pp 495–513
39. Roberts RL (2015) Pipeline cleaning. In: Revie RW (ed) Oil and gas pipelines: integrity and safety handbook. Wiley, Hoboken, pp 601–607
40. Sharland SM, Tasker PW (1988) A mathematical model of crevice and pitting corrosion—I. Phys Model, Corros Sci 28(6):603–620
41. Shirazi SA, Mclaury BS, Shadley JR, Roberts KP, Rybicki EF, Rincon HE, Hassani S, Al-Mutahar FM, Al-Aithan GH (2015) Erosion-corrosion in oil and gas pipelines. In: Revie RW (ed) Oil and gas pipelines: integrity and safety handbook. Wiley, Hoboken, pp 399–421
42. Singh B, Poblett B (2015) Offshore pipeline risk corrosion, and integrity management. In: Revie RW (ed) Oil and gas pipelines: integrity and safety handbook. Wiley, Hoboken, pp 727–757
43. Stewart MG, Melchers RE (1997) Probabilistic risk assessment for engineering systems. Chapman & Hall, London
44. Stipanicev M, Turcu F, Esnault L, Rosas O, Basseguy R, Sztyler M, Beech IB (2014) Corrosion of carbon steel by bacteria from North Sea offshore seawater injection systems: laboratory investigation. Bioelectrochemistry 97:76–88
45. Stott JFD (2012) Implementation of nitrate treatment for reservoir souring control: complexities and pitfalls. In: SPE international conference and exhibition on oilfield corrosion held in Aberdeen, UK, 28–29 May 2012
46. Uzelac NI (2015) In-line inspection (ILI) ("intelligent pigging"). In: Revie RW (ed) Oil and gas pipelines: integrity and safety handbook. Wiley, Hoboken, pp 515–536
47. Waslen D (2015) External coatings. In: Revie RW (ed) Oil and gas pipelines: integrity and safety handbook. Wiley, Hoboken, pp 439–446
48. Webmac (2020) Nord stream, explore the world of piping. http://www.wermac.org/nordstream/nordstream_part1.htm. Last accessed 3 Nov 2020
49. Wranglen G (1974) Pitting and sulphide inclusions in steel. Corros Sci 14:331–349

# Chapter 18
# Reliability Assessment of Corroded Pipelines Subjected to Seismic Activity


**Rafael Amaya-Gómez, Mauricio Sánchez-Silva, and Emilio Bastidas-Arteaga**

**Abstract** Corrosion and natural events are some of the more significant threats for onshore pipelines because of their frequency and potential severity. Corrosion defects reduce the wall thickness and can lead to a burst due to the internal pressure. Extreme events after seismic activity, either by transient (TGD) or permanent ground deformations (PGD), can also affect pipeline integrity, e.g., tension failure. This chapter proposes a combined reliability assessment for a corroded pipeline subjected to TGD using Monte Carlo simulations. It contemplates simulated seismic activity using two Poisson Processes based on historical records and an attenuation law to evaluate a tension failure. The corrosion degradation implements a Lévy Process based on data from In-Line Inspections (ILI), with the possibility of new defects appearing between inspections and the formation of corrosion colonies to determine a burst failure. The proposed approach is illustrated using a real case study.

## 18.1 Introduction

Onshore pipelines are the most widely used and cost-effective means for hydrocarbon transportation. Given the hazardous nature of the fluid (i.e., flammable, toxic, and explosive), a loss of the pipeline containment may dramatically impact the environment and threaten surrounding lives and property. Onshore pipelines frequently experience inner and outer corrosion degradation due to the aggressiveness of the surrounding soil, flaws at the protective coating, or the corrosiveness caused by the

R. Amaya-Gómez (✉) · M. Sánchez-Silva
Department of Civil and Environmental Engineering, Universidad de los Andes, Cr 1E # 19A-40, 111711 Bogotá, Colombia
e-mail: r.amaya29@uniandes.edu.co

M. Sánchez-Silva
e-mail: msanchez@uniandes.edu.co

E. Bastidas-Arteaga
Laboratory of Engineering Sciences for Environment, La Rochelle University, UMR CNRS 7356, La Rochelle, France
e-mail: ebastida@univ-lr.fr



M. G. Stewart and D. V. Rosowsky (eds.), *Engineering for Extremes*, Springer Tracts in Civil Engineering, https://doi.org/10.1007/978-3-030-85018-0_18

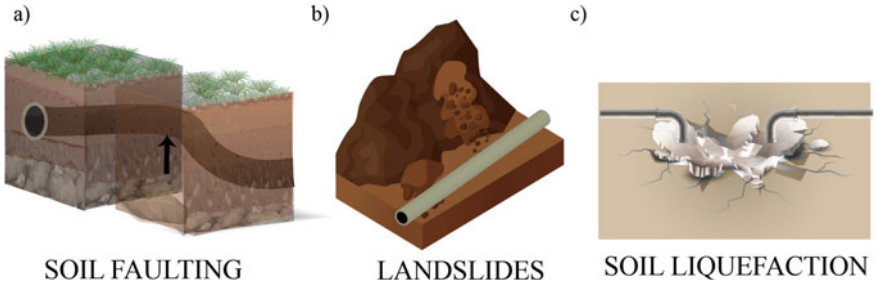


**Fig. 18.1** Schematic failures of a pipeline due to a **a**) soil faulting, **b**) landslide, and **c**) soil liquefaction

transporting fluid [1–3]. The consequent reduction in the wall thickness and the changes in the pipeline properties lead to either leak, bursts, or pipeline ruptures.

Besides corrosion, extreme events associated with a seismic activity or climate change (e.g., heavy rainfall, floods) could also disturb pipelines integrity [4, 5]. These events include transient and permanent ground deformations such as ground shaking, soil faulting, landslides, or soil liquefaction (Fig. 18.1). Although these extreme events are also considered on pipeline risk management, support engineering decisions from a risk-based perspective is challenging due to the uncertainties surrounding each natural event. For instance, after an earthquake occurs, it produces a seismic activity associated with surface or body waves with the ability to alter the pipeline integrity, which can be highly affected depending on how close it is located from the epicenter. In this regard, when and where an earthquake occurs is uncertain, as well on how the seismic waves are going to be attenuated.

The seismic risk for buried pipelines is usually assessed using empirical fragility functions. These functions are obtained based on data from past events or general probabilistic approximations. They are used to estimate the repair rate of a given pipeline (i.e., No. Repairs/km) given a seismic load [6]. These repair rates (RR) are useful for estimating a preliminary failure probability and supporting the further design and protection decisions. However, as noted in the review of Tsinidis et al. [6], the RR does not give further information about how the pipeline would be affected nor what type of repairs would be required, e.g., replacement, recoating, welding the joints. Some exceptions consider a probabilistic approach or a multi-hazard perspective. Two relevant examples include a multi-hazard failure probability of a gas pipeline due to an earthquake shaking, ground failure, and a fire scenario [7], and a GIS model for water pipeline failure probability due to ground shaking and ground failure [8].

This chapter presents a strategy to support the risk assessment of corroded pipelines subjected to seismic activity, considering the information obtained from consecutive In-Line Inspections (ILI) (NACE RP0102-2002 Standard). These inspections provide a clear perspective of the pipe's inner and outer corroded condition using magnetic (MFL) or ultrasonic (UT) tools. These inspections are commonly valuable

to define maintenance policies based on the pipeline condition [9, 10]. The strategy focuses on evaluating burst failure triggered by the metal loss and the internal pressure and tension stresses generated from a Transient Ground Deformation. The corrosion assessment considers the appearance of new defects between inspections and the formation of corrosion colonies (i.e., clusters). The chapter is structured as follows: first, it describes a general context in terms of corrosion (Sect. 18.2) and natural hazards (Sect. 18.3) for onshore pipelines. Section 18.4 presents the proposed methodology and Sect. 18.5 the case study. Finally, Sect. 18.6 presents and discusses the main results and Sect. 18.7 some concluding remarks.

## 18.2 Corrosion Assessment Based on In-Line Measurements

ILI inspections provide valuable information about the condition of the pipeline to support operating and maintenance decisions. An ILI inspection results shall contain a pipe tally, a list of anomalies, and a list of clusters [11]. The pipe tally presents a list of all pipeline and anomaly features associated with: (i) Location and orientation parameters, (ii) structural parameters, and (iii) primary descriptors of the detected anomalies. The location parameters cover the log-distance (i.e., pipeline abscissa), latitude/longitude position, the height above the sea level, and the inclination of the joint. The structural and geometric parameters contemplate the yield and ultimate strengths, the wall thickness, and the pipeline diameter. The list of anomalies describes the imperfections and flaws found above the reporting threshold of the inspection tool. This list of anomalies includes information on the geometric extent of the metal loss (i.e., width, length, and depth), the location, and orientation using a clock-position analogy. This analogy implements the relative circumferential direction of the defects using a 12 h-clock [11]. Figure 18.2 illustrates these parameters, considering a rectangular shape that identifies the maximum extent of the defect.

### *18.2.1 Deterioration Caused by Corrosion*

Corrosion is a progressive degradation mechanism, i.e., it is the result of the capacity being continuously reduced at a rate that may change over time. Growth corrosion models describe the geometric evolution of defects, mainly the depth-increments. Thus, a sequence of ILI measurements can be used to identify the stochastic process that describes their evolution through time, considering the location and orientation of the defects, which allow modeling the corrosion process as different possible sample paths, as illustrated in Fig. 18.3.

Some of the common stochastic processes to model corrosion include the Gamma Process and the Inverse Gaussian Process. They are jump-processes with indepen-

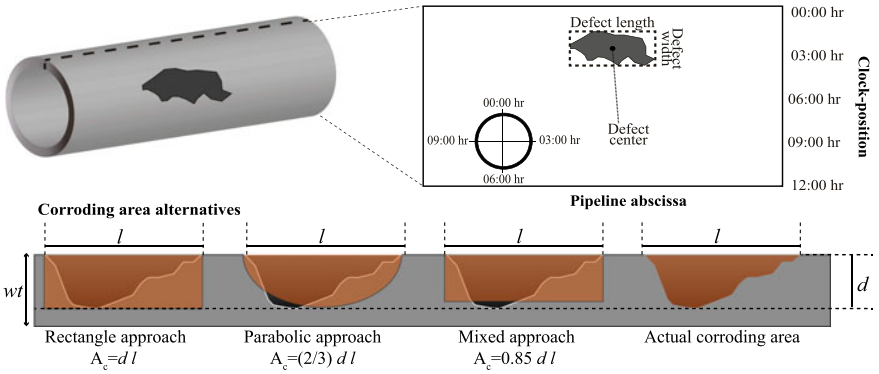


**Fig. 18.2** Schematic location of a corrosion defect. Adapted from [12, 13]

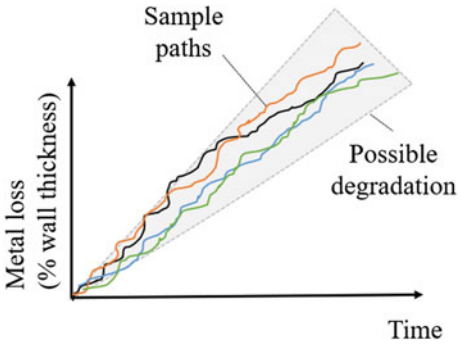


**Fig. 18.3** Schematic degradation of corroded pipelines

dent increments, with non-negative jumps that happen infinitely often in any finite time interval; these properties make them suitable to model progressive degradation. Further details of these processes can be found elsewhere; see, for instance, Amaya-Gómez et al. [12, 14, 15].

### *18.2.2 Failure Modes and Limit States*

In the design of pipelines, the wall thickness is selected to withstand the fluid pressure based on the pipe's material and geometric properties; this is usually evaluated considering Barlow's formula:

$$P = \frac{2\sigma_h \, wt}{D}. \tag{18.1}$$

where $P$ is the internal pressure, $D$ is the pipe diameter, $wt$ is the wall thickness, and $\sigma_h$ is the hoop or tangential stress.[1] The corrosion process reduces the pipeline's effective wall thickness; hence, the pipeline may not withstand the loads coming from the internal operating pressure and make it more prone to fail depending on the extent of the defect. For a pipeline with a corrosion defect with a depth $d$ and a length $l$, the hoop stress is replaced by a flow stress $\sigma_{flow}$ and a term that represents the strength reduction of the pipeline due to the growth of the corrosion area [17, 18]; i.e.,

$$\sigma_{hf} = \sigma_{flow}\left[\frac{1-(A_c/A_o)}{1-(A_c/A_o)M^{-1}}\right], \tag{18.2}$$

where $M$ is known as the Folias or bulging factor, $A_o$ is the intact longitudinal area before the corrosion defect takes place (i.e., $A_o = wt \cdot l$), and $A_c$ is the corroded area, which is a function of the defect depth and length. These areas correspond to metal loss projections in the longitudinal plane based on the wall thickness [19]. Different defect shapes such as parabolic ($(2/3)d \cdot l$), rectangular ($d \cdot l$), or mixed ($0.85d \cdot l$) approaches have been proposed (Fig. 18.2); they are commonly used to determine the pipeline resistance for a plastic collapse or a burst pressure ($P_b$). Some recommendations of the burst pressure models depending on the material toughness can be found in [13]. Besides a burst, a metal loss of the pipeline could lead to a leak or a total rupture. According to the CSA Z662, a small leak occurs when the maximum defect depth mostly exceeds the wall thickness, but it is sufficiently narrow to prevent a burst, whereas a rupture happens after an initial burst and an unstable growth [20].

The shape and evolution of defects have proven to be critical in the reliability evaluation of pipelines; in particular, the amount and the proximity among defects play a significant role. If the defects are located close to each other – known as "corrosion colonies"– the chances of failure causing loss of containment become critical; in this case, the interaction of individual defects acts as a single larger defect (Fig. 18.4). There are several grouping criteria between adjacent corrosion defects, where the most used are those from standards such as DNV RP F-101, BS 7910, CSA Z184, ASMEB31G, or API579-1/ASME FFS-1 [21, 22]. The relevance of the *corrosion colonies* lies in the fact that they affect reliability predictions such as the Mean Time to Failure (MTTF), which in turn, are useful to support further decision-making processes [23].

## 18.3 Seismic Hazards for Buried Onshore Pipelines

Seismic hazards are related to waves propagating through earth generated by seismic faulting, or surface waves that travel along the surface ground from the reflection and

[1] It is commonly replaced by the yield ($\sigma_y$) or ultimate ($\sigma_u$) strength multiplied by a safety factor [16].

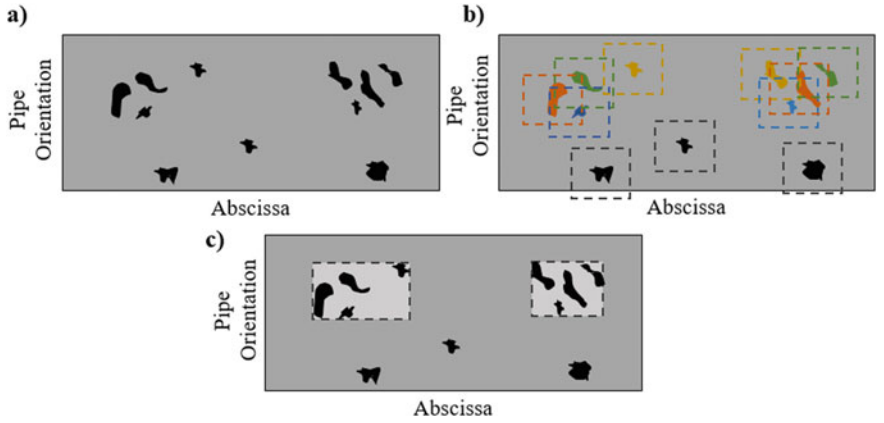


**Fig. 18.4** Schematic **a**) location of corrosion defects, **b**) the clustering criterion, and **c**) the obtained clusters

refraction of body and shear waves. Onshore pipelines are commonly buried, which makes them highly exposed to wave propagation through the surrounding soil [6]. On the one hand, buried pipelines are susceptible to failure due to a Permanent Ground Deformation (PGD), which can be classified into fault movements, landslides, or soil liquefaction (Fig. 18.1). Faulting refers to a discontinuity between two earth layer portions with relative movements; landslides are massive ground movements that may be caused by seismic activity, and liquefaction refers to a liquid soil behavior due to earthquake motions [5]. The latter phenomenon is expected in soils without cohesion and in the presence of high humidity [24]. On the other hand, onshore pipelines may also fail as a consequence of Transient Ground Deformations (TGD) that result from seismic wave propagation [5]. Some strains reported on pipelines are depicted in Table 18.1. This table illustrates the effect of various deformation types on pipelines and the corresponding failure modes.

**Table 18.1** Failure modes of underground pipelines subjected to seismic waves propagation. Adapted from Podimata [25]

| Deformation type | Description | Strain | Risk factors | |
|---|---|---|---|---|
| | | | Liquefaction | Landslide |
| Permanent ground deformation | Longitudinal | Tension | Rupture[a] | Rupture[a] |
| | | Compression | Local buckling[b] | Local buckling[b] |
| | Transverse | Tension | - | Rupture |
| | | Bending | Local buckling[c] | Local buckling |
| | Random | Tension and bending | Rupture[c] | |
| | | Compression and bending | Local buckling[c] | |
| Deformation type | Description | Strain | Risk factors | |
| | | | Shear body waves | Surface waves |
| Transient ground deformation (Wave propagation) | Longitudinal | Tension | Rupture | - |
| | | Compression | Buckling | - |
| | | Bending | - | Buckling |
| | Transverse | Bending | Buckling | |
| | | Tension | Rupture | |
| | Combined | Compression | Buckling | |
| | | Bending | Buckling | |

[a] At the head of PGD, [b] At the tow of PGD, [c] At the flanks of the PGD

Several empirical correlations have been proposed between ground motion properties and pipeline failures; these are known as Ground Motion Prediction (GMP) correlation functions [26]. For seismic waves, this intensity may include the Modified Mercalli Intensity, Peak Ground Acceleration (PGA), Peak Ground Velocity (PGV), and the Arias Intensity, whereas the PGD is associated with the total ground displacement. As noted by Lanzano et al. [26], these parameters are descriptors of the seismic motions but do not describe the entire ground motion. Because these measurements are obtained from instrumented sites, the GMP correlations are proposed to describe the damage at different locations.

Pipeline damage is commonly described in terms of a Repair Rate (RR), representing the number of repairs for a unit of length of a pipeline after an earthquake occurs. Overall, these Repair Rates can be defined as a function of Intensity Measures and some constants based on the pipeline material. O'Rourke and Liu [5] and Toprak and Taskin [27] compared some of these approaches in more detail. Based on this Repair Rate and assuming that the number of repairs follows a Poisson distribution, the probability of failure $P_f$ could be estimated as:

$$P_f = 1 - \mathbb{P}(N = 0) = 1 - \exp\{RR \cdot L\} \tag{18.3}$$

where $L$ is the length of the segment and $\mathbb{P}(N = n_r)$ is the probability of having $n_r$ repairs. Note that if the pipeline is modeled as a series system, failure occurs after the first break.

As remarked by Tsinidis et al. [6], the Repair Rate does not provide much information about damage severity; however, 80% of cases for the TGD are associated with leaks and 20% with breaks, whereas for PGD, it is the other way around. Therefore, some researchers prefer reliability evaluations using a limit state perspective. In this case, estimates of the maximum axial strain are implemented with a limit resistance between 2 and 3% of maximum accumulated strain, following the previous reported recommendations [28, 29]. This approach will be explained in more detail below.

### *18.3.1 Permanent Ground Deformation (PGD)*

The ground deformation could follow a parallel (Longitudinal) or transverse direction regarding the pipeline orientation, a PGD due to fault movement, or buoyancy as a result of Liquefaction. When the ground movement is parallel to the pipeline, the axial stresses would prevail, and the maximum axial tension strain $\epsilon_a$ can be calculated as follows [29]:

$$\epsilon_a = \frac{T_u\, L_p}{2\pi\, D\, wt\, E}\left[1 + \frac{n_{RO}}{1 + r_{RO}}\left(\frac{T_u\, L_p}{2\pi\, D\, wt\, \sigma_y}\right)^{r_{RO}}\right] \tag{18.4}$$

where $T_u$ is a Peak Friction Factor per unit length, $D$ is the outside pipe diameter, $wt$ is the pipe wall thickness, $L_p$ is the length of the PGD zone, $n_{RO}$ and $r_{RO}$ are the Ramberg-Osgood parameters, $\sigma_y$ is the yield strength, and $E$ is the Modulus of Elasticity of the pipe material. According to Dash and Jain [29], the $T_u$ can be estimated using the soil cohesion, the burial depth of the pipeline, the effective unit weight of the soil, the coefficient of the earth pressure at rest, the interface angle of the friction for the pipe and soil, the internal friction angle of the soil, and a coating factor.

For the case of a transverse PGD, the pipeline would be subjected to a bending force when it tries to adjust to the ground movement. In this case, a conservative maximum bending strain of the pipe $\epsilon_b$ can be estimated as follows [29]:

$$\epsilon_b = \frac{P_u\, W_p^2}{3\pi\, E\, wt\, D^2} \tag{18.5}$$

where $W_p$ is the width of the PGD and $P_u$ is the maximum lateral soil resistance per unit length. $P_u$ can be estimated using the horizontal and vertical bending capacity factors at which are tabulated (and interpolation can be used if required), the soil cohesion, the effective unit weight of the soil, the burial depth, and the pipeline diameter.

Note that these equations require many detailed parameters, including the length or the width of the PGD. These parameters represent a significant source of uncertainty, considering that the extent of the PGD would also depend on possible soil instability and topography; see, for instance, the approach proposed by Ref. [4].

### *18.3.2 Transient Ground Deformation*

The maximum axial strain for buried pipelines due to wave propagation is given by [29]:

$$\epsilon_c = \frac{PGV}{\alpha C_s} \tag{18.6}$$

where $PGV$ is the peak ground velocity generated by the ground movement, $C_s$ is the apparent propagation velocity, which could be assumed as 2 km/s to be conservative, and $\alpha$ is a constant parameter that depends if the shear waves are implemented or not.

## 18.4 Reliability Assessment for Corroded Pipelines Subjected to Seismic Activity

The proposed methodology comprises three main stages. First, the continuous degradation process due to corrosion is based on ILI measurements. This stage includes generating new defects, assessing the possibility of the formation of corrosion colonies, and the corrosion degradation model. The second stage describes the shock-based degradation associated with ground shaking from a TGD. This stage covers the seismic characterization of the region and the estimated strains imposed on the pipeline. The final stage is concerned with the reliability assessment based on the burst pressure and the tension failure induced by the seismic movement. The three stages will be explained in more detail in the following sections.

### *18.4.1 Corrosion-Based Continuous Degradation*

Despite their technology, ILI measurements are not entirely accurate and precise. The inspection sensors detect and measure depths above a given threshold (commonly taken as 10% of wall thickness). Therefore, the actual number of defects would be higher than the reported from the ILI report, so a generation rate should be considered. For this purpose, the number and the initiation time of the new defects were determined following a Poisson Process and Monte Carlo simulations [30].

Consider a continuous time-dependent function $\Lambda(t_i)$ representing the expected number of defects generated over the time interval $[0, t_i]$, which is obtained from an instantaneous rate of new defects for a reference pipe segment ($\lambda(\tau)$). This instantaneous rate can be assumed to follow a power-law as $\lambda(\tau) = \lambda_0 \tau^b$, where $\lambda_0$ and $b$ are parameters that can be determined from inspection results. Given $\Lambda(t_i)$, the number of defects up to the time $t_i$ follows the Poisson distribution [30]. The instantaneous rate was determined using the average generation rate between two consecutive inspections for equally spaced segments. Furthermore, a homogeneous process is considered (i.e., $\Lambda(t_i) = \lambda_0 t_i$), but in case a third inspection is available, a non-homogeneous rate can be used instead.

The initiation time was determined using Monte Carlo Simulations, as reported by Ref. [30], whereas the location of the new defects were randomly determined using the distributions of the defects' location along the abscissa and the clock-position. After the new and detected defects are obtained and located (at the inner and outer walls), they are clustered using the DNV RP-F101 criterion. This criterion was selected because of its interesting results against other limit distance criteria and supervised/unsupervised learning methods [23, 31].

Finally, for the degradation process, we consider a Lévy Process denoted by $X_t$ per cluster. It is a stochastic process with: (i) independent increments from the past, (ii) stationary increments, namely, $X_t - X_s$ has the same distribution as $X_{t-s}$ with $0 \leq s \leq t \leq \infty$, and (iii) $X_t$ is continuous in likelihood. For systems that are degraded continuously, the Lévy Process can be described by a deterministic drift and a Lévy measure [32]. Some recognized sub-processes of the Lévy Process are the Gamma Process and the Inverse Gaussian Process, but for this purpose, the Gamma Process is considered due to the possibility of calculating the lifetime and MTTF; further details about this process can be found in [12, 15].

### *18.4.2 Seismic-Based Shock Degradation*

A shock-based degradation process occurs when discrete amounts of the system's capacity are removed at distinct points in time due to sudden and independent events like earthquakes; then, in this case, $X_t$ should follow a shock-based approach [33]. These shocks are assumed to occur randomly over time accordingly to some physical mechanism, and two stochastic processes describe them: (i) inter-arrival time between shocks $\{T_i\}_i^\infty$ and (ii) the damage of each shock $\{Y_i\}_i^\infty$. A particular case of a shock-based mechanism is a Compound Poisson Process, whose $T_i$ are $iid$ distributed exponentially. Figure 18.5 shows a scheme of the proposed methodology based on historic seismic records.

The times at which seismic events occur are modeled by a Poisson Process. The locations are simulated using an Inhomogeneous Poisson Point Process that depends on an intensity $\tilde{\lambda}(x)$ (i.e., the density of points) upon to a given location $x$. The intensity is determined using a kernel smoothing estimator, which can be thought of as a chocolate bar over the points that melt and form an undulating surface, depending

on the points' density. A Gaussian Kernel with the Diggle edge correction was implemented for this work, considering that many authors commonly recommended it. Further details are available in [34].

After the location and the time when these events take place are determined, the damage to the pipeline should be estimated, depending on two principal elements: the magnitude of the event and how the wave propagates to the different sections of the pipeline. In the first place, consider historical seismic data around the pipeline to determine the probability of exceedance of the earthquake magnitude based on the following expression [35]:

$$f_M(m|m > M_{\min}) = \frac{\dfrac{w}{M_u - u}\left(\dfrac{M_u - m}{M_u - u}\right)^{w-1} \exp\left[-\left(\dfrac{M_u - m}{M_u - u}\right)^{w}\right]}{1 - \exp\left[-\left(\dfrac{M_u - M_{\min}}{M_u - u}\right)^{w}\right]}, \quad m \leq M_u \tag{18.7}$$

where $w$ and $u$ are parameters fitted with the seismic data, and $M_{\min}$ and $M_u$ are the minimum and maximum earthquake magnitudes, respectively. The PGA is estimated using the attenuation law reported by [35] that depends on the magnitude $m$ and the distance to the epicenter $R$. Figure 18.6 illustrates this attenuation law for a magnitude between 4.5 and 7.5 and a distance from 0 to 200 km.

Finally, the PGV is estimated following the Guidelines for Seismic Design of Buried Pipelines or appropriate PGV versus PGA correlations to calculate the tensile strain in Eq. 18.6 for each simulated event. An additional axial strain due to the internal pressure is also contemplated to deal with the corroded wall, after applying the Ramberg-Osgood and the Barlow's formula (Eq. 18.1), as described by [29].

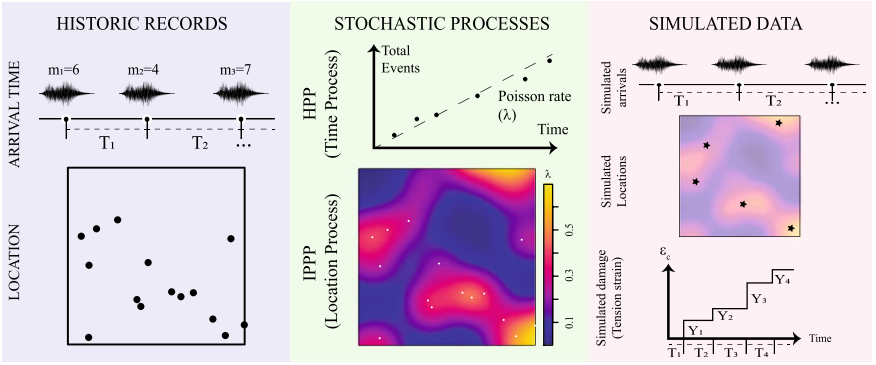


**Fig. 18.5** Description of the seismic model implemented

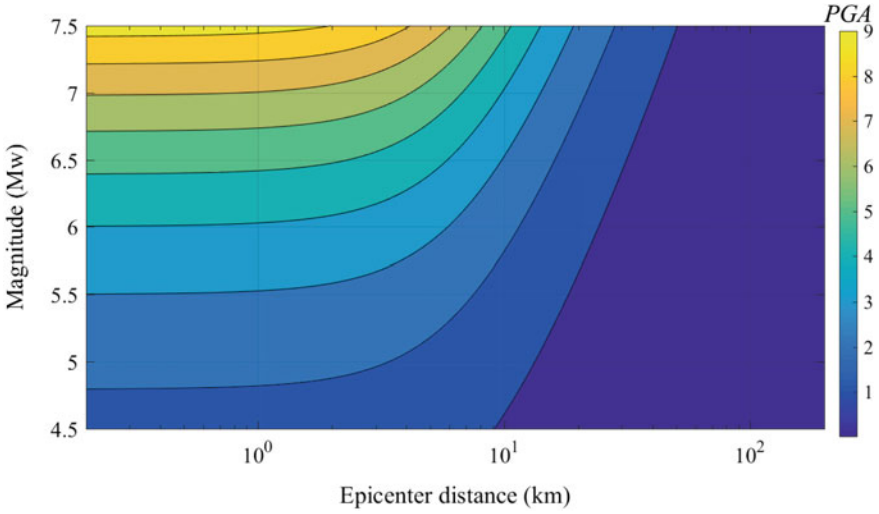


**Fig. 18.6** Contours of the attenuation law reported by [35]

### *18.4.3 Reliability Assessment*

The pipeline reliability is evaluated for a burst criterion and tension failure due to a TGD. To this end, the burst pressure is evaluated using the approach proposed by Netto et al. [36], and the maximum axial tension strain for buried pipelines due to wave propagation. This burst pressure model is selected because it is less conservative among other approaches such as ASMEB31G or CSA Z-662, and it has been recommended for *moderate* toughness materials [13]. This criterion approximates the pipeline's burst pressure, which is later used in the burst limit state function (i.e., $g_P = P_b - P$). The tension failure considers the limit state function of $g_T = 3\% - \epsilon_c*$, where $\epsilon_c*$ is described in Eq. 18.6, including the strain from the internal pressure [29]. In both cases, a failure state occurs when $g \leq 0$, whereas the pipeline is in a safe zone for $g > 0$. The failure probability is then calculated with Monte Carlo simulations using a combined criterion as follows. Let $\mathcal{A}$ corresponds to the pressure failure event and $\mathcal{B}$ is the tension failure event, then the combined failure approach is estimated by the union of these two events, i.e., $\mathbb{P}(\mathcal{A} \cup \mathcal{B}) = \mathbb{P}(\mathcal{A}) + \mathbb{P}(\mathcal{B}) - \mathbb{P}(\mathcal{A} \cap \mathcal{B})$. The failure probability is determined for each pipe segment between consecutive welding joints, considering the maximum defect depth per segment.

**Table 18.2** Summary of corrosion defects along the abscissa

| Parameter | Mean (Coefficient of variation) | | | |
|---|---|---|---|---|
| | ILI-1 Inner wall | ILI-2 Inner wall | ILI-1 Outer wall | ILI-2 Outer wall |
| Average depth (%wt) | 5.49 (0.26) | 5.29 (0.27) | 7.28 (0.49) | 6.77 (0.46) |
| Maximum depth (%wt) | 11.54 (0.21) | 11.14 (0.19) | 15.84 (0.46) | 14.62 (0.43) |
| Length (mm) | 26.07 (0.49) | 26.07 (0.43) | 28.07 (0.48) | 27.37 (0.44) |
| Width (mm) | 22.5 (0.40) | 25.92 (0.53) | 28.81 (0.67) | 32.60 (0.75) |
| Number of defects | 23,708 | 43,399 | 2862 | 4264 |

## 18.5 Case Study

The case study considers an API 5LX52 pipeline carrying different refined products. This pipeline is 45km long, and it has six main valves. The pipeline is mainly localized in relatively flat terrain (i.e., most inclinations $<7°$), but it crosses two mountain sections and two urban zones. A river crossing is located near kilometer 33, and the last 10 km are close to urban zones. For confidential agreements, further details about the location of the case study cannot be provided. The climate is mainly cold dry, but there are also cold-humid zones. The pipeline has a nominal wall thickness of 6.35 mm and an external diameter of 273.1 mm (10-inch nominal). It has a bituminous coating of coal tar and an Impressed Current Cathodic Protection system.

The pipeline condition assessment in terms of corrosion defects is based on two consecutive ILI measurements (two years apart); the ILI measuring tool was a Magnetic Flux Leakage (MFL). The majority of defects are located in the inner wall, as depicted in Table 18.2. Because further information about defects shape is not available in ILI, the maximum rather than the average depth for each defect will be considered from now on. Following the categories reported by the Pipeline Operator Forum [11], it was obtained that general and pitting corrosion cover around 90% in both inspections and pipe walls; the remaining defects were classified as axial and circumferential grooving. For further details, please refer to [37].

Regarding the seismic history, previous earthquake information was determined using Geological Services records. For this purpose, only seismic events with a magnitude greater than 4.5 and a radius of 200 km were considered, obtaining an average magnitude of 5.08 and a standard deviation of 0.63. These events have a rate of occurrence of 2.54 years, and the magnitude probability of exceedance shown in Fig. 18.7.

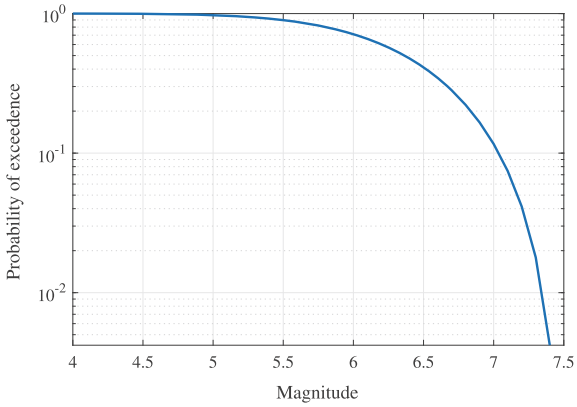


**Fig. 18.7** Probability of exceedance of earthquake magnitudes

## 18.6 Results and Discussion

Based on the two ILI inspections, the expected number of new defects (per kilometer) up-to-time $t_i$ was estimated as $\Lambda(t_i) = 266.3t_i$. Because the time between inspections is about 4 to 6 years, it is assumed that inspections will occur every 5 years. In every inspection, the number of defects and their extent should be updated.

After the generation process, the total of defects was 92,691 in 44 km with 9,023 clusters determined using the DNV criterion, with an average number of 4 defects per cluster. The degradation model was limited to a homogeneous Lévy Processes for each cluster and the assessments of the mean corrosion increments for isolated defects. Their parameters were determined using the last inspection and the installation year [12]. For the isolated cases, the mean degradation of the pipeline was used instead.

Regarding the seismic activity, previous earthquakes' location is usually reported on longitude and latitude coordinates, so a Mercator projection was used. It projects the earth into a cylinder and then to a plane, which has been widely used as a navigation map, but it may produce high distortions near both poles. For this case, the pipeline is near the equator, so the distortion is negligible. The projected earthquakes and the kernel smoothing results (melting chocolate over the points) are depicted in Fig. 18.8. Note that several earthquakes have been reported close to the pipeline, which illustrates how the pipeline is vulnerable to damage from seismic waves. This approach allows us to generate new seismic epicenters based on the information of reported events and those sections where an event has not occurred yet, in a lower probability.

The failure probability was evaluated considering the pressure and tension failure probabilities based on the following considerations and random variables shown in Table 18.3:

- The geometric, material, and corrosion extent are obtained from the ILI measurements of the case study.

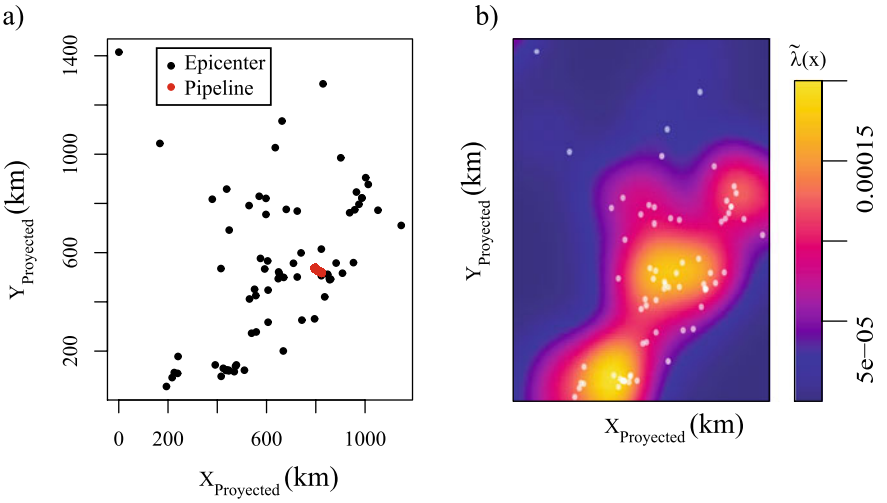


**Fig. 18.8** **a** Location of previous earthquakes and **b** Kernel Smoothing results

**Table 18.3** Main random variables for the reliability assessment

| Parameter | Type | Mean | CoV |
|---|---|---|---|
| $D$ | Normal[a] | 273 | 0.001 |
| $P$ | Gumbel | 11.30 | 0.08 |
| $wt$ | Normal | 6.35 | 0.05 |
| $\zeta_{PGA}$ | Lognormal | 1 | 0.6 |
| $\zeta_{A2V}$ | Lognormal | 1 | 0.49 |
| $\sigma_y$ | Lognormal | 358.53 | 0.005 |

[a]Normal variables were truncated at 0

- Based on the recommendations of CSA Z662-07 [20], the operating pressure is assumed to follow a Gumbel distribution. Parameters for this distribution were obtained from the methodology discussed by Hasan et al. [16].
- After a simulated earthquake occurs, the magnitude of the event is estimated with inverse sampling, and the attenuation law is used to determine the PGA to each segment of the pipeline between consecutive welding joints (Fig. 18.9). For this law, an uncertainty parameter of a lognormal random variable $\zeta_{PGA}$ is considered.
- A correlation based on near accelerogram records is implemented to estimate the PGV to assess tensile strain. This correlation is $PGV = 198.96\, PGA^{1.1149}$ for PGV in cm/s and PGA in %g. This correlation includes a lognormal random variable $\zeta_{A2V}$ to account for the reported variability.

The failure probability of the burst and tension failure probabilities were determined, obtaining the results depicted in Fig. 18.10. This figure indicates that for the first 15 years, the differences between the three failure probabilities are impercepti-

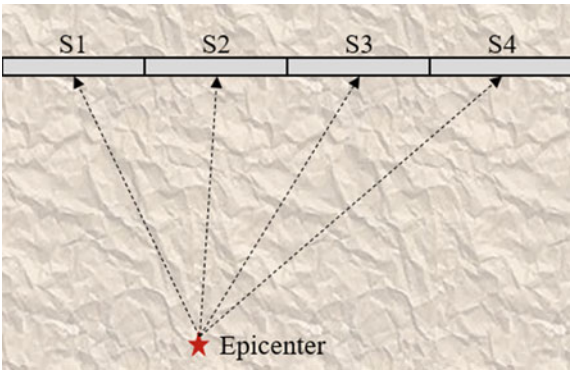


**Fig. 18.9** Schematic attenuated wave propagating to each pipe segment

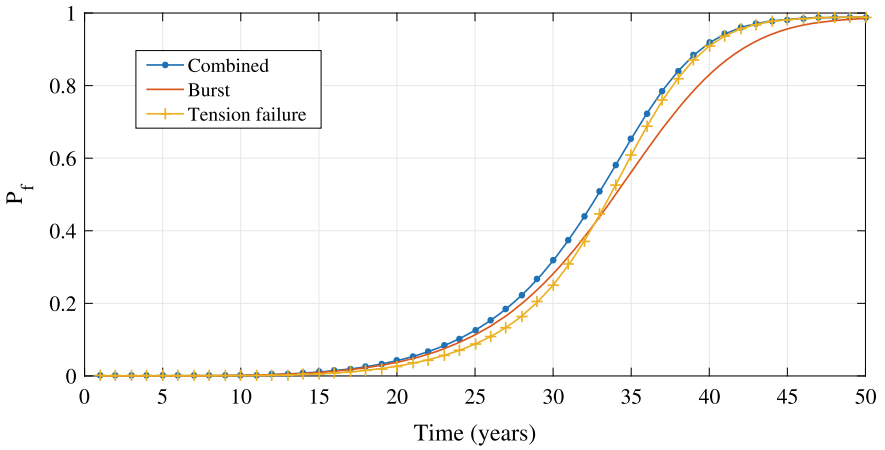


**Fig. 18.10** Combined mean failure probability results

ble. However, after the 35th year, the burst failure results differ significantly from the tension and combined results. In this year, the cumulative strain from the previous earthquakes, as well as the strain from the operating conditions, make the pipeline more susceptible to a Loss of Containment. This result illustrates the relevance of contemplating extreme events such as those from seismic activity to support further decisions. Overall, seismic failures should be considered to prevent conservative predictions of the pipeline condition, i.e., prevent unanticipated loss of containments, burst, or tension failures affecting its environment. This work focused on a TGD due to seismic activity, but other failures as landslides or complete ground motion, which can aggravate this probability, can also be contemplated.

## 18.7 Conclusions

This chapter presented an approach to assess the failure probability of corroded pipelines subjected to seismic activity. Burst and tension failure modes were considered based on previous inspections (ILI) and historic seismic records. The approach used a Lévy process to predict the corrosion degradation process, considering the appearance of new defects between inspections and the possibility of corrosion clusters. The seismic activity was simulated based on the number of events, their magnitude, and location.

The results showed a time-dependent failure probability for burst, tension, and combined failure effects. It was observed that at the beginning, the failure probability of these three mechanisms is almost imperceptible. The proposed approach evaluated only the maximum strain coming from a Transient Ground Deformation (TGD), but other alternatives from Permanent Ground Deformations (PGD) such as landslides or liquefaction could be contemplated. These extreme events cover several modeling uncertainties, including the extent of the longitudinal or traverse ground displacement.

The results also show the importance of frequent monitoring and regular inspections to update the model and evaluate the generation rates of new defects. Although In-Line Inspections provide an initial perspective of the condition at the inner and outer wall of the pipe, the uncertainties on the detection, evolution, and location of the defects demand the use of stochastic rather than deterministic methods. This work evaluates different approaches to simulate new defects, their location, and their evolution in time.

**Acknowledgements** R. Amaya-Gómez thanks the National Department of Science, Technology, and Innovation of Colombia for the Ph.D. scholarship (COLCIENCIAS Grant No. 727, 2015) and the French Ministry for Europe and Foreign Affairs and Campus France for the Eiffel Excellence Program (2018).

## References

1. Arriba-Rodriguez L, Villanueva-Balsera J, Ortega-Fernandez F, Rodriguez-Perez F (2018) Methods to evaluate corrosion in buried steel structures: a review. Metals 8(5):334
2. Li X, Rosas O, Castaneda H (2016) Deterministic modeling of API5L X52 steel in a coal-tar-coating/cathodic-protection system in soil. Int J Pressure Vessels Piping 146:161–170
3. Zhang N, Zeng D, Zhang Z, Zhao W, Yao G (2018) Effect of flow velocity on pipeline steel corrosion behaviour in $H_2S/CO_2$ environment with sulphur deposition. Corros Eng Sci Technol 53(5):370–377
4. Alvarado-Franco J, Castro D, Estrada N, Caicedo B, Sánchez-Silva M, Camacho L, Muñoz F (2017) Quantitative-mechanistic model for assessing landslide probability and pipeline failure probability due to landslides. Eng Geol 222:212–224
5. O'Rourke M, Liu X (1999) Response of buried pipelines subject to earthquake effects. MCEER monograph, Multidisciplinary Center for Earthquake Engineering Research

6. Tsinidis G, Di Sarno L, Sextos A, Furtner P (2019) A critical review on the vulnerability assessment of natural gas pipelines subjected to seismic wave propagation. Part 2: Pipe analysis aspects. Tunneling and underground space technology 92:103056
7. Omidvar B, Kivi H (2016) Multi-hazard failure probability analysis of gas pipelines for earthquake shaking, ground failure and fire following earthquake. Nat Hazards 82(1):703–720
8. Eskandari M, Omidvar B, Modiri M, Nekooie M, Alesheikh A (2017) Geospatial analysis of earthquake damage probability of water pipelines due to multi-hazard failure. ISPRS Int J Geo-Inf 6(6)
9. Gomes W, Beck A (2014) Optimal inspection and design of onshore pipelines under external corrosion process. Struct Saf 47:48–58
10. Sahraoui Y, Khelif R, Chateauneuf A (2013) Maintenance planning under imperfect inspections of corroded pipelines. Int J Pressure Vessels Piping 104:76–82
11. POF (2008) Specifications and requirements for intelligent pig inspection of pipelines. Technical report, Pipeline Operators Forum
12. Amaya-Gómez R, Riascos-Ochoa J, Muñoz F, Bastidas-Arteaga E, Schoefs F, Sánchez-Silva M (2019) Modeling of pipeline corrosion degradation mechanism with a Lévy process based on ILI (In-Line) inspections. Int J Pressure Vessels Piping 172:261–271
13. Amaya-Gómez R, Sánchez-Silva M, Bastidas-Arteaga E, Schoefs F, Muñoz F (2019) Reliability assessments of corroded pipelines based on internal pressure - A review. Eng Fail Anal 98:190–214
14. Qin H, Zhang S, Zhou W (2013) Inverse Gaussian process-based corrosion growth modeling and its application in the reliability analysis for energy pipelines. Front Struct Civ Eng 7(3):276–287
15. van Noortwijk J (2009) A survey of the application of gamma processes in maintenance. Reliab Eng Syst Saf 94(1):2–21. Maintenance Modeling and Application
16. Hasan S, Khan F, Kenny S (2012) Probability assessment of burst limit state due to internal corrosion. Int J Pressure Vessels Piping 89:48–58
17. Kiefner J, Duffy A (1971) Summary of research to determine the strength of corroded areas in line pipe. Technical report, Battelle Columbus Laboratories
18. Maxey W, Kiefner J, Eiber R, ARD (1971) Ductile fracture initiation, propagation and arrest in cylindrical vessels. Fracture Toughness, Technical report ASTM STP514
19. Benjamin A, Freire J, Vieira R, de Andrade E (2006) Burst tests on pipeline containing closely spaced corrosion defects. In: 25th international conference on offshore mechanics and artic engineering, Hamburg, Germany. OMAE2006-92131
20. CSA (2007) CSA Z662–07: limit state equation for burst of large leaks and rupture for corrosion defect. Technical report, Canadian Standard Association
21. Chauhan V, Sloterdijk W (2004) Advances in interaction rules for corrosion defects in pipelines. In: International gas research conference IGRC Vancouver
22. Silva R, Guerreiro J, Loula A (2007) A study of pipe interacting corrosion defects using the FEM and neural networks. Adv Eng Softw 38(11 and 12):868 – 875. Engineering Computational Technology
23. Amaya-Gómez R, Sánchez-Silva M, Muñoz F (2016) Pattern recognition techniques implementation on data from In-Line Inspection (ILI). J Loss Prevent Process Ind 44:735–747
24. Manshoori M (2011) Evaluation of seismic vulnerability and failure modes for pipelines. Proc Eng 14:3042–3049. The Proceedings of the Twelfth East Asia-Pacific Conference on Structural Engineering and Construction
25. Podimata M (2016) Methodological approach to EIA due to gas pipeline failure after an earthquake. The case study of the Trans Adriatic Pipeline. J Nat Gas Sci Eng 35:1200–1206
26. Lanzano G, Salzano E, Santucci de Magistris F, Fabbrocino G (2014) Seismic vulnerability of gas and liquid buried pipelines. J Loss Prevent Process Ind 28:72–78. European Process Safety Pioneers
27. Toprak S, Taskin F (2007) Estimation of earthquake damage to buried pipelines caused by ground shaking. Nat Hazards 40(1):1–24

28. American Lifelines Alliance (2001) Guidelines for the design of buried steel pipe. Technical report, American Society of Civil Engineers
29. Dash S, Jain S (2007) IITK-GSDMA guidelines for seismic design of buried pipelines. Technical report, Indian Institute of Technology Kanpur, Kanpur, India
30. Zhang S, Zhou W (2014) Cost-based optimal maintenance decisions for corroding natural gas pipelines based on stochastic degradation models. Eng Struct 74:74–85
31. Amaya-Gómez R, Sánchez-Silva M, Muñoz F (2019) Integrity assessment of corroded pipelines using dynamic segmentation and clustering. Process Safety Env Protect 128:284–294
32. Riascos-Ochoa J, Sánchez-Silva M, Klutke G-A (2016) Modeling and reliability analysis of systems subject to multiple sources of degradation based on Lévy processes. Prob Eng Mech 45:164–176
33. Sánchez-Silva M, Klutke G-A (2016) Reliability and life-cycle analysis of deteriorating systems. Springer series in Reliability Engineering. Springer
34. Baddeley A, Rubak E, Turner R (2016) Spatial point patterns-methodology and applications with R. CRC Press, Chapman & Hall Interdisciplinary Statistics Series
35. Sánchez-Silva M, Rackwitz R (2004) Socioeconomic implications of life quality index in design of optimum structures to withstand earthquakes. J Struct Eng 130(6):969–977
36. Netto T, Ferraz U, Estefen S (2005) The effect of corrosion defects on the burst pressure of pipelines. J Construct Steel Res 61(8):1185–1204. Second Brazilian special issue
37. Amaya-Gómez R, Bastidas-Arteaga E, Schoefs F, Muñoz F, Sánchez-Silva M (2020) A condition-based dynamic segmentation of large systems using a Changepoints algorithm: a corroding pipeline case. Struct Safety 84:101912

# Chapter 19
# Climate Change Impact for Bridges Subject to Flooding


**Boulent Imam**

**Abstract** Scour is one of the most widespread causes of bridge failure worldwide. The magnitude of the river flow at the bridge location is a key factor which directly affects the scour hole depth. Climate change may cause changes in the flow characteristics in a river due to changes in the precipitation patterns and catchment characteristics. In this paper, statistical analysis of the expected maximum annual flow of rivers is combined with the Monte Carlo simulation to estimate the probability of local scour failure. Climate change is assumed to manifest itself through gradual changes in the statistical characteristics of the expected maximum annual flow distributions. Results are presented from a case study using a bridge in the UK, which revealed that a time-dependent increase in the mean of the expected maximum annual flow has a more pronounced effect on scour performance as compared to an increase of its variability alone. Amongst the cases examined, however, the most adverse effect on local scour performance is observed from the simultaneous increase in both mean and variability of the expected maximum annual flow. The results also highlighted the significance of the foundation depth and local scour model parameter in relation to the changing flow characteristics.

## 19.1 Introduction

The built infrastructure, including buildings, transport systems and bridges can be adversely affected by climate change [1–4]. Natural disasters such as hurricanes, extreme precipitation and flooding can have major socioeconomic impacts, including among others loss of life and damage to the built infrastructure (e.g. loss of service in transport and other infrastructure systems, damage to buildings/bridges, etc.) leading to potentially significant macro-economic effects [5], Swiss [6].

Bridges are most vulnerable to natural hazards such as flooding, storms, hurricanes and winds. Statistics on bridge collapses worldwide reveal that natural hazards are

B. Imam (✉)
Department of Civil and Environmental Engineering, University of Surrey, Guildford GU2 7XH, Surrey, UK
e-mail: b.imam@surrey.ac.uk



M. G. Stewart and D. V. Rosowsky (eds.), *Engineering for Extremes*, Springer Tracts in Civil Engineering, https://doi.org/10.1007/978-3-030-85018-0_19

the predominant cause of failure [7]. This demonstrates, bearing in mind the adverse climate change impacts, the high risk present in the future for bridge structures and transport networks with respect to weather–related extreme events. One of the key effects of climate change on the bridge population will be the increased risk of scour of bridge piers and abutments [8, 9]. This will arise from more frequent and more intense river flooding due to the expected increases in precipitation in the future. Scour is caused by the erosive action of flowing water, removing sediment from around bridge foundations. This has been one of the most common causes of bridge collapses in the past as per the failure statistics reported by [7, 10–12]. A past risk assessment has shown that bridge scour depths may increase by between 5 and 50% over the present value by the 2080s in the UK, depending on the local bridge site conditions [13].

Changing environmental conditions are important for the safety and economy of *transport infrastructure*. The vast value of transport infrastructure assets shows the risk for large economic losses due to the effects of both climate change and extreme weather conditions. For example, the highway and railway networks in the UK alone have asset values in excess of £87 and £54 billion, respectively [14, 15]. Extreme environmental conditions can have a significant impact in the short term by disrupting road and rail networks [16–18] that can lead to noticeable economic losses [19, 20]. In many cases, elements of the transportation infrastructure (e.g. bridge structures) also form part of electricity, telephone, water and gas networks. Therefore, the economic cost of transport asset and network failures may extend far wider than the boundaries of transportation systems to other forms of critical infrastructure [21].

The aim of this chapter is to present a probabilistic framework that has been developed to assess the potential impacts of climate change on bridge scour due to extreme river flooding. This risk framework captures probabilistically uncertainties within the wider problem of scour and can be used to identify adaptation strategies in the future. A case study will be presented to show the applicability of the framework.

## 19.2 Climate Change Impacts on Bridge Scour

### *19.2.1 Background*

Scour is characterised by the erosion/removal of (underwater) river bed material in the vicinity of the piers and abutments [22], leading to the development of scour holes. Scour hole depths exceeding the foundation depth of the piers/abutments can lead to structural instability and sudden bridge failure [23, 24]. A number of factors are associated with the scour depths which may potentially develop at the pier and/or abutments of a bridge including, among others, the geometrical characteristics of the pier/abutment, the river characteristics including bed material and angle of attack as well as the flow magnitude at the bridge location. The scour phenomenon has

been extensively investigated and a number of—mainly empirical—models are available which allow the quantification of scour depths considering the most significant influencing factors such as pier geometry, river and flow characteristics [22, 25–28].

The prediction of scour depths in practice involves significant uncertainty caused by the variability associated with the different influencing factors, including bridge, river and flow characteristics as well as the scour prediction models themselves, which have been developed empirically through small-scale laboratory experiments. A source of uncertainty which is becoming increasingly relevant when predicting future scour performance of bridges is the potential influence of climate change. The increased risk of scour of bridges due to climate change has been recognised worldwide [8, 9, 13]. The potential consequences of climate change on bridge scour performance are currently not well known, on a quantitative basis, and need to be investigated to assist the development and implementation of adaptation strategies [3]. Hence, capturing the aforementioned uncertainties in the analysis would allow a more reliable performance assessment of scour prone bridges and assist towards more efficient decision-making under conditions of uncertainty.

A number of past studies examined the probability of scour failure, without, however, considering the potential influence of climate change in performance assessment [29–35]. On the other hand, risk-based frameworks considering the impact of climate risks on the long-term performance of civil engineering structures are becoming increasingly relevant within the context of infrastructure management [36]. To this end, a number of recent studies have attempted to capture, within risk-based frameworks, climate change effects on bridge scour [37–39].

An important parameter which directly affects the depth of the developing scour hole is the magnitude of the flow which may potentially be encountered in a river at the bridge location. The flow magnitude in a river is governed by a several factors such as catchment characteristics, precipitation patterns, etc. Climate change is predicted to cause changes in the river flow characteristics due to changes in the precipitation patterns and catchment characteristics [40].

In this chapter, a methodology is presented for the reliability assessment of scour prone bridges considering the potential effects of climate change. Statistical analysis of the expected maximum annual flow is combined with Monte Carlo simulation (MCS) to compute the probability of scour failure, through scenario-based modelling. The Flood Estimation Handbook (FEH) and the statistical software WINFAP-FEH 3 are used to estimate the statistical properties of the expected maximum annual flow of the river. The potential influence of climate change on the flow characteristics is considered through gradual changes in the mean and variability (i.e. standard deviation) of the expected maximum annual flow distribution to assess the sensitivity of the probability of failure of the bridge to such changes. The uncertainties associated with the different factors which influence scour performance are taken into account through suitable distributions. Results are presented from a case study using a bridge in the UK, in which scour reliability profiles are presented for a number of scenarios which assume time-dependent changes in the distribution of the expected maximum annual flow. Furthermore, the influence of foundation depth and local scour model parameters are also investigated in relation to the changing flow characteristics.

### 19.2.2 Climate Change and River Flows

Alterations in the climatic and weather conditions due to climate change can potentially increase the uncertainty associated with the magnitude as well as the prediction of extreme weather events including extreme precipitation and river flows [41]. The available evidence suggests that these changes may prevail as temporal changes in the statistical properties and distribution of key climatic parameters such as temperature and precipitation [41, 42]. To enable both the quantification of the potential effects of climate change and the development of future adaptation strategies, a number of potential emission scenarios have been devised by the IPCC which cover a period up to the end of the 21st Century [43]. Increasing flood frequency and magnitude due to increasing precipitation and/or changes to the catchment characteristics can have a significant effect on the scour performance of bridges.

In the UK, during the years 1961–1995, an increase was observed in the extreme precipitation events during winter [44]. A decreasing annual trend of rainfall due to climate change in a particular area can include significant increases in precipitation associated with seasonal trends (e.g. during winter). In general, the climatic projections for the UK [45] indicate this situation. The impacts of climate change, however, are catchment specific and their magnitude can differ remarkably even for catchments located close to each other [46]. A nationally consistent assessment of the sensitivity of flood peaks across Britain to climatic changes has been carried out by [40]. The most recent UK climate change projections (UKCP18) have been considered to provide location-specific information on the potential range of impacts on floods across the country, for three flood return periods, three future time-slices and four emissions scenarios.

### 19.2.3 Local Scour Prediction Model

A number of models have been proposed in literature for the estimation of local scour in bridge piers [28]. Here, local scour is estimated using the HEC-18 design equation [47], given by Eq. 19.1, which considers scour as a time-independent process, i.e. temporal effects of local scour development are not modelled [48].

$$y_{\max} = 2y_0 K_1 K_2 K_3 K_4 \left(\frac{D}{y_0}\right)^{0.65} F_0^{0.43} \tag{19.1}$$

where, $y_{max}$ is the maximum scour depth (m), $y_0$ is the depth (m) of the flow upstream of the bridge pier, $K_1$, $K_2$, $K_3$ and $K_4$ are coefficients which allow for pier shape, angle of attack, streambed conditions and the river bed material size, $D$ is the pier diameter and $F_0$ is the Froude number given by:

$$F_0 = \frac{V}{(g y_0)^{0.5}} \tag{19.2}$$

where, $g$ is the gravity acceleration and $V$ is flow velocity given by:

$$V = \frac{Q}{B y_0} \tag{19.3}$$

and the flow depth $y_0$ is given by [49]:

$$y_0 = \left( \frac{n Q}{B s^{1/2}} \right)^{3/5} \tag{19.4}$$

where, $Q$ is the flow ($m^3/s$), $B$ is the river width (m), $n$ is the Manning's coefficient and $s$ is the longitudinal slope of the channel.

$K_1$ depends on the pier nose shape and it can take the following values: 1.1 for a square nose, 1.0 for round nose or circular cylinder, 0.9 for a sharp nose. Coefficient $K_2$ is a function of the angle of attack of the river flow with respect to the pier [47]. $K_3$ depends on whether there is clear-water scour or the river bed is plane ($K_3 = 1.1$) as opposed to the case of having dune bed configurations with different dune heights ($K_3$ ranging between 1.1 and 1.3 depending on the dune height). $K_4$ depends on the diameter of the river bed material and can range between 0.4 (fine material) to 1.0 (coarse material).

Equation 19.4 can be used for wide rivers with ratios $B/y_0$ exceeding about 10, giving conservative predictions for cases where this is less than about 10 [49]. In this chapter, the flow $Q$ is estimated using the statistical analysis procedures implemented in the software WINFAP-FEH 3 [50].

### *19.2.4 Probabilistic Assessment of Local Scour*

Reliability analysis allows the estimation of the failure probability, $p_f$, of a structure for different limit states. The performance function for the limit state of a bridge is given by:

$$G(t) = R - S(t) \tag{19.5}$$

where, $G(t)$ is the time-dependent safety margin, $R$ and $S(t)$ are the resistance (i.e. foundation depth) and time-dependent load effects (i.e. maximum scour depth given as a function of flow magnitude, river and pier characteristics, etc.), respectively. The performance function for local scour in bridge piers is given by:

$$G(t) = D_F - y_{\max}(t) = D_F - \left[ 2y_0(t)K_1K_2K_3K_4\left(\frac{D}{y_0(t)}\right)^{0.65} F_0(t)^{0.43} \right] \quad (19.6)$$

where, $D_F$ is the foundation depth. $G(t) \leq 0$ indicates the failure realization of the limit state. Using the statistical properties, including distribution type, for the random variables of Eq. 19.6 and assuming that the resistance $D_F$ and the load effects $y_{max}(t)$, are statistically independent, the instantaneous (annual) probability of failure, $p_f(t)$, is given by:

$$p_f(t) = P[G(t) \leq 0] = P\left\{ \left[ D_F - \left[ 2y_0(t)K_1K_2K_3K_4\left(\frac{D}{y_0(t)}\right)^{0.65} F_0(t)^{0.43} \right] \right] \leq 0 \right\} \quad (19.7)$$

Here, Eq. 19.7 is evaluated using Monte Carlo simulation (MCS) implemented in MATLAB software. Alternatively, the availability of a closed form expression for the limit state function enables the use of other reliability analysis methods (e.g. FORM). The use of MCS, however, allows to estimate the failure probability as well as to obtain the distribution of the scour depth Eq. 19.1—which is not known *a-priori*—for the analysis cases examined. The cumulative probability of failure, at any point within a time period, is given by Eq. 19.7, provided that the failures are statistically independent.

The uncertainties associated with the random variables of Eq. 19.7, can be separated as aleatory and epistemic uncertainties [51]. Within the context of scour assessment under changing flow magnitude (i.e. expected maximum annual flow) due to climate change, the variability of flow magnitude is associated with both natural variability and epistemic uncertainty. Aleatory uncertainty in relation to flow modelling is due to the lack of a specific emission scenario for future climate change since climate change itself is a function of several variables which are not always possible to be objectively quantified such as future global population, government policy, technological breakthroughs etc. On the other hand, epistemic uncertainty is caused by the lack of understanding of how a specific climate change scenario (e.g. increased precipitation, etc.) will affect the flow conditions of a particular catchment. Furthermore, the available models for scour are associated with epistemic uncertainty, since the inherently complex nature of scour is modelled through approximations developed from laboratory experiments of small-scale pier models (e.g. Equation 19.1). This uncertainty type can be reduced by developing more accurate models of the phenomenon through, for instance, additional experimentation (this is discussed later in this chapter).

The Monte Carlo based procedure for the probabilistic assessment of local scour considering the potential effects of climate change is implemented in MATLAB using a sample size of $N = 2 \times 10^6$ per year. A number of methods have been devised to

predict the potential flow in a particular river, for instance through statistical analysis of historic flow records or alternatively using the rainfall-runoff method which requires knowledge of the precipitation patterns and the catchment descriptors [50]. The statistical analysis of historic flow records through the widely-used WINFAP-FEH 3 software, which has been used for this case study allows the estimation of the statistical properties of the expected maximum annual flow for any river in the UK. Flow events in different years are assumed to be independent. The expected maximum annual flow, which is denoted here as QMED, is modelled by fitting a suitable distribution to flood data using the statistical procedures implemented in WINFAP-FEH 3 [50]. This approach is based on the creation and analysis of a pooling group of several catchments of similar hydrological characteristics, with the available years of flow records for each station (in the different catchments) contributing to the total number of station years.

Equations 19.2–19.4 are used to calculate the Froude number, flow velocity and flow depth, respectively, while Eq. 19.1 is used to compute the depth of local scour, for each set of the $N$ randomly generated values for the variables (e.g. expected maximum annual flow, pier width, river slope, etc.) in each year. Equations 19.5–19.8 are used to calculate the annual and time-dependent (cumulative) failure probability for a specific value of foundation depth. The foundation depth and the load effects $y(t)$, i.e. the scour depth, are assumed to be statistically independent. In actual bridges, the foundation depth is governed by several factors, one of which is the maximum expected scour depth. However, this correlation is not considered in the present analysis due to the lack of sufficient information. The procedure is demonstrated through a case study; the different analysis cases examined are discussed in subsequent sections of this chapter.

### *19.2.5 Bridge Case Study*

The bridge considered in this case study is assumed to be located on the river Earn in Scotland, UK, assuming alluvial riverbed conditions. Initially, the location of the examined bridge is established on the maps and the available nearby river water level stations are identified. This station is then used in WINFAP-FEH 3 software to create the pooling group using stations from similar catchments with a total of 1000 station years (annual maxima series). WINFAP-FEH 3 provides a number of options for estimating QMED, which is the maximum annual flow with a return period T = 2 years, for instance using the catchment descriptors or annual maxima (AM) series (for more details see [50]. In this chapter, a QMED of 250.2 $m^3/s$ is estimated from AM series of the station.

Analysis of pooling group flood data (i.e. annual maxima series) using the WINFAP-FEH 3 software indicates that the generalized extreme value (GEV) distribution, given by Eq. 19.8 [52], is the most suitable distribution for modelling the magnitude of the expected maximum annual flow, the cumulative distribution function is expressed as follows:

$$F_{X\max} = \exp\left\{-\left[1 - \frac{k(x-\varepsilon)}{\alpha}\right]^{1/k}\right\} \tag{19.8}$$

where, $k$ is the shape parameter, $\varepsilon$ is the location parameter and $\alpha$ is the scale parameter. The GEV distribution parameters obtained from the statistical analysis of stations in similar catchments (i.e. pooling group) in WINFAP are $\alpha = 0.222$, $\varepsilon = 0.919$ and $k = 0.002$. The scale and location parameters of the GEV distribution are given by Eqs. 19.9 and 19.10, respectively [52].

$$\alpha = \sqrt{\frac{k^2\sigma^2}{\Gamma(1+2k) - \Gamma^2(1+k)}} \tag{19.9}$$

$$\varepsilon = \mu - \frac{\alpha}{k}[1 - \Gamma(1+k)] \tag{19.10}$$

where, $\mu$ is the sample mean, $\sigma$ is the sample standard deviation and $k$, $\varepsilon$ and $\alpha$ are the shape, location and scale parameters of the generalized extreme value distribution, respectively [52], and $\Gamma$ is the gamma function.

The potential effects of climate change on scour are examined through a parametric study in which the scale and location parameters are gradually changed for increasing values in the mean $\mu$ and variability (i.e. standard deviation $\sigma$) of the flood magnitude in Eqs. 19.9 and 19.10.

Within the probabilistic framework developed, several variables associated with the bridge and river characteristics are treated as random. Table 19.1 summarises the statistical properties of the random variables considered in this case study. In this study, the bed material is assumed to be deterministic and time invariant; however, over time, changing flow properties may change the size of bed material. The river and pier dimensions (i.e. widths of the river and pier, respectively) are also treated as random. Examination of historic drawings from existing bridges have assisted

**Table 19.1** Statistical properties of variables for scour analysis

| Variables | | Mean | COV | Distribution | Reference |
|---|---|---|---|---|---|
| River | Width (m) | 65 | 0.05 | Normal | Assumed |
| | Streambed conditions (Coef. $K_3$) | 1.1 | 0.05 | Uniform | [34] |
| | Bed material size ($K_4$) | 1.0 | – | – | – |
| | Slope | 0.0032 | 0.05 | Lognormal | Assumed |
| | Manning's coefficient | 0.035 | 0.28 | Lognormal | [34] |
| Bridge piers | Foundation depth (m) | 4.5 | – | – | Assumed |
| | Pier nose shape (Coef. $K_1$) | 1.0 | – | – | – |
| | Angle of attack (Coef. $K_2$) | 1.0 | – | – | – |
| | Pier width, $D$ (m) | 2 | 0.05 | Normal | Assumed |

**Table 19.2** Analysis cases for assessing the influence of assumed changes in the expected maximum annual flow

| Analysis case | Foundation depth (m) | Mean, $\mu$ (Eq. 19.9) | Standard deviation, $\sigma$ (Eq. 19.10) |
|---|---|---|---|
| 45M0000 | 4.5 | No change | |
| 45M2000 | | 20% increase | no change |
| 45M4000 | | 40% increase | no change |
| 45M6000 | | 60% increase | no change |
| 45M0020 | | No change | 20% increase |
| 45M0040 | | No change | 40% increase |
| 45M0060 | | No change | 60% increase |
| 45M2020 | | 20% increase | 20% increase |
| 45M4040 | | 40% increase | 40% increase |
| 45M6060 | | 60% increase | 60% increase |

the selection of the mean values for these variables, with the selected bridge being considered as a representative example for this area. Actual measurements taken during a site visit could allow for deterministic values to be used for these variables. To this end, actual measurements on several (similar) piers within the same bridge may be associated with some degree of variability. Similarly, the river width is not constant and its value depends on the location that the measurement is obtained.

Climate change is likely to impact the precipitation patterns and catchment characteristics of a specific area which in turn may affect the magnitude and frequency of expected maximum annual flow. In this study, it is assumed that climate change will cause a certain amount of temporal changes in the statistical properties of the flood predicted using the FEH (e.g. 20% increase of sample mean). The different analysis cases examined in relation to changing flow conditions are summarised in Table 19.2. These changes are assumed to evolve linearly with time over a 60-year period. In this way, the effects of climate change on the precipitation patterns and catchment descriptors and hence on the flood frequency and magnitude are implicitly considered in the analysis of the different scenarios examined. A foundation depth (FD) of 4.5 m is assumed to facilitate the estimation of the scour failure probability; the effect of this variable is investigated later in this chapter.

## 19.3 Results and Discussion

### *19.3.1 Effect of Changing Flow Characteristics on Pier Scour Failure Probability*

Figures 19.1, 19.2 and 19.3 show the annual and cumulative probabilities of pier scour failure for the scenarios examined with increasing mean, increasing variability

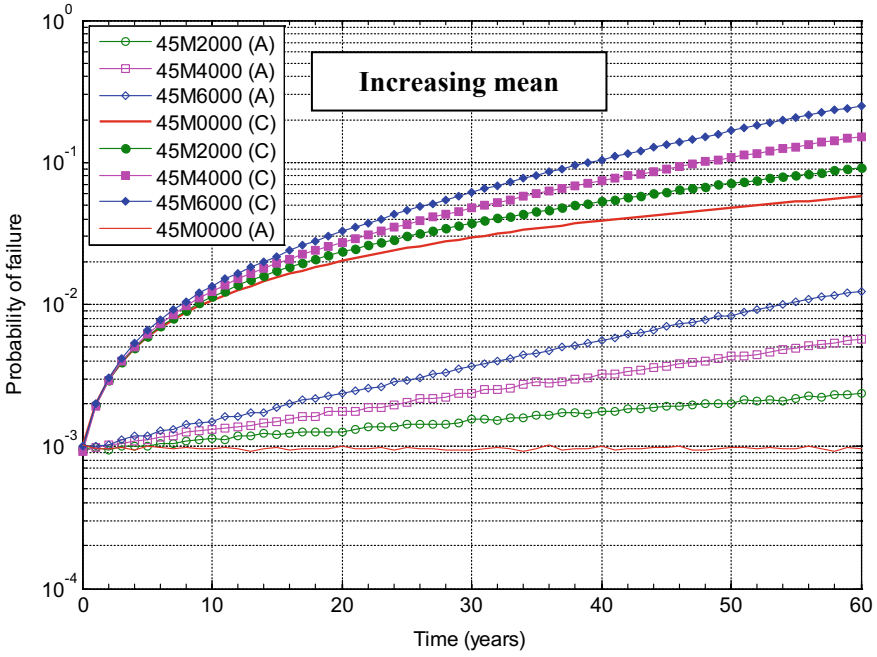


**Fig. 19.1** Effect of increasing mean in the expected maximum annual flow on the annual (A) and cumulative time-dependent (C) probabilities of scour failure

and simultaneous increase of mean and variability in the expected maximum annual flow, respectively, for a given foundation depth equal to 4.5 m. In all figures, (A) and (C) refer to annual and cumulative failure probability, respectively. The effect of foundation depth on the predictions is investigated later in this chapter.

The results in Fig. 19.1 show the effect of increasing mean (Eq. 19.9) in the expected maximum annual flow on the annual and cumulative probabilities of failure for the scenarios with mean increases of 20, 40 and 60% over a 60-year period. The results in this figure indicate that the effect of increasing mean is relatively small for the initial 10 years and it gradually becomes noticeable between 10 and 20 years and significant beyond the initial 20-year period. At the end of the examined period the cumulative probabilities of failure for the scenarios with 20, 40 and 60% increase in mean (i.e. see Fig. 19.1 for cases 45M2000, 45M4000 and 45M6000; in this nomenclature, 45 stands for foundation depth of 4.5 m, M stands for Model and 2000 stands for 20% increase in mean and 0% increase in variability) are predicted to be 59%, 176% and 337%, respectively, higher than the base line scenario which assumes no changes in the statistical properties of the expected maximum annual flow over time, i.e. no change in climate.

The results in Fig. 19.2 show the effect of increasing variability (Eq. 19.10) in the expected maximum annual flow on the annual and cumulative probabilities of failure for the scenarios with variability increases of 20, 40 and 60% over a 60 year

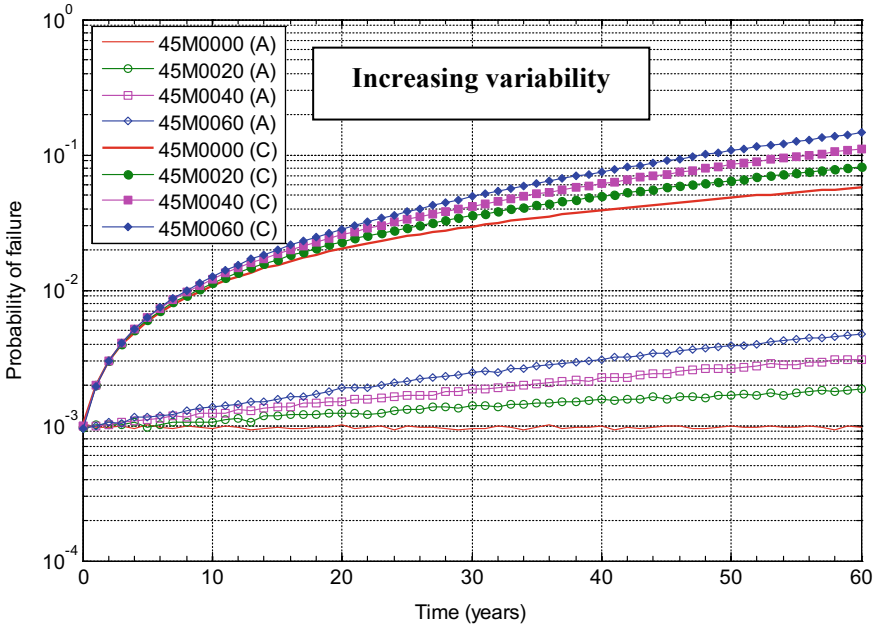


**Fig. 19.2** Effect of increasing variability (standard deviation, σ) in the expected maximum annual flow on the annual (A) and cumulative time-dependent (C) probabilities of scour failure

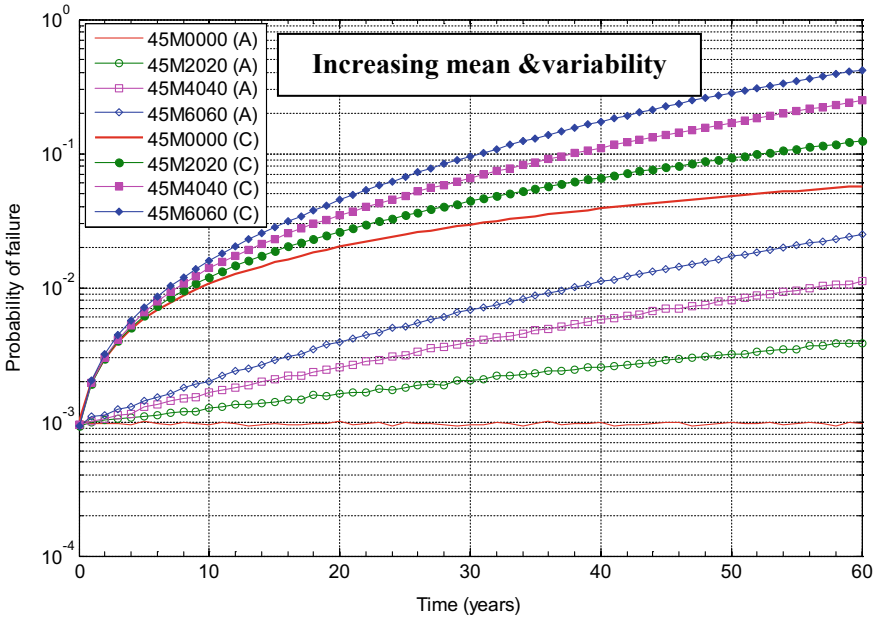


**Fig. 19.3** Effect of simultaneous increase of mean andvariability in the expected maximum annual flow on the annual (A) and cumulative time-dependent (C) probabilities of scour failure

period. The results in this figure indicate that the effect of increasing variability is relatively small for the initial 15 years and it gradually becomes significant beyond the initial 20-year period. For the analysis cases examined, the effect of increasing variability in the expected maximum annual flow is predicted to have a relatively smaller effect on the failure probabilities compared to the previous case of assuming a gradually increasing mean. In general, the results in Fig. 19.2 follow a similar trend to the results obtained for increasing mean (Fig. 19.1); that is as the variability of the expected maximum annual flow increases, the probability of failure also increases (cumulative failure probabilities at the end of the 60-year period are predicted to increase by approximately 41, 92 and 153% for cases 45M0020, 45M4040 and 45M0060, respectively relative to the base line case 45M0000, see Fig. 19.2).

The results in Fig. 19.3 show the effect of simultaneously increasing mean and standard deviation up to 60% (see Eqs. 19.9 and 19.10) of the expected maximum annual flow on the annual and cumulative probabilities of failure for scenarios 45M2020, 45M4040 and 45M6060 (see Table 19.2). The results in this figure indicate that the combined effect is relatively small for the initial 10-year period and it gradually becomes significant beyond 15 years. For the cases examined, the effect of simultaneous increase of mean and variability has the highest relative effect on the predicted probabilities of local scour failure. More specifically, the results for cases 45M2020, 45M4040 and 45M6060 show that at the end of the 60-year period, an increase in the cumulative failure probabilities by approximately 117%, 332% and 633%, respectively, compared to the base-line case 45M0000. It is interesting to note that the combined effects of increasing mean and variability associated with the maximum expected annual flow (i.e. analysis cases 45M2020, 45M4040 and 45M6060) is greater than the sum of the individual effects (i.e. cases where the increasing mean and variability are considered separately), see Figs. 19.1 and 19.2. Based on these observations it can be concluded that the combined effects of increasing mean and variability have the greatest effect on the probability of local scour failure. When considering the impact of increasing mean or variability individually, increasing mean in the maximum expected annual flow is predicted to have a more significant (adverse) effect on the predictions compared to the increasing variability.

The cumulative failure probability profiles have been developed assuming that the flow characteristics occur gradually (linearly) over a 60-year time period. It would be interesting to investigate the effect of potentially sudden changes in the statistical properties of the expected maximum annual flow—due to climate change—on the scour probability of failure. Furthermore, the preceding analyses assume that the distribution type (i.e. generalised extreme value) of the expected maximum annual flow remains the same throughout the examined period. At present, however, it is not possible to confidently predict the timing and magnitude of potentially sudden changes in the flow characteristics that may occur in the future [41]. One of the key challenges that still remain is to establish a link between the altered precipitation patterns and/or catchment properties (due to climate change) with the flow (i.e. expected maximum annual flow) characteristics. To this end, significant uncertainty still exists as to which climate change scenario will be realised.

### 19.3.2 *Effect of Foundation Depth on Scour Probability of Failure*

A common challenge with existing bridges is that the foundation depth is often unknown even if the original drawings of the superstructure are available [53]. The results presented in the previous sections have been obtained by assuming, conservatively, a foundation depth of 4.5 m. A number of additional analysis cases are considered to investigate the influence of assuming foundation depth, due to having unknown foundations, on the cumulative probability of scour failure. The foundation depths examined are 4 and 5 m. These foundations depths are examined for a number of cases which assume increasing mean or/and variability of the expected maximum annual flow distribution; these are: (a) a case of 40% increase in mean, (b) 40% increase of variability and (c) simultaneous increase of mean and variability by 40%.

Figure 19.4 shows the cumulative probabilities of scour failure for the analysis cases with varying assumed foundation depths. As expected, the results in this figure clearly show the influence of foundation depth on the predicted cumulative $p_f$; with smaller foundation depths having higher probabilities of failure. For the case of FD = 4 m the effect of changes in the statistical properties of the flow (i.e. increasing mean or/and variability) have a very small effect on the cumulative probabilities of scour failure. The results in Fig. 19.4 indicate that, for the FD = 4 m case, scour failure becomes almost certain during the last 5 years (of the 60-year period) for the cases with increasing mean and simultaneous increase of mean and variability of the expected maximum annual flow distribution.

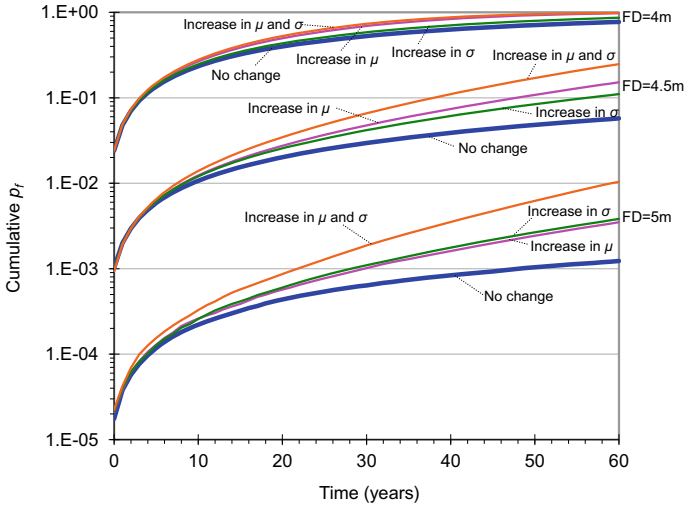


**Fig. 19.4** Effect of foundation depth on time-dependent probability of scour failure under changing expected maximum annual flow

As the foundation depth (FD) increases the probabilities of scour failure decrease as shown in Fig. 19.4. The results in Fig. 19.4 further indicate that the effect of increasing mean and/or variability is not constant when different foundations depths are considered. For example, for the case of FD = 5 m, the increasing variability of the expected maximum annual flow has a greater effect than the increasing mean. Conversely, the increasing mean of the expected maximum annual flow distribution has a greater effect compared to the effect of increasing variability for decreasing foundation depths. As shown in Fig. 19.4, the simultaneous increase of mean and variability of the flow distribution produces the highest probabilities of failure in all cases examined. The influence of the simultaneous increase of mean and variability of the expected maximum annual flow reduces for decreasing foundation depths.

These results indicate that foundation depth has a significant effect on the predictions. In practice, this variable is deemed with high uncertainty while in many cases no data is available on the actual foundation type and depth of a particular bridge [10]. In such cases, conservative values of FD are recommended in assessing scour performance [10]. To this end, the systematic collection of actual foundation depth measurements of piers in scour prone bridges would reduce the uncertainty and hence improve the accuracy of the scour failure predictions during assessments.

### *19.3.3 Effect of Model Parameter $\lambda_{sc}$ on Predicted Scour Depths and Failure Probabilities*

It has been shown that the scour equation (Eq. 19.1) of HEC-18 leads to conservative predictions of local scour [34, 54]. This is due to the fact that the scour prediction models used in codes of practice have been developed through small-scale laboratory experiments. Comparisons of these prediction models with field measurements of scour depths on real bridges have shown that there is a discrepancy between them. It has been suggested that a model parameter $\lambda_{sc}$ can be introduced in Eq. 19.1 to reduce its conservatism [34] inherently taking into account epistemic uncertainty. The local scour model is now given by:

$$y_{\max}(t) = 2\lambda_{sc} y_0(t) K_1 K_2 K_3 K_4 \left(\frac{D}{y_0(t)}\right)^{0.65} F_0(t)^{0.43} \tag{19.11}$$

Several values have been proposed for the statistical properties of $\lambda_{sc}$; for a summary see [34]. To investigate the influence of this parameter a number of scenarios are considered using values for the statistical properties of $\lambda_{sc}$ suggested in [34]. The analysis cases in this section assume a 40% gradual increase in mean, standard deviation and the simultaneous increase of both for the expected maximum annual flow considering two foundation depths of 4.5 and 5 m. The model parameter $\lambda_{sc}$ is modelled using a normal distribution with mean = 0.55 and COV = 52% [34]. In this way comparisons can be made with results presented in previous sections.

Figure 19.5a, b show the predicted time-dependent failure probabilities for the analysis cases with foundation depths 4.5 m and 5 m, respectively. The results in these figures indicate that although the mean value of $\lambda_{sc}$ is less than 1 (i.e. mean value of $\lambda_{sc} = 0.55$), the introduction of this model parameter causes an increase of the predicted time-dependent failure probabilities. This observation can be explained by considering the influence of $\lambda_{sc}$ on the predicted scour depths in Figs. 19.6 and 19.7. More specifically, the results in Figs. 19.6 and 19.7 indicate that the high variability

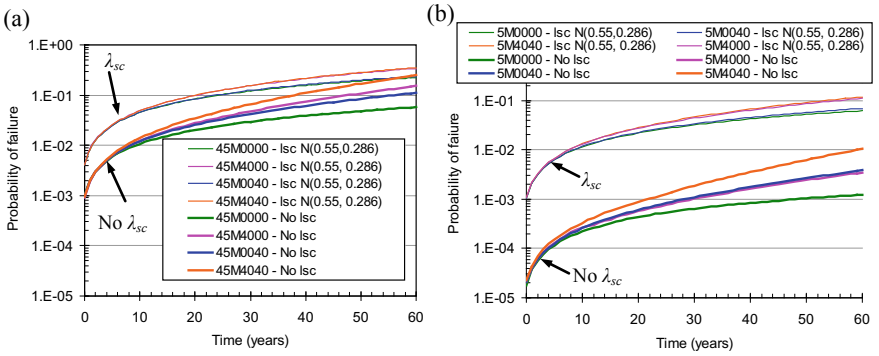


**Fig. 19.5** Effect of model parameter $\lambda_{sc}$ on the time-dependent probabilities of local scour failure for up to 40% increase in the mean or/and variability of the expected maximum annual flow distribution: **a** foundation depth = 4.5 m and **b** foundation depth = 5 m. N (mean, COV) stands for normal distribution with the mean and COV values indicated inside the parentheses

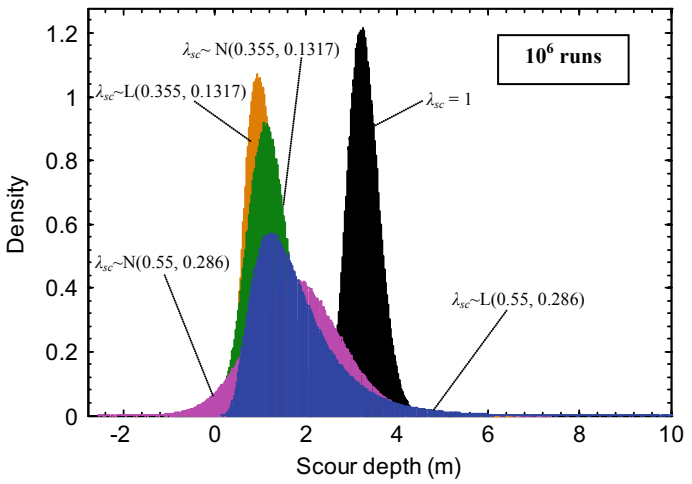


**Fig. 19.6** Effect of model parameter $\lambda_{sc}$ (Eq. 19.11) on the predicted scour depths for cases with no changes in the distribution of the expected maximum annual flow. N (mean, COV) and L (mean, COV) stands for normal and lognormal distribution, respectively, with the mean and COV values indicated inside the parentheses

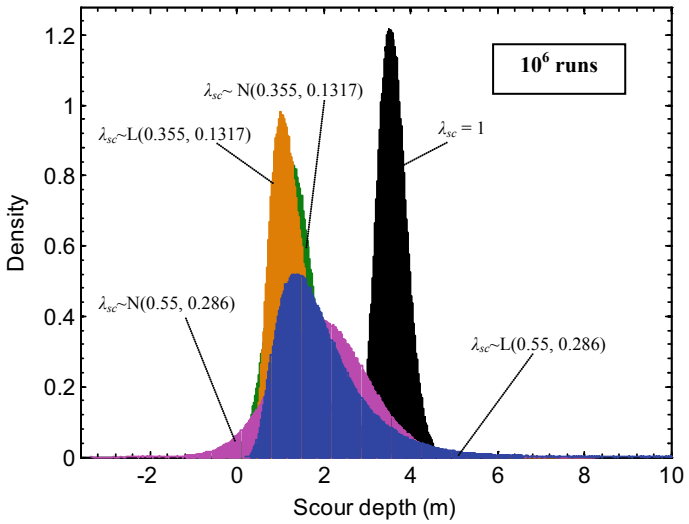


**Fig. 19.7** Effect of model parameter $\lambda_{sc}$ (Eq. 19.11) on the predicted scour depths for cases with 40% increase in the mean of the expected maximum annual flowdistribution. N (mean, COV) and L (mean, COV) stands for normal and lognormal distribution, respectively, with the mean and COV values indicated inside the parentheses

associated with model parameter $\lambda_{sc}$ results in an increase of the scour depth values exceeding 4.5 and 5 m (generated using MCS in MATLAB). As expected, the mean value of the predicted scour depths is lower than the predicted scour depths when $\lambda_{sc} = 1$. The results in Fig. 19.5a, b also indicate that the very high variability of the model parameter $\lambda_{sc}$ (COV = 0.52) overshadows the effect of the assumed increasing variability in the expected maximum annual flow on the predicted time-dependent probabilities of failure (i.e. in Fig. 19.5 the increasing variability of flow is predicted to have an insignificant effect on cumulative $p_f$).

The effect of different statistical properties and distribution types for $\lambda_{sc}$ on the predicted scour depths was also investigated and the results are shown in Figs. 19.6 and 19.7. The results indicate that negative scour depths are predicted in the cases where $\lambda_{sc}$ is modelled using normal distribution, which is not acceptable from a physical point of view. In contrary, $\lambda_{sc}$ remains positive when a lognormal distribution is used for its modelling; in this case however the magnitudes of the predicted maximum scour depths (near the upper tail) are significantly larger than the cases where a normal distribution is used.

Based on the results presented in this section it can be concluded that the use of $\lambda_{sc}$, which is a source of epistemic uncertainty, has a significant effect on the predictions. However, at present the available statistical properties for this variable are not consistent (e.g. negative or very large scour depths) with actual observations. To this end, further research is needed to obtain accurate statistical properties including

the distribution type for this variable through additional field measurements and comparison with the code predictions.

## 19.4 Conclusions

This chapter presented a probabilistic framework that can be used to capture the potential impact of climate change on bridge scour. A case study capturing changes on the magnitude and/or frequency of extreme events of a typical UK bridge has been used to demonstrate the applicability of the framework. The framework that quantifies the time-dependent reliability can be integrated within wider climate change adaptation and mitigation planning frameworks for decision making in the long-term.

**Acknowledgements** The financial support (Grants EP/I00744X/1 and EP/G037612) provided by the Engineering and Physical Sciences Research Council (EPSRC) for this project in the UK is gratefully acknowledged.

## References

1. Kirshen P, Ruth M, Anderson W (2008) Interdependencies of urban climate change impacts and adaptation strategies: a case study of Metropolitan Boston USA. Clim Change 86:105–122
2. Kumar P, Imam B (2013) Footprints of air pollution and changing environment on the sustainability of built infrastructure. Sci Total Environ 444:85–101
3. Meyer MD, Weigel B (2011) Climate change and transport engineering: preparing for a sustainable future. J Transp Eng 137(6):393–403
4. Posey J (2012) Climate change impacts on transportation in the Midwest. U.S. national climate assessment midwest technical input report, Winkler J, Andresen J, Hatfield J, Bidwell D, Brown D. Coordinators
5. Lehner B, Doll P, Alcamo J, Henrichs T, Kaspar F (2006) Estimating the impact of global change on flood and drought risks in Europe: a continental integrated analysis. Clim Change 75:273–299
6. Swiss Re (2013) Mind the risk—a global ranking of cities under treat from natural disasters. Swiss Reinsurance Company Ltd, Switzerland
7. Imhof D (2004) Risk assessment of existing bridge structures. PhD Thesis, University of Cambridge, U.K
8. Dawson RJ, Thompson D, Johns D, Gosling S, Chapman L, Darch G, Watson G, Powrie W, Bell S, Paulson K, Hughes P, Wood R (2016) UK climate change risk assessment evidence report: chapter 4, infrastructure. report prepared for the adaptation sub-committee of the committee on climate change, London
9. Transportation Research Board (TRB) (2008) Potential impacts of climate change on U.S. transportation. Transportation research board special report 290, committee on climate change and U.S. transportation, National Research Council, Washington D.C
10. JBA (2004) Scour & flood risk at railway structures. Infrastructure integrity (4) research theme: project number T112, Final Report, JBA Consulting, Rail Safety & Standards Board
11. Wardhana K, Hadipriono FC (2003) Analysis of recent bridge failures in the United States. J Perform Constr Facil 17(3):144–150

12. Imam BM, Chryssanthopoulos MK (2012) Causes and consequences of metallic bridge failures. Struct Eng Int 22(1):93–98
13. DEFRA (2012) The UK climate change risk assessment 2012 evidence report. Committee on climate change, London, UK
14. Highways Agency (2009) Climate change adaptation strategy and framework. Department for transport, UK
15. Network Rail (2015) A short guide to network rail. National Audit Office, UK
16. Booij MJ (2005) Impact of climate change on river flooding assessed with different spatial model resolutions. J Hydrol 303:176–198
17. Nicholls RJ (2004) Coastal flooding and wetland loss in the 21st century: changes under the SRES climate and socio-economic scenarios. Glob Environ Chang 14:69–86
18. UNEP (2007) Buildings and climate change: status, challenges and opportunities. United nations environment programme ISBN: 978–92–807–2795–1
19. Lamb R, Garside P, Pant R, Hall JW (2019) A probabilistic model of the economic risk to Britain's railway network from bridge scour during floods. Risk Anal 39(11):2457–2478
20. Larsen PH, Goldsmith S, Smith O, Wilson ML, Strzepek K, Chinowsky P, Saylor B (2008) Estimating future costs for Alaska public infrastructure at risk from climate change. Glob Environ Chang 18:442–457
21. ICE (2009) The state of the nation: defending critical infrastructure. Institution of civil engineers, UK
22. Melville BW, Coleman, SE (2000) Bridge scour. Water Resources Publications, LLC
23. Maddison B (2012) Scour failure of bridges. Proceedings of the institution of civil Engineers—Forensic Engineering 165(1):39–52
24. Van Leeuwen Z, Lamb R (2014) Flood and scour related failure incidents at railway assets between 1846 and 2013. Project W13–4224, JBA Trust Limited, UK
25. Breusers HNC, Nicollet G, Shen HW (1977) Local scour around cylindrical piers. J Hydraul Res 15(3):211–252
26. Melville BW (1997) Pier and abutment scour: integrated approach. J Hydraul Eng ASCE 123(2):125–136
27. Richardson EV, Davis SR (2001) Evaluating scour at bridges, 4th edn. United States department of transportation, Federal Highway Administration, Washington, USA
28. Sheppard DM, Melville B, Demir H (2014) Evaluation of existing equations for local scour at bridge piers. J Hydraul Eng 140(1):14–23
29. Briaud JL, Brandimarte L, Wang J, D'Odorico P (2007) Probability of scour depth exceedance owing to hydrologic uncertainty. Georisk: Assessment and Management of Risk for Engineered Systems and Geohazards 1(2):77–88
30. Briaud JL, Gardoni P, Yao C (2014) Statistical, risk and reliability analyses of bridge scour. J Geotech Geoenviron Eng 140(2):04013011
31. Deco A, Frangopol DM (2011) Risk assessment of highway bridges under multiple hazards. J Risk Res 14(9):1057–1089
32. Johnson PA (1992) Reliability-based pier scour engineering. J Hydraul Eng 118(10):1344–1358
33. Muzzammil M, Siddiqui NA (2009) A reliability-based assessment of bridge pier scour in non-uniform sediments. J Hydraul Res 47(3):372–380
34. NCHRP (2003) Design of highway bridges for extreme events. Report 489, National cooperative highway research program, Transportation Research Board, New York
35. Stein SM, Young GK, Trent RE, Pearson DR (1999) Prioritizing scour vulnerable bridges using risk. J Infrastruct Syst 5(3):95–101
36. Stewart MG, Deng X (2015) Climate impact risks and climate adaptation engineering for built infrastructure. ASCE-ASME J Risk U A 1(1):04014001
37. Devendiran DK, Banerjee S, Mondal A (2021) Impact of climate change on multihazard performance of river-crossing bridges: risk, resilience, and adaptation. J Perform Constr Facil 35(1):04020127
38. Liu L, Yang DY, Frangopol DM (2020) Network-level risk-based framework for optimal bridge adaptation management considering scour and climate change. J Infrastruct Syst 26(1):04019037

39. Yang DY, Frangopol DM (2019) Physics-based assessment of climate change impact on long-term regional bridge scour risk using hydrologic modeling: application to Lehigh river watershed. J Bridge Eng (ASCE) 24(11):04019099
40. Kay AL, Rudd AC, Fry M, Nash, Allen S (2021) Climate change impacts on peak river flows: combining national-scale hydrological modelling and probabilistic projections. Clim Risk Manag 31:100263
41. IPCC (2012) Managing the risks of extreme events and disasters to advance climate change adaptation. In: Field CB, Barros V, Stocker TF, Qin D, Dokken DJ, Ebi KL, Mastrandrea MD, Mach KJ, Plattner GK, Allen SK, Tignor M, Midgley PM (eds) A special report of working Groups I and II of the intergovernmental panel on climate change. Cambridge University Press, Cambridge, UK, and New York, NY, USA
42. Katz RW (1993) Towards a statistical paradigm for climate change. Climate Res 2:167–175
43. IPCC (2013) Summary for Policymakers. In: Stocker TF, Qin D, Plattner GK, Tignor M, Allen SK, Boschung J, Nauels A, Xia Y, Bex V. Midgley PM (eds) Climate change 2013: the physical basis, contribution of working Group I to the Fifth assessment report of the intergovernmental panel on climate change. Cambridge University Press, Cambridge, United Kingdom, and New York, NY, USA. 2013
44. Osborn TJ, Hulme M, Jones PD, Basnett TA (2000) Observed trends in the daily intensity of United Kingdom precipitation. Int J Climatol 20:347–364
45. UKCP18, 2018. UK Climate Projections. Accessible online at: http://ukclimateprojections.metoffice.gov.uk/ /. Department for environment, food and rural affairs (Defra), Crown Copyright. UK
46. Prudhomme C, Kay AL, Crooks S, Reynard N (2013) Climate change and river flooding: part 2 sensitivity characterisation for British catchments and example vulnerability assessments. Clim Change 119:949–964
47. Arneson LA, Zevenbergen LW, Lagasse PF, Clopper, PE (2012) Evaluating scour at bridges, 5th edn. Hydraulic engineering circular no. 18 (HEC-18), FHWA-HIF-12–003, U.S. department of transportation, Federal Highway Administration, USA
48. Melville BW, Chiew YM (1999) Time scale for local scour at bridge piers. J Hydraul Eng 125(1):59–65
49. BD 97/12 (2012) The assessment of scour and other hydraulic actions at highway structures. Design manual for roads and bridges, highway structures: inspection and maintenance assessment, Vol 3, Section 4, Part 21, UK
50. Robson A, Reed D (1999) Statistical procedures for flood frequency estimation. Flood estimation handbook, Vol 3. Centre for ecology & hydrology, natural environment research council, Wallingford, Oxfordshire, UK
51. Merz B, Thieken AH (2005) Separating natural and epistemic uncertainty in flood frequency analysis. J Hydrol 209:114–132
52. Kottegoda NT, Rosso R (1997) Statistics, probability and reliability for civil and environmental engineers. McGraw-Hill
53. Rail Safety & Standards Board (RSSB) (2005) Safe management of railway structures—flooding and scour risk. Final Report. JBA Consulting, London
54. Landers MN, Mueller DS (1996) Channel scour at bridges in the United States. Report no. FHWA-RD-95–184, U.S. Department of transportation, Federal Highway Administration

# Chapter 20
# Bushfire and Climate Change Risks to Electricity Transmission Networks


**Chi-Hsiang Wang**

**Abstract** Electricity transmission networks, as a critical component of energy systems that drive daily activities in modern society, have often been impacted by bushfires, as evidenced after the 2018 wildfires, California, USA, and the 2019–2020 Black Summer, Australia, both are record-setting in size and destructiveness in their respective regions. Even though the quantitative risk of bushfires to electricity transmission networks are difficult to model and assess as it consists of complex interplay of weather, climate, topography and vegetation, human activities, and the specific characteristics of the network, some recently developed models using physics-based approaches and statistical methods combined with satellite remote sensing technologies have been applied to and shown promising results in case studies. This chapter describes the interaction of bushfire and transmission network, discusses state-of-the-art models of bushfire risk to transmission networks, and provides some thoughts on adaptation and conceptual resilience framework for transmission networks under bushfire attack.

## 20.1 Introduction

Fire has been a natural phenomenon on Earth for the last 420 million years, soon after the appearance of terrestrial plants [1]. Bushfires (also called wildfires, wildland fires, forest fires, or biomass burning, among others) occur almost every year around the world, many of them inflict devastating damages to facilities and cause casualties. The size of fires, and losses thereof, over the time has been made worse not only by human activities such as constructing houses and facilities next to or inside the forests, but also by the changing climate, as evidenced in countries such as Australia, Canada, the United States, China, Brazil, and the Mediterranean [2]. In addition, occurrence of bushfires outside the seasons of high bushfire weather may be affected by local culture such as the lunar new year period, tomb-sweeping festival and spring ploughing in China, during which burning of sacrificial paper money dedicated to

C.-H. Wang (✉)
CSIRO Energy, Melbourne, Australia
e-mail: chi-hsiang.wang@csiro.au



M. G. Stewart and D. V. Rosowsky (eds.), *Engineering for Extremes*, Springer Tracts in Civil Engineering, https://doi.org/10.1007/978-3-030-85018-0_20

the ancestors and dried rice straw as fertiliser inadvertently ignite uncontrolled fires [3]. According to the [4], as many as 90% of wildfires in the U.S. have been caused by human activities.

Since the industrial revolution in the 1750's, anthropogenic climate change is altering precipitation patterns and increasing temperature globally, resulting in more extreme wildfire events. For example, the estimated direct and indirect damages in California, USA, wildfires in 2018 totalled US$148.5 billion [5], and the 2019–2020 Australian Black Summer, likely the most costly natural disaster in Australia, inflicted an estimated total of tangible and intangible costs of AU$230 billion [6].

In Australia, energy transmission and distribution networks consist of over 900,000 km supplying 11 million customer connections, and the distribution network alone comprises more than seven million power poles [7]. Under normal service conditions, high-voltage overhead transmission lines are the most cost-effective method for long-distance transmission of large-quantity electric energy. However, the devastating 2019–2020 bushfires in New South Wales and Victoria destroyed more than 5000 power poles, damaged thousands of kilometres of the network, causing more than 80,000 power outages across the National Electricity Market (NEM) of Australia. The efforts of network restoration have been herculean. For example, Essential Energy had 1.5 million hectares of its network footprint impacted, an area larger than the entire Greater Sydney Region. And this is just one of the five network operators impacted.

Powerline faults are known also to be a source for bushfire ignition. While the average number of fires started by powerlines is relatively low (around 2.7% of bushfires), powerlines are thought to have started a disproportionately high number of major bushfires and on average burned larger areas than those from other causes (except lightning), especially in heightened fire-danger days [8]. The primary causes of bushfires started by powerlines in the Februaries of 1977, 1983, and 2009 bushfires in Victoria include vegetation touching live wires, fuses producing hot metal particles when they operated, and clashing wires emitting hot metal particles. Under-maintained private overhead powerlines were implicated in many of the fires [9]. Around the world, electricity networks are aging because of under-maintenance and in some places are reaching the end of their design lives. As a result, the probability of electric-induced wildfires is increasing as the aging assets become more prone to faults.

In the remaining of this chapter, the fundamentals of bushfire behaviour are described briefly, followed by the effects of weather and climate on bushfires. The impact mechanisms of bushfires such as the attacks of fire flames, plume, and smoke to electric transmission networks is introduced, and then some modelling and assessment methods of bushfire risk to transmission networks currently in literature are reviewed. Finally, the approaches and thoughts for transmission network adaptation to bushfires and resilience concepts applied to transmission networks are given, followed by some concluding remarks.

## 20.2 Fundamentals of Bushfire Behaviour

Before the appearance of humans, fire regimes and organisms had evolved specialised strategies to resist, promote or recover from natural landscape fire disturbance. The fire-wielding humans since about two million years ago have introduced much more complexity into timing, location, extent and behaviour of vegetation fires [10]. Pre-industrial agriculturalists, for example, used fire to clear land and burn crop debris, and humans of modern era shape fire regimes by suppressing natural ignitions, modifying landscapes and fuel loads through controlled burns, land clearing, urbanisation, cultivation of non-native plants and animal husbandry. Moreover, fires could be set accidently or maliciously that result in devastating wildfires. Worldwide, very few vegetated environments are unaffected by human-induced fires [11].

Despite increased reporting of extreme wildfire events such as the 2018 and 2020 California, USA, wildfires and the 2019–2020 Australian Black Summer catastrophes, until recently it has not been evident if these events are related to climate change. The uncertainty is partly because of only short historical records which are only available in a few nations [12]. Furthermore, uncertainty arises due to substantial variation in fire activity among biomes, which requires regional rather than global studies. Notwithstanding these observational shortages, there is an emerging pattern of global fire activities that reveal the importance of regional-scale variation, climate change and anthropogenic interference [13].

Regional investigations are essential to establish bushfire trends. In Australia, the displacement of aboriginal people from most of the region since European colonisation has changed fire regimes and the composition of vegetation. It is difficult to separate the effects of climate change from that of the termination of more than 45,000 years of aboriginal fire management [14]. Nevertheless, increase in the number of extreme fire events has appeared to be related to climate change [15], and the number of lightning-ignited fires in western Tasmania, Australia, has also sharply increased, with an annual average of burned area of 100 hectares in early 1980s to over 200,000 hectare in 2019 [16].

With regards to extreme fire events, a particularly challenging task is the projections of variability and frequency as well as attribution of these events to anthropogenic climate change. This originates from the inherent uncertainties in coupling interdisciplinary models and the increased level of uncertainty and ‘sampling error’ due to spatiotemporal scarcity of the extremes [17]. With hindsight, the unprecedented 2019–2020 Australian Black Summer was a combination of prolonged drought, unusual conjunction of interannual climate modes, localised lightning storms, and human ignitions. The fact that the losses inflicted by the Australian Black Summer go beyond what is simulated highlights the inadequacy of the current methodologies. If we aspire to capture such improbable combinations of climate and human factors to satisfactorily predict extreme events, further understanding and development of coupled Earth System simulations must be a high priority [18].

Development of a bushfire hazard and risk methodology suitable for assessing the implications of climate change projections requires an appreciation of factors that

influence bushfire behaviour (fire weather severity, topography and vegetation) and the impact of bushfire events on electric transmission networks. The methodology for bushfire risk assessment and associated mitigation strategies needs to be tailored to the combination of these factors.

## 20.3 Effects of Weather and Climate on Bushfire Behaviour

To express the fire hazard posed by weather and climate, a number of fire danger indices have been developed and applied around the world. A brief description of fire danger indices and fireline intensity, a critical component of fire behaviour and damage modelling, is presented in the next subsections.

### *20.3.1 Fire Danger Indices*

Several fire danger indices have been developed based on meteorological variables combined with characteristics of fuels and soil moisture. In general, the purpose of a fire danger rating is to describe the potential of wildfire occurrence and/or the fire behaviour and severity if it occurs. Examples of some developed methods are: (1) Nesterov Index developed for the boreal forests of Russia; (2) Angstrom Index primarily used in Sweden; (3) Baumgartner Index used in Germany and Slovakia; (4) Fosberg's Fire Weather Index for California forests; (5) the US National Fire Danger Rating System; (6) the Fire Weather Index developed based on a Canadian empirical model; and (7) McArthur's Forest Fire Danger Index (FFDI) and Grassland Fire Danger Index [19].

While the Canadian Fire Weather Index is recognised as the most widely used fire danger system [20], this section presents the computation of McArthur's FFDI commonly used by all state governments of Australia.

Noble et al. [21] used statistical methods to derive an equation for FFDI which was originally developed by [22] via circular slide rules:

$$FFDI = 2\exp(-0.45 + 0.987\ln D - 0.0345H + 0.0338T + 0.0264V) \quad (20.1)$$

where $H$ is the relative humidity (%), $T$ is the temperature in degrees Celsius, $V$ is the average wind speed in the open at a height of 10 m (km/h) and $D$ is a fuel drought factor based on the equation:

$$D = \frac{0.191(I + 104)(N + 1)^{3/2}}{3.52(N + 1)^{3/2} + P - 1} \quad (20.2)$$

where $N$ is the time since rain (days), $P$ is the amount of precipitation for the last rain event (mm), and $I$ is the Keetch-Byram Drought Index [23] or Mount's Soil Dryness Index [24]. Plucinski et al. [25] found no statistical difference between Keetch-Byram's and Mount's indices for FFDI.

The FFDI is most sensitive to wind speed [26], which is associated with fire spread rates, ember attack, fanning of smoldering combustion, and suppression difficulty. Temperature and relative humidity are used to implicitly account for the effect of fuel moisture, the amount of water in the fine litter or grass fuels, which can retard combustion.

Notwithstanding its usefulness, the FFDI was based on science more than 60 years ago. The Australian federal and states governments funded development of a new Australian Fire Danger Rating System (AFDRS) that introduces significant change to fire danger forecasting [27]. The AFDRS combines the latest science experience and data to strengthen the ability to support government and emergency services decisions and give communities, industry and business clear and timely information in which they can have confidence. Preparation is underway for changes to legislation, policy and procedures for the AFDRS rollout across Australia in 2022.

### *20.3.2 Fireline Intensity*

Fireline intensity is defined as the rate of heat transfer per unit length of the fire line and represents the radiant energy release in the flaming front. Usually inferred by flame length, it expresses how likely the fire propagates and how difficult it is supressed.

Byram [28] proposed fireline intensity, $I_B$ (kJ/m-s), as the rate of heat released from a linear segment at any point or portion of the fire perimeter:

$$I_B = H \times w \times R \tag{20.3}$$

where $H$ is the heat yield of the fuel (kJ/kg), $w$ is the fuel load (kg/m$^2$), and $R$ is the rate of fire spread (m/s).

Accurate determination of $I_B$ depends on accurate measurements of $w$ and $R$. A physics-based model for rate of fire spread that takes into account the hill slope as well as the convective and radiative heat transfer [29] may be used to determine $R$. The relationships between $I_B$ and flame length as well as between $I_B$ and crown scorch height have been proposed through numerous experimental and observational studies [30].

Potential fuel loads may be estimated based on vegetation and land use classes. In Australia, for example, the vegetation classification may be informed by the following two products:

- National vegetation information system (NVIS), major vegetation subgroups (MVS) version 6.0 [31], and

- The Landsat coverages of Australia, which is processed to develop the national carbon accounting system (NCAS) for forest and non-forest (FNF) products as described by [32].

The NVIS is an ongoing collaborative initiative between the Australian and state and territory governments to manage national vegetation data to help improve vegetation planning and management within Australia. It was developed to enable the compilation of a nationally consistent vegetation dataset from data collected by states and territories in order to assist in managing biodiversity conservation, salinity control, improving water quality and fuel-load management. The NCAS provides a high-resolution binary national grid at 25 m resolution. Cells described as forest represent vegetation that is more than 20% foliage cover at least 2 m in height and at least 0.2 ha in area. The potential fuel load assigned to each vegetation class is based on the eight vegetation classifications specified in Table B3 of the Australian standard, AS 3959:2018 [33].

### *20.3.3 Climate Change on Bushfires and Electricity Transmission*

Bushfire conditions in recent decades have been more devastating than ever and, as discussed in previous sections, these are most likely because of climate change as it brings more frequent extreme fire weather due to more frequent drought, higher temperature, drier vegetation and in some regions more lightning. During the 2019–2020 Australian Black Summer, catastrophic rating, the highest fire danger rating in Australia, were declared for Greater Sydney for the first time. Climate change was found to make the conditions of the Black Summer bushfires at least 30% more likely [34]. Dry lightning without significant rainfall is the primary source of natural ignition for Australian bushfires, and there is a significant trend in southern Australia towards more days with weather conditions conductive to extreme bushfires that produce pyro-cumulonimbus thunderstorms as observed during the 2003 Canberra bushfires and the 2019–2020 Black Summer [35, 36].

The most direct link between harsher bushfire weather and climate change comes from observed and projected increasing temperature, which makes days hotter, heatwaves longer, and droughts more frequent. The average global temperature for 2020 is 1.2 °C above pre-industrial level [37], and Australia's climate has warmed on average by 1.44 °C since national records began in 1910 [35]. In addition, climate change is lengthening the bushfire season. This means that the northern and southern hemisphere seasons are overlapping, making pooling resources for firefighting difficult and, with globally all year-round bushfires, limiting the time window for effective prescribed burning. A review conducted by Science Brief in September 2020 revealed that, well over 100 studies published since 2013 show strong consensus that climate change enhances weather conditions conducive to wildfires. Climate change

is hence concluded to play an unequivocal and pervasive role in increasing the length and intensity of fire weather conditions.

Because of climate change, the range and frequency of threats impacting electricity networks are growing. For instance, Pacific Gas & Electric Co. (PG&E), an electricity and gas network service provider in California, cut power in October 2019 to approximately 2 million people in attempt to avoid sparking wildfires. PG&E was suggested to be the first major corporate bankruptcy caused by climate change [38]. The 2019–2020 Australian bushfires cut transmission lines and isolated communities, with some customers across the southeast coast of Australia losing electricity supply for several consecutive days. Projected temperature rise will increase sagging of overhead conductors, reduce ambient cooling of transformers and decrease the efficiency of electric power transmission; these all add to the electric network susceptibility to bushfire attack.

## 20.4 Bushfire Impact Mechanisms to Electricity Transmission

The key mechanisms of bushfire attack are (a) flame, (b) radiant heat, (c) burning tree branches, (d) wind attack, (e) convective heat, and (f) smoke and hot gases. These mechanisms usually operate in combination, even though they can also occur in isolation. The probabilities of attacks by flame, radiant heat, and convective heat can be greatly reduced by the clearance of vegetation along the transmission line routes as bushfire buffer, although this operation is time-consuming and highly costly.

Large quantities of smoke, flying ashes, and hot gases produced during a bushfire reduce the dielectric strength of the air gap, posing serious threats to the performance of the external insulation of transmission lines. They create a low resistance path in the surrounding air of an air insulated system, providing a potential for flashovers. Smoke particles of partially burnt fuel may deposit on ceramic insulator surfaces, reducing the values of expected creepage (i.e. shortest possible conductive path over an insular surface). Effects of smoke and hot gases generated by a bushfire under transmission spans are a considerable risk for un-intended power flow in transmission shutdowns (e.g. offline maintenance). This scenario can result in catastrophic consequences. In addition to tripping or line failure, heat can also cause conductor melting and structural strength reduction of supporting poles and towers.

Ground slope influences the rate of spread of a bushfire, moving faster up slope and slower down slope. As a rule of thumb by the Victorian Country Fire Authority, every ten degrees of increase in slope doubles the rate of spread of the fire and a corresponding doubling of the fire intensity compared to its behaviour on flat land. However, characteristics of different fuels such as grass, chaparral, and ponderosa pine forests have a significant effect on the rate of fire spread and perimeter shape of the fires on both level ground and smooth hill topography [39]. Vegetation and

topographic slope interact with bushfire behaviour in many complicated ways, which remains an active research topic.

## 20.5 Methods for Assessing Bushfire Risk to Electricity Transmission Lines

The parameters related to fuels, weather, topography, electric conductors and their supporting structures are the fundamental parameters for modelling bushfire attack to electricity transmission networks. Because of its complexity in nature, however, it is difficult to model and predict accurately when, where, and how bushfires will impact electricity transmission networks. For example, when a large number of bushfires erupts, the likely combination of single and multiple line trips becomes hugely complex. Nonetheless, this modelling task has been attempted through various approaches, including physics-based modelling and statistical methods. We briefly review below some of the proposed methods that may be used as a blueprint for further development.

### *20.5.1 Physics-Based Assessment Methods*

At current stage, the development of physics-based bushfire attack models has been limited. A physics-based assessment method requires realistic modelling of the physical parameters of bushfire flames, plume, smoke, burning progress, and their interaction with fuels as well as topographical features such as burning over hills, under the influence of weather parameters such as wind speed and rainfall. When attacking an electric network, it then considers the mechanisms of conductor breakdown and possible damages to the supporting structures.

A critical impact mechanism of bushfires is via air-gap insulation breakdown of live conductors. Because of the dielectric properties of air, air gaps act effectively as insulation media between live conductors and between the ground and live conductors. During a bushfire event, however, the air-gap insulation can be broken by three mechanisms: (a) reduction of air density due to the temperature increase caused by the fire; (b) change of air properties due to fuel oxidation reaction and thermal ionisation of the air caused by fire flames; and (c) reduction of breakdown voltage due to the presence of smoke particulates. The first two mechanisms are thought to be responsible for the majority of insulation breakdown of high-voltage transmission lines [40].

At the heart of a physics-based method is a risk assessment model that takes into account all the fire-progressing and conductor parameters that affect the electricity-carrying capacity of conductors. Two supplementary models, namely, the bushfire spread model and the air-insulation breakdown model, are required to obtain the flame

height, the rate of fire spread, fire line intensity, plume height, plume temperature, and the air-gap insulation breakdown voltage. The idea is to estimate whether or not the flames engulf the conductors based on the physical and electrical parameters of the transmission towers, transmission lines, and flames.

The bushfire spread model provides estimates about flame height and plume temperature profile. An empirical bushfire spread model such as that by [41] may be applied along with an appropriate fire danger index such as the FFDI to obtain the rate of fire spread, flame height, fire line intensity, and plume temperature profile.

The air-insulation breakdown model provides estimates about the air-gap insulation breakdown voltage. The clean air breakdown voltage at around 15 °C is about 250 kV/m. With contamination of the air by fire flame or plume, dependent on the fuel type, the breakdown voltage could be reduced to as low as 35 kV/m [42], increasing the possibility of phase-to-ground and phase-to-phase flashovers.

A case study carried out to compare the prediction and observed breakdown event of a transmission line in China shows promising results with the physics-based modelling approach [43].

### *20.5.2 Statistical Assessment Methods*

Because of inherent randomness in fire events, and the fact that low-probability, high-consequence events have long been modelled successfully by statistical methods [44], it is natural that statistical methods have been applied to estimate bushfire risks. Statistical methods rely heavily on observed data to determine appropriate probability models and the associated model parameters, hence unsurprisingly almost all probabilistic and statistical methods make use of time series data for bushfire risk modelling. For example, with time series bushfire occurrences and burned areas, Ghosh and Dutta [45] used seasonal autoregressive integrated moving average (SARIMA) and a regional fire risk modelling and power flow optimisation framework to assess the impact of bushfires on energy policies. The forecast bushfires from time series analysis is then combined with regional vegetation and risk mapping to detect downed conductors and high impedance fault. This method was applied to estimate wildfire risk to the conterminous U.S.

To estimate the probability of multiple line tripping and to avoid the pitfalls of assuming a specific probability distribution for line tripping probability, Lu et al. [46] used Markov Chain Monte Carlo to obtain the probability of individual transmission line tripping. The trip probability of each transmission line was modelled by logistic distribution. Assuming that the trips among the transmission lines are independent, the transmission network trip risk was expressed in terms of risk index [47, 48] and determined by summing up the risks of all transmission lines in the network. This method was used to assess the trip risks of the transmission network in Hunan Province, China, during the period of the annual Tomb-sweeping Festival and Lunar New Year Festival, the two time periods of most frequent fire events in the province [46].

It is noted that soft computing methods have been attempted in recent years. Dian et al. [49], for example, used cellular automata to simulate the spatiotemporal processes of wildfires and a line outage model taking into account conductor breakdowns due to Flame/plume temperature and smoke. The probability of air insulation breakdown voltage was assumed to follow a normal distribution. This method was applied to a case study for a 500 kV transmission line near Miyi County, China, as part of a wildfire early warning system. Combining fault tree and fuzzy logic with expert opinion and considering the transmission line tripping by wildfires as a sequence of events, Chen et al. [50] used event tree to model wildfire ignition and fault trees to model the events of wildfire early-warning, extinguishing, spreading, line tripping and line re-close failure. The probabilities of consequence of each branch of the event tree was then computed. This method was used to test its applicability to the transmission network in Xiangxi, China.

## 20.6 Adaptation and Resilience

After assessing the bushfire hazard and identifying the transmission network risk to bushfire attack, the questions that follows are how to constrain and minimise the bushfire hazard, how to manage and retrofit the existing network or design a new network such that the transmission infrastructure better copes with bushfire attack, and for serving future energy needs how to make the network more resilient under future bushfires influenced by climate and anthropogenic changes. We conclude the chapter with a review of some state-of-the-art thoughts to address these questions.

### *20.6.1 Adaptation of Transmission Network*

To avoid bushfire attack, the overhead transmission lines can be moved below the ground or the transmission tower height can be increased to compensate the reduced height of ground clearance due to conductor sagging. However, the costs of these approaches are often considered prohibitive. Indeed, upgrading existing infrastructure may be more costly compared to constructing new distributed electric sources [51].

With increase in temperature and heat-stress days, transmission and distribution may require more distributed energy resources to reduce congestion to avoid costly transmission network expansion. However, the efficiency of some renewable energy generation such as solar photovoltaics will be compromised under high temperature conditions. Finding a balanced optimal electric supply network has become an issue under climate change [51].

Electricity networks are a source of ignition for bushfires, particularly under extreme weather conditions [8]. Network-induced fires could be due to asset failures or contact events, representing about 57% and 43%, respectively, of the network

fires in Victoria, Australia, with 50% of asset fires in Victoria becoming ground fires [52]. Asset fires can be managed by the network operators as shown by the utilities in Victoria after 2009 Black Saturday bushfires [53], with techniques including 'spark-less' fuses, ground faults neutralisers and novel automatic reclosers to reduce the possibility of igniting a fire. One approach that prevents a network to start fires is to pre-emptively de-energise the network under extreme fire weather conditions. De-energising a network is not taken lightly though, as it cuts off power supplies to customers.

"Smart grids" is a term used to describe various technologies that may need to be developed to enable future electricity networks to function more safely and efficiently. Smart sensors are key components in smart grids and, when applied specifically to bushfire applications, sufficient quantity and allocation of smart sensors are critical to monitor temperature, wind speed and direction, humidity, transmission line current and voltage. The current and voltage need to be monitored at a frequency up to 10 kHz to enable detection of bushfire eruption [54]. Even though the current smart grid technologies may not yet be capable of reliably detecting wildfires, ongoing improvement of the technologies will make them one of the most efficient solutions for minimising bushfire impact to the power networks.

### *20.6.2 Resilience Assessment for Transmission Networks*

The concept of resilience has been applied since the 1960s for ecological, infrastructure, and organisational systems management and adaptation to disasters. Namely, the emphasis of resilience has been on three aspects: (a) resilience against crossing a system performance threshold; (b) resilience for system response and recovery after damaging impact; and (c) resilience for adaptive capacity and management to avert or alleviate the consequence of future impact [55]. A definition of resilience for power system suggests it as the ability to limit the extent, severity and duration of system degradation following an extreme event [56].

Raoufi et al. [57] conducted an extensive review on the development of power systems resilience metrics with a focus on disasters caused by high-impact, low-frequency events, and concluded that, in the power system literature, no standardised resilience metrics and no general agreement about the necessary capabilities or about the measurement method as well as their relation to the desired outcome. Based on their review, they define the resilience of power systems as: "… the ability of this (power) system to withstand disasters (low-frequency high impact incidents) efficiently while ensuring the least possible interruption in the supply of electricity, sustain critical social services, and enabling a quick recovery and restoration to the normal operational state." With this definition, Raoufi et al. [57] focused on the resilience related to resistance, adaptation, and recovery, combined a variety of resilience metric concepts from the literature, and proposed a general conceptual framework for the classification of resilience metrics related to energy generation, transmission, and distribution.

For a resilience metric to be practicable, ideally the resilience metrics should be quantifiable, hence the specific performance metrics grouped in power, duration, frequency, probability, and curve should be based on quantity and mathematical concepts. In turn, quantitative performance metrics can be used to facilitate quantitative consequence metrics related to economic, social, geographic, as well as safety and health aspects. It is noted that, except the economic metrics, only limited number of metrics for other three aspects have been proposed; more research is required for these metrics to be effectively utilised.

It was remarked that the concept of probability cannot be defined for most of high-impact, low-frequency disasters, hence defining any resilience metric based on disaster probability is controversial [57]. However, successful modelling of such disaster events by extreme-value theory [44] have existed since the 1960s [58–60], and codified probabilistic representations have been widely implemented in design of, for example, construction under extreme hazards such as extreme winds, earthquakes, and flooding [61–63] as well as terrorism in aviation security [64]. In addition, probabilistic/statistical methods have been indispensable for modelling and quantifying the reliability of critical infrastructure systems for as long as that of housing construction [65]. With the increase in knowledge of the high-impact, low-frequency events over the time, probabilistic methods should be included as one of the tools for resilient planning, design, and management of transmission networks.

## 20.7 Conclusions

Every bushfire and its associated impact are unique as the extent of impact is shaped by the weather, climate, topography, human activities, and natural as well as built assets of the location. Extreme bushfire events are particularly challenging events to anticipate because of their scarcity of occurrence and large uncertainty of changing climate that are projected to play a major role to shape such events. Nevertheless, the scientific research of bushfires risk is taking up the pace. This chapter reviews recent development of modelling and assessment efforts of bushfire impact on electricity transmission networks and points out areas that require further research.

Sufficient and reliable energy supply is a must for daily activities of modern society, in this vein all transmission networks should be regarded as critical infrastructure with appropriate consideration in all levels of government planning instruments to ensure they are treated with appropriate priority. It is hence necessary to recognise both the critical nature of transmission infrastructure and the potential for community benefit.

The Australian federal government announced in 2019 that it will invest more than AU$88 million over 10 years to establish a dedicated national research centre for natural hazards, bushfires and climate risks. The aim is to conduct evidence-based research to support the needs of emergency services and communities across Australia to reduce climate and disaster risks, and prepare for, respond to and recover

from future natural disasters. As part of the announcement, the government dedicated AU$2 million of the funds to immediately investigate key issues arising from the 2019/2020 bushfire season. Lessons learned, it is now time to search for better answers for disaster risk reduction and disaster resilience.

## References


1. Bowman DMJS, Balch JK, Artaxo P, Bond WJ, Cochrane MA, D'Antonio CM et al (2009) The human dimension of fire regimes on Earth. J Biogeography 38:2223–2236
2. Ribeiro LM, Viegas DX, Almeida M et al (2020) Chapter 2: extreme wildfires and disasters around the world: lessons to be learned. In: Tedim F, Leone V, McGee TK (eds) Extreme wildfire events and disasters. Elsevier, Amsterdam, Netherlands, pp 31–51
3. Liang Y, Zhou L, Chen J, Huang Y, Wei R, Zhou E (2020) Monitoring and risk assessment of wildfires in the corridors of high-voltage transmission lines. IEEE Access 8:170057–170069
4. U.S. Department of Interior. (2017)7 Burning questions: Wildfires and public lands. https://www.doi.gov/blog/7-burning-questions-wildfires-public-lands. Accessed 13 Jan 2021
5. Wang D, Guan D, Zhu S, Kinnon MM, Geng G et al (2020) Economic footprint of California wildfires in 2018. Nat Sustain
6. Read P, Denniss R (2020) With costs approaching $100 billion, the fires are Australia's costliest natural disaster. The Conversation (https://theconversation.com/with-costs-approaching-100-billion-the-fires-are-australias-costliest-natural-disaster-129433)
7. Energy Networks Australia (2021) Guide to Australia's energy networks. https://www.energynetworks.com.au/resources/fact-sheets/guide-to-australias-energy-networks/. Accessed 10 Feb 2021
8. Miller C, Plucinski M, Sullivan A, Stephenson A, Huston C, Charman K, Prakash M, Dunstall S (2017) Electrically caused wildfires in Victoria, Australia are over-represented when fire danger is elevated. Landsc Urban Plan 167:267–274
9. SA Power Networks (2011) Powerline bushfire safety taskforce: Final report. Attachment 11.7. https://www.aer.gov.au/system/files/SAPN%20-%2011.7%20PUBLIC%20-%20Powerline%20Bushfire%20Safety%20Taskforce%20Final%20Report%20September%202011.pdf. Accessed 9 September 2021
10. Glikson AY, Groves C (2016) Climate, fire and human evolution: the deep time dimensions of the Anthropocene. Springer, ISBN 978-3-319-22511-1
11. Le Page Y, Oom D, Silva JMN, Jonsson P, Pereira JM (2010) Seasonality of vegetation fires as modified by human action: observing the deviation from eco-climatic fire regimes. Global Ecol Biogeogr 19:575–588
12. Bowman DMJS (2018) Wildfire science is at a loss for comprehensive data. Nature 560:7–8
13. Bowman DMJS, Kolden CA, Abatzoglou JT, Johnston FH, van der Werf GR, Flannigan M (2020) Vegetation fires in the Anthropocene. Nat Rev Earth Environ 1:500–515
14. Bowman DM, Walsh A, Prior LD (2004) Landscape analysis of Aboriginal fire management in Central Arnhem Land, north Australia. J Biogeogr 31:207–223
15. Sharples JJ, Cary GJ, Fox-Hughes P, Mooney S, Evens JP, Fletcher M-S, Fromm M, Grierson PF, McRae R, Baker P (2016) Natural hazards in Australia: extreme bushfire. Clim Change 139:85–99
16. Styger J, Marsden-Smedley J, Kirkpatrick J (2018) Changes in lightning fire incidence in the Tasmanian Wilderness world heritage area, 1980–2016. Fire 1(3):38
17. Simiu E, Bietry J, Filliben JJ (1978) Sampling errors in estimation of extreme winds. J Struct Div ASCE 104(ST3):491–501
18. Sanderson BM, Fisher RA (2020) A fiery wake- up call for climate science. Nat Clim Change 10:175–177

19. Pereira MG, Parente J, Amraoui M, Oliveira A, Fernandes PM (2020) Chapter 3: the role of weather and climate conditions on extreme wildfires. In: Tedim F, Leone V, McGee TK (eds) Extreme wildfire events and disasters. Elsevier, Amsterdam, Netherlands, pp 55–72
20. National Aeronautics and Space Administration (2020) Global fire weather database (GFWED). https://data.giss.nasa.gov/impacts/gfwed/. Accessed 14 Jan 2021
21. Noble IR, Bary GAV, Gill AM (1980) McArthur's fire-danger meters expressed as equations. Aust J Ecol 5:201–203
22. McArthur AG (1967) Fire behaviour in eucalypt forests. Forest Research Institute, Forestry and Timber Bureau, Department of National Development, Australia, Leaflet No. 107
23. Keetch JJ, Byram GM (1968) A drought index for forest fire control. USDA Forest Service, Southeastern Forest Experiment Station, Research Paper No. SE-38
24. Mount AB (1972) The derivation and testing of a soil dryness index using runoff data. State Government of Tasmania, Tasmanian Forestry Commission, Australia
25. Plucinski MP, Sullivan AL, McCaw WL (2020) (2020) Comparing the performance of daily forest fire danger summary metrics for estimating fire activity in southern Australian forests. Int J Wildland Fire 29:926–938
26. Dowdy AJ, Mills GA, Finkele K, de Groot W (2010) Index sensitivity analysis applied to the Canadian forest fire weather index and the McArthur forest fire danger index. Meteorol Appl 17:298–312
27. National Council for Fire and Emergency Services (2021) Australian fire danger rating system. https://www.afac.com.au/initiative/afdrs. Accessed 29 Mar 2021
28. Byram GM (1959) Combustion of forest fuels. In: Davis KP (ed) Forest fire: control and use. pp 61–89, 554–555
29. Balbi JH, Chatelon FJ, Morvan D, Rossi JL et al (2020) A convective–radiative propagation model for wildland fires. Int J Wildland Fire 29:723–738
30. Alexander ME, Cruz MG (2021) Corrigendum to: Interdependencies between flame length and fireline intensity in predicting crown fire initiation and crown scorch height. Int J Wildland Fire 30(1):70–70
31. National Vegetation Information System (2020) National vegetation information system V6.0 © Australian government department of agriculture, water and the environment (https://www.environment.gov.au/land/native-vegetation/national-vegetation-information-system). Accessed 3 Mar 2021
32. Furby S (2002) Land cover change: specification for remote sensing analysis. National Carbon Accounting System Technical Report No.9. Australian Greenhouse Office
33. Australia S (2018) Construction of buildings n bushfire-prone areas. Australian/New Zealand Standard, AS 3959:2018
34. van Oldenborgh GJ, Krikken F, Lewis S, Leach NJ, Lehner F et al (2020) Attribution of the Australian bushfire risk to anthropogenic climate change. Natural Hazards and Earth System Sciences. Preprint 11 Mar 2020
35. Bureau of Meteorology (2020) State of the climate 2020. CSIRO and Bureau of Meteorology, Australia
36. McRae RH, Sharples JJ, Wilkes SR, Walker A (2013) An Australian pyro-tornadogenesis event. Nat Hazards 65:1801–1811
37. World Meteorological Organization (2020) State of the global climate 2020 — Provisional report. World Meteorological Organization
38. Wall Street Journal (2019) PG&E: the first climate-change bankruptcy, probably not the last. https://www.wsj.com/articles/pg-e-wildfires-and-the-first-climate-change-bankruptcy-11547820006. Accessed 4 Jan 2021
39. Linn RR, Winterkamp JL, Weise DR, Edminster C (2010) A numerical study of slope and fuel structure effects on coupled wildfire behaviour. Int J Wildland Fire 19:179–201
40. Sukhnandan A, Hoch DA (2002) Fire induced flashovers of transmission lines: theoretical models. IEEE AFRICON. 6th Africon, George, South Africa, 2–4 Jan 2003, pp 617–622
41. Sullivan AL (2009) Wildland surface fire spread modelling, 1990–2007. 2: empirical and quasi-empirical models. Int J Wildland Fire 18:369–386

42. Vosloo HF (2004) The need for and contents of a life cycle management plan for Eskom transmission line servitudes. M.S. Thesis, Rand Afrikaans University, South Africa
43. Chen H, Zhang Y, Zhang L (2018) A method to assess the wildfire induced breakdown of high-voltage transmission lines. J Phys: Conf Ser 1074:012152
44. Wang C-H, Holmes JD (2020) Exceedance rate, exceedance probability, and the duality of GEV and GPD for extreme hazard analysis. Nat Hazards 102:1305–1321
45. Ghosh S, Dutta S (2020) A comprehensive forecasting, risk modelling and optimization framework for electric grid hardening and wildfire prevention in the US. Int J Energy Eng 10(3):80–89
46. Lu J, Guo J, Jian Z, Xu X (2019) Research and application of efficient risk analysis method for electric power grid multiple faults under widespread wildfire disasters. Int Trans Electr Energ Syst 29(9), e12055
47. Xue Y, Van Cutsem T, Ribbens-Pavella M (1988) A simple direct method for fast transient stability assessment of large power systems. IEEE Trans Power Syst 3(2):400–412
48. Xue Y, Van Cutsem T, Ribbens-Pavella M (1989) Extended equal area criterion justifications, generalizations, applications. IEEE Trans Power Syst 4(1):44–52
49. Dian S, Cheng P, Ye Q, Wu J, Luo R et al (2019) Integrating wildfires propagation prediction into early warning of electrical transmission line outages. IEEE Access 7:27586–27603
50. Chen C, Xu T, Zhao D, Lei P (2019) Risk analysis for evolution of transmission lines tripping fault induced by wildfires located in Xiangxi, China. IOP Conf Series: Mater Sci Eng 677:042029
51. Ratnam EL, Baldwin KG, Mancarella P, Howden M, Seebeck L (2020) Electricity system resilience in a world of increased climate change and cybersecurity risk. Electr J 33:106833
52. Energy Safe Victoria (2018) Safety performance report on Victorian electricity networks. State Government of Victoria, Australia
53. Cainey JM (2019) Resilience and reliability for electricity networks. Roy Soc Victoria 131:44–52
54. Jazebi S, de León F, Nelson A (2020) Review of wildfire management techniques—part ii: urgent call for investment in research and development of preventative solutions. IEEE Trans Power Delivery 35(1):440–450
55. Wang C-H, Blackmore JM (2009) Resilience concepts for water resource systems. J Water Resour Plan Manage 135(6):528–536
56. Ciapessoni E, Cirio D, Pitto A, Panteli M, Harte MV, Mak C (2019) Defining power system resilience. RP_306_1, Electra, CIGRE
57. Raoufi H, Vahidinasab V, Mehran K (2020) Power systems resilience metrics: a comprehensive review of challenges and outlook. Sustainability 12(22):9698. https://doi.org/10.3390/su12229698
58. Cornell CA (1968) Engineering seismic risk analysis. Bull Seismol Soc Am 58(5):1583–1606
59. Davenport AG (1960) Rationale for determining design wind velocities. J Struct Div ASCE 86:39–68
60. Wang C-H, Wang X, Khoo YB (2013) Extreme wind gust hazard in Australia and its sensitivity to climate change. Nat Hazards 67:549–567
61. American Society of Civil Engineers (2017) Minimum design loads and associated criteria for buildings and other structures : ASCE/SEI 7–16. American Society of Civil Engineers, Reston, Virginia, USA
62. Standards Australia (2007) Structural design actions. Part 4: Earthquake actions in Australia. Australian/New Zealand Standard, AS/NZS 1170.2:2011
63. Standards Australia (2011) Structural design actions. Part 2: Wind actions. Australian/New Zealand Standard, AS/NZS 1170.2:2011
64. Stewart MG, Mueller J (2018) Are we safe enough? Measuring and assessing aviation security. Elsevier, Amsterdam, Netherlands
65. Stewart MG, Melchers RE (1997) Probabilistic risk assessment of engineering systems. Chapman & Hall, London, UK

# Chapter 21
# Provisions for Climate Change in Structural Design Standards


**Johan Retief and Celeste Viljoen**

**Abstract** Designers of building and civil engineering structures, using design standards for an extensive scope of common structures, are confronted with the advent of a global climate that is changing at an accelerating rate. This chapter considers the possibilities for the adaptation of the basis of structural design to account for the exceptional uncertainties introduced by climate change. The case study is limited to building structures exposed to relatively mild climate loading, by assessing climate change in the context of the South African Loading Code SANS 10160. Standardized decision-making, based on vulnerability resistant robustness concepts, are demonstrated to be effective against a severely uncertain or ambiguous future climate. The risk and reliability basis of semi-probabilistic limit states design is adapted to account for the ambiguity of the climate during the service life of the structure. The design basis for wind loading is used to review information on climate change, to determine the vulnerabilities of structures and identify related design situations. Adaptation of standard procedures can then be applied in accordance with climate robustness classes. Strategies for advancing the design base for climate change in tandem with advancement of associated information, are proposed to be incorporated into the agendas of committees and organizations involved in the advancement of standards for structural design.

**Keywords** Structural standards · Climate change · Uncertainty · Ambiguity · Wind load · Design basis · Structural reliability · Decisions-making

## 21.1 Introduction

Structural design standards are established as an instrument for decision-making under uncertainty by using semi-probabilistic procedures as derived from risk and

J. Retief (✉) · C. Viljoen
Department of Civil Engineering, Stellenbosch University, Stellenbosch, South Africa
e-mail: jvr@sun.ac.za

C. Viljoen
e-mail: celesteviljoen@sun.ac.za



M. G. Stewart and D. V. Rosowsky (eds.), *Engineering for Extremes*, Springer Tracts in Civil Engineering, https://doi.org/10.1007/978-3-030-85018-0_21

reliability concepts [1–3]. Climate change that is forced by anthropogenic greenhouse gas (GHG) release and accumulation into the atmosphere is now confirmed [4]. This introduces an additional dimension to the sources of uncertainty to be reflected in the provisions for structural performance in design practice. An increase in global temperature of the order of 0.8 °C above pre-industrial levels is indicated for the decade ending by 2015; rates of increase of the order of 0.2 °C/decade are obtained as determined from a suite of coupled global climate models (cGCM) [5]. Projections of future climate conditions based on agreement with historic records indicate changes in the extreme climate conditions that will impact on structural performance through changes to the climate actions on structures even for the present generation of structures during their service life. This chapter explores a possible strategy for incorporating provisions for climate change into the operational decision-making process employed by design standards as implemented by the design basis (DB) of the South African Loading Code SANS 10160 [6].

The challenge of reducing the dynamic, even fluid nature of the development of understanding climate change, down to standardized procedures for decision-making on structural performance is truly daunting. However, from the perspective of professional responsibility it is an imperative. The challenge is nevertheless not unlike the efforts required to establish and implement semi-probabilistic limit states design during the pioneering era, albeit on a different scale, but with different levels of technology, resources and experience this time.

The selection of the SANS 10160 for this case study is intended to simplify and constrain the investigation. The scope of the standard is limited to building structures; the primary climate load to be considered is wind loading for a mildly complex extreme wind climate under semi-arid subtropical conditions; for example, tropical cyclones are excluded. The standard is nevertheless harmonized with international practice through reference to Eurocode EN 1990 [7], complying with international standards based on risk and reliability principles such as SANS 2394 [8]. It is sufficiently relevant to situations in many countries and consider issues that could even be of interest to countries exposed to more complex climatic conditions.

Whilst focusing on South African design practice, the case study identifies decision-making issues relevant to the full hierarchy of standards development infrastructure. National to international standardization and professional organizations should have an interest in fundamental and global aspects of structural design in relation to decision-making for climate change. Such a perspective is consistent with the approach proposed for Climate Adaptation Engineering (CAE) to include engagement of stakeholders, a clear path for the flow of information, tools and resources managed in an institutional arrangement for the development of climate decision-making approaches [9].

Scaling across many orders of magnitude down to design standards, from the global phenomenon to the decisions by the designer on a specific structure, poses quite a challenge. Whilst realizing the urgent need for creating decision relevant responses to the unimaginable complex challenges of climate modeling, Weaver et al. [10] proposes an approach to *seek robust solutions* by identifying the greatest vulnerabilities across a range of futures to formulate policies that function reasonably

well across this range. Helgeson [11] classifies this approach as *bottom-up* from well-defined objectives and policies and work backwards to determine the climate conditions where thresholds will be met in *robust decision-making*. The climate robust approach considers climate modeling simply as prediction instruments for scenario generation, sources of insight into complex system behavior and critical thinking to aid decision-making by bottom-up identification of vulnerabilities against multiple views of the future for adopting appropriate responses. The search for tailored climate information is applied to inform specific questions related to the vulnerability of the system under consideration. It is not particularly demanding of climate models. Case studies are useful to explore this approach.

The climate robust approach is evidently suited to considering the adaptation of structural standards as response to climate change. This approach is therefore adopted in the case study. In the following sections the relationship between structural design and the climate provides the framework for extracting relevant information from the growing literature on climate change. A review of the reliability basis provides the background to the standardized basis of structural design for South Africa. Confirmation of anthropogenic climate change (ACC), its projection into the future and downscaling to the country and associated decision-making approaches under uncertainty are subsequently reviewed. Scenarios to reflect ACC in a conceptual format that is consistent with design provisions are then formulated. An outline of the design basis to enhance ACC robustness is derived from on an assessment of vulnerabilities to changing climate actions. The parameters that have an influence on ACC robustness for adaptation of the standard and its application in design are finally reviewed.

## 21.2 Design Basis for Wind Load

It can be expected that ACC conditions will have a significant impact on structural design practice due to shifts in socioeconomic conditions and priorities, such as sustainability and the carbon footprint of the construction industry. The scope of this case study is however limited to the design of building structures in accordance with SANS 10160 [6]. Partial factor limit states design as applied in the standard is based on the principles of risk and reliability. Design values for structural resistance to loading are specified to be sufficiently biased to achieve annual exceedance probabilities of the order of $10^{-5}$ as the approximately cost optimal level of reliability. The exceptionally high reliability levels required for structures, relative to the performance of civil engineering systems and most other capital investments in general, reflect the socioeconomic importance of structural performance. These stringent requirements serve as reference in the characterization of ACC and its future impact. The design basis for structures is summarized as background to the following review of ACC, with the emphasis on wind load as the primary climate condition.

The path from considering processes having an impact on structural performance at stated levels of reliability can broadly be classed into three levels of decision-making under uncertainty, as derived from concepts of structural risk, reliability and

operational discrete or semi-probabilistic procedures. Following the inverse approach of vulnerability resistance, the design basis for wind load is summarized here in the order of design, standardization, lastly reliability and risk.

The design wind load ($Q_d$) on a structure is expressed by Eq. 21.1 as:

$$Q_d = \gamma_w Q_k = \gamma_w c_w (v_k)^2 \tag{21.1}$$

The two reliability elements of Eq. 21.1 are the partial factor ($\gamma_w$) that is calibrated to achieve the required structural reliability under wind loading and ($v_k$) is the characteristic wind speed specified for the given geographical location of the structure. The coefficient ($c_w$) represents procedures for accounting for terrain and structural geometry to convert the free-field wind into the load distribution across the structure, as based on principles of wind engineering.

Design basis standardization is concerned with determining values for the reliability elements ($\gamma_w$; $v_k$) in accordance the target reliability ($\beta_t$) that is related to the probability of failure $P_F = \Phi(-\beta_t)$ where $\Phi$ is the normal probability distribution, of prescribed limit states for representative design situations. Values for the reliability elements are derived from background investigations. The reference reliability target $\beta_{50} = 3.0$–$3.5$ for a 50 year reference period was originally determined from calibration to existing practice [12] and confirmed for the current standard [13]. This translates to exceedance probabilities around $10^{-6}$ per year and associated wind speed values around the $10^{-3}$/y fractile.

The progressive development of the wind load provisions, and representation of the extreme wind climate for the country, is significant when the impact of ACC is considered. The relative simplicity of the representation of the reliability elements needs to be stressed: a single $\gamma_w$-value accounts for an extensive scope that includes the wind climate across the country, in addition to the range of structures and geometries, albeit for a given reliability class and limit state [14], the contribution of model uncertainties introduced by the wind engineering coefficient $c_w$ is not negligible, in particular due to systematic bias [14], the map of $v_k$-values is a highly simplified rendering of the complex climate across the country [15, 16]. Notably the procedures for calculating $c_w$-values led to substantial and systematic increases in wind loading for SANS 10160–3 in comparison to the previous standard [17].

The reliability-based design parameters $\gamma_w$ and $v_k$ are informed by the extreme wind climate for the country, which was investigated in several campaigns. Extreme value models were determined for 14 major centers in the country as input to the 1989 loading code [18]. A new extreme wind set of models was determined for 74 recording stations for the current loading standard SANS 10160 [19], which was further extended to a total of 3500 annual extreme observations [20]. The latest sets of observations made it possible to resolve the extreme wind climate in terms of the wind generating mechanisms, consisting of extratropical cyclonic systems towards the southern parts of the country, mesoscale convective events towards the north, with a wide intermediate range of mixed climate conditions [16, 19, 20].

The wind map for the first-generation standard essentially stipulated a $v_k$-value of 40 m/s for the characteristic gust wind speed across the country [18]. The map for SANS 10160 was completely revised in 2018 by specifying $v_k$-values per municipal district at four levels from 32 m/s to 44 m/s gust speed at 2% fractile value [15], with an update by [20], see Fig. 21.1. Notably the simplification of representing $v_k$-values in 4 m/s intervals is intended to reflect the uncertainty of the underlying extreme value models, temporally due to the extrapolation from limited record lengths of around 20 years, spatially due to the interpolation between the sparse set of recording stations. A review of the historic development of the South African strong wind map is provided by [21].

The review of ACC literature should therefore extract information related to future spatial and temporal probabilities for extreme wind conditions for South Africa over the next century. The central role of wind load as the primary environmental load condition implies that future conditions may have fundamental consequences for determining future optimal and required design reliability levels. The immediate requirement, however, is to provide a transition between the current DB and future conditions, in tandem with evolving ACC conditions.

## 21.3 Review of Anthropogenic Climate Change

Information on extreme wind climate conditions in South Africa is required to define scenarios that can be applied to consider the robustness of structures against the reigning conditions over their service lives. A review of anthropogenic climate change (ACC) provides the background for developing standardized design procedures for appropriate structural resistance and as a primer on the topic to future users, to be able to make informed decisions. Issues of principle and policy also emerge, requiring attention at all levels of decision-making related to structural standards and practice. Information currently available on projected ACC conditions is of critical importance for decisions on either taking early action or to await further clarification on GHG forcing pathways and related extreme conditions.

The review follows the flow of information as it emerges and is reported in the series of IPCC Assessment Reports AR4 [22], AR5 [4] and some previews of AR6 and complementary literature [23]. Key issues are confirmation of the human origins of global climate change, forcing pathways of GHG accumulation, mitigation measures and associated climate projections, vulnerability and impact on human and natural systems, adaptation, and its effectiveness, finally scaling down to the South African extreme wind climate. Economic assessment provides useful information on uncertainties about the state of ACC information and its implications for decision-making.

Key findings reflect progress and shifts in main issues under consideration in subsequent ARs: AR5 concludes that the accumulation of evidence on the phenomenon of global warming since the pre-industrial era is confirmed as unequivocal, that the link to anthropogenic increase in GHG concentrations in the atmosphere

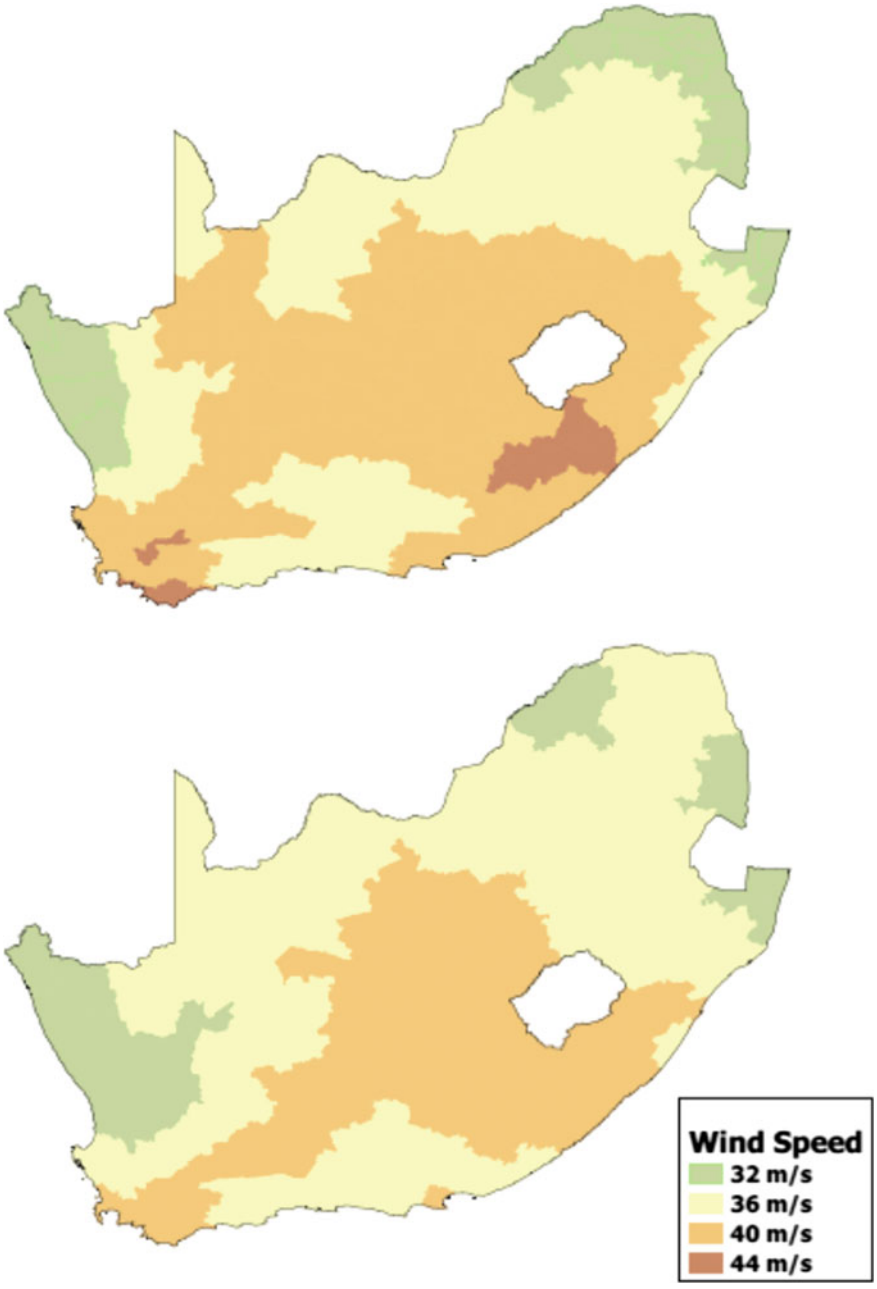


**Fig. 21.1** Characteristic wind speed zones for South Africa: Current map (top), proposed updated map (below) [15, 20]

is extremely likely. An assessment of the implications and effects of the 2015 Paris Agreement with the goal to limit global warming to well below 2 °C, preferably to 1.5 °C compared to pre-industrial levels, is provided in the IPCC Special Report [5]. This goal will require urgent mitigation measures, leading to zero carbon emissions by mid-century, or equivalent drastic measures, with a limited time window to achieve.

### *21.3.1 Forcing Pathways*

The state of information on ACC is reflected by scenarios for the advancement of GHG accumulation depending on the effectiveness of mitigation measures and the resulting global climate [24]. The set of forcing representative concentration pathways (RCP) compiled for AR5 [25] project global temperature increases since the pre-industrial era by 2080–2100 at mean/likely range of 3.7/2.6–4.8 °C for the *high baseline* (do-nothing) scenario RCP8.5; and 1.0/0.3–1.7 °C for RCP2.6, the *lowest mitigation scenario* in the literature. An update, provided by Special Report [5], provides confirmation of an average temperature increase from pre-industrial levels of 0.87/0.75–0.99 °C for the decade ending 2015, with a match within 20% between estimates and observations, and a rate of increase of 0.2°/0.1–0.3 °C per decade. Recent updates based on a new framework of shared socioeconomic pathways (SSP) indicate temperature increases of 1.3 °C by 2020, and values of 2.7/1.4–4.8 °C for 2100 for the range of nine scenarios [23]. The results confirm global incremental temperature rise and its human roots. The dependence of projections on pathway models, mitigation scenarios, and tolerances are clearly demonstrated.

### *21.3.2 Natural and Forced Pathways*

A measure of the effect of GHG accumulation on climatic conditions can be obtained by considering the internally generated variance of the natural climate and GHG forced climate variance as signal [26]. The ratio of forced to total (forced + internal) variance histories is obtained from a set of cGCM histories for the range of RCP2.6, RCP4.5 and RCP6 scenarios. Over the period of observation, the ratio rises slowly to below 20% up to the decade around the year 2000, rising rapidly to above 50% at about 2050; tapering off to between 70 and 90% by 2100. Similar ratios are predicted for the range of RCP scenarios, except for convergence towards the upper range for RCP6 on approaching 2100. The low forced ratio up to the present indicate an observable but subdued effect of radiative forcing. Notably, over the next few decades an accelerated transition can be expected, reaching dominance of forced variance during the last few decades of the century.

### 21.3.3 Socioeconomic Decision-Making

Since socioeconomic decision processes integrate all the elements of the complex process of climate modeling, mitigation pathways, impact, and adaptation analysis, it serves to take a measure on the state of information as it progressed to date.

The findings of the scientific investigations of AR5 are expressed in terms of levels of confidence as derived from modelled results. This implies a frequentist result, considering the central part of the set of outcomes of multiple models. Application of model outcomes to combined scientific and economic Integrated Assessment Model (IAM) *expected utility* decision-making, does not account for tail-end results that pose risks due to possible adverse outcomes.

Much more severe outcomes need to be considered by considering the so-called *fat tail* or *ambiguous* distributions [27–30]. Weitzman [30, 31] asserts that probability estimates of the distribution tails become diffuse, because the frequencies of rare events cannot be estimated from previous experience. Conclusions tend towards application of the *precautionary principle*.

Consequently, consideration of large-consequence/low-probability outcomes is becoming an important component of ACC assessment and decision-making. The dynamic interaction between various modes of climate variability is an example of a source of ACC uncertainty [32]. Estimates of economic damages often increases by an order of magnitude when low probability outcomes are considered, compared to the expected utility framework estimates [33].

Surveys of alternative decision-making approaches applicable to ACC conditions, are instructive, especially when compared to approaches applied to structural standards and design, Helgeson [11, 34–39]. Decision-modes are dependent on context, including the level under consideration, ranging from operational to strategic leadership perspectives. Iterative development is required under dynamic and transitional conditions.

Confirmation can nevertheless be inferred from the literature that structural engineering decision-making is fully compatible and able to deal with ACC situations.

### 21.3.4 Regional Scale Extreme Climate Risk

Recent investigators indicated the need to provide information required for risk assessment by identifying what is possible, not merely what is likely [10, 40–42]. The high confidence on projections of global temperatures is not extended to regional levels and to extreme conditions that poses the highest risks, such as for extratropical regions that form an important part of global atmospheric circulation systems and where significant impact could be expected [43, 44].

Alternative approaches are used for projections of extratropical cyclones (ETC) as important indicators of future extreme conditions [45], specifically for European severe storms [43, 46] and southern hemisphere ETC [47, 48].

These advanced methodologies confirm the limitations of AR5 models for projecting regional conditions, even scaling to alternative pathways. Influencing factors and their relative sensitivities are demonstrated. Indications of increased damage projections for Europe are reported by [44, 49], with a significant increase in the frequency of ETC with extreme wind for the southern hemisphere, in contrast to AR5 reported by [47].

### *21.3.5 Down-Scaled Projections for South Africa*

Application of global climate trends to South African conditions require down-scaling to establish the influence of regional response to radiative forcing [50, 51]. This could be done at various scales and stages in time, as is done by [52] on a continental scale for Africa, Jury [53] on a regional scale for southern Africa, with an updated version for South Africa covering the sub-region 33°–25°S, 22°–32°E [54], to establish general trends, or to assess specific interests such as for water resources of southern Africa [55] and for the western Cape [56].

Early investigations obtain rates of temperature increase of 0.2–0.5 °C/decade across the African continent for four SRES forcing scenarios from AR4, but with some fundamental limitations of not accounting for El Niño cycles, land cover and aerosol loadings [52]. The vulnerability of southern Africa to climate change is related to the arid nature of the region [50], with projected temperature increases of around 3 °C, maximum temperature increasing faster than minimums, rates of 0.2–0.5 °C/decade over the central southern land mass [55]. The acceleration of warming of 0.01–0.02 °C/y is found for southern Africa; a poleward shift of sub-tropical South Atlantic anticyclones, acceleration of the Agulhas current on the east coast having regional impacts [53]. Historic rates of > 0.02 °C/y up to 1980 are projected to increase to 0.028 °C/y by 2050 for RCP6, with a rate of < 0.01 °C/y for the south eastern quadrant of the country, up to 0.04 °C/y for the north west and intermediate higher than average values for the north east and south west are obtained by [54, 57]. Whilst local ACC patterns fit into global trends, regional effects such as its sub-tropical latitude, effects of adjacent oceans, the high elevation inland plateau, semi-arid climate, all have a marked effect on the geographical distribution of climate changes.

The two main extreme wind climate mechanisms of synoptic and convective windstorms may be significantly influenced by indicated changes in subtropic high pressure systems and intensification of precipitation.

## 21.4 Design Situation for ACC Conditions

The review of the progression of ACC confirms that during their service life, structures designed in accordance with SANS 10160 will be subjected to climate conditions that deviate substantially from that on which the standard is based, due to the complex relationship between global warming and regional extreme conditions shown by the review above.

By defining design situations from appropriate ACC scenarios for extreme wind conditions in the country, vulnerabilities of structures provide an indication of the requirements for providing ACC robustness in standardized procedures. ACC vulnerabilities can be assessed relative to the intrinsic robustness of the current design basis for wind loading for the sustained ultimate limit state.

### *21.4.1 ACC Scenarios as Design Situation*

A design situation for AAC should indicate a condition under which the effect of extreme wind conditions deviate from that on which the wind load provisions are based. An *ACC design situation* can then be used to specify robustness requirements. Representative stages for assessment of *ACC robustness* are used to standardize the transitionary nature of ACC. The current situation as outlined in Sect. 21.2 serves as benchmark for initial conditions. The dates 2060 and 2100 will represent the situation at 80% of the service life of *common* and *essential* class structures, representing the latter half of their respective service period.

The benchmark of current extreme wind conditions accounts for the recent increase of wind load characteristic values [17], an increase in the partial factor and improved reflection of extreme wind climate conditions across the country [14]. The ACC2060 situation will be reached by a steep transition to conditions and ambiguity where forced variance takes over from natural variance, but with limited dependence on mitigation forcing pathways. The current ACC2100 ambiguity will be dominated by the realization of mitigation measures. In both scenarios, decision-making on acceptable performance will have the benefit of the unfolding climate up to the date of assessment.

### *21.4.2 Vulnerability Assessment*

ACC vulnerability should be expressed as the impact of extreme wind conditions on compliance to the ultimate limit state requirements for the sustained design situation. The progressive nature of ACC implies that the design working life of the structure becomes vulnerable to noncompliance. The undifferentiated classes of building structures and reliability classes mask vulnerabilities and consequences under an envelope

of conservative design bias, with its own dose of ambiguity. Inconsistent reliability levels for variable loads in general, and specifically for wind load, indicate a more detailed level of vulnerability. Identified inconsistencies include lack of unification with load classes such as snow load and materials-based resistance, marginal reliability for dominating wind load design cases, dependence on substructure systems, the influence of model uncertainties [14, 20, 58, 59].

## 21.5 Design Basis for ACC Situation

The requirement for accounting for ACC conditions arise from the projected change in global climate conditions that will affect the severe wind conditions in South Africa during the service life of structures in the scope of the standard. These conditions could have an impact on the reliability of the structures that exceed the compliance requirements of the standard. Alternatively, it may impair the intended service life of structures. A formulation of the design basis for an ACC design situation is presented in the format of model clauses followed by commentary.

### *21.5.1 General Requirements*

A design basis is introduced to account for changing climatic conditions during the service life of the structure. The design basis is intended to enhance the robustness of the structure against changing extreme wind conditions. The design basis for wind loading is adapted to provide additional robustness against changes to the extreme wind expected during the service life of the structure.

The objective of the ACC design basis is to achieve effective and optimal ACC robustness in a standardized approach, without engaging in the complexities of ACC extreme wind conditions. ACC robustness should be increased to levels that are consistent with the impact on the reliability, functionality, and service life of the structure. The design basis for ACC should enable the designer to account for the ambiguity of impending extreme wind conditions in a systematic manner. The approach is sufficiently general to make it possible to include ACC robustness in the design optimization processes.

The sustained ultimate limit state level of reliability serves as reference to changing extreme wind ambiguity levels. Requirements and provisions should be adjusted to ACC2060 or ACC2100 design situations respectively for application to the assessment of common and essential structures.

ACC conditions are represented by a set of two states that reflect the situation towards the latter half of the service life of the structure. The ACC states are used as cases for which appropriate levels of robustness against extreme wind conditions should be assessed. An indicative Category 3 service life of 50y is used for common

structures. Category 4 service life of 100y applies to essential structures and structures that are of strategic importance or designed for long-term capital investment. Associated reference classes ACC2060 and ACC2100 represent the conditions used to assess robustness requirements. The classes are intended to reflect ambiguous conditions as uncertain extreme wind states. The classes are based on descriptive attributes derived from the projected ACC environment across the country at the assessment stage. Considering the initial South African extreme wind climate as *moderate*, indicative climate descriptors for the ACC states may need to be restated as more severe, to reflect the large uncertainties in magnitude and geographical distribution.

### *21.5.2 Design Requirements*

Changed climate situations should be classified as accidental design situations to indicate the exceedance of the sustained ultimate limit state. Limiting criteria are that human safety should not be compromised; disproportionate damage should be inhibited.

The ambiguity of the ACC state is considered relative to the design base extreme wind state, to imply some degree of normalization or standardization. Notably, the current design wind state has a significant degree of ambiguity, due to intrinsic uncertainties of extreme wind probabilities, approximations of reliability by the stipulated design procedure, across the scope of wind load design situations.

The design service life of the structure should be treated as a design requirement if the sensitivity of structural performance to the ambiguity classes ACC2060 or ACC2100 would have an impact on the expected service life. Classes of severity of the impact may account for the economic, socioeconomic, or strategic impact, depending on the function of the structure.

ACC introduces another level of uncertainty beyond that for which partial factor limit states design provide. ACC uncertainties are classified as ambiguous since probability distribution parameters are unknown, or at least uncertain itself. The reserve wind load resistance can however be utilized by relating ACC impact to exceedance of the limit state, activating the reliability margin above the failure state. This condition resembles an accidental design situation. Accordingly, requirements are specified per case.

### *21.5.3 ACC Robustness Verification*

Design verification should be specified, as based on criteria determined by sensitivity assessment of increased wind load, beyond sustained ultimate limit state values, with associated impairment of safety, functionality, and economic consequences of failure.

The robustness margin depends on the economic justification or affordability of additional capacity, expressed as *ACC robustness*. The ACC design situation is consequently directed to provide robustness specifically against *ACC extreme wind conditions*. The sustained ultimate limit state could then be applied to determine the sensitivity of the structure to extreme wind conditions, assess the marginal cost of increasing robustness and inform decision-making on affordable to optimum ACC robustness, in accordance with the function of the structure.

## 21.6 Application of ACC Design Base

The ACC design situation is a special case of the accidental design situation. Full use can be made of design procedures for wind loading by adding the notion of ambiguity to standard reliability procedures. Although criteria for the assessment of ACC robustness at the reference stage are not clarified, it can be assumed that ambiguity will be reduced over the first half of the service life of the structure to inform decision-making at later stages.

The ACC design situation can be based on adjustment of provisions of the partial wind load factor ($\gamma_w$) or the characteristic wind speed ($v_k$) of the current persistent limit state.

- The required reliability level can be increased by adjusting the Reliability Class by one level. The wind load can be adjusted by raising the reliability class by one level or an increment of $\Delta\beta = 0.5$ through multiplying $\gamma_w$ by a factor of $K_F = 1.1$, equivalent to increasing $v_k$ by a factor of $(K_F)^{½} = 1.05$, for example by increasing $v_k$ from 36 to 38 m/s for ACC robustness design.
- Ambiguity in extreme wind conditions can be introduced by increasing the $v_k$-value by one increment of 4 m/s, for example from 36 to 40 m/s or an increase in the load by a factor of $(40/36)^2 = 1.25$. Such an adjustment should be considered for advancing the boundaries between mapped zones into lower wind speed zones. Standardized guidance could be based on re-mapping of adjusted $v_k$-values for the ACC design situation.

These adjustments indicate that increased reliability is relatively inexpensive, but quite sensitive to the applied $v_k$-value.

More refined adjustment of wind load provisions for the ACC design situation could be derived from the background information on wind loads. Equation (21.2) models $\gamma_W$, based on a Gumbel probability distribution of the free-field wind pressure, normalized to $v_k$-value.

$$\gamma_X = \mu_Q + \sigma_Q\left(-0.45 + 0.78\,\mathrm{LN}\left(-\mathrm{LN}\left(\Phi\left(\alpha_Q\beta\right)\right)\right)\right) = \mu_Q + \sigma_Q\theta_\beta \qquad (21.2)$$

The mean bias $\mu_Q = 0.9$ and standard deviation for wind pressure $\sigma_Q = 0.3$ can be derived from the results for the South African extreme wind climate [14]. Considering the case for $\beta = 3.0$ (Reliability Class 2) and a wind load sensitivity

**Table 21.1** Sensitivity ($\Delta_X/\delta_X$) of the wind load to incremental changes $\delta_X$ in distribution parameters ($X$) to obtain adjusted load factor $\mu_{W,adj}$

| Sensitivity Parameter $X$ | Reference value | Increment $\delta_X$ | Sensitivity $\Delta_X/\delta_X$ |
|---|---|---|---|
| Mean annual extreme wind speed ($\mu_Q$) | 25 m/s | 1 m/s | 1.08 |
| Standard deviation of wind pressure ($\sigma_Q$) | 0.25 | 0.01 | 1.02 |
| Reliability target ($\beta$) | 3.0 | 0.1 | 1.03 |
| Wind load sensitivity factor ($\alpha_Q$) | 0.7 | 0.1 | 1.1 |
| Combined factor | – | – | 1.25 |

factor $\alpha_Q = 0.7$, the probability $(1–P_F) = \Phi(\alpha_Q\beta) = 0.982$, results in $\theta_\beta = 2.68$. The sensitivity of the wind load to the various parameters ($X$) of Eq. (21.2) can be obtained by varying each parameter by an increment $\delta_X$ and apply the ratio $\Delta_X/\delta_X = \gamma_{X+\delta}/\gamma_X$ to the load factor $\gamma_{W,adj} = \gamma_W\ \Delta_X/\delta_X$ as tabulated in Table 21.1.

The sensitivity parameters represent different sources of information and related decision making. Trends in mean annual extreme wind speed, indicated by $\mu_Q$ should be the most direct observation to be made, reflecting the intensity in windstorms for the regional climate zones of the country [20]. Shifts in extreme wind climate, reflected by $\sigma_Q$, could be projected from existing conditions [15]. Engagement with climatologists at an early stage on identifying wind parameter trends is a distinct advantage of a vulnerability policy [39].

Adjustment of the reliability target $\beta$ could be used to adjust the reference value for existing structures [60], or as basic decision parameter to measure the effectiveness of additional robustness. The wind load sensitivity factor $\alpha_Q$ reflects the level of reliability analysis on which decisions are based. Adjustments could be applied at design, or generically to the provisions for the ACC design situation.

The sensitivity of wind load to the load distribution factor ($c_w$), see Eq. (21.1), could also be considered. Probability models for the components of $c_w$, terrain roughness ($c_r$), pressure coefficients ($c_p$), are provided by [14], by [58] for differentiation of wind resistant substructures, by [59] for wind directionality ($c_d$).

## 21.7 Conclusions

The case study considered the feasibility of adapting the design basis for building structures in South Africa to anticipate the impact of anthropogenic changes to the climate during the service life of building structures. Adaptation of the design base for climate loading to minimize the vulnerability of the structure against future ambiguous climate conditions appears to provide a feasible approach. A design situation for climate change is introduced to achieve additional robustness as an accidental design situation. Standardized procedures for loading are adapted to account for climate ambiguity, using the partial factor limit states format. Additional climate

robustness can be provided against possible changes to account for changes in wind speed, its variability, reliability modeling and requirements.

Several advantages, related to standards development and design, arise from introducing a design base for a climate change design situation. Recognition is given at an early stage to this indefinite threat to structures by the changing climate. Designers are guided to make decisions on climate vulnerability that can be identified and optimized for a specific project and its life cycle requirements. This practice is projected to a significant class of capital investment across the country through standardization.

Maximum use is made of available information to counter the ambiguity of the future situation. This is to the benefit of both users and standards developers. Critical components of the design base for wind loading are scrutinized for reinterpretation. The required information on climate change is identified for application in reliability and ambiguity research and engagement with climatologists. Guidance on decision-making under ambiguity of low probability conditions, including criteria and methodologies will follow from early measures. Reassessment of the current design base is bound to refine requirements and verification procedures of the current standard.

The main conclusion of this case study is that the first steps are possible to incorporate provisions for ACC into the South African standard, based on principles of limit states design. Immediate measures can effectively be introduced against arguably the most significant source of uncertainty challenging structural performance, even for the present generation of structures. Differentiated action can be taken by the designer in operational decision-making; in standardization by recognizing the importance of the situation and to provide an appropriate approach; at professional level by collective efforts to keep pace with the evolvement of adverse conditions that forms part and parcel of the Anthropocene epoch that we live in.

## References

1. ISO 2394 (2015) General principles on reliability for structures. International Organization for Standardization.
2. ISO 13824 (2020) Bases for design of structures—general principles on risk assessment of systems involving structures. International Organization for Standardization
3. ISO 22111 (2019) Basis for design of structures—general requirements. International Organization for Standardization
4. IPCC (2014) 5th assessment report (AR5). Climate change 2014: synthesis report. In: Pachauri RK, Meyer LA (eds) Contribution of working Groups I, II and III to the fifth assessment report of the intergovernmental panel on climate change. IPCC, Geneva, Switzerland, pp 151
5. IPCC (2018) Global warming of 1.5°C. An IPCC special report. summary for policymakers. World meteorological organization, Geneva, Switzerland, p 32
6. SABS (2019) SANS 10160:2019. Basis of structural design and actions for buildings and industrial structures. SABS Standards Division, South Africa
7. CEN (2002) European commission for standardization EN 1990:2002. Eurocode—basis for structural design. Brussels
8. SABS (2016) SANS 2394:2016, ISO 2394:2015. General principles on reliability for structures. SABS Standards Division, South Africa

9. Bastidas-Arteaga E, Stewart MG (2019) Climate adaptation engineering: risk and economics for infrastructure decision-making. Elsevier-Butterworth-Heinemann
10. Weaver CP, Lempert RJ, Brown C, Hall JA, Revell D, Sarewitz D (2013) Improving the contribution of climate model information to decision making: the value and demands of robust decision frameworks. WIREs Clim Chang 4:39–60. https://doi.org/10.1002/wcc.202
11. Helgeson C, 2018. Structuring decisions under deep uncertainty. Topoi, published online 14 August 2018. https://doi.org/10.1007/s11245-018-9584-y
12. Milford RV (1988) Target safety and SABS 0160 load factors. The Civil Engineer in South Africa 30(10):475–481
13. Retief JV, Dunaiski PE (2009) The limit states basis of design for SANS 10160–1. In Retief JV, Dunaiski PE (eds), Background to SANS 10160. Sun Media. ISBN 978–1–920338–10–7
14. Botha J, Retief JV, Viljoen C (2018) Uncertainties in the South African wind load design formulation, 16–29. Reliability assessment of the South African wind load design formulation, 30–40. J SAICE 60(3)
15. Kruger AC, Retief JV, Goliger AM (2017) Development of an updated fundamental basic wind speed map for SANS 10160–3 J SAICE 59(4):12–25
16. Kruger AC, Goliger AM, Retief JV, Sekele S (2010) Strong wind climatic zones in South Africa. Wind Struct J 13(1):37–55
17. Goliger AM, Retief JV, Dunaiski PE, Kruger AC (2009) Revised wind-loading design procedures for SANS 10160. In: Retief JV, Dunaiski PE (eds) Background to SANS 10160. Sun Media, pp 149–166
18. Milford RV (1987) Annual maximum wind speed for South Africa. The Civil Engineer in South Africa 29(1):15–19
19. Kruger AC, Retief JV, Goliger AM (2013) Strong wind in South Africa—part 1 application of estimation methods; part 2 mapping of updated statistics. J SAICE 55(2):29–58
20. Bakker FP (2020) Characterisation of the South African extreme wind environment relevant to standardisation. PhD Dissertation submitted to Stellenbosch University
21. Goliger AM, Retief JV, Kruger AC (2017) Review of climatic input data for wind load design in accordance with SANS 10160–3. Journal SAICE 59(4):2–11
22. IPCC (2007) Summary for policymakers. In: Climate change 2007: the physical science basis. AR4. Fourth assessment report of the intergovernmental panel on climate change. Cambridge University Press, Cambridge, United Kingdom and New York, NY, USA
23. Gidden MJ, Riahi K, Smith SJ et al (2019) Global emissions pathways under different socioeconomic scenarios for use in CMIP6: a dataset of harmonized emissions trajectories through the end of the century. Geosci Model Dev 12:1443–1475. https://doi.org/10.5194/gmd-12-1443-2019
24. Meehl GA, Zwiers F, Evans J, Knutson T, Mearns L, Whetton P (2000) Trends in extreme weather and climate events: issues related to modeling extremes in projections of future climate change. Bullet AMS 87(3):427–436
25. Van Vuuren DP, Edmomds J, Kainuma M et al (2011) The representative pathways: an overview. Clim Change 109:5–1
26. Lyu K, Zhang X, Church JA, Hu J (2015) Quantifying internally generated and externally forced climate signals at regional scales in CMIP5 models. Geophys Res Lett 42:9394–9403. https://doi.org/10.1002/2015GL065508
27. Ackerman F,·DeCanio SJ, Howarth RB, Sheeran K (2009) Limitations of integrated assessment models of climate change. Clim Change 95:297–315
28. Nordhaus WD (2007) A review of the Stern review on the economics of climate change. J Econ Lit XLV:686–702
29. Nordhaus WD (2011) The economics of tail events with an application to climate change. Rev Environ Econ Policy 5(2):240–257. https://doi.org/10.1093/reep/rer004
30. Weitzman ML (2007) A review of the Stern review. J of Economic Literature XLV:703–724
31. Weitzman ML (2009) On modeling and interpreting the economics of catastrophic climate change. Rev Econ Stat 91(1):1–19

32. Dilling L, Daly M, Travis WR, Wilhelm OV, Klein RA (2015) The dynamics of vulnerability: why adapting to climate variability will not always prepare us for climate change. WIREs Clim Chang. https://doi.org/10.1002/wcc.341
33. Stoerk T, Wagner G, Ward RET (2018) Policy brief—recommendations for improving the treatment of risk and uncertainty in economic estimates of climate impacts in the sixth intergovernmental panel on climate change assessment report. Rev Environ Econ Policy 12(2):371–376. Summer 2018
34. Auld HE (2008) Adaptation by design: the impact of changing climate on infrastructure. J Public Works & Infrastructure. 1(3):276–288
35. Hallegatte S (2009) Strategies to adapt to an uncertain climate change. Glob Environ Chang 19:240–247
36. Heal G, Millner A (2013) Uncertainty and decision making in climate change economics. The author 2013. Oxford University Press on behalf of the Association of Environmental and Resource
37. Katz RW (2010) Statistics of extremes in climate change. Clim Change 2010(100):71–76. https://doi.org/10.1007/s10584-010-9834-5
38. Kunreuther H, Heal G, Allen M, Edenhofer O, Field CB, Yohe G (2012) Risk management and climate change. Working Paper 18607 National Bureau of Economic Research, Cambridge, Ma. http://www.nber.org/papers/w18607
39. Socolow RH (2011) High-consequence outcomes and internal disagreements. Clim Change 108:775–790
40. Shepherd TG, Boyd E, Calel RA, Chapman SC, Dessai S et al (2018) Storylines: An alternative approach to representing uncertainty in physical aspects of climate change. Clim Change 151:555–571. https://doi.org/10.1007/s10584-018-2317-9
41. Sutton RT (2019) Climate science needs to take risk assessment more seriously. Bullet AMS:1637–1642
42. Weaver CP, Moss RH, Ebi KL, Gleick PH, Stern PC, Tebaldi C, Wilson RS, Arvai JL (2017) Re-framing climate change assessments around risk: recommendations for the US national climate assessment. Environ Res Lett 12**:**080201. https://doi.org/10.1088/1748-9326/aa7494
43. Trzeciak TM, Knippertz P, Pirret JSR, Williams KD (2016) Can we trust climate models to realistically represent severe European windstorms? Clim Dyn 46:3432–3451
44. Zappa G (2019) Regional climate impacts of future changes in the mid-latitude atmospheric circulation: a storyline view. Curr Clim Chang Rep 5:358–371
45. Catto JL, Ackerley D, Booth JF et al (2019) The future of midlatitude cyclones. Curr clim change Rep 5:407–420
46. Raible CC, Pinto JG, Ludwig P, Messmer M (2020) A review of past changes in extratropical cyclones in the northern hemisphere and what can be learned for the future. WIREs Clim Chang. https://doi.org/10.1002/wcc.680
47. Chang EKM (2017) Projected significant increase in the number of extreme extratropical cyclones in the southern hemisphere. J Clim 30:4915–4935
48. Reboita MS, Reale M, da Rocha RP, Giorgi F et al (2020) Future changes in the wintertime cyclonic activity over the CORDEX-CORE southern hemisphere domains in a multi-model approach. Clim Dyn. https://doi.org/10.1007/s00382-020-05317-z
49. Bouwer LM (2011) Have disaster losses increased due to anthropogenic climate change? Bull Am Meteor Soc 92(1):39–46
50. Engelbrecht FA, Landman 1 WA, Engelbrecht CJ, Landman S, Bopape MM, Roux B, McGregor JL, Thatcher M (2011) Multi-scale climate modelling over Southern Africa using a variable-resolution global model. Water SA 37(5). WRC 40-Year Celebration Special Edition 2011
51. Landman W, Engelbrecht F, Hewitson B, van der Merwe J, Malherbe J (2017) Towards bridging the gap between climate change projections and maize producers in South Africa. Theor Appl Climatol. https://doi.org/10.1007/s00704-017-2168-8
52. Hulme M, Doherty R, Todd N, New M, Lister D (2001) African climate change: 1900–2100. Clim Res 17:145–168
53. Jury MR (2013) Climate trends in Southern Africa. S Afr J Sci 109:53–63

54. Jury MR (2017) Climate trends across South Africa since 1980. Water SA (3(4):297–307
55. Kusangaya D, Warburton ML, Archer van Garderen E, Hewitt GPW (2014) Impacts of climate change on water resources in southern Africa. Phys Chem Earth 67–69:47–54
56. Jury MR (2020) Climate trends in the Cape Town area, South Africa. Water SA 46(3):438–447. https://doi.org/10.17159/wsa/2020.v46.i3.8654
57. Jury MR (2019) South Africa's future climate: trends and projections. Springer, The Geography of South Africa
58. Hansen SE, Pedersen ML, Sorensen JD (2015) Probability based calibration of pressure coefficients. In: ICWE14, Fourteenth International Conference on Wind Engineering, Port Alegre, Brazil
59. McAllister TP, Wang N, Ellingwood BR (2018) Risk-informed mean recurrence intervals for updated wind maps in ASCE. J Struct Eng 144(5):7–16
60. Holický M, Retief JV, Viljoen C (2021) Reliability basis for assessment of existing building structures with reference to SANS 10160. J SAICE 63(1):2–10

# Part IV
# Conclusions and Recommendations

# Chapter 22
# Conclusions for Engineers and Policy Makers


**David V. Rosowsky and Mark G. Stewart**

**Abstract** This closing chapter provides a discussion of the political, economic and social imperatives that affect the policy making decision process for extreme events. It shows that the tools are available to inform policy makers to make calm and considered decisions based on risk assessments that considers the preferences of all stakeholders including the public. However, challenges remain if risk-based decisions are to become truly mainstream in the education of engineers and the engineering practice more broadly.

This book brings together leading scholars in risk-based decision around civil infrastructure engineering topics, case studies reflecting current challenges and state-of-the-art in risk-based decision (including both design and assessment), and indications of where risk-based decision is heading is a rapidly maturing multi-disciplinary space when considering often large, often distributed engineering systems subject to extreme loads. These loads include both those arising from natural hazards as well as manmade or technological hazards.

Extreme loads such as those arising from environmental or structural actions for which long records may exist have been long studied and well characterized probabilistically for decades. These models of extreme loads were essential to the development of robust (and now widely used) reliability-based load standards and design codes for wind, seismic, snow, impact and other hazards. Robust statistical models of extreme loads (demands) on structures and infrastructure systems also are required to fully realize the emerging performance-based engineering methodologies (and other multi-objective design philosophies) being developed by several countries.

In cases where records (or other data) are not available, the modeling of predicted extremes becomes more difficult, relying more on engineering judgement and expert

D. V. Rosowsky (✉)
Kansas State University, Manhattan, KS, USA
e-mail: rosowsky@ksu.edu

M. G. Stewart
The University of Newcastle, Newcastle, Australia
e-mail: mark.stewart@newcastle.edu.au



M. G. Stewart and D. V. Rosowsky (eds.), *Engineering for Extremes*, Springer Tracts in Civil Engineering, https://doi.org/10.1007/978-3-030-85018-0_22

opinion (individual or collective, *i.e.* via Delphi method or committee consensus). Such is the case when new or previously unconsidered loads/actions become important in the design process, as in the case of terrorist blast or biological release, for example. It may also be the case in extreme loads for which few data exist, as in the case of extreme flood levels in a region projected to be impacted by the changing climate in the decades ahead.

The case studies in this book include consideration of all of these issues around characterization of extreme loads, and demonstrate how both the intrinsic variability (aleatoric uncertainty) and the uncertainty arising from incomplete information (epistemic uncertainty) can be taken into account in a risk analysis framework intended to inform/guide decision.

While the focus of this book is on the application of risk-based decision to the design or assessment of civil infrastructure systems, the concepts apply (and can scale) to many other engineering fields and applications. Importantly, we make clear that risk-based decision is relatively mature in civil engineering applications, perhaps due in part to the fact that much of the early work in the application of probability, statistics, and risk analysis was by civil engineers. As a result, structural design codes have been formulated using reliability methods for decades in many parts of the world. Still, the contributions in this book also make clear that considerable work remains if risk-based decision is to become truly mainstream in the education of engineers and the engineering practice more broadly.

Despite our efforts to establish a common lexicon, for example, the variations in terminology and nomenclature in the chapters points to another essential need. In order for risk-based decision to become a true part of the engineer's toolbox (and that of the decision-maker), a common language will need to be established, along with a common (well understood and accepted) set of tools/techniques, and even a common framework for risk-based decision. One such definition might be the distinction between risk-*informed* decision versus risk-*based* decision. This remains an area for future work, *e.g.*, how to include and balance quantitative vs. qualitative information, predictive (but incomplete or imperfect) models vs. engineering judgment, etc.

Risk-based (or informed) decision nearly always implies a combination of quantitative and qualitative analysis. Engineers will need to become comfortable with that duality and be able to properly contextualize both. Qualitative analyses (or statements of fact) may be biased by their nature. However, quantitative models yield results that are biased through incompleteness, inaccuracies, simplifications, or model limitations. The engineer, stakeholders and decision maker must understand the power (role, importance/value) and the limitations (biases, risk of erroneous conclusion) of both.

When we started thinking about this book, and again as it was being written, we carefully considered whether a global pandemic should be addressed explicitly (*e.g.*, as a global health crisis, with associated demands on infrastructure and other engineered systems). This was, sadly, all too present on everyone's mind in 2020 and 2021. While we opted not to include pandemics (or any global health or bioterrorism events), it seems clear that many of the same techniques described in this chapter may be applicable. The global public health community, as well as

biohazard/bioterrorism/biosecurity experts worldwide are well versed in risk-based methodologies and this could easily fill another book.

The analysis of extremes will continue to be challenged by politics and policies, despite best efforts to let data and experts inform science, and science inform policy. Perhaps the two ways this is most true would be: (1) the politicization of climate change and associated impacts, and (2) the government response to domestic and international terrorism activity. In one case, our ability to develop responsible, science-based predictive models may be hampered, while in the other case we may see entirely new extreme events developed and used by bad actors and those who would seek to maximize damage to iconic structures, disruption to critical facilities, or harm to populations where countering these threats may undermine our freedom.

Regardless, engineers—and civil engineers in particular—will need to be able to assess risk, temper model predicted results (and risks), and merge them with experience-based judgement to make decisions affecting the safety and performance of critical facilities. This is true when designing, building, assessing, or retrofitting those facilities, whether in the face of new materials or systems, incomplete information about extreme events, and even new or future hazards that are yet to be identified.

There is much to be optimistic about. As this book shows, risk-based approaches to infrastructure design, construction, maintenance and management have led to safer and more resilient infrastructure. At least in the developed world, a building or bridge collapse is almost unheard of, as are dam failures, aircraft crashes, or mass casualties. To be sure, there are challenges to be faced. Climate change and sustainability foremost among them. However, the science and the tools are available to inform policy makers to make calm and considered decisions (science-based and data-informed) based on risk assessments that considers the preferences of all stakeholders including the public. We hope this book has provided some useful guidance about how best to examine, assess, and manage these important challenges.

# Correction to: Extreme Vehicles and Bridge Safety


**Colin Caprani and Mayer Melhem**

**Correction to:**
**Chapter 13 in: M. G. Stewart and D. V. Rosowsky (eds.), *Engineering for Extremes*, Springer Tracts in Civil Engineering, https://doi.org/10.1007/978-3-030-85018-0_13**

The book was inadvertently published with errors in chapter 13. These errors have now been updated with the correction chapter.

The updated version of this chapter can be found at
https://doi.org/10.1007/978-3-030-85018-0_13



M. G. Stewart and D. V. Rosowsky (eds.), *Engineering for Extremes*, Springer Tracts in Civil Engineering, https://doi.org/10.1007/978-3-030-85018-0_23